
[All ETDs from UAB](#)

[UAB Theses & Dissertations](#)

2014

Drag Coefficients for Highway Variable Message Sign Structures

Joseph Phillips
University of Alabama at Birmingham

Follow this and additional works at: <https://digitalcommons.library.uab.edu/etd-collection>

Recommended Citation

Phillips, Joseph, "Drag Coefficients for Highway Variable Message Sign Structures" (2014). *All ETDs from UAB*. 2722.

<https://digitalcommons.library.uab.edu/etd-collection/2722>

This content has been accepted for inclusion by an authorized administrator of the UAB Digital Commons, and is provided as a free open access item. All inquiries regarding this item or the UAB Digital Commons should be directed to the [UAB Libraries Office of Scholarly Communication](#).

DRAG COEFFICIENTS FOR HIGHWAY VARIABLE MESSAGE SIGN
STRUCTURES

by

JOSEPH A. PHILLIPS

FOUAD H. FOUAD, COMMITTEE CHAIR
IAN E. HOSCH
JASON T. KIRBY

A THESIS

Submitted to the graduate faculty of The University of Alabama at Birmingham,
in partial fulfillment of the requirements for the degree of
Master of Science

BIRMINGHAM, ALABAMA

2014

Copyright by
Joseph A. Phillips
2014

DRAG COEFFICIENTS FOR HIGHWAY VARIABLE MESSAGE SIGN STRUCTURES

JOSEPH A. PHILLIPS

DEPARTMENT OF CIVIL, CONSTRUCTION, AND ENVIRONMENTAL
ENGINEERING

ABSTRACT

Variable Message Signs (VMS) are becoming an integral part of transportation infrastructure on US interstates and highways. VMS structures are vital in ensuring the safety of motorists by relaying messages concerning potential road hazards such as fog, traffic congestion, highway construction, and lane closures. These structures are larger and heavier than typical flat panel signs, and thus behave differently when subjected to wind loads. The design of VMS structures is specified in the 2013 edition of the American Association of State Highway and Transportation Officials (AASHTO) *Standard Specifications for Structural Supports for Highway Signs, Luminaires, and Traffic Signals*.

The AASHTO Supports Specifications currently provide a single drag coefficient for all VMS applications: “A value of 1.7 is suggested for Variable Message Signs (VMS) until research efforts can provide precise drag coefficients.” However, the actual drag coefficient varies depending on a number of factors, including: wind speed, wind direction, structural geometry, and vibration characteristics. The drag coefficient for VMS structures provided in the AASHTO Supports Specifications is an estimate which does not account for the variability of wind loading and structure properties. Accurate drag coefficients for VMS structures are not available to designers, potentially leading to unsafe or inefficient designs.

The objective of this study was to develop accurate drag coefficients for VMS to be incorporated in the AASHTO Supports Specifications. Experimental testing was performed at the FIU Wall of Wind testing facility to develop a table of drag coefficients for VMS organized according to aspect and depth ratios. The accuracy of the drag coefficients was verified at UAB using experimental data and FEA dynamic modeling. The analyses showed that the current VMS drag coefficient of 1.7 specified in the AASHTO Supports Specifications is overly conservative. In addition, a sensitivity study was conducted to investigate the impact of the new VMS drag coefficients on the design of sign structures. It was determined that the new VMS drag coefficients significantly reduced the design stresses for both extreme event wind and fatigue level wind. The effects of corner modifications were also investigated and found to cause additional reductions in the VMS drag coefficients.

DEDICATION

This Thesis is dedicated to my family and friends for their continuous support and encouragement over the years. I am especially grateful to my parents, Ted and Karen Phillips, for providing me with an excellent education and helping to prepare me for my future career.

ACKNOWLEDGMENTS

I would like to thank my advisor and mentor, Dr. Fouad H. Fouad, who guided me through the research involved with this project. I am very grateful to Dr. Fouad for investing his time and insight in this project, and also providing me with this research opportunity. I also want to thank Dr. Ian E. Hosch for assisting in the work performed on this project and providing his expertise throughout the entire research process. In addition, I am appreciative of Barbara Clements for her valuable input on the design aspects of this project. Finally, I want to thank Dr. Fouad, Dr. Hosch, and Dr. Jason T. Kirby for serving on my Thesis committee and providing valuable feedback on my research work.

TABLE OF CONTENTS

ABSTRACT	iii
DEDICATION.....	v
ACKNOWLEDGEMENTS.....	vi
LIST OF TABLES.....	xi
LIST OF FIGURES	xiv
LIST OF ABBREVIATIONS.....	xxi
CHAPTER 1 INTRODUCTION.....	1
1.1 Problem Statement.....	1
1.2 Research Objectives.....	2
1.3 Research Methodology.....	3
1.4 Report Outline.....	6
CHAPTER 2 BACKGROUND AND LITERATURE REVIEW ON DRAG.....	9
2.1 Chapter Overview.....	9
2.2 Background.....	9
2.2.1 Drag on Bluff Bodies.....	9
2.2.2 Application of Drag to VMS Structures.....	12
2.3 Literature Review for Drag on Sign Structures.....	13
2.3.1 Ginger et al (1998).....	14
2.3.2 Letchford (2001).....	17
2.3.3 Quinn et al (2001).....	20
2.3.4 Smith et al (2014).....	23
2.3.5 Zuo (2014).....	25
2.3.6 Literature Review Summary.....	30
CHAPTER 3 WALL OF WIND TESTING AT FIU TO DEVELOP DRAG COEFFICIENTS	33
3.1 Chapter Overview.....	33
3.2 Experimental Testing.....	33
3.2.1 FIU Wall of Wind.....	34

3.2.2	VMS Test Models	35
3.2.3	Calibration Tests	37
3.2.4	Drag Coefficient Tests	39
3.2.5	Testing Summary	43
3.3	Test Results	44
3.3.1	Calculation of Drag Coefficients	44
3.3.2	Effect of Aspect Ratio	47
3.3.3	Effect of Depth Ratio	50
3.3.4	Effect of Wind Direction	53
3.3.5	Effect of Corner Modifications	55
3.3.6	Other Considerations	56
3.3.7	Comparison with Literature	57
3.4	Summary Table of Drag Coefficients	59
3.5	Conclusions from Wall of Wind Study	59
CHAPTER 4 VMS STRUCTURES		62
4.1	Chapter Overview	62
4.2	Site Locations	62
4.3	Structure A – Alabaster VMS Structure	64
4.3.1	Overview of Structure	64
4.3.2	Geometric Properties	68
4.3.3	Material Properties	68
4.4	Structure B – Birmingham VMS Structure	71
4.4.1	Overview of Structure	71
4.4.2	Geometric Properties	74
4.4.3	Material Properties	74
4.5	Variable Message Signs	77
CHAPTER 5 FINITE ELEMENT MODELING		78
5.1	Chapter Overview	78
5.2	SAP2000 Software Program	78
5.3	Finite Element Models of VMS Structures	79
5.3.1	Structural Frame	81
5.3.2	Variable Message Sign	83
5.3.3	Support Conditions	84
5.3.4	Access Ladder and Track	86
5.4	Modal Analyses	87
5.4.1	Structure A – Alabaster VMS Structure	87
5.4.2	Structure B – Birmingham VMS Structure	89
CHAPTER 6 COMPARISON OF DRAG COEFFICIENTS USING EXPERIMENTAL DATA AND FEA DYNAMIC MODELING		92
6.1	Chapter Overview	92

6.2	Experimental Analysis	92
6.2.1	Experimental Study of Structure A	93
6.2.2	Experimental Data Selected for Verification Study	104
6.2.3	Experimental Modal Analysis	106
6.3	SAP Dynamic Analyses	113
6.3.1	Wind Pressure Calculations	114
6.3.2	SAP Wind Loading	119
6.3.3	SAP Structural Response	120
6.4	Experimental Data vs. SAP Results	121
6.4.1	Selection of Analysis Intervals	121
6.4.2	Selection of Quasi-static Stress Response	122
6.4.3	Plots of Stress Range vs. Average Wind Velocity	124
6.4.4	Stress Range Tables	128
6.5	Conclusions of Drag Coefficient Verification Study	130
CHAPTER 7 SENSITIVITY STUDY		131
7.1	Chapter Overview	131
7.2	Parameters of Sensitivity Study	131
7.3	SAP Static Analyses	132
7.3.1	Wind Pressure Calculations	133
7.3.2	SAP Load Combinations	139
7.3.3	SAP Structural Response	141
7.4	Stress Reduction	173
7.4.1	Summary of Stress Ratios	173
7.4.2	Discussion of Stress Ratio Results	175
7.5	Analysis of Study Parameters	178
7.6	Conclusions of Sensitivity Study	184
CHAPTER 8 PROPOSED CODE LANGUAGE AND COMMENTARY		186
8.1	Chapter Overview	186
8.2	Proposed Drag Coefficients for AASHTO Supports Specifications	186
8.3	Proposed Commentary for AASHTO Supports Specifications	187
CHAPTER 9 CONCLUSIONS AND FUTURE RESEARCH		188
9.1	Chapter Overview	188
9.2	Summary of Findings	188
9.2.1	Wall of Wind Testing at FIU	188
9.2.2	Drag Coefficient Verification Study at UAB	189
9.2.3	Sensitivity Study at UAB	190
9.3	Recommendations for Future Research	191
LIST OF REFERENCES		193

APPENDIX	197
A SHOP DRAWINGS OF VMS STRUCTURES	197
B PRESSURE CALCULATIONS	210
C SAP STRESS DIAGRAMS FOR SENSITIVITY STUDY	220

LIST OF TABLES

<i>Table</i>	<i>Page</i>
2-1 Selected drag coefficients for fences (Ginger 1998).....	16
2-2 Drag coefficients for hoardings (Ginger 1998).....	16
2-3 Selected drag coefficients for wind normal to hoardings (Letchford 2001).....	18
2-4 Selected drag coefficient results for wind normal to sign (Quinn 2001).....	22
2-5 Critical mean and pseudo-steady force coefficients of five sign models tested by Zuo et al (2014)	29
3-1 Model Dimensions and Geometric Ratios (Meyer 2014).....	36
3-2 Testing Summary (Meyer 2014).....	44
3-3 Summary of mean force coefficient results for the 0° wind direction (Meyer 2014)	46
3-4 Summary of mean force coefficient results for the 45° wind direction (Meyer 2014)	46
3-5 Drag Coefficient Design Matrix for C_{Fx} (Meyer 2014).....	59
4-1 Geometric Properties for Structure A	70
4-2 Material Properties for Structure A.....	70
4-3 Member Properties for Structure B.....	76
4-4 Material Properties for Structure B.....	76
5-1 SAP Mode Shapes for Structure A	89
5-2 Mode Shapes for Structure B.....	91
6-1 ALDOT Data Collection Schedule	104

6-2	Frequency Comparison	109
6-3	Modal Damping Values for Structure A	113
6-4	Drag Coefficients from FIU Wall of Wind Testing.....	118
6-5	Drag Coefficients used for SAP Analyses	119
6-6	Stress Range Values for Strain Gauge 2 Location.....	129
6-7	Stress Range Values for Strain Gauge 4 Location.....	129
6-8	Stress Range Values for Strain Gauge 6 Location.....	129
6-9	Stress Range Values for Strain Gauge 8 Location.....	130
7-1	Parameters for Sensitivity Study.....	132
7-2	K_z Factors for Structure A	135
7-3	K_z Factors for Structure B.....	135
7-4	Drag Coefficients for Sensitivity Analysis	138
7-5	AASHTO Group Load Combinations	139
7-6	Extreme Wind Load Cases.....	140
7-7	Fatigue Wind Load Cases	141
7-8	Member Stresses (psi) for Load Cases 1-3 (Structure A, V = 90 mph).....	149
7-9	Member Stresses (psi) for Load Cases 4-6 (Structure A, V = 150 mph).....	150
7-10	Member Stresses σ (psi) for Load Cases 7-9 (Structure B, V = 90 mph).....	151
7-11	Member Stresses (psi) for Load Cases 10-12 (Structure B, V = 150 mph)	152
7-12	Maximum Stresses for Load Cases 1-12	160
7-13	Member Stress Ranges (psi) for Load Cases 13-15 (Structure A).....	166
7-14	Member Stress Ranges (psi) for Load Cases 16-18 (Structure B).....	167
7-15	Maximum Stress Ranges for Load Cases 13-18.....	171

7-16	Stress Ratios for Extreme Wind (Load Cases 1-12).....	174
7-17	Stress Ratios for Fatigue Wind (Load Cases 13-18).....	174
8-1	VMS Drag Coefficients, C_d	186

LIST OF FIGURES

<i>Figure</i>		<i>Page</i>
1-1	Variable Message Sign (VMS).....	2
1-2	Flow chart for research methodology of VMS project	5
2-1	Flow around streamlined and bluff bodies (Holmes 2001)	10
2-2	Dimensions for sign ratios	13
2-3	Fence and Hoarding Configurations (Ginger 1998)	14
2-4	Drag coefficient vs. wind direction for $c/h = 0.57$ (Ginger 1998)	16
2-5	Mean drag coefficient comparison for elevated panels (Letchford 2001)	19
2-6	Mean drag coefficients for panels with aspect ratio = 2 as a function of wind direction (Letchford 2001).....	20
2-7	Photo of 750 mm square sign mounted on support frame (Quinn 2001).....	21
2-8	Full-scale sign used for experimental study (Smith 2014)	24
2-9	Full-scale drag coefficients compared with wind tunnel studies (Smith 2014)....	25
2-10	Sign models tested in phase 2 of the wind tunnel experiments (Zuo 2014)	26
2-11	Mean force coefficient vs. yaw angle for 5 sign models (Zuo 2014)	28
2-12	Pseudo-steady force coefficient vs. yaw angle for 5 sign models (Zuo 2014)	29
3-1	FIU Wall of Wind (Meyer 2014)	34
3-2	Tare test Setup B for 45° configuration (Meyer 2014)	38
3-3	Tare test Setup A for 0° configuration (Meyer 2014).....	38
3-4	Force coefficient test setup for the 0° wind direction (Meyer 2014)	40

3-5	Force coefficient test setup for the 45° wind direction (Meyer 2014)	40
3-6	Round edge test setup (Meyer 2014)	42
3-7	Chamfer edge test setup (Meyer 2014).....	42
3-8	Galloping test setup for -4.5° angle (Meyer 2014).....	43
3-9	Effect of aspect ratio (b/c) on normal force coefficient for 0° wind direction at 15 m/s (Meyer 2014).....	48
3-10	Effect of aspect ratio (b/c) on normal force coefficient for 0° wind direction at 40 m/s (Meyer 2014).....	49
3-11	Effect of aspect ratio (b/c) on the normal force coefficient for the 45° wind direction at 15 m/s (Meyer 2014).....	49
3-12	Effect of aspect ratio (b/c) on the normal force coefficient for the 45° wind direction at 40 m/s (Meyer 2014).....	50
3-13	Effect of depth ratio (d/c) on the normal force coefficient for the 0° wind direction at 15 m/s (Meyer 2014).....	51
3-14	Effect of depth ratio (d/c) on the normal force coefficient for the 0° wind direction at 40 m/s (Meyer 2014).....	52
3-15	Effect of depth ratio (d/c) on the normal force coefficient for the 45° wind direction at 15 m/s (Meyer 2014).....	52
3-16	Effect of depth ratio (d/c) on the normal force coefficient for the 45° wind direction at 40 m/s (Meyer 2014).....	53
3-17	Comparison of normal force coefficients for the 0° and 45° wind directions at 15 m/s (Meyer 2014).....	54
3-18	Comparison of normal force coefficients for the 0° and 45° wind directions at 40 m/s (Meyer 2014).....	54
3-19	Comparison of sharp (model 9) and modified corner (Models 10 and 11) results for 0° wind direction (Meyer 2014).....	55
3-20	Comparison of sharp (model 9) and modified corner (Models 10 and 11) results for 45° wind direction (Meyer 2014).....	56
3-21	Comparison of FIU WOW and past research results for normal force coefficient (Meyer 2014)	58

4-1	Front View of Structure A (Alabaster VMS Structure)	63
4-2	Front View of Structure B (Birmingham VMS Structure)	64
4-3	Truss Splice Connection of Structure A	65
4-4	Truss to Upright Connection of Structure A.....	66
4-5	Left Upright Splice Connection of Structure A	66
4-6	Base Plate and Foundation of Structure A.....	67
4-7	Access Ladder and Track of Structure A	67
4-8	Structure A - 3D view	69
4-9	Structure A - Front View	69
4-10	Truss Splice Connection of Structure B.....	72
4-11	Truss to Upright Connection of Structure B	72
4-12	Base Plates and Foundation of Structure B.....	73
4-13	Access Ladder and Track of Structure B	73
4-14	Structure B - 3D View	75
4-15	Structure B - Front View.....	75
4-16	VMS Front and Side View.....	77
5-1	SAP Model of Structure A.....	80
5-2	SAP Model of Structure B	80
5-3	Structural Frame Model for Structure A.....	81
5-4	Splice Connections for Left Upright.....	82
5-5	Connections between Truss Chords and Upright.....	83
5-6	Connection of Z-bars to Truss Chords.....	83
5-7	Connection of VMS to Z-bars.....	84

5-8	Base Plates, Anchor Bolts, and Foundations for Structure A	85
5-9	Access Ladder and Track for Structure A.....	86
5-10	Structure A Mode Shape 1 – Longitudinal	88
5-11	Structure A Mode Shape 2 – Horizontal.....	88
5-12	Structure A Mode Shape 3 – Vertical	89
5-13	Structure B Mode Shape 1 – Horizontal	90
5-14	Structure B Mode Shape 2 – Longitudinal	91
5-15	Structure B Mode Shape 3 – Vertical	91
6-1	Strain Gauge Placement on Upright Posts (Adapted from Fouad 2011)	95
6-2	Strain Gauges Attached to Upright at Location 1 (Fouad 2011)	96
6-3	Strain Gauges Attached to Upright with Tape at Location 2 (Fouad 2011)	96
6-4	Strain Gauge Placement on Truss Chord (Adapted from Fouad 2011)	97
6-5	Strain Gauges Attached to Truss Chord (Fouad 2011).....	97
6-6	Accelerometer Placement on Truss Chords and WT Section (Adapted from Fouad 2011)	99
6-7	Attachment of Accelerometer 4H to Truss Chord (Fouad 2011)	99
6-8	Anemometer Placement on Structure (F. H. Fouad 2011).....	101
6-9	Anemometers Connected to Structure with Steel Extension (Fouad 2011)	101
6-10	ALDOT Van with Instrumentation Wiring (Fouad 2011).....	102
6-11	Wind Velocity Time History from Anemometer 1	103
6-12	Strain Time History from Strain Gauge 2.....	103
6-13	Acceleration Time History from Accelerometer 3H	103
6-14	Wind Rose for Run 16	105
6-15	Mode Shapes of Structure A	106

6-16	Response Spectrum of Longitudinal (Mode 1) Acceleration	107
6-17	Response Spectrum of Horizontal (Mode 2) Acceleration	108
6-18	Response Spectrum of Vertical (Mode 3) Acceleration	108
6-19	Sample of Acceleration Response Time History for Damping Calculations	111
6-20	Exponential Decay Curve used to Calculate Damping	111
6-21	Exponential Decay Function for Acceleration Peaks	112
6-22	Wind Velocity Profile for $V_{33} = 20$ mph	115
6-23	Member Centroid Heights for Determining Wind Velocity Magnitude.....	116
6-24	Wind Velocity Excitation Spectrum for Run 16.....	122
6-25	Response Spectrum of Strain Gauge 4 Data for Run 16.....	123
6-26	Unfiltered and Filtered Stress for Strain Gauge 4.....	124
6-27	Quasi-static Stress Range for Sample 100 Second Interval.....	125
6-28	Average Wind Velocity for Sample 100 Second Interval	125
6-29	Stress Response at Strain Gauge 2 Location.....	126
6-30	Stress Response at Strain Gauge 4 Location.....	127
6-31	Stress Response at Strain Gauge 6 Location.....	127
6-32	Stress Response at Strain Gauge 8 Location.....	128
7-1	Basic Wind Speed m/s (mph) for Southeastern United States (AASHTO 2013).....	136
7-2	Structure A Sections	143
7-3	Structure A Section 1	144
7-4	Structure A Section 2	144
7-5	Structure B Sections.....	145
7-6	Structure B Section 1	145

7-7	Structure B Section 2	145
7-8	Structure B Section 3	146
7-9	Structure B Section 4	146
7-10	Stress Envelopes for Post 4 of Structure A.....	147
7-11	Max stress locations for load case 1 (Structure A, V = 90 mph, C _d = 1.7).....	154
7-12	Max stress locations for load case 2 (Structure A, V = 90 mph, C _d = 1.7).....	155
7-13	Max stress locations for load case 3 (Structure A, V = 90 mph, C _d = 1.0).....	155
7-14	Max stress locations for load case 4 (Structure A, V = 150 mph, C _d = 1.7).....	156
7-15	Max stress locations for load case 5 (Structure A, V = 150 mph, C _d = 1.22).....	156
7-16	Max stress locations for load case 6 (Structure A, V = 150 mph, C _d = 1.0).....	157
7-17	Max stress locations for load case 7 (Structure B, V = 90 mph, C _d = 1.7).....	157
7-18	Max stress locations for load case 8 (Structure B, V = 90 mph, C _d = 1.22).....	157
7-19	Max stress locations for load case 9 (Structure B, V = 90 mph, C _d = 1.0).....	158
7-20	Max stress locations for load case 10 (Structure B, V = 150 mph, C _d = 1.7).....	158
7-21	Max stress locations for load case 11 (Structure B, V = 150 mph, C _d = 1.22)....	158
7-22	Max stress locations for load case 12 (Structure B, V = 150 mph, C _d = 1.0).....	159
7-23	Max Member Stresses for Load Cases 1-3 (Structure A, V = 90 mph).....	161
7-24	Max Member Stresses for Load Cases 4-6 (Structure A, V = 150 mph).....	161
7-25	Max Member Stresses for Load Cases 7-9 (Structure B, V = 90 mph).....	162
7-26	Max Member Stresses for Load Cases 10-12 (Structure B, V = 150 mph).....	162
7-27	Fatigue Details for Analysis (AASHTO 2013).....	163
7-28	Stress Envelopes for Post 4 of Structure A.....	164
7-29	Fatigue stress locations for load case 13 (Structure A, C _d = 1.7).....	169

7-30	Fatigue stress locations for load case 14 (Structure A, $C_d = 1.22$)	169
7-31	Fatigue stress locations for load case 15 (Structure A, $C_d = 1.0$)	170
7-32	Fatigue stress locations for load case 16 (Structure B, $C_d = 1.7$)	170
7-33	Fatigue stress locations for load case 17 (Structure B, $C_d = 1.22$)	170
7-34	Fatigue stress locations for load case 18 (Structure B, $C_d = 1.0$)	171
7-35	Max Connection Stresses for Load Cases 13-15 (Structure A)	172
7-36	Max Connection Stresses for Load Cases 16-18 (Structure B)	173
7-37	Effect of Structure Span on Stress Ratios for Upright Posts	180
7-38	Effect of Structure Span on Stress Ratios for Truss Chords	180
7-39	Effect of Structure Span on Stress Ratios for Truss Diagonals	181
7-40	Effect of Wind Speed on Stress Ratios for Upright Posts	181
7-41	Effect of Wind Speed on Stress Ratios for Truss Chords	182
7-42	Effect of Wind Speed on Stress Ratios for Truss Diagonals	182
7-43	Effect of VMS Drag Coefficient on Stress Ratios for Upright Posts	183
7-44	Effect of VMS Drag Coefficient on Stress Ratios for Truss Chords	183
7-45	Effect of VMS Drag Coefficient on Stress Ratios for Truss Diagonals	184

LIST OF ABBREVIATIONS

AASHTO	American Association of State Highway and Transportation Officials
ALDOT	Alabama Department of Transportation
FEA	finite element analysis
FFT	Fast Fourier Transform
FIU	Florida International University
NA	not available
UAB	University of Alabama at Birmingham
VMS	variable message sign
WOW	Wall of Wind

CHAPTER 1 INTRODUCTION

1.1 Problem Statement

Variable Message Signs (VMS) are becoming an integral part of transportation infrastructure on US interstates and highways. VMS structures are vital in ensuring the safety of motorists by relaying messages concerning potential road hazards such as fog, traffic congestion, highway construction, and lane closures. These structures are larger and heavier than typical flat panel signs, and thus behave differently when subjected to wind loads. Figure 1-1 shows a photo of a typical VMS structure installed over a two lane interstate. The design of VMS structures is specified in the 2013 edition of the American Association of State Highway and Transportation Officials (AASHTO) *Standard Specifications for Structural Supports for Highway Signs, Luminaires, and Traffic Signals*.

The AASHTO Supports Specifications currently provide a single drag coefficient for all VMS applications: “A value of 1.7 is suggested for Variable Message Signs (VMS) until research efforts can provide precise drag coefficients.” This drag coefficient value of 1.7 is used for both fatigue and extreme event wind loading scenarios. However, the effect of wind drag on a structure varies depending on a number of factors, including: wind speed, wind direction, structural geometry, and vibration characteristics. The drag coefficient for VMS structures provided in the *Supports Specifications* is an estimate which does not account for the variability of wind loading and structure properties.

Accurate drag coefficients for VMS structures are not available to designers, potentially leading to unsafe or inefficient designs.



Figure 1-1: Variable Message Sign (VMS)

1.2 Research Objectives

The overall purpose of this project was to develop accurate drag coefficients for VMS structures for incorporation into the AASHTO Supports Specifications to promote safer and more economical designs. Wall of Wind testing was conducted at FIU to develop a table of drag coefficients based on the geometric dimensions of VMS sign panels. These drag coefficients were analyzed at UAB to accomplish the following research objectives:

1. Verify the accuracy of the drag coefficient results from the FIU Wall of Wind testing by comparing experimental field data to finite element analyses of a VMS structure.

2. Investigate the impact of the new VMS drag coefficients on the design of sign structures by performing finite element modeling to develop stress reduction ratios for extreme wind design and fatigue wind design.

1.3 Research Methodology

A comprehensive literature review of drag on sign structures was conducted throughout the duration of the project. Past research studies which developed drag coefficients for sign structures were identified and reviewed with a particular focus placed on studies which examined drag on 3-dimensional signs. The results of the FIU Wall of Wind testing were also reviewed to study the experimental testing procedure and select drag coefficients for analysis at UAB.

Two existing VMS structures were selected to analyze the drag coefficient results of the Wall of Wind testing. Both structures were overhead bridge-type structures with four-chord box pipe trusses supporting in-service VMS signs. One structure was located in Alabaster, AL and the other was located in Birmingham, AL. For the purposes of this report, the Alabaster VMS structure was designated as Structure A and the Birmingham VMS Structure was designated as Structure B. Structure A spanned 71 ft over two lanes of traffic, while Structure B spanned 145 ft over six lanes and a median. Drawings, specifications, and photos of the structures were examined to obtain the geometric and material properties of each structure.

Three-dimensional finite element models were developed for both VMS structures using SAP2000. Each model consisted of a structural support frame, a VMS

sign, support conditions, and an access ladder and track. The structural support frame, access ladder, and access track were created in SAP using frame elements, while the VMS sign was modeled using solid elements. Body constraints were commonly used for connections. Once the models were created, modal analyses were run in SAP to determine the dynamic properties of the VMS structures.

Once the SAP models were developed, a study was conducted to verify the drag coefficient results from the FIU Wall of Wind testing using experimental data. The SAP model of Structure A was used for this study. The study compared experimental field data from the Alabaster VMS structure (Structure A) to analytical results obtained from the SAP model of the structure. The experimental data was collected in a previous ALDOT study which examined the response of Structure A due to dynamic wind loading. The same dynamic wind loading which was measured in the field was applied to the SAP model of the structure using a drag coefficient of 1.22 from the FIU testing results for the VMS. The experimental stress response of the structure was compared to the analytical stress response to verify the accuracy of the VMS drag coefficient.

Next, a sensitivity study was conducted to examine the impact of the newly developed VMS drag coefficients on the design of sign structures. The SAP models of both Structures A and B were used for this study. Static analyses were run in SAP to analyze and compare the stress response of the structures due to wind loadings with different VMS drag coefficients. Three VMS drag coefficients were used in this study: $C_d = 1.7$ from the AASHTO Supports Specifications, $C_d = 1.22$ for a standard VMS, and $C_d = 1.0$ for a modified VMS with chamfered corners. The analyses incorporated the AASHTO code requirements for both extreme wind and fatigue wind. Stress ratios were

developed to quantify the amount of stress reduction in critical support members and connections due to the new drag coefficients.

Finally, code language and commentary was developed for incorporation of the new VMS drag coefficients in the AASHTO Supports Specifications. A flow chart summarizing the research methodology for the verification study and sensitivity study of the VMS project is shown in Figure 1-2.

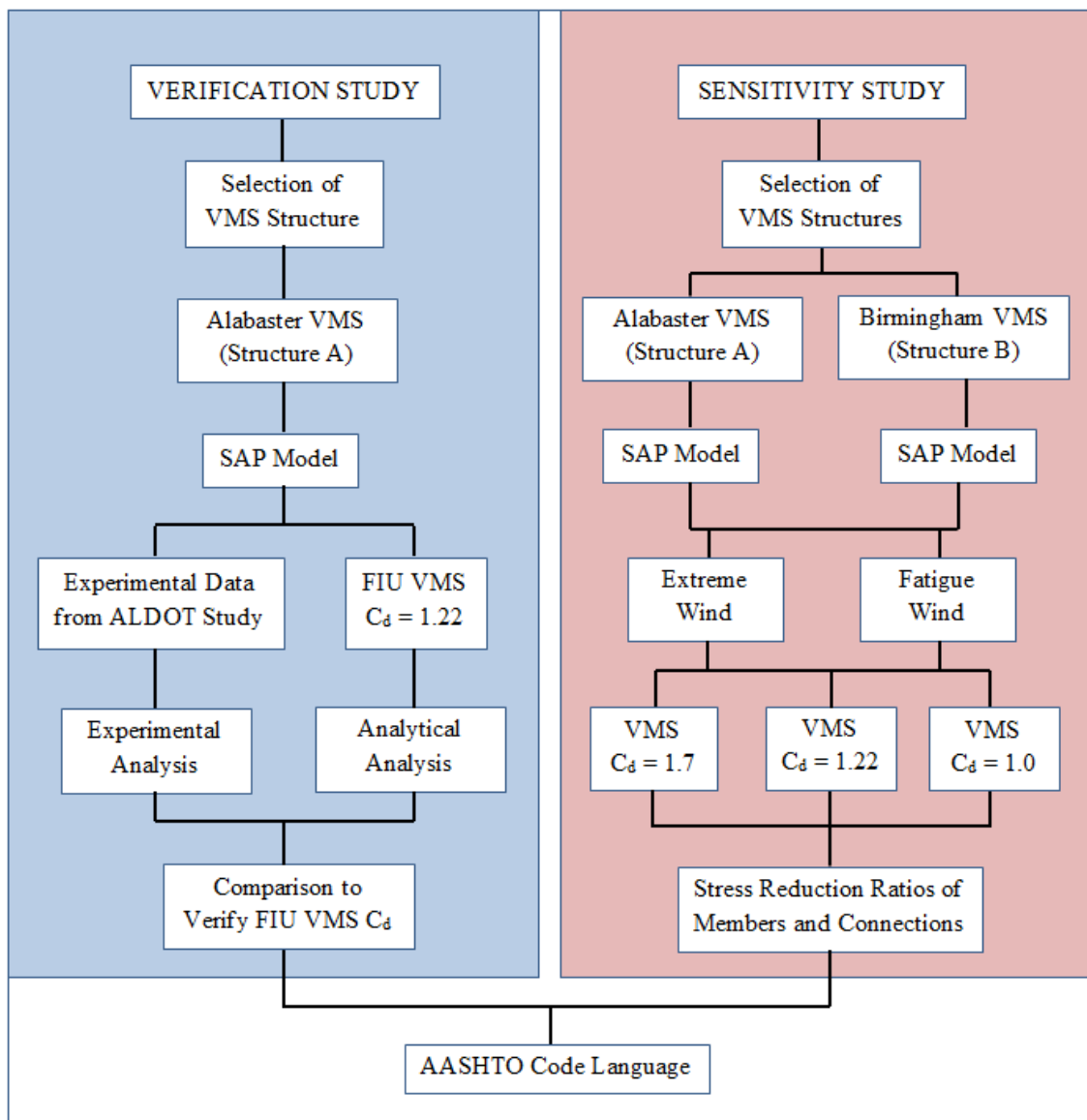


Figure 1-2: Flow chart for research methodology of VMS project

1.4 Report Outline

This report is organized according to the chapters listed below. A short description of each chapter is provided.

Chapter 1 Introduction: The problem statement addressed by the VMS project is discussed and the UAB research objectives for the project are stated.

Chapter 2 Background and Literature Review on Drag: A general background on the physics of drag and its applicability to sign structures is discussed along with a comprehensive literature review on drag for sign structures.

Chapter 3 Wall of Wind Testing at FIU to Develop Drag Coefficients: A detailed description of the experimental test set-up, analysis, and results from the FIU Wall of Wind testing is provided.

Chapter 4 VMS Structures: A detailed description of the two VMS structures used for analyzing the Wall of Wind drag coefficients is provided. Photos of the structures and their support components are included. The geometric and material properties of each structure are presented and discussed.

Chapter 5 Finite Element Modeling: A detailed description of the finite element modeling process of the two VMS structures in SAP2000 is provided. A modal

analysis of each structure is presented along with the resulting mode shapes and natural frequencies.

Chapter 6 Comparison of Drag Coefficients Using Experimental Data and FEA

Dynamic Modeling: A study was conducted to verify the accuracy of the VMS drag coefficient results from the FIU Wall of Wind testing. The study compared experimental field data from a previous study to analytical results obtained from finite element modeling of a VMS structure.

Chapter 7 Sensitivity Study: A sensitivity study was conducted to examine the impact of the new VMS drag coefficients on the design of sign structures. Finite element analyses of VMS structures were used to develop stress reduction ratios for critical support members and fatigue connections.

Chapter 8 Proposed Code Language: Code language and commentary was developed for inclusion of the new VMS drag coefficients in the AASHTO Supports Specifications.

Chapter 9 Conclusions and Future Research: A summary of the conclusions from the Wall of Wind testing at FIU and the experimental and analytical studies conducted at UAB for the VMS project is provided. Recommendations for future research are also discussed.

References: A list of references used in preparation of the report is provided.

Appendix: Additional information and calculations used for the project are provided.

CHAPTER 2 BACKGROUND AND LITERATURE REVIEW ON DRAG

2.1 Chapter Overview

This chapter begins with a brief background concerning the physics of drag and how it relates to wind loads on sign structures. This is followed by a comprehensive literature review of previous research studies which focused on developing drag coefficients for signs. The findings of the research studies are summarized and compared to draw general conclusions regarding the variables which control the behavior of drag on signs.

2.2 Background

2.2.1 *Drag on Bluff Bodies*

Drag is the force induced on an object by a moving fluid due to pressure differentials and viscous action. In most practical applications, the fluid inducing the drag force is either air or water. For the purposes of this study, the fluid is taken as air flow due to natural wind. The drag on an object depends on a number of factors, including the density and velocity of the air flow interacting with the object, as well as the object's size and shape. The drag force is defined by Equation 2-1.

$$F_D = \frac{1}{2} \rho V^2 C_d A \quad (\text{Eqn. 2-1})$$

Where:

- F_D = drag force
- ρ = air density
- V = mean wind velocity
- C_d = drag coefficient
- A = surface area of object

The drag coefficient is a measure of the aerodynamic characteristics of an object. Objects which are more aerodynamic in shape have lower drag coefficients and thus lower drag forces under the same wind velocities than objects which are less aerodynamic in shape.

Objects in free stream flow can be classified as either streamlined bodies or bluff bodies. Streamlined bodies are more aerodynamic in shape and have smaller drag forces than bluff bodies. An airfoil is an example of a streamlined body, while a flat plate or sign would be classified as bluff bodies. Figure 2-1 shows the differences in free stream flow around streamlined and bluff bodies.

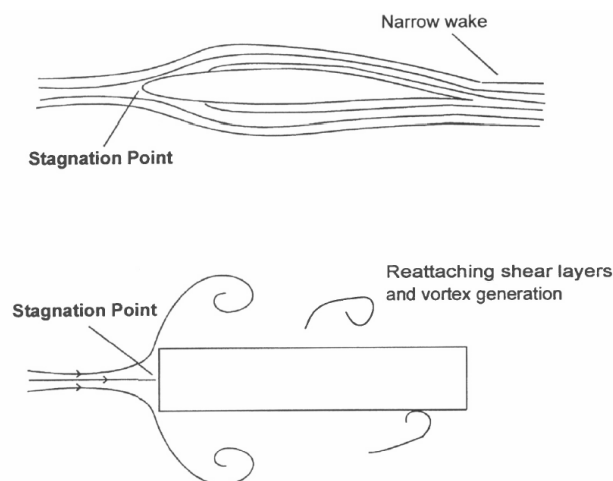


Figure 2-1: Flow around streamlined and bluff bodies (Holmes 2001)

When air flows over the surface of a streamlined body, a very thin boundary layer is created as the flow follows the contours of the body. The boundary layer extends from the surface of the object where the flow has zero velocity to the point where the flow velocity matches that of free stream flow. The flow remains attached to the surface of the body without being disrupted along the entire length of the body. Since there is no significant drop in pressure as air flows around a streamlined body, the drag forces on the body are primarily due to the viscous action of the fluid on the body (Holmes 2001, Larose 2006).

The interaction of air flow with bluff bodies is very different than the aerodynamic behavior of streamlined bodies. When air flow strikes a bluff body, the flow stagnates on the front surface as it tries to find a path around the body. A boundary layer is developed between the object's surface and the free stream flow as in the case of a streamlined body. However, as the flow passes over the leading edge corners of the bluff body, the boundary layer becomes separated from the object's surface. This creates a new layer of high shear and vorticity known as the free shear layer. Unlike the boundary layer on a streamlined body, the free shear layer surrounding a bluff body is very turbulent and not attached to the object's surface. This gap between the free shear layer and the object's surface results in a large region of separated flow downstream of the bluff body. The region of separated flow results in higher drag on the bluff body due to the significant pressure drop behind the body (Munshi 1997). Eventually, the vortices created by the free shear layer are shed downstream and the free stream flow comes back together to envelope the bluff body. For bluff bodies with long after-body lengths (objects that are more 3-dimensional) the free shear layer will sometimes re-attach to the

surface, thus reducing the region of separated flow and the corresponding drag on the body (Holmes 2001).

2.2.2 Application of Drag to VMS Structures

Drag forces can develop on sign structures due to natural wind buffeting and truck-induced wind gusts. Natural wind produces a drag force on signs as positive pressure builds up on the front face of the sign and negative pressure or suction draws on the rear face of the sign. The magnitude of the drag force varies with the velocity and turbulence of the wind. Truck-induced wind gusts can also develop drag forces on signs as vertical uplift from passing trucks creates positive pressures and/or suction on the bottom of signs. Variable Message Signs (VMS) are particularly susceptible to truck-induced drag due to their extended depth. This study uses natural wind loading to develop drag coefficients for VMS structures. However, the same drag coefficients apply for the scenario of truck-induced wind gusts.

The magnitude of the drag coefficient for a sign depends on the relative geometric dimensions of the sign. Figure 2-2 shows the geometric dimensions of a typical 3-dimensional rectangular sign. The dimensions and elevation of a sign are usually expressed in terms of three ratios for testing and analysis purposes: the aspect ratio (b/c), the clearance ratio (c/h), and the depth ratio (d/c). This notation for the geometric ratios is used throughout the report. The drag coefficient of a sign is dependent on each of these ratios, as will be discussed in the following literature review for drag on sign structures.

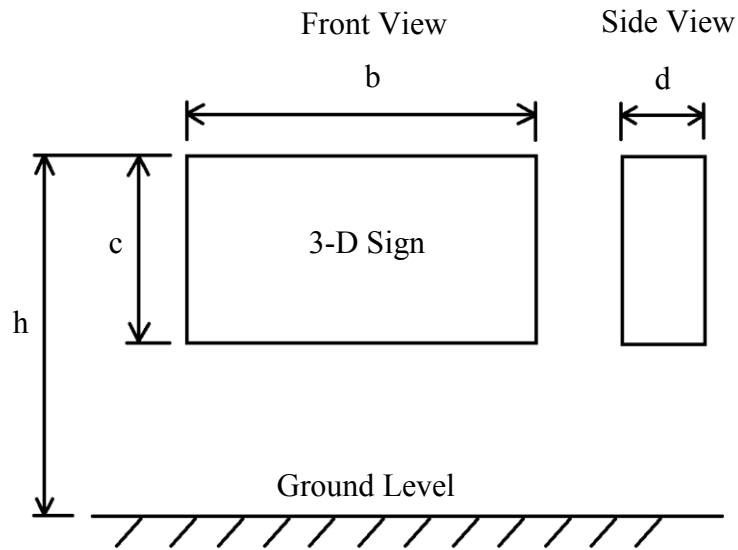


Figure 2-2: Dimensions for sign ratios

2.3 Literature Review for Drag on Sign Structures

A comprehensive literature review was conducted to examine previous research findings related to drag on sign structures. The literature was initially searched in an attempt to find studies which involved measuring the drag coefficient for Variable Message Signs (VMS). However, no such studies were found. The VMS drag coefficient of 1.7 provided in the AASHTO Supports Specifications is not referenced to any particular study and appears to just be a conservative estimate for use in design until research efforts can provide more accurate results. Thus, the literature review was broadened to examine more general findings related to drag on sign structures.

The effect of drag on sign structures has been a topic of study for many decades. Some of the earliest research which studied drag on sign structures was conducted by Flachsbart in the 1930s. Flachsbart's research formed the framework for a series of experimental studies over the following years to refine and more accurately calculate

drag coefficients for different parameters. This literature review focuses on several of the more recent research studies for drag on rectangular sign structures which are relevant to the current study. These studies include both field testing and wind tunnel testing of sign structures. The experimental procedures and findings of each study are discussed, and general conclusions are established by comparing the results of each study.

2.3.1 *Ginger et al (1998)*

Ginger et al (1998) conducted a wind tunnel study at the Cyclone Structural Testing Station (CSTS) at James Cook University to determine the net pressure coefficients on a selection of fences and hoardings. The research also identified different fence and hoarding configurations which experienced large loads. Various parameters were investigated for the different wind tunnel tests. The aspect ratio and wind direction were investigated for the fences, while the clearance ratio and wind direction were considered for the hoardings (the aspect ratio was fixed at 2). Figure 2-3 shows the configurations used by Ginger et al (1998) for the fence and hoarding tests.

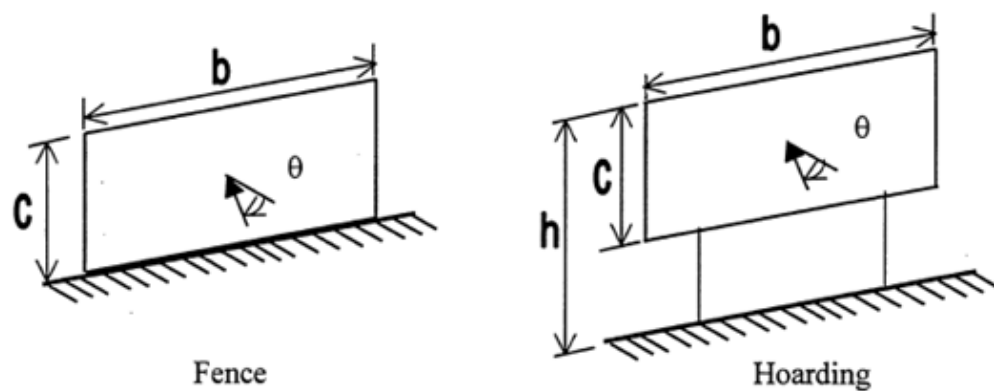


Figure 2-3: Fence and Hoarding Configurations (Ginger 1998)

Ginger et al (1998) constructed a rectangular pressure tapped model panel for use in the wind tunnel testing. The panel model had a length scale of 1:50 (80 mm high x 160 mm long x 8 mm thick). The panel model was divided into four sections with pressure transducers attached to each section. For testing of the fence models, additional panels were secured next to the pressure tapped panel to increase the aspect ratio. The fence tests were conducted using aspect ratios ranging from 2 to 12. For testing of the hoarding models, the pressure tapped model was mounted on legs with varying lengths. The hoarding tests were conducted using clearance ratios of 0.57, 0.67, and 0.80. The wind approach direction was varied from -90° to 90° for the tests.

Table 2-1 shows selected drag coefficient results compiled by Ginger et al (1998) from their own wind tunnel testing, as well as from several other contemporary studies. All of these results are for wind normal to fence panel structures. Ginger et al (1998) concluded that their wind tunnel testing of the fences supported the generally accepted research finding that the mean drag coefficient of fence panels decreases as the aspect ratio increases, with the lowest drag coefficient occurring for an aspect ratio of about 5.

Table 2-2 shows the drag coefficient results from the hoarding tests conducted by Ginger et al (1998). There were not enough hoarding tests to develop a noticeable trend based on the clearance ratio; however, the drag coefficients were in good agreement with Letchford's (1998) equation, which will be presented later. Figure 2-4 shows the drag coefficients measured by Ginger et al (1998) plotted versus the approaching wind direction for the hoarding test with a clearance ratio of 0.57. The figure shows that the drag coefficient decreased as the wind direction increased from 0° to 45° to 90° , which supports the general research findings.

Table 2-1: Selected drag coefficients for fences (Ginger 1998)

Aspect Ratio	Area Averaged Mean Pressure Coefficient					
	Letchford & Holmes (1994)		Letchford & Robertson (1998)		Letchford (1998)	Ginger et al (1998)
	CSIRO	Oxford	Silsoe	Oxford	UQ	CSTS
1		1.13	1.06	1.24	1.15	
1.5	1.17					
2		1.24			1.14	1.25
3		1.22	0.96			
4					1.08	1.12
5	1.07		~0.97	1.17	1.04	
6						1.15
7				1.13		
9			~0.98	1.16		
10	1.13					

Table 2-2: Drag coefficients for hoardings (Ginger 1998)

Clearance Ratio	Mean Net Pressure Coefficients		
	CSTS Study by Ginger et al (1998)		Letchford (1998) Eqn.
	$\theta = 0^\circ$	$\theta = 45^\circ$	$\theta = 0^\circ$
0.57	1.39	1.12	1.41
0.67	1.39	1.27	1.37
0.80	1.43	1.08	1.30

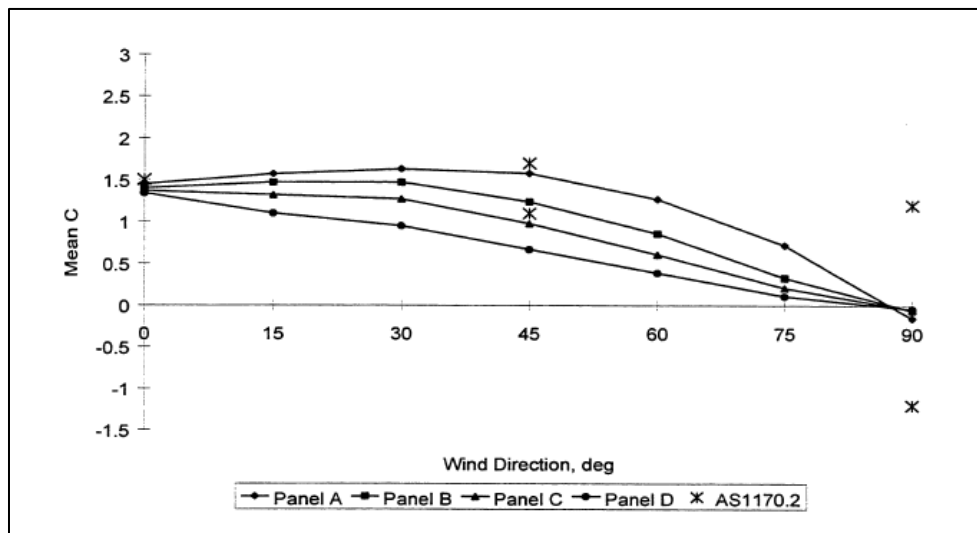


Figure 2-4: Drag coefficient vs. wind direction for $c/h = 0.57$ (Ginger 1998)

2.3.2 Letchford (2001)

Letchford (2001) conducted one of the most extensive studies to date involving the measurement of drag coefficients for different flat panel sign configurations. He used wind tunnel tests to investigate the effect of aspect ratio, clearance ratio, wind direction, and porosity on the magnitude of drag coefficients for signboards and hoardings in turbulent flow. This section provides a summary of the research conducted by Letchford over a period of several years, culminating in his findings published in 2001. The results involving porosity are not discussed here, as they do not pertain to the present study.

Letchford (2001) tested several scaled models, with sizes ranging from 50 mm high x 50 mm wide to 100 mm high x 400 mm wide for different aspect ratios. He also varied the gaps beneath the mounted panels from 5 to 150 mm to create different clearance ratios. The wind speed of the wind tunnel was set to create a Reynolds number of 5×10^4 for all the tests. Pressure transducers were used to measure the resultant drag forces on the panels so that the normal force coefficients could be calculated. The study focused on finding the mean force coefficients since earlier research had indicated that the overall loading on signboards and hoardings behaved quasi-statically for high mean loads.

Multiple hoarding configurations were tested 10 times and the results were averaged for each configuration. The standard error in the mean drag coefficients was approximately 3%. Table 2-3 shows a summary of the testing results for wind normal to the hoardings. Letchford's (2001) results provided a more comprehensive picture of the effect of the clearance ratio on drag coefficients for signs. The drag coefficients generally decreased in magnitude as the aspect ratio increased for signs close to the

ground (high clearance ratios). This trend was in good agreement with the findings of Ginger (1998) and others. However, the drag coefficients generally increased in magnitude as the aspect ratio increased for signs farther away from the ground (low clearance ratios).

Table 2-3: Selected drag coefficients for wind normal to hoardings (Letchford 2001)

Clearance Ratio	Aspect Ratio							
	0.2	0.25	0.5	1	2	4	5	10
1.0	1.42	1.41	1.17	1.15	1.14	1.08	1.04	
0.95	1.43	1.43	1.33	1.27	1.24	1.14		
0.9	1.44	1.45	1.41	1.34	1.33	1.2	1.15	
0.8	1.46	1.49	1.44	1.43	1.39	1.32		
0.67			1.46	1.42	1.38	1.35	1.32	
0.5			1.47	1.38	1.42	1.45	1.44	
0.3				1.42	1.45	1.53	1.57	1.55
0.16					1.48	1.51		1.63

Letchford (2001) compared his results to the original research of Flachsbart (1934), as well as the requirements of the contemporary Australian and US wind load codes as seen in Figure 2-5. Letchford (2001) noted that the code requirements had been largely influenced by Flachsbart’s research. The drag coefficient results of Letchford (2001) were higher than Flachsbart’s results and the corresponding code requirements for the parameters investigated. Letchford (2001) attributed this to the increased turbulence in his wind tunnel study as compared to the relatively smooth flow used by Flachsbart. As a result, the codes have been updated to agree better with Letchford’s (2001) research.

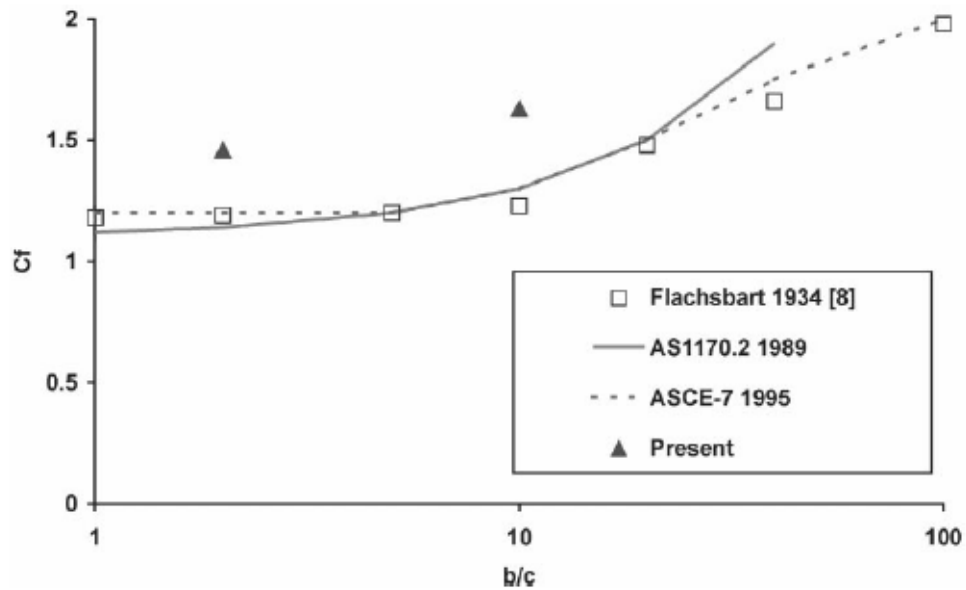


Figure 2-5: Mean drag coefficient comparison for elevated panels (Letchford 2001)

Letchford (2001) also formed conclusions regarding the effect of the approaching wind direction on the drag coefficient magnitude. Figure 2-6 shows the variation of the drag coefficients with changing wind direction for different clearance ratios tested. Letchford (2001) observed that the drag coefficient was relatively constant for wind directions ranging from 0° to 45°, but then decreased dramatically for wind directions above 45°. This trend was in good agreement with the general research findings.

Based on the results of his findings, Letchford (2001) developed Equation 2-2 for the computation of drag coefficients based on the parameters of aspect ratio and depth ratio. The equation fit his drag coefficient results with an error less than $\pm 0.1C_f$ for $0.2 < b/c < 5$ and $0.2 < c/h < 1.0$.

$$C_f = 1.45 + 0.5(0.7 + \log(b/c))(0.5 - (c/h)) \quad (\text{Eqn. 2-2})$$

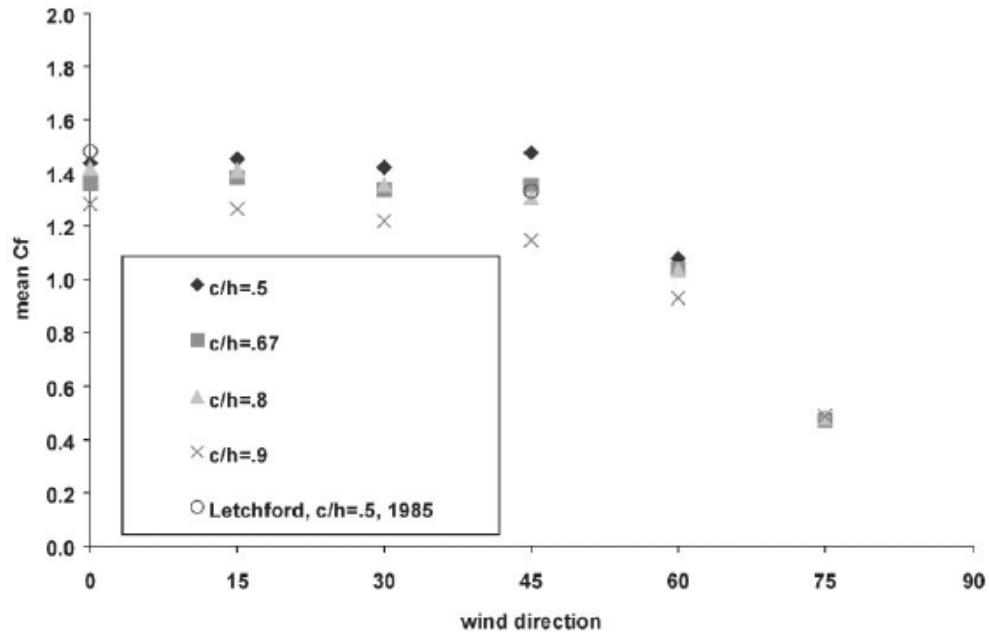


Figure 2-6: Mean drag coefficients for panels with aspect ratio = 2 as a function of wind direction (Letchford 2001)

2.3.3 Quinn et al (2001)

Quinn et al (2001) conducted an experimental study at the Silsoe Research Institute to measure drag coefficients for sign panels subjected to natural wind. The sign panels utilized in the study represented full scale temporary signs often installed along roadways. Quinn et al (2001) selected a range of 750 mm high and 1500 mm high signs for testing, along with a pedestrian sign banner. This section focuses on the drag coefficient results for the 750 and 1500 mm high signs. The parameters of the study included sign shape, size, and inclination angle. Four different sign shapes were studied: rectangular, square, triangular, and circular. The sign panels were tested at inclination angles of 0° and 22.5°.

The forces on each sign panel were measured using three load cells mounted on a triangular steel frame which supported the sign. The wind speed and direction were

measured simultaneously using an ultrasonic anemometer installed close to the sign support frame. Typical wind speeds ranged from 4 to 12 m/s during testing. Drag coefficient values were developed based on 1 minute values for wind speed and force measurements. Figure 2-7 shows a photograph of the experimental test setup with the 750 mm square sign attached to the support frame.



Figure 2-7: Photo of 750 mm square sign mounted on support frame (Quinn 2001)

Table 2-4 shows selected drag coefficient values from the testing by Quinn et al (2001). Quinn made several conclusions regarding the drag coefficient values. The table only presents the results for the square and rectangular signs since these are the only shapes relevant to the current study. However, Quinn did note that the sign shape (rectangular, square, triangular, or circular) did not have a significant effect on the

magnitude of the drag coefficient. Quinn also noted that the wind speed and inclination angle of the sign did not appear to have a significant effect on the drag coefficient.

Quinn observed that the larger signs (1500 mm high) had higher drag coefficients than the smaller signs (750 mm high). He attributed this to the close proximity of the 750 mm signs to the ground, indicating that the clearance ratio has an effect on the drag coefficient. Quinn also concluded that the drag coefficients for the signs mounted at 1 m were dependent on the wind direction according to a cosine-like function for small wind angles, while the signs mounted at 2 m had a more constant drag coefficient with varying wind angles. The addition of the frame around the square 750 mm sign increased the drag coefficient due to disruption of the flow around the sign. This indicated that the edge conditions of a sign have a significant effect on the drag coefficient.

Quinn conducted a spectral analysis of the sign response to determine how well the experimental data matched with wind tunnel testing results for flat plates. He concluded that the field data and wind tunnel results were generally in good agreement, except that the field data had an increased response in the frequency range of 0.1 to 1 Hz.

Table 2-4: Selected drag coefficient results for wind normal to sign (Quinn 2001)

Sign Shape	Sign Size	Elevation to center of sign (m)	Inclination Angle	C_w (0°) value
Square	750 mm	1	0°	1.05
Rectangle	750 mm x 1050 mm	1	0°	1.03
Square	750 mm	1	22.5°	1.10
Rectangle	750 mm x 1050 mm	1	22.5°	1.14
Square + Frame	750 mm	1	0°	1.25
Square + Frame	750 mm	1	22.5°	1.45
Square	750 mm	2	0°	1.08
Rectangle	1500 mm x 2000 mm	2	0°	1.22
Rectangle	1500 mm x 2000 mm	2	22.5°	1.39

2.3.4 *Smith et al (2014)*

Smith et al (2014) conducted an experimental study at the Reese Technology Center in Lubbock, Texas, to measure the long-term response of a full-scale billboard sign to natural wind loading. The field data was analyzed to develop an experimental drag coefficient for the billboard sign. The results of the study would be used to establish a benchmark for testing sign models in a wind tunnel as a part of the research performed by Zuo et al (2014).

The full-scale sign had a width of 7.5 m, a height of 3.75 m, and a depth of 1.75 m, resulting in an aspect ratio of 2, a clearance ratio of 0.5, and a depth ratio of 0.47. The sign was mounted on a 10 inch diameter standard steel pipe section. Figure 2-8 shows a photograph of the sign tested in the field. Pressure transducers were spaced evenly across the surface area of the sign to measure the net pressures induced by the wind loading on the sign. The wind speed and direction was measured by an anemometer attached to another pole adjacent to the sign structure. The wind excitation and corresponding pressure on the sign were measured whenever the mean wind speed exceeded 15 mph (6.7 m/s). A total of 470 15 minute intervals were measured during the study.



Figure 2-8: Full-scale sign used for experimental study (Smith 2014)

Smith et al (2014) used the measured pressure data to calculate drag coefficients for each interval of data. Figure 2-9 shows the experimental drag coefficient results vs. the corresponding angle of wind attack for the full-scale field testing plotted along with results of various wind tunnel tests, including studies performed by Letchford (2001) and Zuo et al (2014). The full-scale data presented a steady correlation between the drag coefficient and wind direction, with the largest drag coefficient occurring for a wind direction approximately normal to the sign and having an average magnitude of about 1.25. Smith et al (2014) noted that the drag coefficient results of Letchford (2001) for flat plate signs formed an upper boundary to the full-scale testing results and were significantly larger for most wind directions. This indicated that the drag coefficient for a

box-shaped sign is smaller than for a flat plate sign. Smith et al (2014) also concluded that the full-scale testing results agreed well with the wind tunnel tests conducted by Zuo et al (2014), which will be discussed next.

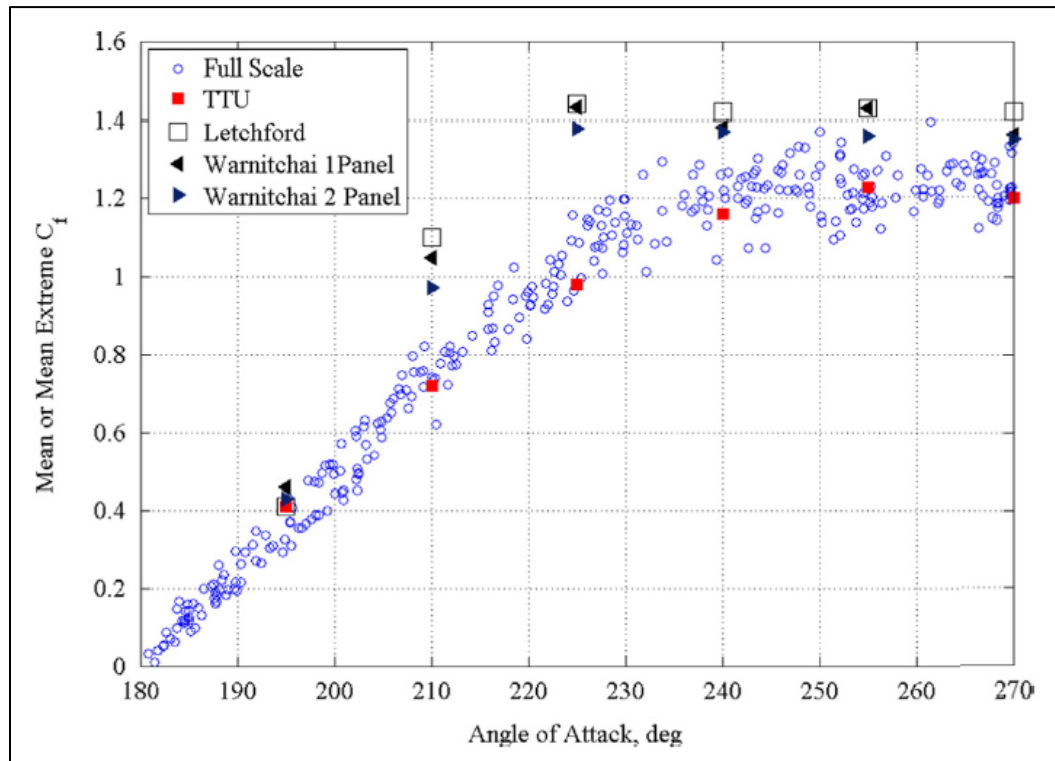


Figure 2-9: Full-scale drag coefficients compared with wind tunnel studies (Smith 2014)

2.3.5 Zuo (2014)

Zuo et al (2014) conducted an extensive wind tunnel study at Texas Tech University to develop drag coefficients for different types of rectangular signs. The study included three main phases of research. Phase 1 compared model-scale wind tunnel measurements to the full-scale field testing results of the experimental study by Smith et al (2014) to verify the accuracy of the wind tunnel results. Phase 2 examined wind tunnel loadings on five different configurations of rectangular signs to determine the effect of

the sign configuration on the drag coefficient. Finally, phase 3 focused exclusively on wind tunnel testing of box sign configurations to determine the effects of aspect ratio and clearance ratio on the drag coefficients for the box signs.

All of the models which were tested in the wind tunnel had a length scale of 1:50. In phase 1 of the wind tunnel testing, a box sign model was created with model dimensions which corresponded to the full-scale sign dimensions of the structure tested by Smith et al (2014) in the field. In phase 2 of the testing, five different configurations of rectangular signs were selected for testing. The configurations included a box sign, a single-plate sign, a double-plate sign, a 30° V-shaped sign, and a 10° V-shaped sign. Figure 2-10 shows the five sign configurations with model dimensions. In the figure, $b = 15.2$ cm, $h = c = 7.6$ cm, and $t = 3.7$ cm. These dimensions corresponded to an aspect ratio of 2, a clearance ratio of 0.5, and a depth ratio for the box sign of 0.49. The box sign model had the same dimensions as the model used for phase 1 of the testing.

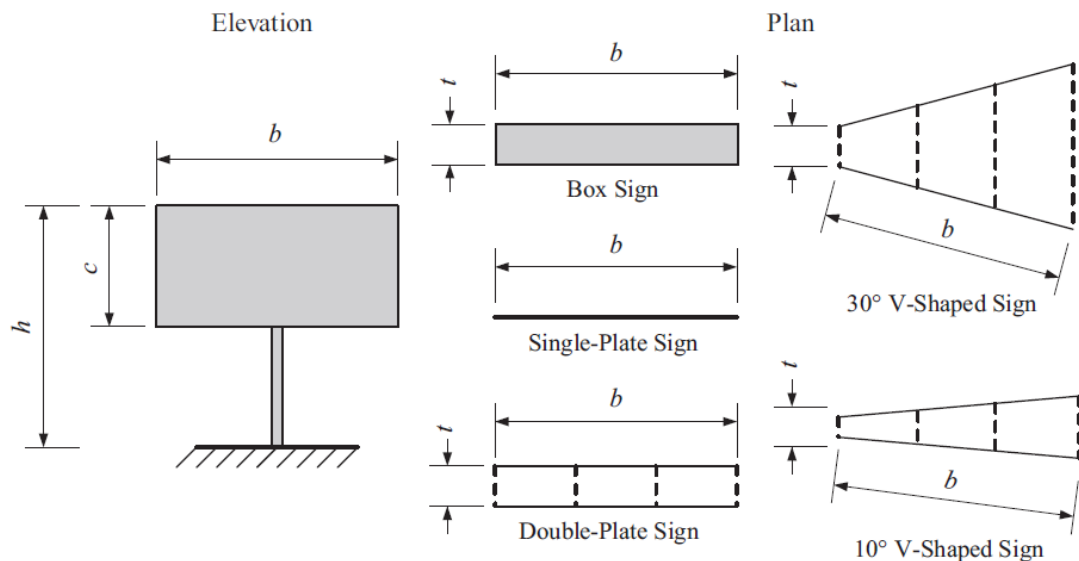


Figure 2-10: Sign models tested in phase 2 of the wind tunnel experiments (Zuo 2014)

In phase 3 of the wind tunnel testing, a total of 39 rectangular box sign models with varying aspect and clearance ratios were tested. The depth of the models was held constant at 3.7 cm, as Zuo et al (2014) noted that this model depth was common for many sign applications, such as Variable Message Signs (VMS), and it was not practical for them to test enough models to accurately quantify the effect of the depth ratio on the drag coefficient.

In all three phases of the wind tunnel testing, the box sign, single-plate sign, and double-plate sign models were tested at 6 different orientations ranging from 0° to 75° in 15° increments. The V-shaped models were tested at additional orientations. A total of 10 tests were conducted for each model at each orientation. The mean and pseudo-steady force coefficients were calculated for each scenario by averaging the results measured by the force transducers for each set of 10 tests.

The results of the phase 1 testing indicated that the model-scale drag coefficients were in good agreement with the full-scale results measured in the field by Smith et al (2014). This was shown earlier in the summary of the study conducted by Smith et al (2014).

The phase 2 testing led Zuo et al (2014) to several conclusions regarding the effect of model configuration on the drag coefficient. Figure 2-11 and Figure 2-12 show the mean and pseudo-steady force coefficients for the five different sign model configurations at varying wind angles of attack. Based on these plots, Zuo et al (2014) concluded that the mean and pseudo-steady force coefficients for single-plate and box sign models are relatively close for low yaw angles. The force coefficients for the single-

plate and box sign models were relatively constant for yaw angles ranging from 0° to 30°, but then decreased drastically once the yaw angle increased above 45°.

Zuo et al (2014) also concluded that the mean and pseudo-steady force coefficients for the box sign model were consistently lower than for the single-plate sign model, except for the 75° orientation. Zuo et al (2014) attributed this decrease in the drag coefficient to the partial reattachment of flow that occurs on the extended depth of the box sign model. They also concluded that since the current design standards were based on wind tunnel testing of flat signs, using the codified drag coefficients for box signs would result in overly conservative designs.

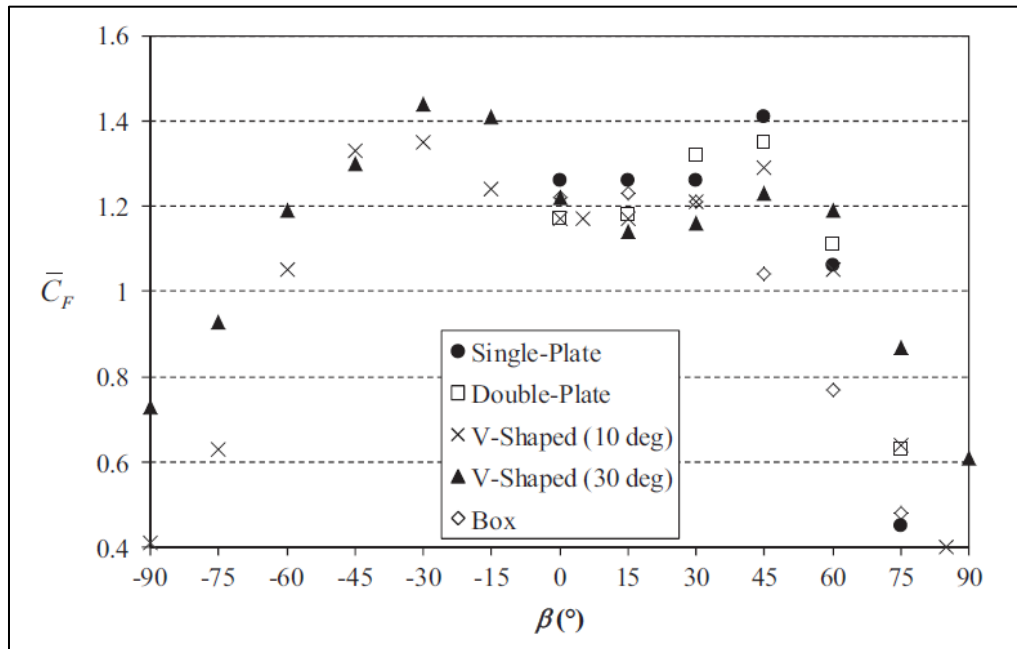


Figure 2-11: Mean force coefficient vs. yaw angle for 5 sign models (Zuo 2014)

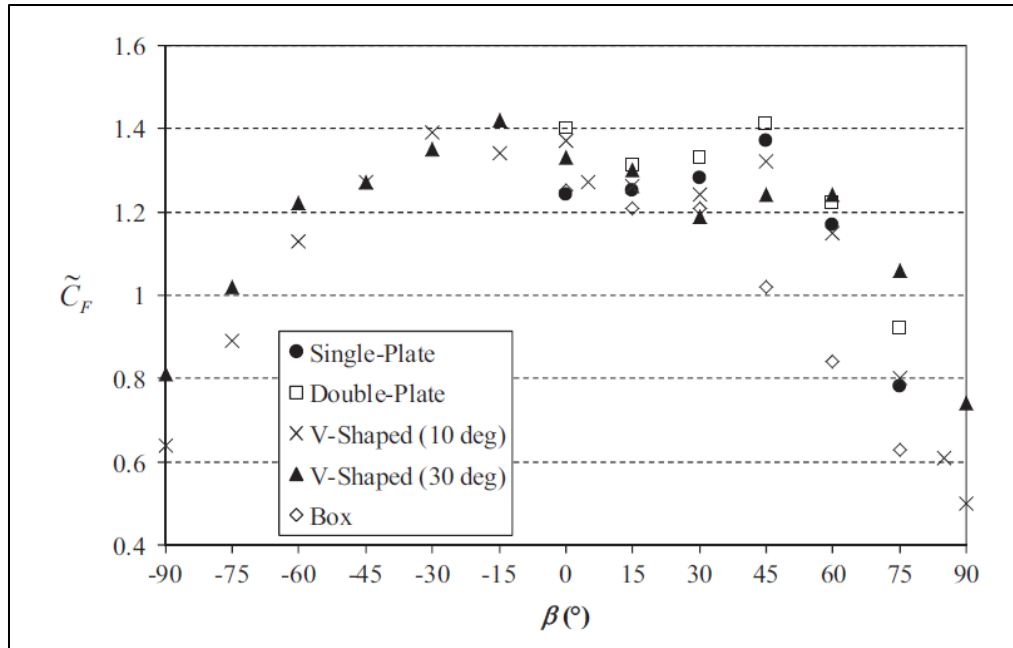


Figure 2-12: Pseudo-steady force coefficient vs. yaw angle for 5 sign models (Zuo 2014)

Table 2-5 summarizes the critical mean and pseudo-steady force coefficients for the five sign model configurations. Zuo et al (2014) noted that the critical drag coefficients for the single-plate were close to the values reported by Letchford (2001) for models with similar aspect and clearance ratios. The critical drag coefficients for the box sign model were 1.23 and 1.25 for the mean and pseudo-steady calculations, respectively.

Table 2-5: Critical mean and pseudo-steady force coefficients of five sign models tested by Zuo et al (2014)

	Single-plate	Double-plate	10 ⁰ V-shaped	30 ⁰ V-shaped	Box
Mean Coefficient	1.41 [45 ⁰]	1.35 [45 ⁰]	1.35 [-30 ⁰]	1.44 [-30 ⁰]	1.23 [15 ⁰]
Pseudo-steady Coefficient	1.37 [45 ⁰]	1.41 [45 ⁰]	1.39[-30 ⁰]	1.42 [-15 ⁰]	1.25 [0 ⁰]

Zuo et al (2014) compared the phase 3 testing results for the box sign models to the results reported by Letchford (2001) for flat sign models with similar aspect and clearance ratios. Zuo et al concluded in each case that the drag coefficients for the box

sign models were significantly lower than the drag coefficients for the flat sign models. Zuo et al (2014) also concluded that the drag coefficient generally decreases with increasing aspect ratio when the sign is relatively close to the ground (clearance ratio is less than 0.5), but increases with increasing aspect ratio when the sign is elevated higher.

2.3.6 Literature Review Summary

Based on the literature review for drag on sign structures, several general conclusions can be drawn regarding the behavior of drag coefficients for signs. First, the drag coefficient depends on the aspect ratio of the sign. The wind tunnel studies by Ginger et al (1998), Letchford (2001), and Zuo et al (2014) all concluded that the drag coefficient of a rectangular sign panel generally decreases with increasing aspect ratio when the sign is close to the ground (high clearance ratio), but increases with increasing aspect ratio when the sign is further elevated (low clearance ratio). This second scenario (low clearance ratio) is prevalent for variable message signs spanning across highways and interstates.

Second, the drag coefficient depends on the clearance ratio of the sign. Letchford (2001) and Zuo et al (2014) thoroughly investigated the effects of the clearance ratio on the drag coefficient and made similar observations. They noted that the drag coefficient generally increases as the clearance ratio is decreased (as the sign is elevated higher above to the ground). However, the effect of the clearance ratio on the magnitude of the drag coefficient becomes less significant when the sign is at a considerable elevation, as in the case of variable message signs installed over highways. Thus, the effect of the clearance ratio was not considered in the current study.

Third, the drag coefficient depends on the depth ratio of the sign. The combined findings of the field study by Smith et al (2014) and the wind tunnel study by Zuo et al (2014) demonstrated that the drag coefficient decreases as the depth ratio is increased (as the sign becomes thicker). The box shaped signs tested by Smith et al (2014) and Zuo et al (2014) had smaller drag coefficients than those reported for flat plate signs with the same aspect and clearance ratios. The decrease in the drag coefficient for the box shaped signs was attributed to partial reattachment of flow on the extended depth of the box signs. Based on these results, Zuo et al (2014) concluded that the current design standards over-estimate the drag coefficient for the design of three-dimensional rectangular signs, such as variable message signs, since the standards were based on testing of flat plate signs.

Fourth, the drag coefficient depends on the angle of attack of the wind. The researchers who studied the effect of wind direction on drag all concluded that the drag coefficient is usually the largest when the wind is approximately normal to the sign for typical flat plate or box shaped signs. As the wind angle of attack increases relative to the normal direction, the drag coefficient either initially remains constant or decreases in relation to the wind angle.

Fifth, the effect of wind speed on the drag coefficient is not as clear. During the experimental studies by Quinn et al (2001) and Smith et al (2014), the wind speed did not appear to significantly affect the magnitude of the drag coefficient. However, Letchford (2001) did note that the increased turbulence at higher wind speeds can increase the drag coefficient. Drag coefficients should be developed and compared for both fatigue level

winds and extreme event winds to determine the effect of wind speed on the drag coefficient.

Finally, the drag coefficient can depend on the edge characteristics of rectangular signs. Quinn et al (2001) observed during field testing that adding a frame around a rectangular sign increased the drag coefficient due to disruption of the wind flow around the sign. This indicated that the edge conditions of a sign have a significant effect on the drag coefficient. Based on this observation, it would seem accurate to assume that smoothing the edges of a sign so that they are not as sharp would potentially decrease the drag coefficient.

CHAPTER 3 WALL OF WIND TESTING AT FIU TO DEVELOP DRAG COEFFICIENTS

3.1 Chapter Overview

Experimental testing was performed at the FIU Wall of Wind facility to develop drag coefficients for Variable Message Signs (VMS). VMS models with varying geometric properties were constructed and tested for different wind speeds, wind directions, and other wind-related phenomena. The testing results were used to calculate drag coefficients for different VMS configurations. This chapter summarizes the general findings of the Wall of Wind study at FIU. All figures, tables, and other numerical results contained in this chapter were obtained from the FIU project report authored by Debbie Meyer, Dr. Amir Mirmiran, and Dr. Arindam Gan Chowdury. All findings were based on the Wall of Wind test results. Further details, analysis, and findings of the Wall of Wind study can be found in the FIU project report (Meyer 2014).

3.2 Experimental Testing

Experimental testing of VMS models was performed at the FIU Wall of Wind facility. The models were designed and constructed with geometric properties comparative to full-scale VMS panels. Some of the models were constructed with round and chamfered edges, instead of the sharp edges which are standard for most VMS panels. Multiple tests were conducted to determine the force coefficients for standard VMS panels, as well as for VMS panels with modified edges. This was done for both

fatigue winds and extreme winds. The testing also examined the effects of galloping and wind driven rain.

3.2.1 FIU Wall of Wind

The Wall of Wind system at FIU is 6.1 m wide by 4.3 m high and composed of two rows of six electric fans controlled by variable frequency drives. Each fan is capable of generating air flow of 113.3 m³/s, resulting in potential wind speeds in excess of 60 m/s (Meyer 2014). Figure 3-1 shows the intake side of the Wall of Wind in the testing lab at FIU.



Figure 3-1: FIU Wall of Wind (Meyer 2014)

3.2.2 *VMS Test Models*

Model sizes were selected for testing at the Wall of Wind facility based on typical dimensions of Variable Message Signs provided by sign manufacturers. The models were sized based on their aspect and depth ratios. Three aspect ratios b/c (1, 3, and 5) and three depth ratios d/c (0.1, 0.4, and 0.7) were selected to represent a wide range of VMS configurations. A clearance ratio of $c/h = 0.24$ was used for all models. This clearance ratio was selected to represent the elevation of full-size VMS panels in the field. All of the models were scaled using a length scale of 1:3 so that the largest model would fit inside the effective wind field created by the Wall of Wind (Meyer 2014).

A total of 13 models were constructed for testing at the Wall of Wind facility. Table 3-1 shows the scaled dimensions of each model along with the corresponding aspect and depth ratios. Models 1 through 9 were constructed with sharp edges, while model 10 was constructed with round edges and model 11 was constructed with chamfered edges. The round and chamfered edge dimensions of models 10 and 11 were designed to be 5% of the vertical height of the models. Models 1 through 11 were assembled as three-dimensional boxes using plywood reinforced with stud framing. Models 12 and 13 were constructed as flat panels using a single sheet of plywood. These last two models were used solely for the blockage test (Meyer 2014).

Table 3-1: Model Dimensions and Geometric Ratios (Meyer 2014)

Model No.	Width b (m)	Height c (m)	Depth d (m)	Aspect Ratio b/c	Depth Ratio d/c
1	0.6	0.6	0.06	1	0.1
2	1.8	0.6	0.06	3	0.1
3	3.0	0.6	0.06	5	0.1
4	0.6	0.6	0.2	1	0.4
5	1.8	0.6	0.2	3	0.4
6	3.0	0.6	0.2	5	0.4
7	0.6	0.6	0.4	1	0.7
8	1.8	0.6	0.4	3	0.7
9	3.0	0.6	0.4	5	0.7
10	3.0	0.6	0.4	5	0.7
11	3.0	0.6	0.4	5	0.7
12	3.0	0.6	0.013	5	0.021
13	1.5	0.3	0.013	5	0.042

Two different cantilever systems were constructed from vertical and horizontal steel tubes to support the models during testing: a single cantilever system and a double cantilever system. Both cantilever systems were constructed as rigid frames which were bolted to the Wall of Wind floor during testing. The single cantilever system was used to support the smaller models (1, 4, and 7), while the double cantilever system was used to support the larger models (2, 3, 5, 6, and 8-13). The plywood models were mounted to the cantilever systems using steel plates and bolts (Meyer 2014).

The cantilever support systems were instrumented with multi-axis load cells at the top of each vertical support to measure forces, moments, and torques induced in the structure by the test wind loading on the models. Cobra probes were placed above the models to measure the wind velocity and turbulence in three orthogonal directions. The

probes were placed at a sufficient height so that the measured wind speeds were not affected by flow turbulence around the models (Meyer 2014).

3.2.3 Calibration Tests

Tare tests were performed on all of the models to isolate and correct for the secondary aerodynamic forces applied to the cantilever support system. Two different configurations were used to accommodate the range of model sizes: Setup A and Setup B. Setup A was used to determine the tare correction for the single support system, and was applied to the smaller models (1, 4, and 7). Setup B was used to determine the tare correction for the double support system, and was applied to the larger models (2, 3, 5, 6, and 8-13). Both tare test setups were tested for horizontal wind directions of 0° and 45° normal to the front surface of the model. Figure 3-2 shows tare test Setup A at a 45° configuration. Figure 3-3 shows tare test Setup B at a 0° configuration (Meyer 2014).

Blockage tests were conducted using the flat panel models (12 and 13) in order to make sure that the wind speed measurements were sampled at a far enough distance away from the top of the models and also to correct for local flow effects. Blockage correction factors were calculated for the different model configurations (Meyer 2014).



Figure 3-2: Tare test Setup B for 45° configuration (Meyer 2014)



Figure 3-3: Tare test Setup A for 0° configuration (Meyer 2014)

3.2.4 Drag Coefficient Tests

Multiple tests were performed on the VMS models in the Wall of Wind facility to determine drag coefficients for different configurations (models with sharp, round, and chamfered edges), and to investigate unique phenomena such as galloping and wind driven rain. The drag coefficients were measured for both fatigue winds and extreme winds.

3.2.4.1 Force Coefficient Tests

Force coefficient tests were performed to determine the drag coefficients for the different aspect and depth ratios selected for the study. Models 1 through 9 were tested for horizontal wind directions of 0° and 45° , resulting in a total of 18 model configurations. Figure shows the force coefficient test setup for the 0° wind direction, and Figure shows the setup for the 45° wind direction. The models were tested at fan motor speeds of 15 m/s (fatigue wind) and 40 m/s (extreme wind). Test data was collected from the load cells and cobra probes at a sampling frequency of 100 Hz for 1 minute intervals. The appropriate factors for tare correction, blockage correction, and wind speed adjustment were applied to all of the test data (Meyer 2014).



Figure 3-4: Force coefficient test setup for the 0° wind direction (Meyer 2014)

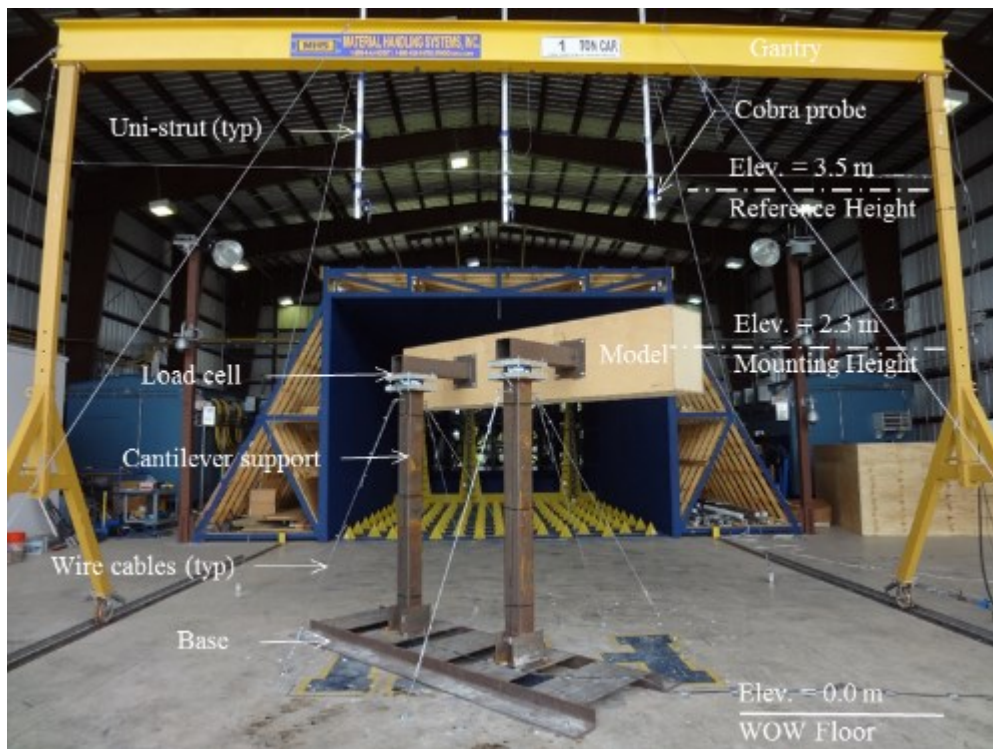


Figure 3-5: Force coefficient test setup for the 45° wind direction (Meyer 2014)

3.2.4.2 Corner Modification Tests

Corner modification tests were performed to investigate the effects of using round and chamfered edges instead of sharp edges on the models. Model 10 (round edges) and model 11 (chamfered edges) were used for these tests. Figure 3-6 shows a close-up view of model 10 with the round edges. Figure 3-7 shows a close-up view of model 11 with the chamfered edges. The corner modification tests were conducted following the same configurations and parameters for calibration and data collection as the force coefficient tests (Meyer 2014).

3.2.4.3 Galloping Tests

Galloping tests were performed using model 9 to investigate the galloping potential of the VMS model. Conditions conducive for the onset of galloping were created by inserting a series of wedges between the model and the cantilever support system. The wedges varied the angle of attack of the wind on the model. The angle of attack was varied from -4.5° to 4.5° in several increments for the galloping tests. Figure 3-8 shows the galloping test setup with the wedges between the model and cantilever support system (Meyer 2014).



Figure 3-6: Round edge test setup (Meyer 2014)



Figure 3-7: Chamfer edge test setup (Meyer 2014)



Figure 3-8: Galloping test setup for -4.5° angle (Meyer 2014)

3.2.4.4 Wind Driven Rain Test

A wind driven rain test was performed on model 8 by mounting spray nozzles in front of the Wall of Wind fans. The test was conducted to determine if wind driven rain significantly affected the drag coefficient for the model (Meyer 2014).

3.2.5 Testing Summary

Testing of the VMS models was performed at the FIU Wall of Wind facility from May 28, 2013 to June 7, 2013. The models were tested at various wind speeds representing fatigue winds and extreme winds as well as different wind approach angles. Table 3-2 provides a summary of the different test conditions for each model.

Table 3-2: Testing Summary (Meyer 2014)

Model No.	Test Speed						Wind Approach	
	20% 12 m/s	25% 15 m/s	30% 18 m/s	50% 30 m/s	60% 37 m/s	65% 40 m/s	0°	45°
1	✓	✓				✓	✓	✓
2	✓					✓	✓	✓
3	✓					✓	✓	✓
4	✓	✓				✓	✓	✓
5	✓					✓	✓	✓
6	✓	✓				✓	✓	✓
7	✓	✓				✓	✓	✓
8	✓	✓	✓	✓	✓	✓	✓	✓
9	✓	✓				✓	✓	✓
10	✓	✓		✓		✓	✓	✓
11	✓	✓		✓		✓	✓	✓
12			✓				✓	✓
13					✓		✓	✓

3.3 Test Results

3.3.1 Calculation of Drag Coefficients

The mean force coefficients were calculated for each model from the test data. The mean normal force coefficient (C_{Fx}) was calculated using Equation 3-1, the mean lateral force coefficient (C_{Fy}) was calculated using Equation 3-2, and the mean vertical lift force coefficient (C_{Fz}) was calculated using Equation 3-3.

$$C_{Fx} = \frac{F_x}{\frac{1}{2}\rho V^2(bc)} \quad (\text{Eqn. 3-1})$$

$$C_{Fy} = \frac{F_y}{\frac{1}{2}\rho V^2(bc)} \quad (\text{Eqn. 3-2})$$

$$C_{Fz} = \frac{F_z}{\frac{1}{2}\rho V^2(bc)} \quad (\text{Eqn. 3-3})$$

Where:

- F_x , F_y , and F_z are the resultant forces measured by the load cells along the x, y, and z axis, respectively,
- ρ is the air density (assumed to be 1.225 kg/m³),
- V (m/s) is the mean wind speed measured by the cobra probes,
- b (m) is the lateral length of the VMS model,
- and c (m) is the height of the VMS model

Table 3-3 presents a summary of the mean force coefficients for the tests with wind in the 0° direction. Table 3-4 presents a summary of the mean force coefficients for the tests with wind in the 45° direction. Both tables list the force coefficients for fatigue winds (15 m/s) as well as extreme winds (40 m/s). In the following sections, only the conclusions related to the normal force coefficients (C_{Fx}) are discussed as these were used to develop drag coefficients for VMS. An in-depth discussion of the lateral force coefficients (C_{Fy}) and vertical lift force coefficients (C_{Fz}) can be found in the original report on the Wall of Wind testing by Debbie Meyer (2014).

Table 3-3: Summary of mean force coefficient results for the 0° wind direction (Meyer 2014)

Model No.	b (m)	d (m)	c (m)	Aspect Ratio b/c	Depth Ratio d/c	0° Wind Direction					
						15 m/s			40 m/s		
						C _{Fx}	C _{Fy}	C _{Fz}	C _{Fx}	C _{Fy}	C _{Fz}
1	0.6	0.06	0.61	1	0.1	1.16	0.00	-0.06	1.15	0.00	-0.05
2	1.8	0.06	0.61	3	0.1	1.20	0.03	-0.08	1.22	0.01	-0.01
3	3.0	0.06	0.61	5	0.1	1.24	0.01	-0.07	1.28	0.01	0.00
4	0.6	0.24	0.61	1	0.4	1.05	0.03	-0.12	1.12	0.00	-0.03
5	1.8	0.24	0.61	3	0.4	1.17	0.03	-0.07	1.21	0.02	0.00
6	3.0	0.24	0.61	5	0.4	1.23	0.00	-0.06	1.25	0.00	0.00
7	0.6	0.43	0.61	1	0.7	0.97	0.00	0.00	0.98	0.01	0.01
8	1.8	0.43	0.61	3	0.7	1.12	-0.01	-0.05	1.16	0.02	0.04
9	3.0	0.43	0.61	5	0.7	1.19	0.00	-0.05	1.22	0.01	0.03
10	3.0	0.43	0.61	5	0.7	0.85	0.03	0.24	1.06	0.04	0.12
11	3.0	0.43	0.61	5	0.7	0.97	0.03	0.04	1.01	0.04	0.12
12	3.0	0.01	0.61	5	0.02	1.27	0.01	-0.04	-	-	-
13	1.5	0.01	0.30	5	0.04	-	-	-	1.27	0.01	0.06

Table 3-4: Summary of mean force coefficient results for the 45° wind direction (Meyer 2014)

Model No.	b (m)	d (m)	c (m)	Aspect Ratio b/c	Depth Ratio d/c	45° Wind Direction					
						15 m/s			40 m/s		
						C _{Fx}	C _{Fy}	C _{Fz}	C _{Fx}	C _{Fy}	C _{Fz}
1	0.6	0.06	0.61	1	0.1	1.23	-0.12	-0.02	1.24	-0.10	0.06
2	1.8	0.06	0.61	3	0.1	1.13	-0.03	0.00	1.18	-0.06	0.04
3	3.0	0.06	0.61	5	0.1	1.02	-0.01	-0.04	1.11	-0.04	0.02
4	0.6	0.24	0.61	1	0.4	0.99	-0.35	-0.08	1.02	-0.36	0.01
5	1.8	0.24	0.61	3	0.4	1.03	-0.13	-0.06	1.06	-0.16	-0.01
6	3.0	0.24	0.61	5	0.4	0.99	-0.04	-0.05	1.03	-0.07	-0.04
7	0.6	0.43	0.61	1	0.7	0.93	-0.54	-0.07	0.94	-0.56	0.01
8	1.8	0.43	0.61	3	0.7	0.93	-0.21	0.05	0.95	-0.22	0.08
9	3.0	0.43	0.61	5	0.7	0.89	-0.11	0.02	0.91	-0.11	0.04
10	3.0	0.43	0.61	5	0.7	0.69	-0.07	0.00	0.74	-0.11	0.03
11	3.0	0.43	0.61	5	0.7	0.74	-0.06	0.10	0.72	-0.10	-0.06
12	3.0	0.01	0.61	5	0.02	1.04	-0.11	0.04	-	-	-
13	1.5	0.01	0.30	5	0.04	-	-	-	1.04	-0.47	0.22

3.3.2 Effect of Aspect Ratio

3.3.2.1 0° Horizontal Wind Direction

Figure 3-9 shows the normal force coefficient plotted versus the aspect ratio (b/c) for the 0° horizontal wind direction and 15 m/s wind speed. Individual plots are provided for each selected depth ratio ($d/c = 0.1, 0.4, \text{ and } 0.7$). Figure 3-10 shows the same normal force coefficient versus aspect ratio plots, but for the 40 m/s wind speed. Both of these figures clearly show that the drag coefficient increased with the aspect ratio. This correlation was attributed to the model becoming more two-dimensional at higher aspect ratios. For small aspect ratios ($b/c = 1$), the narrow shape allows flow to travel evenly around the sides, top, and base of the model, resulting in a narrow wake region and lower drag coefficient. As the aspect ratio increases ($b/c = 3$ and $b/c = 5$), the extended length of the model forces the flow to travel faster over the top and base of the model, resulting in a wider wake region and higher drag coefficient. The lowest drag coefficient was found to occur for model 7, which had the lowest aspect ratio ($b/c = 1$) and the highest depth ratio ($d/c = 0.7$). This model had the lowest drag coefficient because it had the narrowest wake region due to its 3-D shape and also had the potential for partial reattachment of flow (Meyer 2014).

3.3.2.2 45° Horizontal Wind Direction

Figure 3-11 shows the normal force coefficient plotted versus the aspect ratio (b/c) for the 45° horizontal wind direction and 15 m/s wind speed. Individual plots are provided for each selected depth ratio ($d/c = 0.1, 0.4, \text{ and } 0.7$). Figure 3-12 shows the same normal force coefficient versus aspect ratio plots, but for the 40 m/s wind speed.

Both of these figures show that the behavior of the aspect ratio depended on the depth ratio. For models with a depth ratio of 0.1, the drag coefficient decreased almost linearly as the aspect ratio increased. However, for models with depth ratios of 0.4 and 0.7, the drag coefficient first increased slightly as the aspect ratio moved from 1 to 3 but then decreased as the aspect ratio moved from 3 to 5 (Meyer 2014).

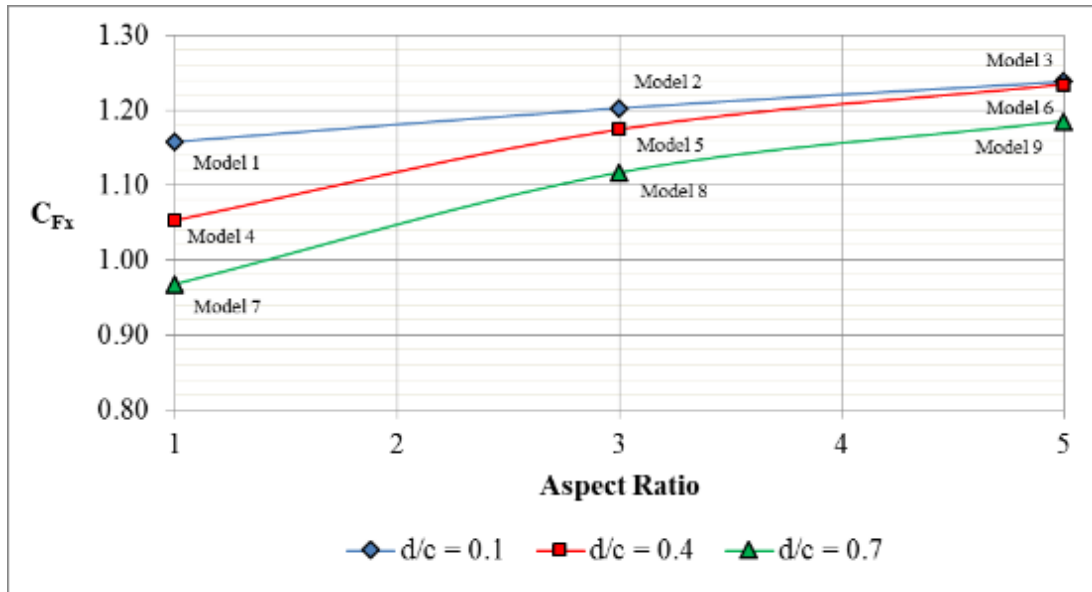


Figure 3-9: Effect of aspect ratio (b/c) on normal force coefficient for 0° wind direction at 15 m/s (Meyer 2014)

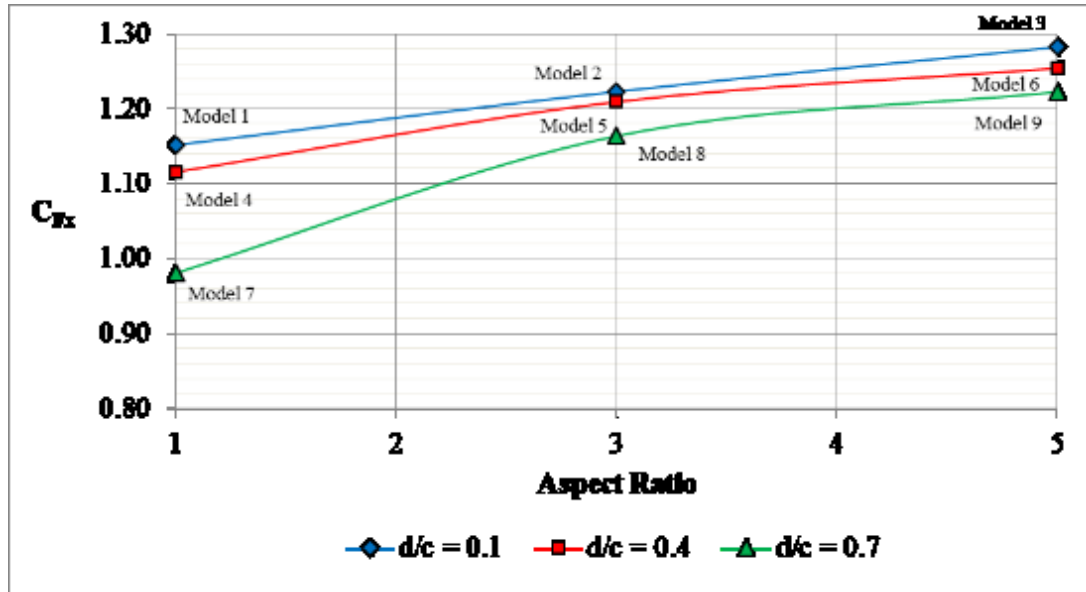


Figure 3-10: Effect of aspect ratio (b/c) on normal force coefficient for 0° wind direction at 40 m/s (Meyer 2014)

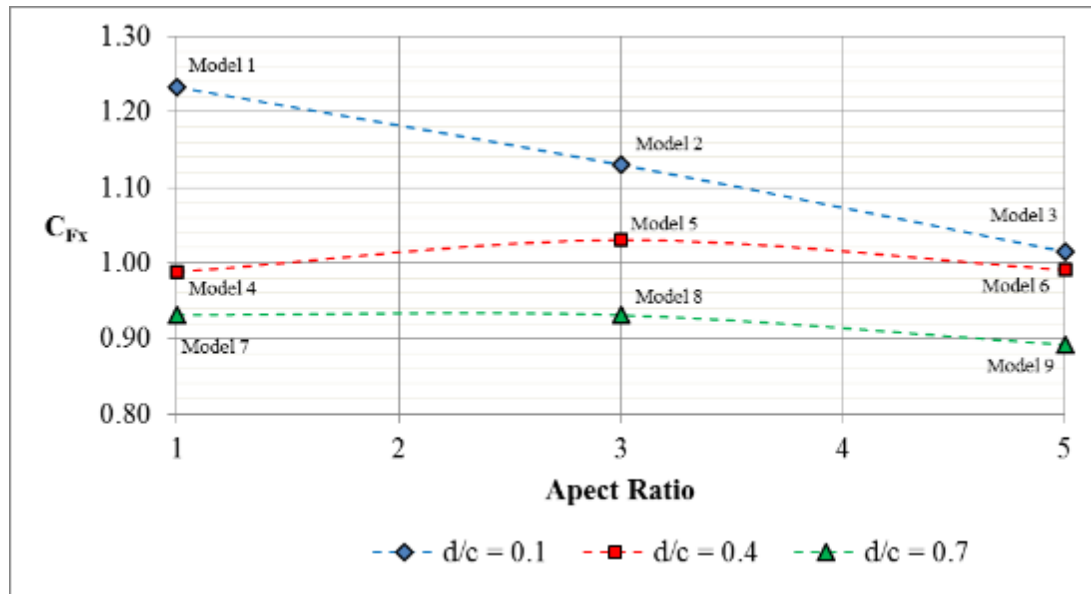


Figure 3-11: Effect of aspect ratio (b/c) on the normal force coefficient for the 45° wind direction at 15 m/s (Meyer 2014)

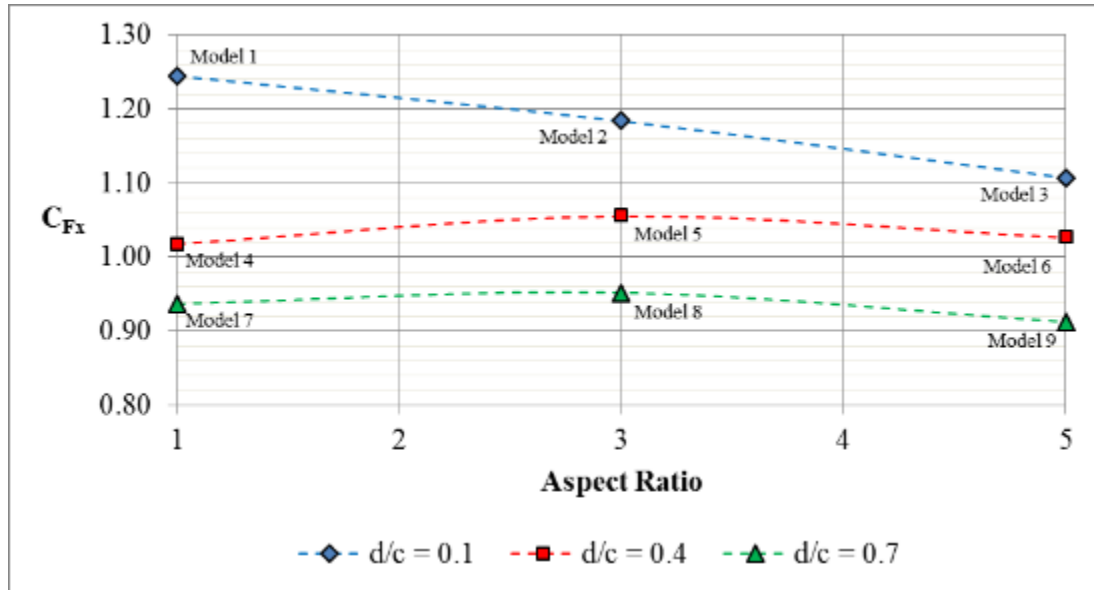


Figure 3-12: Effect of aspect ratio (b/c) on the normal force coefficient for the 45° wind direction at 40 m/s (Meyer 2014)

3.3.3 Effect of Depth Ratio

3.3.3.1 0° Horizontal Wind Direction

Figure 3-13 shows the normal force coefficient plotted versus the depth ratio (d/c) for the 0° horizontal wind direction and 15 m/s wind speed. Individual plots are provided for each selected aspect ratio ($b/c = 1, 3, \text{ and } 5$). Figure 3-14 shows the same normal force coefficient versus depth ratio plots, but for the 40 m/s wind speed. Both of these figures show that the drag coefficient decreased as the depth ratio increased for the selected aspect ratios. This decrease in the drag coefficient for higher depth ratios was likely due to partial reattachment of flow on the sides of the models with larger depths. The square models ($b/c = 1$) had the lowest drag coefficients due to the narrow wake region and partial reattachment of flow created by the narrow widths and extended depths of the models (Meyer 2014).

3.3.3.2 45° Horizontal Wind Direction

Figure 3-15 shows the normal force coefficient plotted versus the depth ratio (d/c) for the 45° horizontal wind direction and 15 m/s wind speed. Individual plots are provided for each selected aspect ratio ($b/c = 1, 3, \text{ and } 5$). Figure 3-16 shows the same normal force coefficient versus depth ratio plots, but for the 40 m/s wind speed. Both of these figures show that the drag coefficient decreased as the depth ratio increased for the selected aspect ratios. These results are similar to the results for the 0° wind direction (Meyer 2014).

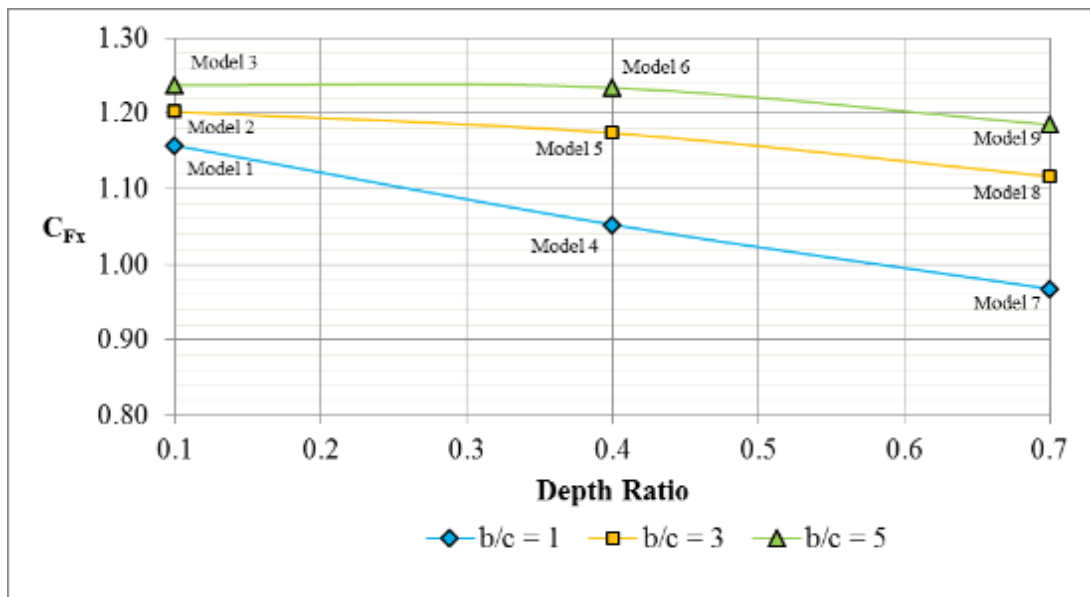


Figure 3-13: Effect of depth ratio (d/c) on the normal force coefficient for the 0° wind direction at 15 m/s (Meyer 2014)

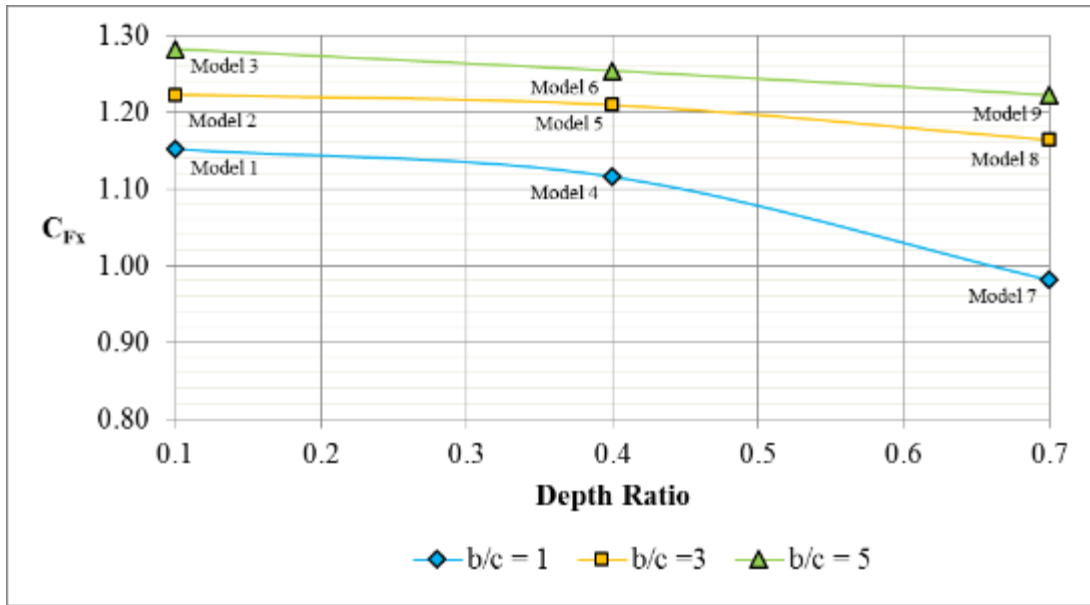


Figure 3-14: Effect of depth ratio (d/c) on the normal force coefficient for the 0° wind direction at 40 m/s (Meyer 2014)

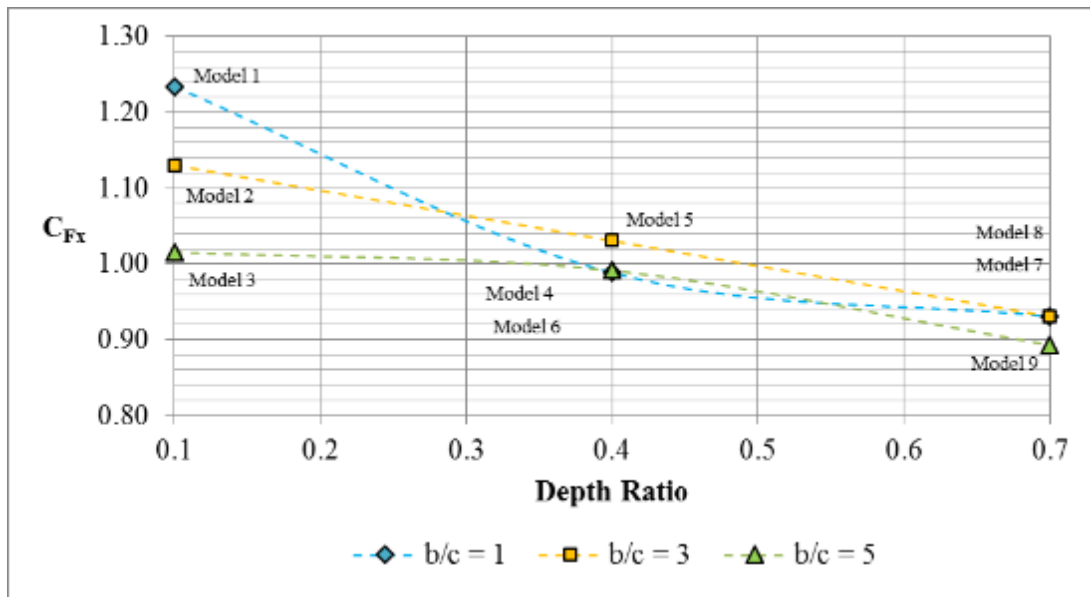


Figure 3-15: Effect of depth ratio (d/c) on the normal force coefficient for the 45° wind direction at 15 m/s (Meyer 2014)

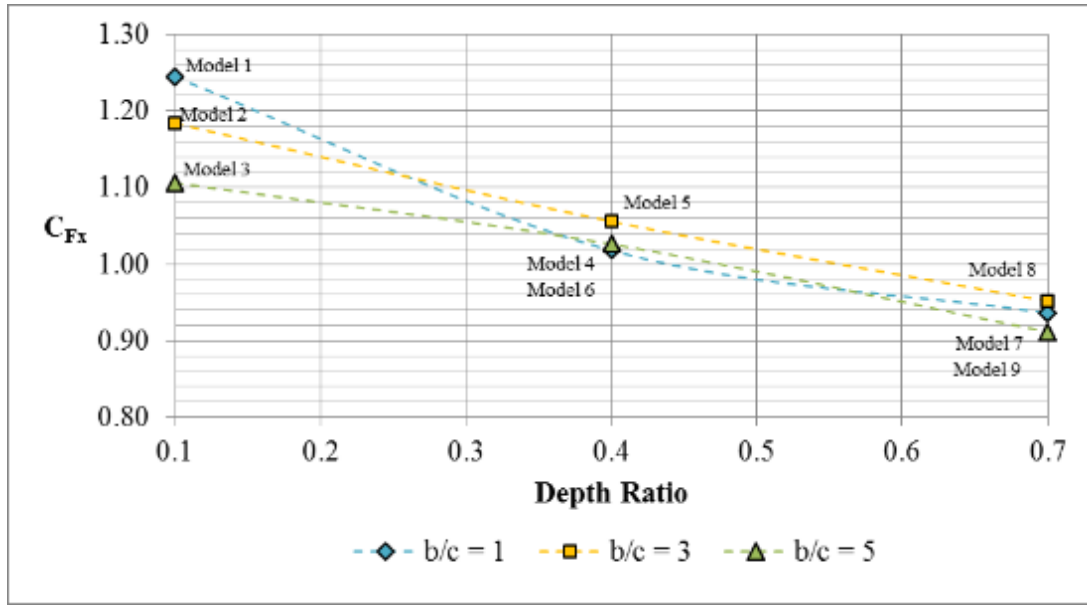


Figure 3-16: Effect of depth ratio (d/c) on the normal force coefficient for the 45° wind direction at 40 m/s (Meyer 2014)

3.3.4 Effect of Wind Direction

Figure 3-17 and Figure 3-18 show comparisons of the drag coefficients measured for the 0° and 45° wind directions, respectively. The drag coefficients of all the models were greater for the wind in the 0° direction than wind in the 45° direction, except for model 1. Model 1 had the smallest aspect and depth ratios compared to the other models. The higher drag coefficient in the 45° wind direction was attributed to possible negative pressure build-up on the rear leading edge of the model (Meyer 2014).

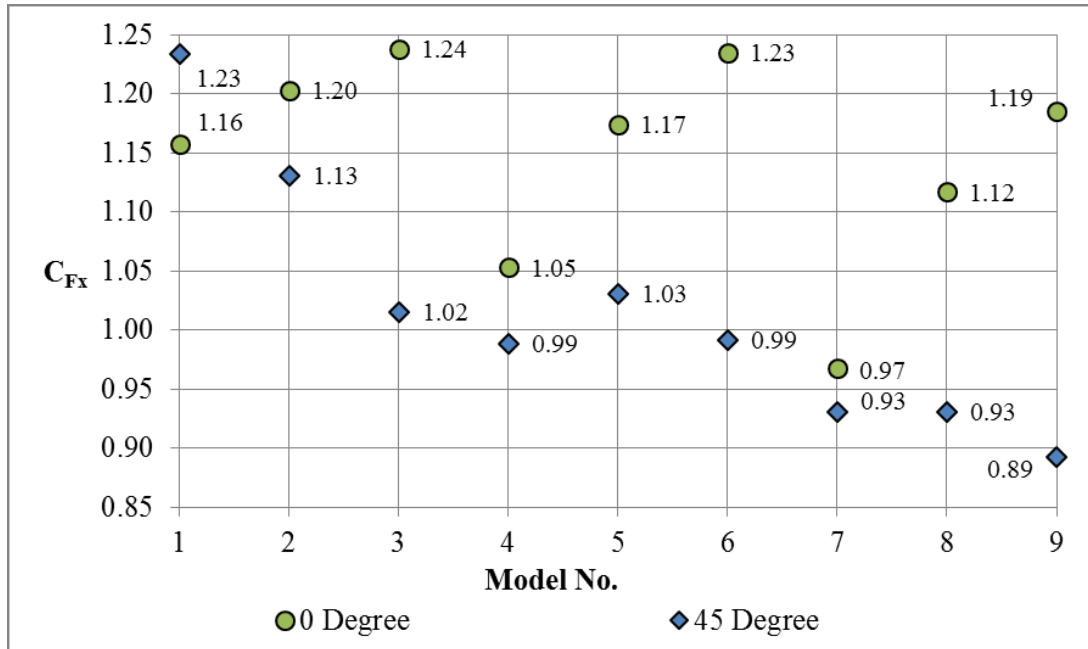


Figure 3-17: Comparison of normal force coefficients for the 0° and 45° wind directions at 15 m/s (Meyer 2014)

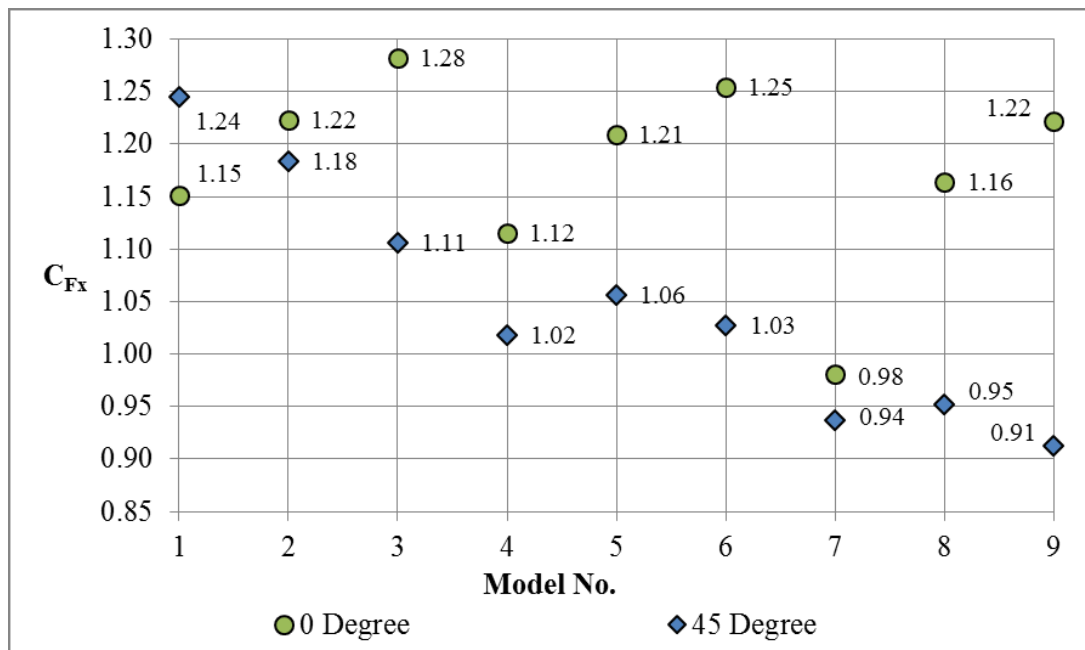


Figure 3-18: Comparison of normal force coefficients for the 0° and 45° wind directions at 40 m/s (Meyer 2014)

3.3.5 Effect of Corner Modifications

Models 10 and 11 were modified to have round edges and chamfered edges, respectively, instead of sharp edges. These models had the same overall dimensions as model 9 (aspect ratio $b/c = 5$, depth ratio $d/c = 0.7$). The modified drag coefficients for models 10 and 11 were plotted as a function of wind speed in Figure 3-19 for the 0° wind direction and in Figure 3-20 for the 45° wind direction. Plots of the drag coefficients for model 9 with sharp edges were included in the figures for comparison purposes. The figures show that the drag coefficients are much lower for the models with modified edges for both wind directions (0° and 45°) as well as for both fatigue and extreme wind speeds. This suggests that the round and chamfered corners reduce the wake width surrounding the model, resulting in less drag (Meyer 2014).

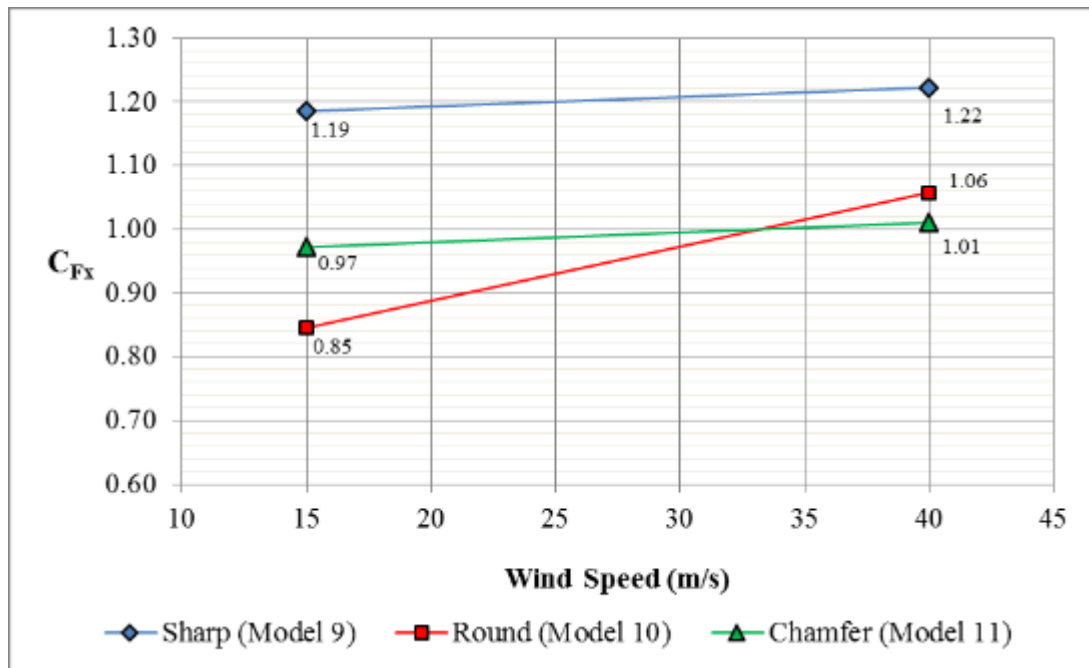


Figure 3-19: Comparison of sharp (model 9) and modified corner (Models 10 and 11) results for 0° wind direction (Meyer 2014)

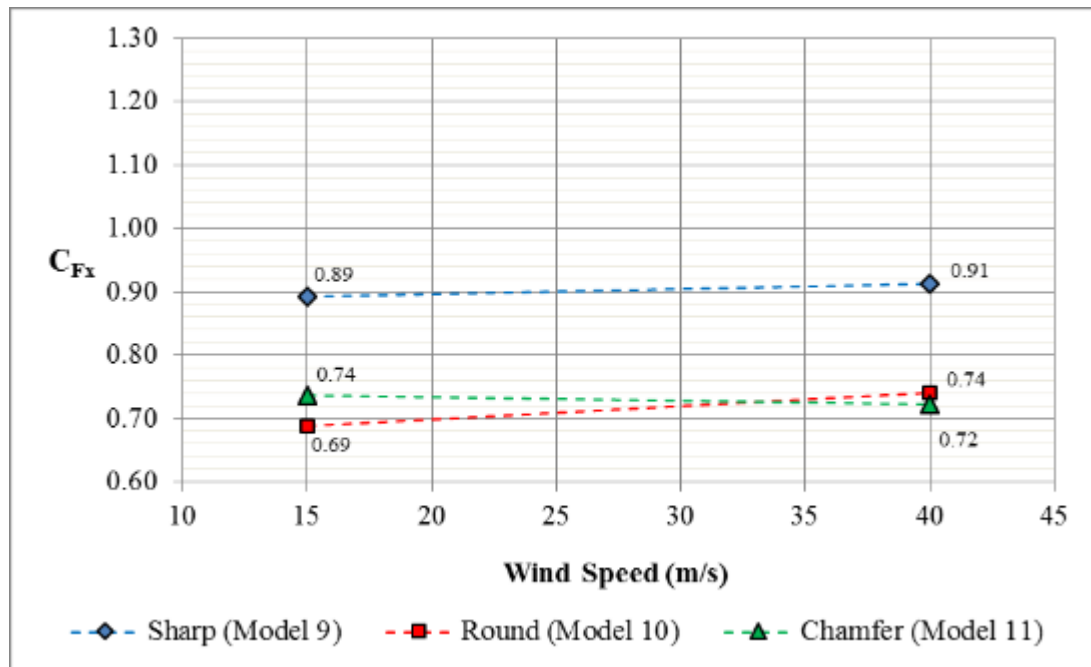


Figure 3-20: Comparison of sharp (model 9) and modified corner (Models 10 and 11) results for 45° wind direction (Meyer 2014)

3.3.6 Other Considerations

In addition to the effects of aspect ratios, depth ratios, and corner modifications on the magnitude of VMS drag coefficients, the Wall of Wind study also examined several other conditions which could potentially affect drag. These conditions included Reynolds number effects, wind driven rain, and galloping potential.

All of the models were tested at both fatigue level winds (15 m/s) and extreme level winds (40 m/s) to determine the effects of changing the Reynolds number on the drag coefficient. The wind levels used for testing corresponded to a Reynolds number range of 5.96×10^5 to 1.59×10^6 . The results of the Wall of Wind testing indicated a small increase in the normal force coefficient (C_{Fx}) with increasing wind speed for the standard sharp edge models. This increase in C_{Fx} was thought to be due to additional

vibration in the structure support system at higher wind speeds. As a result, Reynolds number effects were not considered in the Wall of Wind study (Meyer 2014).

The effect of wind driven rain on the drag coefficient was investigated for model 8. The model was subjected to wind driven rain conditions by mounting spray nozzles to the Wall of Wind fans. This test was conducted for the 45° wind direction but not the 0° wind direction. The drag coefficient results for the model with and without wind driven rain did not vary by much, so it was concluded that wind driven rain did not have any significant effect on the drag coefficient (Meyer 2014).

The potential for galloping of VMS panels was investigated by adjusting the test setup to vary the angle of attack of the wind on Model 9. The wind angle of attack was varied from -4.5° to 4.5° by installing wedges between the model and the support system. Testing was performed for fatigue and extreme winds. Evaluation of the Den Hartog criterion using the test results indicated that the model was susceptible to galloping (Meyer 2014).

3.3.7 Comparison with Literature

The drag coefficient results from the Wall of Wind study were compared to previous findings in the literature. Figure 3-21 plots the Wall of Wind drag coefficients along with the drag coefficient results from other research studies for different types of signs. The Wall of Wind results compare very well with the findings of Zuo et al. (2014) and Smith et al. (2014), which are for 3-D box sign configurations similar to VMS panels. The results of Letchford (2001) are more conservative than the Wall of Wind results as they represent drag coefficients for flat panel signs. The Wall of Wind drag coefficients are lower due to the extended depth of the sign models, leading to smaller

wake regions and partial reattachment of flow. It can also be seen from the comparisons that the current drag coefficient of 1.7 used in the AASHTO design of VMS panels is overly conservative (Meyer 2014).

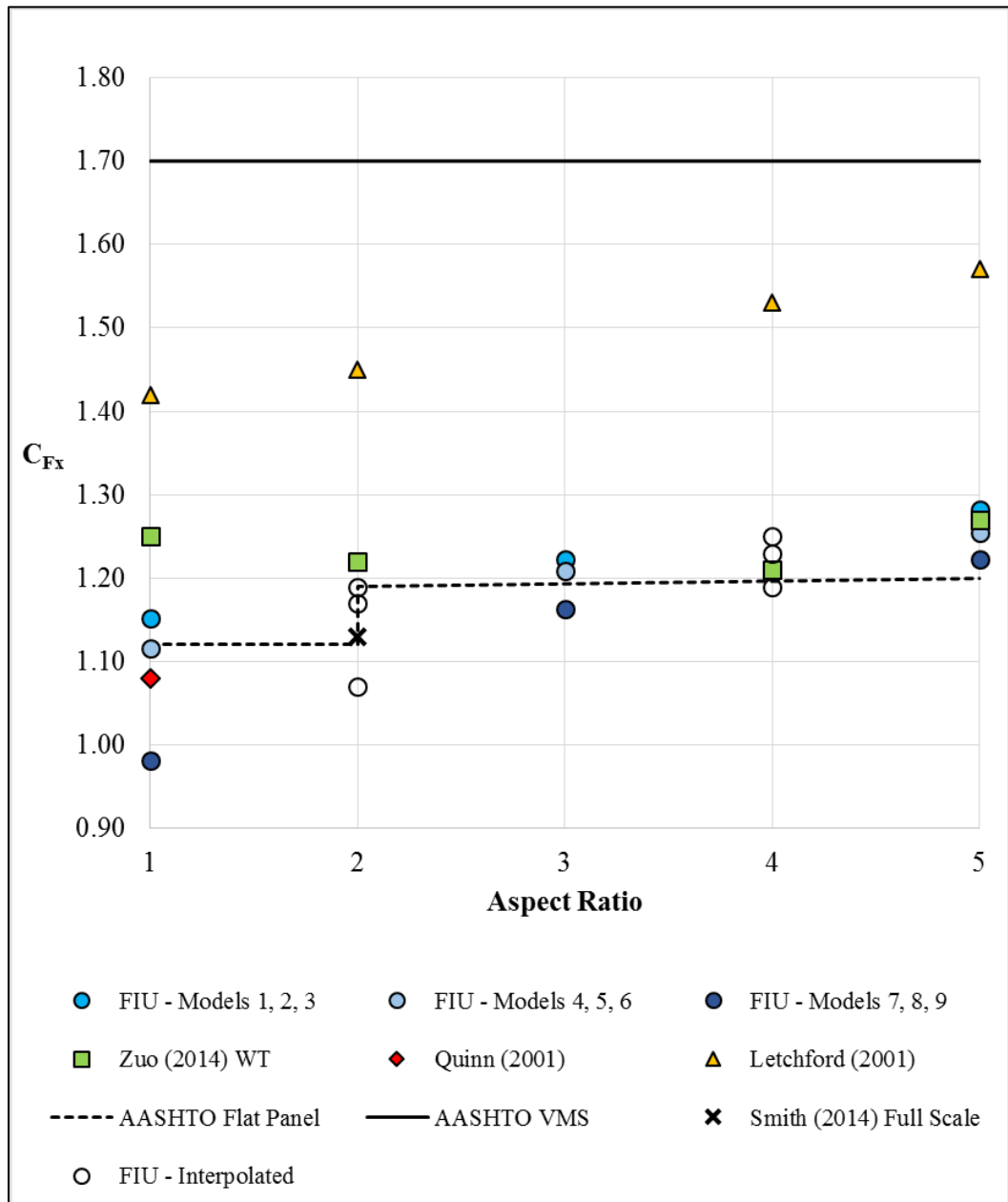


Figure 3-21: Comparison of FIU WOW and past research results for normal force coefficient (Meyer 2014)

3.4 Summary Table of Drag Coefficients

Table 3-5 provides a summary of the drag coefficients developed by the Wall of Wind study for various aspect and depth ratios. A single table is provided for both fatigue level winds and extreme event winds since the drag coefficient results were very close for the 15 m/s and 40 m/s wind speeds. The drag coefficient values were selected to be the largest of all the cases for wind speed and wind direction. The results for the 40 m/s wind speed at a 0° wind direction typically controlled the magnitude of the drag coefficients. The results corresponding to aspect ratios of 1, 3, and 5 and depth ratios of 0.1, 0.4, and 0.7 were obtained from the Wall of Wind test data, and all other drag coefficient values in the table were interpolated (Meyer 2014).

Table 3-5: Drag Coefficient Design Matrix for C_{Fx} (Meyer 2014)

Aspect Ratio (b/c)	Depth Ratio (d/c)						
	0.1	0.2	0.3	0.4	0.5	0.6	0.7
1.0	1.21	1.18	1.15	1.12	1.08	1.04	0.98
2.0	1.21	1.20	1.18	1.17	1.14	1.11	1.09
3.0	1.22	1.22	1.22	1.21	1.20	1.18	1.16
4.0	1.25	1.25	1.24	1.24	1.23	1.22	1.21
5.0	1.28	1.27	1.26	1.25	1.24	1.23	1.22

3.5 Conclusions from Wall of Wind Study

Experimental testing was conducted at the FIU Wall of Wind facility to develop drag coefficients for VMS panels. Multiple models with varying aspect and depth ratios were constructed for testing. The models were tested at different wind speeds and directions of wind approach. The study also examined the effects of edge modifications (round and chamfered edges) on the reduction of the drag coefficient. Additional testing

was performed to determine the effects of Reynolds number and wind driven rain on the models, as well as to investigate galloping potential (Meyer 2014).

The Wall of Wind testing yielded several findings regarding the dependency of the drag coefficient on the VMS size, shape, and orientation with respect to the wind direction. The testing demonstrated that the drag coefficient increases with increasing aspect ratio as the flow becomes more two-dimensional and the end effects are reduced. On the other hand, it was determined that the drag coefficient decreases with increasing depth ratio due to the smaller wake region and reattachment of flow. In addition, the study showed that the drag coefficient is generally larger when the wind direction is normal to the front face of the VMS (0°) than when the wind direction is at an angle to the VMS ($\sim 45^\circ$) (Meyer 2014).

The study also concluded that constructing VMS panels with round or chamfered edges instead of sharp edges would significantly decrease the magnitude of the drag coefficient. This development could potentially lead to economic savings in the design of sign support structures for VMS panels (Meyer 2014).

The Wall of Wind study also determined that the drag coefficient for VMS panels is not significantly affected by Reynolds number or wind driven rain. However, it was observed that VMS panels could be susceptible to galloping for certain configurations (Meyer 2014).

The results of the Wall of Wind study were generally in good agreement with the research findings of previous studies on drag coefficients for signs. It was also determined that the drag coefficient value of 1.7 for the design of VMS panels in the current ASSHTO Supports Specifications is too conservative. A summary table listing

drag coefficient values for VMS panels based on aspect and depth ratios was provided for consideration (Meyer 2014).

CHAPTER 4 VMS STRUCTURES

4.1 Chapter Overview

Two existing VMS structures were selected for analysis. Both structures are overhead bridge-type structures with four-chord box pipe trusses supporting in-service VMS signs. One structure is located in Alabaster, AL (Structure A) and the other is located in Birmingham, AL (Structure B). This chapter provides a description of the two VMS structures selected for analysis. A detailed overview of each support structure including a discussion of the frame members, connections, and support conditions is presented along with photos. In addition, the geometric and material properties of each structure are provided in graphical and tabular form. Finally, the properties of the VMS signs installed on the two structures are discussed.

4.2 Site Locations

Two in-service VMS structures were examined in this project. The first structure is located on I-65 Northbound near Alabaster, Alabama between exits 234 and 238. This structure is designated as Structure A throughout this report. Structure A is a steel overhead bridge structure that spans 71 ft across the two northbound lanes of traffic. This structure was selected for analysis because it was the subject of a previous ALDOT study which collected response data of the structure due to wind excitation. The data from the

ALDOT study was used to validate the methods used in this project. Figure 4-1 shows a northbound view on I-65 of Structure A.

The second VMS structure examined in this project is a steel overhead bridge structure located on U.S. Highway 280 near Birmingham, Alabama. This structure is designated as Structure B throughout this report. Structure B is situated about a mile east of the junction between Hwy 280 and I-459, with the VMS facing the Hwy 280 westbound traffic. The overhead bridge spans 145 ft across all six lanes of traffic in both directions as well as the median. This structure was selected for analysis because it has a very long span length compared to most VMS structures. Figure 4-2 shows a westbound view on Hwy 280 of Structure B.



Figure 4-1: Front View of Structure A (Alabaster VMS Structure)



Figure 4-2: Front View of Structure B (Birmingham VMS Structure)

4.3 Structure A – Alabaster VMS Structure

4.3.1 Overview of Structure

Structure A consists of a four chord box truss supported on each end by uprights. The four chords of the truss are framed with fillet welded struts and diagonal webs. The truss is spliced in the center with bolted transverse steel plates so that it is symmetric on each side. Figure 4-3 shows the four chord truss with the splice connection in the center. The ends of the bottom truss chords rest on WT sections which are welded to the upright posts. The bottom truss chords are connected to the WT sections using U-bolts and the top truss chords are connected to the upright posts using U-bolts as shown in Figure 4-4.

The uprights of the support structure consist of two vertical posts which are framed with fillet welded struts and diagonal webs in addition to the WT section. For the purposes of this study, the uprights are designated as either the “left upright” or “right upright” according to their position when viewed from the front of the VMS structure.

The right upright of Structure A is continuous from the base plates to the top of the truss. However, the posts of the left upright are spliced about 7 ft above the base plates with bolted transverse steel plates. This splice connection of the left upright posts is shown in Figure 4-5. The upright posts are supported by steel base plates and reinforced concrete foundations as shown in Figure 4-6. Each upright post is fillet welded to a square base plate, which in turn is anchor bolted to a cylindrical concrete foundation.

The VMS is connected to the front of the truss structure with aluminum Z-bars and U-bolts. The VMS is bolted to six Z-bars at the top, middle, and bottom of the bars. The Z-bars are then secured to the front top and bottom truss chords using U-bolts. The structure also includes an access ladder and track leading to the VMS for maintenance purposes as shown in Figure 4-7.



Figure 4-3: Truss Splice Connection of Structure A



Figure 4-4: Truss to Upright Connection of Structure A



Figure 4-5: Left Upright Splice Connection of Structure A



Figure 4-6: Base Plate and Foundation of Structure A



Figure 4-7: Access Ladder and Track of Structure A

4.3.2 Geometric Properties

Structure A spans 71 ft across the two northbound lanes of traffic on I-65. Figures 4-8 and 4-9 show a 3-dimensional view and a front view of the support structure with geometric dimensions. These figures show the location of the VMS in reference to the truss. A complete set of shop drawings for Structure A showing all member sizes and dimensions can be found in the appendix.

The upright posts, truss chords, struts, and diagonal webs of the support structure are all made of steel pipe. The upright posts have outside diameters of 8.625 in, and the truss chords have outside diameters of 3.5 in. The diameters of the struts and diagonal webs vary. Table 4-1 provides a summary of the geometric properties of the structure support members. The table lists the outside diameter, thickness, and length of each type of support member, and also provides member quantities.

4.3.3 Material Properties

The upright posts and truss chords of Structure A are made of API-5L-X52 steel pipe with a minimum yield stress of 52 ksi. The struts and diagonal webs are constructed of ASTM A53 Grade B steel pipe with a minimum yield stress of 35 ksi. All steel plates and splices are made of A36 steel. Table 4-2 shows a summary of the material properties for the support structure.

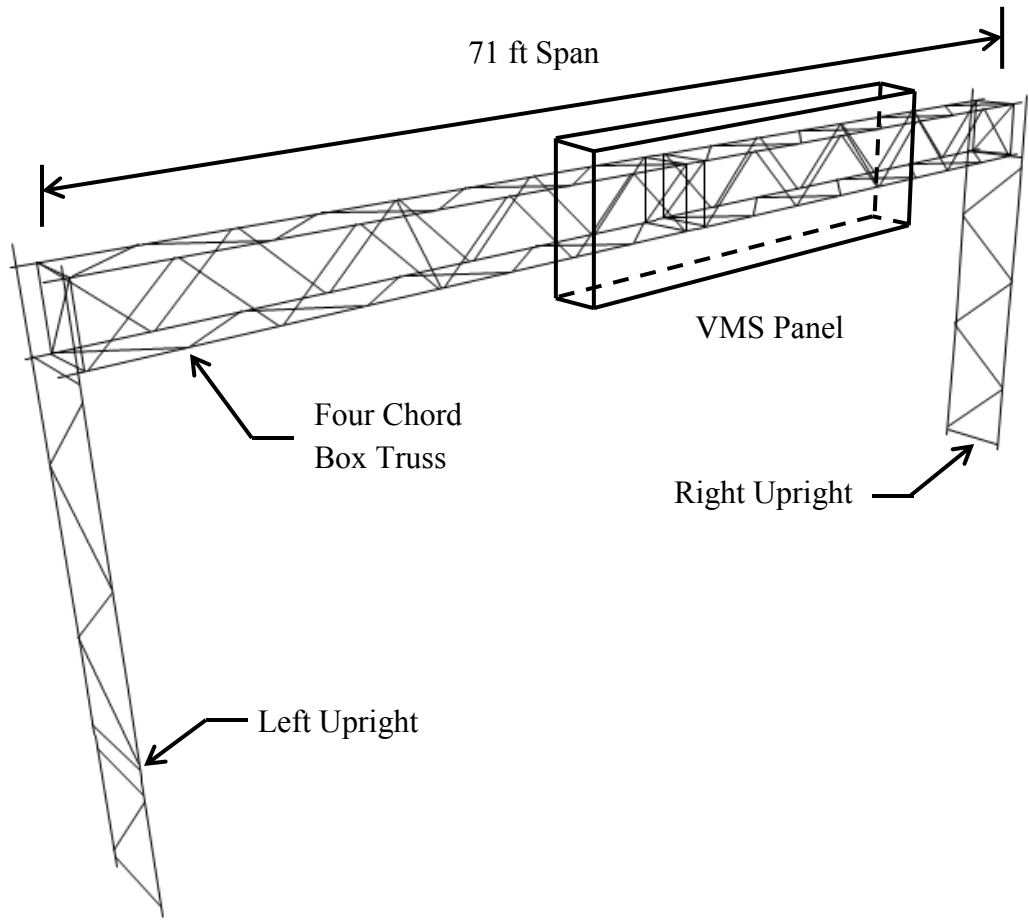


Figure 4-8: Structure A - 3D view

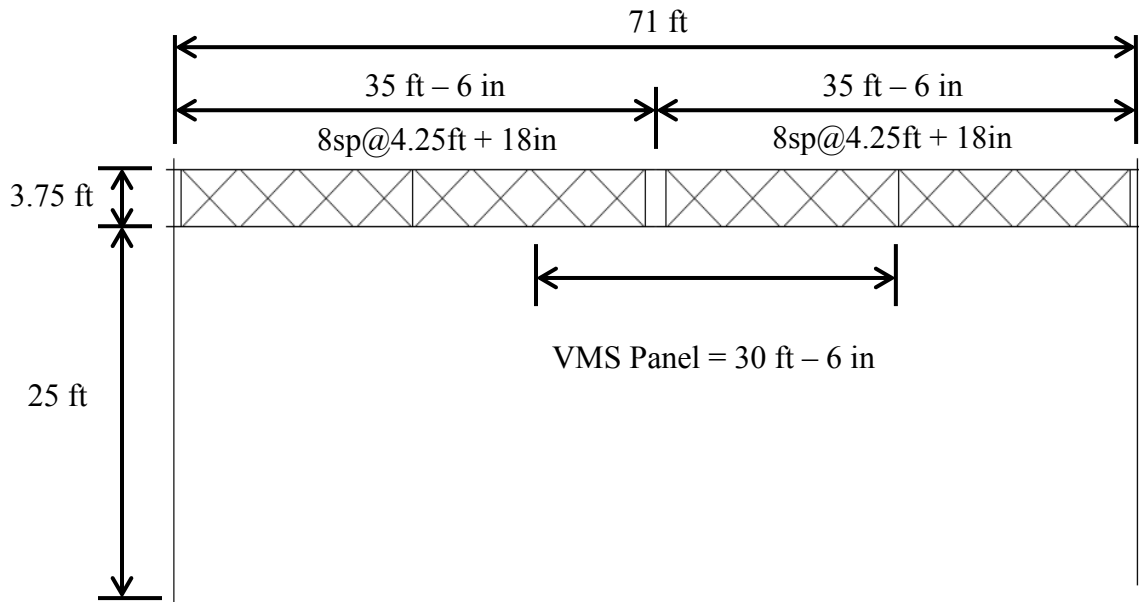


Figure 4-9: Structure A - Front View

Table 4-1: Geometric Properties for Structure A

Member Type		Outside Diameter (in)	Thickness (in)	Length (in)	Quantity	
Upright Support	Post	Left	8.625	0.25	353	2
		Right	8.625	0.25	337	2
	Strut		1.900	0.200	57	4
	Diagonal	Left	1.900	0.200	75	5
		Right	1.900	0.200	77	4
	WT 6 x 13		NA	NA	57	2
Truss	Chord		3.500	0.216	864	4
	Strut	Vertical	1.315	0.133	45	8
		Horizontal	1.315	0.133	39	8
	Diagonal	Vertical	1.900	0.145	67	32
		Horizontal	1.660	0.140	63	32
		Interior	1.315	0.133	60	6

Table 4-2: Material Properties for Structure A

Material	Members	Material Designation	Modulus of Elasticity (ksi)	Min. Yield Stress (ksi)
Steel Pipe	Upright Posts & Truss Chords	API-5L-X52	29000	52
	Struts & Diagonals	ASTM A53 GR. B	29000	35
Steel WT	WT Truss Supports	A36	29000	36
Steel Plate	Base Plates & Frame Splices	A36	29000	36
Steel Rod	Anchor Bolts	AASHTO M314-90 Grade 55	29000	55
Concrete	Foundations	4 ksi Compressive Strength	3600	NA

4.4 Structure B – Birmingham VMS Structure

4.4.1 Overview of Structure

Structure B consists of a four chord box truss supported on each end by uprights. The four chords of the truss are framed with fillet welded struts and diagonal webs. The truss is divided into four sections with each of the four chords spliced together at the connection points using bolted transverse steel plates. The truss is symmetric about the mid-span splice connection. Figure 4-10 shows the four chord truss with a splice connection between two of the truss sections. The ends of the bottom truss chords rest on WT sections which are welded to the upright posts. The bottom truss chords are connected to the WT sections and the top truss chords are connected to the upright posts using U-bolts as shown in Figure 4-11.

The uprights of the support structure consist of two vertical posts which are framed with fillet welded struts and diagonal webs in addition to the WT section. Both the left upright and the right upright are continuous from the base plates to the top of the truss. Each upright is supported by steel base plates and a rectangular reinforced concrete foundation as shown in Figure 4-12. The upright posts are fillet welded to base plates, which in turn are anchor bolted to the concrete foundation.

The VMS is connected to the front of the truss structure with aluminum Z-bars and U-bolts. The VMS is bolted to six Z-bars at the top, middle, and bottom of the bars. The Z-bars are then secured to the front top and bottom truss chords using U-bolts. The structure also includes an access ladder and track leading to the VMS for maintenance purposes as shown in Figure 4-13.



Figure 4-10: Truss Splice Connection of Structure B



Figure 4-11: Truss to Upright Connection of Structure B



Figure 4-12: Base Plates and Foundation of Structure B



Figure 4-13: Access Ladder and Track of Structure B

4.4.2 Geometric Properties

Structure B spans 145 ft across all six lanes of traffic and the median on U.S. Highway 280. Figures 4-14 and 4-15 show a 3-dimensional view and a front view of the support structure with geometric dimensions. These figures show the location of the VMS in reference to the truss. A complete set of shop drawings for Structure B showing all member sizes and dimensions can be found in the appendix.

The upright posts, truss chords, struts, and diagonal webs of the support structure are all made of steel pipe. The upright posts have outside diameters of 8.625 in, and the truss chords have outside diameters of 5.563 in. The diameters of the struts and diagonal webs vary. Table 4-3 provides a summary of the geometric properties of the structure support members. The table lists the outside diameter, thickness, and length of each type of support member, and also provides member quantities.

4.4.3 Material Properties

The structural supports of Structure B have the same material properties as Structure A. A summary of the material properties is repeated in Table 4-4 for reference purposes.

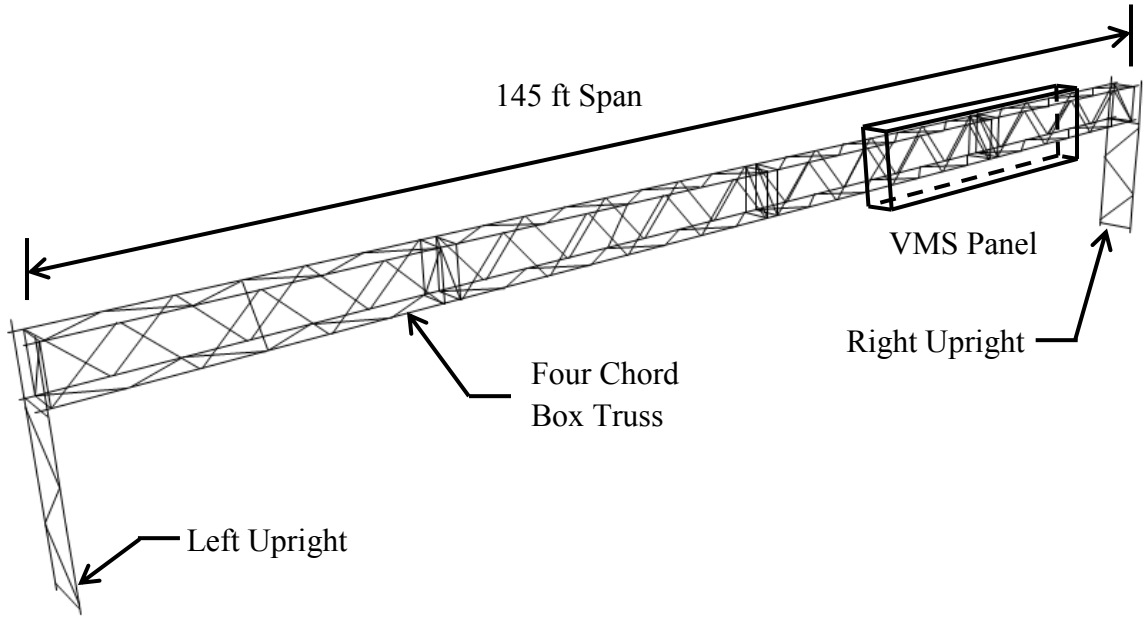


Figure 4-14: Structure B - 3D View

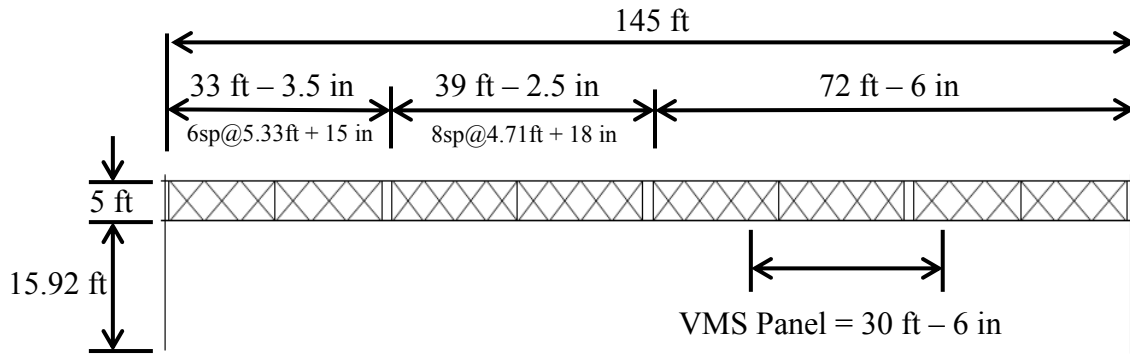


Figure 4-15: Structure B - Front View

Table 4-3: Member Properties for Structure B

Member Type		Outside Diameter (in)	Thickness (in)	Length (in)	Quantity	
Upright Support	Post	Left	8.625	0.25	259	2
		Right	8.625	0.25	262	2
	Strut	Left	1.900	0.200	60	1
		Right	2.375	0.154	60	1
	Diagonal	Left	1.900	0.145	82	3
		Right	2.375	0.154	82	3
	WT 6 x 13		NA	NA	60	2
Truss	Chord		5.563	0.219	1752	4
	Strut	Vertical	1.660	0.140	60	16
		Horizontal	1.660	0.140	39	16
	Diagonal	Vertical (LT & RT Trusses)	2.375	0.154	87	24
		Horizontal (LT & RT Trusses)	1.900	0.145	74	24
		Vertical (Middle Trusses)	2.375	0.154	82	32
		Horizontal (Middle Trusses)	1.900	0.145	68	32
		Interior	1.315	0.133	72	12

Table 4-4: Material Properties for Structure B

Material	Members	Material Designation	Modulus of Elasticity (ksi)	Min. Yield Stress (ksi)
Steel Pipe	Upright Posts & Truss Chords	API-5L-X52	29000	52
	Struts & Diagonals	ASTM A53 GR. B	29000	35
Steel WT	WT Truss Supports	A36	29000	36
Steel Plate	Base Plates & Frame Splices	A36	29000	36
Steel Rod	Anchor Bolts	AASHTO M314-90 Grade 55	29000	55
Concrete	Foundations	4 ksi Compressive Strength	3600	NA

4.5 Variable Message Signs

The VMS signs installed on Structures A and B are both the same size and weight. The signs are constructed of a steel frame covered with exterior aluminum panels. Figure 4-16 shows the front and side views of the VMS signs with dimensions. The weight of each VMS is approximately 4500 lbs including all interior electronics.

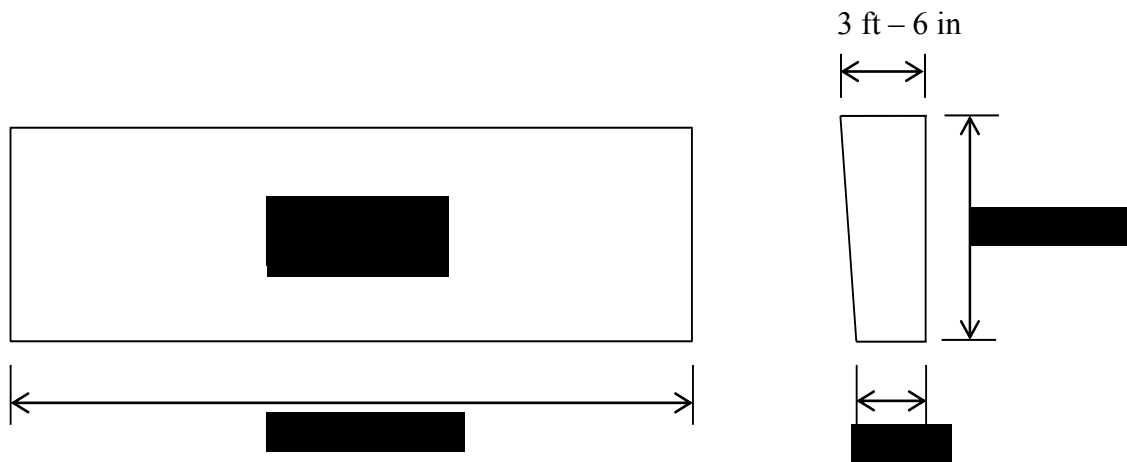


Figure 4-16: VMS Front and Side View

CHAPTER 5 FINITE ELEMENT MODELING

5.1 Chapter Overview

Three-dimensional finite element models were developed for Structures A and B using SAP2000. Each model consisted of a structural support frame, a VMS sign, support conditions, and an access ladder and track. The structural support frame, access ladder, and access track were created using frame elements, while the VMS sign was modeled using solid elements. Body constraints were commonly used for connections. Once the models were created, modal analyses were run in SAP to determine the dynamic properties of the VMS structures. This chapter provides a detailed description of the SAP modeling process and modal analyses for Structures A and B.

5.2 SAP2000 Software Program

SAP2000 is a structural modeling, analysis, and design software package. The program has a graphic user interface which can display 2-dimensional and 3-dimensional views of a structural model. The geometric properties of structural members can be defined using a variety of elements types, including frame elements, solid elements, and shell elements. Material properties can be defined using density, modulus of elasticity, Poisson's ratio, and strength.

SAP can apply point loads, distributed loads, surface loads, and base loads to a structural system, and can also account for the self-weight of the structure. The program

can perform static or dynamic analyses on a structure using either linear or nonlinear methods. Analysis results, including shear, moment, and normal forces and stresses, can be displayed in SAP's user interface or exported to output tables. SAP also integrates updated code requirements from AASHTO, ACI, and AISC for design purposes.

5.3 Finite Element Models of VMS Structures

Finite element models of Structures A and B were created in SAP2000 version 15. The models were developed using the geometric dimensions and material properties outlined in Chapter 4 and included in the shop drawings in the appendix. This section provides a detailed explanation of the modeling process for Structure A. Structure B was modeled following the same process as Structure A with a few exceptions which are noted in the text.

There were four main steps to creating each model. First, the structural frame consisting of the uprights, 4-chord truss, and connections was created. Second, the VMS was modeled and attached to the truss. Third, the support conditions were defined for the structure. Finally, the access ladder and track were modeled to add the extra weight and rigidity experienced by the structure in the field. Figures 5-1 and 5-2 show 3-dimensional extruded views of the SAP models for Structures A and B, respectively.

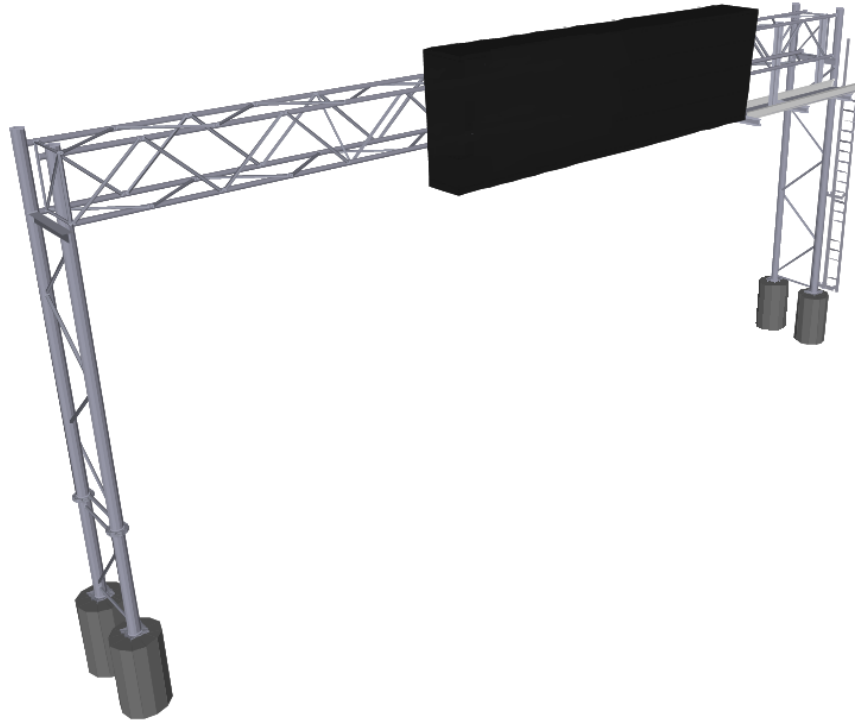


Figure 5-1: SAP Model of Structure A

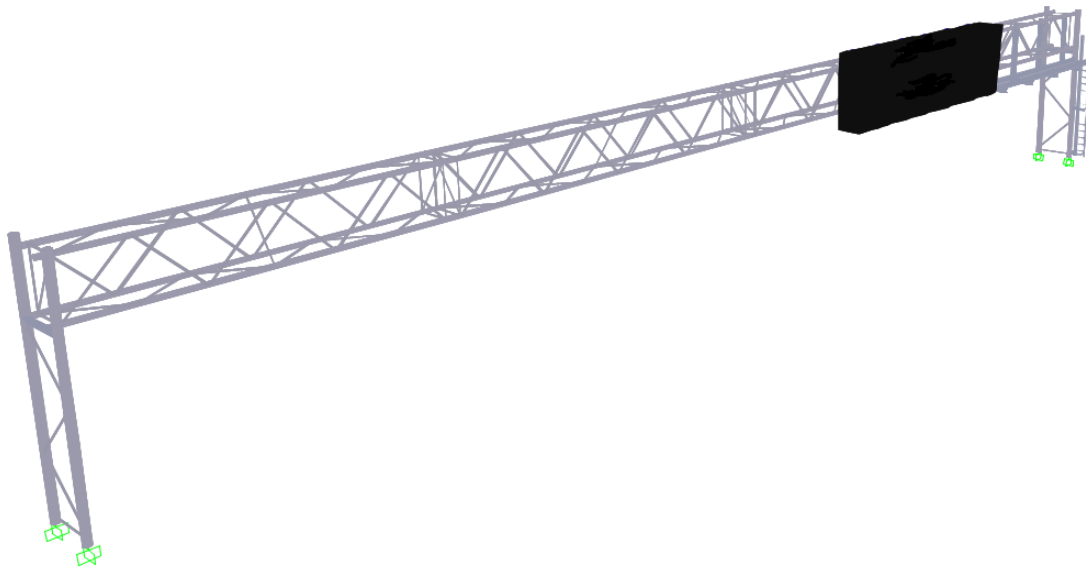


Figure 5-2: SAP Model of Structure B

5.3.1 Structural Frame

The structural frame of Structure A was created in SAP using frame elements, solid elements, and body constraints. The upright posts, truss chords, and web bracing were modeled as frame elements with circular steel pipe cross-sections. The connections of the web bracing members to the upright posts and truss chords were modeled using moment releases to represent limited rigidity of the connections in the field. The WT sections supporting the truss were modeled as frame elements with the cross-section selected from the AISC section properties database in SAP. Fixed connections were applied between the WT sections and the upright posts to represent the welded connection. Figure 5-3 shows the structural frame of Structure A modeled in SAP.

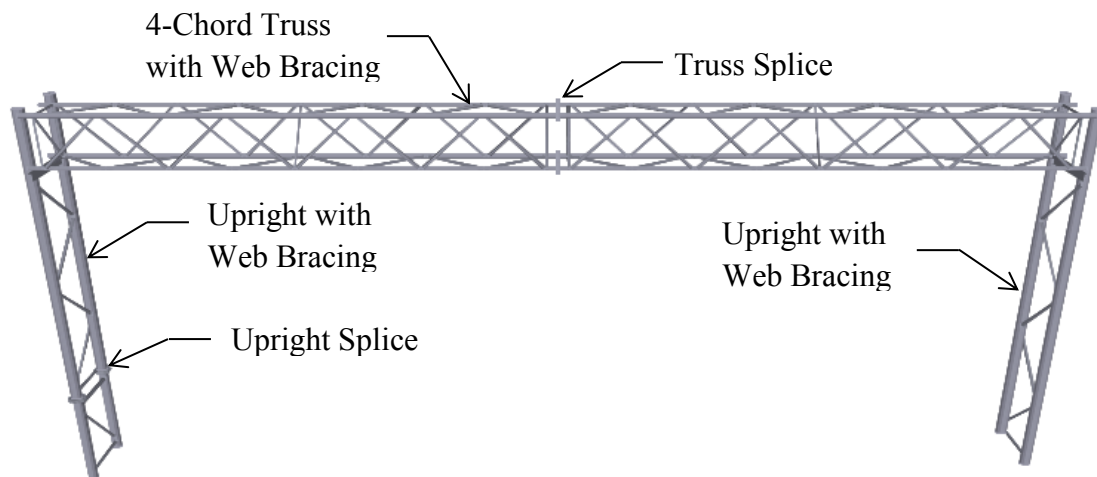


Figure 5-3: Structural Frame Model for Structure A

The upright splices and truss splices of the Structure A were modeled using solid elements and body constraints. Each splice consisted of two adjacent steel plates bolted together and welded to their respective frame supports. The steel plates forming the splice were modeled as solid elements. The solid elements were connected to the frame elements using body constraints with all degrees of freedom constrained to represent the

welded connection between the steel plate and the upright post or truss chord. The bolted connection between the two steel plates was modeled using body constraints at the bolt locations with only the translational degrees of freedom constrained. Figure 5-4 shows the splice connections modeled for the left upright.

Analysis checks of the SAP model for Structure A showed that the truss splices and upright splices created fixed connections between the steel pipes adjacent to each splice. Consequently, the truss splices in the SAP model for Structure B were defined as fixed connections using body constraints with all degrees of freedom constrained.

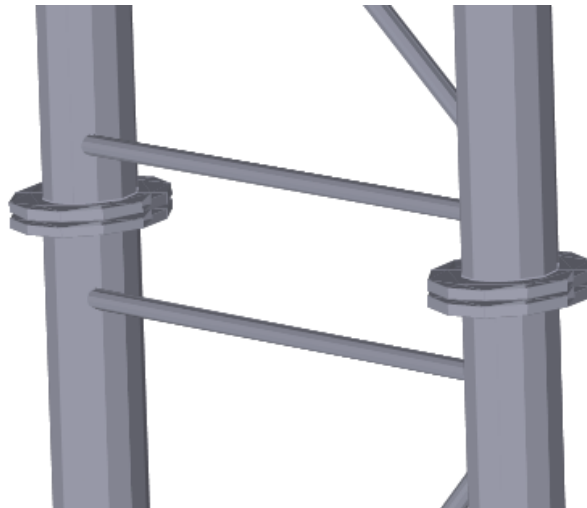


Figure 5-4: Splice Connections for Left Upright

The truss chords of Structure A were connected to the upright posts and WT sections using U-bolts in the field. This connection was modeled in SAP using body constraints with only the translational degrees of freedom constrained. Figure 5-5 shows the connections between the truss chords and the adjacent upright post or WT shape.

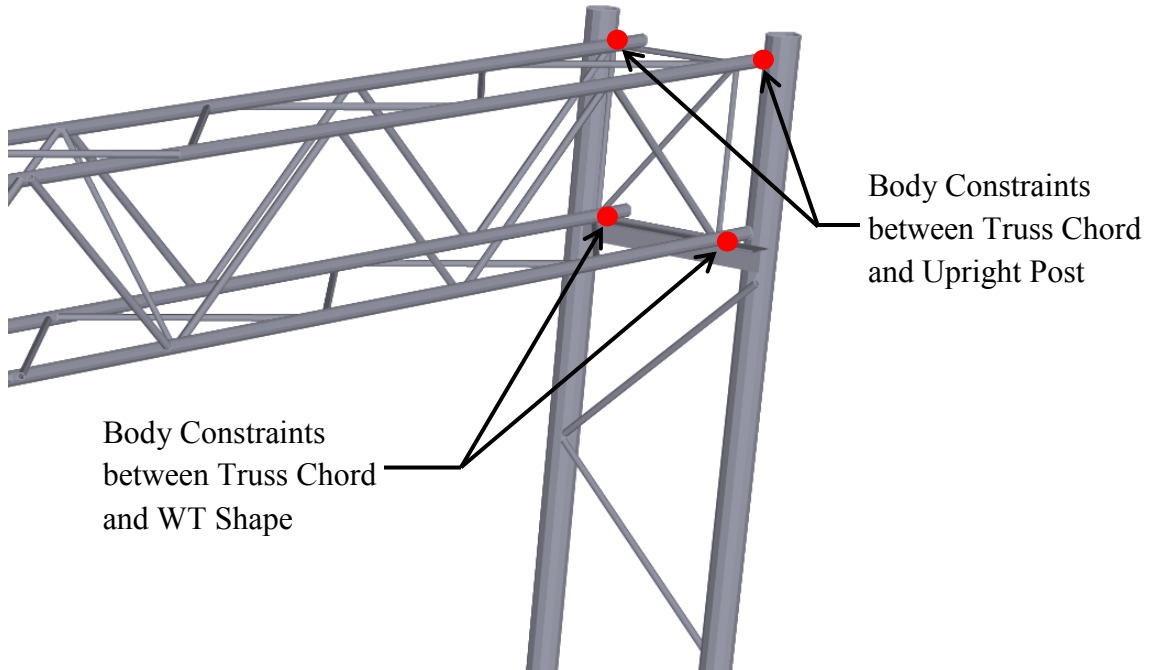


Figure 5-5: Connections between Truss Chords and Upright

5.3.2 *Variable Message Sign*

The VMS was attached to the support structure using six evenly spaced aluminum Z-bars. The Z-bars were connected to the front top and bottom truss chords using U-bolts. These connections were modeled using body constraints with only the translational degrees of freedom constrained. Figure 5-6 shows the locations of the body constraints connecting the Z-bars to the truss chords.

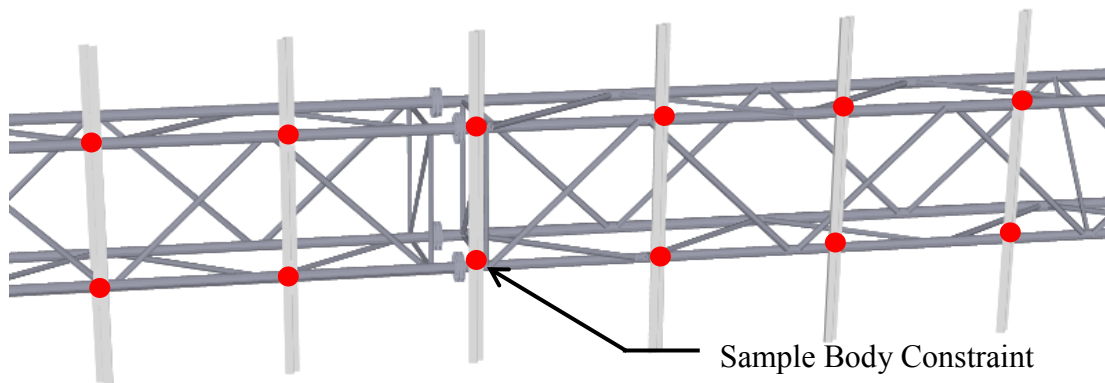


Figure 5-6: Connection of Z-bars to Truss Chords

The VMS was modeled as a 3-D structure of solid elements with an overall density of 5.1 pcf and aluminum isotropic properties. The density was calculated from the estimated weight of the VMS (4500 lbs) and its total volume (884 cf) based on the geometric dimensions provided in Chapter 4. The VMS was attached to the Z-bars using bolted connections at the top, middle, and bottom of the Z-bars. These connections were modeled using body constraints with only the translational degrees of freedom constrained. Figure 5-7 provides a view from the back of the truss structure showing the locations of the body constraints connecting the VMS to the Z-bars.

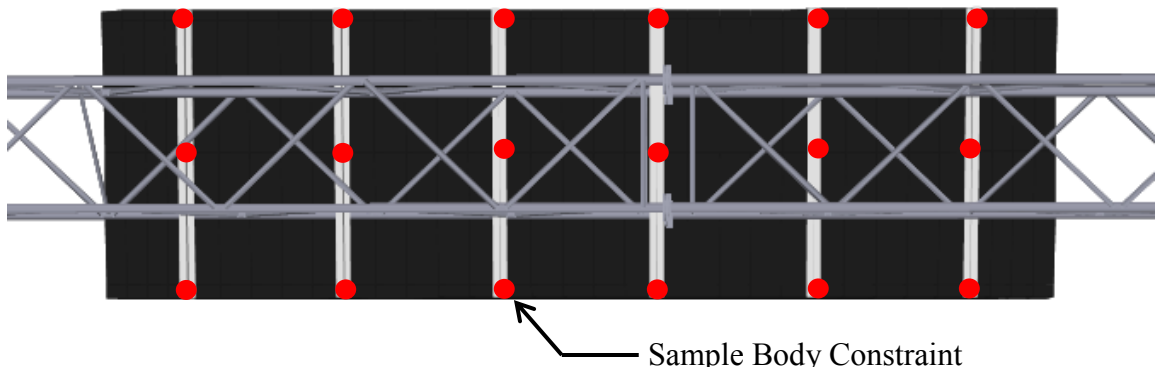


Figure 5-7: Connection of VMS to Z-bars

5.3.3 Support Conditions

The steel base plates and concrete foundations supporting the uprights of Structure A were created in SAP using solid elements. The base plates were welded to the upright posts and connected to the concrete foundation using anchor bolts. The welded connection was modeled using body constraints with all degrees of freedom constrained. The anchor bolts were modeled as frame elements with one end attached to the base plate and the other end embedded in the concrete foundation. A 2 in space was

created between the bottom of the base plates and the top of the foundations as specified in the shop drawings. Finally, the base of each foundation was restrained using fixed supports. Figure 5-8 shows pictures of the base plates, anchor bolts, and foundations modeled in SAP.

Analysis checks of the SAP model for Structure A showed that the connections between the upright posts, base plates, anchor bolts, and concrete foundations were essentially equivalent to fixed support conditions. Consequently, the bases of the four upright posts in the SAP model for Structure B were assigned fixed restraints for support conditions.

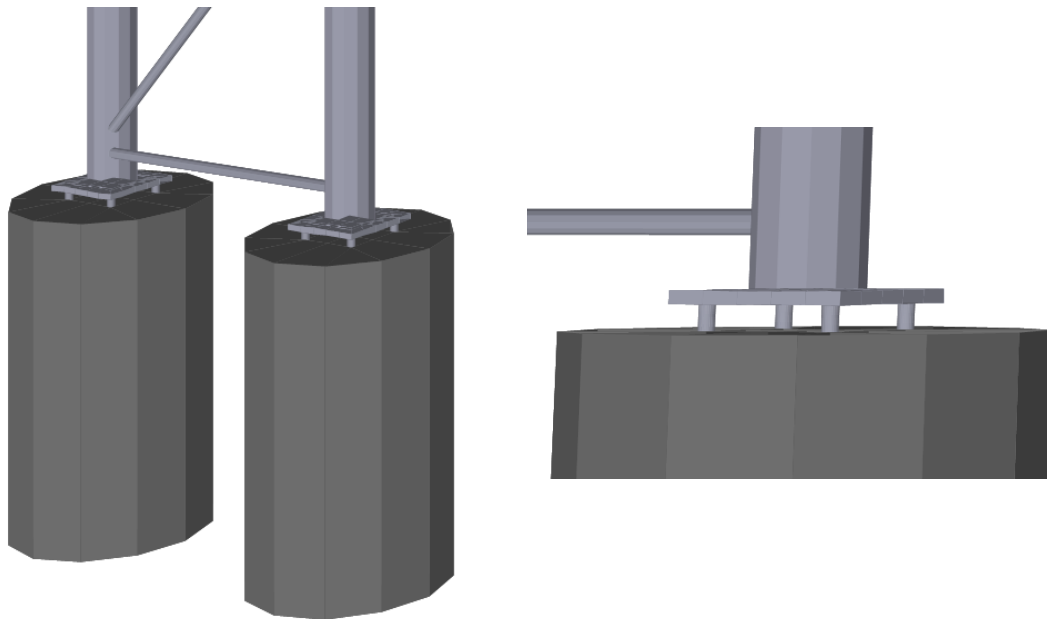


Figure 5-8: Base Plates, Anchor Bolts, and Foundations for Structure A

5.3.4 Access Ladder and Track

The access ladder was modeled in SAP using frame elements. The ladder rails were defined as steel angles and the ladder rungs were defined as steel pipes. The ladder was connected to the right upright post closest to the on-coming traffic using U-bolts and welded angles. These connections were modeled using body constraints.

The access track was modeled using frame elements for the track supports and solid elements for the track grating. The track supports were defined as small steel W-shapes attached to the top and bottom truss chords using body constraints to represent U-bolt connections. Aluminum channels were also modeled on each side of the track grating. Figure 5-9 shows the access ladder and track attached to the support structure.

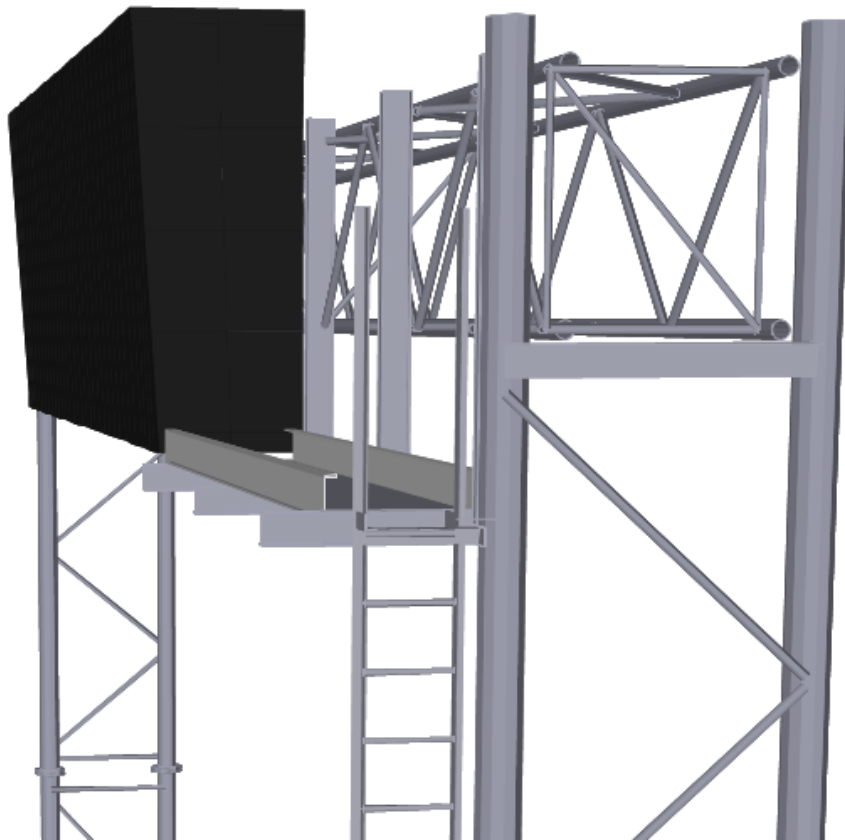


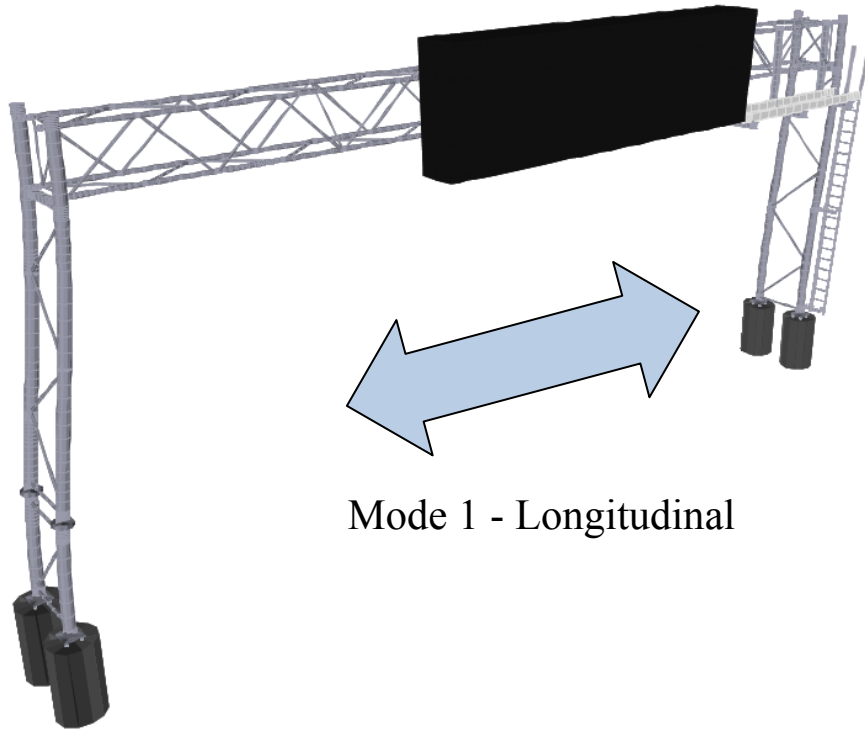
Figure 5-9: Access Ladder and Track for Structure A

5.4 Modal Analyses

Modal analyses were performed in SAP for Structures A and B to determine the dominant mode shapes and natural frequencies for each structure. The dominant mode shapes were those which had the lowest natural frequencies of vibration. The first three mode shapes and natural frequencies for each SAP model are provided in the following sections.

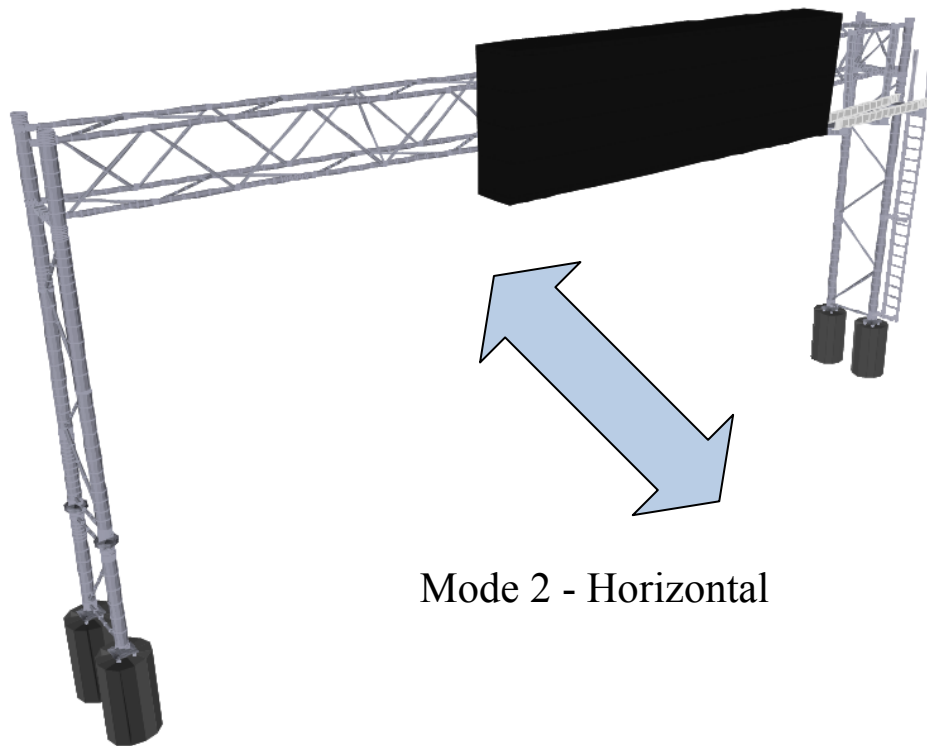
5.4.1 Structure A – Alabaster VMS Structure

The first mode shape of Structure A is shown in Figure 5-10. The first mode involved longitudinal vibration of the structure in the direction perpendicular to traffic due to bending of the uprights (side-to-side in-plane motion). The natural frequency of the first mode was 1.51 Hz. The second mode shape of the structure is shown in Figure 5-11. The second mode was defined by horizontal vibration of the truss structure in the direction parallel to traffic (out-of-plane motion). The natural frequency of the second mode was 3.13 Hz. The third mode shape of the structure is shown in Figure 5-12. The third mode involved vertical vibration of the truss structure in the direction of gravity (up-and-down in-plane motion), as well as torsion of the sign and truss structure. The natural frequency of the third mode was 3.79 Hz. A summary of the first three mode shapes of Structure A with their corresponding natural frequencies and periods is provided in Table 5-1.



Mode 1 - Longitudinal

Figure 5-10: Structure A Mode Shape 1 – Longitudinal



Mode 2 - Horizontal

Figure 5-11: Structure A Mode Shape 2 – Horizontal

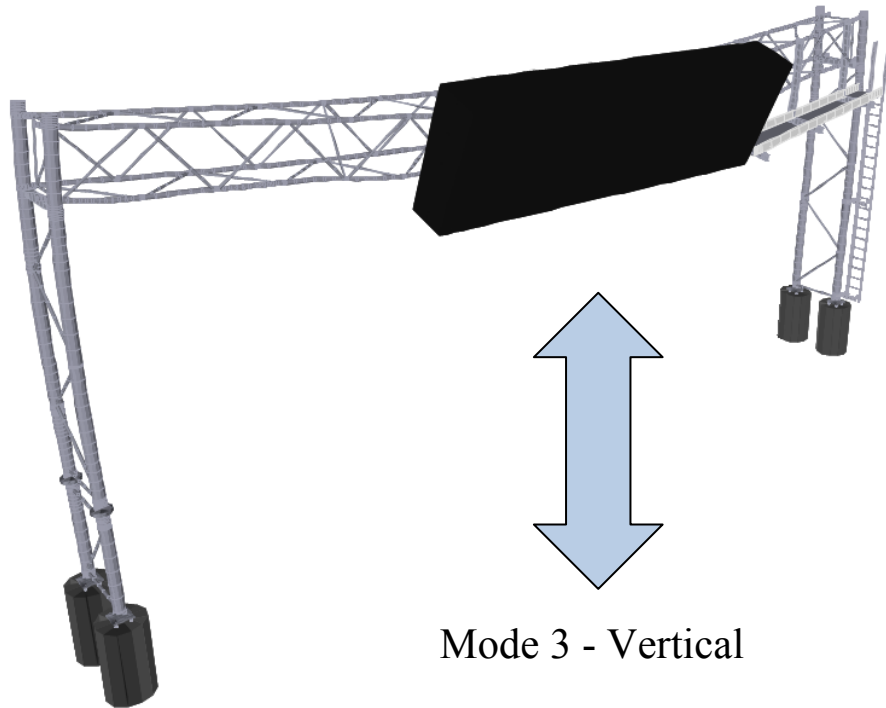


Figure 5-12: Structure A Mode Shape 3 – Vertical

Table 5-1: SAP Mode Shapes for Structure A

Mode	Direction of Vibration	Natural Frequency (Hz)	Natural Period (sec)
1	Longitudinal	1.51	0.662
2	Horizontal	3.13	0.319
3	Vertical	3.79	0.264

5.4.2 Structure B – Birmingham VMS Structure

The first mode shape of Structure B is shown in Figure 5-13. The first mode involved horizontal vibration of the truss structure in the direction parallel to traffic (out-of-plane motion). The natural frequency of the first mode was 1.29 Hz. The second mode shape of the structure is shown in Figure 5-14. The second mode was defined by

longitudinal vibration of the structure in the direction perpendicular to traffic due to bending in the uprights (side-to-side in-plane motion). The natural frequency of the second mode was 1.89 Hz. The third mode shape of the structure is shown in Figure 5-15. The third mode involved vertical vibration of the truss structure in the direction of gravity (up-and-down in-plane motion), as well as torsion of the sign and truss structure. The natural frequency of the third mode was 2.01 Hz. A summary of the first three mode shapes of Structure B with their corresponding natural frequencies and periods is provided in Table 5-2.

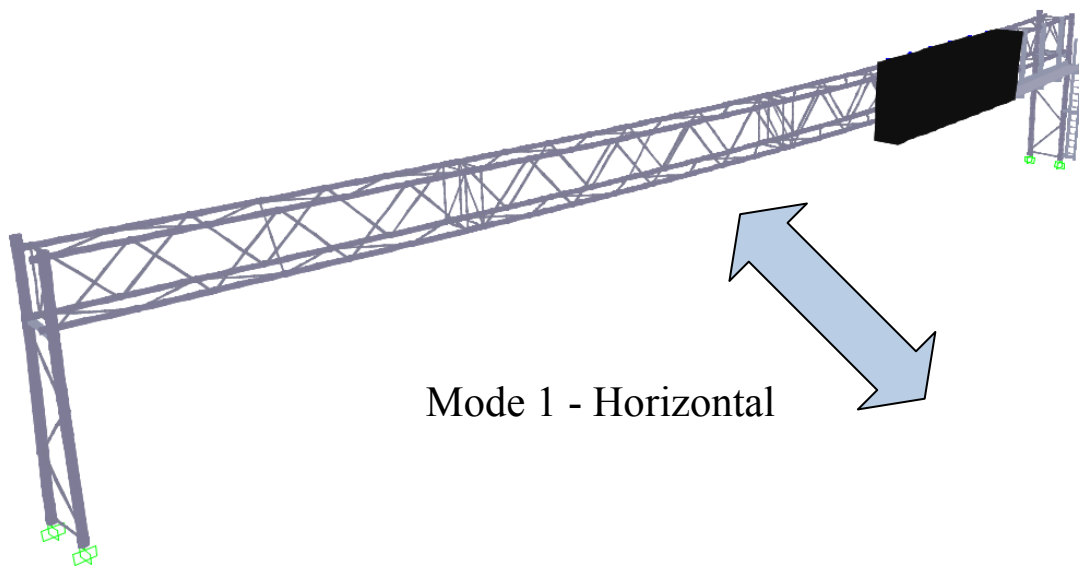


Figure 5-13: Structure B Mode Shape 1 – Horizontal

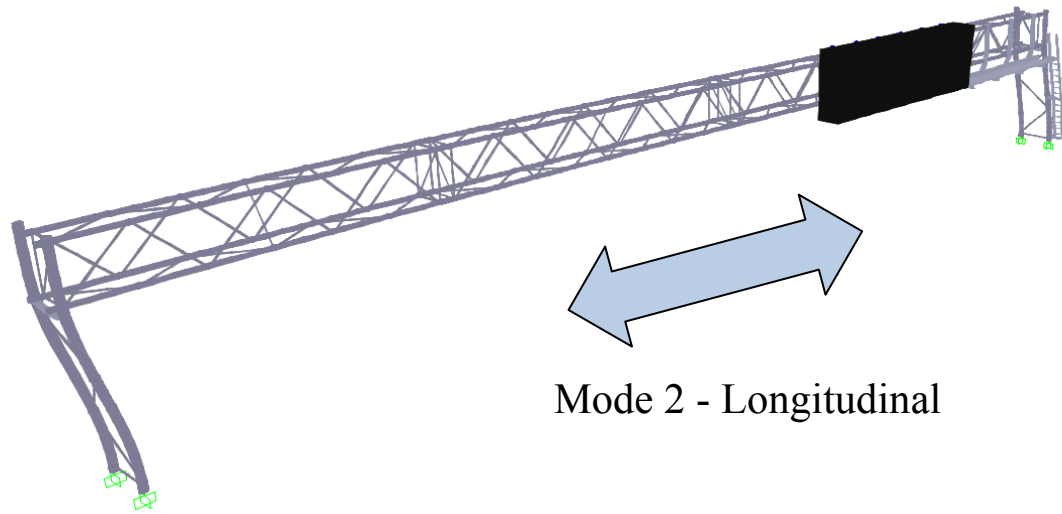


Figure 5-14: Structure B Mode Shape 2 – Longitudinal

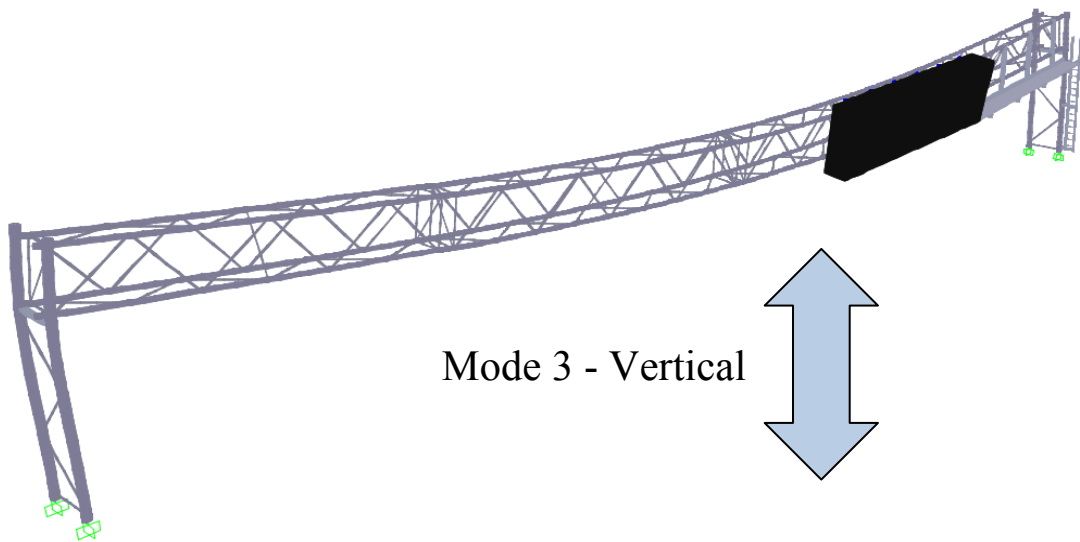


Figure 5-15: Structure B Mode Shape 3 – Vertical

Table 5-2: Mode Shapes for Structure B

Mode	Direction of Vibration	Natural Frequency (Hz)	Natural Period (sec)
1	Horizontal	1.29	0.775
2	Longitudinal	1.89	0.529
3	Vertical	2.01	0.498

CHAPTER 6 COMPARISON OF DRAG COEFFICIENTS USING EXPERIMENTAL DATA AND FEA DYNAMIC MODELING

6.1 Chapter Overview

A study was conducted to verify the VMS drag coefficient results from the FIU Wall of Wind testing. The study compared experimental field data from Structure A to analytical results obtained from the SAP model of the structure. The experimental data was collected in a previous ALDOT study which examined the response of Structure A due to dynamic wind loading. The same dynamic wind loading which was measured in the field was applied to the SAP model of the structure using a VMS drag coefficient from the FIU Wall of Wind testing. The experimental stress response of the structure was compared to the analytical stress response to verify the accuracy of the VMS drag coefficient. This chapter provides a description of the drag coefficient verification study and discusses the results as they apply to the Wall of Wind testing project.

6.2 Experimental Analysis

An experimental analysis was performed using data collected from a previous ALDOT study. The data included measurements for strain and acceleration of the Structure A as well as fatigue wind velocities. Usable data was selected for the drag coefficient verification study based on wind speed and direction criteria. The mode shapes and corresponding natural frequencies of the Structure A were determined from

the experimental data and compared to the mode shapes and frequencies of the SAP model.

6.2.1 Experimental Study of Structure A

ALDOT conducted an experimental study of Structure A from August 2010 to February 2011. The structure was instrumented with strain gauges, accelerometers, and anemometers to collect time history data for analysis purposes. Data was collected for the structure on six different days over a period of several months. The information and pictures presented in this section were obtained from the report “Design of Overhead VMS Structures for Fatigue Loads” by Fouad H. Fouad and Ian E. Hosch.

6.2.1.1 Instrumentation of Structure

Structure A was instrumented with strain gauges, accelerometers, and anemometers to collect time history data. The strain gauges were used to measure the stress response of critical support members under fatigue wind loading. The accelerometers were used to determine the dynamic vibration properties of the structure such as natural frequencies and modal damping. Finally, anemometers were used to measure natural fatigue wind speeds and directions for the structure’s location. All of the data was recorded simultaneously using a data acquisition system.

Strain Gauges

Uniaxial strain gauges were used to determine the stress response of the structure under wind loading. The strain gauges were placed at critical stress locations on two upright posts and one truss chord. The gauges were positioned along the longitudinal

axis of each member so that the normal strain could be measured. A protective coating and tape were used to cover each strain gauge from the environment (Fouad 2011).

Upright Posts

A total of eight strain gauges were attached to the two upright posts located on the right side of the northbound lanes. Four strain gauges were attached to each post at a location of 8 ft - 6 in above the base plates. The strain gauges were placed at intervals of 90 degrees around the circumference of each post. One of the gauges was offset to avoid an existing conduit. Figure 6-1 shows the placement of the strain gauges at locations 1 and 2 on the uprights. Figure 6-2 shows the attached strain gauges at location 1 before the protective coating and tape have been applied. Figure 6-3 shows the attached strain gauges along with the protective coating and tape at location 2 (Fouad 2011).

Truss Chords

Four strain gauges were attached to the bottom truss chord which was closest to the on-coming northbound traffic. The strain gauges were attached to the chord at 22 in from the first vertical truss web on the right side of the structure. The gauges were placed at intervals of 90 degrees around the circumference of the truss chord. Figure 6-4 shows the placement of the strain gauges at location 3 on the truss chord. Figure 6-5 shows the attached strain gauges at location 3 before the protective coating and tape have been applied (Fouad 2011).

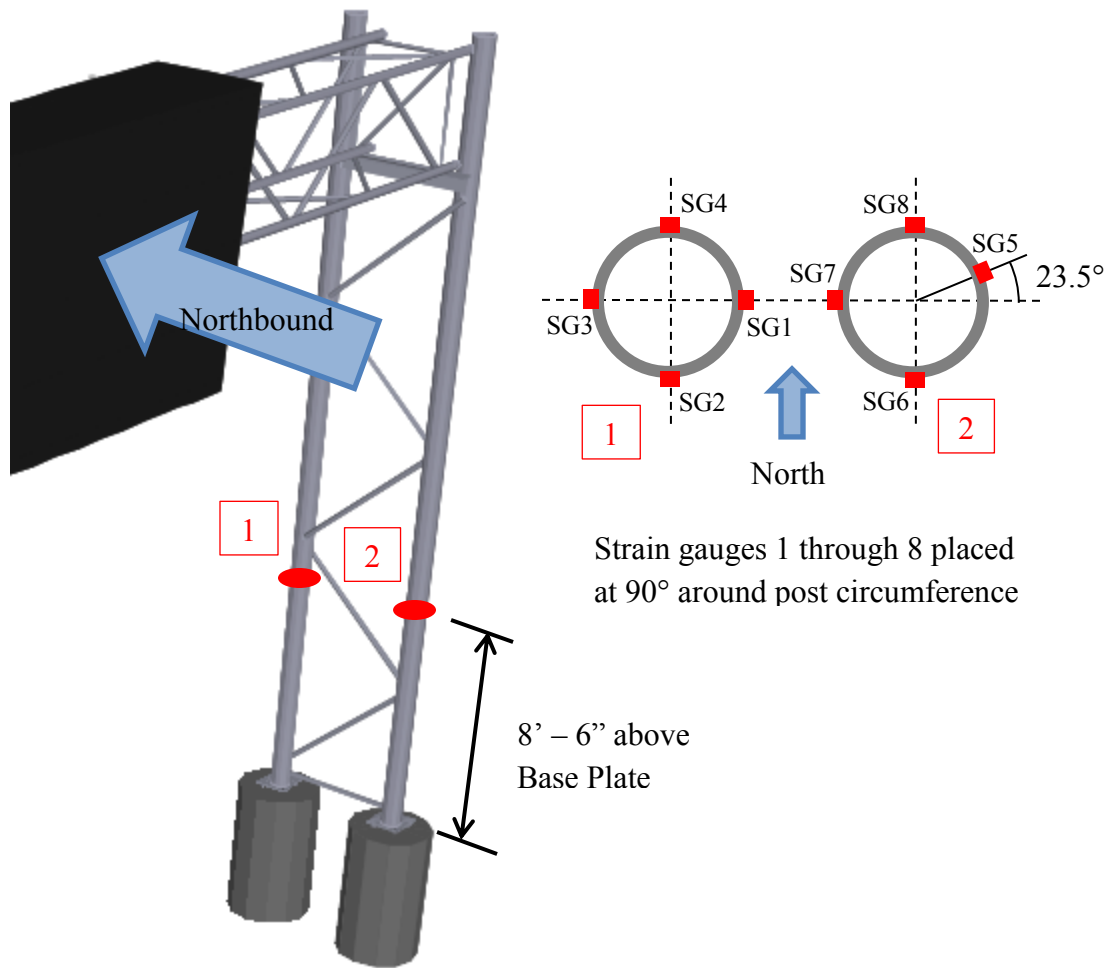


Figure 6-1: Strain Gauge Placement on Upright Posts (Adapted from Fouad 2011)

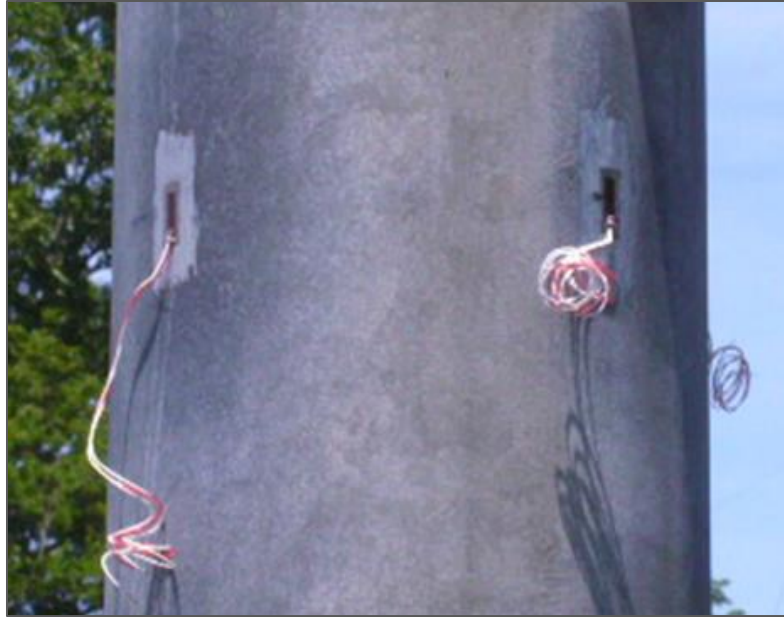


Figure 6-2: Strain Gauges Attached to Upright at Location 1 (Fouad 2011)



Figure 6-3: Strain Gauges Attached to Upright with Tape at Location 2 (Fouad 2011)

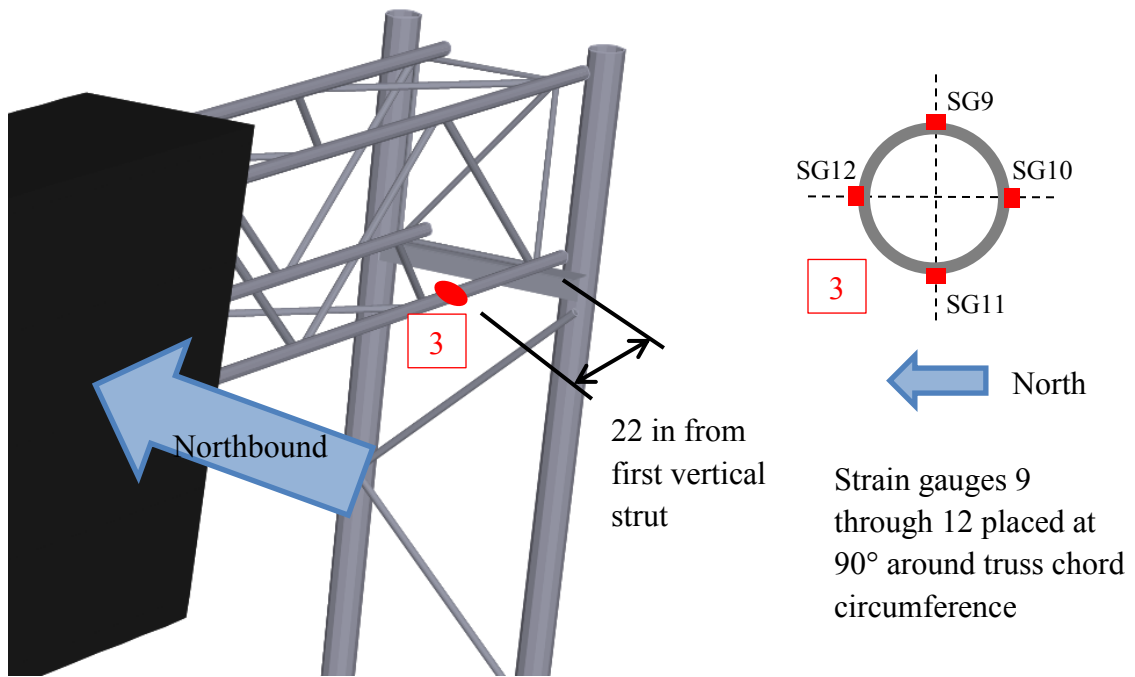


Figure 6-4: Strain Gauge Placement on Truss Chord (Adapted from Fouad 2011)

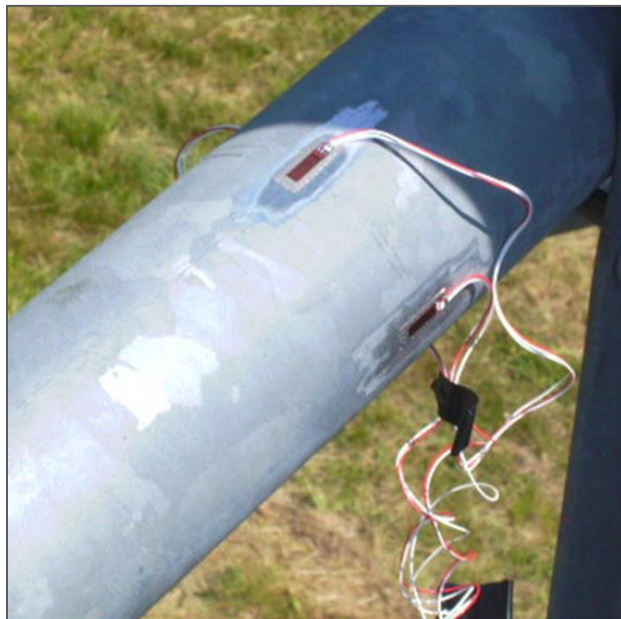


Figure 6-5: Strain Gauges Attached to Truss Chord (Fouad 2011)

Accelerometers

Accelerometers were used to determine the acceleration response of the structure under wind loading. The acceleration response was important in identifying several dynamic properties of the structure such as modes of vibration, natural frequencies, and critical damping percentages. The accelerometers were of the piezoelectric type and had a maximum capacity of 96.5 ft/sec^2 or 3 G (Fouad 2011).

A total of four accelerometers were attached to the structure. The accelerometers were placed at strategic locations determined from preliminary finite element analysis to capture the primary modes of structural vibration. Figure 6-6 shows the placement of the accelerometers. Accelerometer 1L was used to measure the longitudinal acceleration of the structure perpendicular to traffic. Accelerometer 2V recorded the vertical acceleration of the structure, while accelerometer 3H recorded the horizontal acceleration of the structure parallel to traffic. Accelerometer 4H also measured the horizontal acceleration of the structure to identify any torsional behavior of the truss. Figure 6-7 shows the attachment of accelerometer 4H to the truss chord (Fouad 2011).

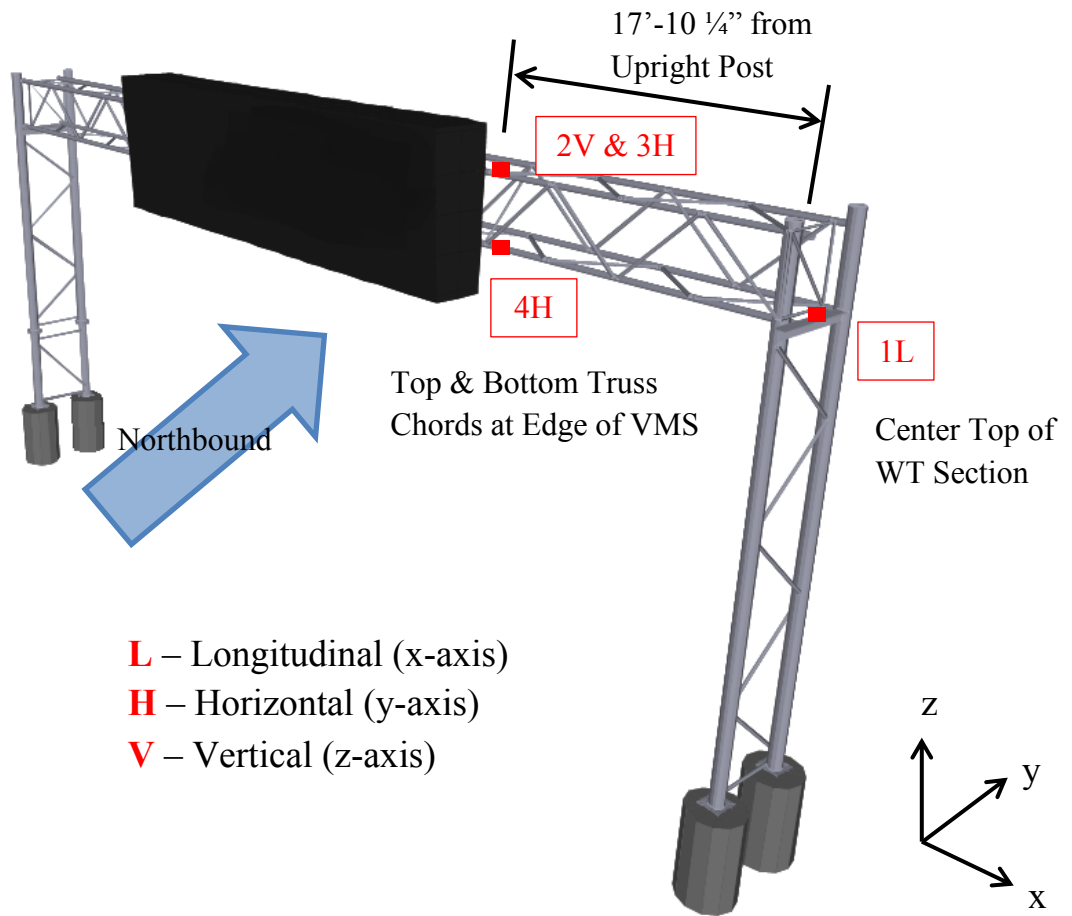


Figure 6-6: Accelerometer Placement on Truss Chords and WT Section (Adapted from Fouad 2011)

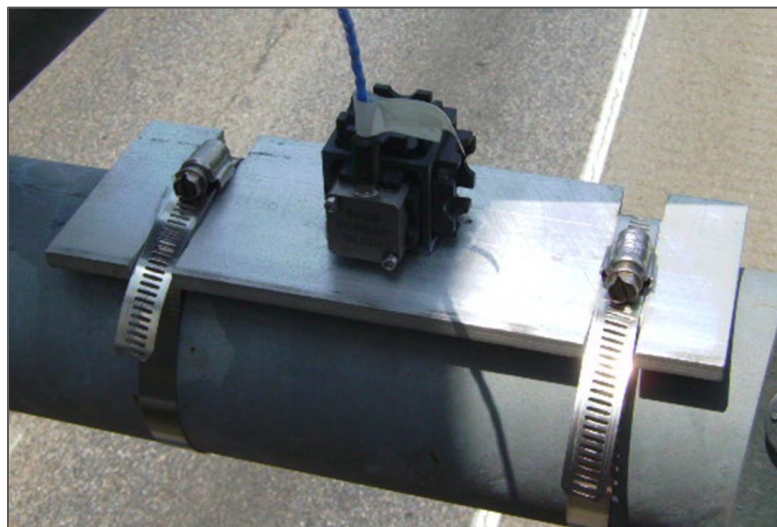


Figure 6-7: Attachment of Accelerometer 4H to Truss Chord (Fouad 2011)

Anemometers

Anemometers were used to measure the natural wind speed and direction for the location of Structure A. The anemometers were WindSonic Ultrasonic Wind Sensors. A total of two anemometers were used: AN-1 and AN-2. Figure 6-8 shows the attachment of the anemometers to the structure. The anemometers were attached to the right upright using a steel rod which extended 4 ft above the top of the truss. This was done to avoid any wind effects such as turbulence and vortices caused by the structure. Figure 6-9 shows pictures of the anemometers attached to the structure with the steel rod extension (Fouad 2011).

Each anemometer measured the wind speed and direction for a different plane. AN-1 measured wind in the horizontal plane, while AN-2 measured wind in the vertical plane. Both anemometers encompassed the full 360 degree range of motion within their respective planes. The south bearing for the anemometers was specified as the side which faced the on-coming traffic (Fouad 2011).

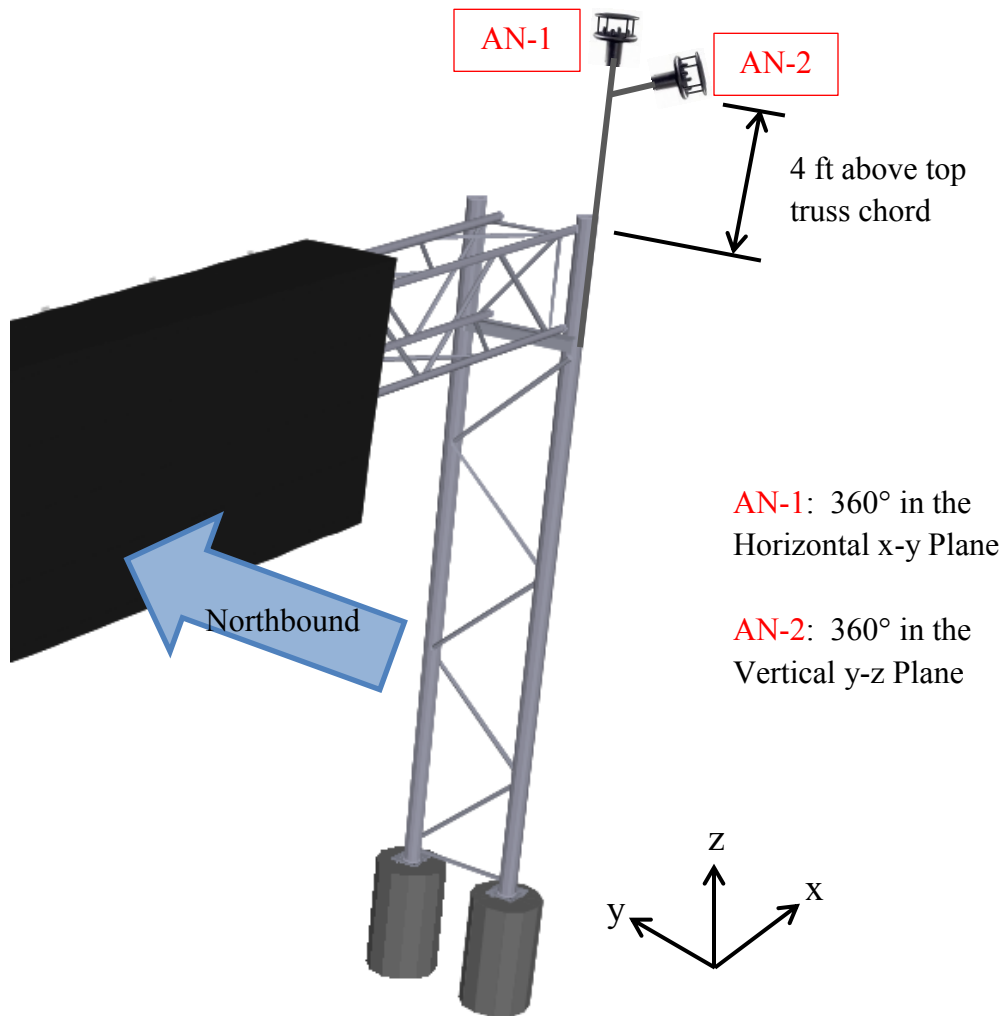


Figure 6-8: Anemometer Placement on Structure (Adapted from Fouad 2011)



Figure 6-9: Anemometers Connected to Structure with Steel Extension (Fouad 2011)

Data Acquisition System

All of the instrumentation was wired into a data acquisition system. The data acquisition system consisted of 20 channels which collected data simultaneously. Each channel collected data from a specific instrument: 12 channels collected data from the strain gages, 4 channels collected data from the accelerometers, and 4 channels collected data from the anemometers (2 for wind speed and 2 for wind direction). Data was collected at a rate of 60 Hz (samples per second), which was much higher than the natural frequencies of the structure. This prevented errors such as aliasing in the data collection process (Fouad 2011).

A van was parked on the side of the interstate near the structure on testing days. The van held the data acquisition system as well as a portable computer to store the data. The instrumentation wiring was fed through a hole in the side of the van and connected to the data acquisition system as shown in Figure 6-10 (Fouad 2011).



Figure 6-10: ALDOT Van with Instrumentation Wiring (Fouad 2011)

Figures 6-11, 6-12, and 6-13 show wind velocity, strain, and acceleration time histories of a sample of data collected simultaneously by the data acquisition system. The wind velocity time history was measured using anemometer 1, the strain time history was measured using strain gauge 2, and the acceleration time history was measured using accelerometer 3H.

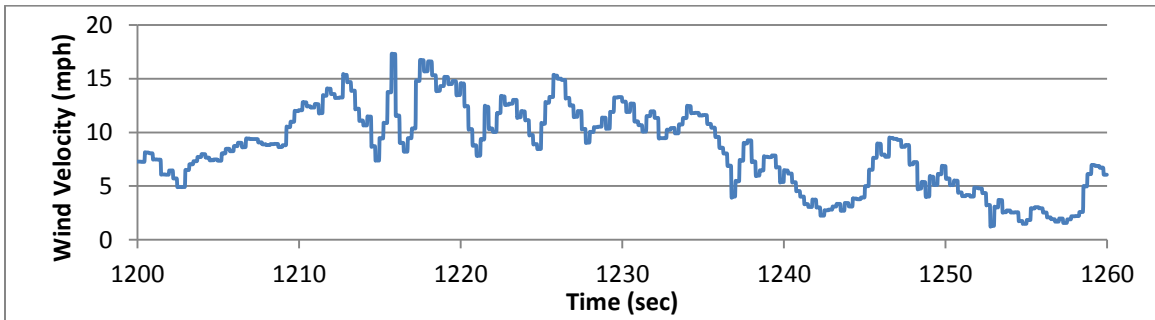


Figure 6-11: Wind Velocity Time History from Anemometer 1

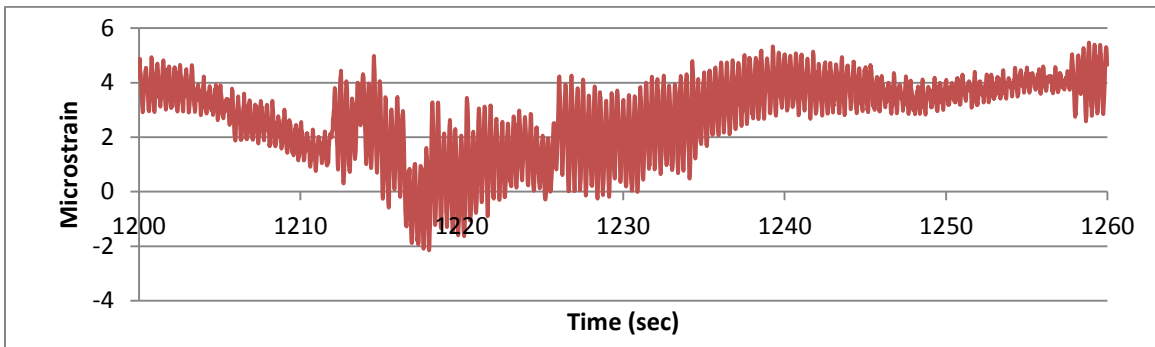


Figure 6-12: Strain Time History from Strain Gauge 2

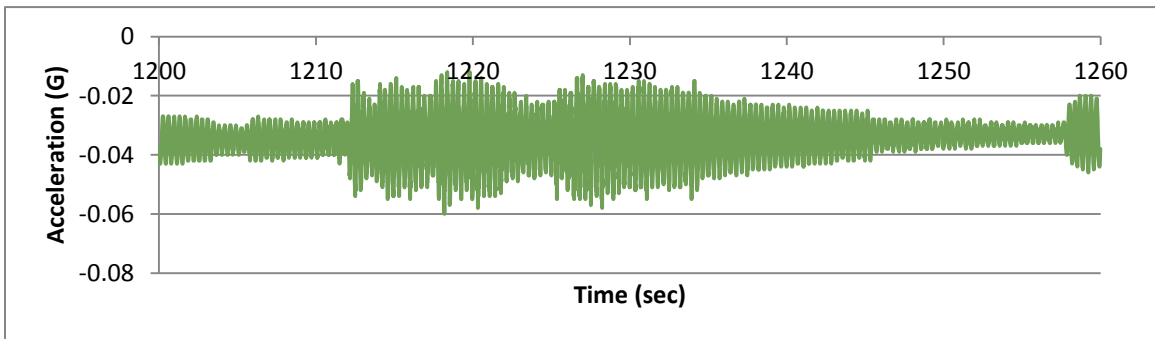


Figure 6-13: Acceleration Time History from Accelerometer 3H

6.2.1.2 Data Collection Schedule

ALDOT collected time history data for Structure A on six different days over a period of several months. Archived history data from NOAA (National Oceanic and Atmospheric Administration) was used to select testing days with potentially high wind speeds. Data collection was started on August 26, 2010 and completed on February 2, 2011. On each day of testing, several runs of data were collected with each run lasting approximately 45 minutes. A total of 31 runs of data were collected during the testing period. Table 6-1 shows ALDOT's data collection schedule with the total time duration of data collected each day. The total amount of time history data collected was almost 24 hours.

Table 6-1: ALDOT Data Collection Schedule

Date	Runs	Duration (minutes)
8/26/2010	1 - 4	195
9/3/2010	5 - 9	240
10/4/2010	10 - 15	285
10/26/2010	16 - 21	270
12/2/2010	22 - 26	215
2/2/2011	27 - 31	225
Total Duration (minutes)		1430
Total Duration (hours)		23.8

6.2.2 Experimental Data Selected for Verification Study

The experimental data collected by ALDOT for Structure A was analyzed to select applicable data for the verification study. Applicable data was considered to consist of extended wind events which satisfied the following criteria: first, the wind

velocity was relatively high, and second, the wind direction was predominantly toward the front face of the VMS. All 31 runs of data collected by ALDOT were examined based on these two criteria. Of the 31 runs, run 16 satisfied the wind velocity and direction criteria the best. Thus, the data in run 16 was selected for all further analysis.

Run 16 had an average wind velocity of 5.2 mph and an average wind direction of 193 degrees (with 180 degrees representing wind normal to the front face of the VMS). Peak wind gusts reached upwards of 25 mph. Run 16 consisted of approximately 45 minutes of data, corresponding to about 162,000 data counts. A wind rose summarizing the wind directional data for run 16 is shown in Figure 6-14.

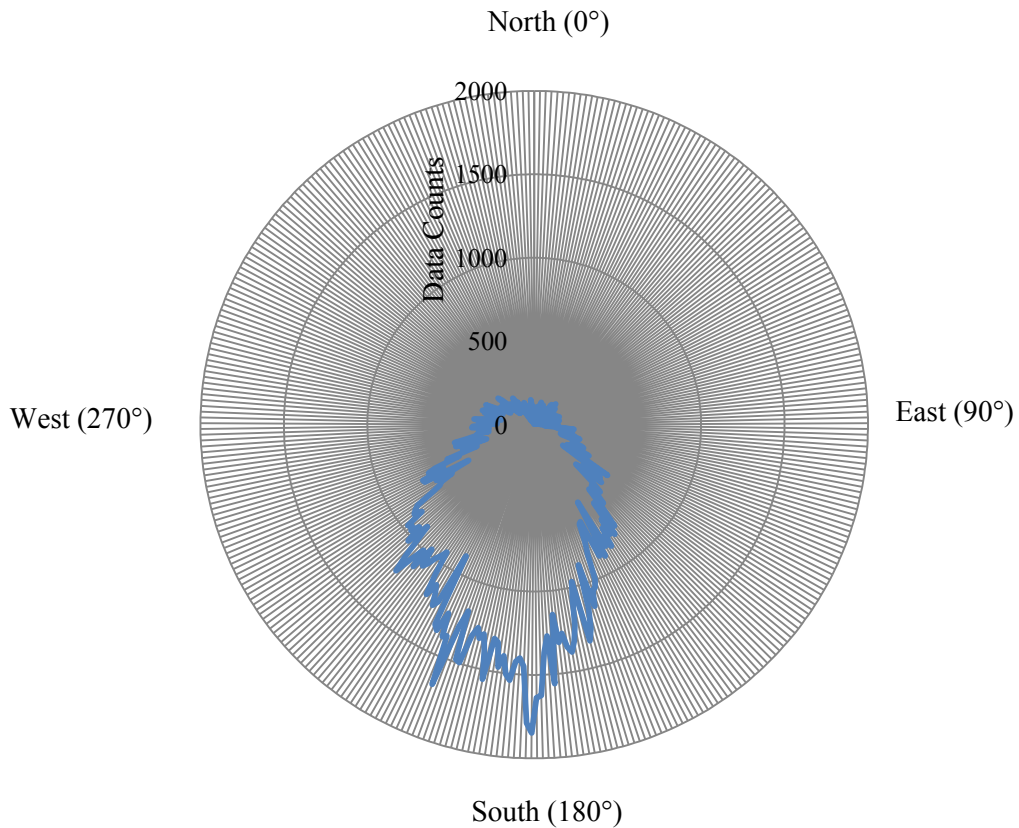


Figure 6-14: Wind Rose for Run 16

6.2.3 Experimental Modal Analysis

An experimental modal analysis of Structure A was performed to determine the dominant mode shapes and corresponding natural frequencies for the structure. The modal analysis was conducted using the experimental acceleration data from run 16 collected by ALDOT. The experimental natural frequencies of Structure A were compared with the SAP natural frequencies computed in Chapter 3 to determine the accuracy of the SAP model.

6.2.3.1 Mode Shapes

Structure A experienced three primary modes of vibration. These mode shapes were the same as the first three mode shapes determined in the SAP modal analysis for the structure. The first mode was longitudinal vibration of the structure in the direction perpendicular to traffic (side-to-side in-plane motion). The second mode was horizontal vibration of the structure in the direction parallel to traffic (out-of-plane motion). The third mode was vertical vibration of the structure in the direction of gravity (up-and-down in-plane motion). Figure 6-15 summarizes the three dominant mode shapes of the structure.

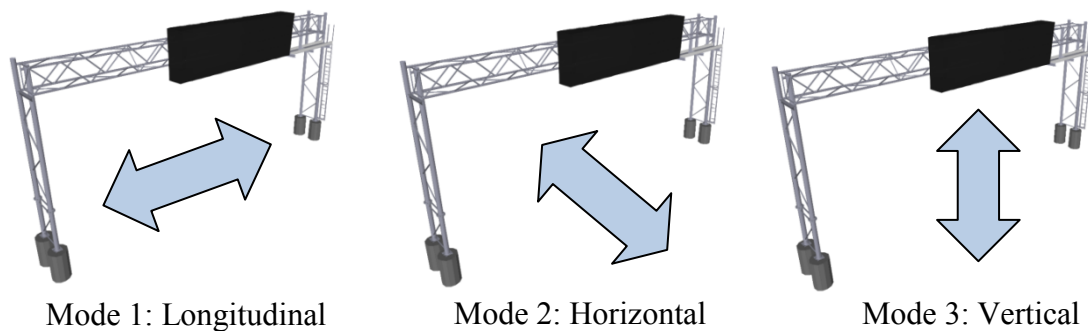


Figure 6-15: Mode Shapes of Structure A

6.2.3.2 Experimental Modal Frequencies

The modal frequencies of Structure A were measured using the acceleration data collected from the accelerometers for run 16. The accelerometers measured the acceleration response time history of the structure for each mode shape (longitudinal, horizontal, and vertical) as the structure was subjected to wind excitation. The acceleration response data for each mode was converted from the time domain to the frequency domain using the Fast Fourier Transform (FFT). The resulting response spectrums yielded the natural frequency of each mode. Figure 6-16 shows the response spectrum for mode 1 (longitudinal vibration). Mode 1 had the lowest natural frequency of the three modes at 1.41 Hz. Figure 6-17 shows the response spectrum for mode 2 (horizontal vibration). The natural frequency of mode 2 was 2.81 Hz. Figure 6-18 shows the response spectrum for mode 3 (vertical vibration). Mode 3 had the highest natural frequency at 3.79 Hz.

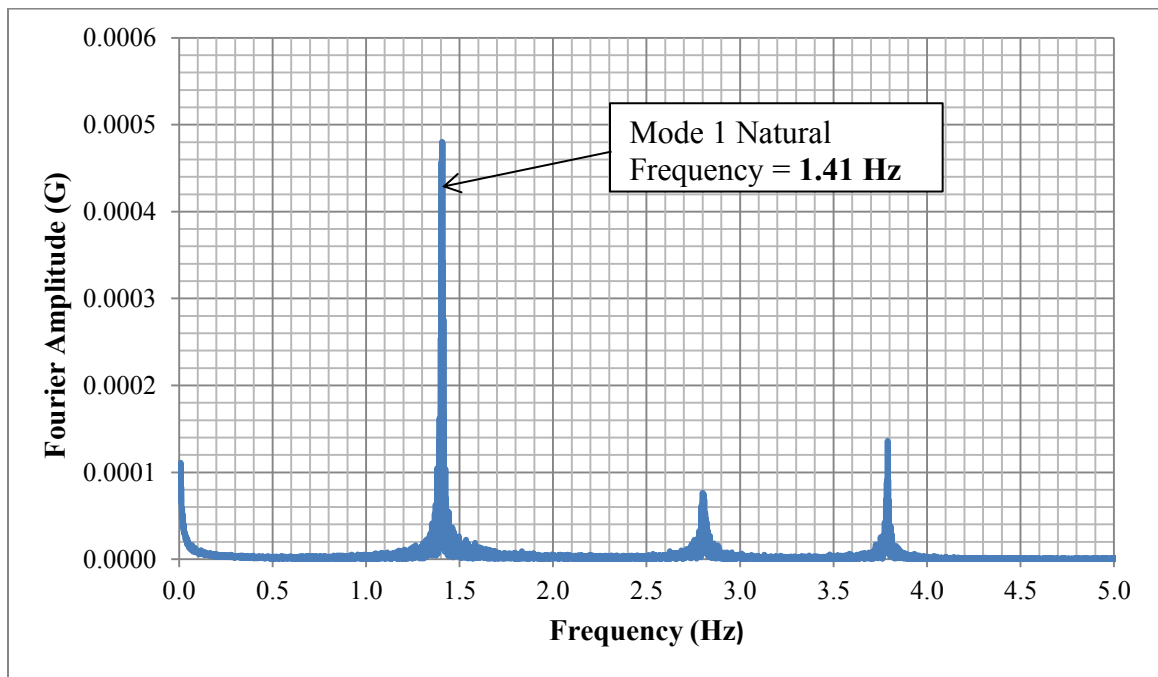


Figure 6-16: Response Spectrum of Longitudinal (Mode 1) Acceleration

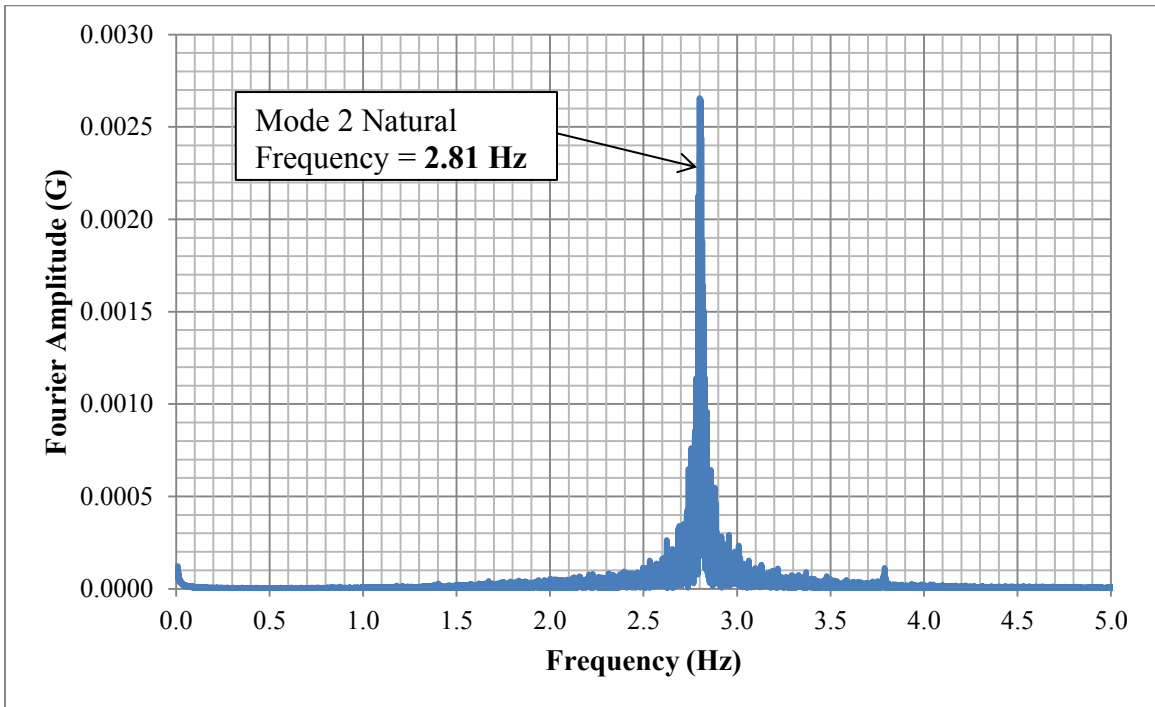


Figure 6-17: Response Spectrum of Horizontal (Mode 2) Acceleration

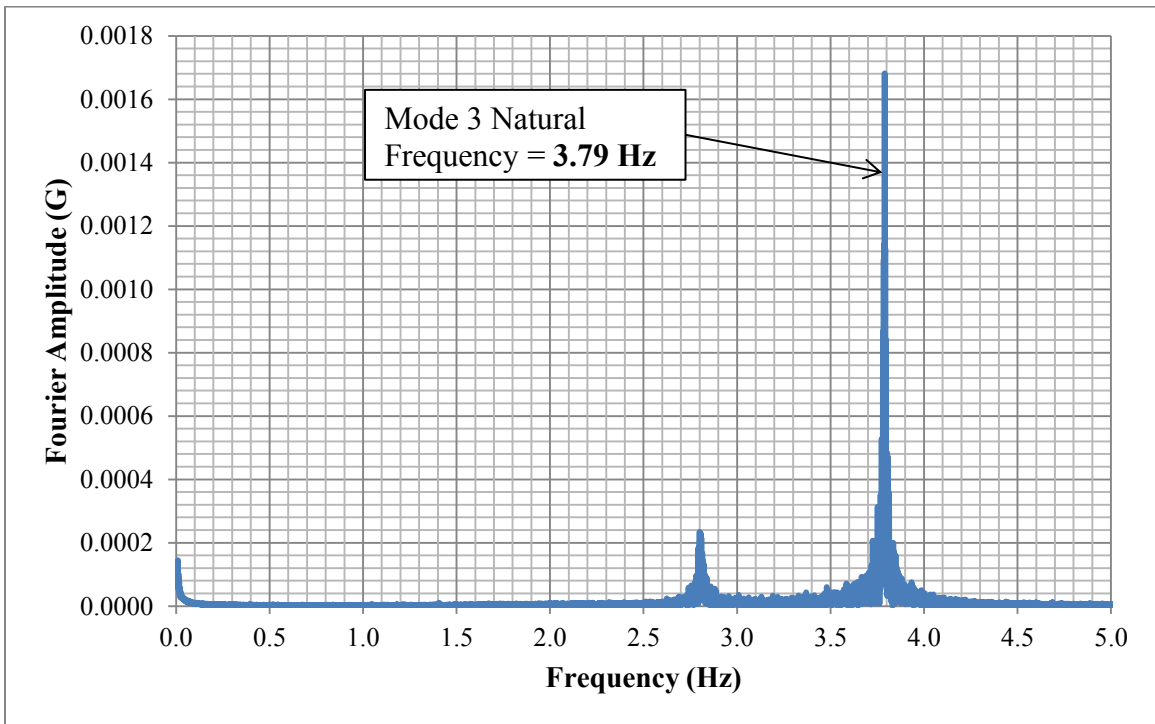


Figure 6-18: Response Spectrum of Vertical (Mode 3) Acceleration

6.2.3.3 Comparison of Modal Frequencies

The experimental modal frequencies of Structure A were compared to the SAP modal frequencies to check the accuracy of the SAP model. Table 6-2 shows the experimental and SAP frequencies for each mode and the percent difference of the frequencies. The SAP frequencies for modes 1 and 2 were higher than the experimental frequencies, but still considered satisfactory since they were within about 10% of the experimental frequencies. The lower experimental frequencies for modes 1 and 2 were attributed to a reduced stiffness of the structure in the field. The SAP frequency for mode 3 was equivalent to the experimental frequency. Thus, the SAP model was considered to be accurate since the percent difference of each modal frequency was relatively low.

Table 6-2: Frequency Comparison

Mode	Modal Frequencies		Percent Difference
	Experimental	SAP2000	
1	1.41	1.51	6.62%
2	2.81	3.13	10.22%
3	3.79	3.79	0.00%

6.2.3.4 Experimental Modal Damping

The modal damping behavior of Structure A was determined using acceleration time histories collected from the accelerometers for run 16. The damping for each of the three dominant modes of vibration was approximated by averaging the damping values from several samples of acceleration response data. The acceleration response of each sample was first filtered using a band-pass filter to select only the acceleration response due to the natural frequency of the mode. For example, the acceleration response of

mode 2 (natural frequency of 2.81 Hz) was filtered to select the response due to frequencies between 2.6 Hz and 3.0 Hz.

The filtered acceleration response for each sample of data was plotted versus time. Figure 6-19 shows an example of the filtered acceleration response of mode 2 for one of the sample time histories. As seen in Figure 6-19, Structure A experienced an oscillatory response to wind loading with spikes and decays in acceleration amplitude due to intermittent wind gusts. The decays in acceleration amplitude can be approximately modeled using exponential decay functions for viscous damping.

Figure 6-20 shows a magnified view of the acceleration response time history with the corresponding exponential decay curve. The acceleration response for this curve started to decay at around the 26 second mark. The exponential decay function for viscous damping can be approximated by Equation 6-1.

$$y = A_0 e^{-\zeta \omega_n t} \quad (\text{Eqn. 6-1})$$

Where:

- y = acceleration amplitude as a function of time of the exponential curve (G)
- A_0 = initial acceleration amplitude of the exponential curve (G)
- ζ = damping ratio
- ω_n = natural frequency of mode (rad/sec)
- t = time (sec)

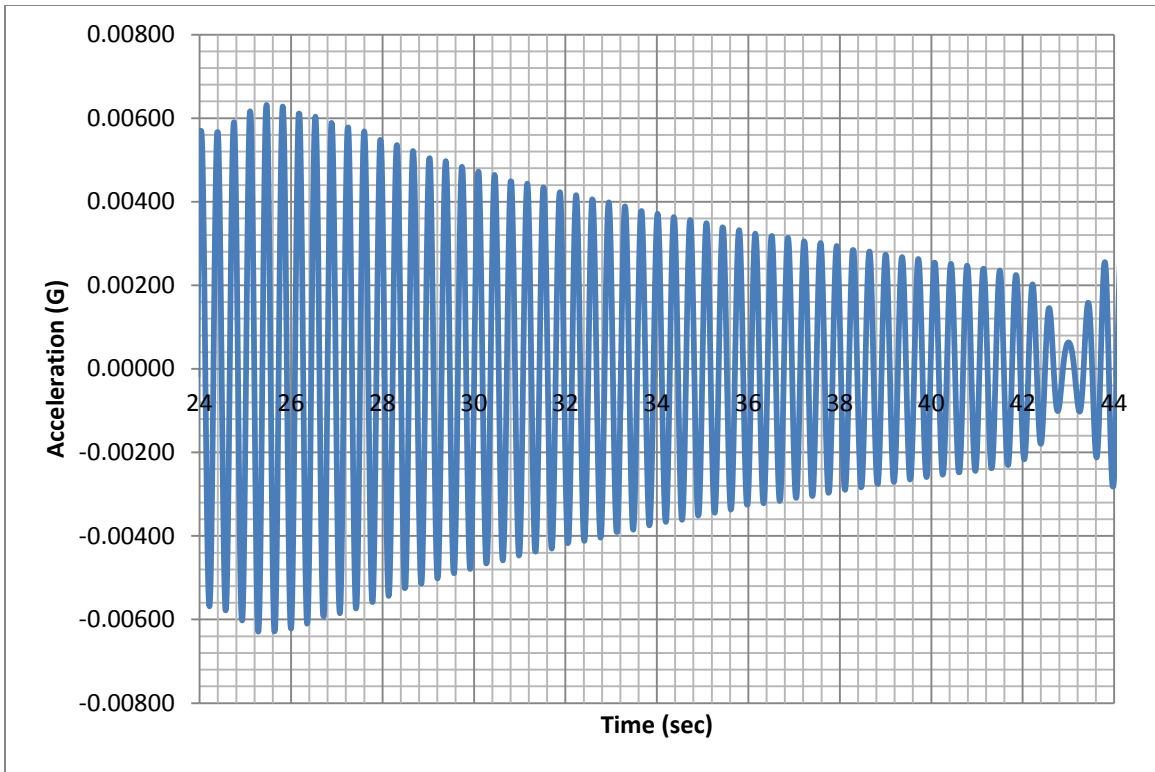


Figure 6-19: Sample of Acceleration Response Time History for Damping Calculations

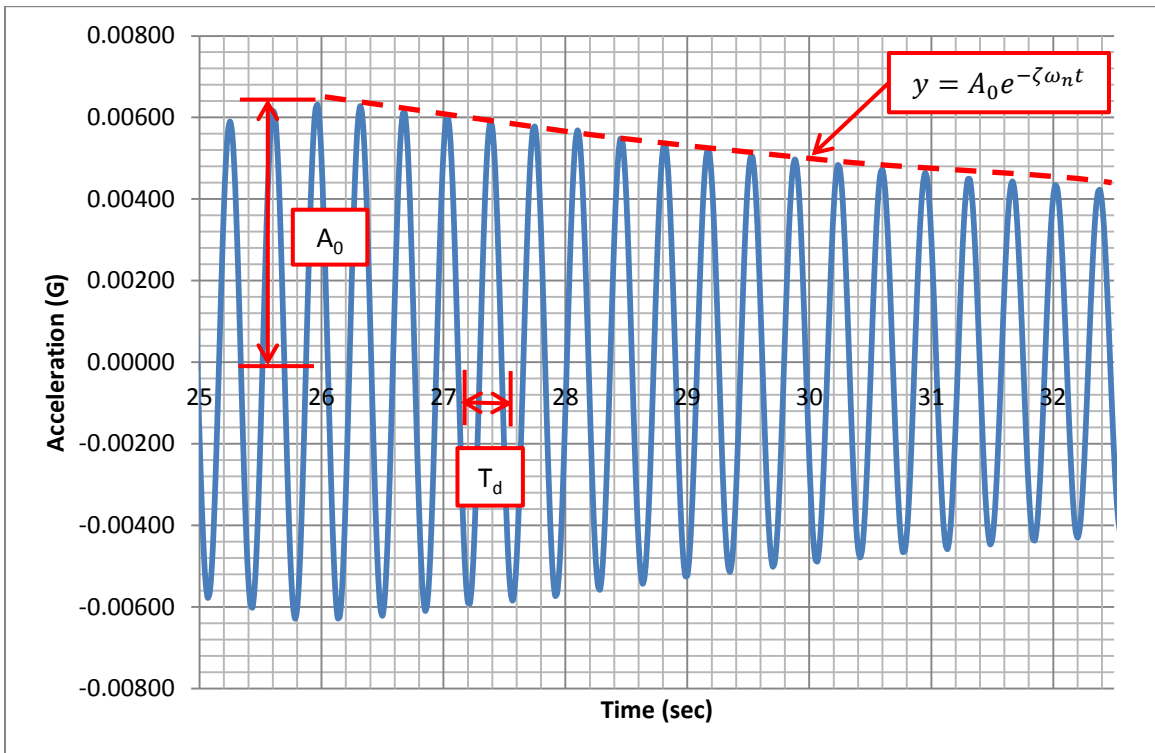


Figure 6-20: Exponential Decay Curve used to Calculate Damping

The positive peaks of the acceleration response were extracted from the time history shown in Figure 6-19 and plotted separately in Figure 6-21. The time of the first peak was set to zero so that the amplitude of the curve could be found. A trendline was plotted to model the acceleration peaks as an exponential decay curve. The equation of the trendline and R^2 value are shown in Figure 6-21.

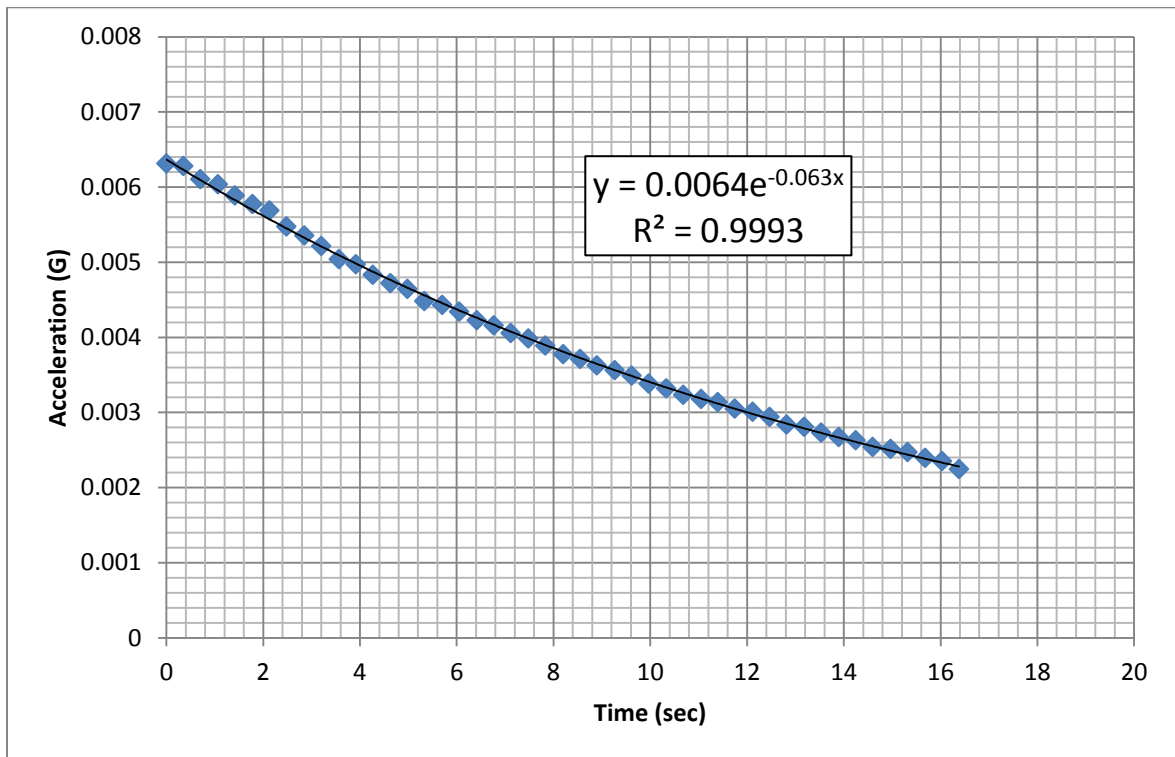


Figure 6-21: Exponential Decay Function for Acceleration Peaks

The damping ratio was calculated from the exponential decay function using the modal natural frequency of the structure determined previously. This calculation assumed that the damping ratio was very low and that the undamped natural frequency of the structure was approximately equal to the damped natural frequency. The calculation for the damping ratio was as follows:

$$\zeta \omega_n = 0.063 \quad (\text{from exp. decay function in Figure 6-21}) \quad (\text{Eqn. 6-2})$$

$$\omega_n = 2\pi f_n = 2\pi(2.81) = 17.66 \text{ rad/sec (mode 2)} \quad (\text{Eqn. 6-3})$$

$$\zeta = \frac{0.063}{\omega_n} = \frac{0.063}{17.66} = 0.00357 \quad (\text{Eqn. 6-4})$$

The above process of filtering the acceleration response data, plotting the acceleration response time history and corresponding exponential decay curve, and calculating the modal damping ratio was performed for five different samples of data for each of the three modes of vibration (longitudinal, horizontal, and vertical). The five damping values calculated for each mode were then averaged to determine the approximate damping of each mode. Table 6-3 summarizes the results of the modal damping analysis. Mode 1 had the highest average damping at 0.616%, mode 2 had an average damping of 0.336%, and mode 3 had the lowest average damping at 0.163%. These average modal damping values were used in the SAP dynamic analyses of Structure A.

Table 6-3: Modal Damping Values for Structure A

Mode	Direction of Vibration	Modal Freq.	Measured Damping from Acceleration Time History Data Samples					Average Damping
1	Longitudinal	1.41	0.00756	0.01005	0.00350	0.00372	0.00598	0.00616
2	Horizontal	2.81	0.00357	0.00329	0.00312	0.00385	0.00300	0.00336
3	Vertical	3.79	0.00134	0.00160	0.00210	0.00189	0.00122	0.00163

6.3 SAP Dynamic Analyses

Two dynamic time history analyses were performed in SAP using the wind data from run 16. The first analysis was conducted using a VMS drag coefficient based on the FIU Wall of Wind testing results, while the second analysis used the VMS drag

coefficient tabulated in the AASHTO Supports Specifications. Both analyses used a time history wind pressure loading calculated from the same 45 minutes of wind velocity and direction data of run 16. The only variable between the two analyses was the drag coefficient used for the VMS.

6.3.1 Wind Pressure Calculations

The wind speed and direction data from run 16 was used to develop wind pressure time histories for wind normal to the front of the VMS (y-direction) and wind parallel to the front of the VMS (x-direction). These wind pressure time histories on Structure A were calculated using Equation 6-5 from basic fluid dynamics (Dexter 2002):

$$P = \frac{1}{2} \rho V^2 C_d \text{ (psf)} \quad \text{(Eqn. 6-5)}$$

Where:

- P = wind pressure time history (psf),
- ρ = standard air density (0.002367 slug/ft³),
- V = wind velocity time history from run 16 (ft/sec), and
- C_d = drag coefficient

6.3.1.1 Wind Velocity

Wind velocity time histories were developed for wind normal to the front of the VMS (y-direction) and wind parallel to the front of the VMS (x-direction). This was accomplished by dividing the wind velocity vectors from run 16 into x- and y-components based on the magnitude and angle of the wind. However, before the wind velocity vectors were divided into their components, the velocity data had to be adjusted

to account for boundary layer effects. Boundary layer effects cause the wind speed to decrease exponentially as the elevation decreases. Equation 6-6 was used to adjust the wind velocity based on the height of sign members above the ground (Dexter 2002):

$$V_z = V_{33} \left(\frac{z}{z_{33}} \right)^{1/7} \quad (\text{Eqn. 6-6})$$

Where:

- V_z = wind velocity at height z above the ground
- V_{33} = wind velocity at height z_{33} above the ground
- $z_{33} = 33$ ft (10 meters)

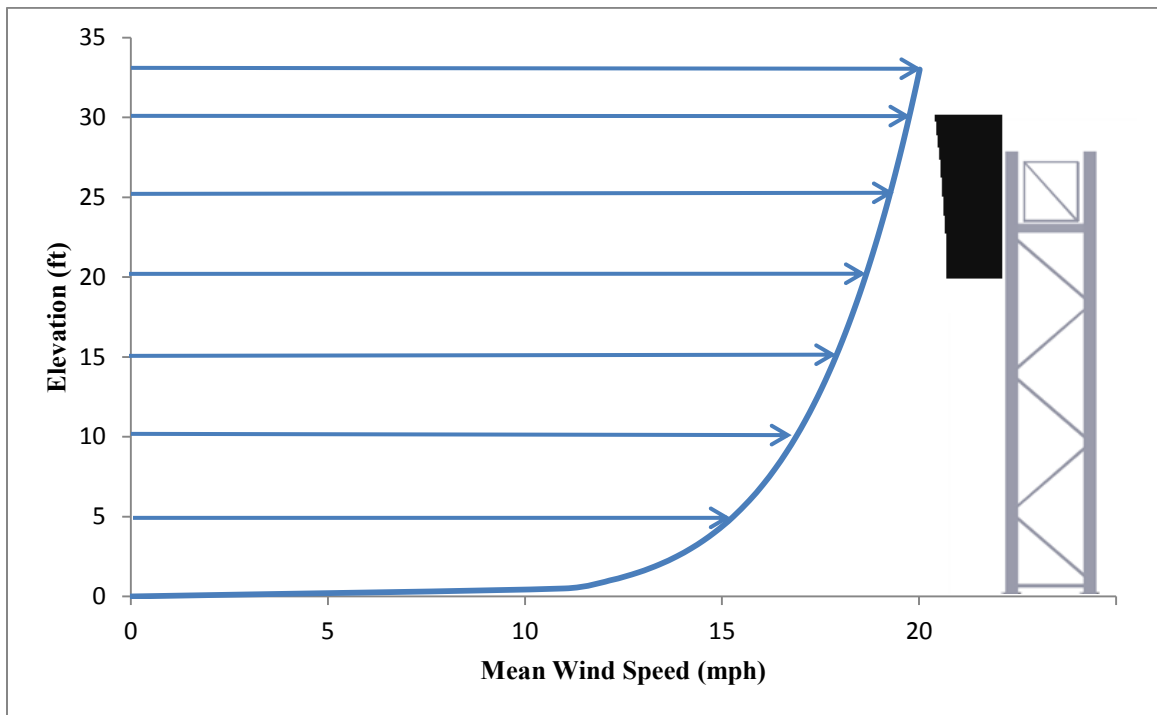


Figure 6-22: Wind Velocity Profile for $V_{33} = 20$ mph

The velocity conversion formula can be represented graphically using a velocity profile. Figure 6-22 shows the velocity profile for a standard wind speed of 20 mph in

reference to Structure A. In order to use the velocity conversion formula, the time history of V_{33} had to be determined. This was done by converting the time history wind velocity data measured at the elevation of the anemometer (30.5 ft) to velocity data for a height of 33 ft. The velocity conversion formula could then be used to determine the wind velocity magnitude at the height of each sign member's centroid.

The height (z) used in the velocity conversion formula was selected as the geometric centroid for the VMS and the support members. All of the support members, except for the upright posts, were assigned a single centroid for calculating the wind velocity magnitude. The upright posts were divided into three sections along their lengths and centroids were assigned for each section to account for the increase in wind velocity from the ground level to the top of the structure. Figure 6-23 shows the centroid heights for each section of the uprights as well as for the other support members and VMS. These centroid heights were the same for both wind velocity in the y -direction and in the x -direction.

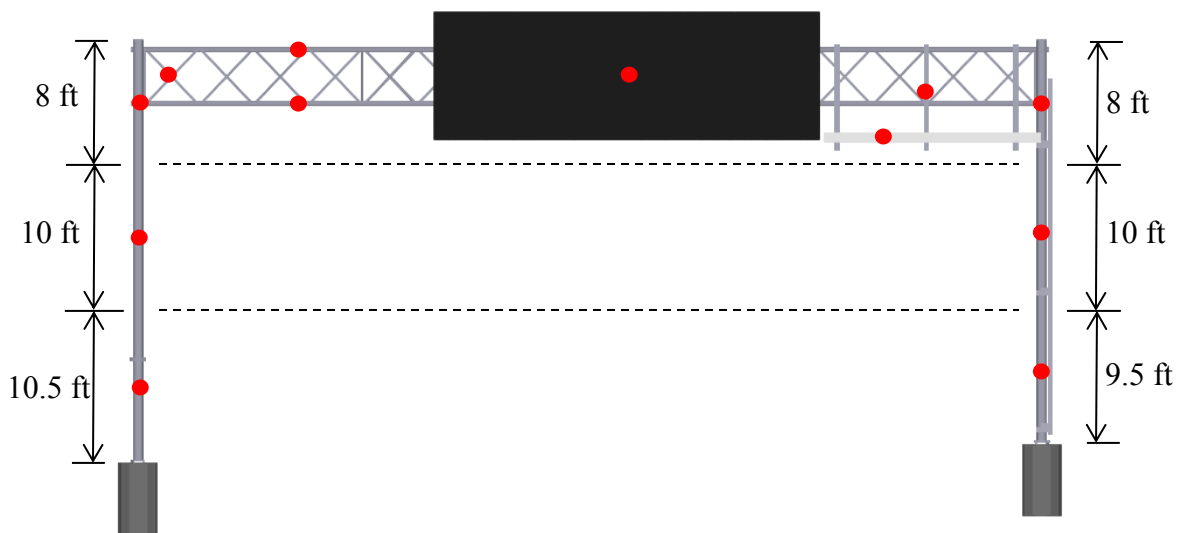


Figure 6-23: Member Centroid Heights for Determining Wind Velocity Magnitude

In order to simplify the SAP analyses, the velocity time histories for all of the support members were referenced to the velocity time history for the VMS using velocity correlation ratios ($V_{\text{Member}} / V_{\text{VMS}}$). The VMS was assigned a base unit velocity, and the velocities of all other support members were scaled to the VMS velocity.

6.3.1.2 Drag Coefficients

Drag coefficients were selected for all members of Structure A for wind normal to the front of the VMS (y-direction) and wind parallel to the front of the VMS (x-direction). For the FIU time history analysis, the VMS drag coefficient in the y-direction was selected based on the sign dimensions provided in Chapter 2. FIU provided a table of drag coefficients organized according to the aspect and depth ratios of a VMS (Table 6-4). This table was based on the results of the Wall of Wind testing. The aspect and depth ratios of the VMS supported by Structure A were calculated using Equations 6-7 and 6-8 as follows:

$$\text{Aspect Ratio} = \frac{\text{Length}}{\text{Height}} = \frac{30.50 \text{ ft}}{8.92 \text{ ft}} = 3.42 \quad (\text{Eqn. 6-7})$$

$$\text{Depth Ratio} = \frac{\text{Depth}}{\text{Height}} = \frac{3.27 \text{ ft}}{8.92 \text{ ft}} = 0.37 \quad (\text{Eqn. 6-8})$$

These aspect and depth ratios were used to interpolate a drag coefficient value from Table 6-4. The drag coefficient for wind normal to the front of the VMS was estimated to be 1.22 for the FIU time history analysis.

Table 6-4: Drag Coefficients from FIU Wall of Wind Testing

Aspect Ratio	Depth Ratio						
	0.1	0.2	0.3	0.4	0.5	0.6	0.7
1.0	1.21	1.18	1.15	1.12	1.08	1.04	0.98
2.0	1.21	1.20	1.18	1.17	1.14	1.11	1.09
3.0	1.22	1.22	1.22	1.21	1.20	1.18	1.16
4.0	1.25	1.25	1.24	1.24	1.23	1.22	1.21
5.0	1.28	1.27	1.26	1.25	1.24	1.23	1.22

For the AASHTO time history analysis, the VMS drag coefficient in the y-direction was selected to be 1.70 from Table 3.8.6-1 of the AASHTO Supports Specifications. For both the FIU and AASHTO time history analyses, the VMS drag coefficient for wind parallel to the front of the sign (x-direction) was approximated to be 1.0 based on the results in Table 6-4.

The drag coefficients for all of the remaining members of the Structure A were selected from Table 3.8.6-1 of the AASHTO Supports Specifications. Drag coefficients were selected for both the x- and y-directions. Table 6-5 provides a summary of the drag coefficients used for the SAP time history analyses.

For all cases where two cylindrical members were next to each other in the same plane as the wind direction, the drag coefficient was selected to be 1.2. Examples of this type of scenario include the uprights and the front and back truss chords for wind in the y-direction. Individual cylindrical members were assigned a drag coefficient of 1.1.

For all cases where two or more flat members were adjacent in the same plane as the wind direction, the drag coefficient was selected to be 2.0. Examples of this type of

scenario include the ladder rail angles for wind in the y-direction and the W-shape supports of the access track for wind in the x-direction. Individual flat members were assigned a drag coefficient of 1.7.

Table 6-5: Drag Coefficients used for SAP Analyses

Members	Drag Coefficients	
	y-direction	x-direction
Upright Posts	1.20	1.10
Truss Chords	1.20	NA
WT Truss Support	NA	1.70
Adjacent Webs	1.20	NA
Individual Webs	1.10	1.10
W-Shape Track Supports	1.70	2.00
Channel Track Rails	2.00	NA
Access Ladder Rails	2.00	1.70
Access Ladder Rungs	NA	1.10
<i>FIU VMS</i>	<i>1.22</i>	<i>1.00</i>
<i>AASHTO VMS</i>	<i>1.70</i>	<i>1.00</i>

6.3.2 SAP Wind Loading

The wind pressure loadings calculated for the x- and y-directions were applied to all exposed surfaces of the Structure A model in SAP. The loadings were applied as surface pressures on the VMS and as distributed loads on all of the supporting frame members. The distributed loads for the frame members were calculated by multiplying the wind pressure time histories by the diameter of each frame member.

The wind pressure time histories for the x- and y- directions were both run simultaneously in the SAP analyses to replicate the wind excitation measured in the field. This was done separately for the pressure loading due to the FIU VMS drag coefficient and the pressure loading due to the AASHTO VMS drag coefficient.

6.3.3 SAP Structural Response

The stress response of Structure A due to the applied wind loading was examined for each analysis. Time histories of the axial force and bending moments for the right upright posts were extracted from SAP. These time histories were recorded at the locations of the strain gauges installed by ALDOT on the upright posts in the experimental study. Normal stress time histories were calculated at selected strain gauge points on the cross-section of support members using Equation 6-9:

$$\sigma = \frac{P}{A} + \frac{Mc}{I} \text{ (psi)} \quad \text{(Eqn. 6-9)}$$

Where:

- σ = Normal stress at strain gauge location (psi),
- P = Axial force at strain gauge location (lbs),
- M = Bending moment in the direction of member curvature (lb-ft),
- A = Cross-sectional area of member (in²),
- c = Distance from neutral axis to outer edge of member (in), and
- I = Moment of Inertia of member (in⁴)

Normal stress time histories were calculated at the locations of strain gauges 2 and 4 for the back right upright post and strain gauges 6 and 8 for the front right upright post (see Figure 6-1 for strain gauge locations).

6.4 Experimental Data vs. SAP Results

The stress response of the uprights and truss chords was examined in order to compare the experimental data to the results of the SAP analyses for both the FIU and AASHTO loadings. This was done by first selecting analysis intervals for the stress data which captured the full response of the VMS structure to wind gusts. Next, the stress data was filtered to remove the resonant stress response, so that only the quasi-static stress response of the structure remained. The quasi-static stress response and corresponding wind excitation velocity were then divided into the appropriate analysis intervals. Finally, the stress range over these intervals was plotted versus the average wind velocity to show the variation of stress with wind excitation. This process was performed for the stress response at several of the strain gauge locations on the upright posts.

6.4.1 Selection of Analysis Intervals

A Fast Fourier Transform was applied to the time history wind velocity data of run 16. The Fast Fourier Transform converted the velocity data from the time domain to the frequency domain. The resulting velocity amplitude versus frequency data was plotted using a logarithmic scale to create a wind excitation spectrum as shown in Figure 6-24. The spectrum was used to determine the dominant wind gust frequency for the 45 minutes of data in run 16. Ignoring the very low frequencies, the dominant wind gust frequency was determined to be approximately 0.01 Hz. A frequency of 0.01 Hz corresponded to a wind gust period of 100 seconds. Thus, analysis time intervals of 100 seconds were selected to capture the full response of the structure to wind gusts.

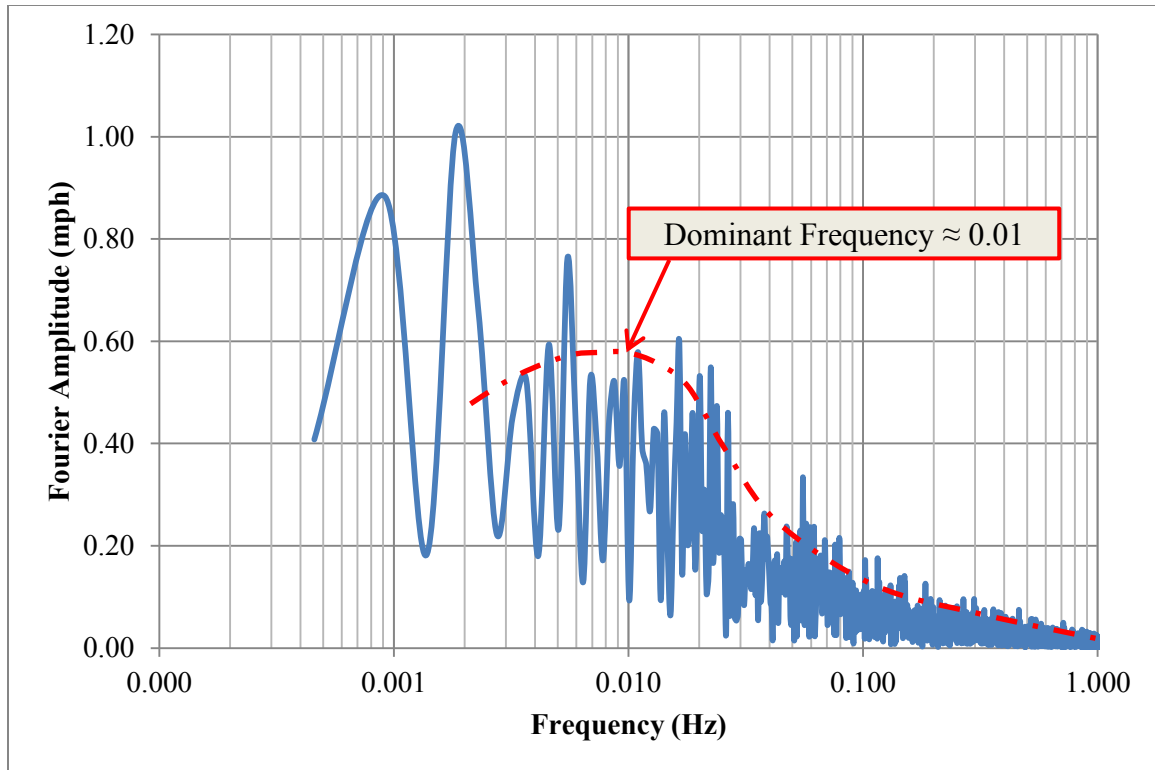


Figure 6-24: Wind Velocity Excitation Spectrum for Run 16

6.4.2 Selection of Quasi-static Stress Response

A Fast Fourier Transform was applied to the time history strain data of run 16. The Fast Fourier Transform converted the strain data from the time domain to the frequency domain. The resulting strain amplitude versus frequency data was plotted using a logarithmic scale to create a response spectrum. Figure 6-25 shows the response spectrum for the data from strain gauge 4. The response spectrum was used to identify and compare the quasi-static response of the structure to the resonant response.

The quasi-static response represented the behavior of the structure due to the variation of the wind gust excitation. The resonant response, on the other hand, represented the vibration of the structure about its own natural frequencies. Since the purpose of this study was to verify the accuracy of the VMS drag coefficient, only the

quasi-static response of the structure was applicable for analysis. The drag coefficient is related to the static wind load on an object and does not account for resonant conditions. Also, the quasi-static response of the structure is not affected by damping in the structure, since damping only applies to the resonant response. Thus, the effects of damping could be ignored in the analyses.

As shown in Figure 6-25, all of the resonant response frequencies of the structure are greater than 1 Hz. These resonant response frequencies are similar to the natural vibration frequencies found previously in the experimental modal analysis. In order to select the quasi-static response of the structure, the strain data was filtered using a low-pass filter to remove all vibration responses with frequencies greater than 1 Hz. This removed the resonant response, leaving only the quasi-static response of the structure.

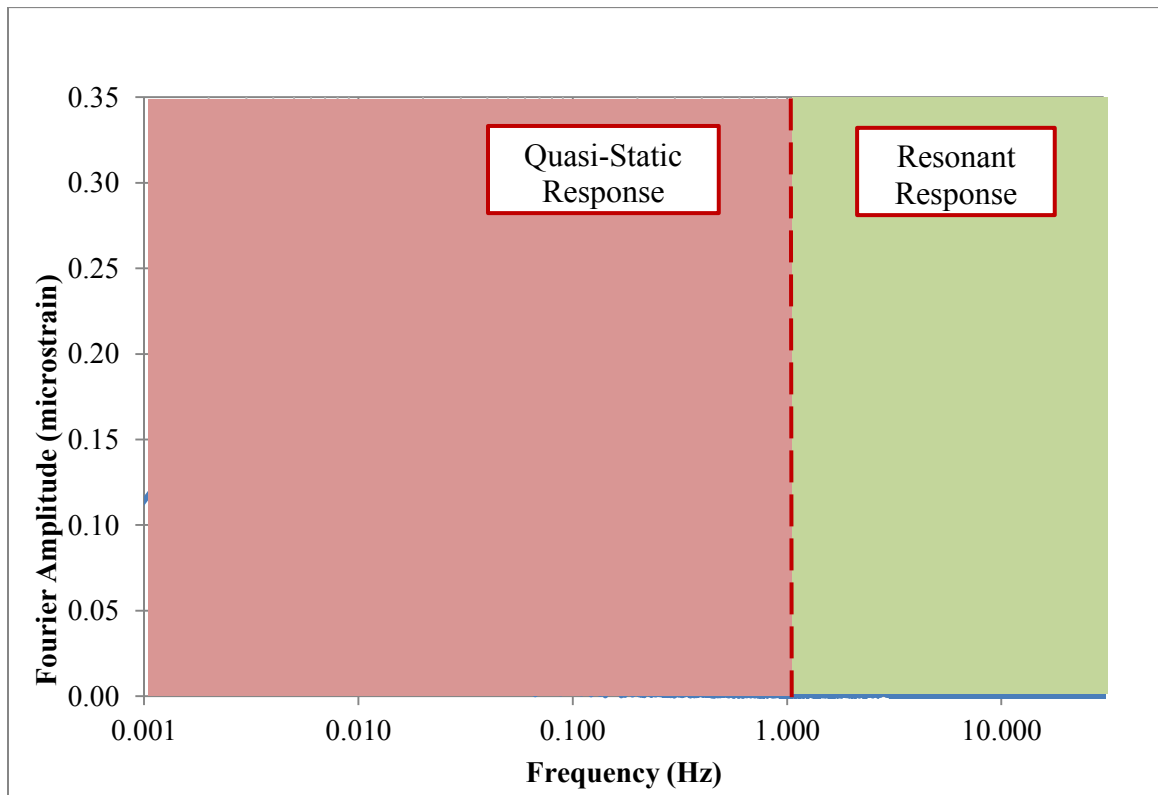


Figure 6-25: Response Spectrum of Strain Gauge 4 Data for Run 16

Figure 6-26 shows a 100 second sample of data from strain gauge 4 which has been converted to stress data. The figure shows plots for both the unfiltered stress and the filtered stress. The plot of filtered stress represents the quasi-static response of the structure, while the plot of unfiltered stress represents the total response of the structure (both the quasi-static response and resonant response).

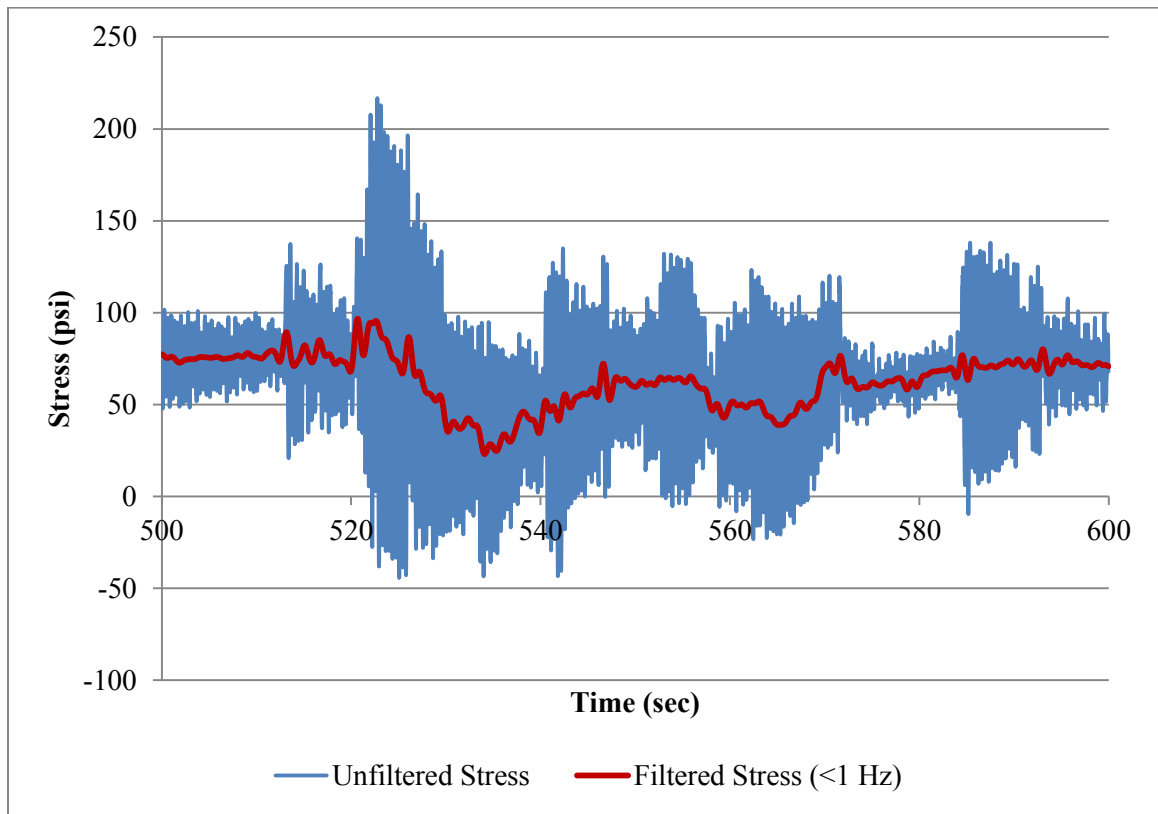


Figure 6-26: Unfiltered and Filtered Stress for Strain Gauge 4

6.4.3 Plots of Stress Range vs. Average Wind Velocity

The quasi-static stress response of the uprights and truss chords was analyzed and compared using plots of stress range versus average wind velocity. The filtered stress data from the experimental and SAP loadings was first divided into 100 second intervals based on the dominant wind gust frequency determined previously. The stress range was

then calculated for each 100 second interval by subtracting the minimum stress over the interval from the maximum stress. Figure 6-27 shows the quasi-static stress range for the sample of data from strain gauge 4 presented previously. In addition, the average wind velocity was calculated for each 100 second interval. Figure 6-28 shows the average wind velocity corresponding to the same time history sample of data.

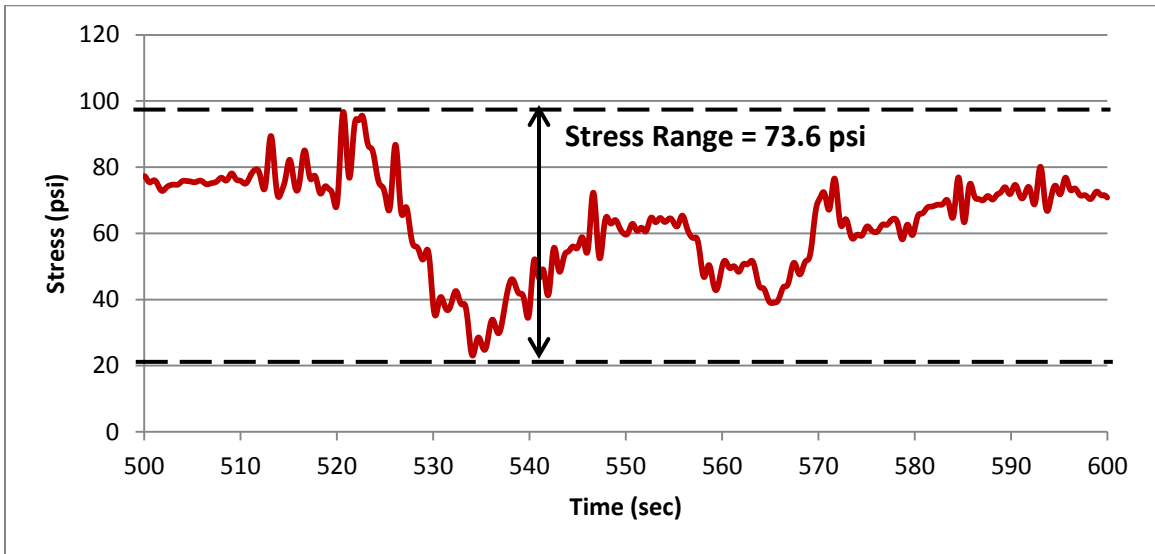


Figure 6-27: Quasi-static Stress Range for Sample 100 Second Interval

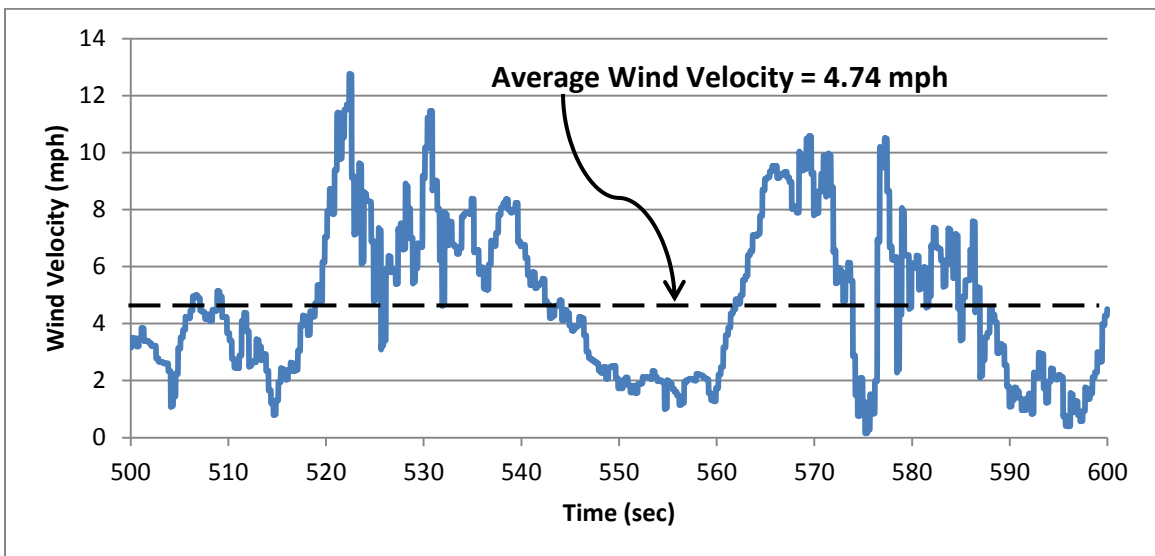


Figure 6-28: Average Wind Velocity for Sample 100 Second Interval

The stress response was examined at the locations of four of the strain gauges installed on the right upright posts of Structure A. For each of the strain gauge locations, the stress range was plotted versus the average wind velocity for the experimental and SAP (FIU and AASHTO) loadings. This was done for all of the 100 second intervals in run 16.

Figures 6-29 and 6-30 show the stress range plots for strain gauges 2 and 4 on the back right upright post. Figures 6-31 and 6-32 show the stress range plots for strain gauges 6 and 8 on the front right upright post. All four of these figures show that the SAP stress response in the upright posts due to the FIU loading accurately portrays the experimental stress response measured in the field, while the SAP stress response due to the AASHTO loading is too conservative.

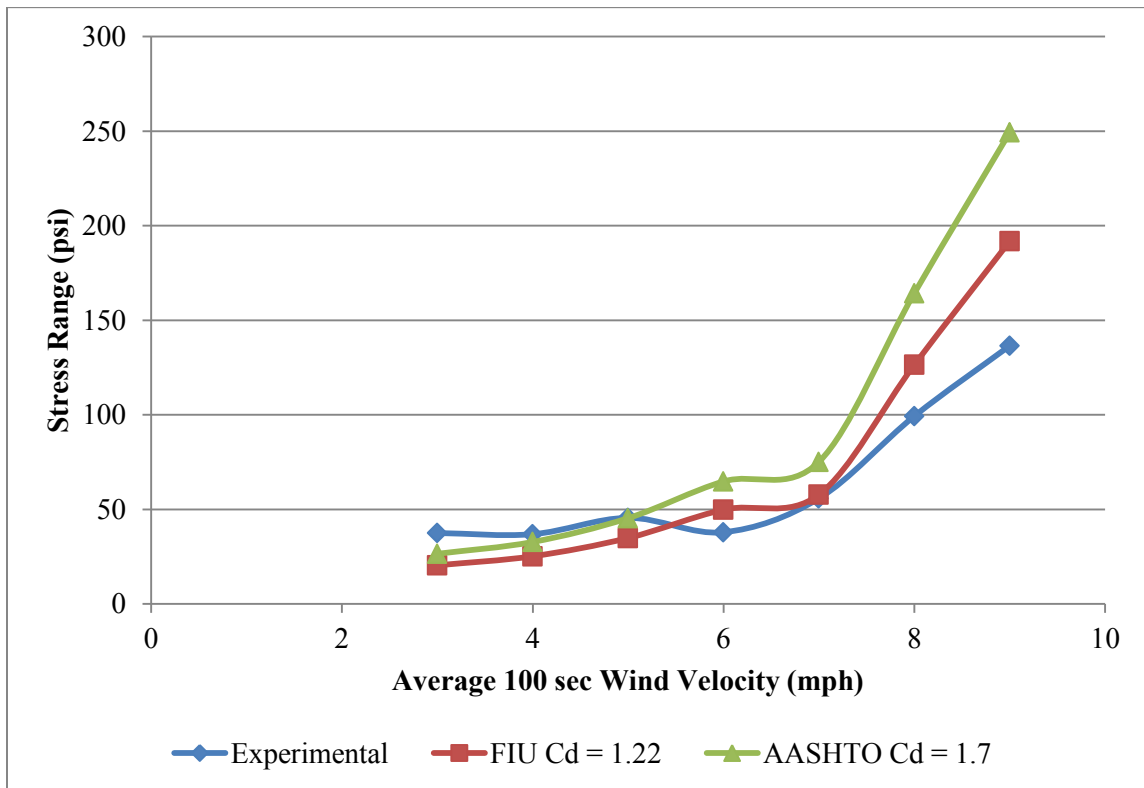


Figure 6-29: Stress Response at Strain Gauge 2 Location

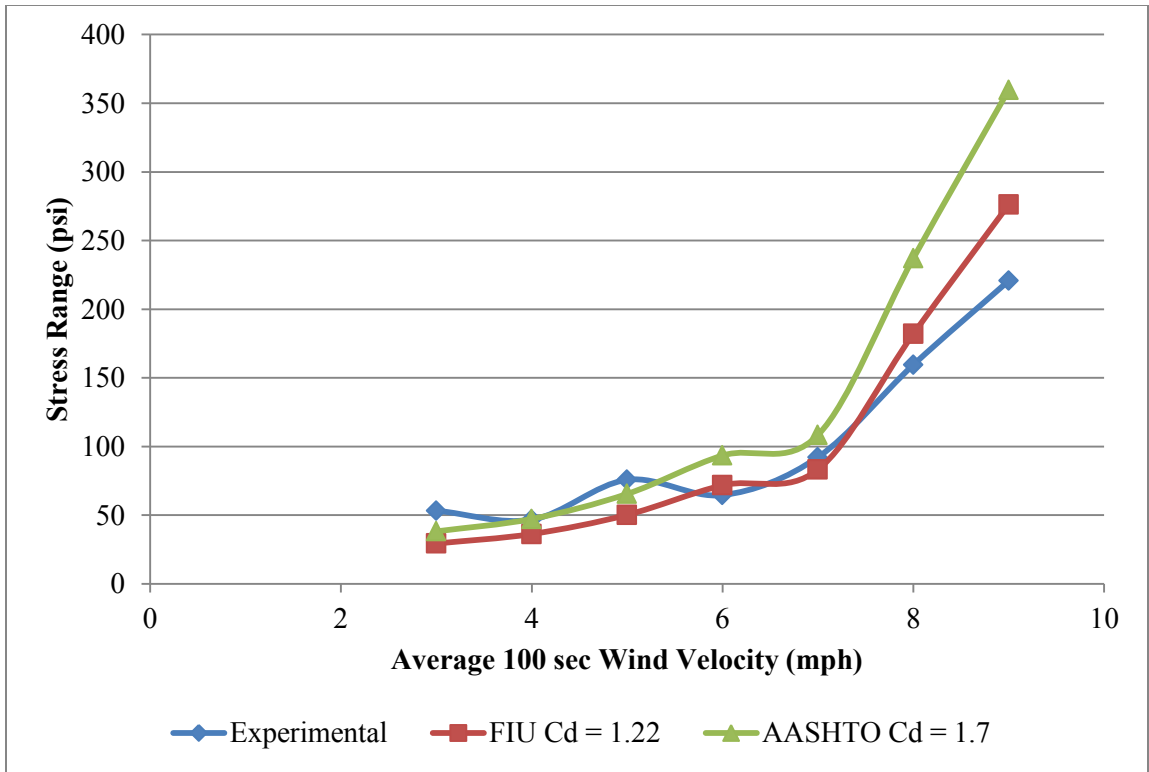


Figure 6-30: Stress Response at Strain Gauge 4 Location

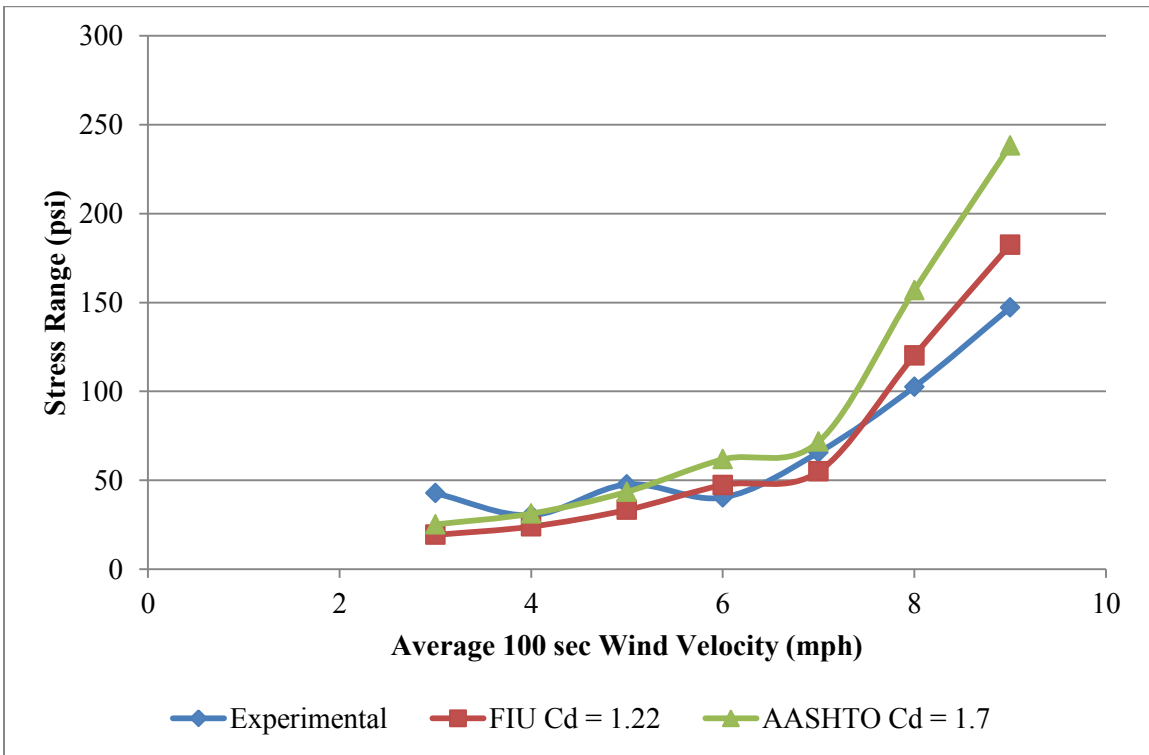


Figure 6-31: Stress Response at Strain Gauge 6 Location

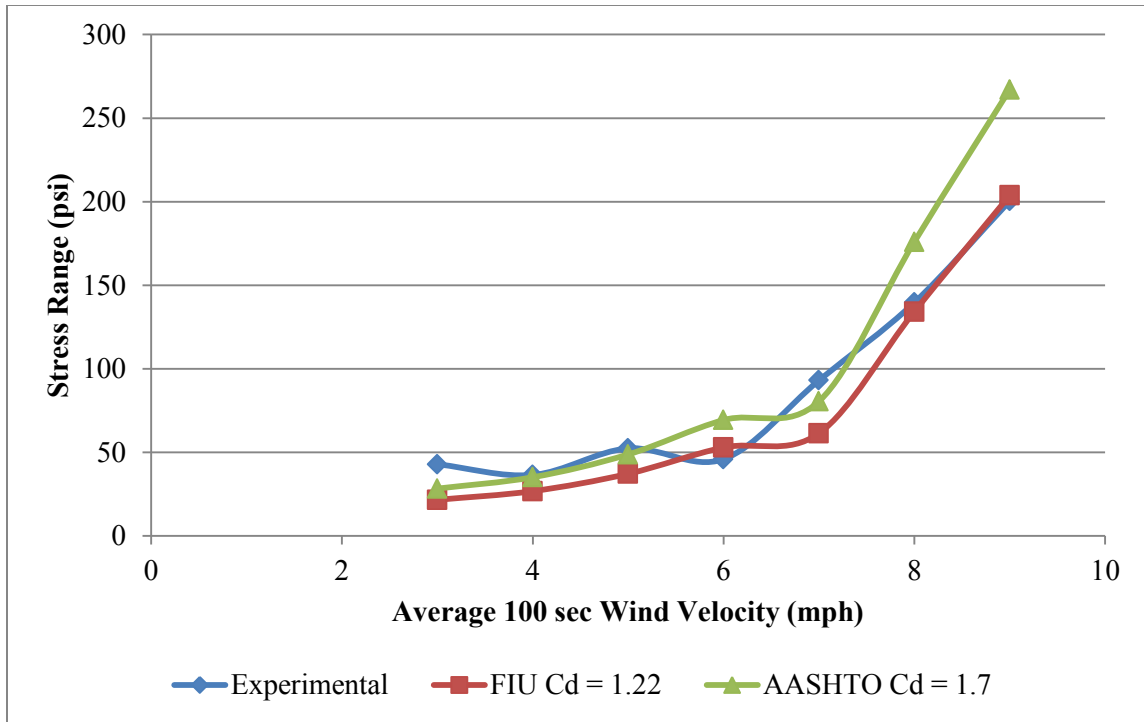


Figure 6-32: Stress Response at Strain Gauge 8 Location

6.4.4 Stress Range Tables

Tables 6-6 through 6-9 show the stress range values for the strain gauge locations plotted in the stress response graphs. The tables also include calculations for the percent differences between the stress ranges for the experimental results and the SAP (FIU and AASHTO) results. As seen in the tables, the AASHTO results generally have the greatest percent differences from the experimental results, especially for the higher average wind velocities. Thus, the FIU results are a more accurate representation of the experimental field data.

Table 6-6: Stress Range Values for Strain Gauge 2 Location

Avg Velocity (mph)	Stress Range (psi)			Percent Difference from Exp.	
	Experimental	FIU C _d	AASHTO C _d	FIU C _d	AASHTO C _d
3	53.33	29.40	38.24	44.9	28.3
4	46.75	36.32	47.30	22.3	1.2
5	75.78	50.25	65.50	33.7	13.6
6	64.67	71.79	93.48	11.0	44.5
7	92.26	83.25	108.42	9.8	17.5
8	159.53	182.06	237.08	14.1	48.6
9	220.74	276.24	359.78	25.1	63.0

Table 6-7: Stress Range Values for Strain Gauge 4 Location

Avg Velocity (mph)	Stress Range (psi)			Percent Difference from Exp.	
	Experimental	FIU C _d	AASHTO C _d	FIU C _d	AASHTO C _d
3	37.51	20.44	26.53	45.5	29.3
4	36.90	25.23	32.79	31.6	11.1
5	45.56	34.89	45.38	23.4	0.4
6	37.94	49.88	64.80	31.5	70.8
7	55.85	57.83	75.16	3.5	34.6
8	99.34	126.46	164.34	27.3	65.4
9	136.54	191.87	249.36	40.5	82.6

Table 6-8: Stress Range Values for Strain Gauge 6 Location

Avg Velocity (mph)	Stress Range (psi)			Percent Difference from Exp.	
	Experimental	FIU C _d	AASHTO C _d	FIU C _d	AASHTO C _d
3	42.73	19.28	25.18	54.9	41.1
4	30.37	23.96	31.28	21.1	3.0
5	47.66	33.34	43.52	30.1	8.7
6	40.31	47.30	61.77	17.3	53.2
7	65.64	54.91	71.69	16.4	9.2
8	102.58	120.20	156.89	17.2	53.0
9	147.11	182.46	238.18	24.0	61.9

Table 6-9: Stress Range Values for Strain Gauge 8 Location

Avg Velocity (mph)	Stress Range (psi)			Percent Difference from Exp.	
	Experimental	FIU C_d	AASHTO C_d	FIU C_d	AASHTO C_d
3	42.87	21.59	28.29	49.6	34.0
4	36.47	26.78	35.10	26.6	3.8
5	52.37	37.17	48.74	29.0	6.9
6	45.93	52.90	69.35	15.2	51.0
7	93.08	61.39	80.48	34.0	13.5
8	139.63	134.24	175.97	3.9	26.0
9	200.42	203.79	267.12	1.7	33.3

6.5 Conclusions of Drag Coefficient Verification Study

A study was conducted to verify the VMS drag coefficient results from the FIU Wall of Wind testing. The study compared experimental field data collected from a VMS structure in Alabaster, AL (Structure A) as part of a previous ALDOT study to analytical results obtained from a SAP model of the structure. Two VMS drag coefficients were used in the analysis: $C_d = 1.22$ from the FIU Wall of Wind testing and $C_d = 1.7$ from the AASHTO Supports Specifications. The drag coefficients were based on the dimensions of the VMS sign panel.

Plots of Quasi-static stress range versus average wind velocity were created for several locations on two upright posts of Structure A. The plots showed that the VMS drag coefficient from the FIU Wall of Wind testing accurately modeled the behavior of the sign structure under fatigue level winds, while the VMS drag coefficient from the AASHTO Supports Specifications was too conservative. Thus, the study concluded that the drag coefficient results from the FIU Wall of Wind testing are relatively accurate and should be considered for incorporation into the AASHTO Supports Specifications.

CHAPTER 7 SENSITIVITY STUDY

7.1 Chapter Overview

A sensitivity study was conducted to examine the impact of the newly developed VMS drag coefficients on the design of sign structures. The SAP models of Structures A and B were used for this study. Static analyses were run in SAP to analyze and compare the stress response of the structures due to wind loadings with different VMS drag coefficients. The analyses incorporated the AASHTO code requirements for both extreme wind and fatigue wind. Stress ratios were developed to quantify the amount of stress reduction in critical support members and connections due to the new drag coefficients. This chapter provides a detailed description of the sensitivity study and discusses the impact of the VMS drag coefficients on the design of sign structures.

7.2 Parameters of Sensitivity Study

The sensitivity study followed four main parameters as outlined in Table 7-1. The first parameter was the span length of the VMS structure. The span length of Structure A was 71 ft, while the span length of Structure B was 145 ft. The second parameter of the sensitivity study was the wind loading applied to the structures. The structures were analyzed for extreme level winds and fatigue level winds. The third parameter of the study was the location and corresponding extreme wind speed for the structures. Two locations with different wind speeds were selected for the study: Birmingham, AL and

Miami, FL. These locations were selected because of the wide variation in their extreme wind speeds. The fourth parameter was the drag coefficient used for the VMS signs. Three unique VMS drag coefficients were used for the sensitivity study: a drag coefficient of 1.7 as specified for a VMS in the AASHTO Supports Specifications, a drag coefficient of 1.22 based on the FIU testing results for a standard VMS, and a drag coefficient of 1.00 based on the FIU results for a VMS with chamfered edges. The VMS drag coefficients were the same for both extreme wind and fatigue wind according to the results from the FIU Wall of Wind testing.

Table 7-1: Parameters for Sensitivity Study

Parameter	Variable	Levels
I	Structure (Span)	Structure A (71 ft)
		Structure B (145 ft)
II	Loading	Extreme Wind
		Fatigue Wind
III	Location (Design Wind Speed)	Birmingham, AL (90 mph)
		Miami, FL (150 mph)
IV	VMS Drag Coefficient	AASHTO $C_d = 1.7$
		Standard FIU $C_d = 1.22$
		Modified FIU $C_d = 1.00$

7.3 SAP Static Analyses

Static analyses were run in SAP for the different parameters of the sensitivity study. The wind loads were calculated for both extreme wind and fatigue wind according to the AASHTO Supports Specifications. The SAP analyses were organized into eighteen different load cases based on the parameters of the study. Each load case was run in SAP and the maximum stress response of critical support members and

connections was recorded. The stress response was used to develop stress reduction ratios which compared the change in stress due to different VMS drag coefficients.

7.3.1 Wind Pressure Calculations

The wind pressure loads on the VMS structures were calculated using the equations for extreme wind and fatigue wind found in the AASHTO Supports Specifications. The extreme wind load was defined by a static wind pressure, while the fatigue wind load was defined by an equivalent static natural wind gust pressure range. Both the extreme wind load and fatigue wind load were calculated for all exposed surfaces of the VMS structures in the horizontal direction.

7.3.1.1 Extreme Wind

The static wind pressure on the VMS structures for the extreme wind analyses was calculated using Equation 7-1 from the AASHTO Supports Specifications:

$$P_z = 0.00256K_zGV^2I_rC_d \text{ (psf)} \quad \text{(Eqn. 7-1)}$$

Where:

- P_z = Static wind pressure at height z above the ground (psf),
- K_z = Height and Exposure Factor,
- G = Gust Effect Factor,
- V = Basic Wind Speed (mph),
- I_r = Wind Importance Factor, and
- C_d = Drag Coefficient

Height and Exposure Factor

The height and exposure factor (K_z) adjusts the effective wind pressure based on the height of a structure above the ground and the local exposure conditions. The frictional drag of the terrain causes the wind speed to decrease close to ground level. The amount of frictional drag depends on the exposure classification of the terrain. The AASHTO Supports Specifications state that all sign structures should be designed for Exposure C site conditions.

The height and exposure factors were calculated for each member of the VMS structures using Equation 7-2 from the AASHTO Supports Specifications. The equation is as follows:

$$K_z = 2.01 \left(\frac{z}{z_g} \right)^{2/\alpha} \quad (\text{Eqn. 7-2})$$

Where:

- K_z = Height and Exposure Factor,
- z = Height above the ground at which the pressure is calculated or 16 ft (whichever is greater),
- z_g = 900 ft for Exposure C, and
- α = 9.5 for Exposure C

The height and exposure factors for the members of both Structures A and B are summarized in Tables 7-2 and 7-3, respectively.

Table 7-2: K_z Factors for Structure A

Member		Height z of Centroid above ground (ft)	K_z
Uprights	0 - 16 ft	16.0	0.860
	16 - 22 ft	19.0	0.892
	22 - 28 ft	25.0	0.945
Access Ladder Rails	0 - 16 ft	16.0	0.860
	16 - 22 ft	19.0	0.892
	22 - 25.3 ft	25.0	0.945
Bottom Truss Chords		22.7	0.926
Top Truss Chords		26.5	0.957
Vertical Truss Webs		24.6	0.942
Vertical Struts		24.6	0.942
W-Shape Track Hangers		23.4	0.932
Channel Track Rails		20.7	0.908
<i>VMS</i>		23.1	0.930

Table 7-3: K_z Factors for Structure B

Member		Height z of Centroid above ground (ft)	K_z
Uprights	0 - 11 ft	16.0	0.860
	11 - 16 ft	18.2	0.884
	16 - 21 ft	23.2	0.931
Access Ladder Rails	0 - 11 ft	16.0	0.860
	11 - 16 ft	18.2	0.884
	16 - 17.2 ft	23.2	0.931
Bottom Truss Chords		20.6	0.908
Top Truss Chords		25.6	0.950
Vertical Truss Webs		23.1	0.930
Vertical Struts		23.1	0.930
W-Shape Track Hangers		22.5	0.925
Channel Track Rails		18.6	0.888
<i>VMS</i>		23.1	0.930

Gust Effect Factor

The gust effect factor (G) adjusts the effective wind pressure to account for the dynamic interaction of the structure with the wind. The AASHTO Supports Specifications state that the gust effect factor shall be taken as a minimum of 1.14.

Basic Wind Speed

The basic wind speed (V) for the design of sign structures is diagrammed using wind speed maps in the AASHTO Supports Specifications. Figure 7-1 shows the wind speed map for the Southeastern United States. This wind speed map was used to determine the design wind speeds for the VMS structures at the locations selected for analysis. The wind speeds for Birmingham, AL and Miami, FL were selected to be 90 mph and 150 mph, respectively.

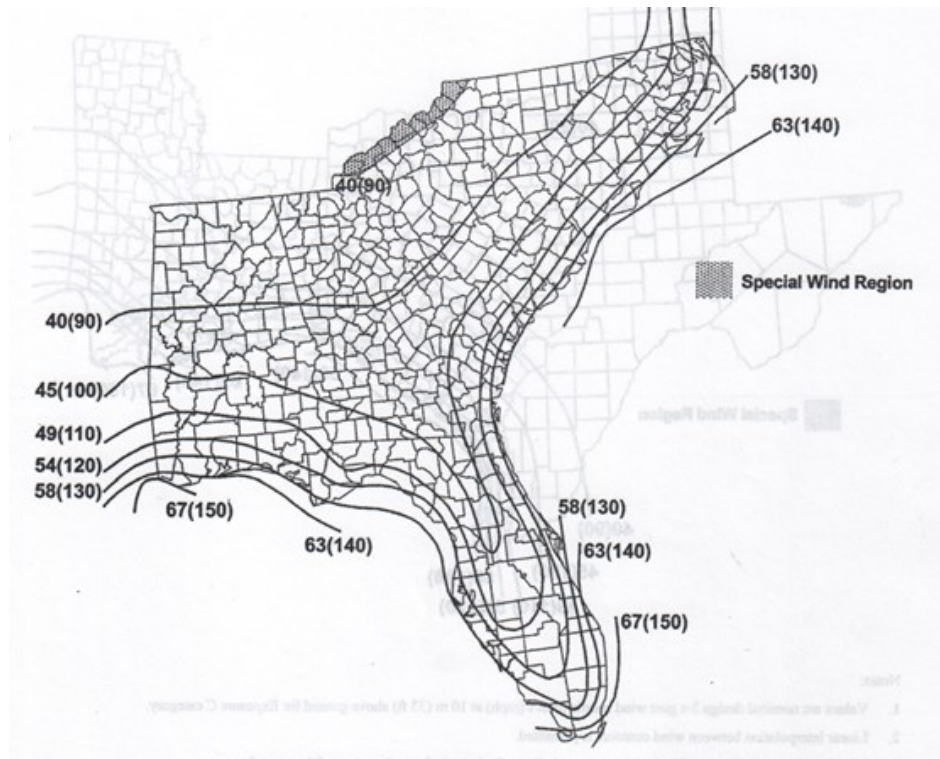


Figure 7-1: Basic Wind Speed m/s (mph) for Southeastern United States (AASHTO 2013)

Wind Importance Factor

The wind importance factor adjusts the effective wind pressure according to the design life of the structure. The AASHTO Supports Specifications recommend a 50 year minimum design life for overhead sign structures. This corresponds to a wind importance factor of 1.00 for both hurricane regions and non-hurricane regions.

Drag Coefficients

The drag coefficients for the support members of the VMS structures were selected from Table 3.8.6-1 of the AASHTO Supports Specifications. For all cases where two cylindrical members were next to each other in the same plane as the wind direction, the drag coefficient was selected to be 1.2. Examples of this type of scenario include the uprights and the front and back truss chords. Individual cylindrical members were assigned a drag coefficient of 1.1. For all cases where two or more flat members were next to each other in the same plane as the wind direction, the drag coefficient was selected to be 2.0. Examples of this type of scenario include the ladder rail angles and track supports. Individual flat members were assigned a drag coefficient of 1.7.

For the AASHTO loading cases, the drag coefficient for the VMS was selected to be 1.70 from Table 3.8.6-1 of the AASHTO Supports Specifications. For the FIU loading cases, the standard VMS was assigned a drag coefficient of 1.22 and the VMS with chamfered edges was assigned a drag coefficient of 1.00. These drag coefficients were based on the FIU Wall of Wind testing results. Table 7-4 provides a summary of the drag coefficients used for the SAP sensitivity analysis.

Table 7-4: Drag Coefficients for Sensitivity Analysis

Members	Drag Coefficients
Upright Posts	1.2
Truss Chords	1.2
Adjacent Webs	1.2
Individual Webs	1.1
W-Shape Track Hangers	1.7
Channel Track Rails	2.0
Access Ladder Rails	2.0
<i>AASHTO VMS</i>	<i>1.7</i>
<i>FIU VMS Standard Edges</i>	<i>1.22</i>
<i>FIU VMS Chamfered Edges</i>	<i>1.0</i>

7.3.1.2 Fatigue Wind

The equivalent static natural wind gust pressure range on the VMS structures for the fatigue wind analyses was calculated using Equation 7-3 from the AASHTO Supports Specifications:

$$P_{NW} = 5.2C_dI_F \text{ (psf)} \quad \text{(Eqn. 7-3)}$$

Where:

- P_{NW} = Equivalent static natural wind gust pressure range (psf),
- C_d = Drag Coefficient, and
- I_F = Fatigue Importance Factor

Drag Coefficients

The drag coefficients used for the fatigue wind analysis of the VMS structures are the same as the drag coefficients used for the extreme wind analysis. Refer to Table 7-4 for the drag coefficients used in the fatigue analysis.

Fatigue Importance Factor

The fatigue importance factor (I_F) accounts for the risk of traffic hazards or property damage that could result from the fatigue failure of sign structures. The fatigue importance factor is dependent on the fatigue importance category. Structures which support variable message signs are classified as Category I structures. According to Table 11.6-1 of the AASHTO Supports Specifications, the fatigue importance factor for Category I non-cantilevered sign structures under natural wind gusts is 1.0.

7.3.2 *SAP Load Combinations*

The AASHTO Supports Specifications provide four load combinations for the design of sign structures. These four load combinations are shown in Table 7-5 which is a reproduction of Table 3.4-1 in the Specifications. The first three load combinations are for extreme wind design, while the fourth is for fatigue wind design. Each of the load combinations for extreme wind design has a corresponding percent increase of allowable stress. For example, load combinations II and III can have design stresses which are 33% greater than the allowable stresses.

Table 7-5: AASHTO Group Load Combinations

Group Load	Load Combination	Percentage of Allowable Stress
I	DL	100
II	DL + W	133
III	DL + Ice + 1/2(W)	133
IV	Fatigue	NA

Since the purpose of the sensitivity study was to examine the impact of the newly developed VMS drag coefficients on the design of sign structures, only load combinations II and IV were utilized. Load combination II was the controlling load combination for extreme wind, and load combination IV was used for fatigue wind.

7.3.2.1 Extreme Wind Load Cases

Extreme wind static load cases were run for both the Structure A and Structure B SAP models. Six load cases were run for each model for a total of twelve load cases. The load cases were developed according to load combination II for extreme wind found in the AASHTO Supports Specifications. All load cases combined the dead load of the VMS and its support structure acting in the direction of gravity with the extreme wind load acting in the horizontal direction. The wind speed and VMS drag coefficient were varied for the different load cases according to the parameters of the sensitivity study. Table 7-6 summarizes the extreme wind load cases run in the SAP analyses.

Table 7-6: Extreme Wind Load Cases

SAP Model	Load Case	Load Combination	Wind Speed (mph)	VMS Drag Coefficient
Structure A	1	DL + W	90	1.7 _{AASHTO}
	2	DL + W	90	1.22 _{FIU}
	3	DL + W	90	1.0 _{FIU}
	4	DL + W	150	1.7 _{AASHTO}
	5	DL + W	150	1.22 _{FIU}
	6	DL + W	150	1.0 _{FIU}
Structure B	7	DL + W	90	1.7 _{AASHTO}
	8	DL + W	90	1.22 _{FIU}
	9	DL + W	90	1.0 _{FIU}
	10	DL + W	150	1.7 _{AASHTO}
	11	DL + W	150	1.22 _{FIU}
	12	DL + W	150	1.0 _{FIU}

7.3.2.2 Fatigue Wind Load Cases

Fatigue wind static load cases were run for both the Structure A and Structure B SAP models. Three load cases were run for each model for a total of six load cases. The load cases were developed according to the load combination for fatigue wind found in the AASHTO Supports Specifications. The fatigue wind loading was based on a yearly mean wind velocity of 11.2 mph which correlated to an equivalent static natural wind gust pressure range according to Equation 7-3. The fatigue wind pressure range was applied to the VMS structure SAP models in the horizontal direction. The VMS drag coefficient was varied for the different load cases according to the parameters of the sensitivity study. Table 7-7 summarizes the fatigue wind load cases run in the SAP analyses.

Table 7-7: Fatigue Wind Load Cases

SAP Model	Load Case	Load Combination	VMS Drag Coefficient
Structure A	13	Fatigue _{NW}	1.7 _{AASHTO}
	14	Fatigue _{NW}	1.22 _{FIU}
	15	Fatigue _{NW}	1.0 _{FIU}
Structure B	16	Fatigue _{NW}	1.7 _{AASHTO}
	17	Fatigue _{NW}	1.22 _{FIU}
	18	Fatigue _{NW}	1.0 _{FIU}

7.3.3 SAP Structural Response

The static stress response of the Structure A and Structure B models was examined for the extreme wind and fatigue wind load cases. The response of each structural model was measured for the different load cases by recording the axial stress in

the frame support members. The axial stress at any point in a frame member can be calculated in SAP using Equation 7-4 (Computers and Structures, Inc. 2011):

$$S_{11} = \frac{P}{A} - x_2 \frac{M_3}{I_{33}} - x_3 \frac{M_2}{I_{22}} \quad (psi) \quad (\text{Eqn. 7-4})$$

Where:

- S_{11} = axial stress at a point in a frame cross-section
- P = Axial force (lb),
- M_3 = Bending moment about the major axis (lb-in),
- M_2 = Bending moment about the minor axis (lb-in),
- A = Cross-sectional area of frame member (in^2),
- I_{33} = Moment of inertia about the major axis (in^4),
- I_{22} = Moment of inertia about the minor axis (in^4),
- x_2 = Distance from the centroid of the section to the point where the stress is calculated along the minor axis (in), and
- x_3 = Distance from the centroid of the section to the point where the stress is calculated along the major axis (in)

SAP uses the equation for S_{11} to calculate the axial stress at eight evenly spaced points around the circumference of a pipe frame element. The maximum and minimum axial stresses along the cross-section can then be extracted from SAP.

7.3.3.1 Critical Support Members

The stress response due to the extreme wind and fatigue wind loadings was recorded for the critical support members of Structures A and B. The critical support members included the four upright posts, the four truss chords, and the horizontal truss diagonals on the ends of each structure. The end horizontal truss diagonals were selected because analyses indicated that they experienced the largest stresses when compared to the rest of the diagonals. The frame members analyzed for Structure A are shown in Figure 7-2 through Figure 7-4, while the frame members analyzed for Structure B are shown in Figure 7-5 through Figure 7-9. The VMS structures were divided into sections to allow for easy diagramming of the support members.

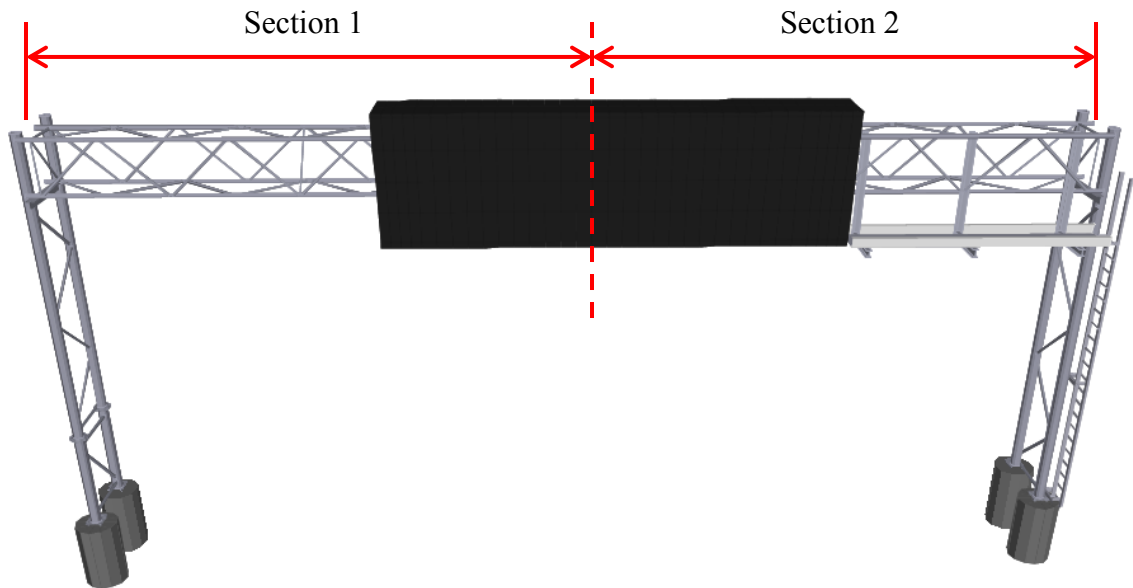


Figure 7-2: Structure A Sections

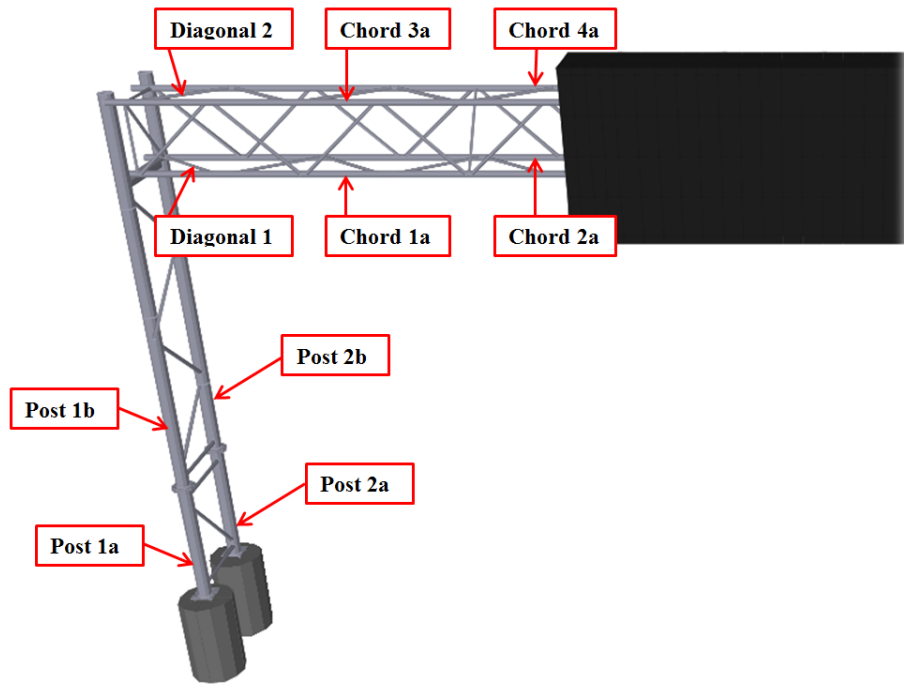


Figure 7-3: Structure A Section 1

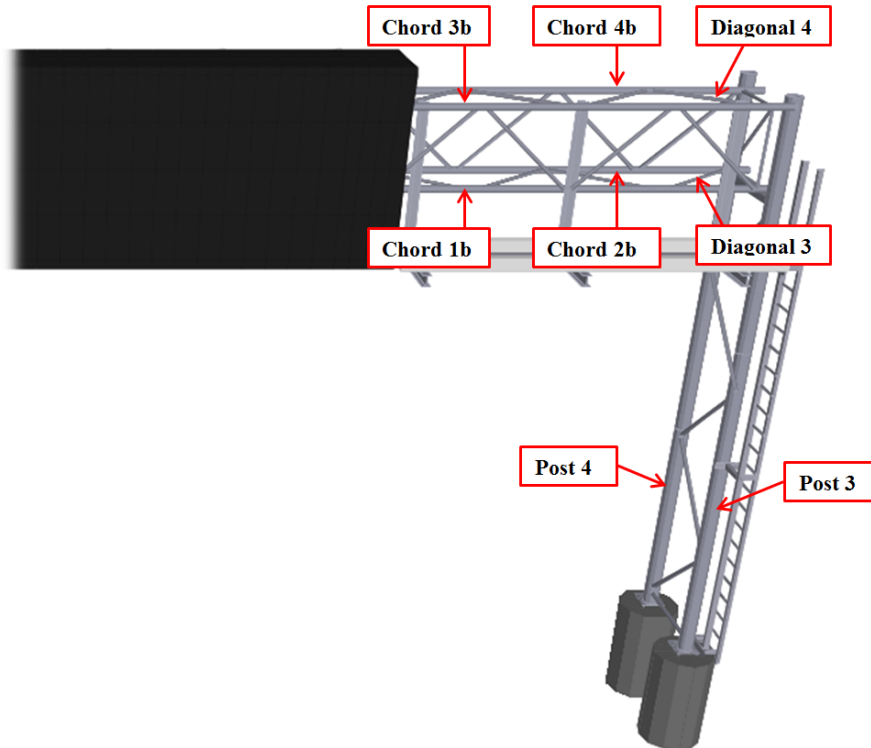


Figure 7-4: Structure A Section 2

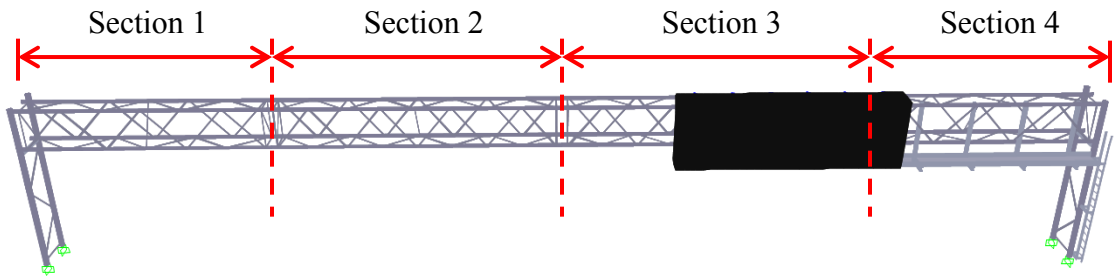


Figure 7-5: Structure B Sections

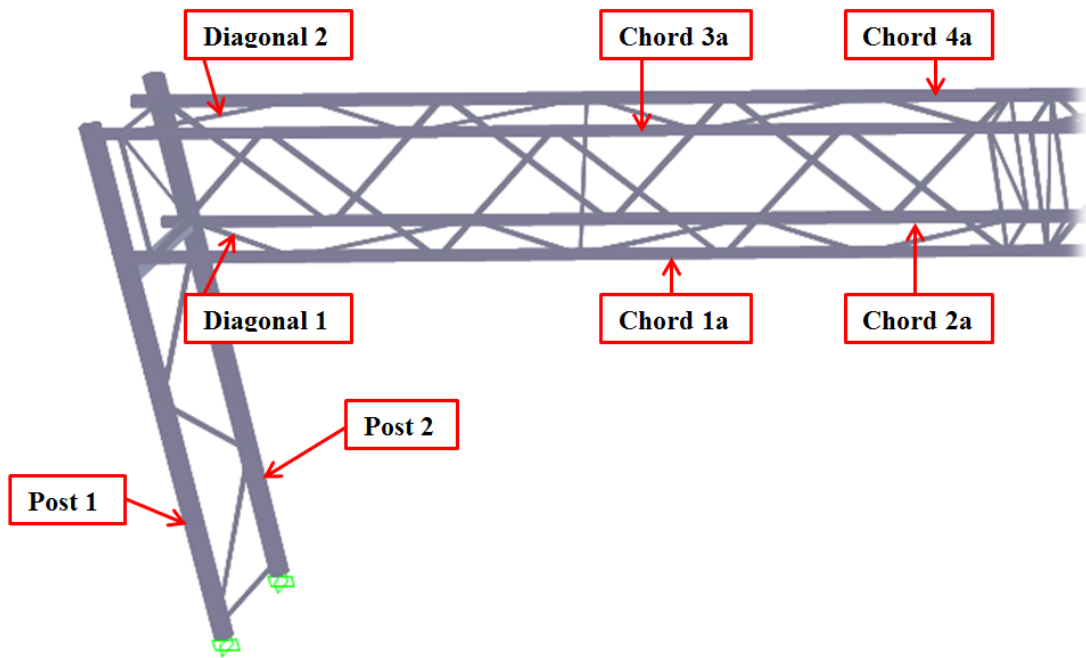


Figure 7-6: Structure B Section 1

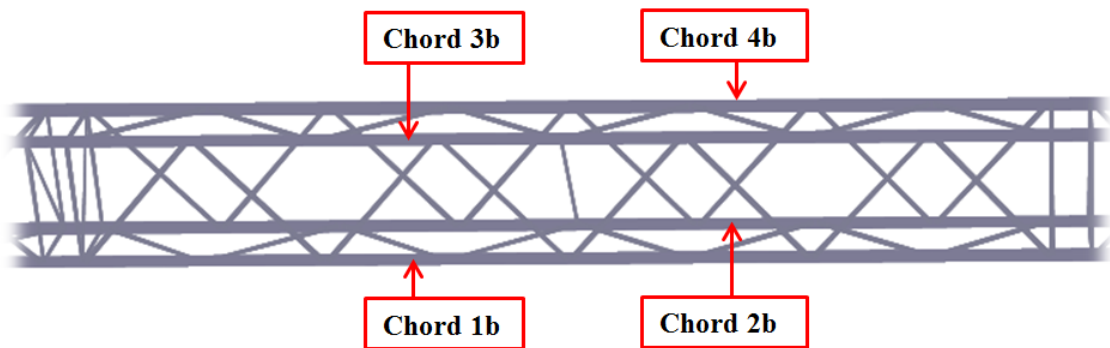


Figure 7-7: Structure B Section 2



Figure 7-8: Structure B Section 3

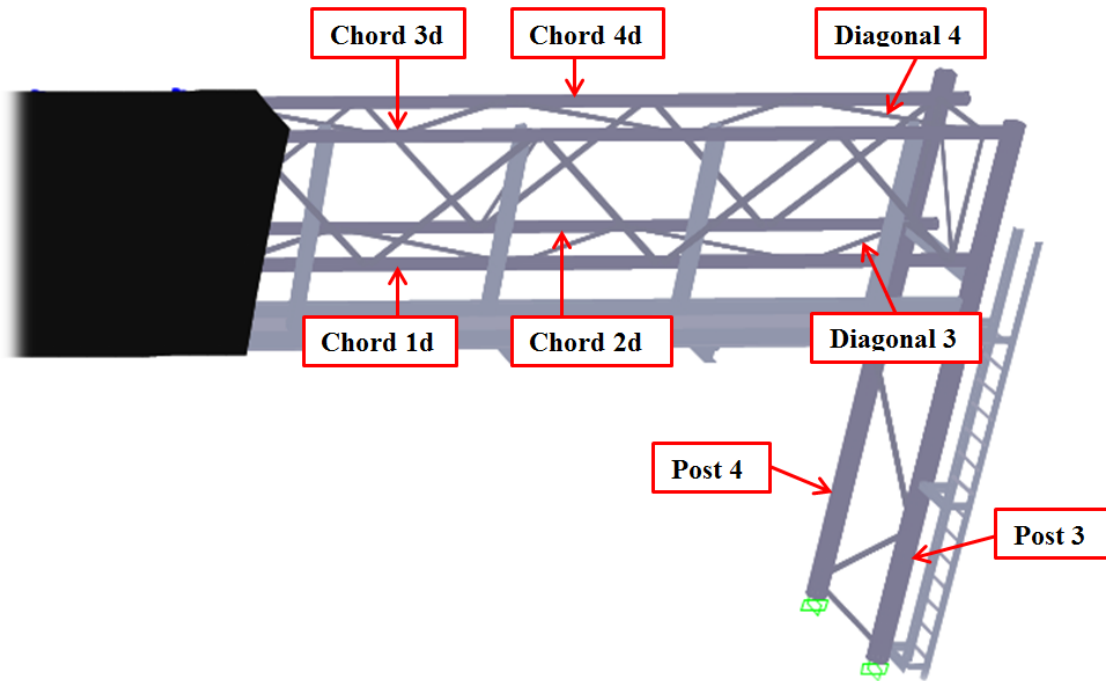


Figure 7-9: Structure B Section 4

7.3.3.2 Extreme Wind Stress Response

The static stress response due to the extreme wind loadings was measured for load cases 1 through 12. For each load case, the envelopes of the maximum and minimum axial stresses (both measured using the formula for S_{11}) were created in SAP for each

critical support member. The stress envelopes for the support members under each load case can be found in Appendix C. As an example, Figure 7-10 shows the stress envelopes for post 4 of the Structure A model for load case 1. The stress envelopes show both the maximum and minimum axial stresses as well as the location of these stresses in the support member. These stress envelopes were used to record the absolute maximum stress and its corresponding location for each support member. For example, the absolute maximum stress for post 4 of the Structure A model under load case 1 was 11308 psi. This stress occurred at the base of the post.

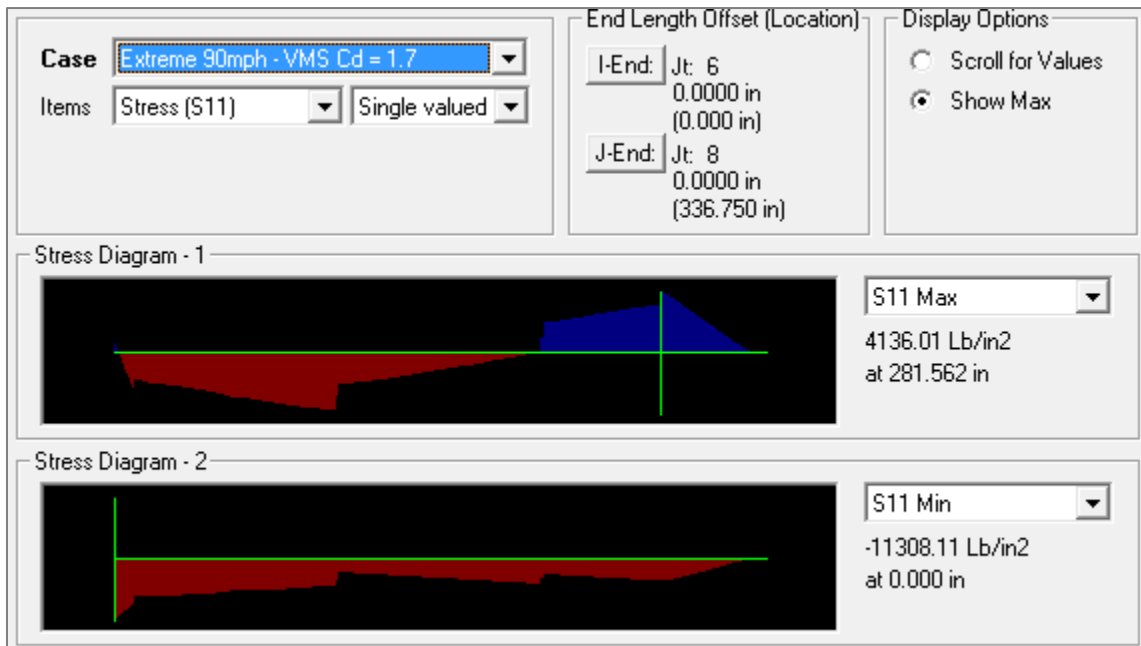


Figure 7-10: Stress Envelopes for Post 4 of Structure A

Member Stresses from SAP

Tables were developed to record the absolute maximum stress for each critical support member under the different load cases for extreme wind. The stress results were grouped so that each table included the results from three load cases which had varying

VMS drag coefficients with all other parameters constant. This was done so that the stress results from the load cases with the new VMS drag coefficients (1.22 and 1.0) could be compared to the stress results from the load cases with the AASHTO VMS drag coefficient (1.7). The comparison between the stress results for the different load cases was performed using stress reduction ratios.

Two sets of stress reduction ratios were calculated for each critical support member. The first set of stress ratios was calculated for a standard VMS by dividing the maximum stress in each support member for the load case with a VMS drag coefficient of 1.22 by the maximum stress for the load case with a VMS drag coefficient of 1.7. The second set of stress ratios was calculated for a VMS with modified edges by dividing the maximum stress in each support member for the load case with a VMS drag coefficient of 1.0 by the maximum stress for the load case with a VMS drag coefficient of 1.7. These stress ratios were included in the tables which record the absolute maximum stresses for the support members.

Tables 7-8, 7-9, 7-10, and 7-11 show the maximum stresses in the critical support members and the corresponding stress ratios for load cases 1-3, 4-6, 7-9, and 10-12, respectively. Each table also includes the overall maximum stress in the upright posts, truss chords, and truss diagonals for each load case as well as the corresponding stress ratios.

Table 7-8: Member Stresses (psi) for Load Cases 1-3 (Structure A, V = 90 mph)

Structure A: Extreme Wind (90 mph)						
	Member ID	Max σ (C_d 1.7)	Max σ (C_d 1.22)	Max σ (C_d 1.0)	σ Ratio (C_d 1.22)	σ Ratio (C_d 1.0)
Uprights	Post 1a	8152	6305	5460	0.77	0.67
	Post 1b	5999	4607	3969	0.77	0.66
	Post 2a	11105	8789	7815	0.79	0.70
	Post 2b	4597	3745	3472	0.81	0.76
	Post 3	9217	6822	5726	0.74	0.62
	Post 4	11308	8771	7669	0.78	0.68
Max Stress for Posts:		11308	8789	7815	0.78	0.69
Truss Chords	Chord 1a	13088	9877	9306	0.75	0.71
	Chord 1b	19442	16632	15366	0.86	0.79
	Chord 2a	15529	12721	11436	0.82	0.74
	Chord 2b	16256	12867	11343	0.79	0.70
	Chord 3a	18688	15723	14382	0.84	0.77
	Chord 3b	24298	20614	18927	0.85	0.78
	Chord 4a	9207	6060	4619	0.66	0.50
	Chord 4b	8508	4448	2642	0.52	0.31
Max Stress for Chords:		24298	20614	18927	0.85	0.78
Horizontal Truss Webs	Diagonal 1	9608	7934	7168	0.83	0.75
	Diagonal 2	5526	3893	3146	0.70	0.57
	Diagonal 3	13836	11050	9775	0.80	0.71
	Diagonal 4	4266	2486	1672	0.58	0.39
Max Stress for Diagonals:		13836	11050	9775	0.80	0.71

Table 7-9: Member Stresses (psi) for Load Cases 4-6 (Structure A, V = 150 mph)

Structure A: Extreme Wind (150 mph)						
	Member ID	Max σ (C_d 1.7)	Max σ (C_d 1.22)	Max σ (C_d 1.0)	σ Ratio (C_d 1.22)	σ Ratio (C_d 1.0)
Uprights	Post 1a	22638	17509	15159	0.77	0.67
	Post 1b	16843	12978	11206	0.77	0.67
	Post 2a	29334	22902	19953	0.78	0.68
	Post 2b	11746	9162	7978	0.78	0.68
	Post 3	28292	21641	18593	0.76	0.66
	Post 4	32193	24951	21631	0.78	0.67
Max Stress for Posts:		32193	24951	21631	0.78	0.67
Truss Chords	Chord 1a	36653	26774	22245	0.73	0.61
	Chord 1b	55050	37539	30415	0.68	0.55
	Chord 2a	34294	26496	22921	0.77	0.67
	Chord 2b	38567	29154	24840	0.76	0.64
	Chord 3a	38994	30760	27079	0.79	0.69
	Chord 3b	49056	38823	34133	0.79	0.70
	Chord 4a	30117	21377	17371	0.71	0.58
	Chord 4b	38176	26900	21732	0.70	0.57
Max Stress for Chords:		55050	38823	34133	0.71	0.62
Horizontal Truss Webs	Diagonal 1	21826	17178	15047	0.79	0.69
	Diagonal 2	17083	12549	10471	0.73	0.61
	Diagonal 3	34344	26609	23063	0.77	0.67
	Diagonal 4	16179	11236	8970	0.69	0.55
Max Stress for Diagonals:		34344	26609	23063	0.77	0.67

Table 7-10: Member Stresses σ (psi) for Load Cases 7-9 (Structure B, V = 90 mph)

Structure B: Extreme Wind (90 mph)						
	Member ID	Max σ (C_d 1.7)	Max σ (C_d 1.22)	Max σ (C_d 1.0)	σ Ratio (C_d 1.22)	σ Ratio (C_d 1.0)
Uprights	Post 1	7748	6531	5974	0.84	0.77
	Post 2	13442	12544	12132	0.93	0.90
	Post 3	9277	7098	6107	0.77	0.66
	Post 4	19688	16546	15107	0.84	0.77
Max Stress for Posts:		19688	16546	15107	0.84	0.77
Truss Chords	Chord 1a	6813	5667	5142	0.83	0.75
	Chord 1b	7963	5566	4917	0.70	0.62
	Chord 1c	16551	12101	10063	0.73	0.61
	Chord 1d	13615	10109	10127	0.74	0.74
	Chord 2a	12372	11105	10526	0.90	0.85
	Chord 2b	21387	18676	17434	0.87	0.82
	Chord 2c	24201	20896	19383	0.86	0.80
	Chord 2d	19423	16453	15094	0.85	0.78
	Chord 3a	12403	11270	10811	0.91	0.87
	Chord 3b	21686	18943	17688	0.87	0.82
	Chord 3c	30556	26742	24996	0.88	0.82
	Chord 3d	25026	22194	21131	0.89	0.84
	Chord 4a	4523	3900	3801	0.86	0.84
	Chord 4b	7174	4197	2834	0.59	0.40
	Chord 4c	8530	4995	3393	0.59	0.40
	Chord 4d	8388	5163	4669	0.62	0.56
Max Stress for Chords:		30556	26742	24996	0.88	0.82
Horizontal Truss Webs	Diagonal 1	9349	8223	7708	0.88	0.82
	Diagonal 2	5567	4525	4048	0.81	0.73
	Diagonal 3	19275	16558	15314	0.86	0.79
	Diagonal 4	7065	4597	3467	0.65	0.49
Max Stress for Diagonals:		19275	16558	15314	0.86	0.79

Table 7-11: Member Stresses (psi) for Load Cases 10-12 (Structure B, V = 150 mph)

Structure B: Extreme Wind (150 mph)						
	Member ID	Max σ (C_d 1.7)	Max σ (C_d 1.22)	Max σ (C_d 1.0)	σ Ratio (C_d 1.22)	σ Ratio (C_d 1.0)
Uprights	Post 1	24860	20085	18018	0.81	0.72
	Post 2	28791	24794	22962	0.86	0.80
	Post 3	33025	25294	21750	0.77	0.66
	Post 4	47986	39259	35259	0.82	0.73
Max Stress for Posts:		47986	39259	35259	0.82	0.73
Truss Chords	Chord 1a	18913	15729	14270	0.83	0.75
	Chord 1b	32846	24704	20972	0.75	0.64
	Chord 1c	55542	40931	34234	0.74	0.62
	Chord 1d	43017	31372	26368	0.73	0.61
	Chord 2a	25629	22112	20500	0.86	0.80
	Chord 2b	45314	37783	34332	0.83	0.76
	Chord 2c	51328	42151	37944	0.82	0.74
	Chord 2d	42349	34102	30321	0.81	0.72
	Chord 3a	25726	21981	20264	0.85	0.79
	Chord 3b	45653	38036	34546	0.83	0.76
	Chord 3c	62685	50900	46045	0.81	0.73
	Chord 3d	50039	39650	36001	0.79	0.72
	Chord 4a	18433	14511	12713	0.79	0.69
	Chord 4b	32678	24352	20536	0.75	0.63
	Chord 4c	37594	27444	22792	0.73	0.61
	Chord 4d	33099	24141	20035	0.73	0.61
Max Stress for Chords:		62685	50900	46045	0.81	0.73
Horizontal Truss Webs	Diagonal 1	22794	19667	18233	0.86	0.80
	Diagonal 2	16997	14104	12778	0.83	0.75
	Diagonal 3	44524	36978	33519	0.83	0.75
	Diagonal 4	26694	19840	16698	0.74	0.63
Max Stress for Diagonals:		44524	36978	33519	0.83	0.75

Member Stress Locations

Figures were created to show the locations of the maximum stresses in the upright posts and truss chords for each extreme wind load case. Stress ratios were included in the figures for the FIU load cases to show the stress reduction in the support members due to the new VMS drag coefficients.

Figure 7-11 through Figure 7-13 show the maximum stress locations for load cases 1 through 3, respectively. These three load cases represent Structure A subject to 90 mph extreme wind with the VMS drag coefficient varying from 1.7 to 1.22 to 1.0. As seen in the figures, the maximum stresses in the upright posts occurred at the bases of posts 2, 3, and 4, and close to the stub connection in post 1. The maximum stresses in the truss chords occurred behind the VMS sign panel at connections between the truss chords and the truss webs and between the front truss chords and the sign.

Figure 7-14 through Figure 7-16 show the maximum stress locations for load cases 4 through 6, respectively. These three load cases represent Structure A subject to 150 mph extreme wind with the VMS drag coefficient varying from 1.7 to 1.22 to 1.0. As seen in the figures, the maximum stresses in the upright posts occurred at the bases of posts 2, 3, and 4, and close to the stub connection in post 1. The maximum stresses in the truss chords occurred behind the right side of the VMS sign panel at connections between the truss chords and the truss webs and between the front truss chords and the sign.

Figure 7-17 through Figure 7-19 show the maximum stress locations for load cases 7 through 9, respectively. These three load cases represent Structure B subject to 90 mph extreme wind with the VMS drag coefficient varying from 1.7 to 1.22 to 1.0. For load cases 7 and 8, the maximum stresses in the upright posts occurred at the bases of

posts 1, 3, and 4, and at the WT truss support connection in post 1. The maximum stresses in the truss chords occurred behind the VMS sign panel at connections between the truss chords and the truss webs and between the front truss chords and the sign. For load case 9, the maximum stresses in the upright posts occurred at the bases of posts 1 and 3, and at the WT truss support connection in posts 2 and 4. The maximum stresses in the truss chords occurred behind the VMS sign panel and close to the ends of the truss chords.

Figure 7-20 through Figure 7-22 show the maximum stress locations for load cases 10 through 12, respectively. These three load cases represent Structure B subject to 150 mph extreme wind with the VMS drag coefficient varying from 1.7 to 1.22 to 1.0. As seen in the figures, the maximum stresses in the upright posts occurred at the bases of the posts. The maximum stresses in the truss chords occurred behind the VMS sign panel at connections between the truss chords and the truss webs and between the front truss chords and the sign.

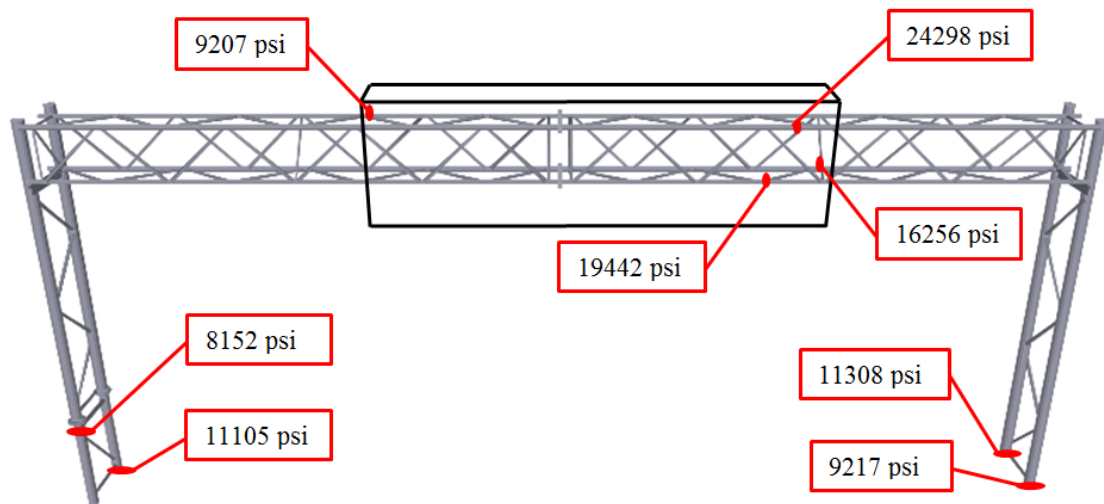


Figure 7-11: Max stress locations for load case 1 (Structure A, $V = 90$ mph, $C_d = 1.7$)

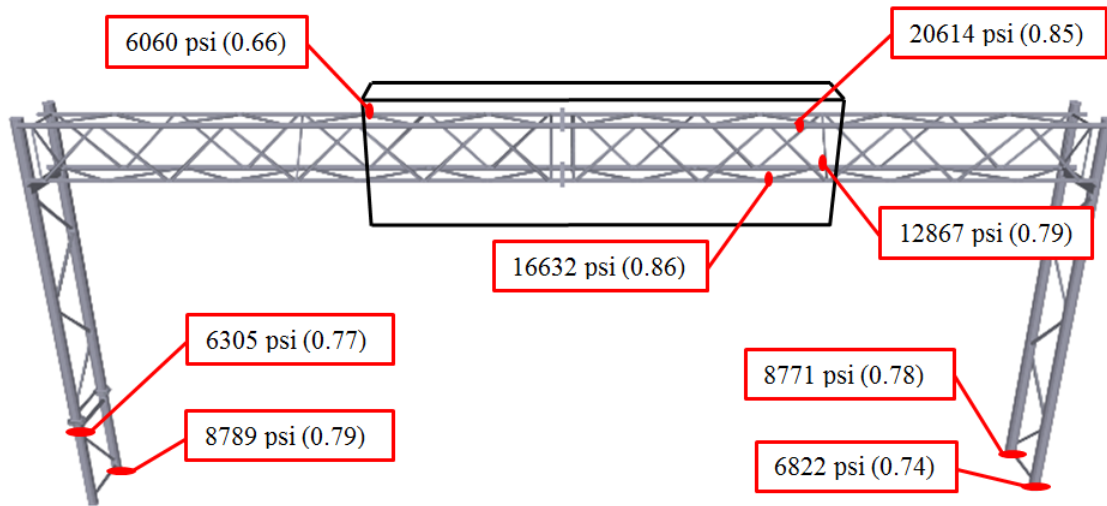


Figure 7-12: Max stress locations for load case 2 (Structure A, V = 90 mph, $C_d = 1.22$)

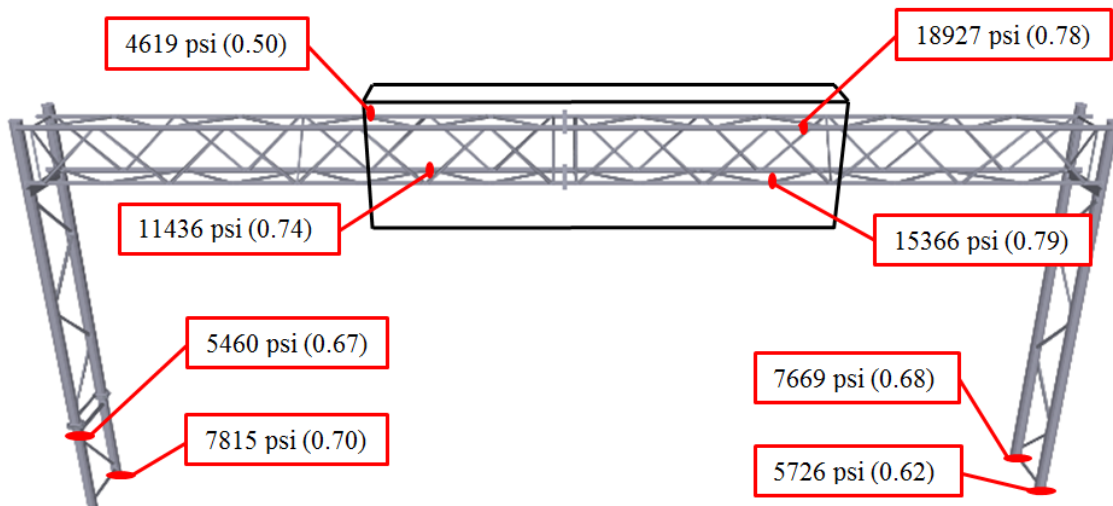


Figure 7-13: Max stress locations for load case 3 (Structure A, V = 90 mph, $C_d = 1.0$)

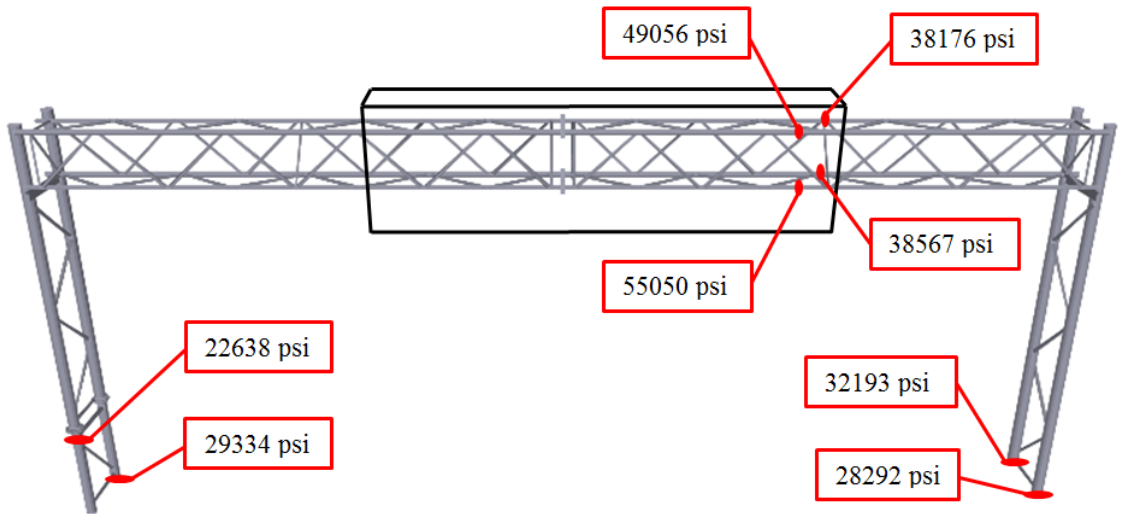


Figure 7-14: Max stress locations for load case 4 (Structure A, $V = 150$ mph, $C_d = 1.7$)

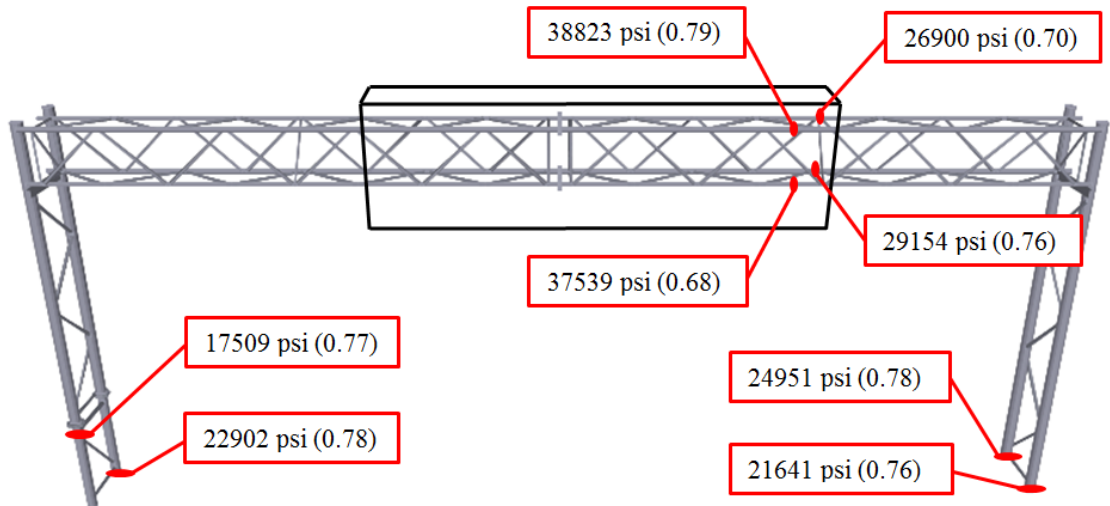


Figure 7-15: Max stress locations for load case 5 (Structure A, $V = 150$ mph, $C_d = 1.22$)

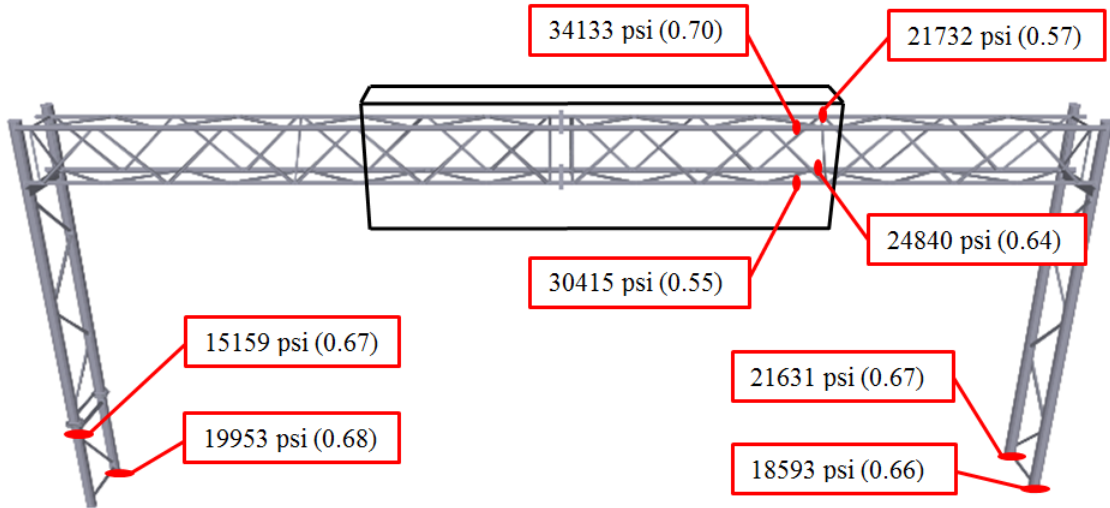


Figure 7-16: Max stress locations for load case 6 (Structure A, $V = 150$ mph, $C_d = 1.0$)

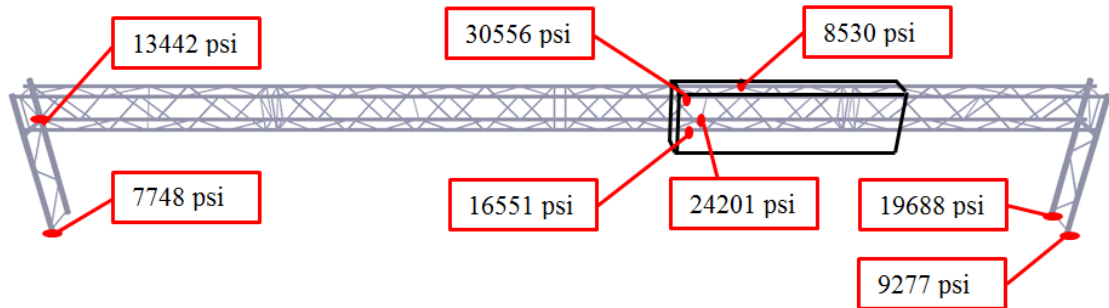


Figure 7-17: Max stress locations for load case 7 (Structure B, $V = 90$ mph, $C_d = 1.7$)

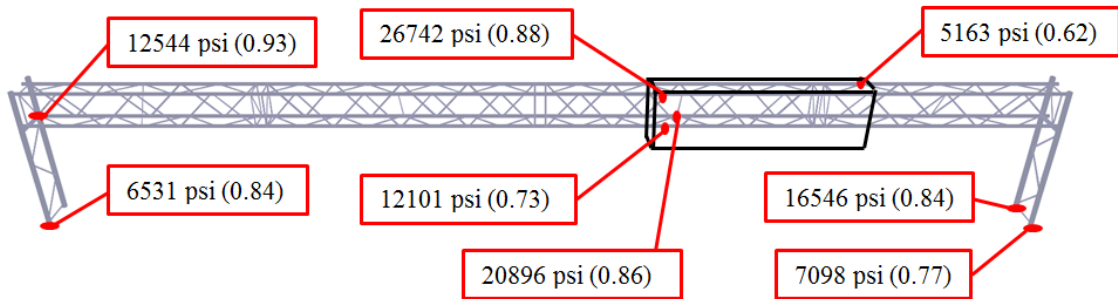


Figure 7-18: Max stress locations for load case 8 (Structure B, $V = 90$ mph, $C_d = 1.22$)

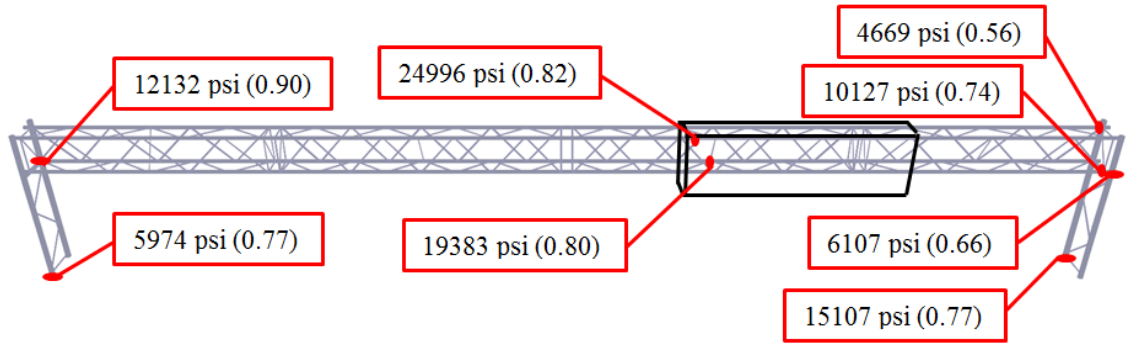


Figure 7-19: Max stress locations for load case 9 (Structure B, V = 90 mph, C_d = 1.0)

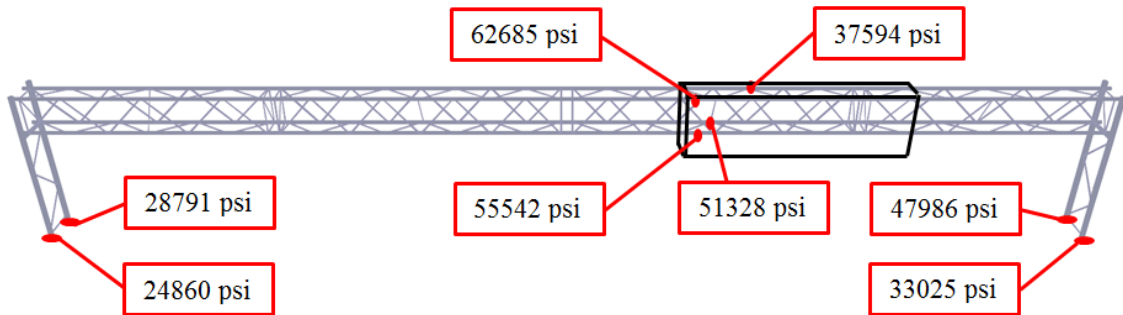


Figure 7-20: Max stress locations for load case 10 (Structure B, V = 150 mph, C_d = 1.7)

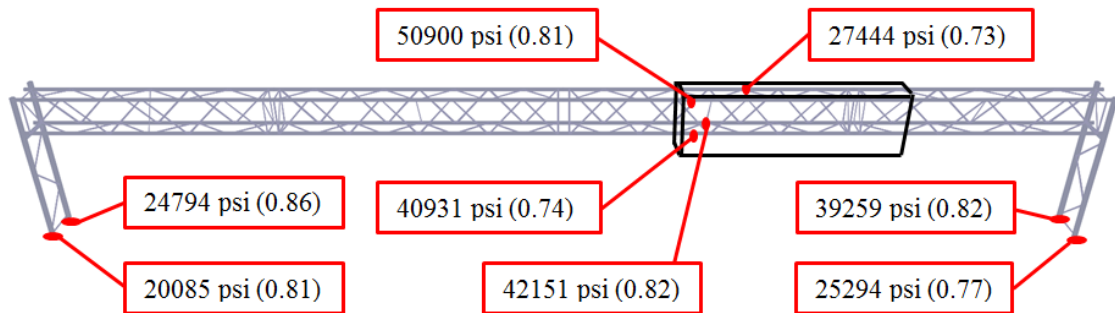


Figure 7-21: Max stress locations for load case 11 (Structure B, V = 150 mph, C_d = 1.22)

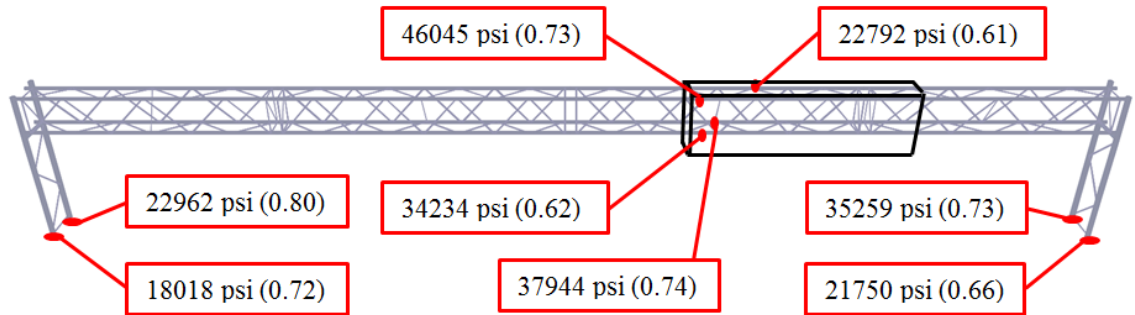


Figure 7-22: Max stress locations for load case 12 (Structure B, V = 150 mph, C_d = 1.0)

Maximum Member Stresses

The SAP stress results were analyzed to select the maximum member stresses for each extreme wind load case. Table 7-12 shows the maximum stresses for the upright posts, truss chords, and truss diagonals organized according to the load cases and parameters, along with the corresponding stress ratios. The maximum post stress for each load case was selected to be the maximum stress of all four upright posts. The maximum chord stress for each load case was selected to be the maximum stress of all four truss chords. Finally, the maximum diagonal stress for each load case was selected to be the maximum stress of all four horizontal truss diagonals which were analyzed.

The maximum member stresses in Table 7-12 are displayed graphically for groups of three load cases in Figures 7-23 through 7-26. The extreme wind load cases were divided into groups of three with the VMS drag coefficient varying from 1.7 to 1.22 to 1.0 for each group of three load cases. Each figure shows the comparison between the maximum member stresses for the posts, chords, and diagonals due to the variation of the VMS drag coefficient, along with the corresponding stress reduction ratios. The maximum member stresses decrease significantly as the VMS drag coefficient decreases.

Also, all of the figures show that the truss chords experience the largest stresses, with the upright posts and truss diagonals experiencing smaller stresses.

Table 7-12: Maximum Stresses for Load Cases 1-12

Load Case	Parameters			Maximum Member Stress (psi)		
	Structure	Wind Speed (mph)	VMS C_d	Upright Posts	Truss Chords	Truss Diagonals
1	A	90	1.7 _{AASHTO}	11308	24298	13836
2	A	90	1.22 _{FIU}	8789 (0.78)	20614 (0.85)	11050 (0.80)
3	A	90	1.0 _{FIU}	7815 (0.69)	18927 (0.78)	9775 (0.71)
4	A	150	1.7 _{AASHTO}	32193	55050	34344
5	A	150	1.22 _{FIU}	24951 (0.78)	38823 (0.71)	26609 (0.77)
6	A	150	1.0 _{FIU}	21631 (0.67)	34133 (0.62)	23063 (0.67)
7	B	90	1.7 _{AASHTO}	19688	30556	19275
8	B	90	1.22 _{FIU}	16546 (0.84)	26742 (0.88)	16558 (0.86)
9	B	90	1.0 _{FIU}	15107 (0.77)	24996 (0.82)	15314 (0.79)
10	B	150	1.7 _{AASHTO}	47986	62685	44524
11	B	150	1.22 _{FIU}	39259 (0.82)	50900 (0.81)	36978 (0.83)
12	B	150	1.0 _{FIU}	35259 (0.73)	46045 (0.73)	33519 (0.75)

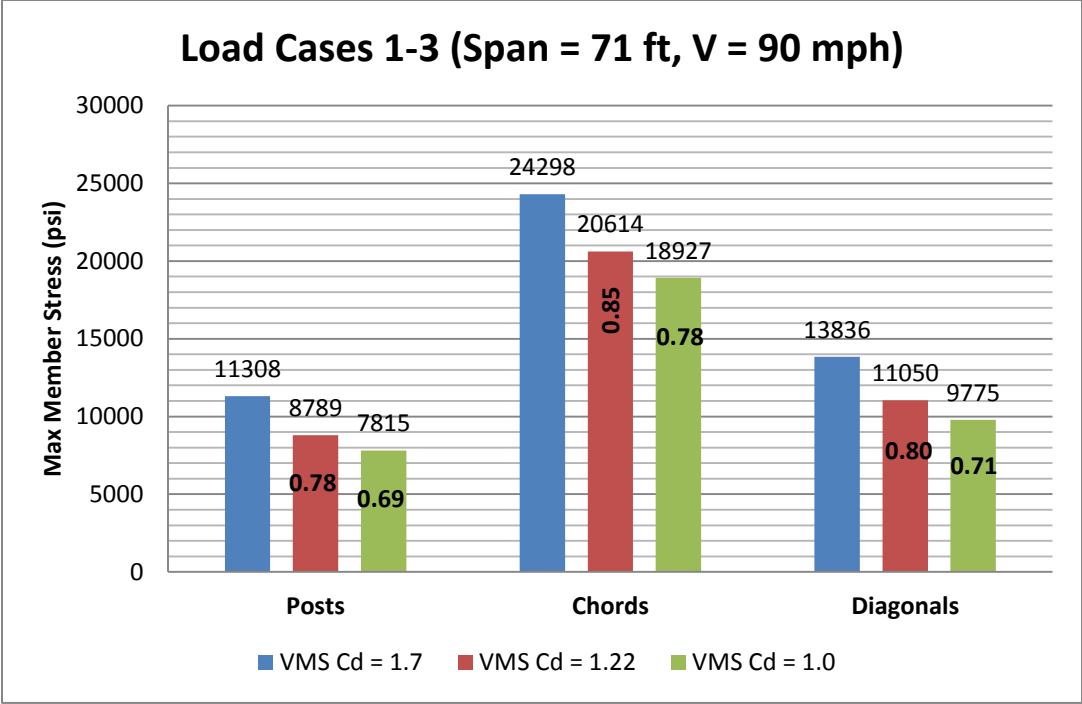


Figure 7-23: Max Member Stresses for Load Cases 1-3 (Structure A, V = 90 mph)

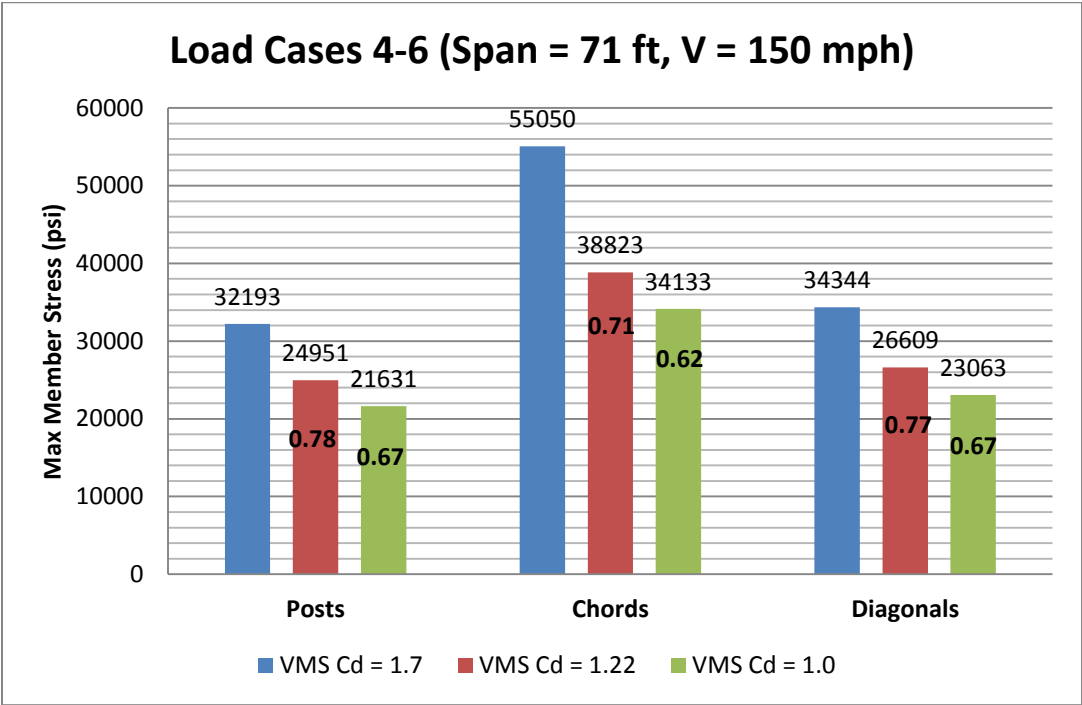


Figure 7-24: Max Member Stresses for Load Cases 4-6 (Structure A, V = 150 mph)

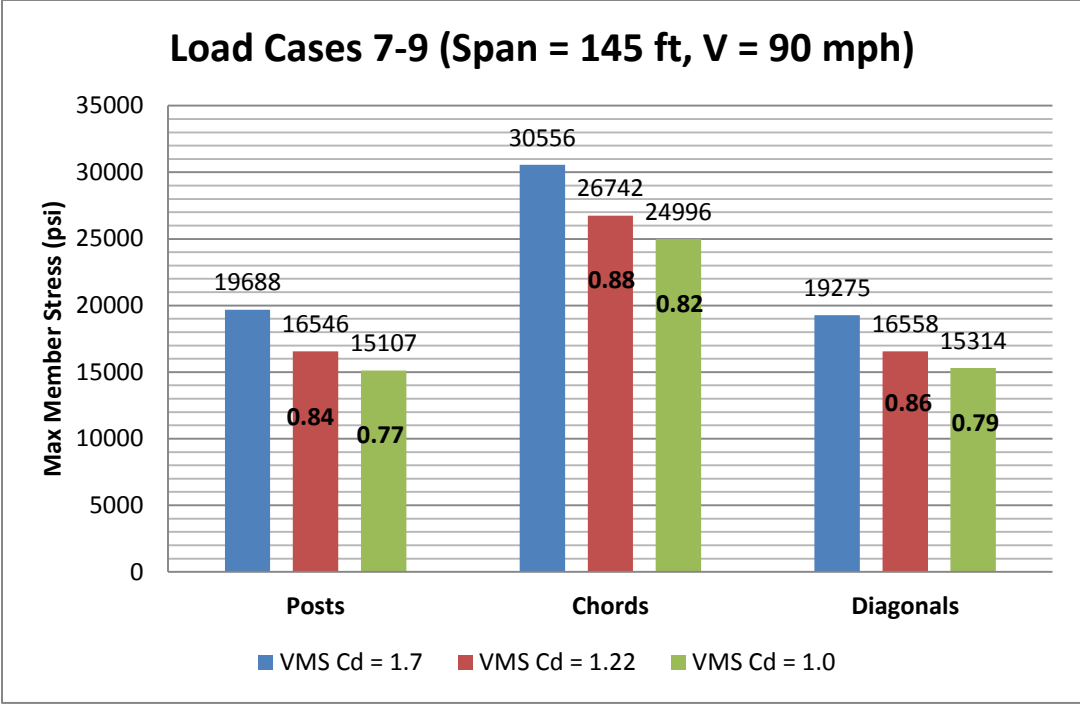


Figure 7-25: Max Member Stresses for Load Cases 7-9 (Structure B, V = 90 mph)

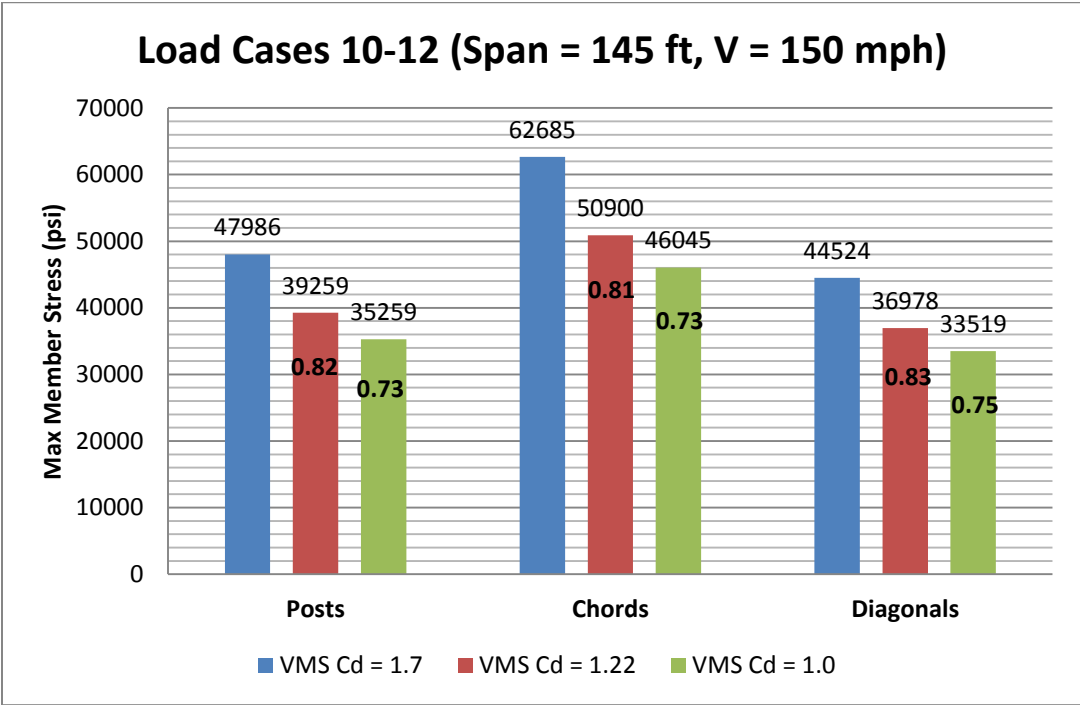
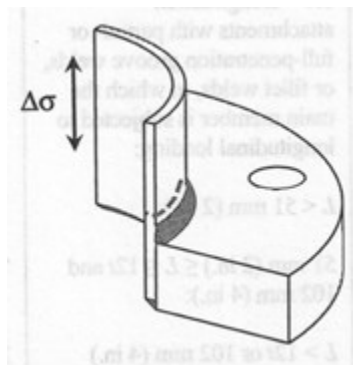


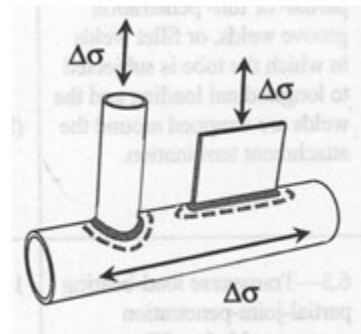
Figure 7-26: Max Member Stresses for Load Cases 10-12 (Structure B, V = 150 mph)

7.3.3.3 Fatigue Wind Stress Response

Critical fatigue connections were analyzed for the fatigue load cases in SAP based on the requirements of the AASHTO Supports Specifications. Chapter 11 of the AASHTO Supports Specifications provides common fatigue details for sign support structures. Two of these fatigue details which are unique to the structures analyzed in SAP are shown in Figure 7-27. Fatigue detail 5.4 was analyzed for the welded connections between the upright posts and the base plates which support the structure. Fatigue detail 5.5 was analyzed for the welded connections between the truss chords and truss diagonal webs. In each of these fatigue details, the axial stress range in the support members at the connection location represented the constant amplitude fatigue threshold (CAFT).



(b) Fatigue Detail 5.4



(a) Fatigue Detail 5.5

Figure 7-27: Fatigue Details for Analysis (AASHTO 2013)

The static stress response due to the fatigue wind loadings was measured for load cases 13 through 18. For each load case, the envelopes of the maximum and minimum axial stresses (both measured using the formula for S_{11}) were created in SAP for each critical support member. The stress envelopes for the support members under each load

case can be found in Appendix C. As an example, Figure 7-28 shows the stress envelopes for post 4 of the Structure A model for load case 13. The stress envelopes show both the maximum and minimum axial stresses at any point along the support member's length. These stress envelopes were used to record the absolute maximum stress at the fatigue connection locations for each support member. For example, the absolute maximum stress at the base of post 4 of the Structure A model under load case 13 was 2788 psi.

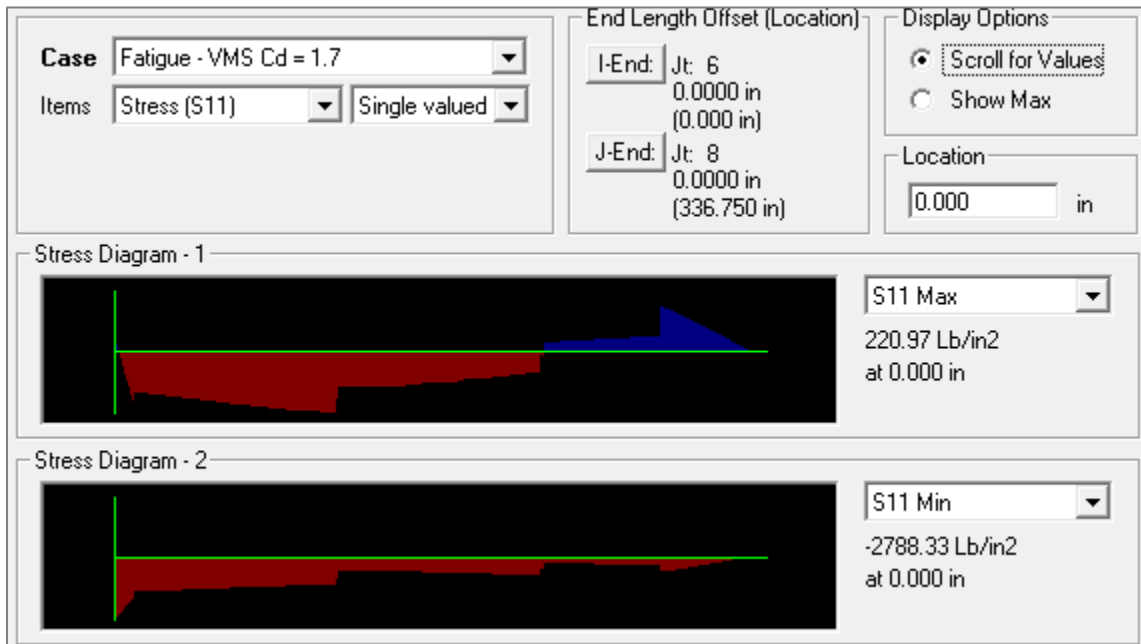


Figure 7-28: Stress Envelopes for Post 4 of Structure A

Fatigue Stresses from SAP

Tables were developed to record the absolute maximum stress at the critical fatigue connection locations for the different load cases of fatigue wind. The stress results were grouped so that each table included the results from three load cases which had varying VMS drag coefficients with all other parameters held constant. This was

done so that the stress results from the load cases with the new VMS drag coefficients (1.22 and 1.0) could be compared to the stress results from the load cases with the AASHTO VMS drag coefficient (1.7). The comparison between the stress results for the different load cases was performed using stress reduction ratios.

Two sets of stress reduction ratios were calculated for each critical fatigue connection location. The first set of stress ratios was calculated for a standard VMS by dividing the maximum stress at each connection location for the load case with a VMS drag coefficient of 1.22 by the maximum stress for the load case with a VMS drag coefficient of 1.7. The second set of stress ratios was calculated for a VMS with modified edges by dividing the maximum stress at each connection location for the load case with a VMS drag coefficient of 1.0 by the maximum stress for the load case with a VMS drag coefficient of 1.7. These stress ratios were included in the tables along with the absolute maximum stresses for the fatigue connection locations.

Tables 7-13 and 7-14 show the maximum stresses at the fatigue connection locations and the corresponding stress ratios for load cases 13-15 and 16-18, respectively. Each table also includes the overall maximum stress at the base of the posts for fatigue detail 5.4 and along the truss chords and diagonals for fatigue detail 5.5, as well as the corresponding stress ratios.

Table 7-13: Member Stress Ranges (psi) for Load Cases 13-15 (Structure A)

Structure A: Fatigue Wind						
	Member ID	σ Range (C_d 1.7)	σ Range (C_d 1.22)	σ Range (C_d 1.0)	σ Ratio (C_d 1.22)	σ Ratio (C_d 1.0)
Fatigue Detail 5.4 (Upright to Base Plate Connection)	Post 1a	1487	1152	1000	0.77	0.67
	Post 2a	2432	1883	1632	0.77	0.67
	Post 3	2547	1979	1720	0.78	0.68
	Post 4	2788	2170	1887	0.78	0.68
	Max Stress:	2788	2170	1887	0.78	0.68
Fatigue Detail 5.5 (Chord to Web Connection)	Chord 1a	3137	2294	1909	0.73	0.61
	Chord 1b	5533	3981	3274	0.72	0.59
	Chord 2a	2498	1832	1558	0.73	0.62
	Chord 2b	2968	2165	1845	0.73	0.62
	Chord 3a	2918	2146	1794	0.74	0.61
	Chord 3b	3999	2932	2445	0.73	0.61
	Chord 4a	2784	2039	1699	0.73	0.61
	Chord 4b	3953	2990	2552	0.76	0.65
	Max Stress:	5533	3981	3274	0.72	0.59
	Diagonal 1	1626	1229	1048	0.76	0.64
Diagonal 2	1537	1150	974	0.75	0.63	
Diagonal 3	2731	2071	1770	0.76	0.65	
Diagonal 4	1582	1160	968	0.73	0.61	
Max Stress:	2731	2071	1770	0.76	0.65	

Table 7-14: Member Stress Ranges (psi) for Load Cases 16-18 (Structure B)

Structure B: Fatigue Wind						
	Member ID	σ Range (C_d 1.7)	σ Range (C_d 1.22)	σ Range (C_d 1.0)	σ Ratio (C_d 1.22)	σ Ratio (C_d 1.0)
Fatigue Detail 5.4 (Upright to Base Plate Connection)	Post 1	2509	2102	1916	0.84	0.76
	Post 2	2104	1763	1608	0.84	0.76
	Post 3	3286	2626	2326	0.80	0.71
	Post 4	3781	3037	2697	0.80	0.71
	Max Stress:	3781	3037	2697	0.80	0.71
Fatigue Detail 5.5 (Chord to Web Connection)	Chord 1a	1808	1491	1347	0.82	0.75
	Chord 1b	3314	2619	2303	0.79	0.69
	Chord 1c	5343	4096	3527	0.77	0.66
	Chord 1d	4089	3096	2643	0.76	0.65
	Chord 2a	1768	1471	1336	0.83	0.76
	Chord 2b	3187	2545	2252	0.80	0.71
	Chord 2c	3657	2865	2505	0.78	0.68
	Chord 2d	3054	2350	2030	0.77	0.66
	Chord 3a	1861	1542	1396	0.83	0.75
	Chord 3b	3194	2544	2248	0.80	0.70
	Chord 3c	4680	3636	3159	0.78	0.68
	Chord 3d	3842	2927	2510	0.76	0.65
	Chord 4a	1897	1562	1410	0.82	0.74
	Chord 4b	3395	2685	2361	0.79	0.70
	Chord 4c	3872	3006	2611	0.78	0.67
	Chord 4d	3293	2528	2180	0.77	0.66
	Max Stress:	5343	4096	3527	0.77	0.66
	Diagonal 1	1798	1531	1409	0.85	0.78
	Diagonal 2	1517	1270	1157	0.84	0.76
	Diagonal 3	3384	2740	2446	0.81	0.72
Diagonal 4	2608	2024	1757	0.78	0.67	
Max Stress:	3384	2740	2446	0.81	0.72	

Fatigue Stress Locations

Figures were created to show the locations of the maximum fatigue stresses in the upright posts and truss chords for each fatigue wind load case. Stress ratios were included in the figures for the FIU load cases to show the stress reduction at the fatigue connection locations due to the new VMS drag coefficients.

Figure 7-29 through Figure 7-31 show the fatigue stress locations for load cases 13 through 15, respectively. These three load cases represent Structure A subject to fatigue wind with the VMS drag coefficient varying from 1.7 to 1.22 to 1.0. As seen in the figures, the fatigue stresses in the upright posts were measured at the bases where the posts connect to the base plates. The maximum fatigue stresses in the truss chords predominantly occurred behind the right side of the VMS sign panel.

Figure 7-32 through Figure 7-34 show the fatigue stress locations for load cases 16 through 18, respectively. These three load cases represent Structure B subject to fatigue wind with the VMS drag coefficient varying from 1.7 to 1.22 to 1.0. As seen in the figures, the fatigue stresses in the upright posts were measured at the bases where the posts connect to the base plates. The maximum fatigue stresses in the truss chords occurred behind the VMS sign panel.

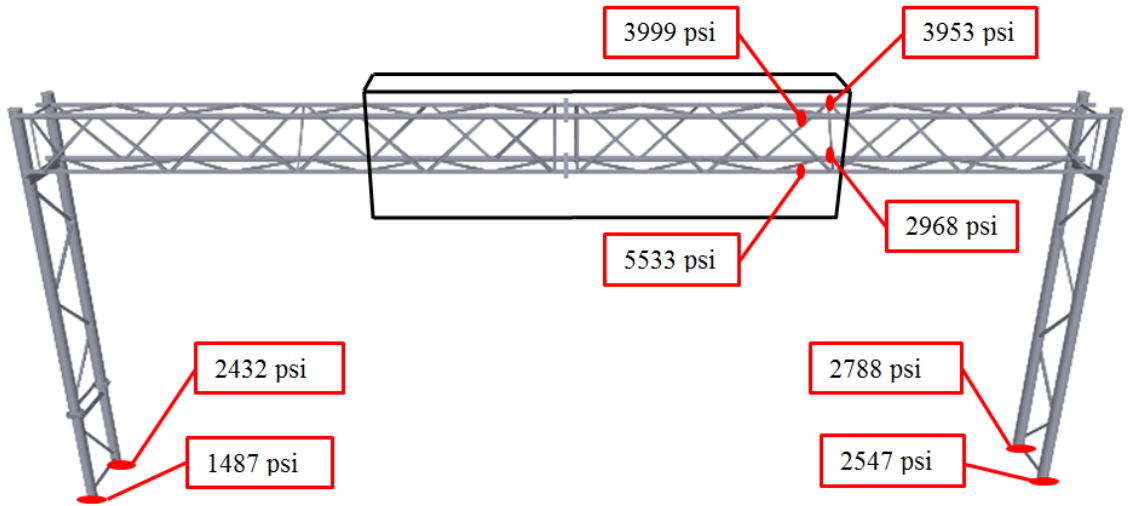


Figure 7-29: Fatigue stress locations for load case 13 (Structure A, $C_d = 1.7$)

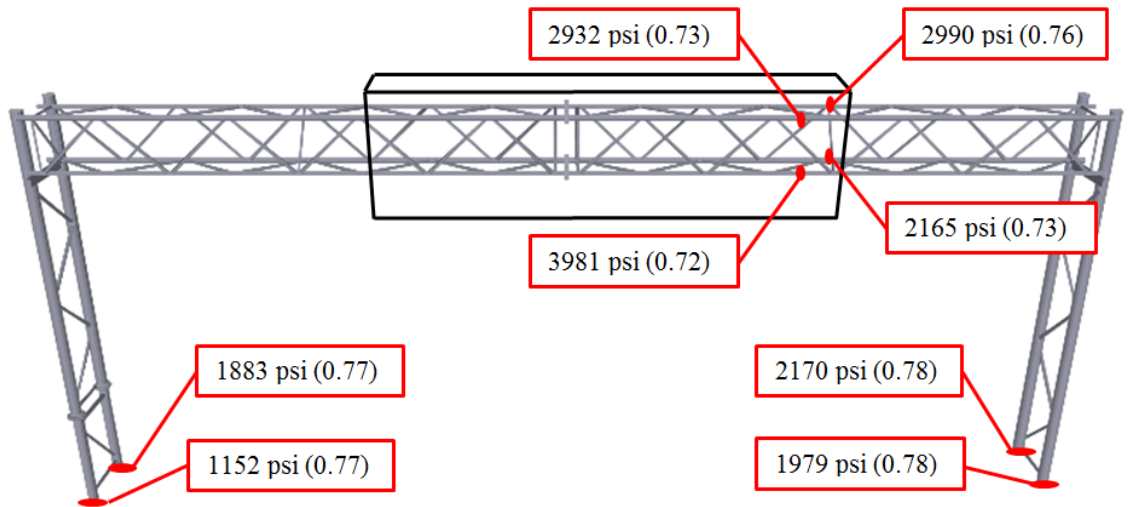


Figure 7-30: Fatigue stress locations for load case 14 (Structure A, $C_d = 1.22$)

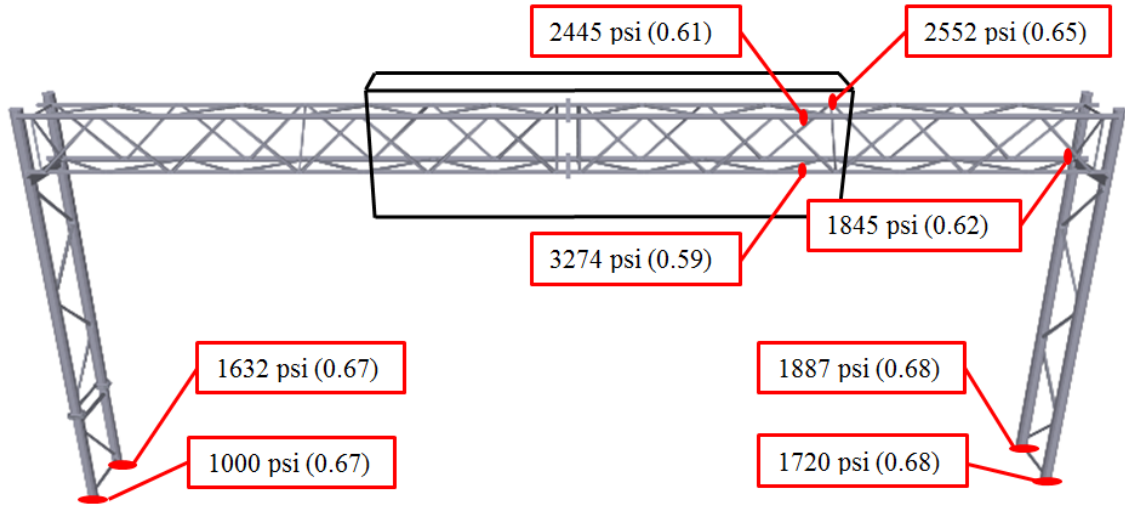


Figure 7-31: Fatigue stress locations for load case 15 (Structure A, $C_d = 1.0$)

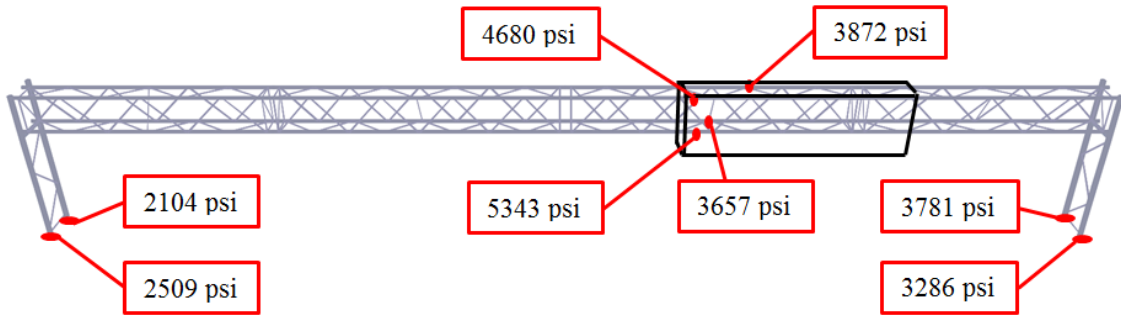


Figure 7-32: Fatigue stress locations for load case 16 (Structure B, $C_d = 1.7$)

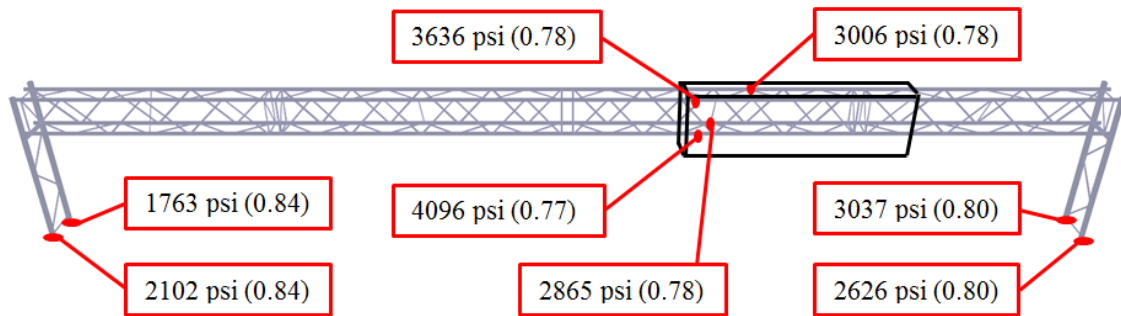


Figure 7-33: Fatigue stress locations for load case 17 (Structure B, $C_d = 1.22$)

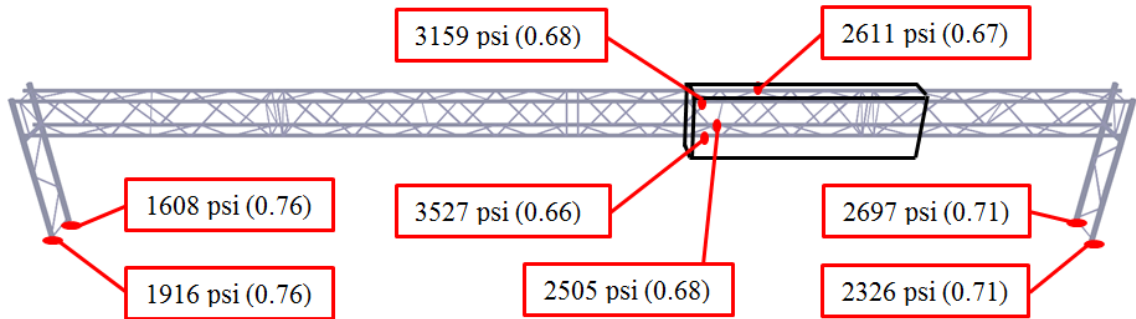


Figure 7-34: Fatigue stress locations for load case 18 (Structure B, $C_d = 1.0$)

Maximum Fatigue Stress Ranges

The SAP stress results were analyzed to select the maximum equivalent stress ranges at the critical connection locations for each fatigue wind load case. Table 7-15 shows the maximum stresses for the upright posts, truss chords, and truss diagonals at the connections organized according to the load cases and parameters, along with the corresponding stress reduction ratios. The maximum stress in the upright posts at the base plate connections for each load case was selected to be the maximum stress of all four base plate connections. The maximum stresses in the truss chords and diagonals at the chord-to-web connection for each load case were selected to be the maximum stresses of all chord-to-web connections.

Table 7-15: Maximum Stress Ranges for Load Cases 13-18

Load Case	Parameters		Maximum Connection Stress Range (psi)		
	Structure	VMS C_d	Fatigue Detail 5.4	Fatigue Detail 5.5	
			Upright Posts	Truss Chords	Truss Diagonals
13	A	1.7 _{AASHTO}	2788	5533	2731
14	A	1.22 _{FIU}	2170 (0.78)	3981 (0.72)	2071 (0.76)
15	A	1.0 _{FIU}	1887 (0.68)	3274 (0.59)	1770 (0.65)
16	B	1.7 _{AASHTO}	3781	5343	3384
17	B	1.22 _{FIU}	3037 (0.80)	4096 (0.77)	2740 (0.81)
18	B	1.0 _{FIU}	2697 (0.71)	3527 (0.66)	2446 (0.72)

The maximum connection stresses in Table 7-15 are displayed graphically for groups of three load cases in Figures 7-35 and 7-36. The fatigue wind load cases were divided into groups of three with the VMS drag coefficient varying from 1.7 to 1.22 to 1.0 for each group of three load cases. Each figure shows the comparison between the maximum connection stresses for the posts, chords, and diagonals due to the variation of the VMS drag coefficient, along with the corresponding stress reduction ratios. The maximum connection stresses decrease significantly as the VMS drag coefficient decreases. Also, both figures show that the truss chords experience the largest fatigue stresses at the chord-to-web connections when compared to the other member connections.

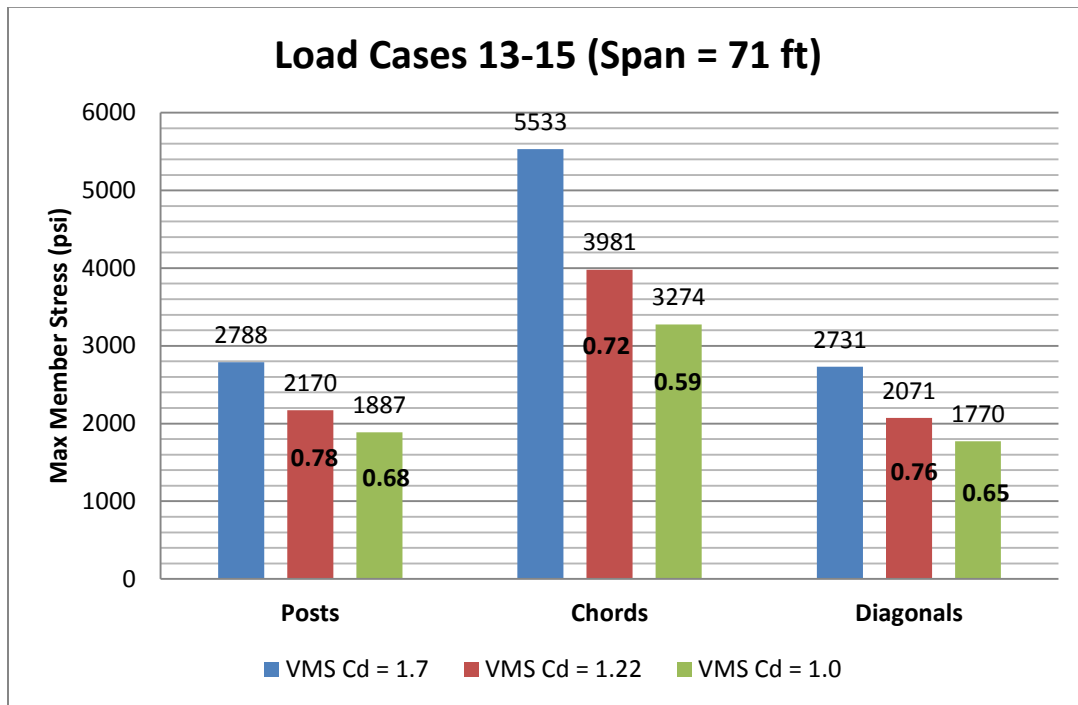


Figure 7-35: Max Connection Stresses for Load Cases 13-15 (Structure A)

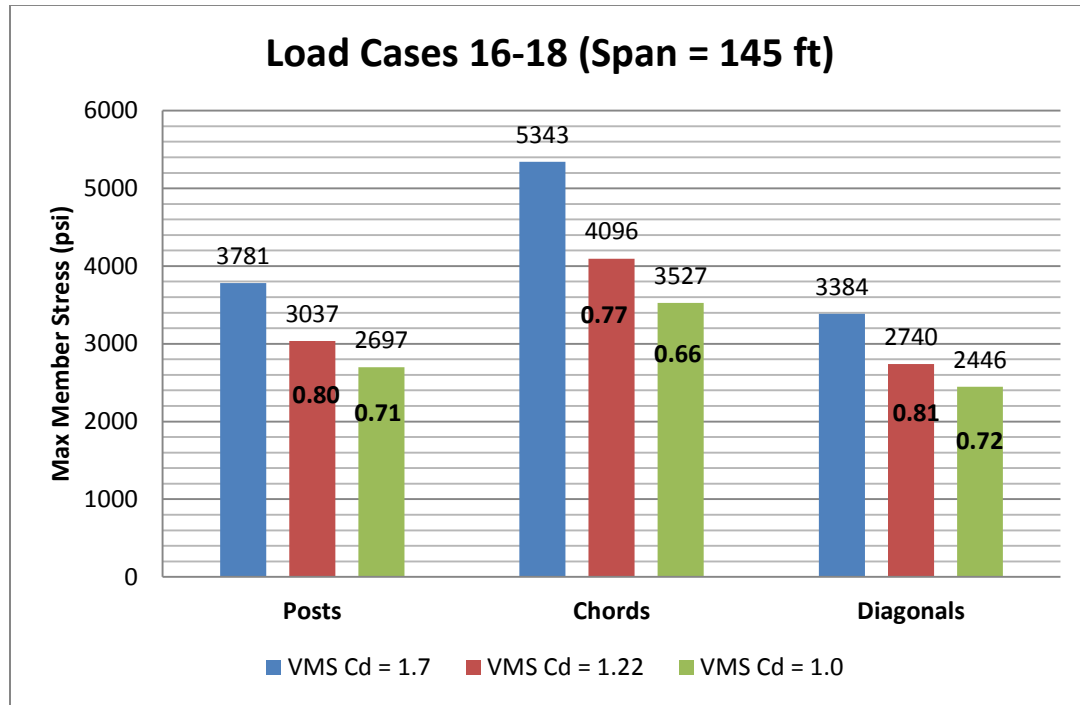


Figure 7-36: Max Connection Stresses for Load Cases 16-18 (Structure B)

7.4 Stress Reduction

7.4.1 Summary of Stress Ratios

The results of the sensitivity analysis were summarized using stress reduction ratios for the critical support members of the VMS structures under both extreme wind and fatigue wind loadings. The AASHTO load cases, with VMS drag coefficients of 1.7, were set as the control load cases. Thus, the stress reduction ratios were calculated by dividing the FIU stresses by the AASHTO stresses.

Table 7-16 shows the stress reduction ratios for the extreme wind load cases. The stress ratios for the support members are organized according to the parameters of the sensitivity study. The parameters for the extreme wind load cases included the VMS drag coefficient, the span of the structure, and the design wind speed. The extreme wind stress ratios were based on the overall maximum stresses in each type of support member

(upright posts, truss chords, and horizontal truss diagonals) due to the varying VMS drag coefficients.

Table 7-17 shows the stress reduction ratios for the fatigue wind load cases, which are also organized according to the parameters of the sensitivity study. The parameters for the fatigue wind load cases included the VMS drag coefficient and the span of the structure. The fatigue wind stress ratios were based on the overall maximum stresses at the fatigue connection locations due to the varying VMS drag coefficients.

Table 7-16: Stress Ratios for Extreme Wind (Load Cases 1-12)

EXTREME WIND					
Parameters			Stress Ratios (FIU stress / AASHTO stress)		
VMS Drag Coefficient	Structure (Span)	Design Wind Speed	Upright Posts	Truss Chords	Horizontal Truss Diagonals
Standard FIU $C_d = 1.22$	Structure A (71 ft)	90 mph	0.78	0.85	0.80
		150 mph	0.78	0.71	0.77
	Structure B (145 ft)	90 mph	0.84	0.88	0.86
		150 mph	0.82	0.81	0.83
Modified FIU $C_d = 1.00$	Structure A (71 ft)	90 mph	0.69	0.78	0.71
		150 mph	0.67	0.62	0.67
	Structure B (145 ft)	90 mph	0.77	0.82	0.79
		150 mph	0.73	0.73	0.75

Table 7-17: Stress Ratios for Fatigue Wind (Load Cases 13-18)

FATIGUE WIND				
Parameters		Stress Ratios (FIU stress / AASHTO stress)		
VMS Drag Coefficient	Structure (Span)	Fatigue Detail 5.4	Fatigue Detail 5.5	
		Base of Upright Posts	Truss Chords	Horizontal Truss Diagonals
Standard FIU $C_d = 1.22$	Structure A (71 ft)	0.78	0.72	0.76
	Structure B (145 ft)	0.80	0.77	0.81
Modified FIU $C_d = 1.00$	Structure A (71 ft)	0.68	0.59	0.65
	Structure B (145 ft)	0.71	0.66	0.72

7.4.2 Discussion of Stress Ratio Results

The stress ratio tables for extreme wind and fatigue wind show that reducing the VMS drag coefficient from 1.7 to 1.22 (for a standard VMS) or 1.0 (for a modified VMS) results in significant stress reductions in critical member supports and at fatigue connections. The amount of stress reduction for each type of support member or fatigue connection depends on the parameters of the sensitivity study.

7.4.2.1 Upright Posts

For the extreme wind load cases with a VMS drag coefficient of 1.22, the stress ratios of the upright posts ranged from 0.78 to 0.84. These stress ratios corresponded to stress reductions of 16% to 22% in the posts. For the extreme wind load cases with a VMS drag coefficient of 1.0, the stress ratios of the upright posts ranged from 0.67 to 0.77. These stress ratios corresponded to stress reductions of 23% to 33% in the posts. Thus, the smaller VMS drag coefficient for extreme wind resulted in greater stress reduction of the upright posts.

For the fatigue wind load cases with a VMS drag coefficient of 1.22, the stress ratios of the upright-to-base plate connections ranged from 0.78 to 0.80. These stress ratios corresponded to stress reductions of 20% to 22% at the post connections. For the fatigue wind load cases with a VMS drag coefficient of 1.0, the stress ratios of the upright-to-base plate connections ranged from 0.68 to 0.71. These stress ratios corresponded to stress reductions of 29% to 32% in the posts. Thus, the smaller VMS drag coefficient for fatigue wind resulted in greater stress reduction of the upright-to-base plate connections.

The upright posts experienced about the same level of stress reduction for both the extreme wind and fatigue wind load cases. However, the extreme wind load cases resulted in a larger range of stress reduction for the upright posts than the fatigue wind load cases. This was attributed in part to the additional variable of design wind speed for the extreme wind load cases.

7.4.2.2 Truss Chords

For the extreme wind load cases with a VMS drag coefficient of 1.22, the stress ratios of the truss chords ranged from 0.71 to 0.88. These stress ratios corresponded to stress reductions of 12% to 29% in the chords. For the extreme wind load cases with a VMS drag coefficient of 1.0, the stress ratios of the truss chords ranged from 0.62 to 0.82. These stress ratios corresponded to stress reductions of 18% to 38% in the chords. Thus, the smaller VMS drag coefficient for extreme wind resulted in greater stress reduction of the truss chords.

For the fatigue wind load cases with a VMS drag coefficient of 1.22, the stress ratios of the chords at the chord-to-web connections ranged from 0.72 to 0.77. These stress ratios corresponded to stress reductions of 23% to 28% in the chords. For the fatigue wind load cases with a VMS drag coefficient of 1.0, the stress ratios of the chords at the chord-to-web connections ranged from 0.59 to 0.66. These stress ratios corresponded to stress reductions of 34% to 41% in the chords. Thus, the smaller VMS drag coefficient for fatigue wind resulted in greater stress reduction of the chords at the chord-to-web connections.

The truss chords experienced slightly more stress reduction at the chord-to-web connections for the fatigue wind load cases than for the extreme wind load cases. Also,

the range of stress reduction of the chords was greater for extreme wind than for fatigue wind.

7.4.2.3 *Truss Diagonals*

For the extreme wind load cases with a VMS drag coefficient of 1.22, the stress ratios of the truss diagonals ranged from 0.77 to 0.86. These stress ratios corresponded to stress reductions of 14% to 23% in the diagonals. For the extreme wind load cases with a VMS drag coefficient of 1.0, the stress ratios of the truss diagonals ranged from 0.67 to 0.79. These stress ratios corresponded to stress reductions of 21% to 33% in the chords. Thus, the smaller VMS drag coefficient for extreme wind resulted in greater stress reduction of the truss diagonals.

For the fatigue wind load cases with a VMS drag coefficient of 1.22, the stress ratios of the diagonals at the chord-to-web connections ranged from 0.76 to 0.81. These stress ratios corresponded to stress reductions of 19% to 24% in the diagonals. For the fatigue wind load cases with a VMS drag coefficient of 1.0, the stress ratios of the diagonals at the chord-to-web connections ranged from 0.65 to 0.72. These stress ratios corresponded to stress reductions of 28% to 35% in the diagonals. Thus, the smaller VMS drag coefficient for fatigue wind resulted in greater stress reduction of the diagonals at the chord-to-web connections.

The truss diagonals experienced slightly more stress reduction at the chord-to-web connections for the fatigue wind load cases than for the extreme wind load cases. Also, the range of stress reduction of the chords was greater for extreme wind than for fatigue wind.

7.4.2.4 Member Comparisons

The upright posts, truss chords, and truss diagonals all experienced significant stress reductions due to the new VMS drag coefficients. Of these three types of members, the truss chords experienced the greatest range of stress reduction based on the parameters of the sensitivity study. The amount of stress reduction in the truss chords ranged from 12% to 38% for extreme wind and from 23% to 41% for fatigue wind. In addition, the truss chords experienced the highest potential for stress reduction of all three types of support members.

7.5 Analysis of Study Parameters

The stress reduction ratios were analyzed to determine the impact of the different parameters of the sensitivity study. This was done by varying a single parameter at a time while holding all others constant, and graphing the increase or decrease in the stress ratios of the upright posts, truss chords, and horizontal truss diagonals.

The first parameter examined was the span of the VMS structures. Figures 7-37, 7-38, and 7-39 show the effect of varying the structure span on the stress ratios for the upright posts, truss chords, and truss diagonals, respectively. Each figure contains six plots, all of which hold the wind speed and VMS drag coefficient constant while varying the structure span. The structure span is set as the independent variable and the stress ratio is set as the dependent variable. In each figure, the stress ratios increase with an increase in the structure span. Thus, increasing the structure span results in less stress reduction of the support members and fatigue connections.

The second parameter examined was the design wind speed. Figures 7-40, 7-41, and 7-42 show the effect of varying the wind speed on the stress ratios for the upright posts, truss chords, and truss diagonals, respectively. Each figure contains four plots, all of which hold the structure span and VMS drag coefficient constant while varying the wind speed (the fatigue load cases are not included since this parameter only applies to extreme wind). The wind speed is set as the independent variable and the stress ratio is set as the dependent variable. In each figure, the stress ratios decrease with an increase in the wind speed. Thus, increasing the design wind speed for a structure results in greater stress reduction of the support members.

The third and final parameter examined was the VMS drag coefficient. Figures 7-43, 7-44, and 7-45 show the effect of varying the VMS drag coefficient on the stress ratios for the upright posts, truss chords, and truss diagonals, respectively. Each figure contains six plots, all of which hold the structure span and wind speed constant while varying the VMS drag coefficient. The VMS drag coefficient is set as the independent variable and the stress ratio is set as the dependent variable. In each figure, the stress ratios increase with an increase in the VMS drag coefficient. Thus, increasing the VMS drag coefficient results in less stress reduction of the support members and fatigue connections.

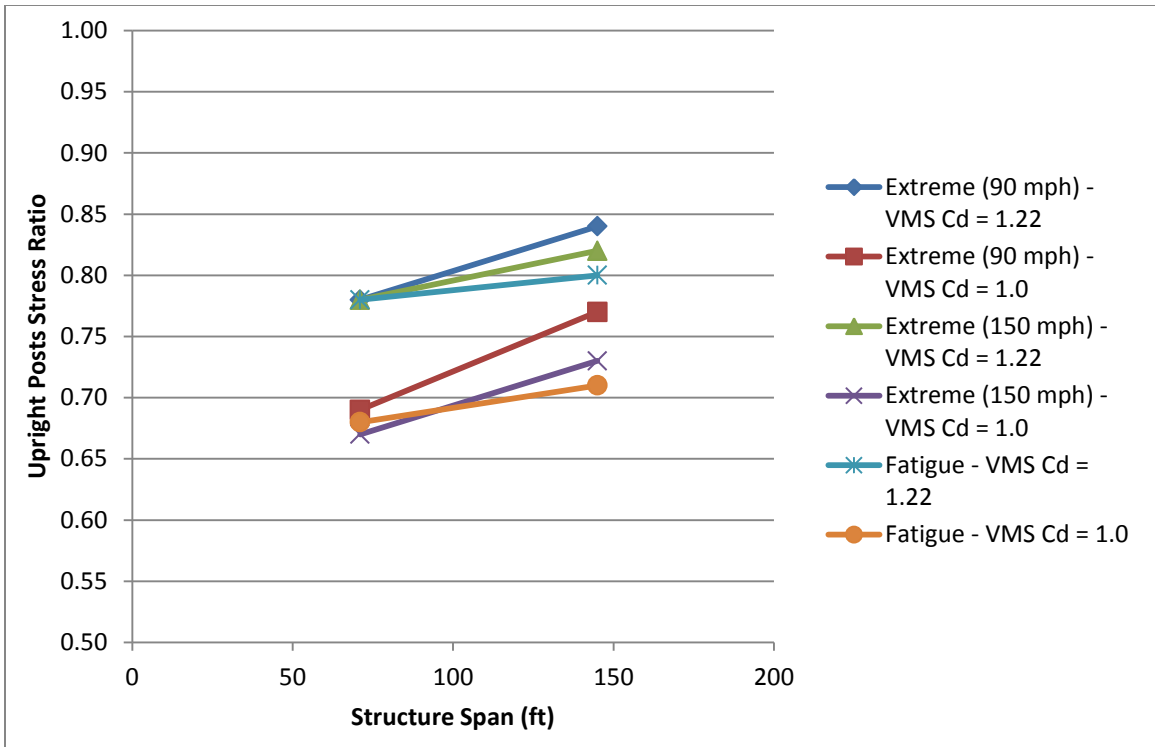


Figure 7-37: Effect of Structure Span on Stress Ratios for Upright Posts

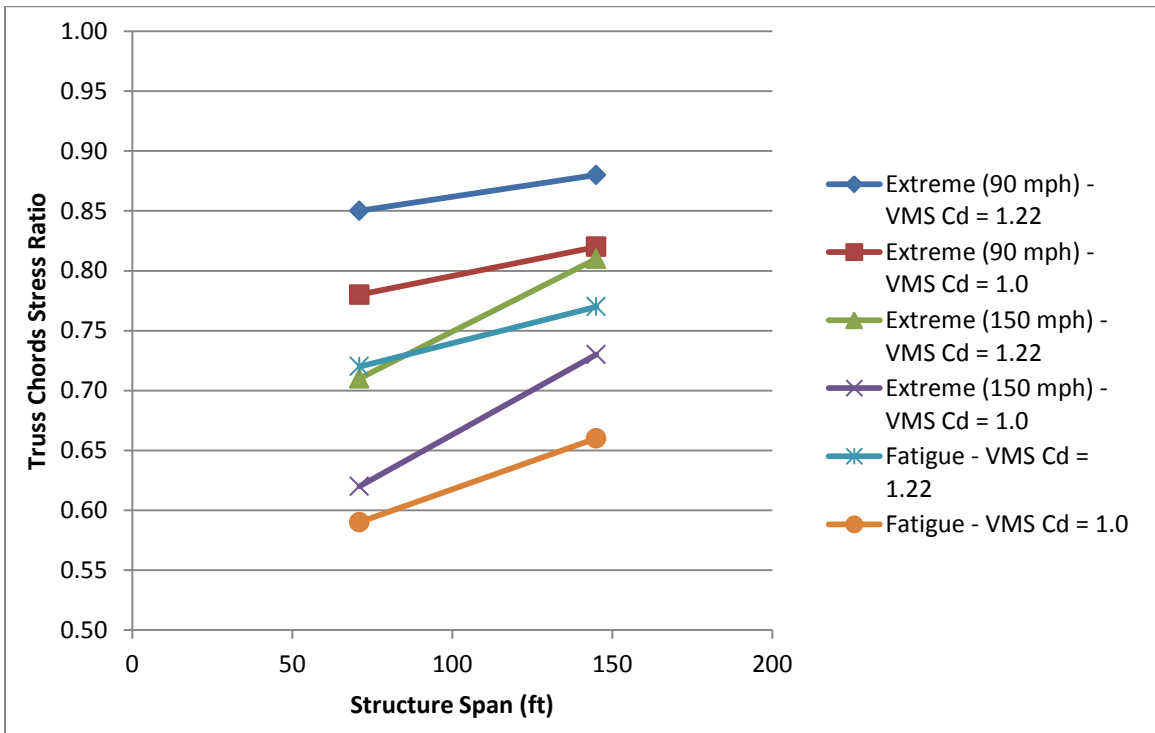


Figure 7-38: Effect of Structure Span on Stress Ratios for Truss Chords

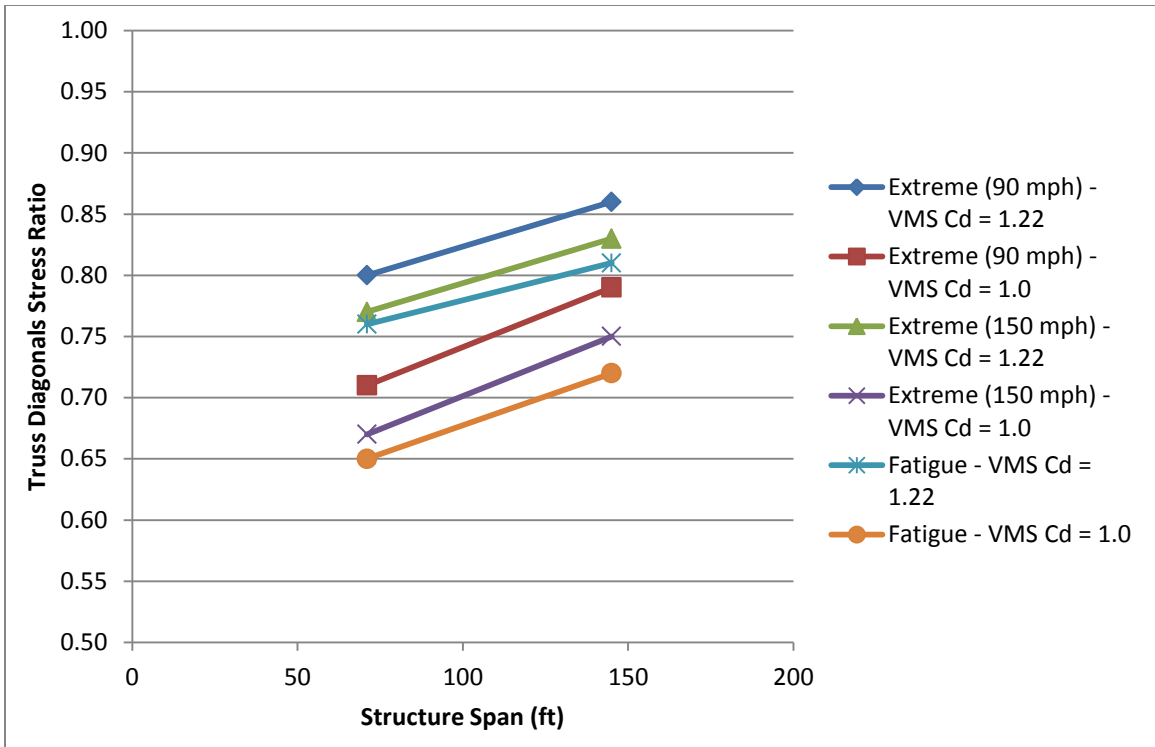


Figure 7-39: Effect of Structure Span on Stress Ratios for Truss Diagonals

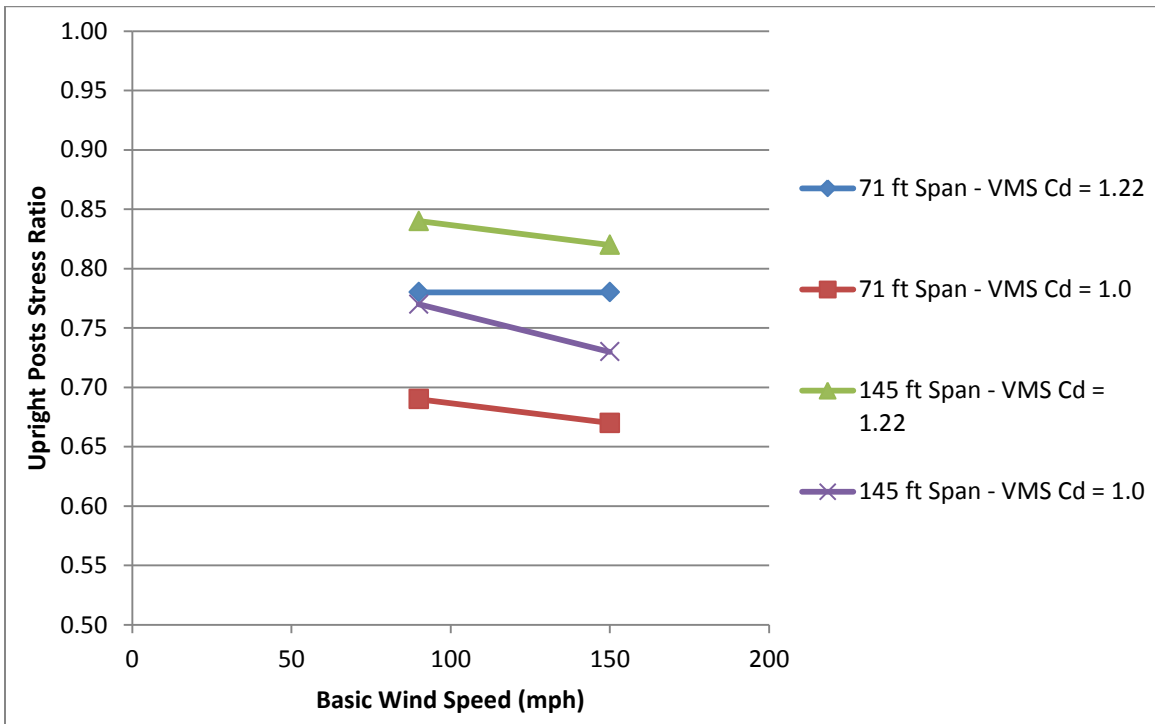


Figure 7-40: Effect of Wind Speed on Stress Ratios for Upright Posts

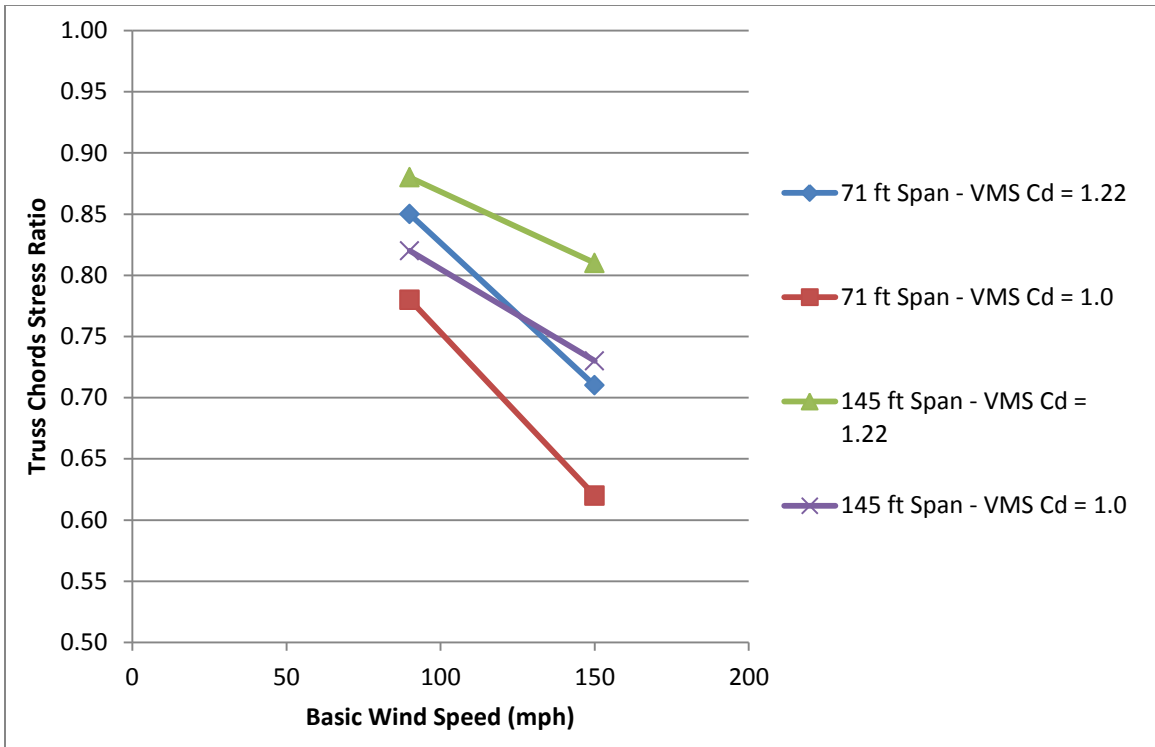


Figure 7-41: Effect of Wind Speed on Stress Ratios for Truss Chords

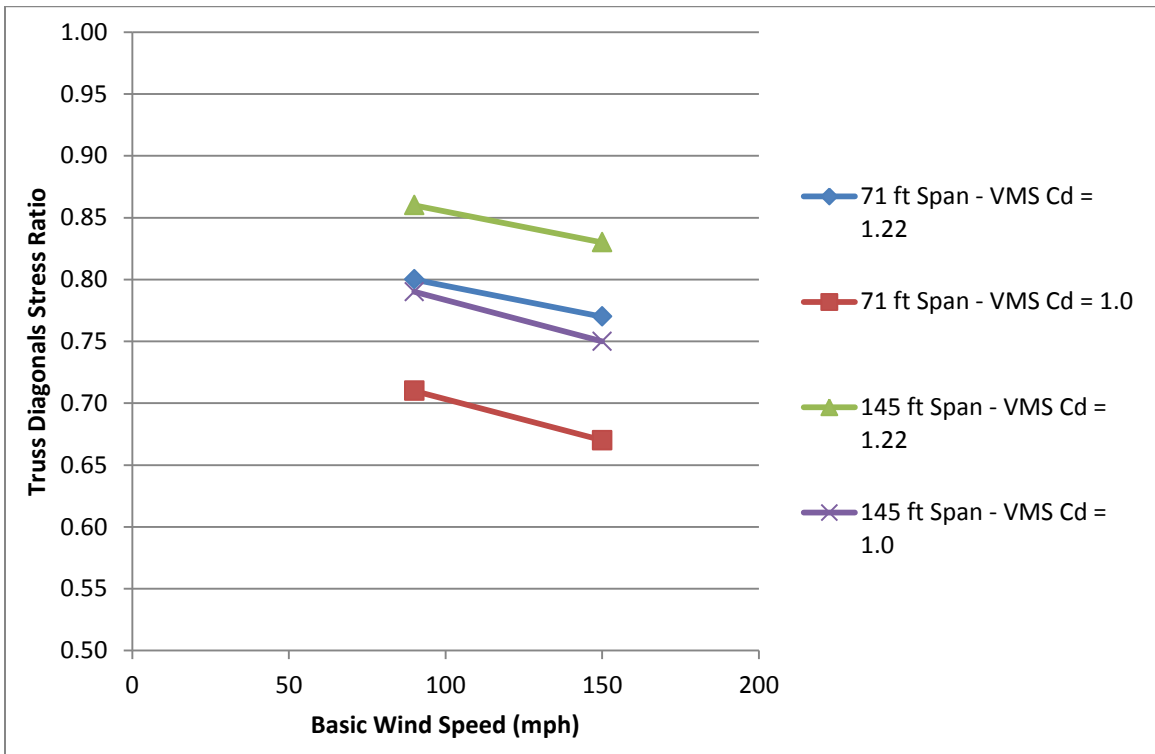


Figure 7-42: Effect of Wind Speed on Stress Ratios for Truss Diagonals

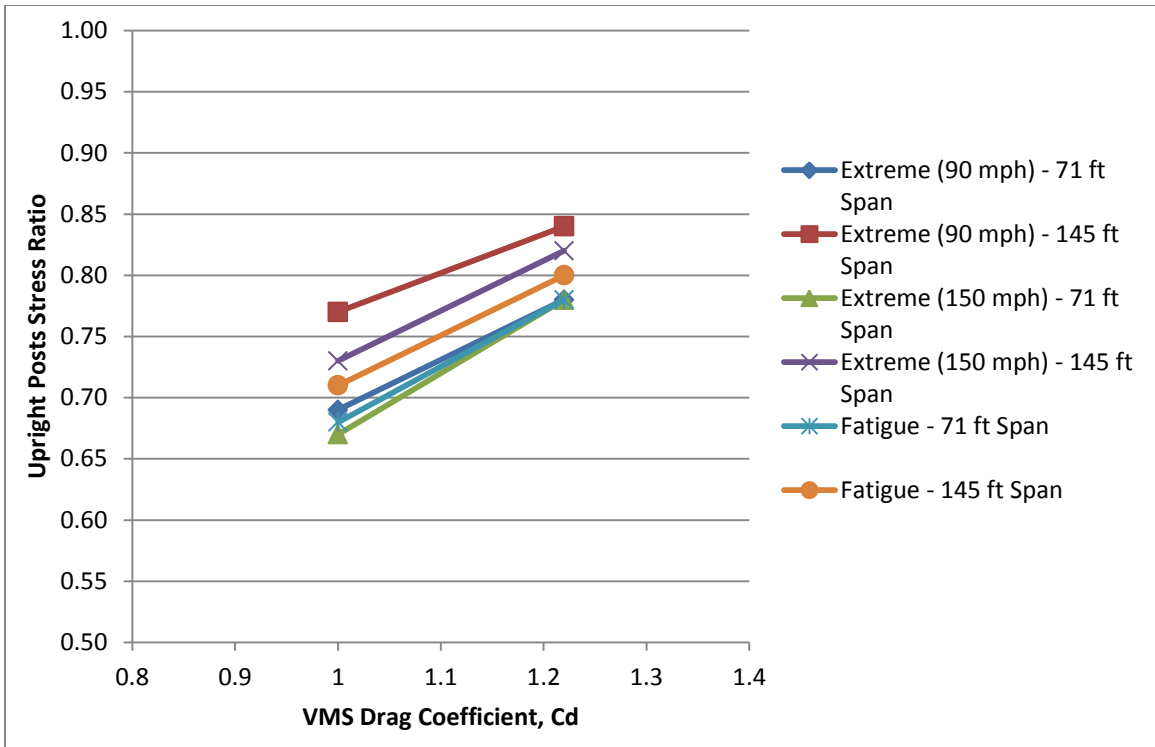


Figure 7-43: Effect of VMS Drag Coefficient on Stress Ratios for Upright Posts

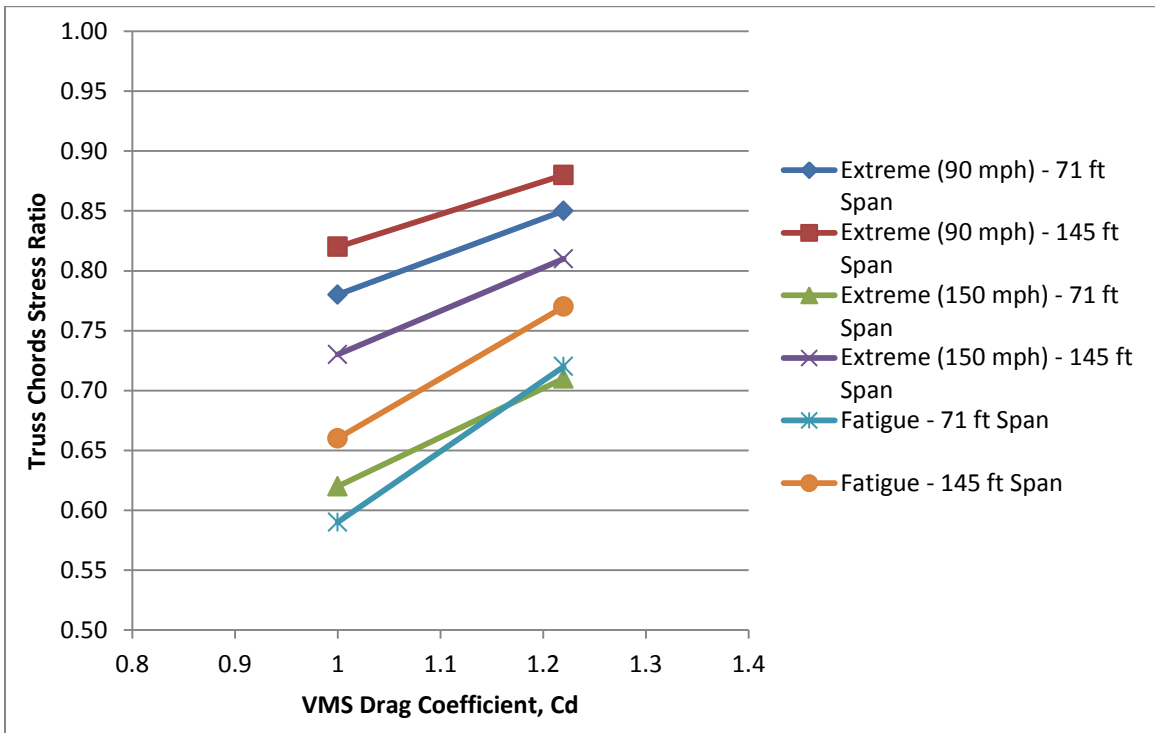


Figure 7-44: Effect of VMS Drag Coefficient on Stress Ratios for Truss Chords

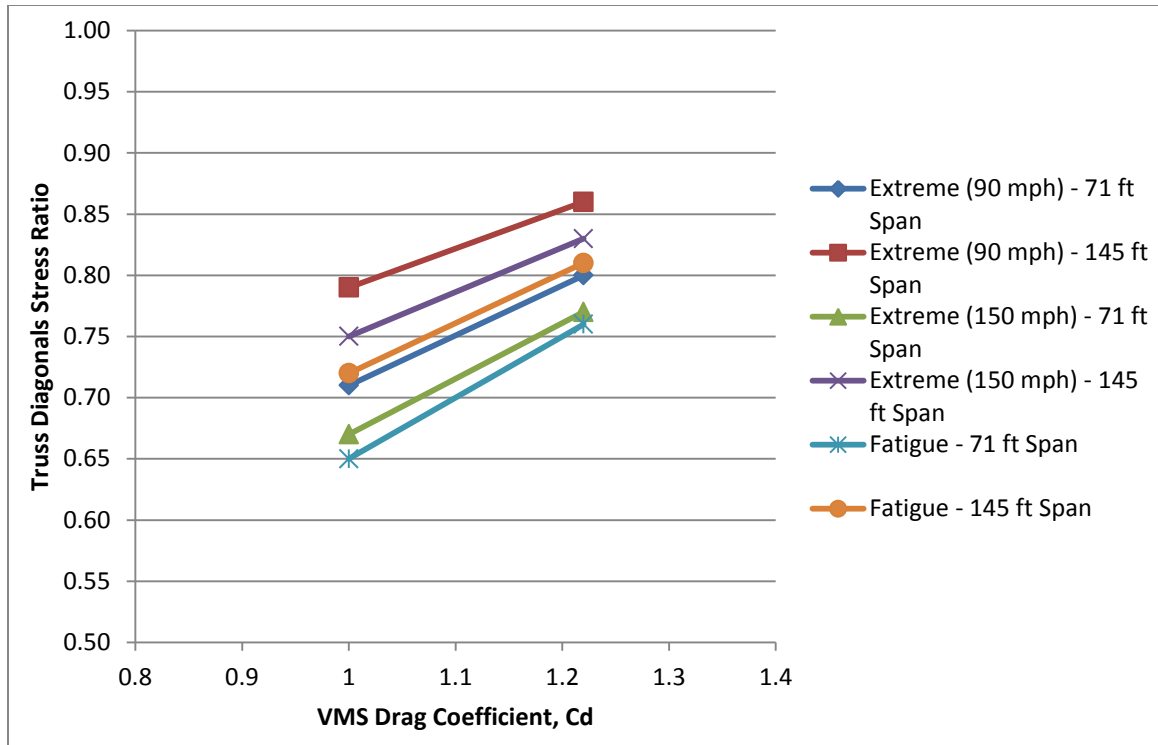


Figure 7-45: Effect of VMS Drag Coefficient on Stress Ratios for Truss Diagonals

7.6 Conclusions of Sensitivity Study

A sensitivity study was conducted to examine the impact of the newly developed VMS drag coefficients on the design of sign structures. Static analyses were performed in SAP to measure the stress response due to wind loadings with varying VMS drag coefficients. The stress response was examined in critical support members for extreme wind load cases and at critical connections for fatigue wind load cases. The study considered three different VMS drag coefficients: $C_d = 1.7$ from the AASHTO Supports Specifications, $C_d = 1.22$ for a standard VMS based on the FIU Wall of Wind testing, and $C_d = 1.0$ for a VMS with modified edges. Other parameters such as structure span and design wind speed were also analyzed.

Stress ratios were developed to quantify the impact of changing the VMS drag coefficients on the design of the sign support structure. These stress ratios were calculated using maximum stresses in the support members and at connection details. The stress ratios showed that the new VMS drag coefficients resulted in significant reduction of member and connection stresses.

For the extreme wind load cases, using a drag coefficient of 1.22 for a standard VMS resulted in member stress reductions ranging from 12 to 29%, while using a drag coefficient of 1.0 for a modified VMS resulted in member stress reductions ranging from 18 to 38%. These reductions in member stresses depended on a number of factors including structure span, design wind speed, and member type (post, chord, or diagonal).

For the fatigue wind load cases, using a drag coefficient of 1.22 for a standard VMS resulted in stress reductions at critical connections ranging from 19 to 28%, while using a drag coefficient of 1.0 for a modified VMS resulted in stress reductions ranging from 28 to 41%. These stress reductions at connection details depended on a number of factors including structure span and connection type (fatigue details 5.4 and 5.5).

The study also concluded that the level of stress reduction due to using the new VMS drag coefficients depends on the following parameters: structure span, design wind speed, and reduction of the drag coefficient. The study found that increasing the structure span will decrease the amount of stress reduction in the support members and connections. On the other hand, increasing the design wind speed for the structure will increase the amount of stress reduction. Finally, decreasing the drag coefficient will increase the amount of stress reduction in the support members and connections.

CHAPTER 8 PROPOSED CODE LANGUAGE AND COMMENTARY

8.1 Chapter Overview

This chapter presents the code language and commentary for incorporation of the proposed VMS drag coefficients into the AASHTO Supports Specifications.

8.2 Proposed Drag Coefficients for AASHTO Supports Specifications

We propose the following changes to the AASHTO Supports Specifications:

1. Remove the drag coefficient of 1.7 for Variable Message Signs (VMS) from Table 3.8.6-1 of the Specifications.
2. Add Table 8-1 to Section 3.8.6 of the Specifications.

Table 8-1: VMS Drag Coefficients, C_d

Aspect Ratio	Depth Ratio						
	0.1	0.2	0.3	0.4	0.5	0.6	0.7
1.0	1.21	1.18	1.15	1.12	1.08	1.04	0.98
2.0	1.21	1.20	1.18	1.17	1.14	1.11	1.09
3.0	1.22	1.22	1.22	1.21	1.20	1.18	1.16
4.0	1.25	1.25	1.24	1.24	1.23	1.22	1.21
5.0	1.28	1.27	1.26	1.25	1.24	1.23	1.22

8.3 Proposed Commentary for AASHTO Supports Specifications

The drag coefficients for Variable Message Signs (VMS) are organized according to aspect and depth ratios. The drag coefficient values were developed through experimental testing and analytical studies at Florida International University (FIU) and the University of Alabama at Birmingham (UAB).

Experimental testing was conducted at the FIU Wall of Wind facility to develop the proposed drag coefficients for VMS. The testing was performed on scaled models of VMS structures for both extreme level winds and fatigue level winds. The study concluded that the same drag coefficients should be used for both extreme wind design and fatigue wind design of VMS structures.

Analytical studies were conducted at UAB to verify the accuracy of the proposed drag coefficients and investigate the impact of the drag coefficients on the design of VMS structures. Finite element modeling was used to compare maximum stresses in VMS structures for the proposed drag coefficients versus the existing drag coefficient of 1.7 specified in Table 3.8.6-1 of the 2013 AASHTO Supports Specifications. The analyses showed potential stress reductions ranging from 12 to 29% for ultimate design of support members and 19 to 28% for fatigue design of critical connections as a result of using the proposed VMS drag coefficients.

The testing and analysis also showed that constructing VMS with rounded or chamfered edges has the potential to even further reduce the drag coefficients for VMS. The development of drag coefficients for VMS with rounded and chamfered edges can be considered for a future research study.

CHAPTER 9 CONCLUSIONS AND FUTURE RESEARCH

9.1 Chapter Overview

This chapter provides a summary of the conclusions from the Wall of Wind testing at FIU and the experimental and analytical studies conducted at UAB for the VMS project. In addition, recommendations for future research are discussed.

9.2 Summary of Findings

9.2.1 Wall of Wind Testing at FIU

Experimental testing was conducted at the FIU Wall of Wind facility to develop drag coefficients for VMS panels. Multiple models with varying aspect and depth ratios were constructed for testing. The models were tested at different wind speeds and directions of wind approach. The study also examined the effects of edge modifications (round and chamfered edges) on the reduction of the drag coefficient. Additional testing was performed to determine the effects of Reynolds number and wind driven rain on the models, as well as to investigate galloping potential.

The Wall of Wind testing yielded several findings regarding the dependency of the drag coefficient on the VMS size, shape, and orientation with respect to the wind direction. The testing demonstrated that the drag coefficient increases with increasing aspect ratio as the flow becomes more two-dimensional and the end effects are reduced. On the other hand, it was determined that the drag coefficient decreases with increasing

depth ratio due to the smaller wake region and reattachment of flow. In addition, the study showed that the drag coefficient is generally larger when the wind direction is normal to the front face of the VMS (0°) than when the wind direction is at an angle to the VMS ($\sim 45^\circ$).

The study also concluded that constructing VMS panels with round or chamfered edges instead of sharp edges would significantly decrease the magnitude of the drag coefficient. This development could potentially lead to economic savings in the design of sign support structures for VMS panels.

The Wall of Wind study also determined that the drag coefficient for VMS panels is not significantly affected by Reynolds number or wind driven rain. However, it was observed that VMS panels could be susceptible to galloping for certain configurations.

The results of the Wall of Wind study were generally in good agreement with the research findings of previous studies on drag coefficients for signs. It was also determined that the drag coefficient value of 1.7 for the design of VMS panels in the current ASSHTO Supports Specifications is too conservative. A summary table listing drag coefficient values for VMS panels based on aspect and depth ratios was provided for consideration.

9.2.2 Drag Coefficient Verification Study at UAB

A study was conducted at UAB to verify the VMS drag coefficient results from the FIU Wall of Wind testing. The study compared experimental field data collected from a VMS structure in Alabaster, AL (Structure A) as part of a previous ALDOT study to analytical results obtained from a SAP model of the structure. Two VMS drag coefficients were used in the analysis: $C_d = 1.22$ from the FIU Wall of Wind testing and

$C_d = 1.7$ from the AASHTO Supports Specifications. The drag coefficients were based on the dimensions of the VMS sign panel.

Plots of quasi-static stress range versus average wind velocity were created for several locations on two upright posts of Structure A. The plots showed that the VMS drag coefficient from the FIU Wall of Wind testing accurately modeled the behavior of the sign structure under fatigue level winds, while the VMS drag coefficient from the AASHTO Supports Specifications was too conservative. Thus, the study concluded that the drag coefficient results from the FIU Wall of Wind testing are relatively accurate and should be considered for incorporation into the AASHTO Supports Specifications.

9.2.3 Sensitivity Study at UAB

A sensitivity study was conducted at UAB to examine the impact of the newly developed VMS drag coefficients on the design of sign structures. Two VMS structures with different span lengths (Structures A and B) were analyzed during the sensitivity study. Static analyses were performed in SAP to measure the stress response due to wind loadings with varying VMS drag coefficients. The stress response was examined in critical support members for extreme wind load cases and at critical connections for fatigue wind load cases. The study considered three different VMS drag coefficients: $C_d = 1.7$ from the AASHTO Supports Specifications, $C_d = 1.22$ for a standard VMS based on the FIU Wall of Wind testing, and $C_d = 1.0$ for a VMS with modified edges. Other parameters such as structure span and design wind speed were also analyzed.

Stress ratios were developed to quantify the impact of changing the VMS drag coefficients on the design of the sign support structure. These stress ratios were calculated using maximum stresses in the support members and at connection details.

The stress ratios showed that the new VMS drag coefficients resulted in significant reduction of member and connection stresses.

For the extreme wind load cases, using a drag coefficient of 1.22 for a standard VMS resulted in member stress reductions ranging from 12 to 29%, while using a drag coefficient of 1.0 for a modified VMS resulted in member stress reductions ranging from 18 to 38%. These reductions in member stresses depended on a number of factors including structure span, design wind speed, and member type (post, chord, or diagonal).

For the fatigue wind load cases, using a drag coefficient of 1.22 for a standard VMS resulted in stress reductions at critical connections ranging from 19 to 28%, while using a drag coefficient of 1.0 for a modified VMS resulted in stress reductions ranging from 28 to 41%. These stress reductions at connection details depended on a number of factors including structure span and connection type (fatigue details 5.4 and 5.5).

The study also concluded that the level of stress reduction due to using the new VMS drag coefficients depends on the following parameters: structure span, design wind speed, and reduction of the drag coefficient. The study found that increasing the structure span will decrease the amount of stress reduction in the support members and connections. On the other hand, increasing the design wind speed for the structure will increase the amount of stress reduction. Finally, decreasing the drag coefficient will increase the amount of stress reduction in the support members and connections.

9.3 Recommendations for Future Research

The research performed for the VMS project was limited to the scope of the study. However, the research findings led to other points of study which can be

considered for future research. Recommendations for future research based on the findings of the VMS project are provided below:

- More extensive testing and analysis can be performed to further investigate the impact of using rounded and chamfered edge modifications on VMS. Further study could lead to new drag coefficients for round and chamfer edge applications which could be incorporated in the AASHTO Supports Specifications.
- More extensive experimental testing of full-scale VMS structures can be conducted to further analyze the behavior of the structures for different wind conditions. The amount of experimental data used for the drag coefficient verification study was limited due to the low wind speeds and varying wind directions measured. Further experimental testing could attempt to collect data during higher wind intervals.
- Wind tunnel testing can be performed for full-scale VMS structures to analyze the behavior of the structures under extreme wind loading conditions. This would require a very large wind testing facility to accommodate the size of full-scale structures.

LIST OF REFERENCES

- AASHTO. *Standard Specifications for Structural Supports for Highway Signs, Luminaires, and Traffic Signals*. 6th Edition. Washington, D.C.: American Association of State Highway and Transportation Officials, 2013.
- Abdalla, Ramy. "Fatigue Resistant Design of Noncantilevered Sign Support Structures." Thesis, University of Alabama at Birmingham, 2000.
- Computers and Structures, Inc. *CSI Analysis Reference Manual*. Berkeley, CA, 2011.
- Cook, R. A., D. Bloomquist, A. M. Agosta, and A. F. Taylor. "Wind Load Data for Variable Message Signs." Report Number 0728-9488, Florida Department of Transportation, 1996.
- Davenport, A. G. "The Spectrum of Horizontal Gustiness Near the Ground in High Winds." Department of Civil Engineering, University of Bristol, 1960.
- DelGrego, M. and J. T. DeWolf. "Field Monitoring and Evaluation for Sign Support Structures Subject to Dynamic Loads." University of Connecticut, 2003.
- Dexter, R. J. and M. J. Ricker. *Fatigue-Resistant Design of Cantilevered Signal, Sign, and Light Supports*. NCHRP Report 469, The Transportation Research Board, Washington, D.C.: National Academy Press, 2002.
- Fisher, J. W., A. Nussbaumer, P. B. Keating, and B. T. Yen. *Resistance of Welded Details Under Variable Amplitude Long-Life Fatigue Loading*. NCHRP Report 354, Transportation Research Board, National Academy Press, 1993.
- Foley, C. M., S. J. Ginal, J. L. Peronto, and R. A. Fournelle. "Structural Analysis of Sign Bridge Structures and Luminaire Supports." WHRP Report No. 04-03, Wisconsin Department of Transportation, 2004.
- Fouad, F. H. and E. Calvert. "AASHTO 2001 Design of Overhead Cantilevered Sign Supports." UTCA Report Number 02216, University Transportation Center for Alabama, 2004.
- Fouad, F. H. and E. Calvert. "Design of Cantilevered Overhead Sign Supports." *Transportation Research Record*, no. Issue No. 1928 (2005): 39-47.

- Fouad, F. H. and E. Calvert. "Evaluating the Design Safety of Highway Structural Supports." UTCA Report Number 00218, University Transportation Center for Alabama, 2001.
- Fouad, F. H. and E. Calvert. "New Wind Design Criteria for Traffic Signal Support Structures." UTCA Report 04219, University Transportation Center for Alabama, 2005.
- Fouad, F. H. and I. E. Hosch. *Design of Overhead VMS Structures for Fatigue Loads*. UTCA Report Number 09203, University Transportation Center for Alabama, 2011.
- Fouad, F. H. et al. "Structural Supports for Highway Signs, Luminaires, and Traffic Signals." NCHRP Report 494, The Transportation Research Board, Washington, D.C., 2003.
- Foutch, D. A., J. A. Rice, J. M. LaFave, S. Valdovinos, and T. W. Kim. "Evaluation of Aluminum Highway Sign Trusses and Standards for Wind and Truck Gust Loadings." Physical Research Report No. 153, Illinois Department of Transportation, Bureau of Materials and Physical Research, 2006.
- Fu, T., A. M. Aly, A. G. Chowdhury, G. Bitsuamlak, D. Yeo, and E. Simiu. "A Proposed Technique for Determining Aerodynamic Pressures on Residential Homes." *Wind and Structures* 12, no. 1 (2012): 27-41.
- Gilani, A. S., J. W. Chavez, and A. S. Whittaker. *Fatigue Life Evaluation of Changeable Message Sign Structures*. University of California at Berkeley, Earthquake Engineering Research Center, 1997.
- Ginal, Scott. "Fatigue Performance of Full-Span Sign Support Structures Considering Truck-Induced Gust and Natural Wind Pressures." Thesis, Marquette University, 2003.
- Ginger, J. D., G. F. Reardon, and B. L. Langtree. "Winds Loads on Fences and Hoardings." Technical Report No 47, James Cook University, 1998.
- Hosch, I. E. and F. H. Fouad. "Fatigue Design of Sign Support Structures for Loading Caused by Natural Wind Loads." *Transportation Research Record*, no. Issue No. 2131 (2009): 15-22.
- Hosch, I. E. *Design of Highway Overhead Cantilever-Type Sign Support Structures for Fatigue Loads*. Dissertation, Ann Arbor, MI: ProQuest LLC, 2010.
- Irvine, Tom. "An Introduction to Random Vibration - Revision B." 2000.
- Irvine, Tom. "Power Spectral Density Units - Revision A." 2000.
- Irvine, Tom. "The Fourier Series of a Rectangular Wave - Revision A." 2005.

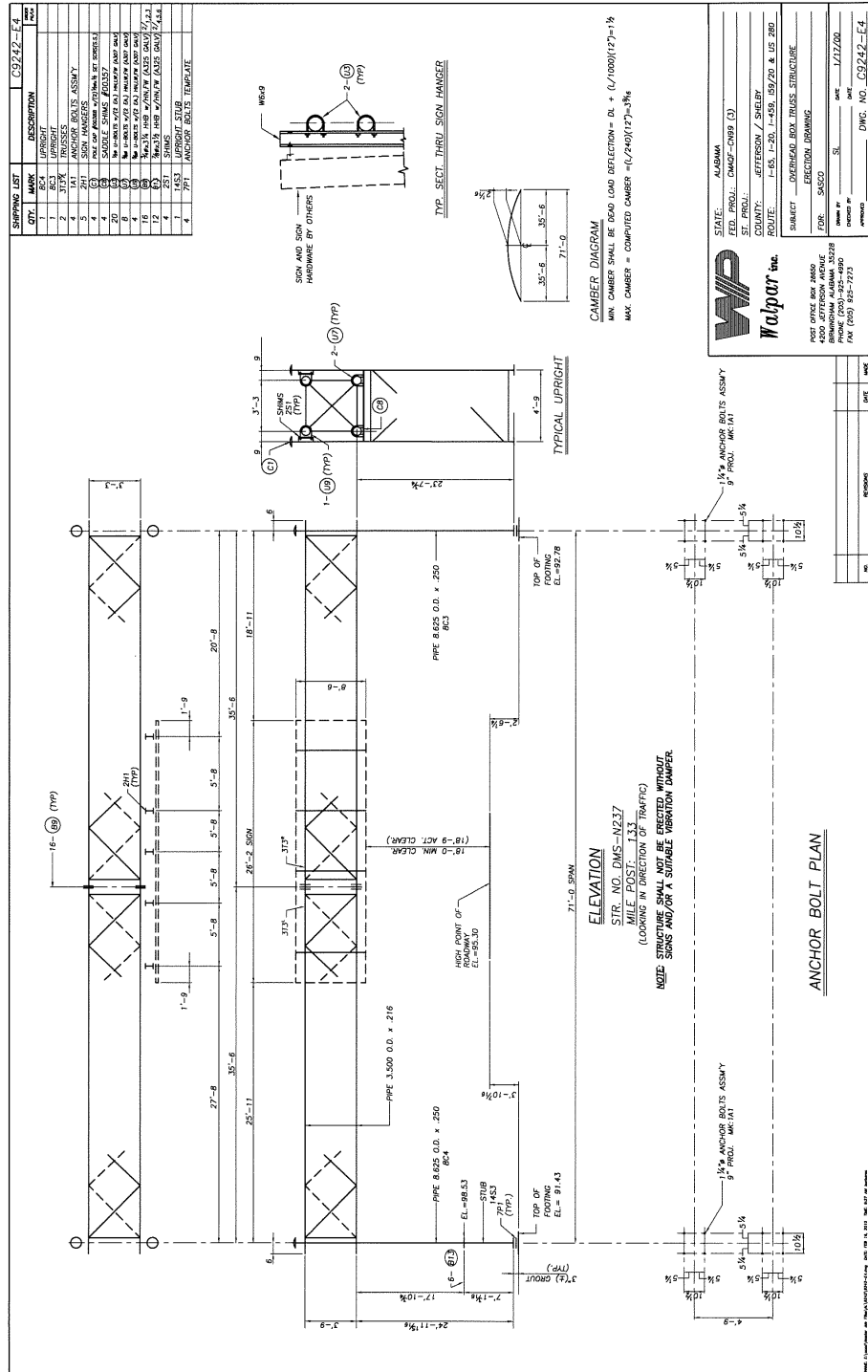
- Irwin, P. A. "Bluff Body Aerodynamics in Wind Engineering." *Journal of Wind Engineering and Industrial Aerodynamics*, no. 96 (2008): 701-712.
- Johns, K. W. and R. J. Dexter. *Fatigue Related Wind Loads on Highway Support Structures*. Lehigh University, ATLSS Reports, 1998.
- Kaczinski, M. R. et al. "Fatigue-Resistant Design of Cantilevered Signal, Sign and Light Supports." NCHRP Report 412, 1998.
- Larose, G. L. and A. D'Auteuil. "Experiments on 2D Rectangular Prisms at High Reynolds Numbers in a Pressurised Wind Tunnel." *Journal of Wind Engineering and Industrial Aerodynamics*, no. 96 (2008): 923-933.
- Larose, G. L. and A. D'Auteuil. "On the Reynolds Number Sensitivity of the Aerodynamics of Bluff Bodies with Sharp Edges." *Journal of Wind Engineering and Industrial Aerodynamics*, no. 94 (2006): 365-376.
- Letchford, C. W. "Wind Loads on Rectangular Signboards and Hoardings." *Journal of Wind Engineering and Industrial Aerodynamics*, no. 89 (2001): 135-151.
- McDonald, J. R., K. C. Mehta, W. Oler, and N. Pulipaka. "Wind Load Effects on Signs, Luminaires, and Traffic Signal Structures." Wind Engineering Research Center, Texas Tech University, 1995.
- McLean, T. W., J. S. Park, and J. M. Stallings. "Fatigue Evaluation of Two Variable Message Sign Structures." Final Report, The Alabama Department of Transportation, Montgomery, AL, 2004.
- Meyer, Debbie. "Aerodynamic Testing of Variable Message Signs." Dissertation (Draft), Florida International University, Miami, FL, 2014.
- Munshi, S. R., V. J. Modi, and T. Yokomizo. "Aerodynamics and Dynamics of Rectangular Prisms with Momentum Injection." *Journal of Fluids and Structures*, no. 11 (1997): 873-892.
- Munshi, S. R., V. J. Modi, and T. Yokomizo. "Fluid Dynamics of Flat Plates and Rectangular Prisms in the Presence of Moving Surface Boundary-layer Control." *Journal of Wind Engineering and Industrial Aerodynamics*, no. 79 (1999): 37-60.
- Park, J. S., T. W. McLean, and M. Stallings. "Wind-Induced Fatigue of VMS Sign Structures." *Building on the Past*, 2004: 407-411.
- Quinn, A. D., C. J. Baker, and N. G. Wright. "Wind and Vehicle Induced Forces on Flat Plates - Part 1: Wind Induced Force." *Journal of Wind Engineering and Industrial Aerodynamics*, no. 89 (2001): 817-829.

- Rice, J. A., D. A. Foutch, J. M. LaFave, and S. Valdovinos. "Field Testing and Analysis of Aluminum Highway Sign Trusses." *Engineering Structures*, no. 34 (2012): 173-186.
- Simiu, E. and R. H. Scanlan. *Wind Effects on Structures*. 2nd Edition. New York: Wiley-Interscience, 1986.
- Smith, D. A., D. Zuo, K. C. Mehta. "Characteristics of Wind Induced Net Force and Torque on a Rectangular Sign Measured in the Field." *Journal of Wind Engineering and Industrial Aerodynamics*, no. 133 (2014): 80-91.
- South, J. M. "Fatigue Analysis of Overhead Sign and Signal Structures." Physical Research Report No. 115, Illinois Department of Transportation, 1994.
- Yu, D. and A. Kareem. "Parametric Study of Flow Around Rectangular Prisms Using LES." *Journal of Wind Engineering and Industrial Aerodynamics*, no. 77&78 (1998): 653-662.
- Zalewski, B. and A. Huckelbridge. "Dynamic Load Environment of Bridge-Mounted Sign Support Structures." Report No. ST/SS/05-002, Office of Research and Development, Ohio Department of Transportation, 2005.
- Zuo, D., D. A. Smith, and K. C. Mehta. "Benchmark Wind Tunnel Study of Wind Loading on Rectangular Sign Structures." *The Seventh International Colloquium on Bluff Body Aerodynamics and Applications*. Shanghai, China, 2012.
- Zuo, D., D. A. Smith, and K. C. Mehta. "Experimental Study of Wind Loading of Rectangular Sign Structures." *Journal of Wind Engineering and Industrial Aerodynamics*, no. 130 (2014): 62-74.

APPENDIX A

SHOP DRAWINGS OF VMS STRUCTURES

Structure A – Alabaster VMS Structure



POLE CAPS
(ALUM 355-F)

PART NO.	REMARKS	QTY.	ADV. BILL
00386	1/2" O.D. 180° APART	55	1/2

U-BOLTS

MARK	QTY.	DIA.	"A"	"B"	RADIUS	THRD.	MATERIAL	ADV. BILL
U3	80	3/8	3 3/4	2 3/8	2 3/8	2	A307	3/2, 3.4
U4	160	1/2	4 3/8	3 3/8	3 3/8	2	A307	3/2, 3.4
U5	40	5/8	5 1/4	4 1/8	4 1/8	2	A307	3/2, 3.4
U6	32	3/4	5 3/8	4 1/8	4 1/8	2	A307	3/2, 3.4
U7	16	7/8	5 3/4	4 1/8	4 1/8	2	A307	3/2, 3.4
U8	16	1	5 3/4	4 1/8	4 1/8	2	A307	3/2, 3.4
U9	16	1 1/8	5 3/4	4 1/8	4 1/8	2	A307	3/2, 3.4
U10	16	1 1/4	5 3/4	4 1/8	4 1/8	2	A307	3/2, 3.4
U11	16	1 3/8	5 3/4	4 1/8	4 1/8	2	A307	3/2, 3.4
U12	16	1 1/2	5 3/4	4 1/8	4 1/8	2	A307	3/2, 3.4
U13	8	1 5/8	5 3/4	4 1/8	4 1/8	2	A307	3/2, 3.4

SADDLE SHIM DETAIL
(ALUM 355-F)

PART NO.	"A"	"B"	"C"	"D"	"E"	"F"	"G"	REMARKS	QTY.	ADV. BILL
00389	6	2	1/2	2 3/4	1 3/4	1 3/4	1 3/4	1/2 O.D.	12	1/2
00387	6	3	1 1/2	1 1/2	1 1/2	1 1/2	1 1/2	1 1/2 O.D.	18	1/2
00388	6	5	2 1/2	1 1/2	2 1/2	2 1/2	2 1/2	1 1/2 O.D.	18	1/2

ANCHOR BOLTS ASSYS
(SEE CHART FOR MARKS)

MARK	QTY.	"A"	"B"	"C"	"D"	"E"	"F"	"G"	REMARKS
1A1	56	1-3/4	7	1-1/2	10	10	10	10	1/2" P.F.R. & A.B.

CS242-1

ANCHOR BOLTS ASSYS
(SEE CHART FOR MARKS)

MARK	QTY.	"A"	"B"	"C"	"D"	"E"	"F"	"G"	REMARKS
1A1	56	1-3/4	7	1-1/2	10	10	10	10	1/2" P.F.R. & A.B.

WALPART INC.

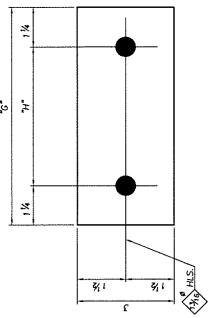
STATE: ALABAMA
 FED. PROJ.: CMDF-089 (3)
 ST. PROJ.: JEFFERSON/SHELBY
 COUNTY: JEFFERSON/SHELBY
 ROUTE: I-65-201-458-59/29 & US 290

SUBJECT: SIGN STRUCTURES
 MSC: DETAILS
 FOR: SASSO
 DRAWN BY: MRF
 DATE: 1/18/00
 CHECKED BY: MRF
 DATE: 1/18/00
 APPROVED: MRF
 DATE: 1/18/00

POST OFFICE BOX 2860
 4700 JEFFERSON AVENUE
 MOBILE, ALABAMA 36688-2860
 Phone: (205) 325-4400
 Fax: (205) 325-7723

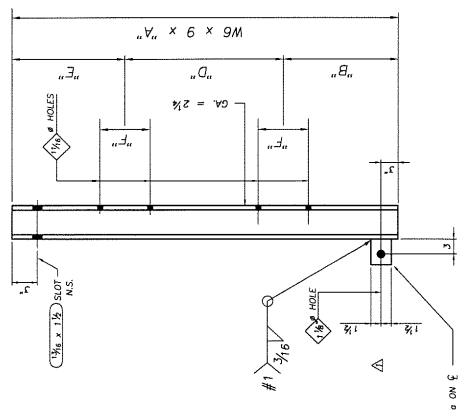
C9242-2

MARK	QTY	DESCRIPTION OF MATERIAL	UNIT
ZH1	20	W	6
ZH2	40	6" x 3"	6
ZH3	5		6
ZH4	5		6
ZH5	5		6
ZH6	5		6
ZH7	5		6
ZH8	5		6
ZH9	5		6
ZH10	5		6
ZH11	5		6
ZH12	5		6
ZH13	5		6
ZH14	5		6
ZH15	5		6
ZH16	5		6
ZH17	5		6
ZH18	5		6
ZH19	5		6
ZH20	5		6
ZH21	5		6
ZH22	5		6
ZH23	5		6
ZH24	5		6
ZH25	5		6
ZH26	5		6
ZH27	5		6
ZH28	5		6
ZH29	5		6
ZH30	5		6
ZH31	5		6
ZH32	5		6
ZH33	5		6
ZH34	5		6
ZH35	5		6
ZH36	5		6
ZH37	5		6
ZH38	5		6
ZH39	5		6
ZH40	5		6
ZH41	5		6
ZH42	5		6
ZH43	5		6
ZH44	5		6
ZH45	5		6
ZH46	5		6
ZH47	5		6
ZH48	5		6
ZH49	5		6
ZH50	5		6



SHIM PLATES

MARK	QTY	SIZE	THICKNESS
ZS1	16	6" x 3"	1/8"
ZS2	32	7" x 3"	1/8"
ZS3	8	8" x 3"	1/8"



SIGN HANGER

MARK	QTY	A"	B"	C"	D"	E"	F"
ZH1	20	8"-6"	2"-4 1/2"	3"-9"	2"-4 1/2"	2"-4 1/2"	4 1/8"
ZH2	40	8"-6"	2"-4 1/2"	3"-9"	2"-4 1/2"	2"-4 1/2"	5 1/8"
ZH3	5	8"-6"	2"-3"	4"-0"	2"-3"	2"-3"	6 1/8"
ZH4	5	8"-6"	1"-9"	5"-0"	1"-9"	1"-9"	6 1/8"

MATERIAL SPECS.
 ALL METL. - ASTM A36
 GALV. AFTER FAB.
 HANGERS PER 01.1 - 1969 & ASHFD 1961
 HOLES SHALL BE 1/8"

REF. E1-E14



POST OFFICE BOX 1800
 BRUNSWICK, ALABAMA 35208
 PHONE (205) 835-4990
 FAX (205) 835-7313

STATE: ALABAMA
 FED. PROJ.: CM07-089 (3)
 ST. PROJ.:
 COUNTY: LEEFLOSW/SHELBY
 ROUTE: I-65-201-491-59/29 & US 280

SUBJECT: SIGN STRUCTURE

FOR: SASSO

DATE: 1/18/00
 DRAWN BY: JPT
 APPROVED: JPT

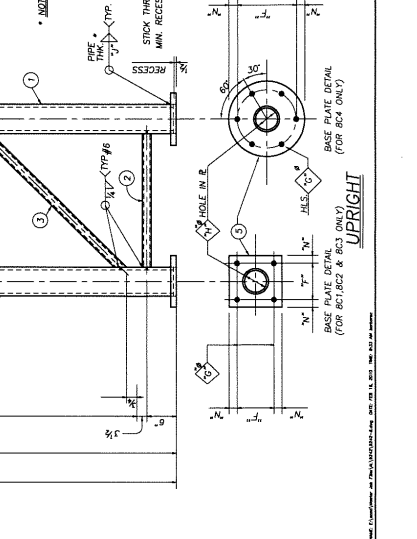
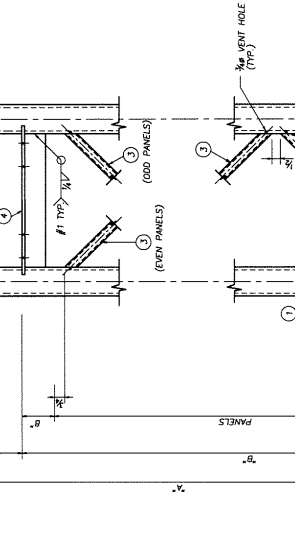
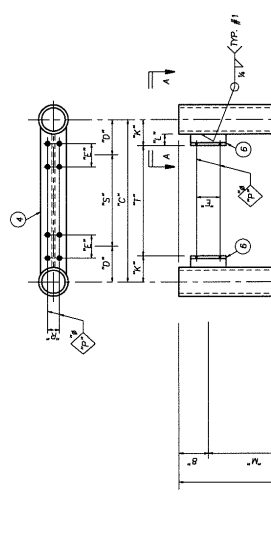
DWG. NO.: C9242-2

NO.	REV. PLATE	DATE	BY	CHK	APP
1		1/18/00	JPT	JPT	

CG242-B

MARK	QTY	DESCRIPTION OF MATERIAL	UNIT	QTY
B01	1	PIPE 8.625 x .250	UPRIGHT	28
B02	1	PIPE 1.900 x .145		4
B03	1	PIPE 1.900 x .145		5
B04	1	PIPE 1.900 x .145		5
B05	1	PIPE 1.900 x .145		5
B06	1	PIPE 1.900 x .145		5
B07	1	PIPE 1.900 x .145		5
B08	1	PIPE 1.900 x .145		5
B09	1	PIPE 1.900 x .145		5
B10	1	PIPE 1.900 x .145		5
B11	1	PIPE 1.900 x .145		5
B12	1	PIPE 1.900 x .145		5
B13	1	PIPE 1.900 x .145		5
B14	1	PIPE 1.900 x .145		5
B15	1	PIPE 1.900 x .145		5
B16	1	PIPE 1.900 x .145		5
B17	1	PIPE 1.900 x .145		5
B18	1	PIPE 1.900 x .145		5
B19	1	PIPE 1.900 x .145		5
B20	1	PIPE 1.900 x .145		5
B21	1	PIPE 1.900 x .145		5
B22	1	PIPE 1.900 x .145		5
B23	1	PIPE 1.900 x .145		5
B24	1	PIPE 1.900 x .145		5
B25	1	PIPE 1.900 x .145		5
B26	1	PIPE 1.900 x .145		5
B27	1	PIPE 1.900 x .145		5
B28	1	PIPE 1.900 x .145		5
B29	1	PIPE 1.900 x .145		5
B30	1	PIPE 1.900 x .145		5
B31	1	PIPE 1.900 x .145		5
B32	1	PIPE 1.900 x .145		5
B33	1	PIPE 1.900 x .145		5
B34	1	PIPE 1.900 x .145		5
B35	1	PIPE 1.900 x .145		5
B36	1	PIPE 1.900 x .145		5
B37	1	PIPE 1.900 x .145		5
B38	1	PIPE 1.900 x .145		5
B39	1	PIPE 1.900 x .145		5
B40	1	PIPE 1.900 x .145		5
B41	1	PIPE 1.900 x .145		5
B42	1	PIPE 1.900 x .145		5
B43	1	PIPE 1.900 x .145		5
B44	1	PIPE 1.900 x .145		5
B45	1	PIPE 1.900 x .145		5
B46	1	PIPE 1.900 x .145		5
B47	1	PIPE 1.900 x .145		5
B48	1	PIPE 1.900 x .145		5
B49	1	PIPE 1.900 x .145		5
B50	1	PIPE 1.900 x .145		5
B51	1	PIPE 1.900 x .145		5
B52	1	PIPE 1.900 x .145		5
B53	1	PIPE 1.900 x .145		5
B54	1	PIPE 1.900 x .145		5
B55	1	PIPE 1.900 x .145		5
B56	1	PIPE 1.900 x .145		5
B57	1	PIPE 1.900 x .145		5
B58	1	PIPE 1.900 x .145		5
B59	1	PIPE 1.900 x .145		5
B60	1	PIPE 1.900 x .145		5
B61	1	PIPE 1.900 x .145		5
B62	1	PIPE 1.900 x .145		5
B63	1	PIPE 1.900 x .145		5
B64	1	PIPE 1.900 x .145		5
B65	1	PIPE 1.900 x .145		5
B66	1	PIPE 1.900 x .145		5
B67	1	PIPE 1.900 x .145		5
B68	1	PIPE 1.900 x .145		5
B69	1	PIPE 1.900 x .145		5
B70	1	PIPE 1.900 x .145		5
B71	1	PIPE 1.900 x .145		5
B72	1	PIPE 1.900 x .145		5
B73	1	PIPE 1.900 x .145		5
B74	1	PIPE 1.900 x .145		5
B75	1	PIPE 1.900 x .145		5
B76	1	PIPE 1.900 x .145		5
B77	1	PIPE 1.900 x .145		5
B78	1	PIPE 1.900 x .145		5
B79	1	PIPE 1.900 x .145		5
B80	1	PIPE 1.900 x .145		5
B81	1	PIPE 1.900 x .145		5
B82	1	PIPE 1.900 x .145		5
B83	1	PIPE 1.900 x .145		5
B84	1	PIPE 1.900 x .145		5
B85	1	PIPE 1.900 x .145		5
B86	1	PIPE 1.900 x .145		5
B87	1	PIPE 1.900 x .145		5
B88	1	PIPE 1.900 x .145		5
B89	1	PIPE 1.900 x .145		5
B90	1	PIPE 1.900 x .145		5
B91	1	PIPE 1.900 x .145		5
B92	1	PIPE 1.900 x .145		5
B93	1	PIPE 1.900 x .145		5
B94	1	PIPE 1.900 x .145		5
B95	1	PIPE 1.900 x .145		5
B96	1	PIPE 1.900 x .145		5
B97	1	PIPE 1.900 x .145		5
B98	1	PIPE 1.900 x .145		5
B99	1	PIPE 1.900 x .145		5
B100	1	PIPE 1.900 x .145		5

MARK	QTY	DESCRIPTION OF MATERIAL	UNIT	QTY
B01	1	PIPE 8.625 x .250	UPRIGHT	28
B02	1	PIPE 1.900 x .145		4
B03	1	PIPE 1.900 x .145		5
B04	1	PIPE 1.900 x .145		5
B05	1	PIPE 1.900 x .145		5
B06	1	PIPE 1.900 x .145		5
B07	1	PIPE 1.900 x .145		5
B08	1	PIPE 1.900 x .145		5
B09	1	PIPE 1.900 x .145		5
B10	1	PIPE 1.900 x .145		5
B11	1	PIPE 1.900 x .145		5
B12	1	PIPE 1.900 x .145		5
B13	1	PIPE 1.900 x .145		5
B14	1	PIPE 1.900 x .145		5
B15	1	PIPE 1.900 x .145		5
B16	1	PIPE 1.900 x .145		5
B17	1	PIPE 1.900 x .145		5
B18	1	PIPE 1.900 x .145		5
B19	1	PIPE 1.900 x .145		5
B20	1	PIPE 1.900 x .145		5
B21	1	PIPE 1.900 x .145		5
B22	1	PIPE 1.900 x .145		5
B23	1	PIPE 1.900 x .145		5
B24	1	PIPE 1.900 x .145		5
B25	1	PIPE 1.900 x .145		5
B26	1	PIPE 1.900 x .145		5
B27	1	PIPE 1.900 x .145		5
B28	1	PIPE 1.900 x .145		5
B29	1	PIPE 1.900 x .145		5
B30	1	PIPE 1.900 x .145		5
B31	1	PIPE 1.900 x .145		5
B32	1	PIPE 1.900 x .145		5
B33	1	PIPE 1.900 x .145		5
B34	1	PIPE 1.900 x .145		5
B35	1	PIPE 1.900 x .145		5
B36	1	PIPE 1.900 x .145		5
B37	1	PIPE 1.900 x .145		5
B38	1	PIPE 1.900 x .145		5
B39	1	PIPE 1.900 x .145		5
B40	1	PIPE 1.900 x .145		5
B41	1	PIPE 1.900 x .145		5
B42	1	PIPE 1.900 x .145		5
B43	1	PIPE 1.900 x .145		5
B44	1	PIPE 1.900 x .145		5
B45	1	PIPE 1.900 x .145		5
B46	1	PIPE 1.900 x .145		5
B47	1	PIPE 1.900 x .145		5
B48	1	PIPE 1.900 x .145		5
B49	1	PIPE 1.900 x .145		5
B50	1	PIPE 1.900 x .145		5
B51	1	PIPE 1.900 x .145		5
B52	1	PIPE 1.900 x .145		5
B53	1	PIPE 1.900 x .145		5
B54	1	PIPE 1.900 x .145		5
B55	1	PIPE 1.900 x .145		5
B56	1	PIPE 1.900 x .145		5
B57	1	PIPE 1.900 x .145		5
B58	1	PIPE 1.900 x .145		5
B59	1	PIPE 1.900 x .145		5
B60	1	PIPE 1.900 x .145		5
B61	1	PIPE 1.900 x .145		5
B62	1	PIPE 1.900 x .145		5
B63	1	PIPE 1.900 x .145		5
B64	1	PIPE 1.900 x .145		5
B65	1	PIPE 1.900 x .145		5
B66	1	PIPE 1.900 x .145		5
B67	1	PIPE 1.900 x .145		5
B68	1	PIPE 1.900 x .145		5
B69	1	PIPE 1.900 x .145		5
B70	1	PIPE 1.900 x .145		5
B71	1	PIPE 1.900 x .145		5
B72	1	PIPE 1.900 x .145		5
B73	1	PIPE 1.900 x .145		5
B74	1	PIPE 1.900 x .145		5
B75	1	PIPE 1.900 x .145		5
B76	1	PIPE 1.900 x .145		5
B77	1	PIPE 1.900 x .145		5
B78	1	PIPE 1.900 x .145		5
B79	1	PIPE 1.900 x .145		5
B80	1	PIPE 1.900 x .145		5
B81	1	PIPE 1.900 x .145		5
B82	1	PIPE 1.900 x .145		5
B83	1	PIPE 1.900 x .145		5
B84	1	PIPE 1.900 x .145		5
B85	1	PIPE 1.900 x .145		5
B86	1	PIPE 1.900 x .145		5
B87	1	PIPE 1.900 x .145		5
B88	1	PIPE 1.900 x .145		5
B89	1	PIPE 1.900 x .145		5
B90	1	PIPE 1.900 x .145		5
B91	1	PIPE 1.900 x .145		5
B92	1	PIPE 1.900 x .145		5
B93	1	PIPE 1.900 x .145		5
B94	1	PIPE 1.900 x .145		5
B95	1	PIPE 1.900 x .145		5
B96	1	PIPE 1.900 x .145		5
B97	1	PIPE 1.900 x .145		5
B98	1	PIPE 1.900 x .145		5
B99	1	PIPE 1.900 x .145		5
B100	1	PIPE 1.900 x .145		5



MATL. SPECS.
 UPRIGHTS-STEEL PIPE - API-5L-X52 (33 KSI MIN. YIELD)
 (SMALL METR ASTM A53, OR 9 SPECS)
 WELDS-STEEL METR ASTM A53, OR 9 SPECS
 PLATES-ASTM-A36
 GALV. ASTM-A123
 GALV. ASTM-A123
 ALL PIPE SIZES ARE OUTSIDE DIAMETER
 GALVANIZING VENT HOLES TO BE REAMED SMOOTH

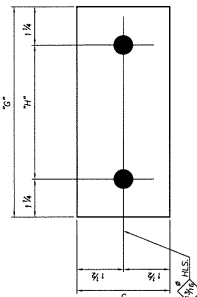
STATE: ALABAMA
 FED. PROJ.: DM47-CM89 (3)
 ST. PROJ.:
 COUNTY: LEEFLOREN / SHELBY
 ROUTE: I-65, I-20, I-459, 89/20 & US 290
 SUBJECT: OVERHEAD SIGN SUPPORT
 DRAWING: CG242-B

POST OFFICE BOX 2800
 BRUSHY CREEK
 BRUSHY CREEK, ALABAMA 35208
 PHONE (205) 825-4990
 FAX (205) 825-7171

DATE: 1/17/00
 DRAWN BY: MRF
 CHECKED BY: MRF
 APPROVED BY: MRF

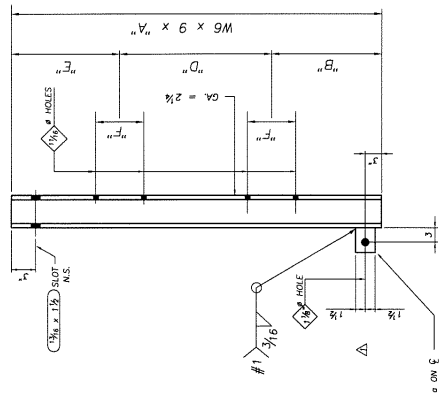
DWG. NO. CG242-B

MARK		QTY		DESCRIPTION OF MATERIAL		C9242-2	
MARK	QTY	MARK	QTY	DESCRIPTION	MARK	QTY	DESCRIPTION
ZH1	20	W	1	SIGN HANGERS	8	6	
ZH2	40	W	1	SIGN HANGERS	8	6	
ZH3	5	W	1	SIGN HANGERS	8	6	
ZH4	5	W	1	SIGN HANGERS	8	6	
ZH5	5	W	1	SIGN HANGERS	8	6	
ZH6	5	W	1	SIGN HANGERS	8	6	
ZH7	5	W	1	SIGN HANGERS	8	6	
ZH8	5	W	1	SIGN HANGERS	8	6	
ZH9	5	W	1	SIGN HANGERS	8	6	
ZH10	5	W	1	SIGN HANGERS	8	6	
ZH11	5	W	1	SIGN HANGERS	8	6	
ZH12	5	W	1	SIGN HANGERS	8	6	
ZH13	5	W	1	SIGN HANGERS	8	6	
ZH14	5	W	1	SIGN HANGERS	8	6	
ZH15	5	W	1	SIGN HANGERS	8	6	
ZH16	5	W	1	SIGN HANGERS	8	6	
ZH17	5	W	1	SIGN HANGERS	8	6	
ZH18	5	W	1	SIGN HANGERS	8	6	
ZH19	5	W	1	SIGN HANGERS	8	6	
ZH20	5	W	1	SIGN HANGERS	8	6	
ZH21	5	W	1	SIGN HANGERS	8	6	
ZH22	5	W	1	SIGN HANGERS	8	6	
ZH23	5	W	1	SIGN HANGERS	8	6	
ZH24	5	W	1	SIGN HANGERS	8	6	
ZH25	5	W	1	SIGN HANGERS	8	6	
ZH26	5	W	1	SIGN HANGERS	8	6	
ZH27	5	W	1	SIGN HANGERS	8	6	
ZH28	5	W	1	SIGN HANGERS	8	6	
ZH29	5	W	1	SIGN HANGERS	8	6	
ZH30	5	W	1	SIGN HANGERS	8	6	
ZH31	5	W	1	SIGN HANGERS	8	6	
ZH32	5	W	1	SIGN HANGERS	8	6	
ZH33	5	W	1	SIGN HANGERS	8	6	
ZH34	5	W	1	SIGN HANGERS	8	6	
ZH35	5	W	1	SIGN HANGERS	8	6	
ZH36	5	W	1	SIGN HANGERS	8	6	
ZH37	5	W	1	SIGN HANGERS	8	6	
ZH38	5	W	1	SIGN HANGERS	8	6	
ZH39	5	W	1	SIGN HANGERS	8	6	
ZH40	5	W	1	SIGN HANGERS	8	6	
ZH41	5	W	1	SIGN HANGERS	8	6	
ZH42	5	W	1	SIGN HANGERS	8	6	
ZH43	5	W	1	SIGN HANGERS	8	6	
ZH44	5	W	1	SIGN HANGERS	8	6	
ZH45	5	W	1	SIGN HANGERS	8	6	
ZH46	5	W	1	SIGN HANGERS	8	6	
ZH47	5	W	1	SIGN HANGERS	8	6	
ZH48	5	W	1	SIGN HANGERS	8	6	
ZH49	5	W	1	SIGN HANGERS	8	6	
ZH50	5	W	1	SIGN HANGERS	8	6	
ZH51	5	W	1	SIGN HANGERS	8	6	
ZH52	5	W	1	SIGN HANGERS	8	6	
ZH53	5	W	1	SIGN HANGERS	8	6	
ZH54	5	W	1	SIGN HANGERS	8	6	
ZH55	5	W	1	SIGN HANGERS	8	6	
ZH56	5	W	1	SIGN HANGERS	8	6	
ZH57	5	W	1	SIGN HANGERS	8	6	
ZH58	5	W	1	SIGN HANGERS	8	6	
ZH59	5	W	1	SIGN HANGERS	8	6	
ZH60	5	W	1	SIGN HANGERS	8	6	
ZH61	5	W	1	SIGN HANGERS	8	6	
ZH62	5	W	1	SIGN HANGERS	8	6	
ZH63	5	W	1	SIGN HANGERS	8	6	
ZH64	5	W	1	SIGN HANGERS	8	6	
ZH65	5	W	1	SIGN HANGERS	8	6	
ZH66	5	W	1	SIGN HANGERS	8	6	
ZH67	5	W	1	SIGN HANGERS	8	6	
ZH68	5	W	1	SIGN HANGERS	8	6	
ZH69	5	W	1	SIGN HANGERS	8	6	
ZH70	5	W	1	SIGN HANGERS	8	6	
ZH71	5	W	1	SIGN HANGERS	8	6	
ZH72	5	W	1	SIGN HANGERS	8	6	
ZH73	5	W	1	SIGN HANGERS	8	6	
ZH74	5	W	1	SIGN HANGERS	8	6	
ZH75	5	W	1	SIGN HANGERS	8	6	
ZH76	5	W	1	SIGN HANGERS	8	6	
ZH77	5	W	1	SIGN HANGERS	8	6	
ZH78	5	W	1	SIGN HANGERS	8	6	
ZH79	5	W	1	SIGN HANGERS	8	6	
ZH80	5	W	1	SIGN HANGERS	8	6	
ZH81	5	W	1	SIGN HANGERS	8	6	
ZH82	5	W	1	SIGN HANGERS	8	6	
ZH83	5	W	1	SIGN HANGERS	8	6	
ZH84	5	W	1	SIGN HANGERS	8	6	
ZH85	5	W	1	SIGN HANGERS	8	6	
ZH86	5	W	1	SIGN HANGERS	8	6	
ZH87	5	W	1	SIGN HANGERS	8	6	
ZH88	5	W	1	SIGN HANGERS	8	6	
ZH89	5	W	1	SIGN HANGERS	8	6	
ZH90	5	W	1	SIGN HANGERS	8	6	
ZH91	5	W	1	SIGN HANGERS	8	6	
ZH92	5	W	1	SIGN HANGERS	8	6	
ZH93	5	W	1	SIGN HANGERS	8	6	
ZH94	5	W	1	SIGN HANGERS	8	6	
ZH95	5	W	1	SIGN HANGERS	8	6	
ZH96	5	W	1	SIGN HANGERS	8	6	
ZH97	5	W	1	SIGN HANGERS	8	6	
ZH98	5	W	1	SIGN HANGERS	8	6	
ZH99	5	W	1	SIGN HANGERS	8	6	
ZH100	5	W	1	SIGN HANGERS	8	6	



SHIM PLATES

MARK	QTY	W	L	T
ZS1	16	6 1/2"	7 1/2"	1/4"
ZS2	32	7 1/2"	5 1/2"	1/4"
ZS3	8	8 1/2"	6 5/8"	1/4"



SIGN HANGER

MARK	QTY	A	B	C	D	E	F
ZH1	20	8'-6"	2'-4 1/2"	3'-9"	2'-4 1/2"	4 1/8"	4 1/8"
ZH2	40	8'-6"	2'-4 1/2"	3'-9"	2'-4 1/2"	5 1/8"	5 1/8"
ZH3	5	8'-6"	2'-3"	4'-0"	2'-3"	6 1/8"	6 1/8"
ZH4	5	8'-6"	1'-9"	5'-0"	1'-9"	6 1/8"	6 1/8"

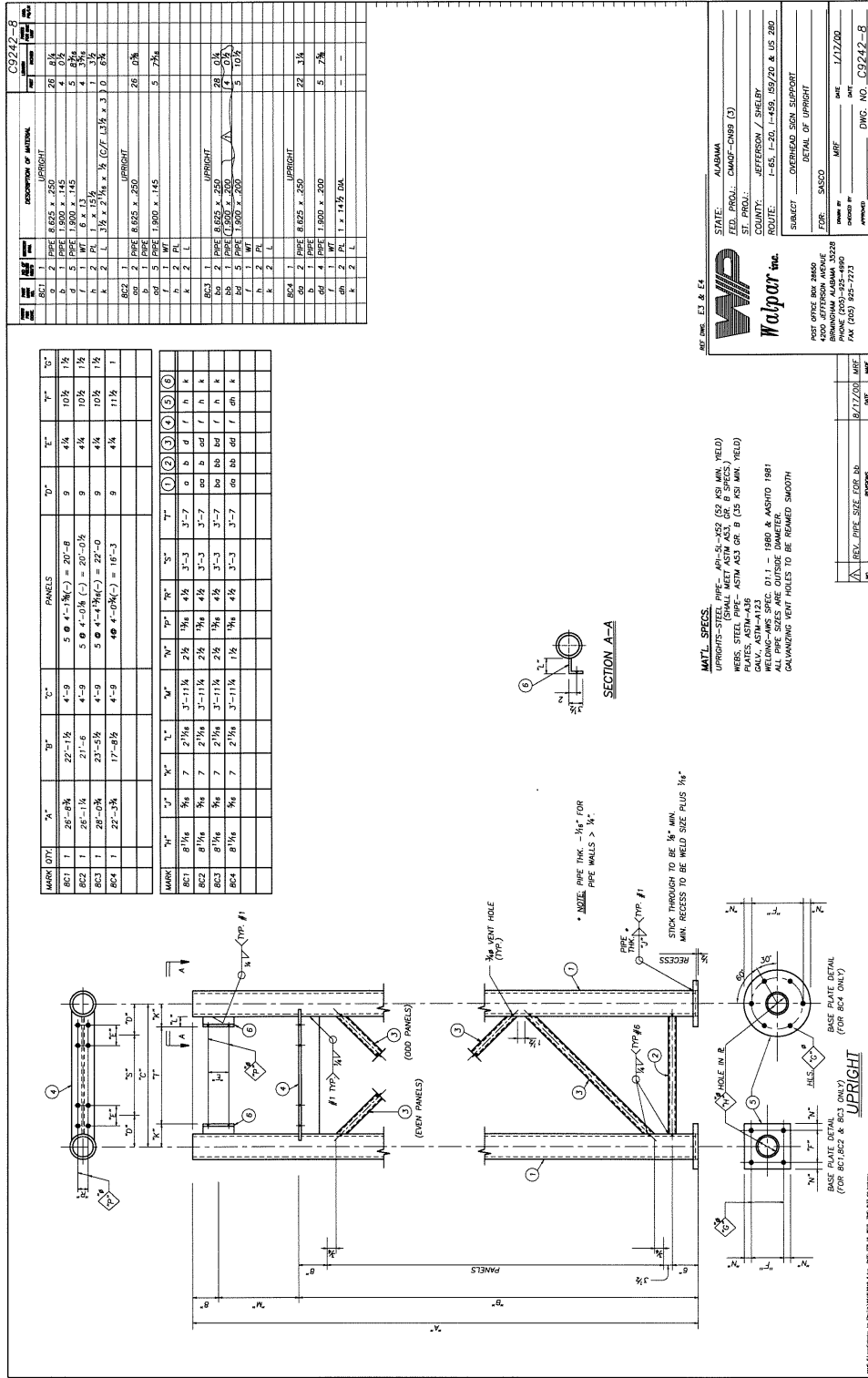
STATE: ALABAMA
 FED. PROJ. CMAS-0992 (3)
 ST. PROJ.: JEFFERSON/SHELBY
 COUNTY: JEFFERSON/SHELBY
 ROUTE: I-65-20-45E-59/20 & I-65 280

WALPOUR inc.
 1000 10th Ave. SE
 Birmingham, Alabama 35228
 Phone: (205) 325-4900
 Fax: (205) 325-4974

DATE: 1/18/00
 DRAWN BY: JPT
 CHECKED BY: JPT
 DWG. NO.: C9242-2

MATERIAL SPECIFICATIONS
 WELDS: AS PER AISC
 GALV. AFTER FAB PER ASTM A123
 WELDING: AWS SPEC D1.1 - 1980 & AWS D1.1
 HOLES: SHALL BE 1/8"

NO.	REV.	DATE	BY	CHK.
1	REV. PLATE 3		JPT	JPT



STATE: ALABAMA
 FED. PROJ.: CMAC-CNSR (3)
 ST. PROJ.: JEFFERSON / SHERID
 COUNTY: JEFFERSON / SHERID
 ROUTE: I-65, I-20, I-45, I-59, I-59/20 & US 280
 SUBJECT: OVERHEAD SIGN SUPPORT

FOR: SASSCO
 DRAWING NO.: C9242-B
 DATE: 1/17/00

POST OFFICE BOX 2800
 BRUNSWICK ALABAMA 36209
 PHONE (205)-325-4990
 FAX (205) 325-7475

APPENDIX B

PRESSURE CALCULATIONS

Pressure Calculations for Drag Coefficient Verification Study

$$P = \frac{1}{2} \rho V^2 C_d \text{ (psf)}$$

$$\rho = 0.002367 \text{ slug/ft}^3$$

$$V_z = V_{10} \left(\frac{z}{z_{10}} \right)^{1/7}$$

$$z_{10} = 32.8 \text{ ft}$$

$$z_{VMS} = 24.6 \text{ ft}$$

$$V_{10}/V_{VMS} = 1.041954$$

Y-direction										
	Uprights 0 - 10 ft	Uprights 10 - 20 ft	Uprights 20 - 28 ft	Bottom Chords	Top Chords	Vertical Truss Webs	End Truss Web	W6x9 Track Hanger	C8x11.5 Track Side Support	Ladder Angle
C_d	1.2	1.2	1.2	1.2	1.2	1.1	1.2	1.7	2.0	2.0
z (ft)	5	15	24	22.7	26.5	24.6	24.6	23.4	20.7	14
(V/V_{VMS})²	0.634	0.868	0.993	0.977	1.021	1.000	1.000	0.986	0.952	0.851
P/V_{VMS}²	0.00090	0.00123	0.00141	0.00138	0.00145	0.00130	0.00142	0.00198	0.00225	0.00201
Diam. (ft)	0.7188	0.7188	0.7188	0.2917	0.2917	0.1583	0.1096	0.3333	0.6667	0.2500
P*d/V_{VMS}²	0.00064	0.00088	0.00101	0.00040	0.00042	0.00020	0.00015	0.000661	0.001502	0.000504
AASHTO VMS Ratio	0.32181	0.44048	0.50379	0.20121	0.21031	0.10245	0.07735	0.32857	0.74661	0.25037
FIU VMS Ratio	0.44843	0.61378	0.70200	0.28037	0.29305	0.14276	0.10779	0.45785	1.04036	0.34887

X-direction									
	Uprights 0 - 10 ft	Uprights 10 - 20 ft	Uprights 20 - 28 ft	Upright Webs	End Truss Web	WT6x13 Truss Support	W6x9 Track Hanger	Ladder Angle	Ladder Rungs
C_d	1.1	1.1	1.1	1.1	1.1	1.7	2.0	1.7	1.1
z (ft)	5	15	24	14	24.6	22.5	23.4	14	14
(V/V_{VMS})²	0.634	0.868	0.993	0.851	1.000	0.975	0.986	0.851	0.851
P/V_{VMS}²	0.000826	0.001130	0.001293	0.001108	0.001302	0.001961	0.002333	0.001713	0.001108
Diam. (ft)	0.7188	0.7188	0.7188	0.1583	0.1096	0.5000	0.5000	0.1667	0.0833
P*d/V_{VMS}²	0.000594	0.000812	0.000929	0.000175	0.000143	0.000981	0.001167	0.000285	0.000092
AASHTO VMS Ratio	0.50149	0.68641	0.78507	0.14826	0.12054	0.82860	0.98581	0.24119	0.07803
FIU VMS Ratio	0.50149	0.68641	0.78507	0.14826	0.12054	0.82860	0.98581	0.24119	0.07803

	Y-direction		X-direction
	AASHTO VMS	FIU VMS	VMS
C_d	1.7	1.22	1.0
z (ft)	24.6	24.6	24.6
(V/V_{VMS})²	1	1	1

Pressure Calculations for Sensitivity Study

Structure A – Alabaster VMS Structure

Extreme Wind (90 mph)

$$P_z = 0.00256K_zGV^2I_rC_d \text{ (psf)}$$

$$K_z = 2.01\left(\frac{z}{900}\right)^{2/9.5}$$

G	1.14
V	90 mph
I _r	1

Y-direction						
	Uprights 0 - 16 ft	Uprights 16 - 22 ft	Uprights 22 - 28 ft	Bottom Chords	Top Chords	Vertical Truss Webs
C _d	1.2	1.2	1.2	1.2	1.2	1.1
z (ft)	16	19	25	22.7	26.5	24.6
K _z	0.860	0.892	0.945	0.926	0.957	0.942
P _z (psf)	24.410	25.309	26.814	26.275	27.145	24.496
Diam. (ft)	0.7188	0.7188	0.7188	0.2917	0.2917	0.1583
P _z *d (plf)	17.544	18.191	19.273	7.664	7.917	3.879

Y-direction (continued)						
	Vertical Struts	W6x9 Track Hangers	C8x11.5 Track Side Support	Ladder Angle 0 - 16 ft	Ladder Angle 16 - 22 ft	Ladder Angle 22 - 25.3 ft
C _d	1.2	1.7	2	2	2	2
z (ft)	24.6	23.4	20.7	16	19	23.7
K _z	0.942	0.932	0.908	0.860	0.892	0.935
P _z (psf)	26.723	37.461	42.949	40.683	42.181	44.191
Diam. (ft)	0.1096	0.3333	0.6667	0.2500	0.2500	0.2500
P _z *d (plf)	2.928	12.486	28.634	10.171	10.545	11.048

	Y-direction		
	AASHTO VMS	Standard FIU VMS	Modified FIU VMS
C_d	1.7	1.22	1.0
z (ft)	23.1	23.1	23.1
K_z	0.930	0.930	0.930
P_z (psf)	37.360	26.811	21.976

Extreme Wind (150 mph)

$$P_z = 0.00256K_zGV^2I_rC_d \text{ (psf)}$$

$$K_z = 2.01\left(\frac{z}{900}\right)^{2/9.5}$$

G	1.14
V	150 mph
I _r	1

Y-direction						
	Uprights 0 - 16 ft	Uprights 16 - 22 ft	Uprights 22 - 28 ft	Bottom Chords	Top Chords	Vertical Truss Webs
C_d	1.2	1.2	1.2	1.2	1.2	1.1
z (ft)	16	19	25	22.7	26.5	24.6
K_z	0.860	0.892	0.945	0.926	0.957	0.942
P_z (psf)	67.804	70.302	74.484	72.986	75.403	68.045
Diam. (ft)	0.7188	0.7188	0.7188	0.2917	0.2917	0.1583
P_z*d (plf)	48.734	50.530	53.535	21.288	21.993	10.774

Y-direction (continued)						
	Vertical Struts	W6x9 Track Hangers	C8x11.5 Track Side Support	Ladder Angle 0 - 16 ft	Ladder Angle 16 - 22 ft	Ladder Angle 22 - 25.3 ft
C_d	1.2	1.7	2	2	2	2
z (ft)	24.6	23.4	20.7	16	19	23.7
K_z	0.942	0.932	0.908	0.860	0.892	0.935
P_z (psf)	74.231	104.060	119.304	113.007	117.171	122.752
Diam. (ft)	0.1096	0.3333	0.6667	0.2500	0.2500	0.2500
P_z*d (plf)	8.135	34.683	79.540	28.252	29.293	30.688

	Y-direction		
	AASHTO VMS	Standard FIU VMS	Modified FIU VMS
C_d	1.7	1.22	1.0
z (ft)	23.1	23.1	23.1
K_z	0.930	0.930	0.930
P_z (psf)	103.777	74.476	61.046

Fatigue Wind

$$P_{NW} = 5.2C_d I_F \text{ (psf)}$$

$$I_F = 1$$

Y-direction							
	Uprights	Truss Chords	Vertical Truss Webs	Vertical Struts	W6x9 Track Hangers	C8x11.5 Track Side Support	Ladder Angle
C_d	1.2	1.2	1.1	1.2	1.7	2	2
P_{NW} (psf)	6.240	6.240	5.720	6.240	8.840	10.400	10.400
Diam. (ft)	0.7188	0.2917	0.1583	0.1096	0.3333	0.6667	0.2500
P_{NW}*d	4.485	1.820	0.906	0.684	2.946	6.934	2.600

	Y-direction		
	AASHTO VMS	Standard FIU VMS	Modified FIU VMS
C_d	1.7	1.22	1.0
P_{NW} (psf)	8.840	6.344	5.200

Structure B – Birmingham VMS Structure

Extreme Wind (90 mph)

$$P_z = 0.00256K_zGV^2I_rC_d \text{ (psf)}$$

$$K_z = 2.01\left(\frac{z}{900}\right)^{2/9.5}$$

G	1.14
V	90 mph
I _r	1

Y-direction						
	Uprights 0 - 11 ft	Uprights 11 - 16 ft	Uprights 16 - 21 ft	Bottom Chords	Top Chords	Vertical Truss Webs
C_d	1.2	1.2	1.2	1.2	1.2	1.1
z (ft)	16	18.2	23.2	20.6	25.6	23.1
K_z	0.860	0.884	0.931	0.908	0.950	0.930
P_z (psf)	24.410	25.081	26.396	25.743	26.948	24.174
Diam. (ft)	0.7188	0.7188	0.7188	0.4636	0.4636	0.1979
P_z*d (plf)	17.544	18.027	18.972	11.934	12.493	4.784

Y-direction (continued)						
	Vertical Struts	W6x9 Track Hangers	C8x11.5 Track Side Support	Ladder Angle 0 - 11 ft	Ladder Angle 11 - 16 ft	Ladder Angle 16 - 17.2 ft
C_d	1.2	1.7	2	2	2	2
z (ft)	23.1	22.5	18.6	16	18.2	21.3
K_z	0.930	0.925	0.888	0.860	0.884	0.914
P_z (psf)	26.372	37.153	41.993	40.683	41.801	43.208
Diam. (ft)	0.1383	0.3333	0.6667	0.2500	0.2500	0.2500
P_z*d (plf)	3.648	12.383	27.997	10.171	10.450	10.802

	Y-direction		
	AASHTO VMS	Standard FIU VMS	Modified FIU VMS
C_d	1.7	1.22	1.0
z (ft)	23.1	23.1	23.1
K_z	0.930	0.930	0.930
P_z (psf)	37.360	26.811	21.976

Extreme Wind (150 mph)

$$P_z = 0.00256K_zGV^2I_rC_d \text{ (psf)}$$

$$K_z = 2.01\left(\frac{z}{900}\right)^{2/9.5}$$

G 1.14
V 150 mph
I_r 1

Y-direction						
	Uprights 0 - 11 ft	Uprights 11 - 16 ft	Uprights 16 - 21 ft	Bottom Chords	Top Chords	Vertical Truss Webs
C_d	1.2	1.2	1.2	1.2	1.2	1.1
z (ft)	16	18.2	23.2	20.6	25.6	23.1
K_z	0.860	0.884	0.931	0.908	0.950	0.930
P_z (psf)	67.804	69.669	73.321	71.509	74.857	67.150
Diam. (ft)	0.7188	0.7188	0.7188	0.4636	0.4636	0.1979
P_z*d (plf)	48.734	50.074	52.700	33.151	34.702	13.290

Y-direction (continued)						
	Vertical Struts	W6x9 Track Hangers	C8x11.5 Track Side Support	Ladder Angle 0 - 11 ft	Ladder Angle 11 - 16 ft	Ladder Angle 16 - 17.2 ft
C_d	1.2	1.7	2	2	2	2
z (ft)	23.1	22.5	18.6	16	18.2	21.3
K_z	0.930	0.925	0.888	0.860	0.884	0.914
P_z (psf)	73.255	103.204	116.647	113.007	116.114	120.024
Diam. (ft)	0.1383	0.3333	0.6667	0.2500	0.2500	0.2500
P_z*d (plf)	10.134	34.398	77.769	28.252	29.029	30.006

	Y-direction		
	AASHTO VMS	Standard FIU VMS	Modified FIU VMS
C_d	1.7	1.22	1.0
z (ft)	23.1	23.1	23.1
K_z	0.930	0.930	0.930
P_z (psf)	103.777	74.476	61.046

Fatigue Wind

$$P_{NW} = 5.2C_d I_F \text{ (psf)}$$

I_F 1

Y-direction							
	Uprights	Truss Chords	Vertical Truss Webs	Vertical Struts	W6x9 Track Hangers	C8x11.5 Track Side Support	Ladder Angle
C_d	1.2	1.2	1.1	1.2	1.7	2	2
P_{NW} (psf)	6.240	6.240	5.720	6.240	8.840	10.400	10.400
Diam. (ft)	0.7188	0.4636	0.1979	0.1383	0.3333	0.6667	0.2500
P_{NW}*d	4.485	2.893	1.132	0.863	2.946	6.934	2.600

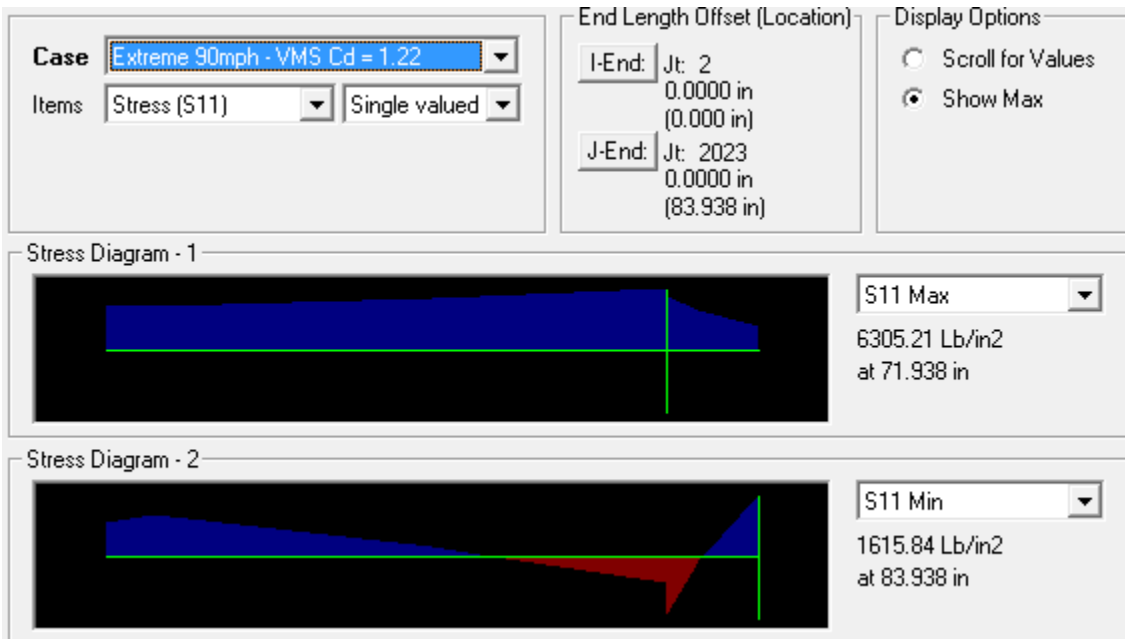
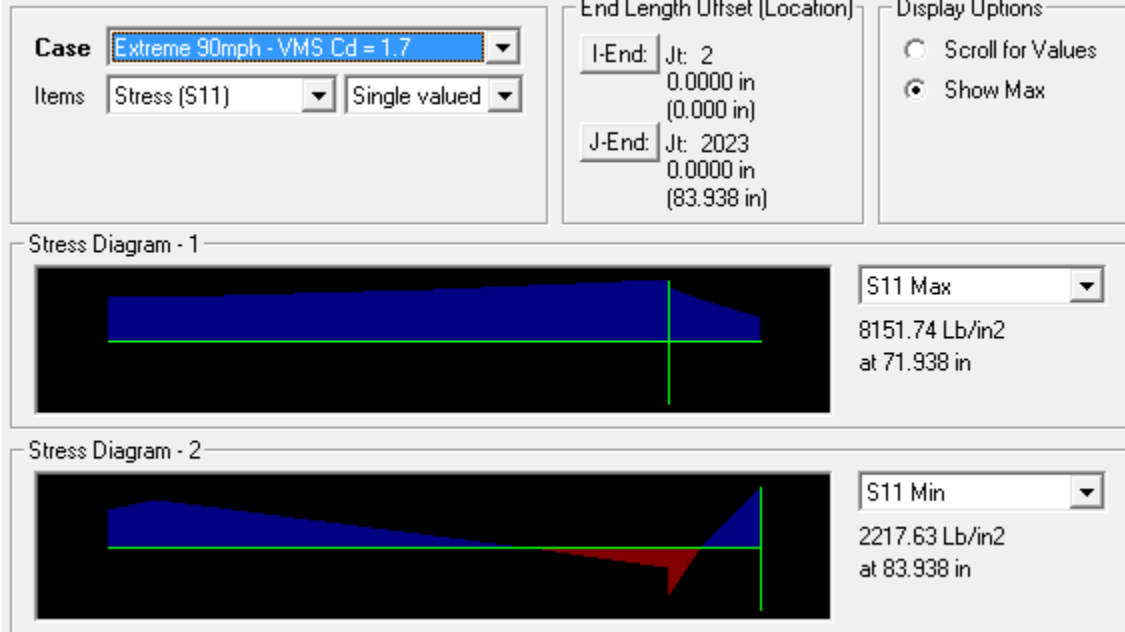
	Y-direction		
	AASHTO VMS	Standard FIU VMS	Modified FIU VMS
C_d	1.7	1.22	1.0
P_{NW} (psf)	8.840	6.344	5.200

APPENDIX C

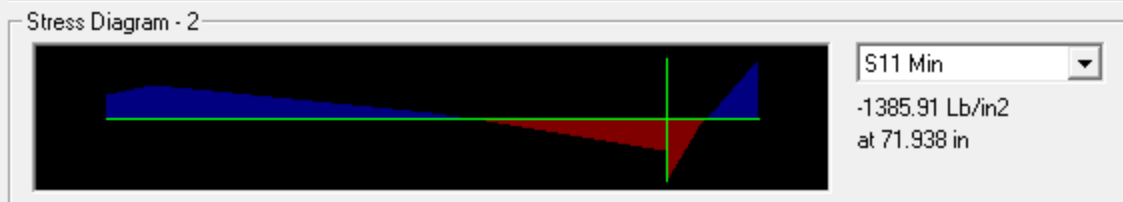
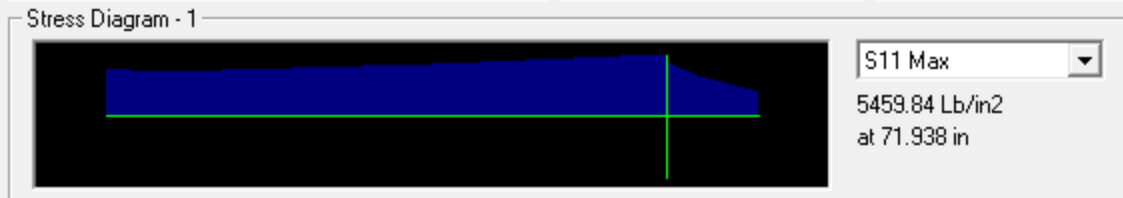
SAP STRESS DIAGRAMMS FOR SENSITIVITY STUDY

Structure A – Alabaster VMS Structure

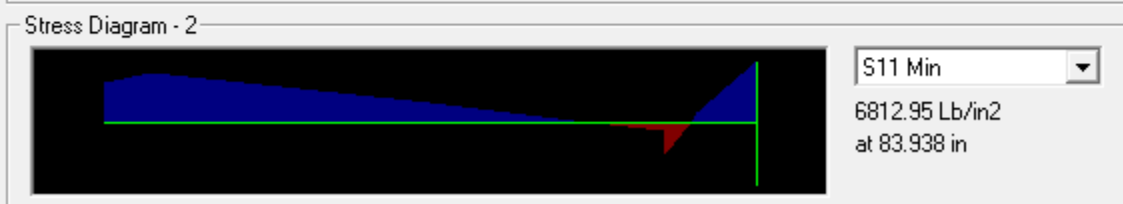
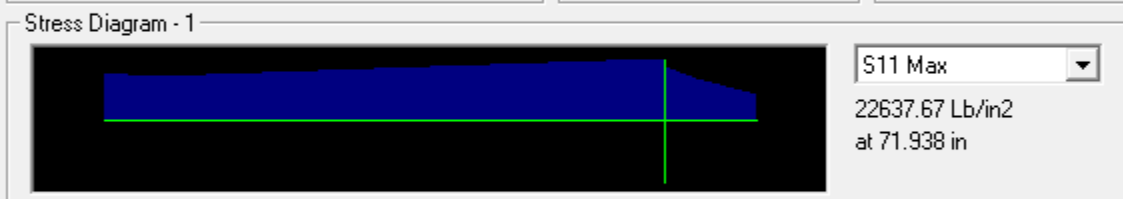
Upright 1a



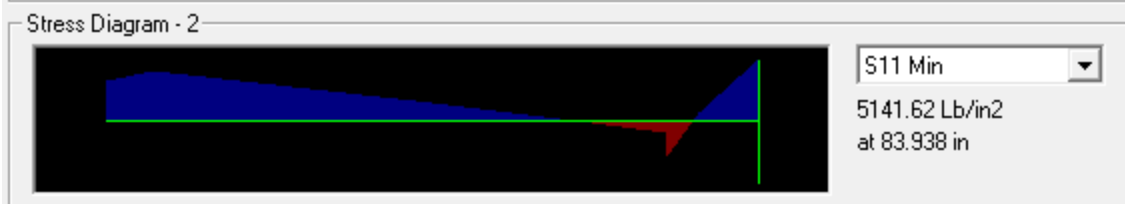
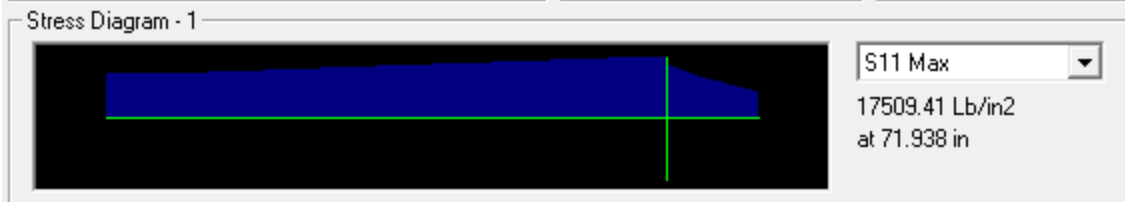
Case Extreme 90mph - VMS Cd = 1.0 Items Stress (S11) Single valued	End Length Offset (Location) I-End: Jt: 2 0.0000 in (0.000 in) J-End: Jt: 2023 0.0000 in (83.938 in)	Display Options <input type="radio"/> Scroll for Values <input checked="" type="radio"/> Show Max
--	---	--



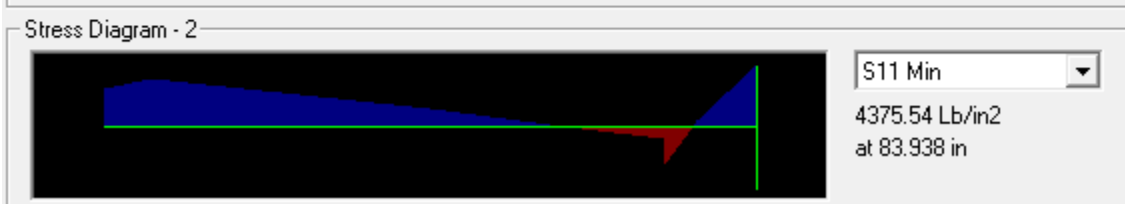
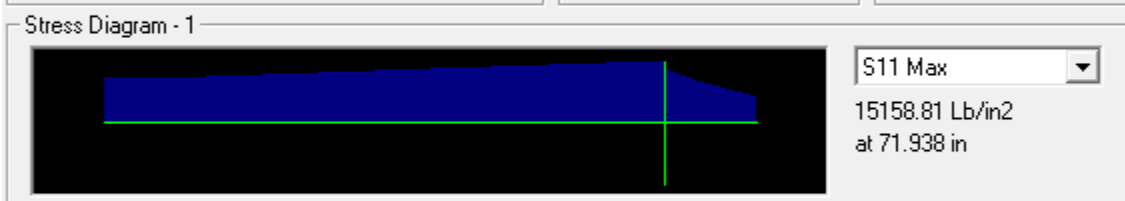
Case Extreme 150mph - VMS Cd = 1.7 Items Stress (S11) Single valued	End Length Offset (Location) I-End: Jt: 2 0.0000 in (0.000 in) J-End: Jt: 2023 0.0000 in (83.938 in)	Display Options <input type="radio"/> Scroll for Values <input checked="" type="radio"/> Show Max
---	---	--



Case Extreme 150mph - VMS Cd = 1.22 Items Stress (S11) Single valued	End Length Offset (Location) I-End: Jt: 2 0.0000 in (0.000 in) J-End: Jt: 2023 0.0000 in (83.938 in)	Display Options <input type="radio"/> Scroll for Values <input checked="" type="radio"/> Show Max
---	---	--



Case Extreme 150mph - VMS Cd = 1.0 Items Stress (S11) Single valued	End Length Offset (Location) I-End: Jt: 2 0.0000 in (0.000 in) J-End: Jt: 2023 0.0000 in (83.938 in)	Display Options <input type="radio"/> Scroll for Values <input checked="" type="radio"/> Show Max
--	---	--



Case Fatigue - VMS Cd = 1.7 Items Stress (S11) Single valued	End Length Offset (Location) I-End: Jt: 2 0.0000 in (0.000 in) J-End: Jt: 2023 0.0000 in (83.938 in)	Display Options <input checked="" type="radio"/> Scroll for Values <input type="radio"/> Show Max Location 0.000 in
---	---	---

Stress Diagram - 1



S11 Max
 1486.56 Lb/in2
 at 0.000 in

Stress Diagram - 2



S11 Min
 410.40 Lb/in2
 at 0.000 in

Case Fatigue - VMS Cd = 1.22 Items Stress (S11) Single valued	End Length Offset (Location) I-End: Jt: 2 0.0000 in (0.000 in) J-End: Jt: 2023 0.0000 in (83.938 in)	Display Options <input checked="" type="radio"/> Scroll for Values <input type="radio"/> Show Max Location 0.000 in
--	---	---

Stress Diagram - 1

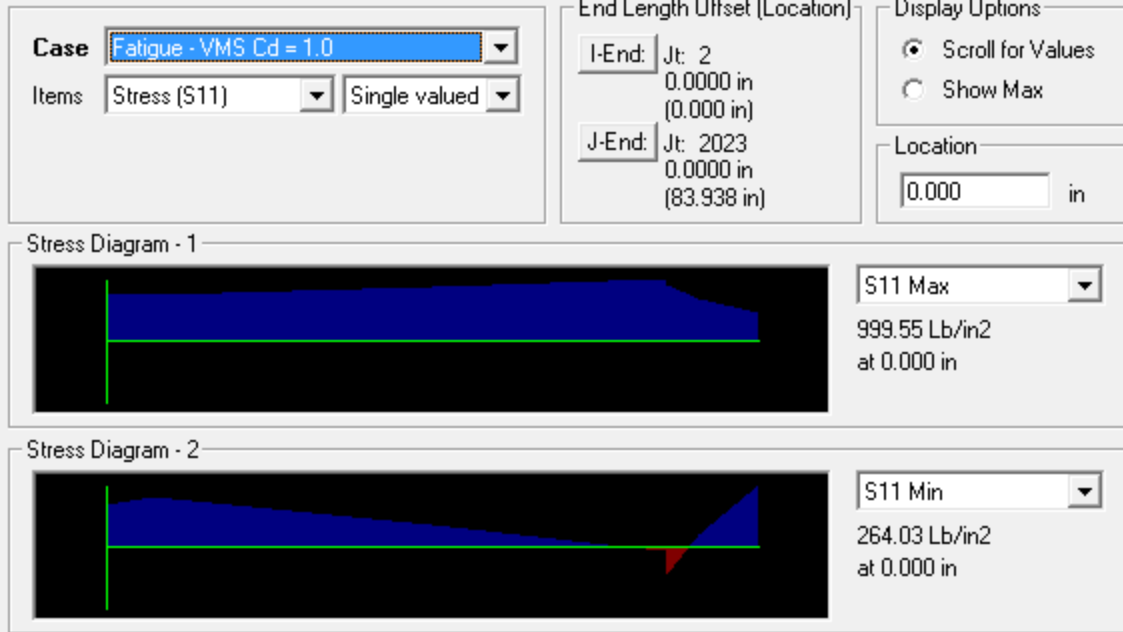


S11 Max
 1152.08 Lb/in2
 at 0.000 in

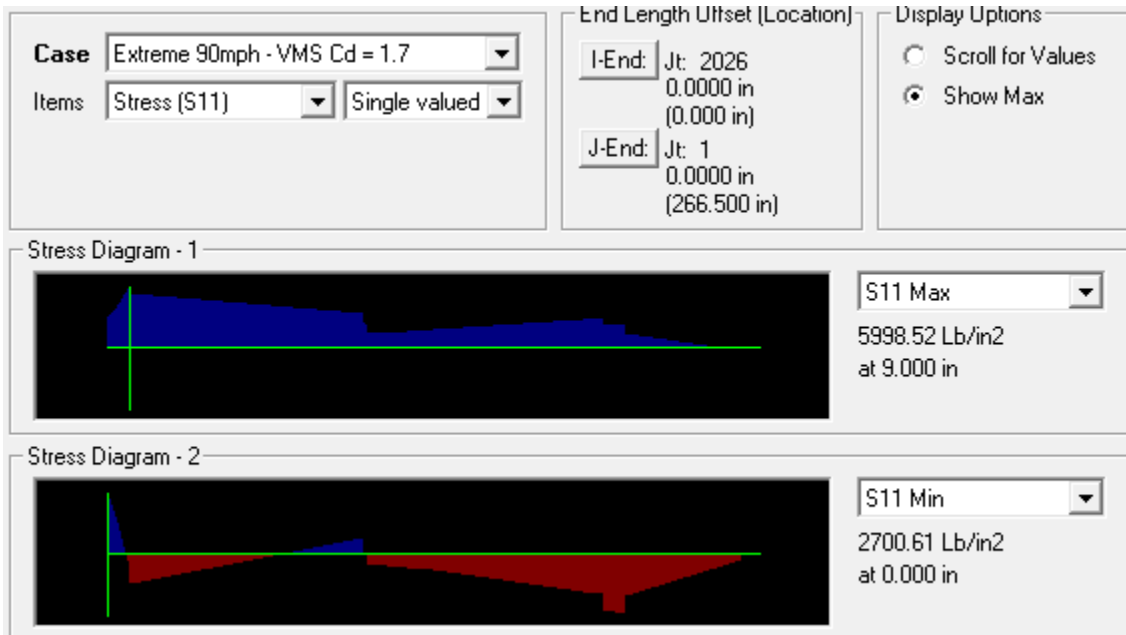
Stress Diagram - 2



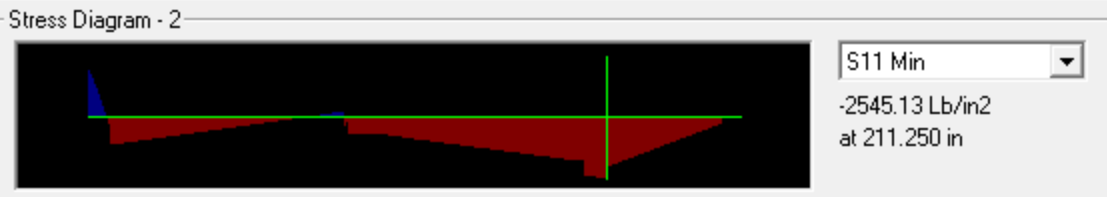
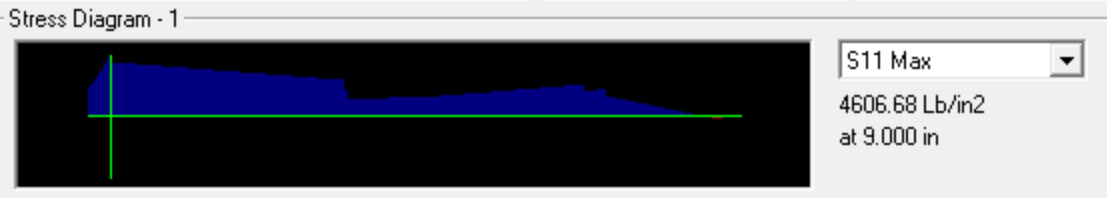
S11 Min
 309.87 Lb/in2
 at 0.000 in



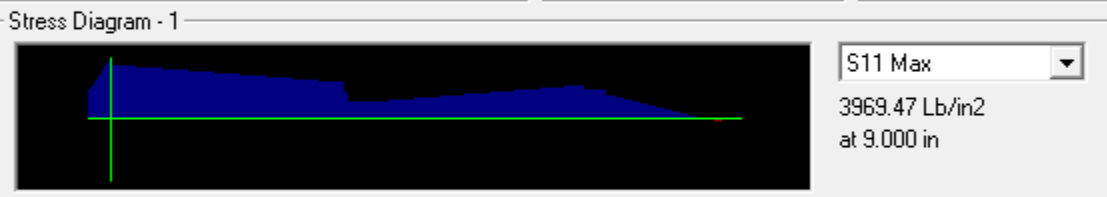
Upright 1b



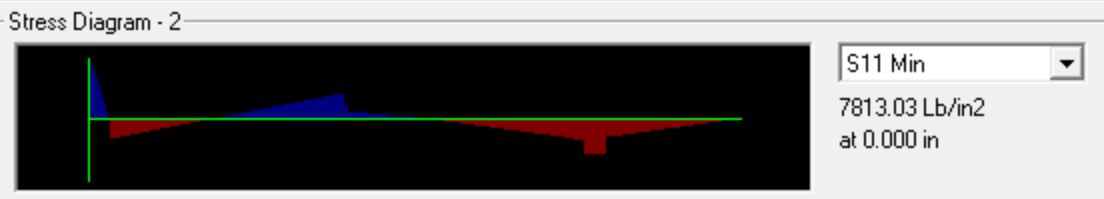
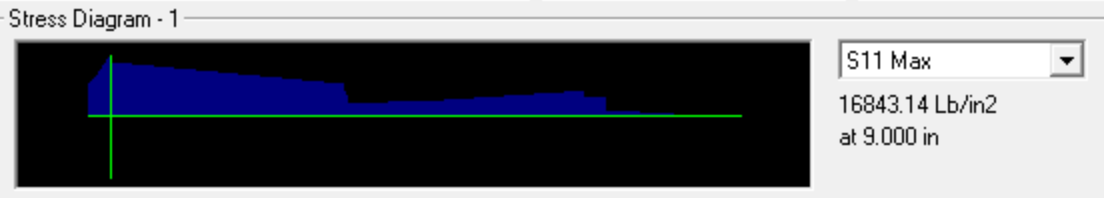
Case Extreme 90mph - VMS Cd = 1.22 Items Stress (S11) Single valued	End Length Offset (Location) I-End: Jt: 2026 0.0000 in (0.000 in) J-End: Jt: 1 0.0000 in (266.500 in)	Display Options <input type="radio"/> Scroll for Values <input checked="" type="radio"/> Show Max
--	--	--



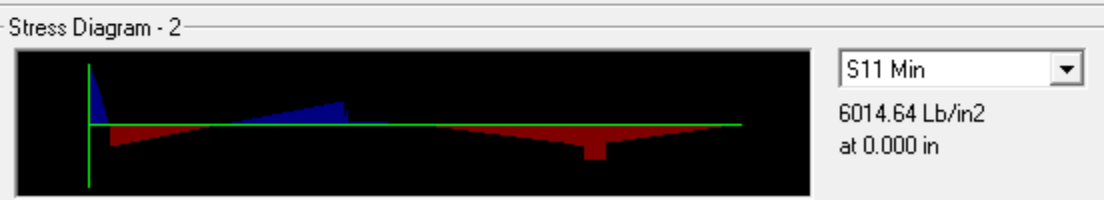
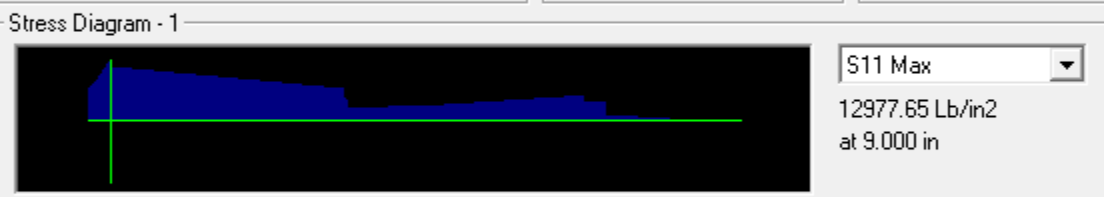
Case Extreme 90mph - VMS Cd = 1.0 Items Stress (S11) Single valued	End Length Offset (Location) I-End: Jt: 2026 0.0000 in (0.000 in) J-End: Jt: 1 0.0000 in (266.500 in)	Display Options <input type="radio"/> Scroll for Values <input checked="" type="radio"/> Show Max
---	--	--

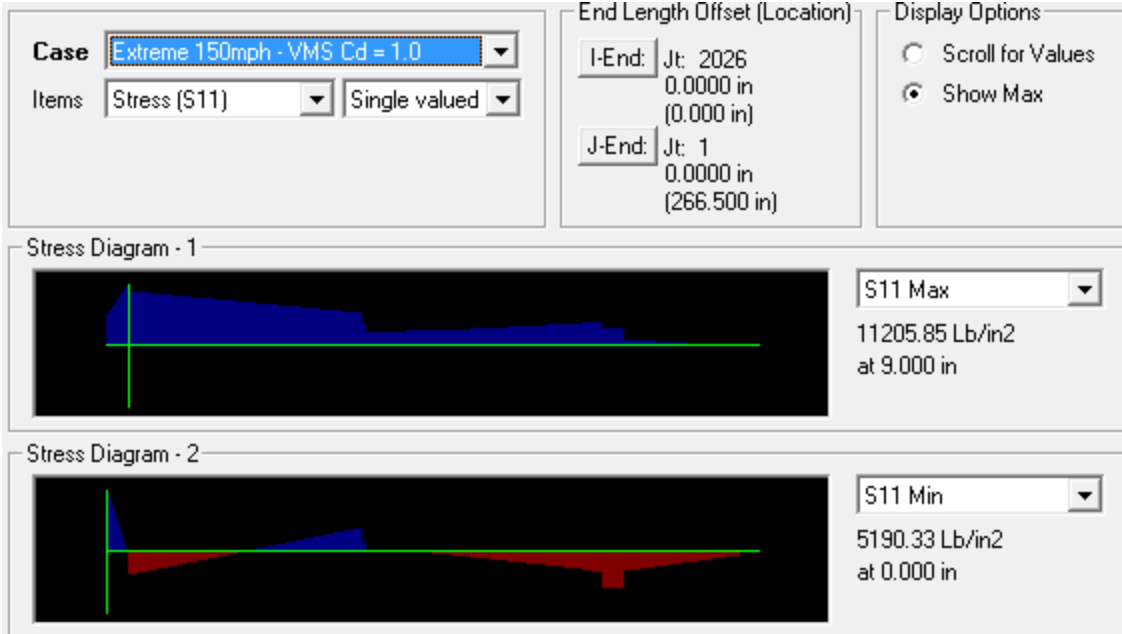


Case Extreme 150mph - VMS Cd = 1.7 Items Stress (S11) Single valued	End Length Offset (Location) I-End: Jt: 2026 0.0000 in (0.000 in) J-End: Jt: 1 0.0000 in (266.500 in)	Display Options <input type="radio"/> Scroll for Values <input checked="" type="radio"/> Show Max
--	--	--

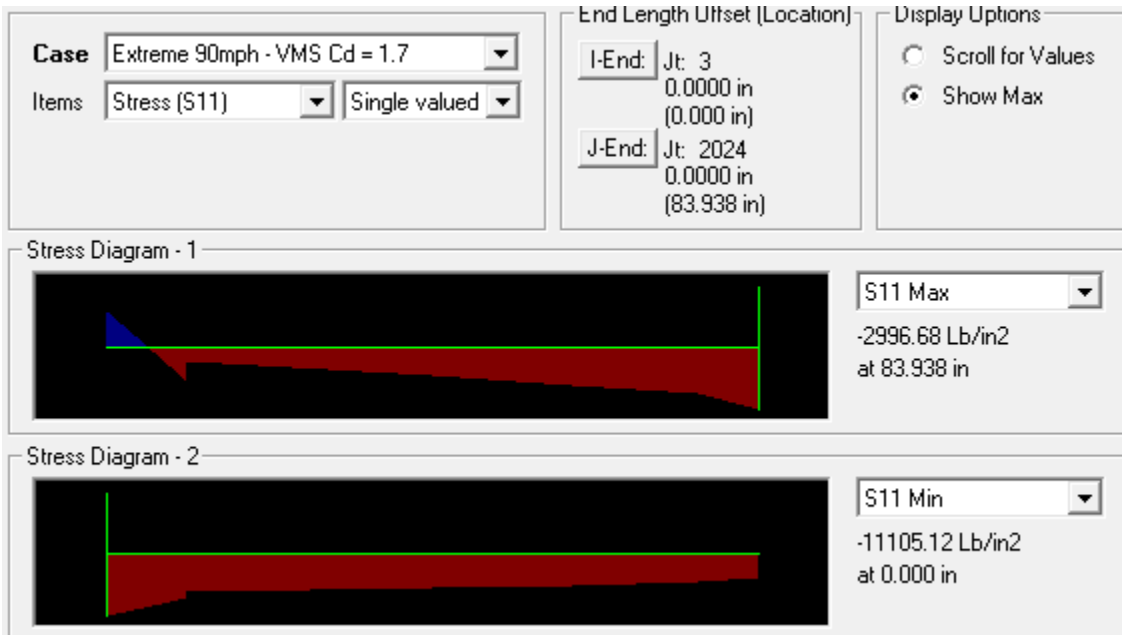


Case Extreme 150mph - VMS Cd = 1.22 Items Stress (S11) Single valued	End Length Offset (Location) I-End: Jt: 2026 0.0000 in (0.000 in) J-End: Jt: 1 0.0000 in (266.500 in)	Display Options <input type="radio"/> Scroll for Values <input checked="" type="radio"/> Show Max
---	--	--

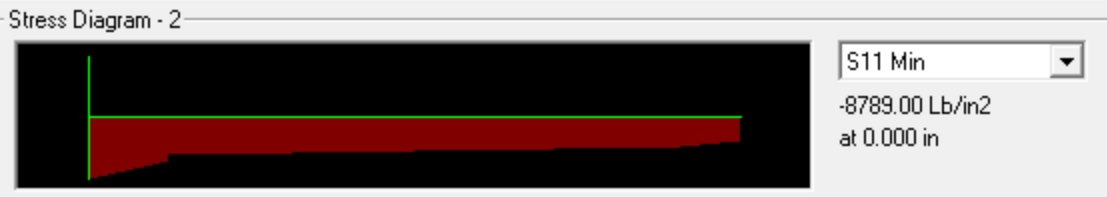
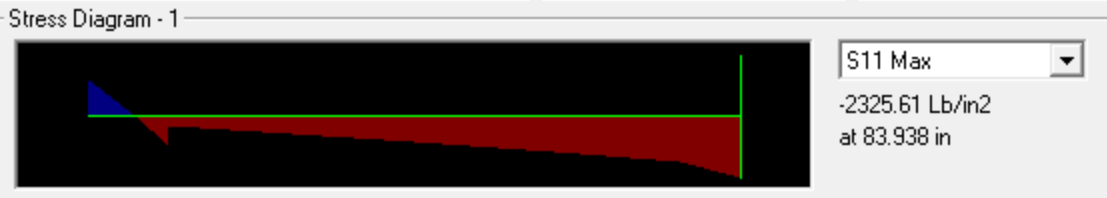




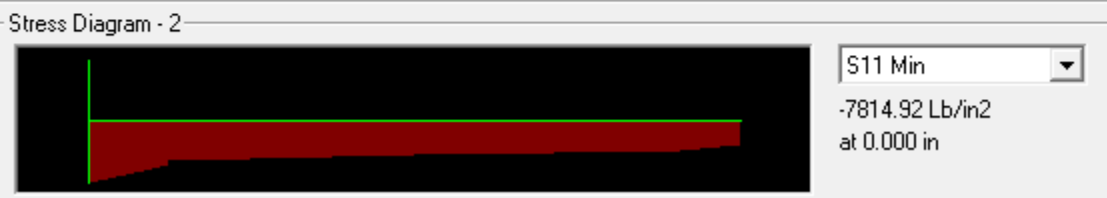
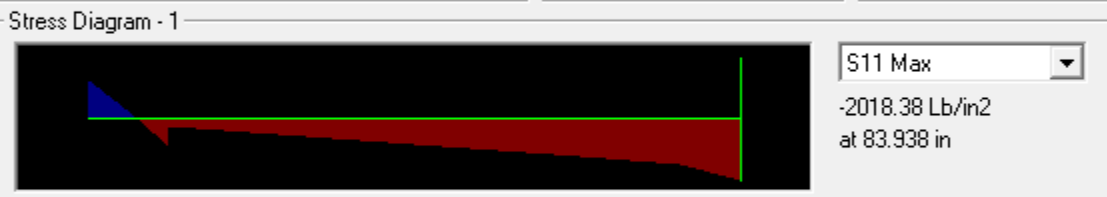
Upright 2a



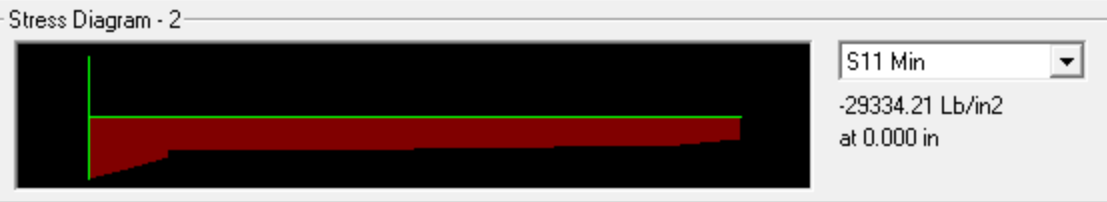
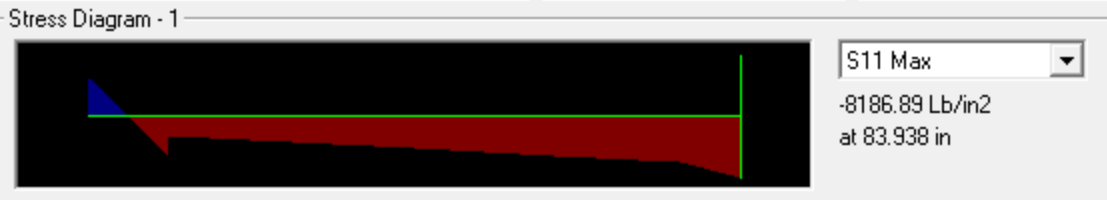
Case Extreme 90mph - VMS Cd = 1.22 Items Stress (S11) Single valued	End Length Offset (Location) I-End: Jt: 3 0.0000 in (0.000 in) J-End: Jt: 2024 0.0000 in (83.938 in)	Display Options <input type="radio"/> Scroll for Values <input checked="" type="radio"/> Show Max
--	---	--



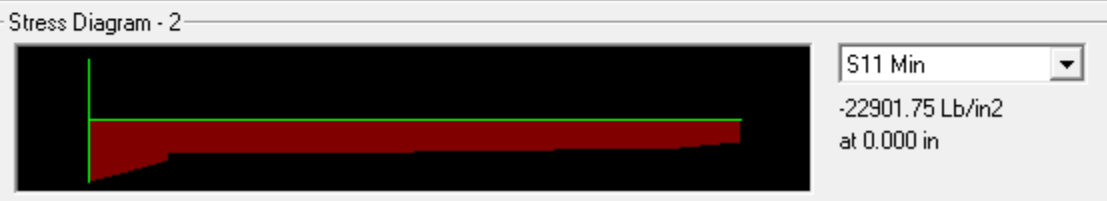
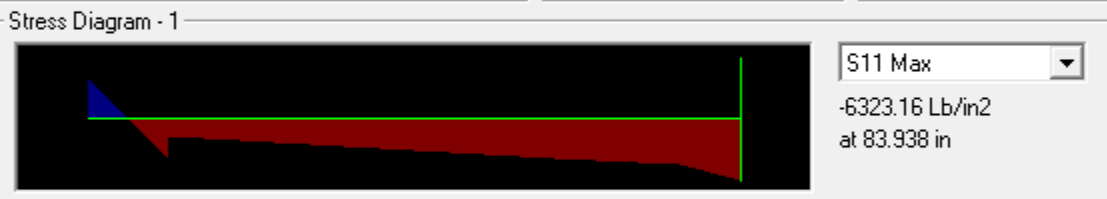
Case Extreme 90mph - VMS Cd = 1.0 Items Stress (S11) Single valued	End Length Offset (Location) I-End: Jt: 3 0.0000 in (0.000 in) J-End: Jt: 2024 0.0000 in (83.938 in)	Display Options <input type="radio"/> Scroll for Values <input checked="" type="radio"/> Show Max
---	---	--



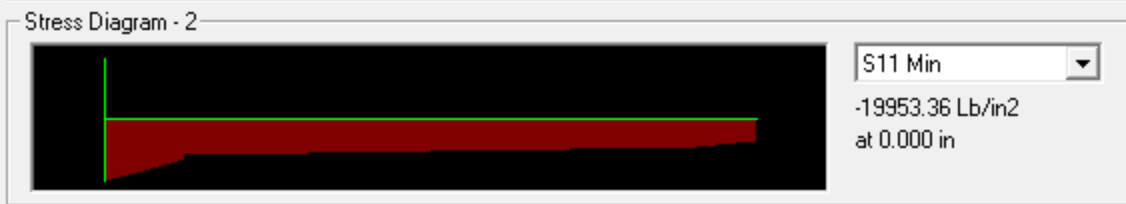
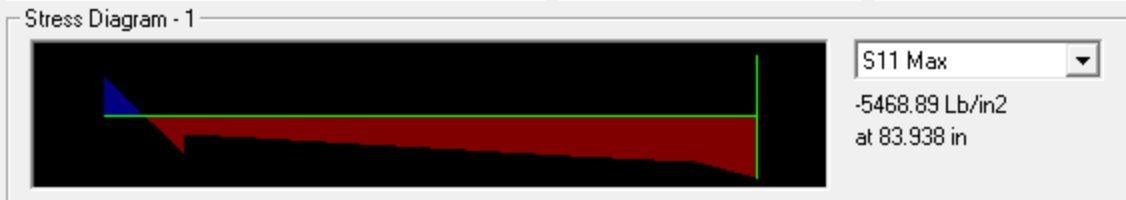
Case Extreme 150mph - VMS Cd = 1.7 Items Stress (S11) Single valued	End Length Offset (Location) I-End: Jt: 3 0.0000 in (0.000 in) J-End: Jt: 2024 0.0000 in (83.938 in)	Display Options <input type="radio"/> Scroll for Values <input checked="" type="radio"/> Show Max
--	---	--



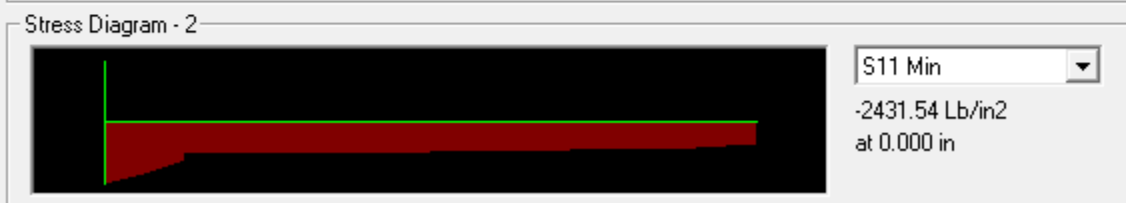
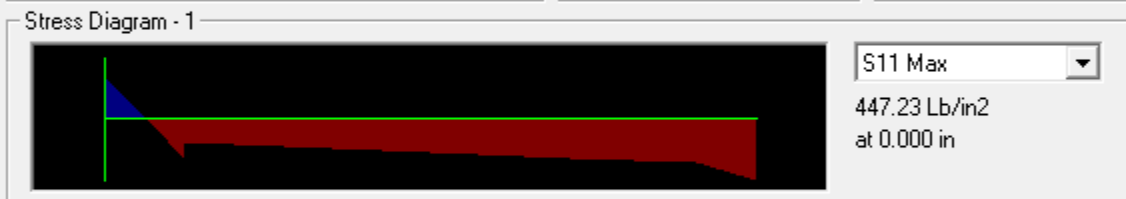
Case Extreme 150mph - VMS Cd = 1.22 Items Stress (S11) Single valued	End Length Offset (Location) I-End: Jt: 3 0.0000 in (0.000 in) J-End: Jt: 2024 0.0000 in (83.938 in)	Display Options <input type="radio"/> Scroll for Values <input checked="" type="radio"/> Show Max
---	---	--



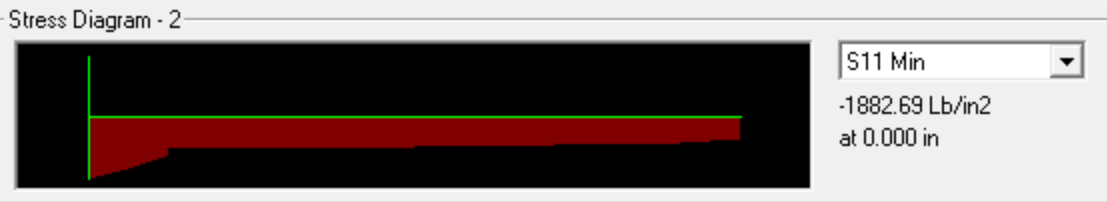
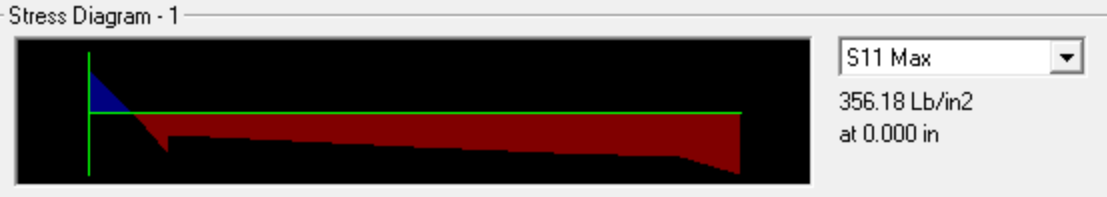
Case Extreme 150mph - VMS Cd = 1.0 Items Stress (S11) Single valued	End Length Offset (Location) I-End: Jt: 3 0.0000 in (0.000 in) J-End: Jt: 2024 0.0000 in (83.938 in)	Display Options <input type="radio"/> Scroll for Values <input checked="" type="radio"/> Show Max
--	---	--



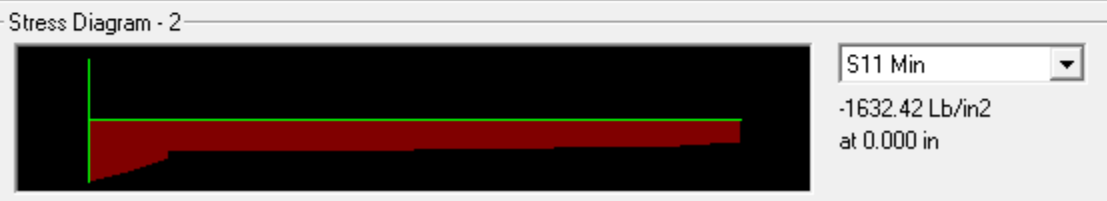
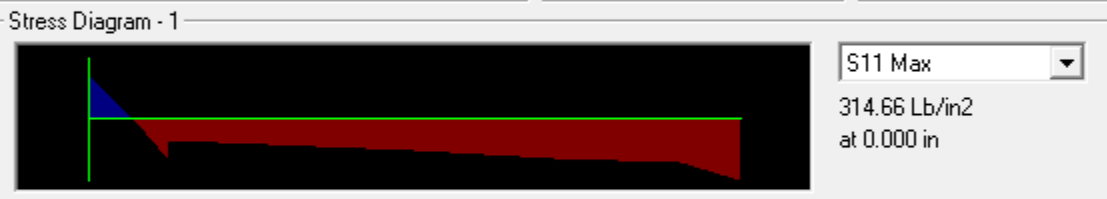
Case Fatigue - VMS Cd = 1.7 Items Stress (S11) Single valued	End Length Offset (Location) I-End: Jt: 3 0.0000 in (0.000 in) J-End: Jt: 2024 0.0000 in (83.938 in)	Display Options <input checked="" type="radio"/> Scroll for Values <input type="radio"/> Show Max Location 0.000 in
---	---	---



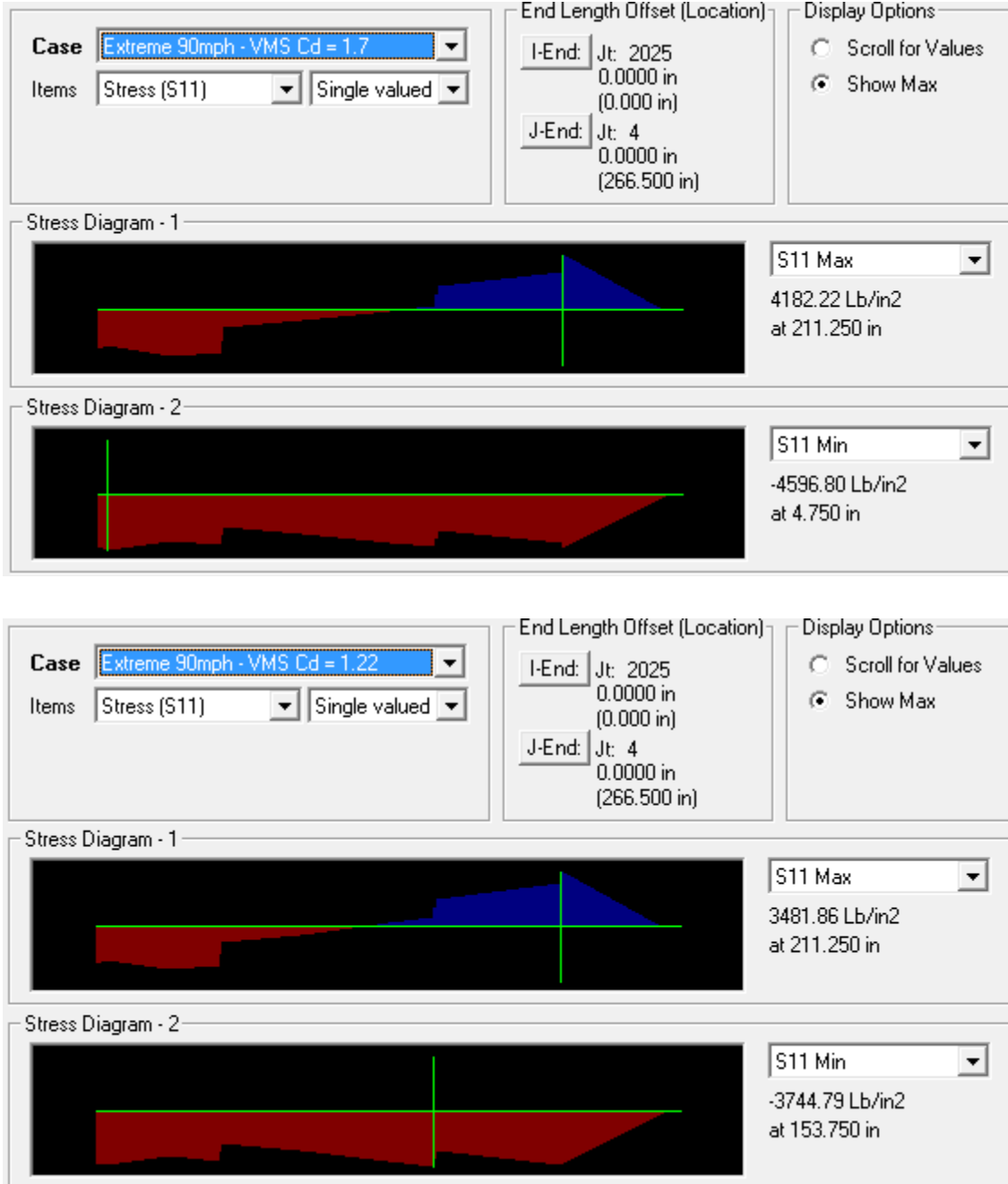
Case Fatigue - VMS Cd = 1.22 Items Stress (S11) Single valued	End Length Offset (Location) I-End: Jt: 3 0.0000 in (0.000 in) J-End: Jt: 2024 0.0000 in (83.938 in)	Display Options <input checked="" type="radio"/> Scroll for Values <input type="radio"/> Show Max Location 0.000 in
--	---	---



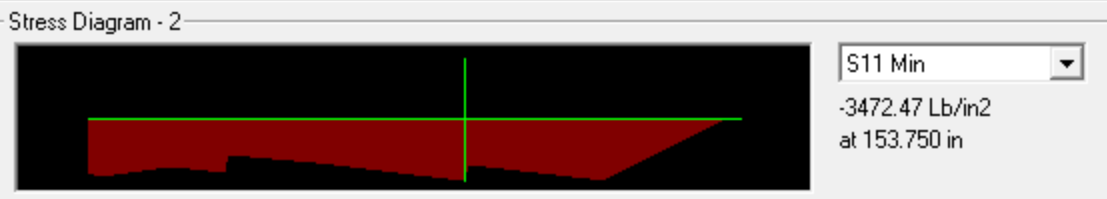
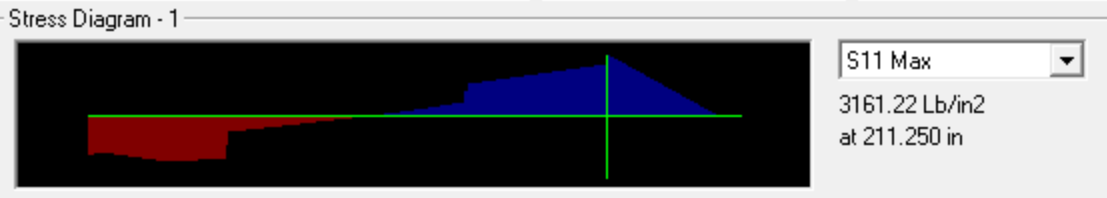
Case Fatigue - VMS Cd = 1.0 Items Stress (S11) Single valued	End Length Offset (Location) I-End: Jt: 3 0.0000 in (0.000 in) J-End: Jt: 2024 0.0000 in (83.938 in)	Display Options <input checked="" type="radio"/> Scroll for Values <input type="radio"/> Show Max Location 0.000 in
---	---	---



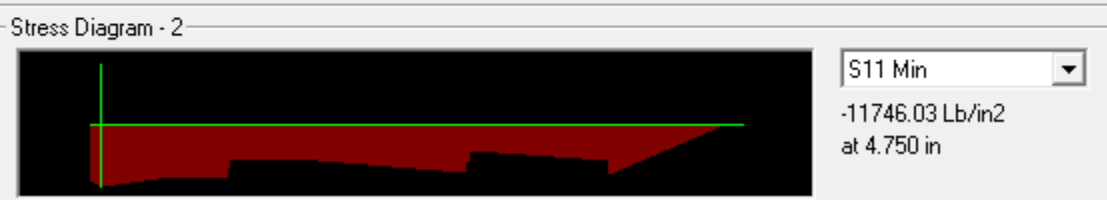
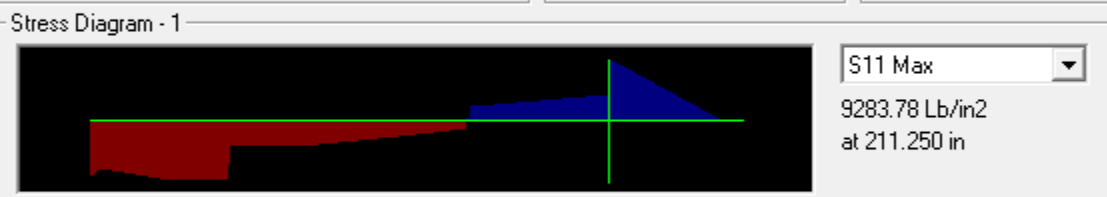
Upright 2b



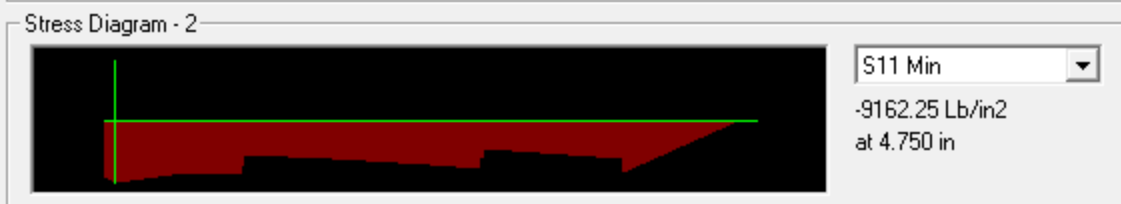
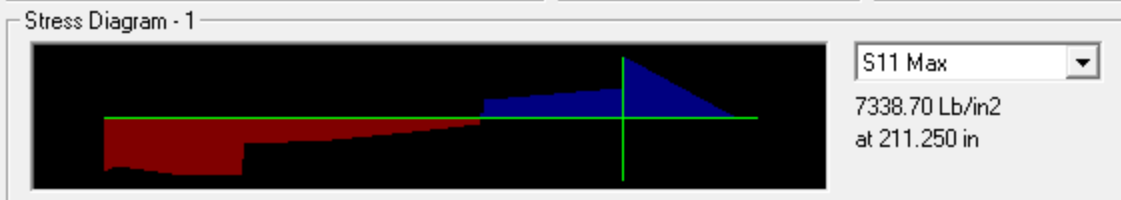
Case Extreme 90mph - VMS Cd = 1.0 Items Stress (S11) Single valued	End Length Offset (Location) I-End: Jt: 2025 0.0000 in (0.000 in) J-End: Jt: 4 0.0000 in (266.500 in)	Display Options <input type="radio"/> Scroll for Values <input checked="" type="radio"/> Show Max
--	--	--



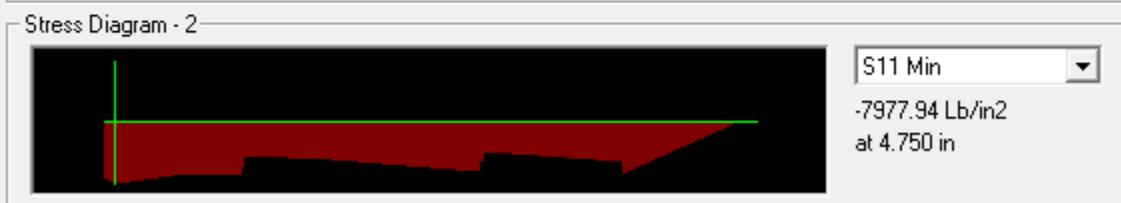
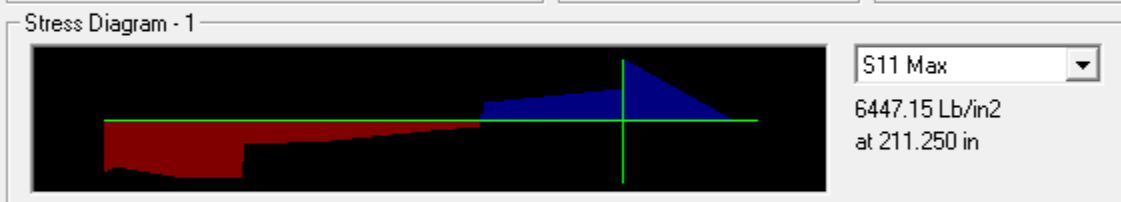
Case Extreme 150mph - VMS Cd = 1.7 Items Stress (S11) Single valued	End Length Offset (Location) I-End: Jt: 2025 0.0000 in (0.000 in) J-End: Jt: 4 0.0000 in (266.500 in)	Display Options <input type="radio"/> Scroll for Values <input checked="" type="radio"/> Show Max
---	--	--



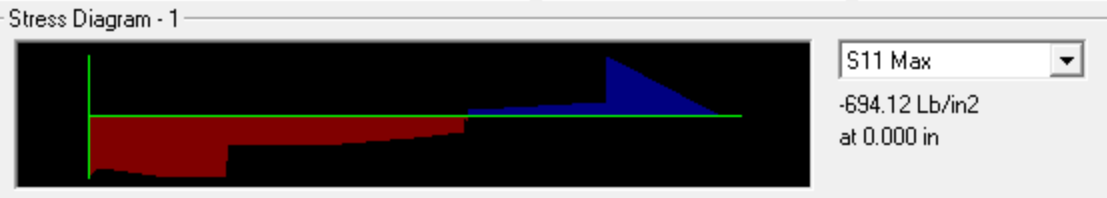
Case Extreme 150mph - VMS Cd = 1.22 Items Stress (S11) Single valued	End Length Offset (Location) I-End: Jt: 2025 0.0000 in (0.000 in) J-End: Jt: 4 0.0000 in (266.500 in)	Display Options <input type="radio"/> Scroll for Values <input checked="" type="radio"/> Show Max
---	--	--



Case Extreme 150mph - VMS Cd = 1.0 Items Stress (S11) Single valued	End Length Offset (Location) I-End: Jt: 2025 0.0000 in (0.000 in) J-End: Jt: 4 0.0000 in (266.500 in)	Display Options <input type="radio"/> Scroll for Values <input checked="" type="radio"/> Show Max
--	--	--

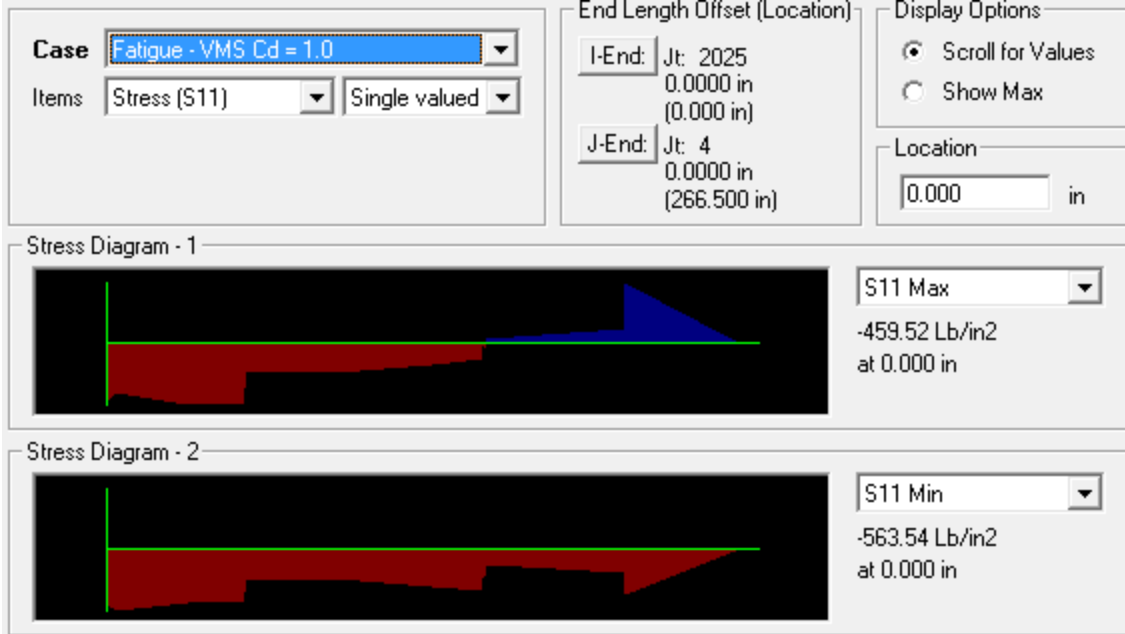


Case Fatigue - VMS Cd = 1.7 Items Stress (S11) Single valued	End Length Offset (Location) I-End: Jt: 2025 0.0000 in (0.000 in) J-End: Jt: 4 0.0000 in (266.500 in)	Display Options <input checked="" type="radio"/> Scroll for Values <input type="radio"/> Show Max Location 0.000 in
--	--	---

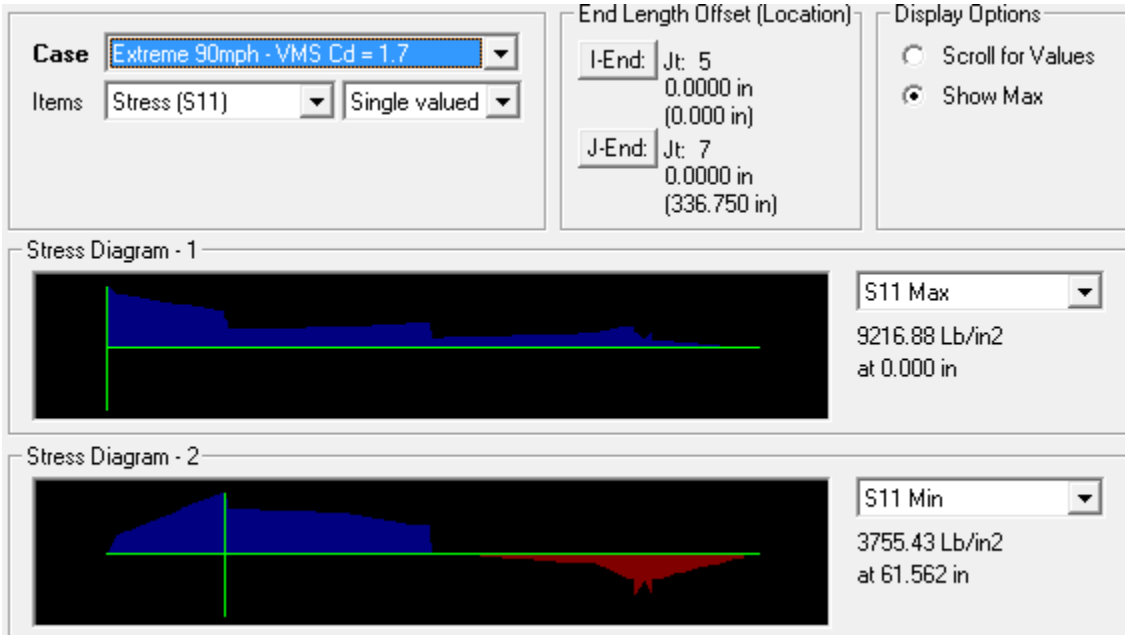


Case Fatigue - VMS Cd = 1.22 Items Stress (S11) Single valued	End Length Offset (Location) I-End: Jt: 2025 0.0000 in (0.000 in) J-End: Jt: 4 0.0000 in (266.500 in)	Display Options <input checked="" type="radio"/> Scroll for Values <input type="radio"/> Show Max Location 0.000 in
---	--	---



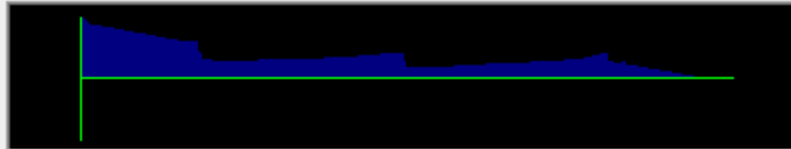


Upright 3



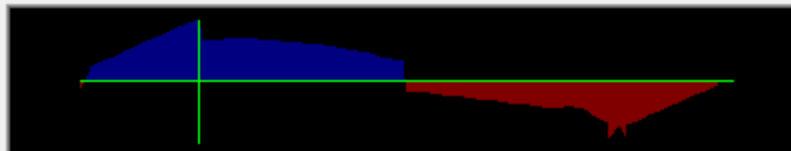
Case Extreme 90mph - VMS Cd = 1.22 Items Stress (S11) Single valued	End Length Offset (Location) I-End: Jt: 5 0.0000 in (0.000 in) J-End: Jt: 7 0.0000 in (336.750 in)	Display Options <input type="radio"/> Scroll for Values <input checked="" type="radio"/> Show Max
--	---	--

Stress Diagram - 1



S11 Max
6822.05 Lb/in2
at 0.000 in

Stress Diagram - 2



S11 Min
2637.15 Lb/in2
at 61.562 in

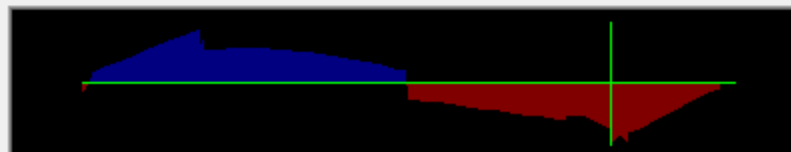
Case Extreme 90mph - VMS Cd = 1.0 Items Stress (S11) Single valued	End Length Offset (Location) I-End: Jt: 5 0.0000 in (0.000 in) J-End: Jt: 7 0.0000 in (336.750 in)	Display Options <input type="radio"/> Scroll for Values <input checked="" type="radio"/> Show Max
---	---	--

Stress Diagram - 1



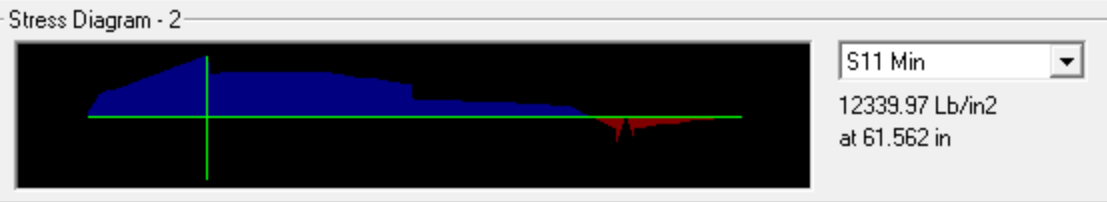
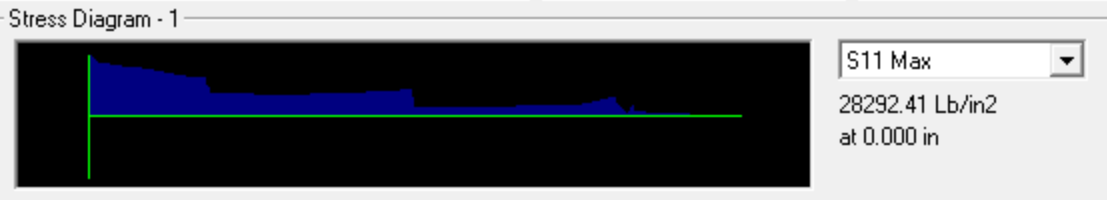
S11 Max
5725.65 Lb/in2
at 0.000 in

Stress Diagram - 2

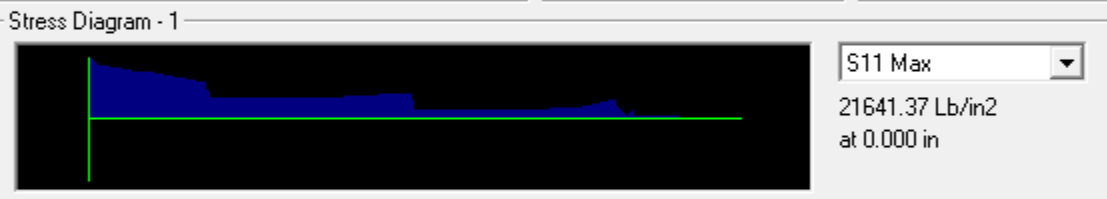


S11 Min
-2462.80 Lb/in2
at 272.812 in

Case Extreme 150mph - VMS Cd = 1.7 Items Stress (S11) Single valued	End Length Offset (Location) I-End: Jt: 5 0.0000 in (0.000 in)	Display Options <input type="radio"/> Scroll for Values <input checked="" type="radio"/> Show Max
	J-End: Jt: 7 0.0000 in (336.750 in)	

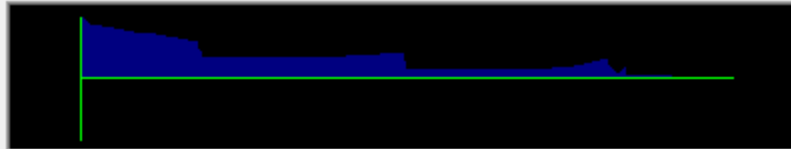


Case Extreme 150mph - VMS Cd = 1.22 Items Stress (S11) Single valued	End Length Offset (Location) I-End: Jt: 5 0.0000 in (0.000 in)	Display Options <input type="radio"/> Scroll for Values <input checked="" type="radio"/> Show Max
	J-End: Jt: 7 0.0000 in (336.750 in)	



Case Extreme 150mph - VMS Cd = 1.0 Items Stress (S11) Single valued	End Length Offset (Location) I-End: Jt: 5 0.0000 in (0.000 in) J-End: Jt: 7 0.0000 in (336.750 in)	Display Options <input type="radio"/> Scroll for Values <input checked="" type="radio"/> Show Max
--	---	--

Stress Diagram - 1



S11 Max
 18592.78 Lb/in2
 at 0.000 in

Stress Diagram - 2



S11 Min
 7810.68 Lb/in2
 at 61.562 in

Case Fatigue - VMS Cd = 1.7 Items Stress (S11) Single valued	End Length Offset (Location) I-End: Jt: 5 0.0000 in (0.000 in) J-End: Jt: 7 0.0000 in (336.750 in)	Display Options <input checked="" type="radio"/> Scroll for Values <input type="radio"/> Show Max Location 0.000 in
---	---	---

Stress Diagram - 1



S11 Max
 2546.62 Lb/in2
 at 0.000 in

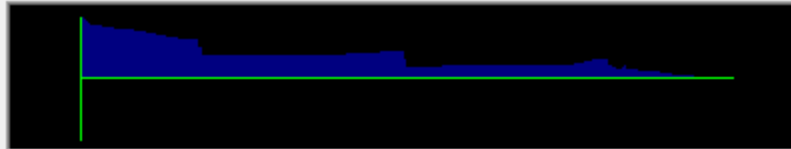
Stress Diagram - 2



S11 Min
 152.74 Lb/in2
 at 0.000 in

Case Fatigue - VMS Cd = 1.22 Items Stress (S11) Single valued	End Length Offset (Location) I-End: Jt: 5 0.0000 in (0.000 in) J-End: Jt: 7 0.0000 in (336.750 in)	Display Options <input checked="" type="radio"/> Scroll for Values <input type="radio"/> Show Max Location 0.000 in
--	---	---

Stress Diagram - 1



S11 Max
 1979.12 Lb/in²
 at 0.000 in

Stress Diagram - 2



S11 Min
 104.14 Lb/in²
 at 0.000 in

Case Fatigue - VMS Cd = 1.0 Items Stress (S11) Single valued	End Length Offset (Location) I-End: Jt: 5 0.0000 in (0.000 in) J-End: Jt: 7 0.0000 in (336.750 in)	Display Options <input checked="" type="radio"/> Scroll for Values <input type="radio"/> Show Max Location 0.000 in
---	---	---

Stress Diagram - 1



S11 Max
 1720.34 Lb/in²
 at 0.000 in

Stress Diagram - 2

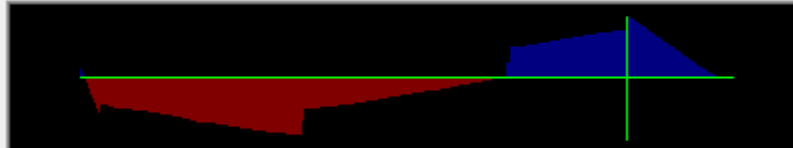


S11 Min
 81.98 Lb/in²
 at 0.000 in

Upright 4

Case Extreme 90mph - VMS Cd = 1.7	End Length Offset (Location)	Display Options
Items Stress (S11) Single valued	I-End: Jt: 6 0.0000 in (0.000 in)	<input type="radio"/> Scroll for Values
	J-End: Jt: 8 0.0000 in (336.750 in)	<input checked="" type="radio"/> Show Max

Stress Diagram - 1



S11 Max

4136.01 Lb/in²
at 281.562 in

Stress Diagram - 2

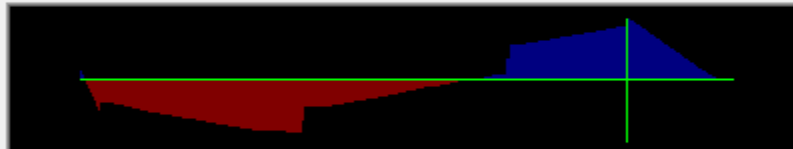


S11 Min

-11308.11 Lb/in²
at 0.000 in

Case Extreme 90mph - VMS Cd = 1.22	End Length Offset (Location)	Display Options
Items Stress (S11) Single valued	I-End: Jt: 6 0.0000 in (0.000 in)	<input type="radio"/> Scroll for Values
	J-End: Jt: 8 0.0000 in (336.750 in)	<input checked="" type="radio"/> Show Max

Stress Diagram - 1



S11 Max

3403.42 Lb/in²
at 281.562 in

Stress Diagram - 2

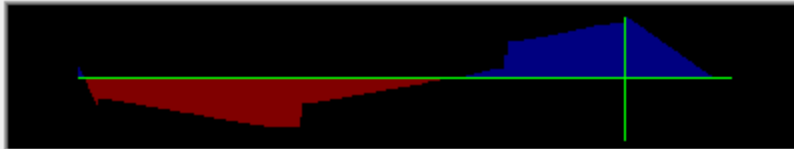


S11 Min

-8771.35 Lb/in²
at 0.000 in

Case Extreme 90mph - VMS Cd = 1.0 Items Stress (S11) Single valued	End Length Offset (Location) I-End: Jt: 6 0.0000 in (0.000 in) J-End: Jt: 8 0.0000 in (336.750 in)	Display Options <input type="radio"/> Scroll for Values <input checked="" type="radio"/> Show Max
--	---	--

Stress Diagram - 1



S11 Max
 3122.49 Lb/in²
 at 281.562 in

Stress Diagram - 2



S11 Min
 -7669.14 Lb/in²
 at 0.000 in

Case Extreme 150mph - VMS Cd = 1.7 Items Stress (S11) Single valued	End Length Offset (Location) I-End: Jt: 6 0.0000 in (0.000 in) J-End: Jt: 8 0.0000 in (336.750 in)	Display Options <input type="radio"/> Scroll for Values <input checked="" type="radio"/> Show Max
---	---	--

Stress Diagram - 1



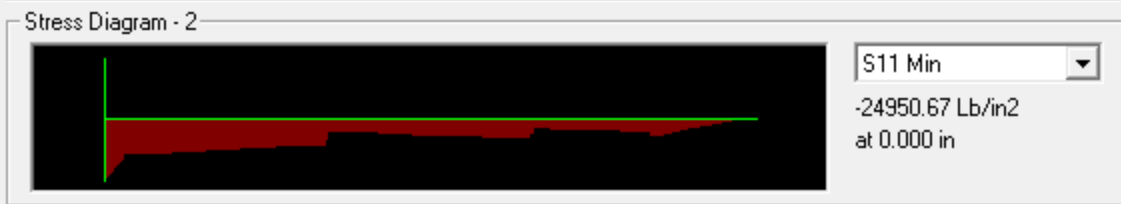
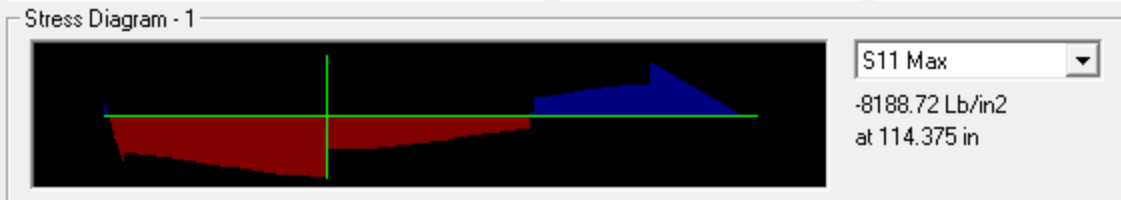
S11 Max
 -10583.95 Lb/in²
 at 114.375 in

Stress Diagram - 2

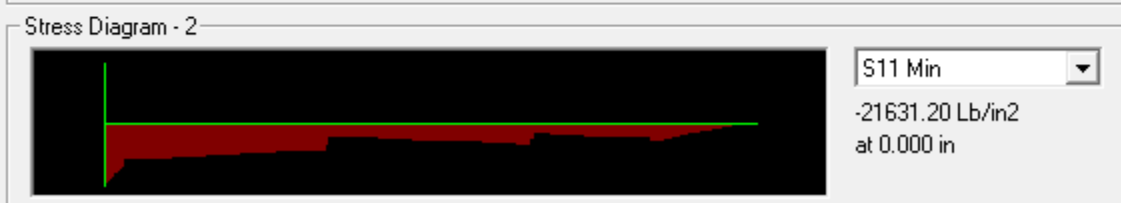
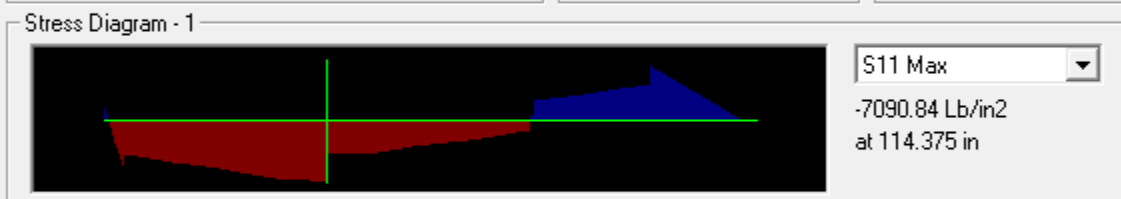


S11 Min
 -32192.72 Lb/in²
 at 0.000 in

Case Extreme 150mph - VMS Cd = 1.22 Items Stress (S11) Single valued	End Length Offset (Location) I-End: Jt: 6 0.0000 in (0.000 in) J-End: Jt: 8 0.0000 in (336.750 in)	Display Options <input type="radio"/> Scroll for Values <input checked="" type="radio"/> Show Max
---	---	--

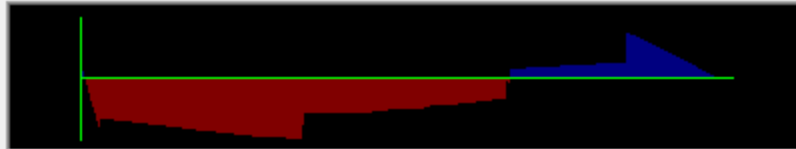


Case Extreme 150mph - VMS Cd = 1.0 Items Stress (S11) Single valued	End Length Offset (Location) I-End: Jt: 6 0.0000 in (0.000 in) J-End: Jt: 8 0.0000 in (336.750 in)	Display Options <input type="radio"/> Scroll for Values <input checked="" type="radio"/> Show Max
--	---	--



Case Fatigue - VMS Cd = 1.7 Items Stress (S11) Single valued	End Length Offset (Location) I-End: Jt: 6 0.0000 in (0.000 in) J-End: Jt: 8 0.0000 in (336.750 in)	Display Options <input checked="" type="radio"/> Scroll for Values <input type="radio"/> Show Max Location 0.000 in
--	---	---

Stress Diagram - 1



S11 Max
 220.97 Lb/in²
 at 0.000 in

Stress Diagram - 2



S11 Min
 -2788.33 Lb/in²
 at 0.000 in

Case Fatigue - VMS Cd = 1.22 Items Stress (S11) Single valued	End Length Offset (Location) I-End: Jt: 6 0.0000 in (0.000 in) J-End: Jt: 8 0.0000 in (336.750 in)	Display Options <input checked="" type="radio"/> Scroll for Values <input type="radio"/> Show Max Location 0.000 in
---	---	---

Stress Diagram - 1



S11 Max
 183.73 Lb/in²
 at 0.000 in

Stress Diagram - 2



S11 Min
 -2170.41 Lb/in²
 at 0.000 in

Case Fatigue - VMS Cd = 1.0

Items Stress (S11) Single valued

End Length Offset (Location)

I-End: Jt: 6
0.0000 in
(0.000 in)

J-End: Jt: 8
0.0000 in
(336.750 in)


Display Options

Scroll for Values
 Show Max

Location

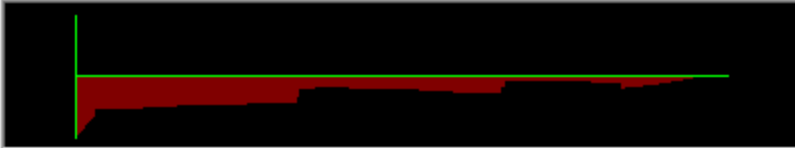
0.000 in

Stress Diagram - 1



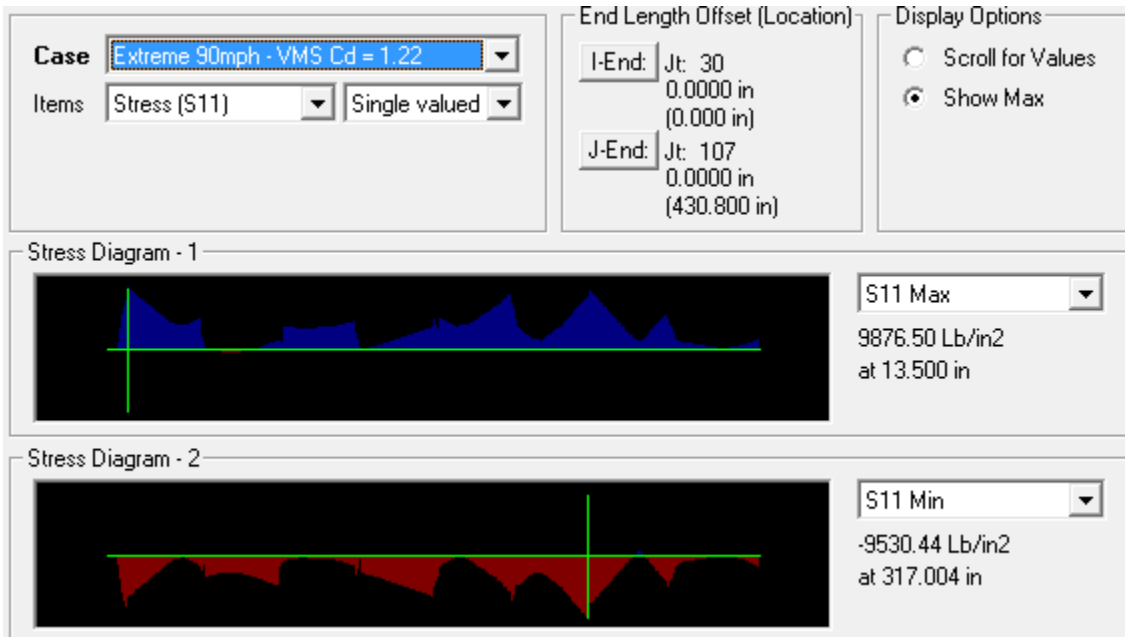
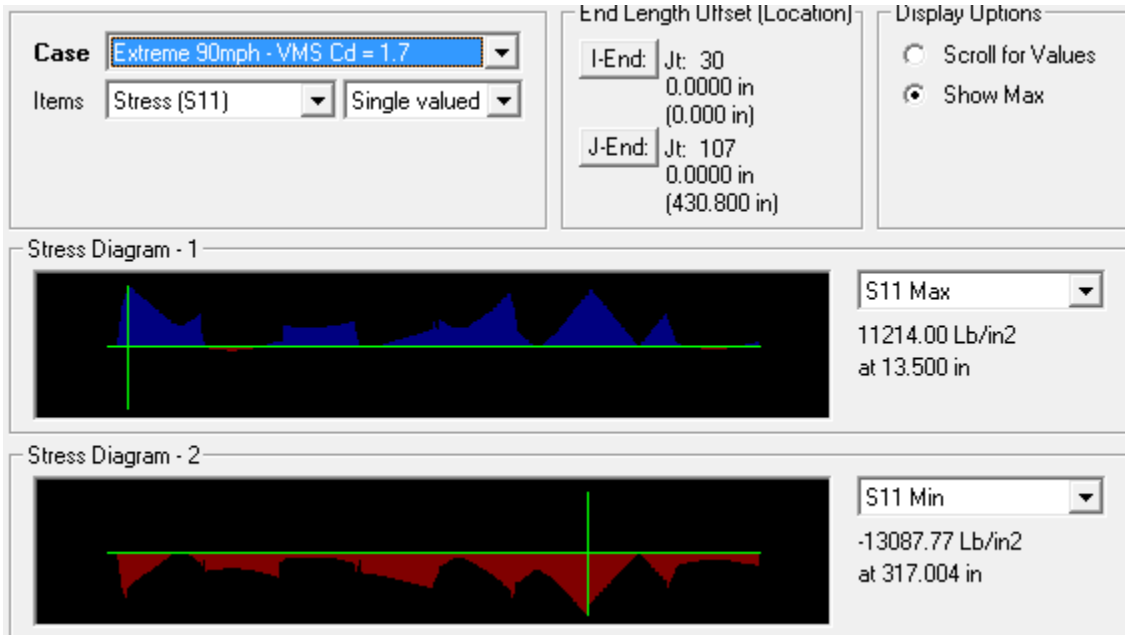
S11 Max
166.75 Lb/in2
at 0.000 in

Stress Diagram - 2



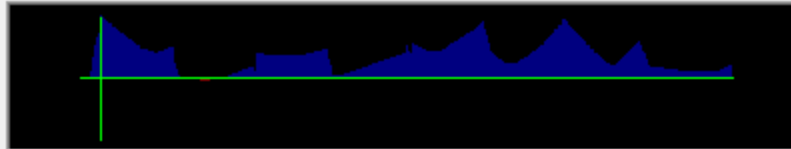
S11 Min
-1888.63 Lb/in2
at 0.000 in

Chord 1a



Case Extreme 90mph - VMS Cd = 1.0 Items Stress (S11) Single valued	End Length Offset (Location) I-End: Jt: 30 0.0000 in (0.000 in) J-End: Jt: 107 0.0000 in (430.800 in)	Display Options <input type="radio"/> Scroll for Values <input checked="" type="radio"/> Show Max
---	--	--

Stress Diagram - 1



S11 Max
9305.06 Lb/in2
at 13.500 in

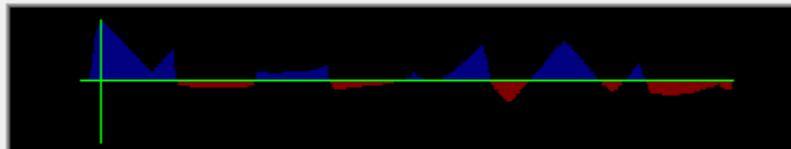
Stress Diagram - 2



S11 Min
-7901.82 Lb/in2
at 317.004 in

Case Extreme 150mph - VMS Cd = 1.7 Items Stress (S11) Single valued	End Length Offset (Location) I-End: Jt: 30 0.0000 in (0.000 in) J-End: Jt: 107 0.0000 in (430.800 in)	Display Options <input type="radio"/> Scroll for Values <input checked="" type="radio"/> Show Max
--	--	--

Stress Diagram - 1

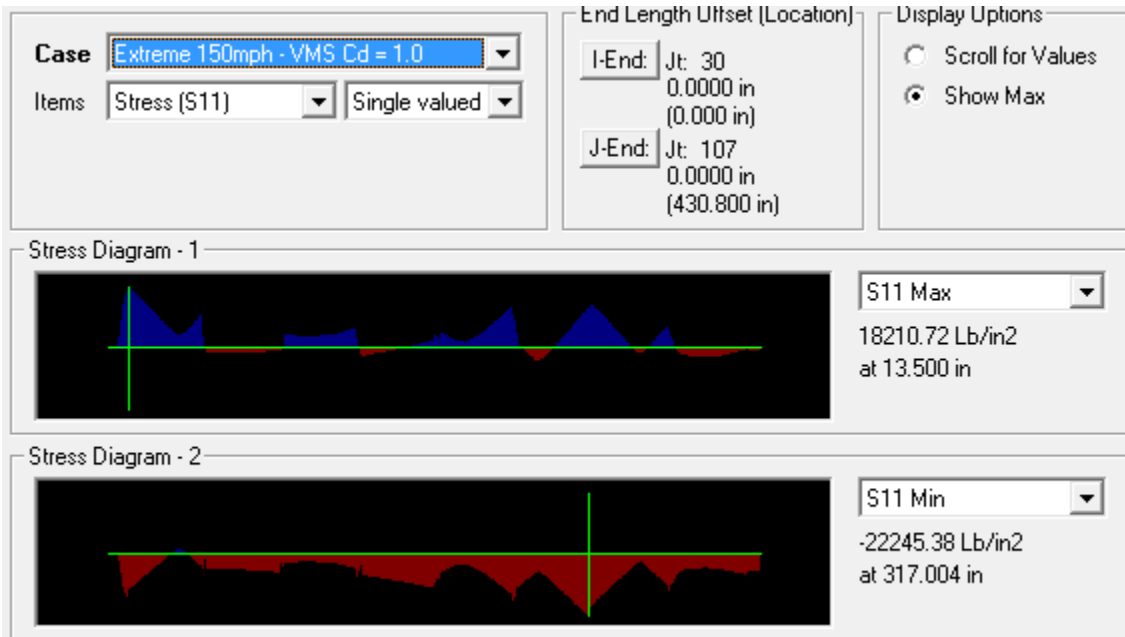
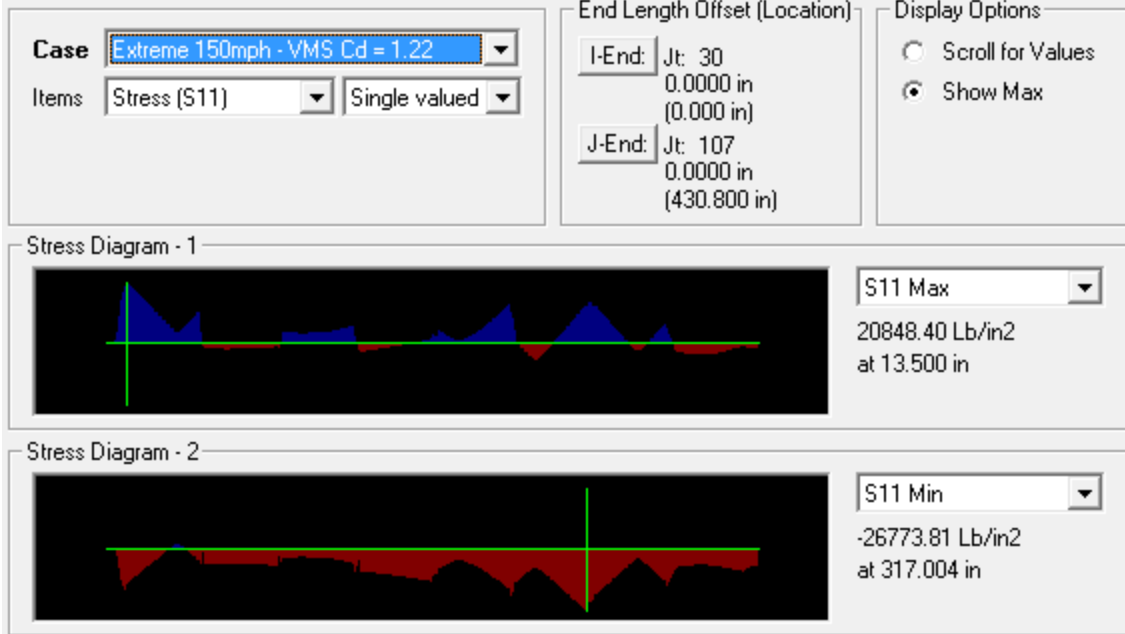


S11 Max
26602.97 Lb/in2
at 13.500 in

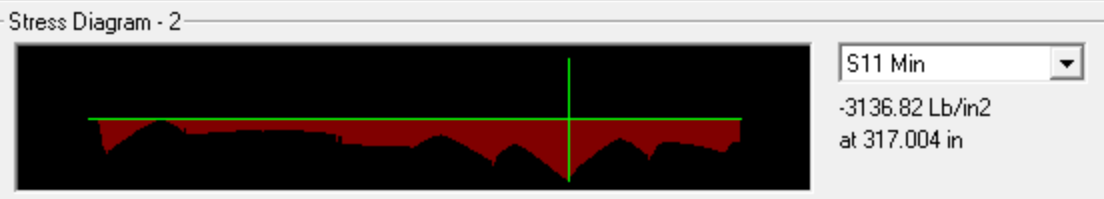
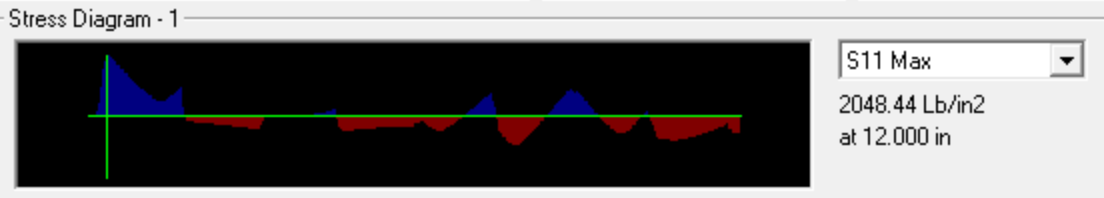
Stress Diagram - 2



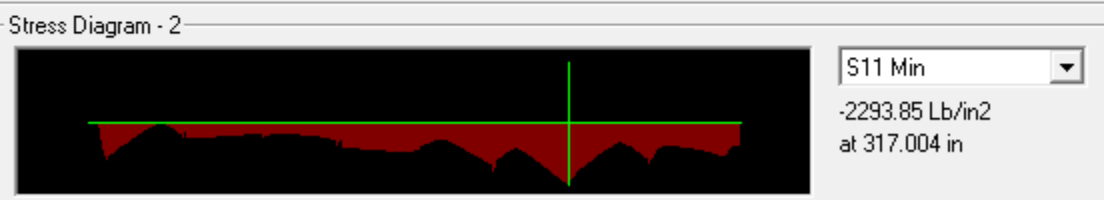
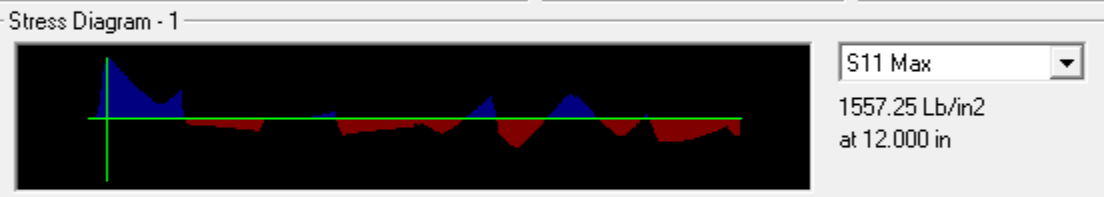
S11 Min
-36653.41 Lb/in2
at 317.004 in

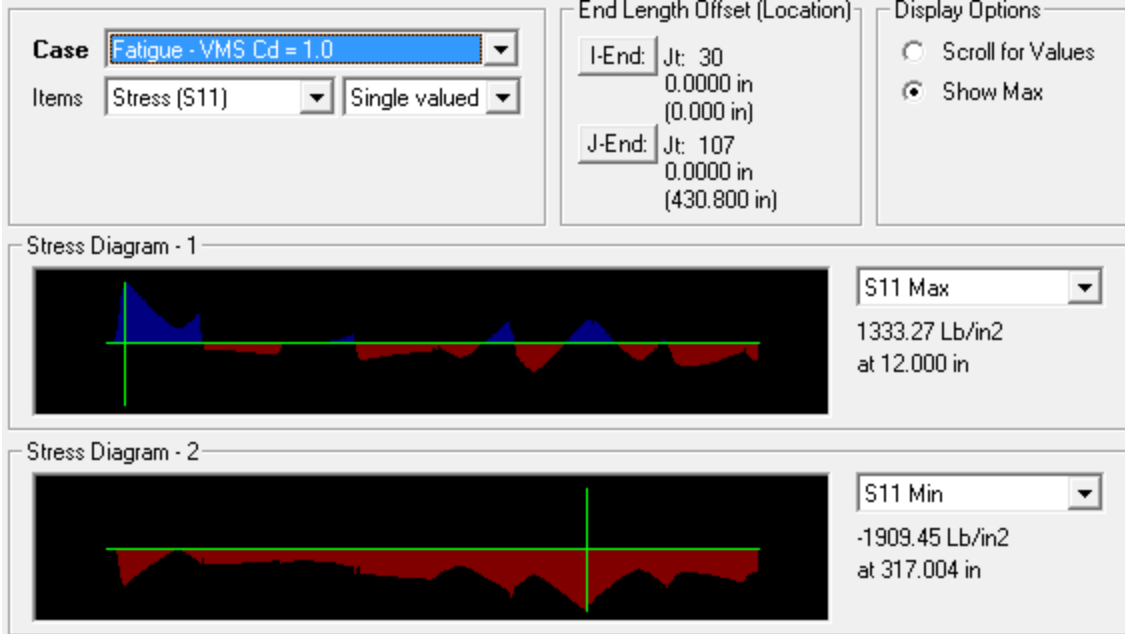


Case Fatigue - VMS Cd = 1.7 Items Stress (S11) Single valued	End Length Offset (Location) I-End: Jt: 30 0.0000 in (0.000 in) J-End: Jt: 107 0.0000 in (430.800 in)	Display Options <input type="radio"/> Scroll for Values <input checked="" type="radio"/> Show Max
--	--	--

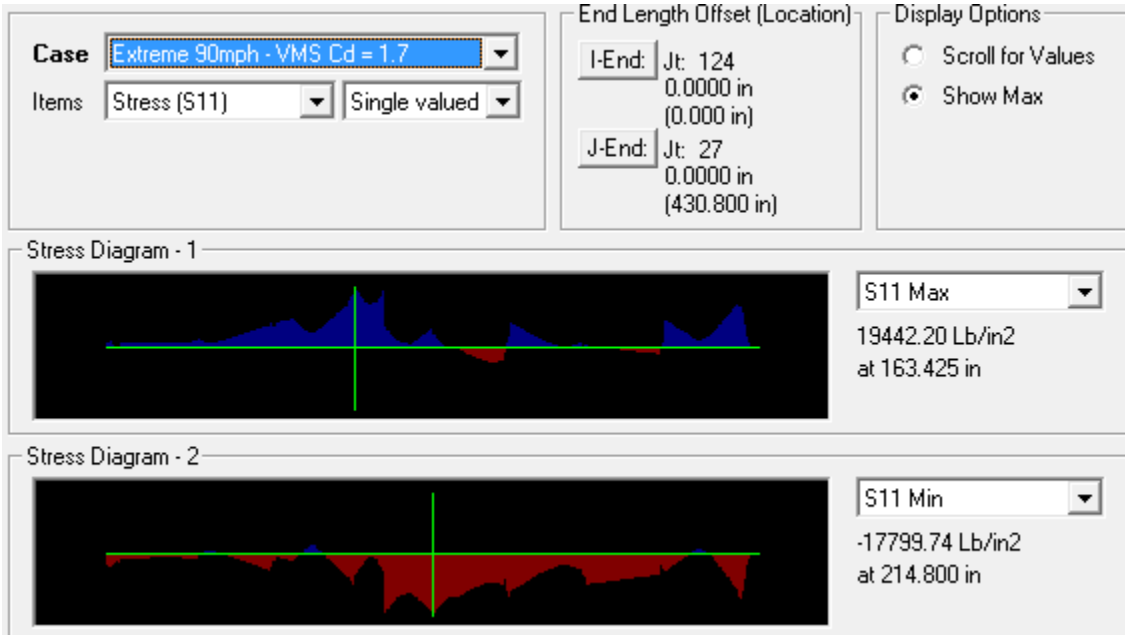


Case Fatigue - VMS Cd = 1.22 Items Stress (S11) Single valued	End Length Offset (Location) I-End: Jt: 30 0.0000 in (0.000 in) J-End: Jt: 107 0.0000 in (430.800 in)	Display Options <input type="radio"/> Scroll for Values <input checked="" type="radio"/> Show Max
---	--	--

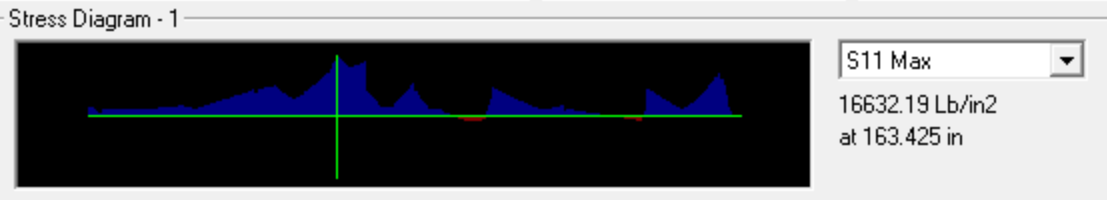




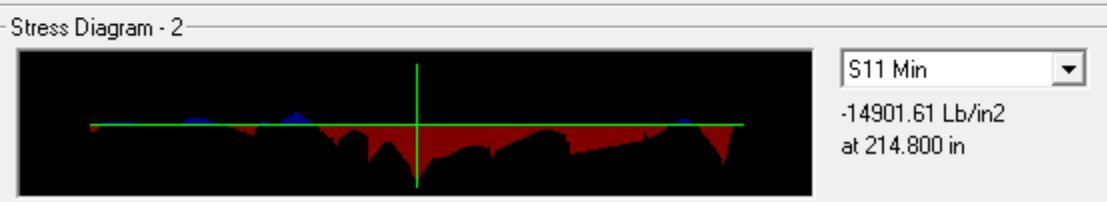
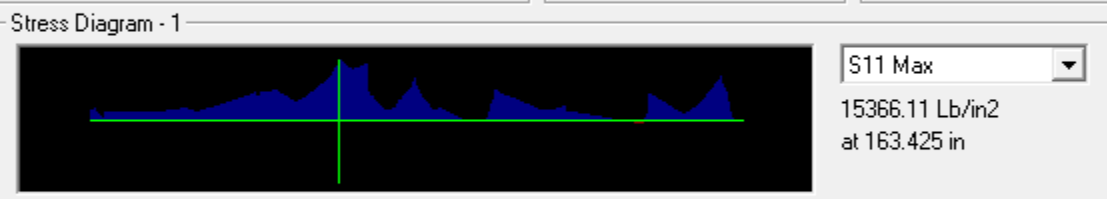
Chord 1b



Case Extreme 90mph - VMS Cd = 1.22 Items Stress (S11) Single valued	End Length Offset (Location) I-End: Jt: 124 0.0000 in (0.000 in) J-End: Jt: 27 0.0000 in (430.800 in)	Display Options <input type="radio"/> Scroll for Values <input checked="" type="radio"/> Show Max
--	--	--



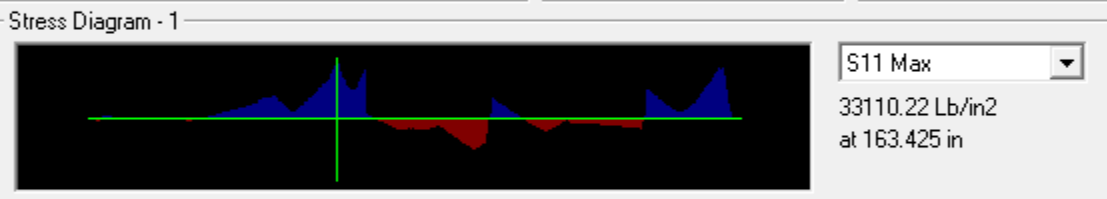
Case Extreme 90mph - VMS Cd = 1.0 Items Stress (S11) Single valued	End Length Offset (Location) I-End: Jt: 124 0.0000 in (0.000 in) J-End: Jt: 27 0.0000 in (430.800 in)	Display Options <input type="radio"/> Scroll for Values <input checked="" type="radio"/> Show Max
---	--	--



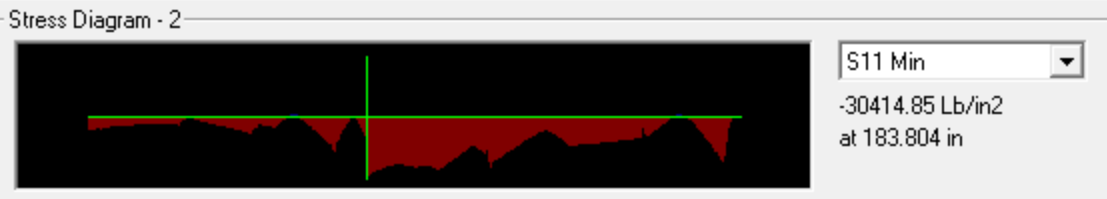
Case Extreme 150mph - VMS Cd = 1.7 Items Stress (S11) Single valued	End Length Offset (Location) I-End: Jt: 124 0.0000 in (0.000 in)	Display Options <input type="radio"/> Scroll for Values <input checked="" type="radio"/> Show Max
	J-End: Jt: 27 0.0000 in (430.800 in)	



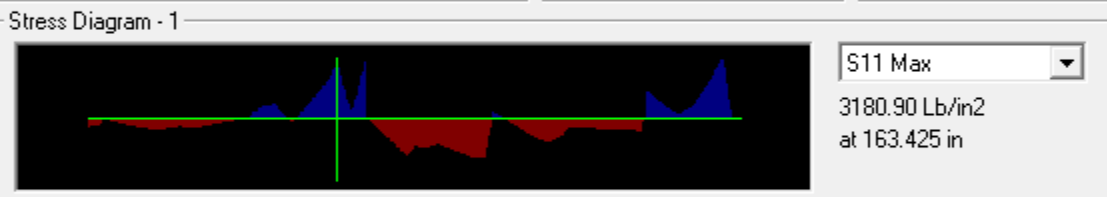
Case Extreme 150mph - VMS Cd = 1.22 Items Stress (S11) Single valued	End Length Offset (Location) I-End: Jt: 124 0.0000 in (0.000 in)	Display Options <input type="radio"/> Scroll for Values <input checked="" type="radio"/> Show Max
	J-End: Jt: 27 0.0000 in (430.800 in)	



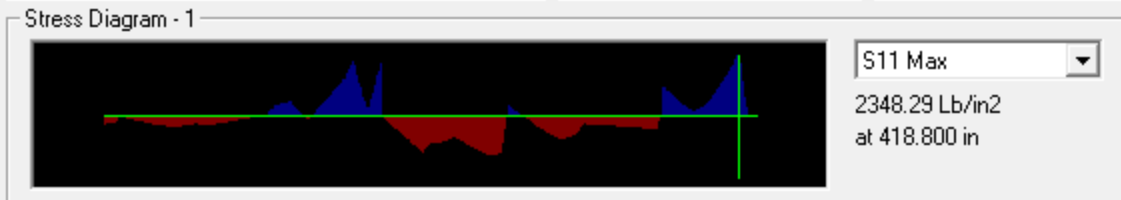
Case Extreme 150mph - VMS Cd = 1.0 Items Stress (S11) Single valued	End Length Offset (Location) I-End: Jt: 124 0.0000 in (0.000 in) J-End: Jt: 27 0.0000 in (430.800 in)	Display Options <input type="radio"/> Scroll for Values <input checked="" type="radio"/> Show Max
--	--	--



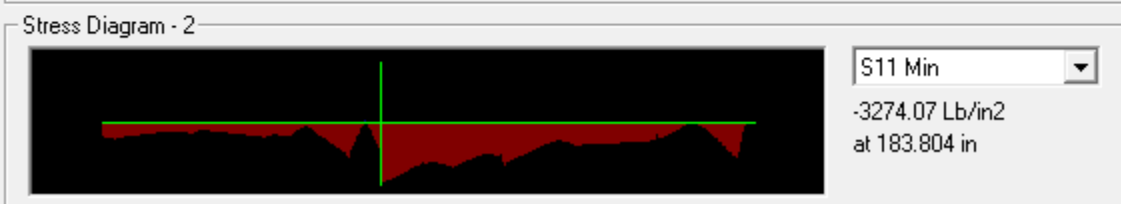
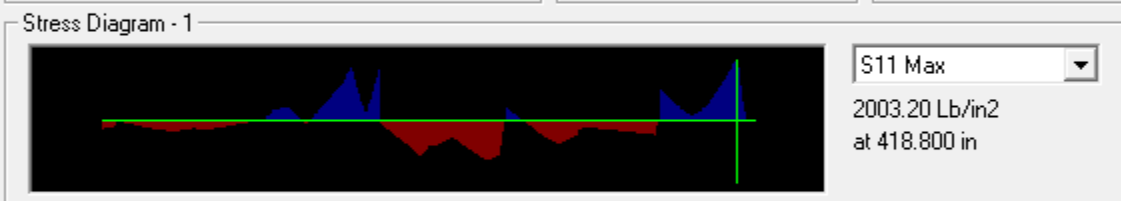
Case Fatigue - VMS Cd = 1.7 Items Stress (S11) Single valued	End Length Offset (Location) I-End: Jt: 124 0.0000 in (0.000 in) J-End: Jt: 27 0.0000 in (430.800 in)	Display Options <input type="radio"/> Scroll for Values <input checked="" type="radio"/> Show Max
---	--	--



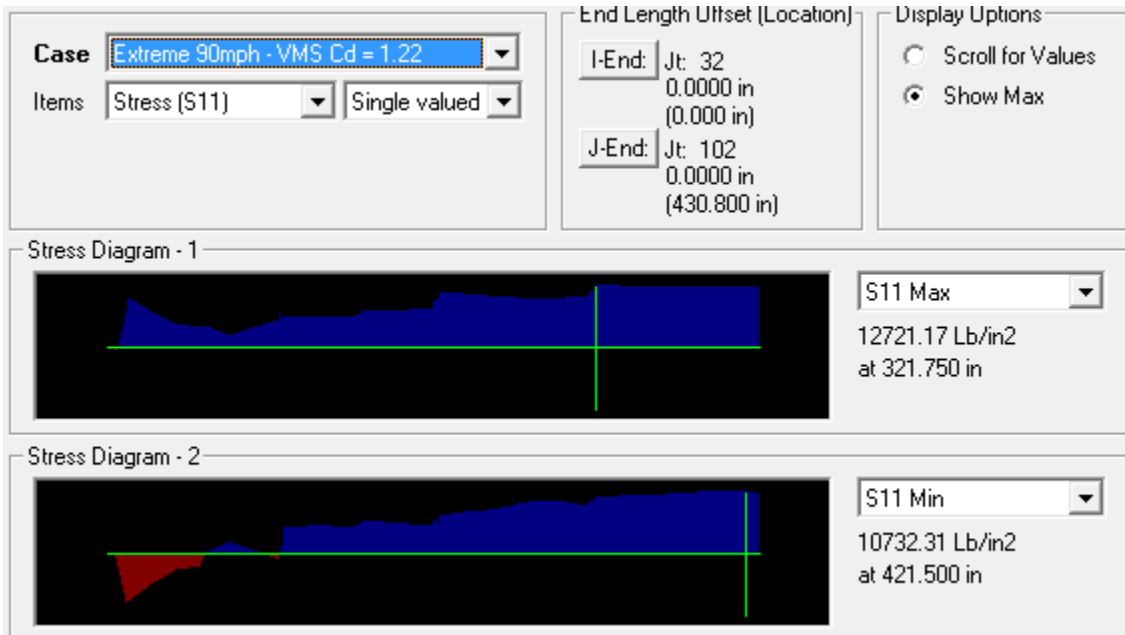
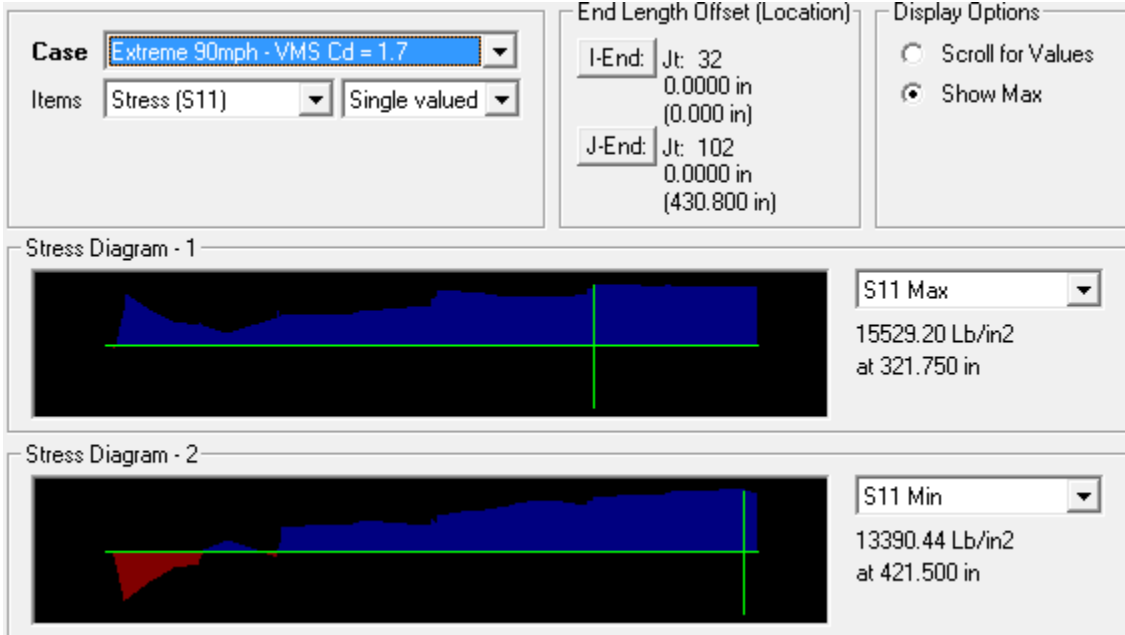
Case Fatigue - VMS Cd = 1.22 Items Stress (S11) Single valued	End Length Offset (Location) I-End: Jt: 124 0.0000 in (0.000 in) J-End: Jt: 27 0.0000 in (430.800 in)	Display Options <input type="radio"/> Scroll for Values <input checked="" type="radio"/> Show Max
---	--	--

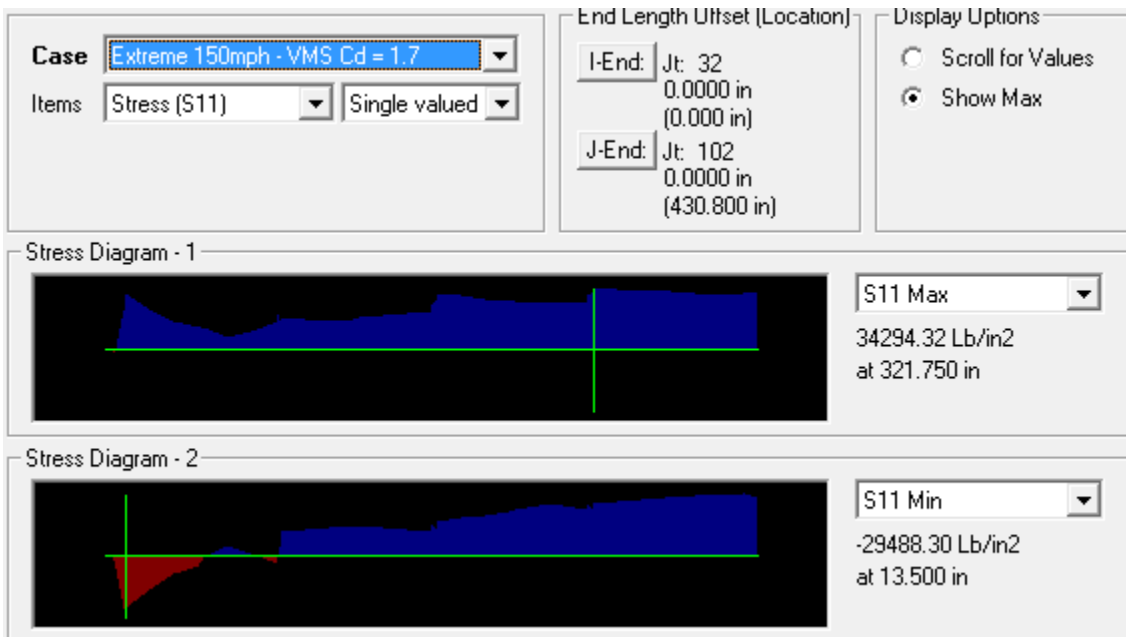
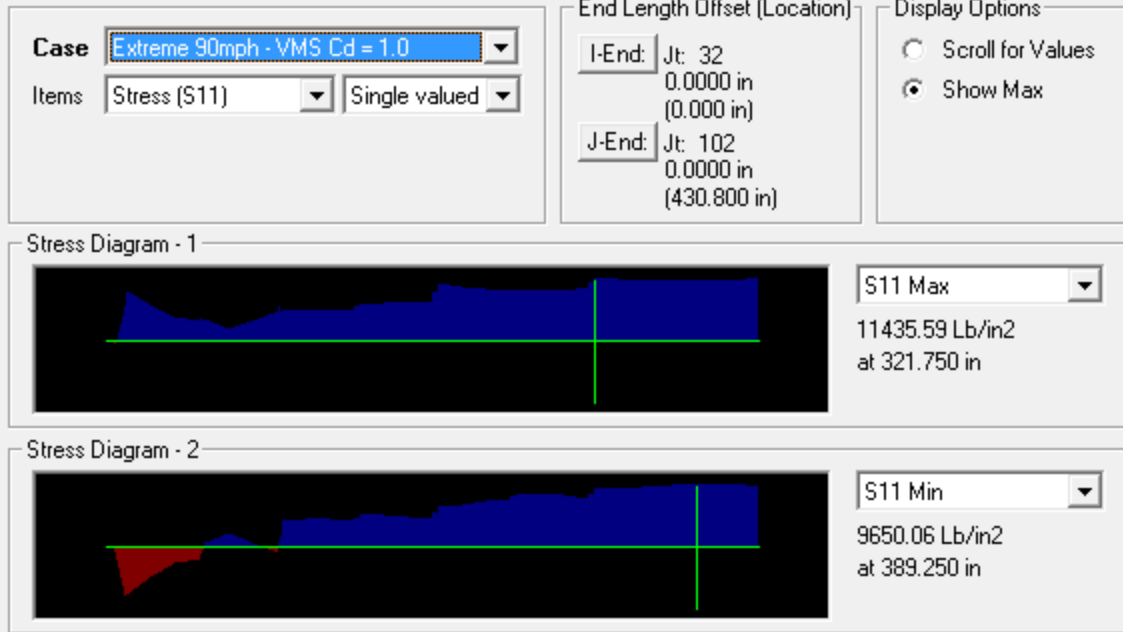


Case Fatigue - VMS Cd = 1.0 Items Stress (S11) Single valued	End Length Offset (Location) I-End: Jt: 124 0.0000 in (0.000 in) J-End: Jt: 27 0.0000 in (430.800 in)	Display Options <input type="radio"/> Scroll for Values <input checked="" type="radio"/> Show Max
--	--	--



Chord 2a





Case Extreme 150mph - VMS Cd = 1.22 Items Stress (S11) Single valued	End Length Offset (Location) I-End: Jt: 32 0.0000 in (0.000 in) J-End: Jt: 102 0.0000 in (430.800 in)	Display Options <input type="radio"/> Scroll for Values <input checked="" type="radio"/> Show Max
---	--	--

Stress Diagram - 1



S11 Max

26495.69 Lb/in2
at 321.750 in

Stress Diagram - 2



S11 Min

23167.24 Lb/in2
at 423.000 in

Case Extreme 150mph - VMS Cd = 1.0 Items Stress (S11) Single valued	End Length Offset (Location) I-End: Jt: 32 0.0000 in (0.000 in) J-End: Jt: 102 0.0000 in (430.800 in)	Display Options <input type="radio"/> Scroll for Values <input checked="" type="radio"/> Show Max
--	--	--

Stress Diagram - 1



S11 Max

22921.10 Lb/in2
at 321.750 in

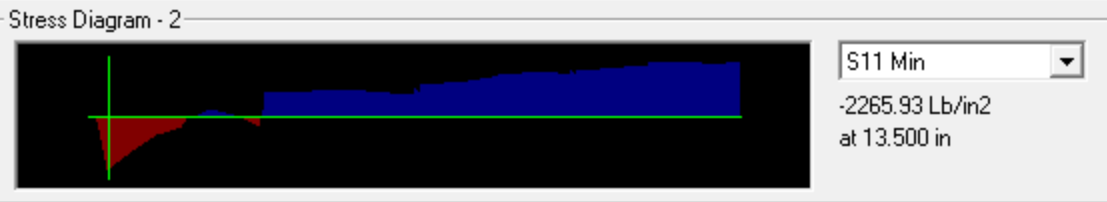
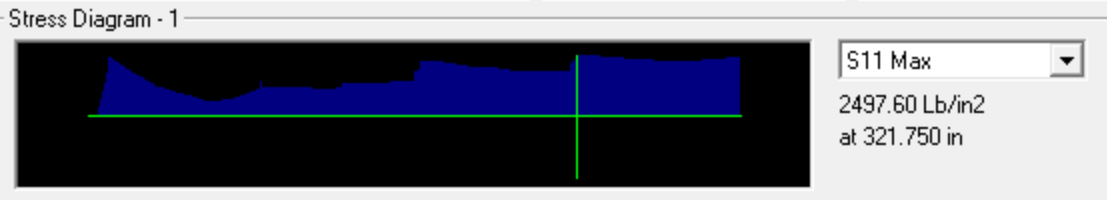
Stress Diagram - 2



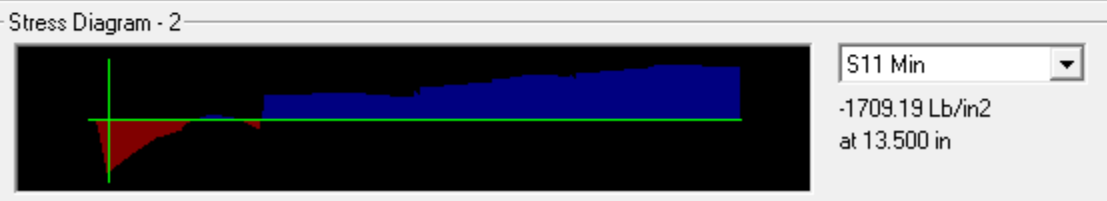
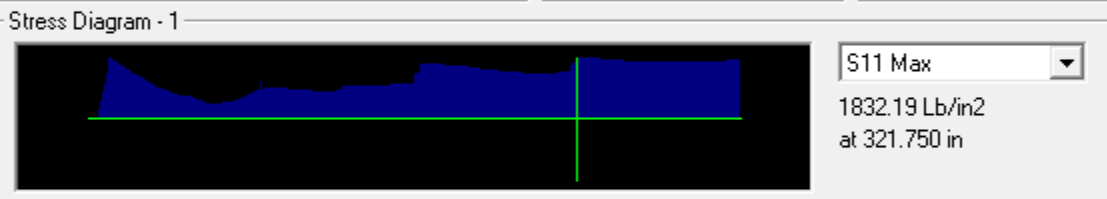
S11 Min

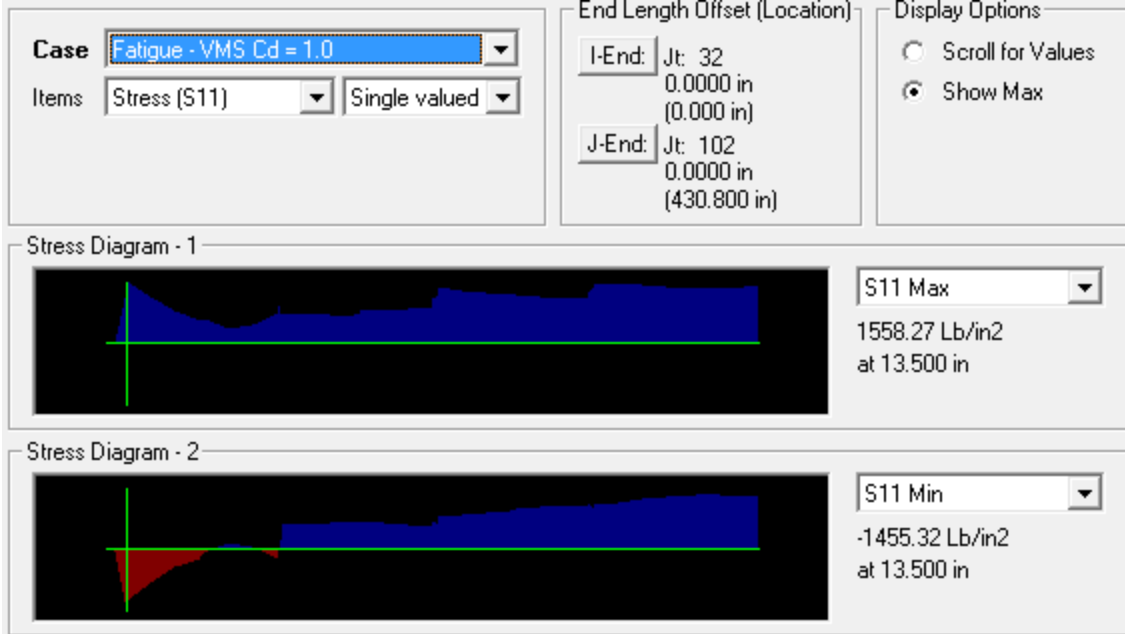
20190.31 Lb/in2
at 421.500 in

Case Fatigue - VMS Cd = 1.7 Items Stress (S11) Single valued	End Length Offset (Location) I-End: Jt: 32 0.0000 in (0.000 in) J-End: Jt: 102 0.0000 in (430.800 in)	Display Options <input type="radio"/> Scroll for Values <input checked="" type="radio"/> Show Max
---	--	--

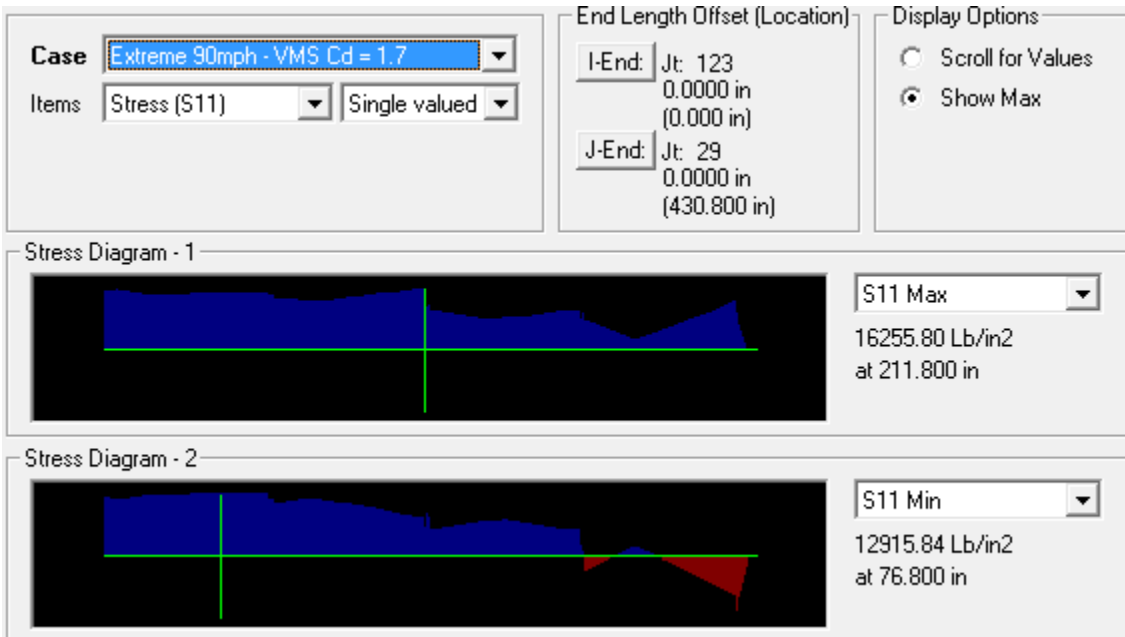


Case Fatigue - VMS Cd = 1.22 Items Stress (S11) Single valued	End Length Offset (Location) I-End: Jt: 32 0.0000 in (0.000 in) J-End: Jt: 102 0.0000 in (430.800 in)	Display Options <input type="radio"/> Scroll for Values <input checked="" type="radio"/> Show Max
--	--	--

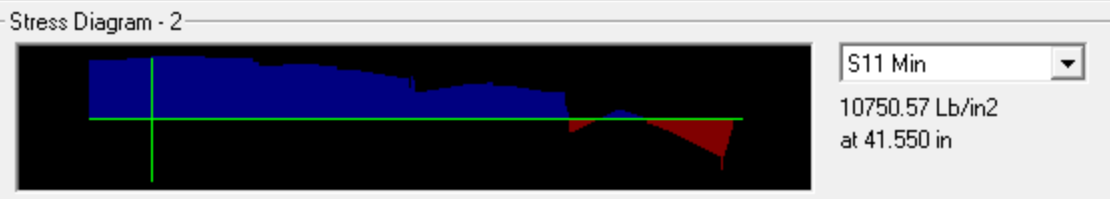
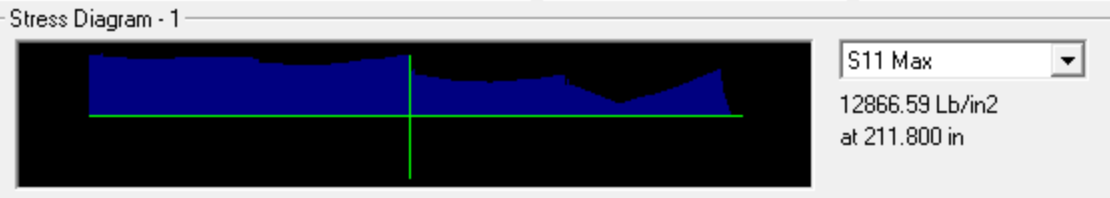




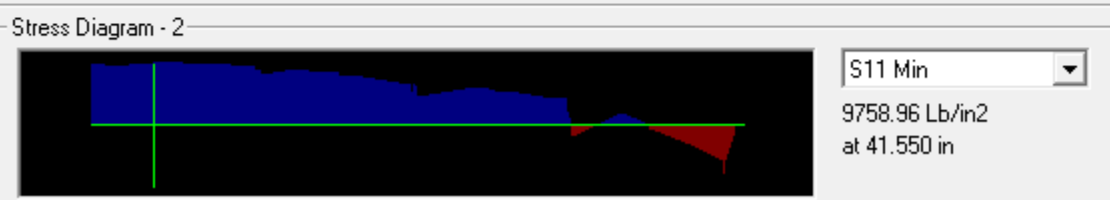
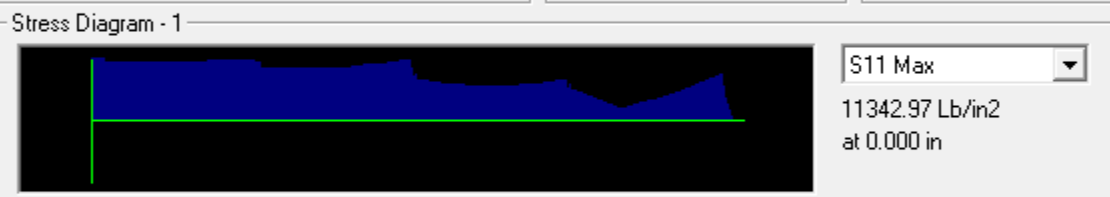
Chord 2b



Case Extreme 90mph - VMS Cd = 1.22 Items Stress (S11) Single valued	End Length Offset (Location) I-End: Jt: 123 0.0000 in (0.000 in) J-End: Jt: 29 0.0000 in (430.800 in)	Display Options <input type="radio"/> Scroll for Values <input checked="" type="radio"/> Show Max
--	--	--

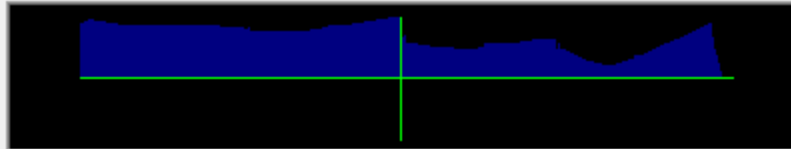


Case Extreme 90mph - VMS Cd = 1.0 Items Stress (S11) Single valued	End Length Offset (Location) I-End: Jt: 123 0.0000 in (0.000 in) J-End: Jt: 29 0.0000 in (430.800 in)	Display Options <input type="radio"/> Scroll for Values <input checked="" type="radio"/> Show Max
---	--	--



Case Extreme 150mph - VMS Cd = 1.7 Items Stress (S11) Single valued	End Length Offset (Location) I-End: Jt: 123 0.0000 in (0.000 in) J-End: Jt: 29 0.0000 in (430.800 in)	Display Options <input type="radio"/> Scroll for Values <input checked="" type="radio"/> Show Max
--	--	--

Stress Diagram - 1



S11 Max
 38567.14 Lb/in2
 at 211.800 in

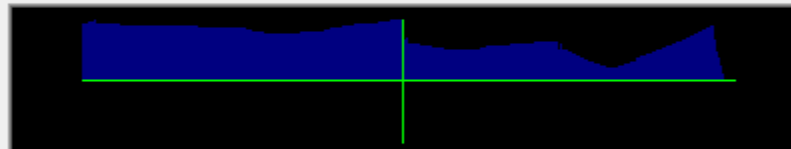
Stress Diagram - 2



S11 Min
 -30186.97 Lb/in2
 at 417.300 in

Case Extreme 150mph - VMS Cd = 1.22 Items Stress (S11) Single valued	End Length Offset (Location) I-End: Jt: 123 0.0000 in (0.000 in) J-End: Jt: 29 0.0000 in (430.800 in)	Display Options <input type="radio"/> Scroll for Values <input checked="" type="radio"/> Show Max
---	--	--

Stress Diagram - 1



S11 Max
 29154.43 Lb/in2
 at 211.800 in

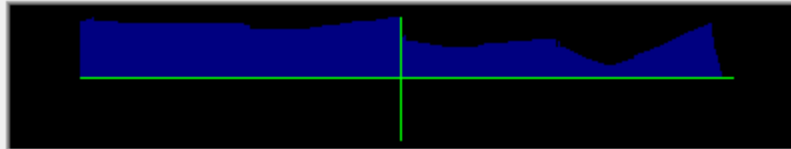
Stress Diagram - 2



S11 Min
 -23028.01 Lb/in2
 at 417.300 in

Case Extreme 150mph - VMS Cd = 1.0 Items Stress (S11) Single valued	End Length Offset (Location) I-End: Jt: 123 0.0000 in (0.000 in) J-End: Jt: 29 0.0000 in (430.800 in)	Display Options <input type="radio"/> Scroll for Values <input checked="" type="radio"/> Show Max
---	--	--

Stress Diagram - 1



S11 Max
 24840.00 Lb/in²
 at 211.800 in

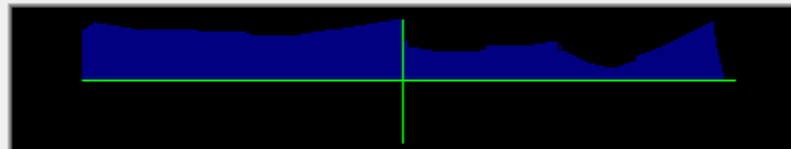
Stress Diagram - 2



S11 Min
 -19746.62 Lb/in²
 at 417.300 in

Case Fatigue - VMS Cd = 1.7 Items Stress (S11) Single valued	End Length Offset (Location) I-End: Jt: 123 0.0000 in (0.000 in) J-End: Jt: 29 0.0000 in (430.800 in)	Display Options <input type="radio"/> Scroll for Values <input checked="" type="radio"/> Show Max
--	--	--

Stress Diagram - 1

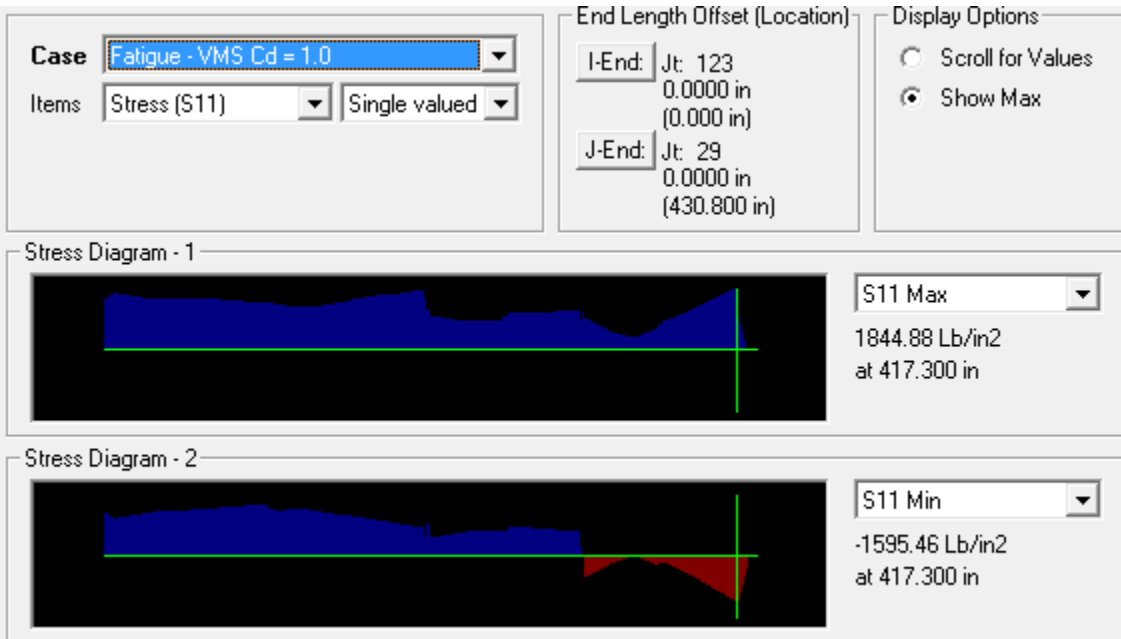
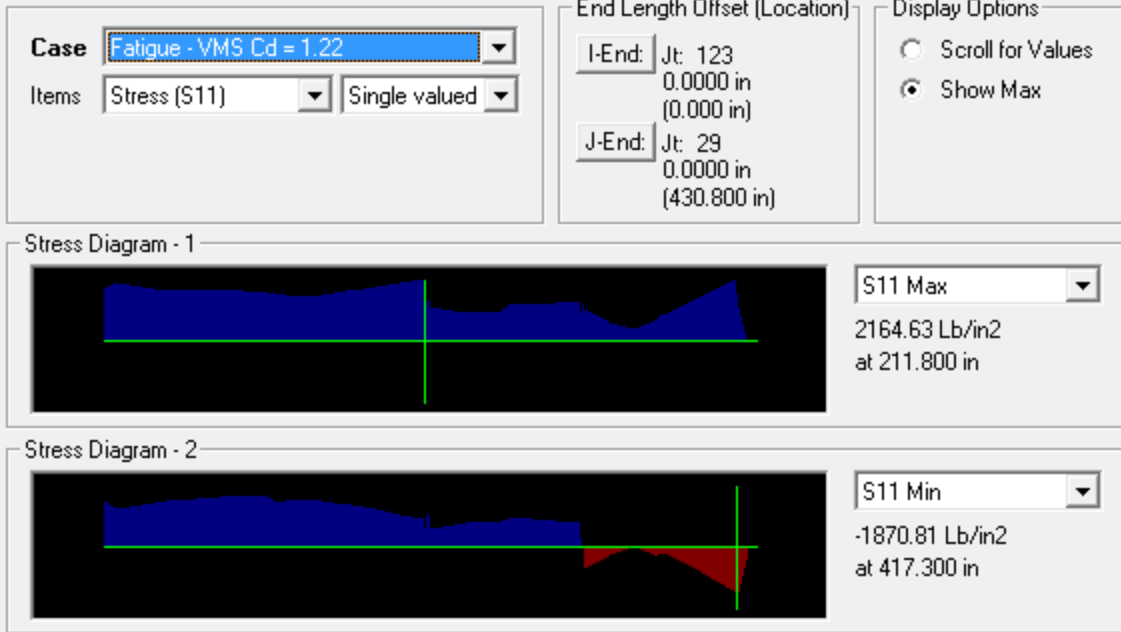


S11 Max
 2967.77 Lb/in²
 at 211.800 in

Stress Diagram - 2



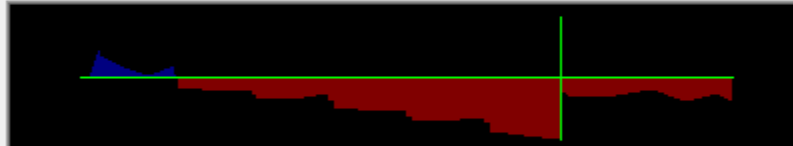
S11 Min
 -2474.64 Lb/in²
 at 417.300 in



Chord 3a

Case Extreme 90mph - VMS Cd = 1.7	End Length Offset (Location)	Display Options
Items Stress (S11) Single valued	I-End: Jt: 25 0.0000 in (0.000 in)	<input type="radio"/> Scroll for Values
	J-End: Jt: 109 0.0000 in (430.800 in)	<input checked="" type="radio"/> Show Max

Stress Diagram - 1



S11 Max

-14610.74 Lb/in2
at 317.004 in

Stress Diagram - 2



S11 Min

-18687.90 Lb/in2
at 270.375 in

Case Extreme 90mph - VMS Cd = 1.22	End Length Offset (Location)	Display Options
Items Stress (S11) Single valued	I-End: Jt: 25 0.0000 in (0.000 in)	<input type="radio"/> Scroll for Values
	J-End: Jt: 109 0.0000 in (430.800 in)	<input checked="" type="radio"/> Show Max

Stress Diagram - 1



S11 Max

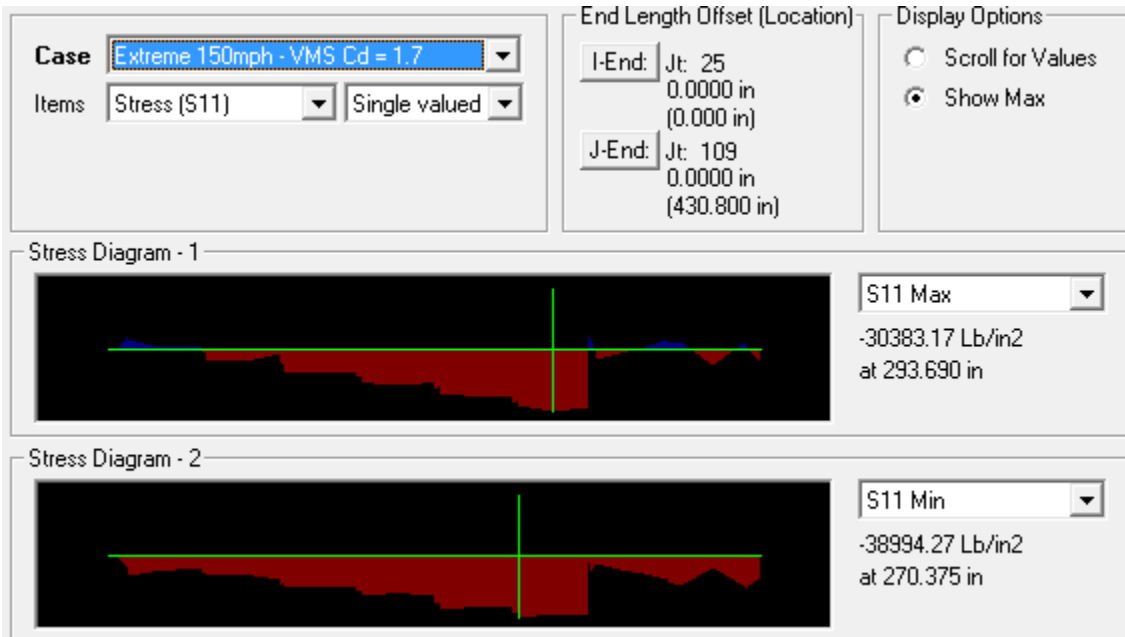
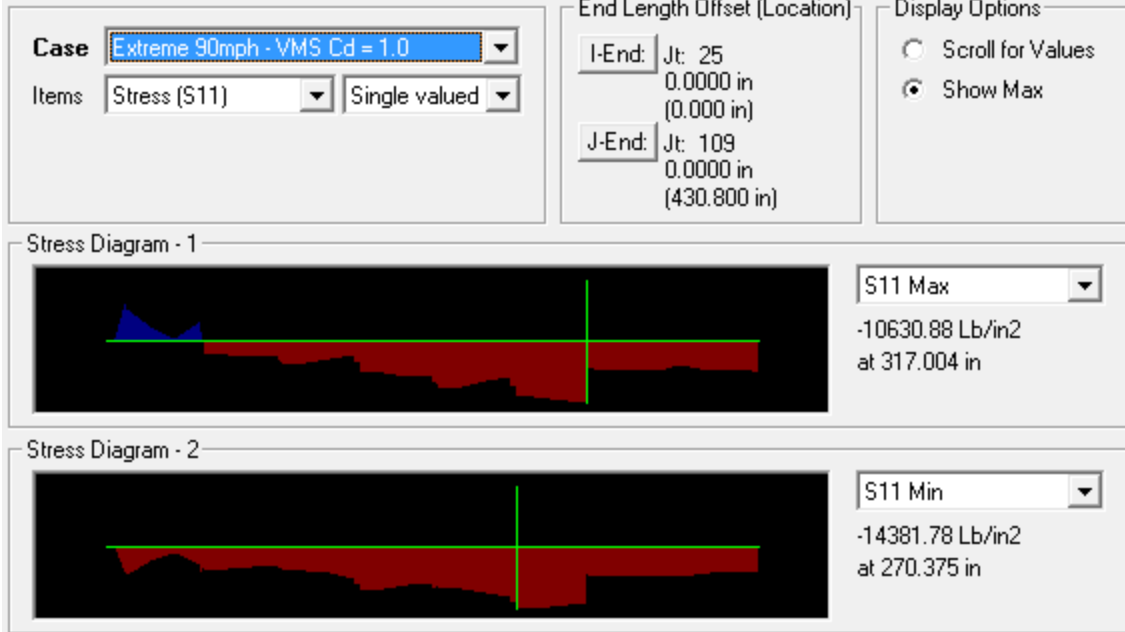
-11906.64 Lb/in2
at 317.004 in

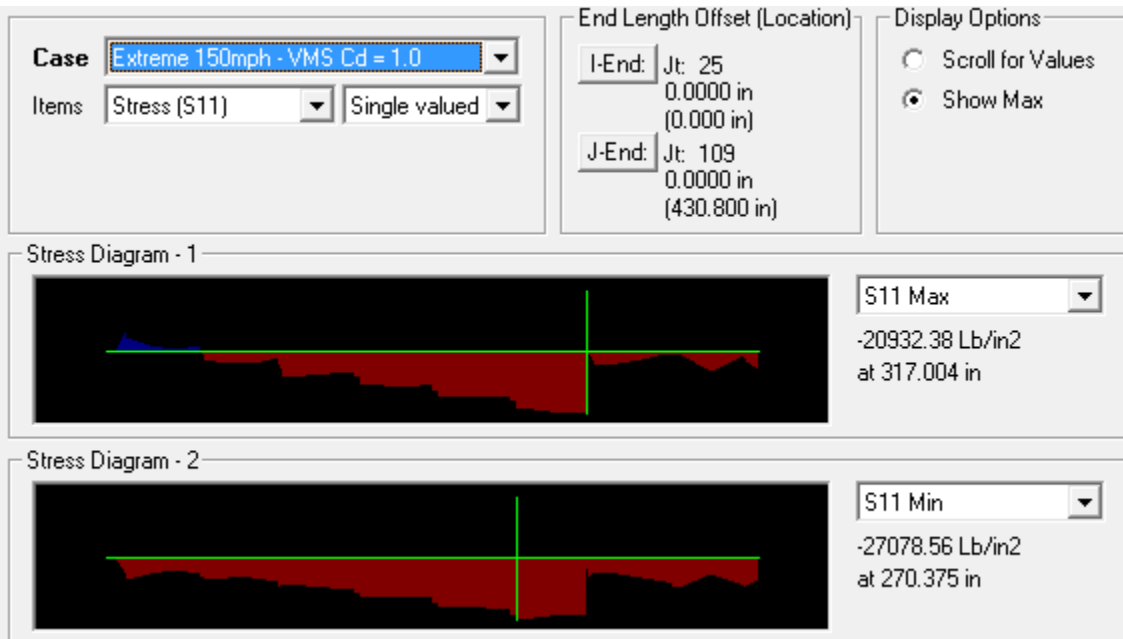
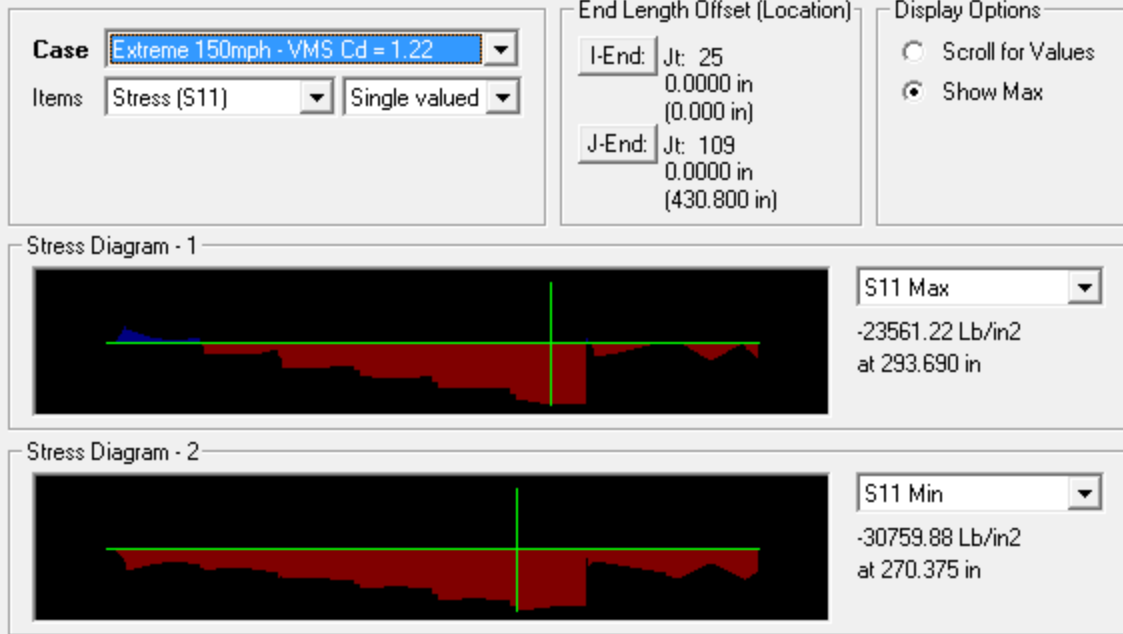
Stress Diagram - 2

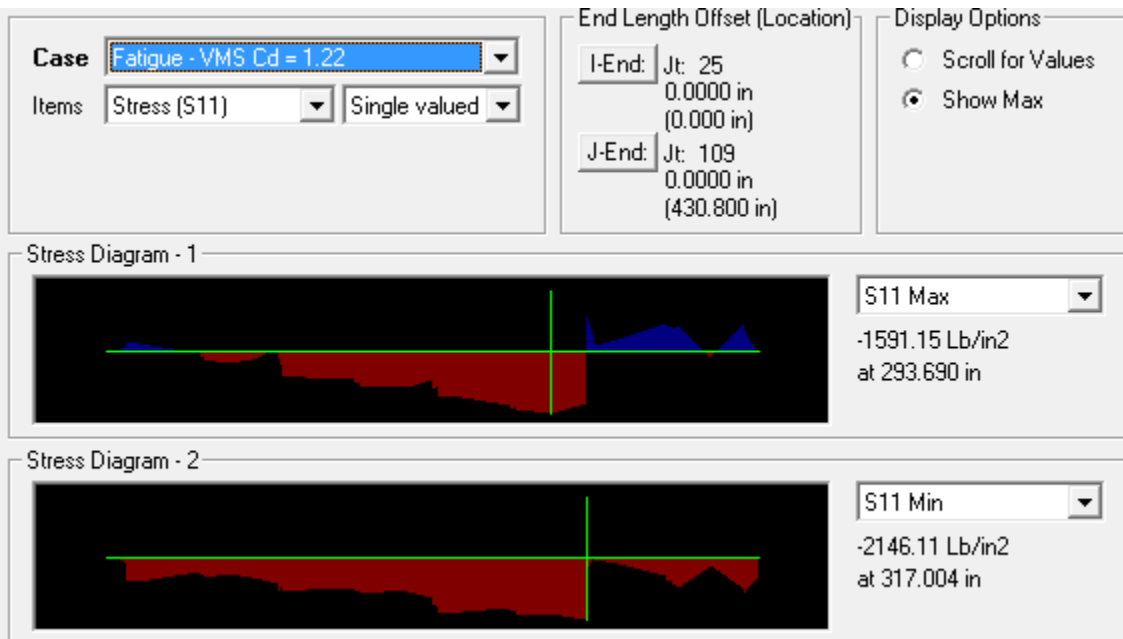
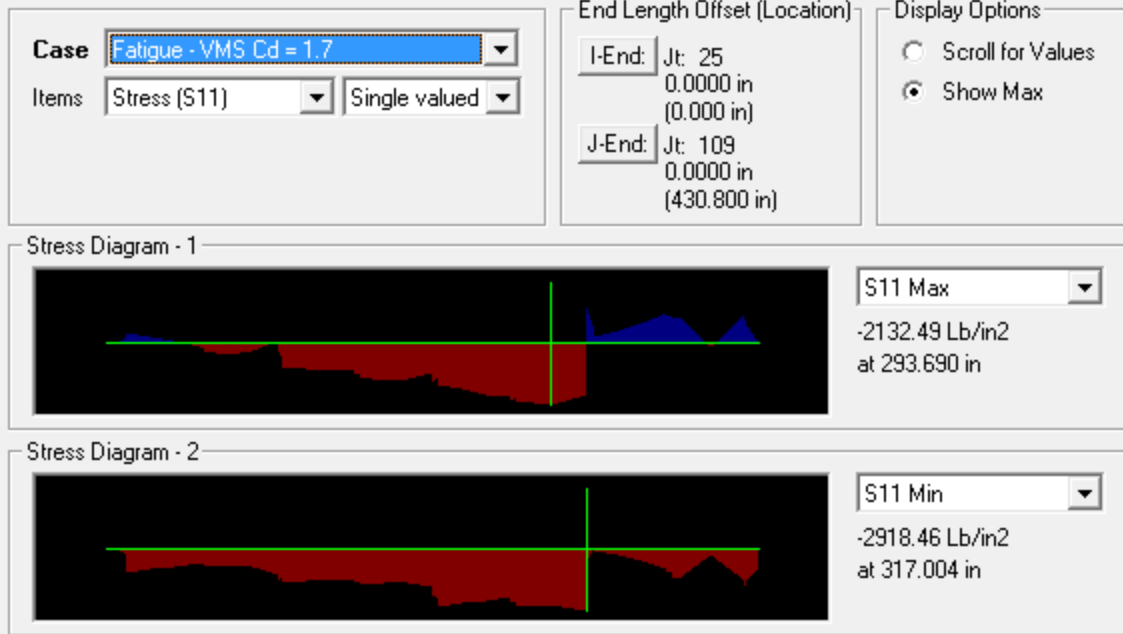


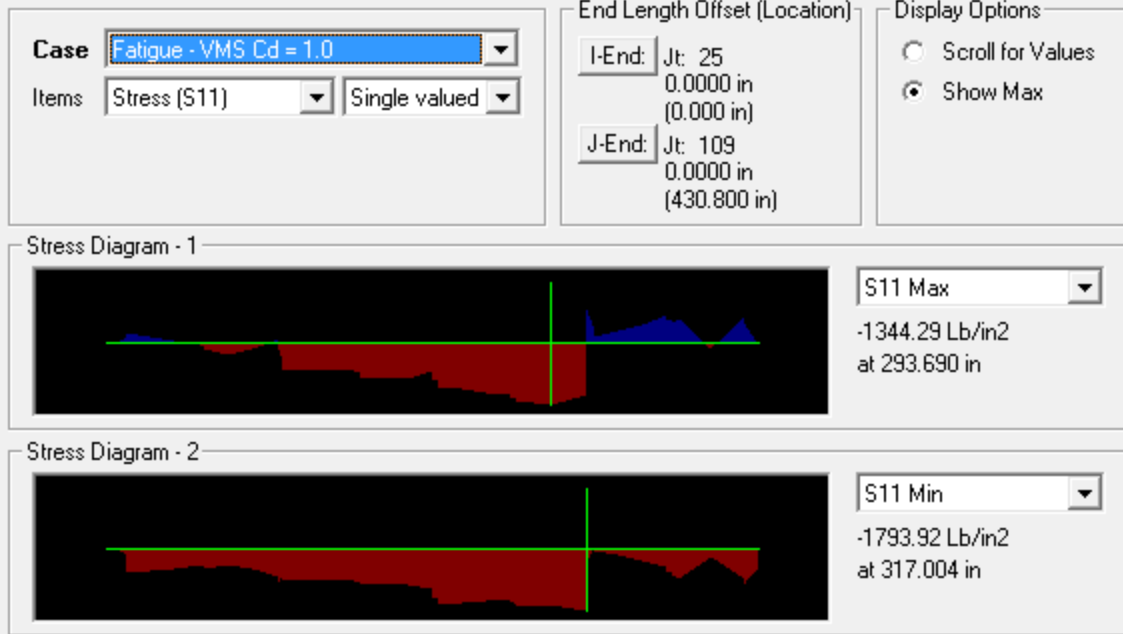
S11 Min

-15722.96 Lb/in2
at 270.375 in

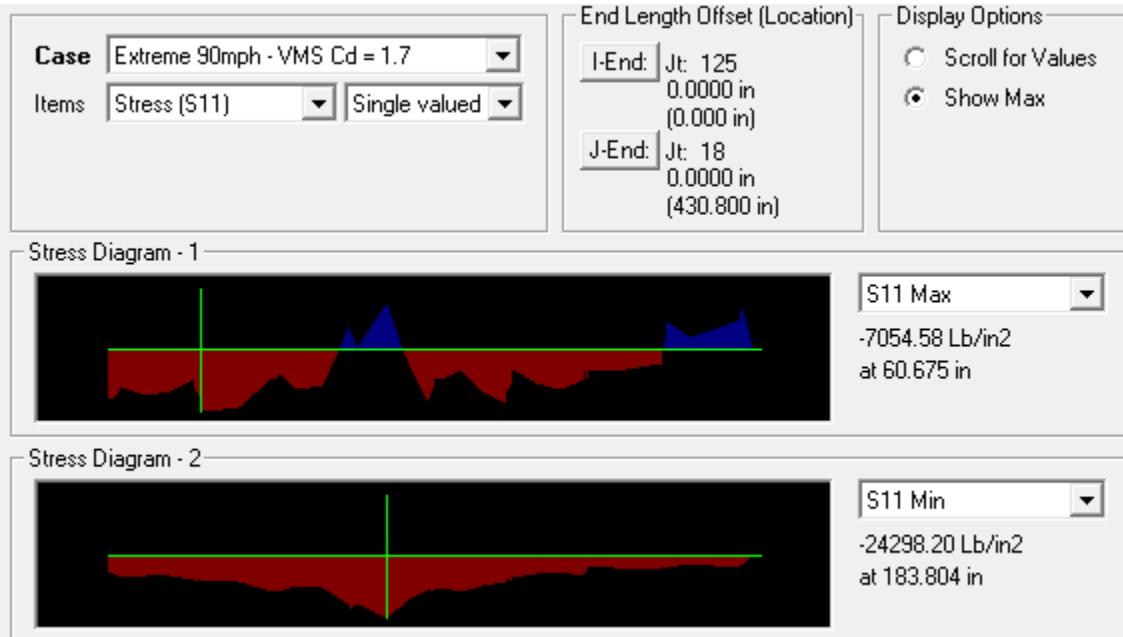




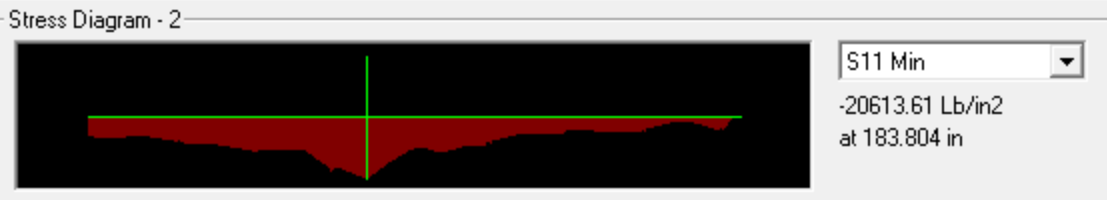
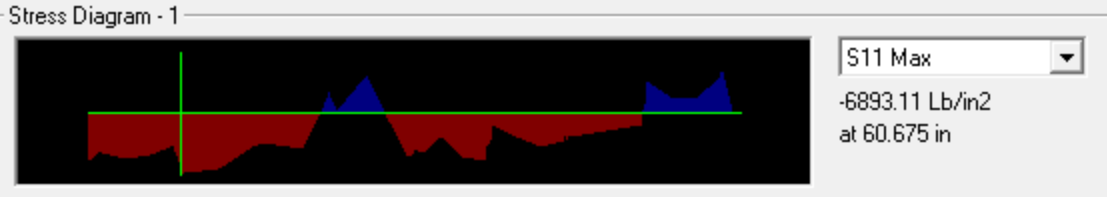




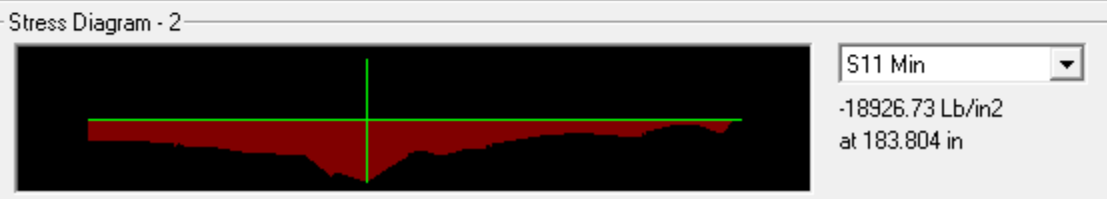
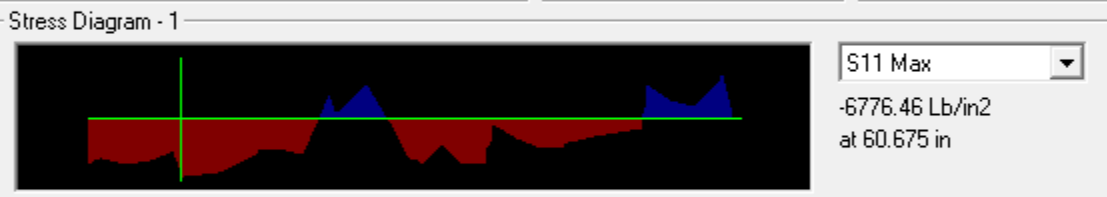
Chord 3b

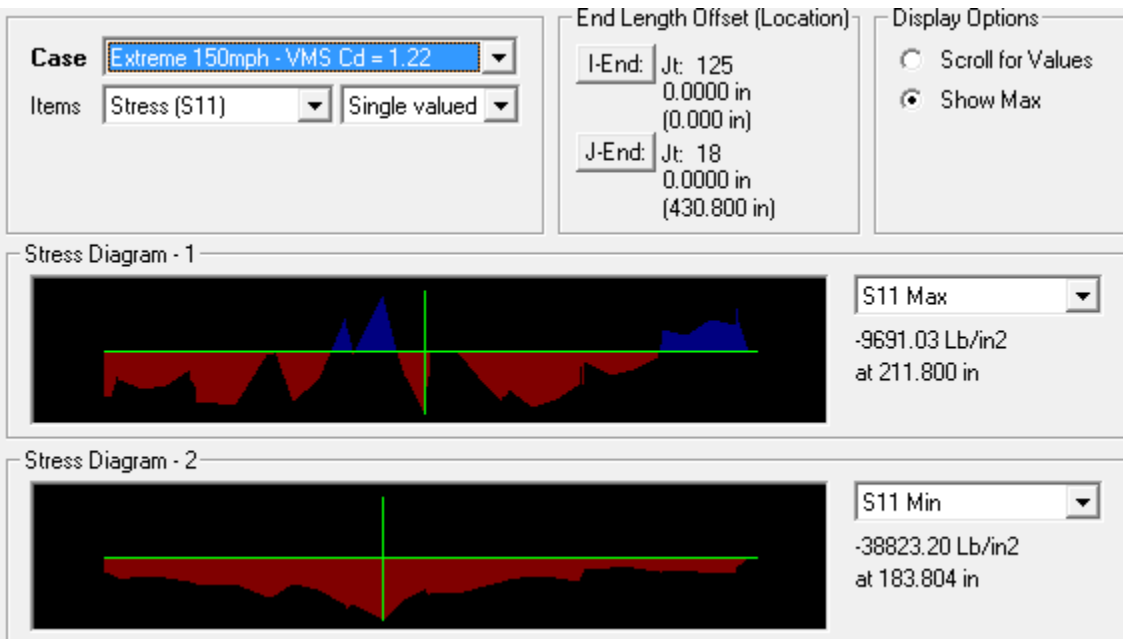
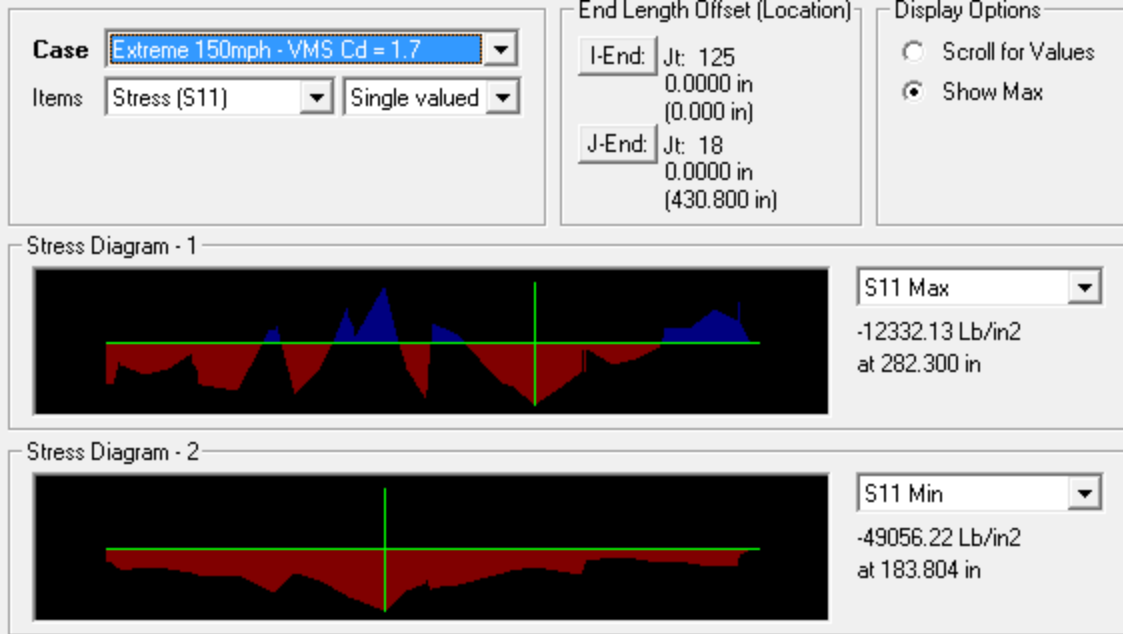


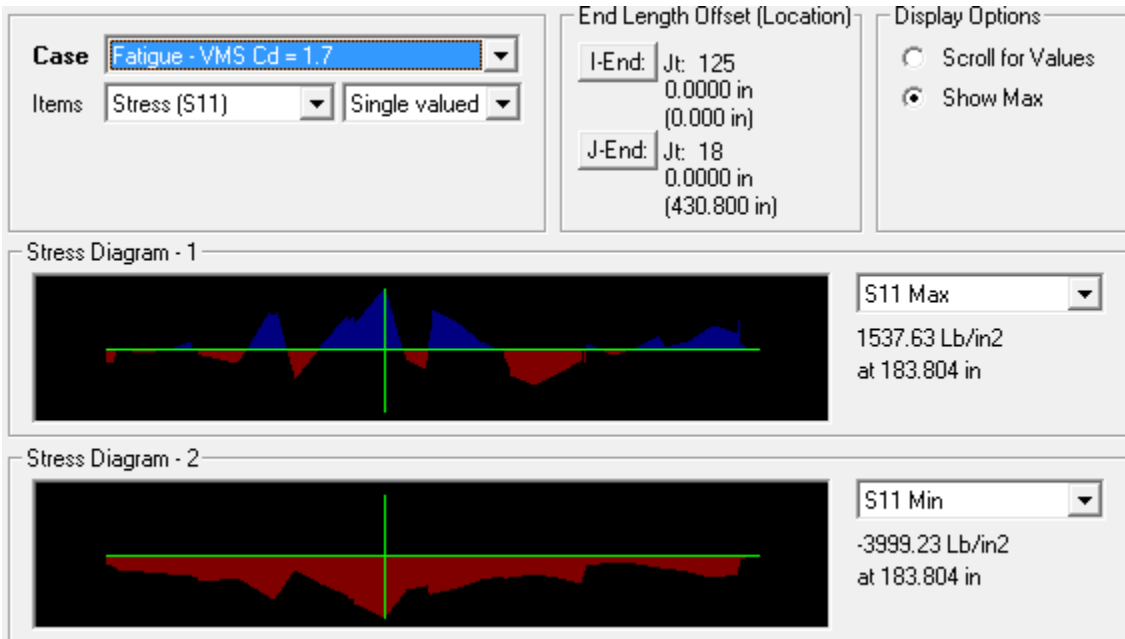
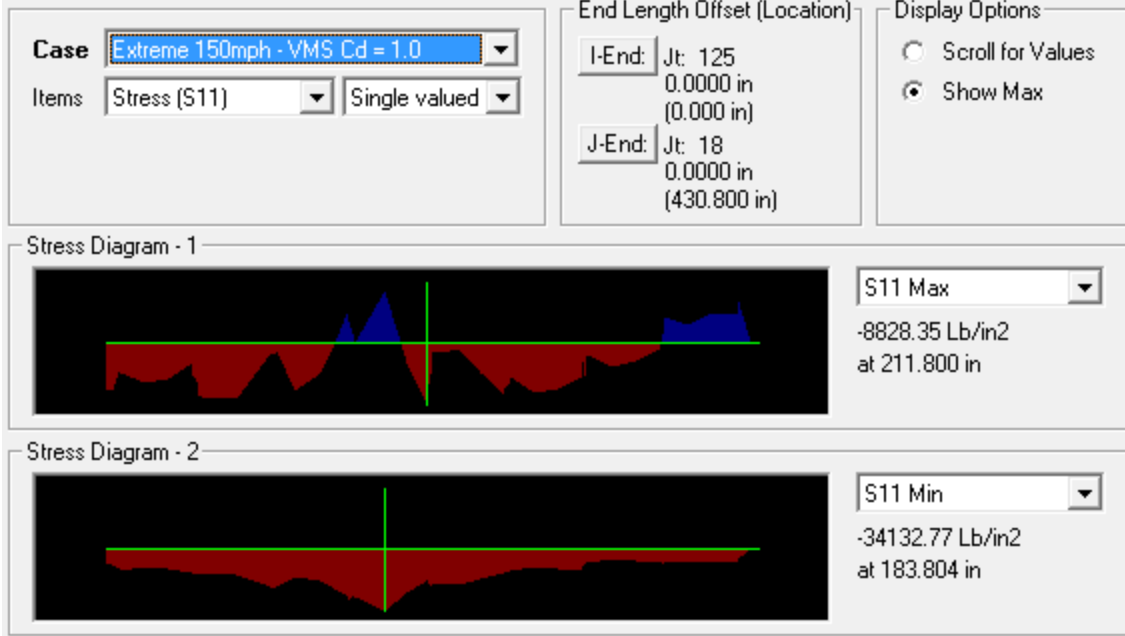
Case Extreme 90mph - VMS Cd = 1.22 Items Stress (S11) Single valued	End Length Offset (Location) I-End: Jt: 125 0.0000 in (0.000 in) J-End: Jt: 18 0.0000 in (430.800 in)	Display Options <input type="radio"/> Scroll for Values <input checked="" type="radio"/> Show Max
--	--	--



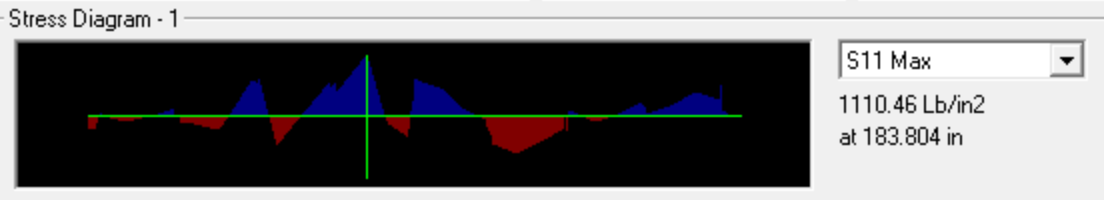
Case Extreme 90mph - VMS Cd = 1.0 Items Stress (S11) Single valued	End Length Offset (Location) I-End: Jt: 125 0.0000 in (0.000 in) J-End: Jt: 18 0.0000 in (430.800 in)	Display Options <input type="radio"/> Scroll for Values <input checked="" type="radio"/> Show Max
---	--	--



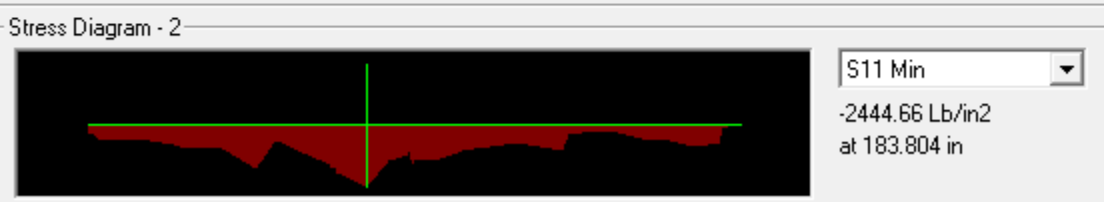
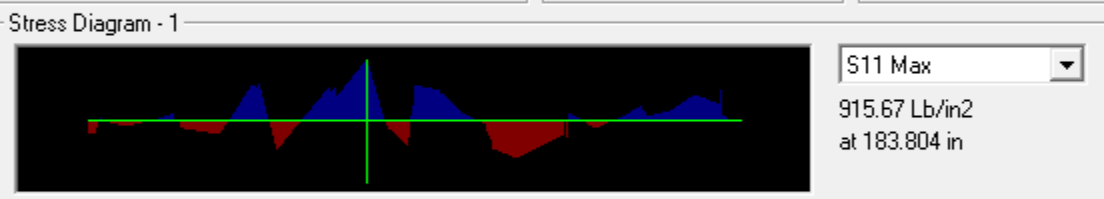




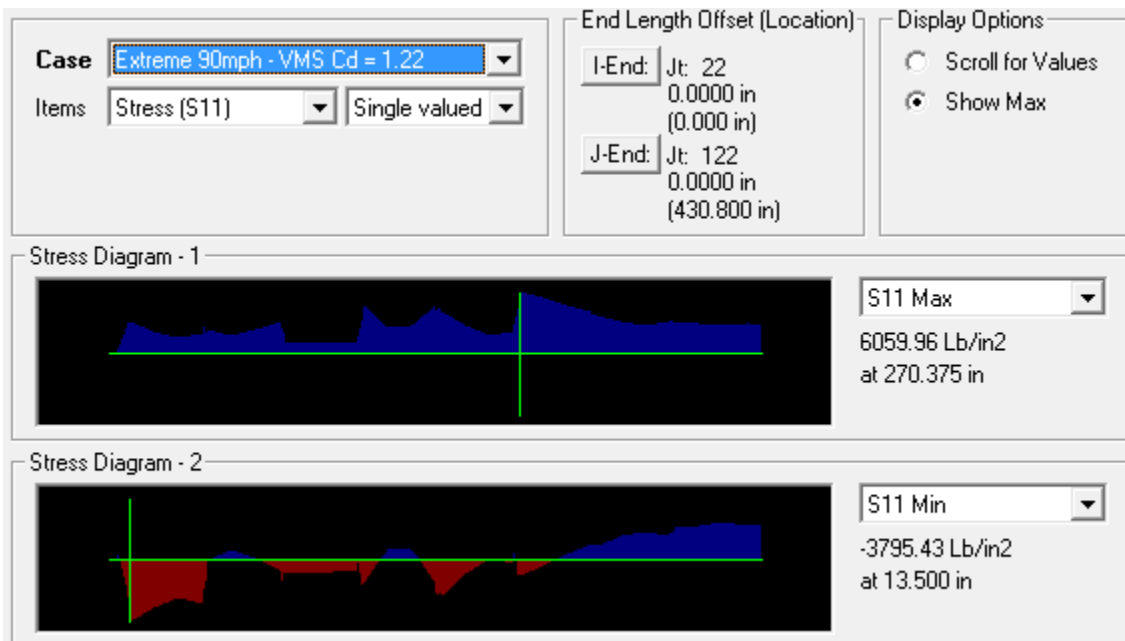
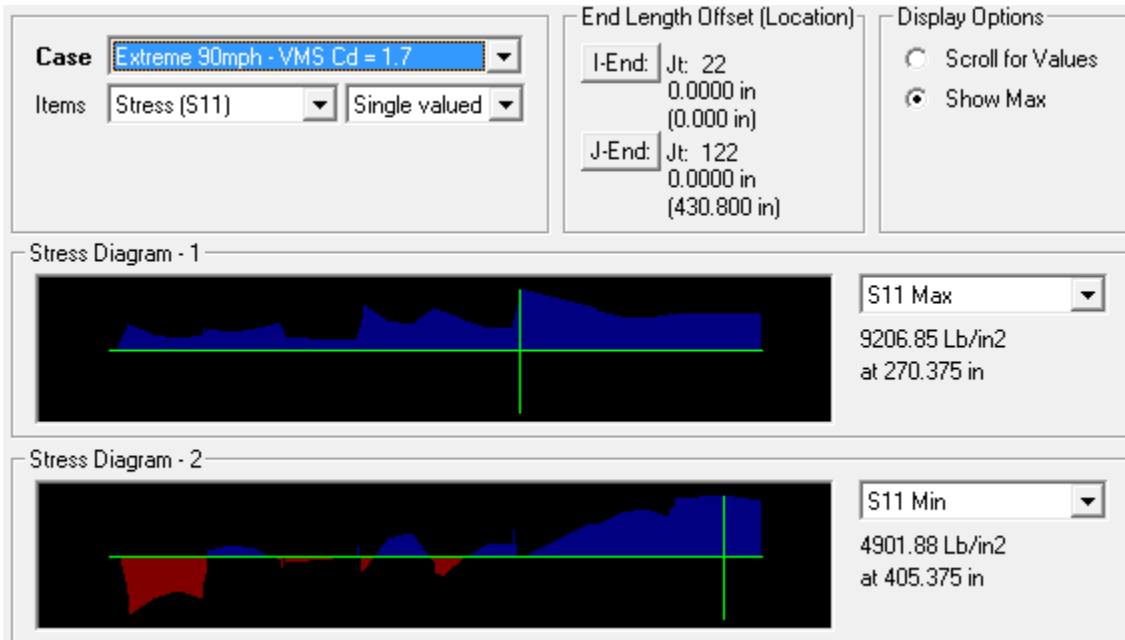
Case Fatigue - VMS Cd = 1.22 Items Stress (S11) Single valued	End Length Offset (Location) I-End: Jt: 125 0.0000 in (0.000 in) J-End: Jt: 18 0.0000 in (430.800 in)	Display Options <input type="radio"/> Scroll for Values <input checked="" type="radio"/> Show Max
--	--	--



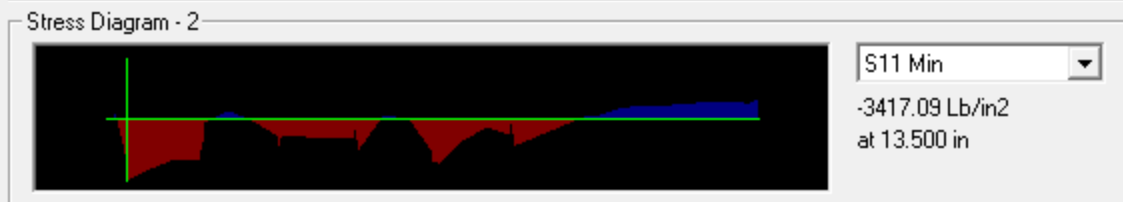
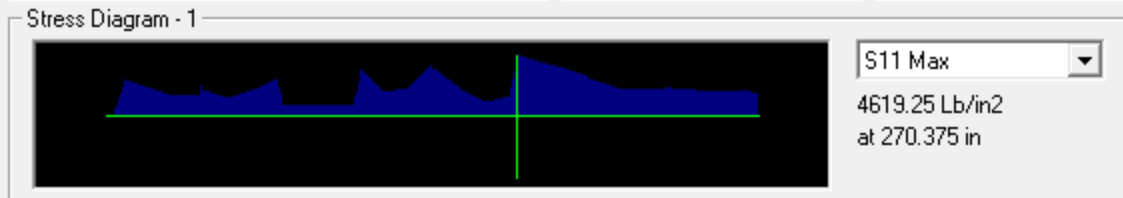
Case Fatigue - VMS Cd = 1.0 Items Stress (S11) Single valued	End Length Offset (Location) I-End: Jt: 125 0.0000 in (0.000 in) J-End: Jt: 18 0.0000 in (430.800 in)	Display Options <input type="radio"/> Scroll for Values <input checked="" type="radio"/> Show Max
---	--	--



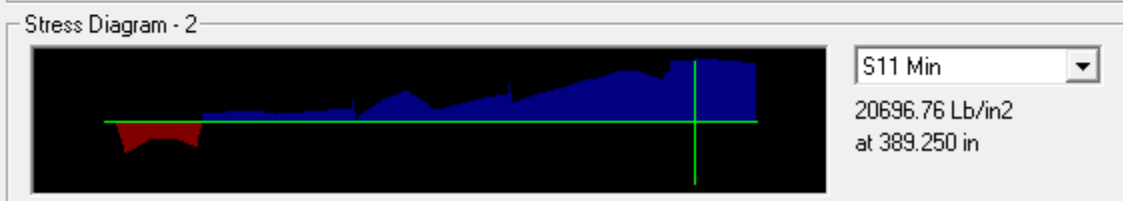
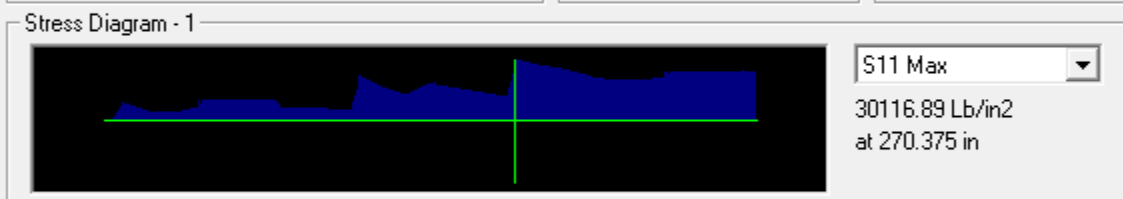
Chord 4a

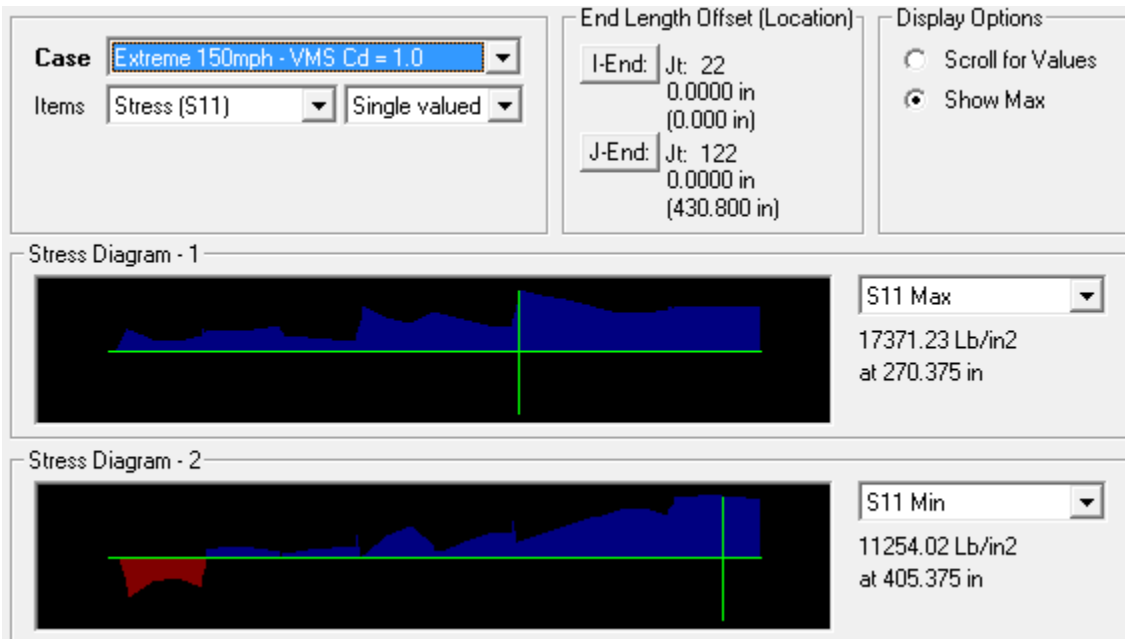
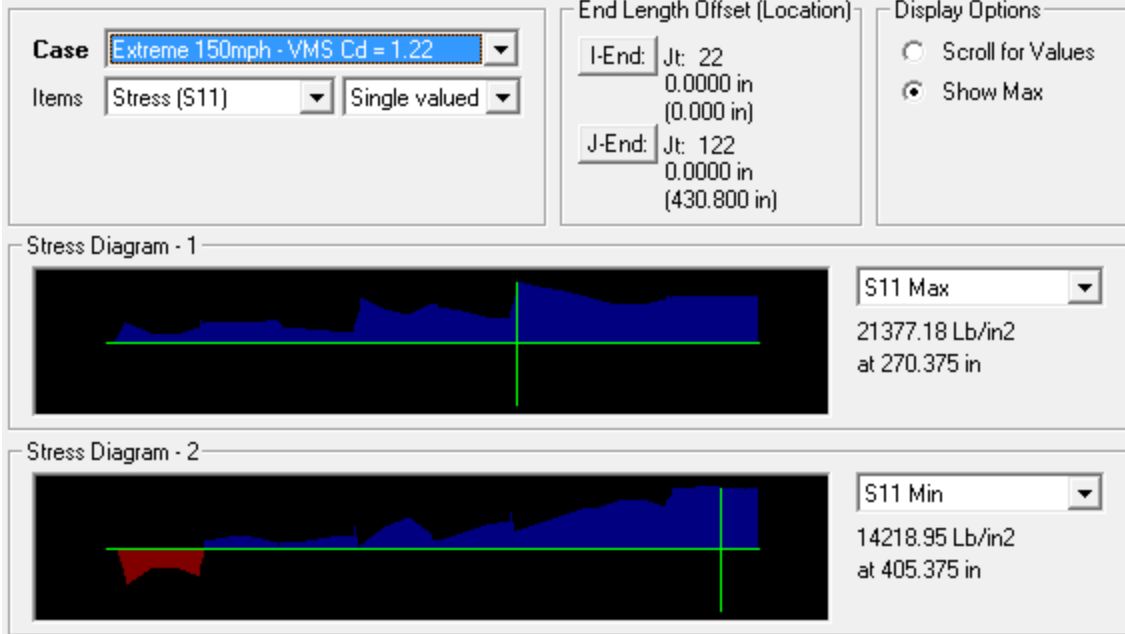


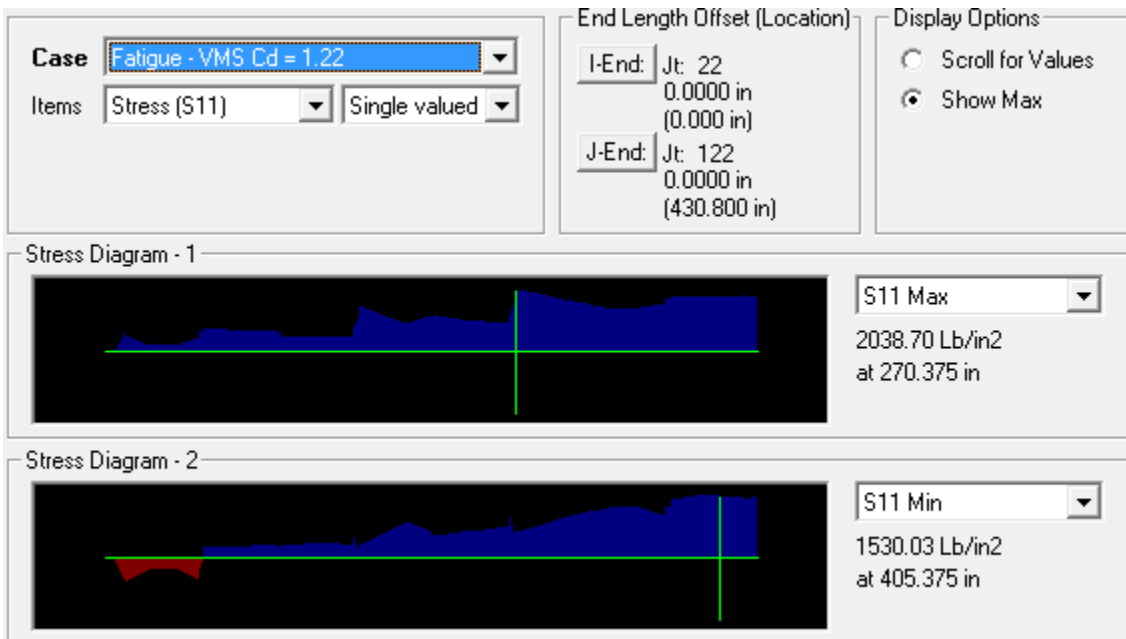
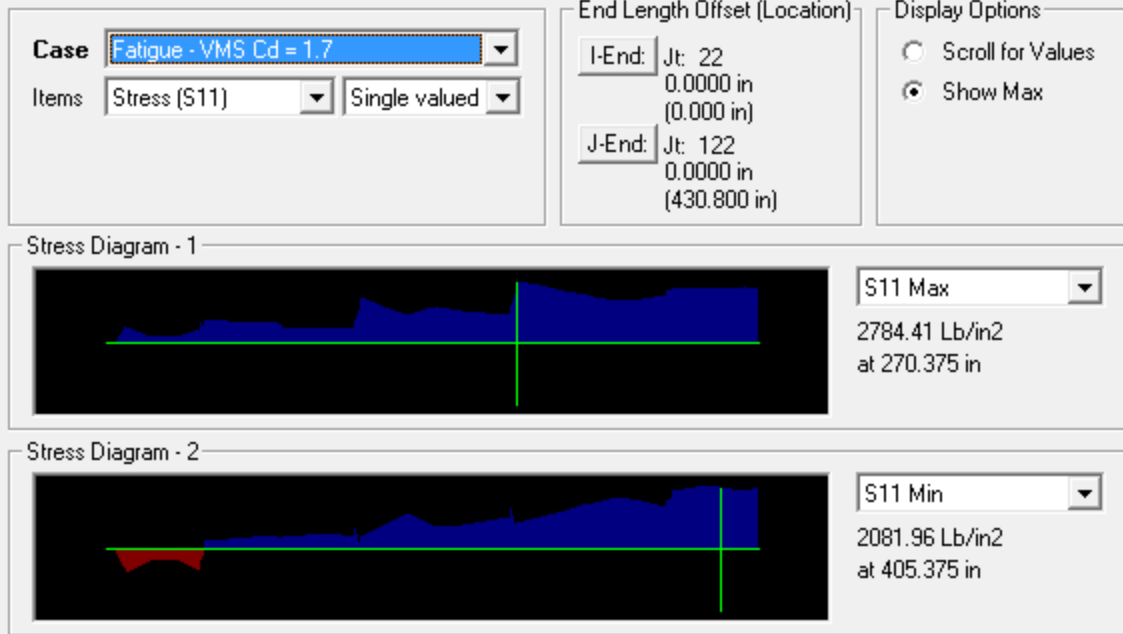
Case Extreme 90mph - VMS Cd = 1.0 Items Stress (S11) Single valued	End Length Offset (Location) I-End: Jt: 22 0.0000 in (0.000 in) J-End: Jt: 122 0.0000 in (430.800 in)	Display Options <input type="radio"/> Scroll for Values <input checked="" type="radio"/> Show Max
---	--	--

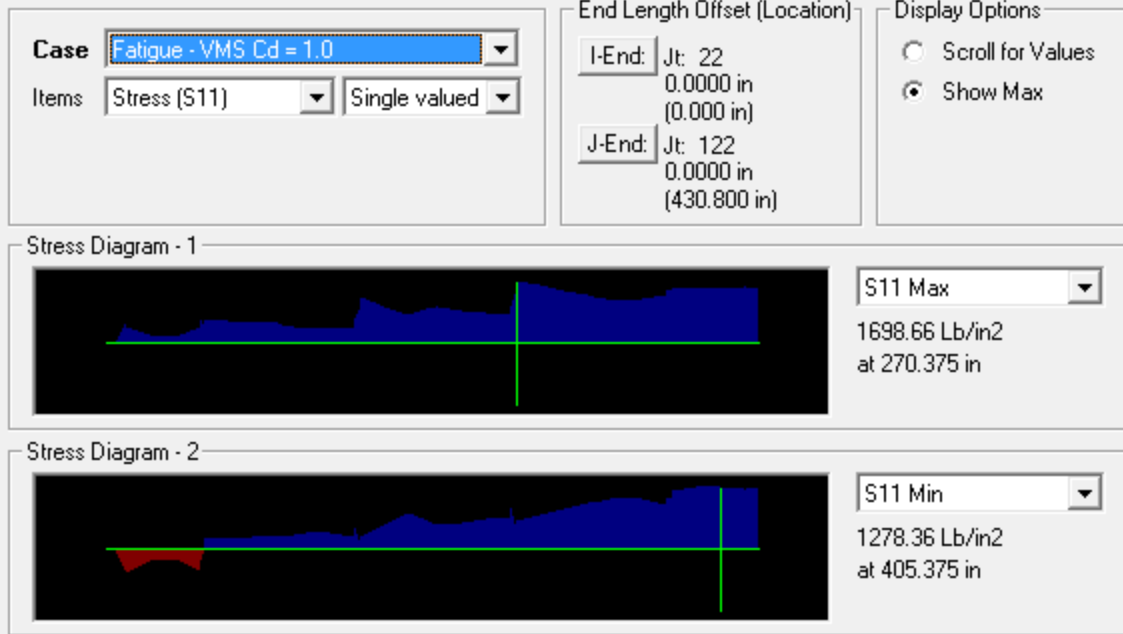


Case Extreme 150mph - VMS Cd = 1.7 Items Stress (S11) Single valued	End Length Offset (Location) I-End: Jt: 22 0.0000 in (0.000 in) J-End: Jt: 122 0.0000 in (430.800 in)	Display Options <input type="radio"/> Scroll for Values <input checked="" type="radio"/> Show Max
--	--	--

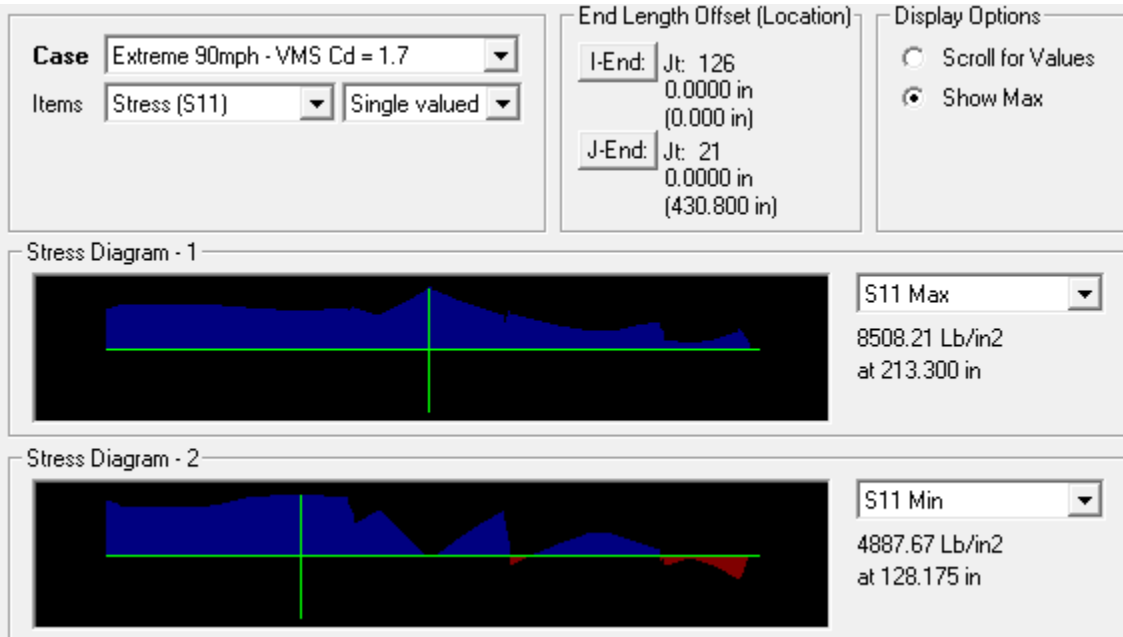




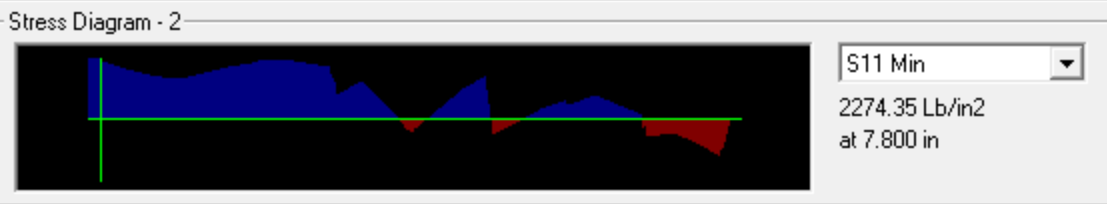
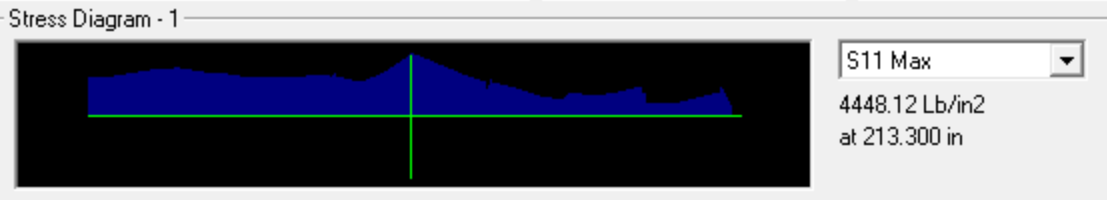




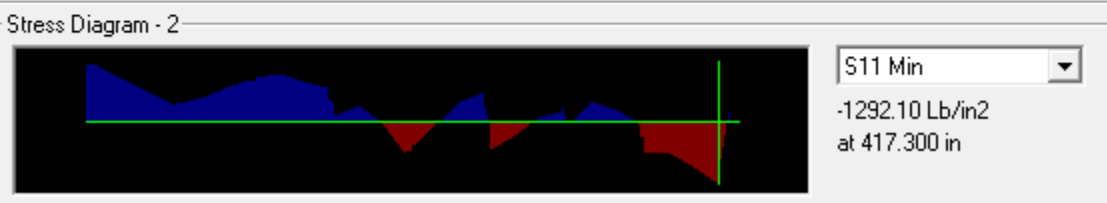
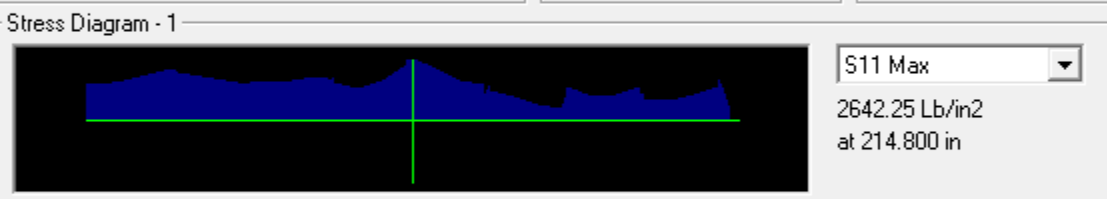
Chord 4b

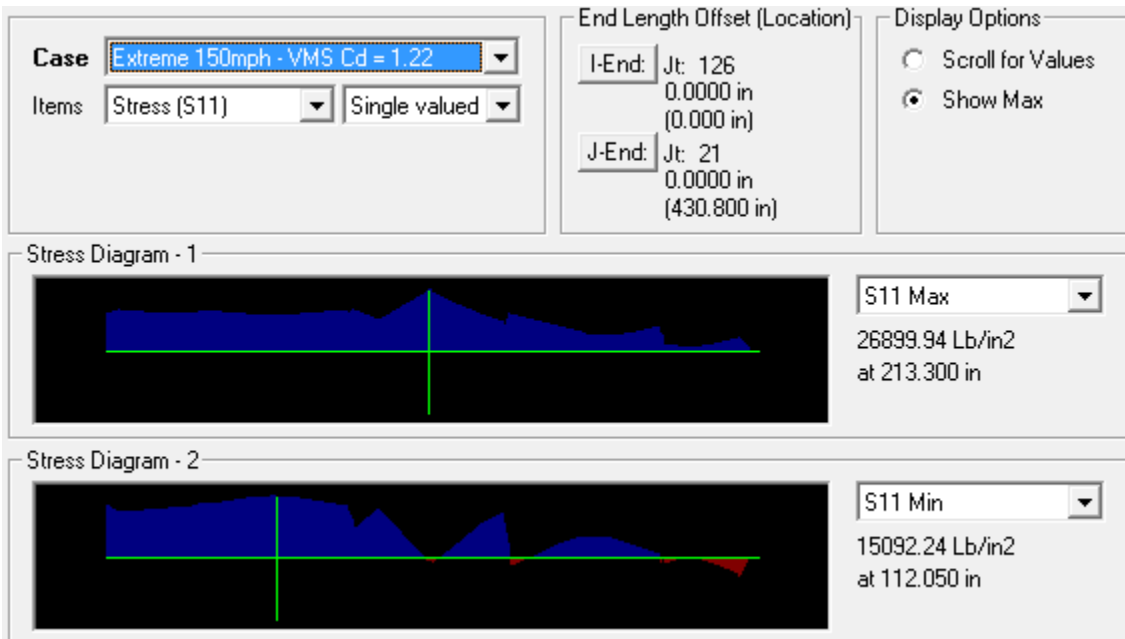
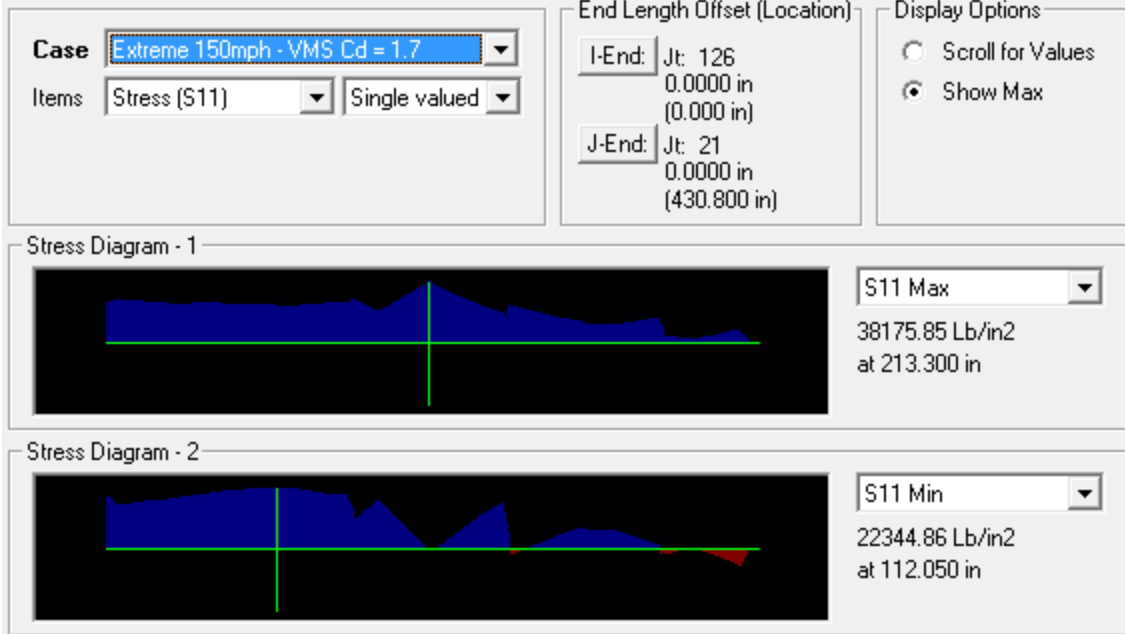


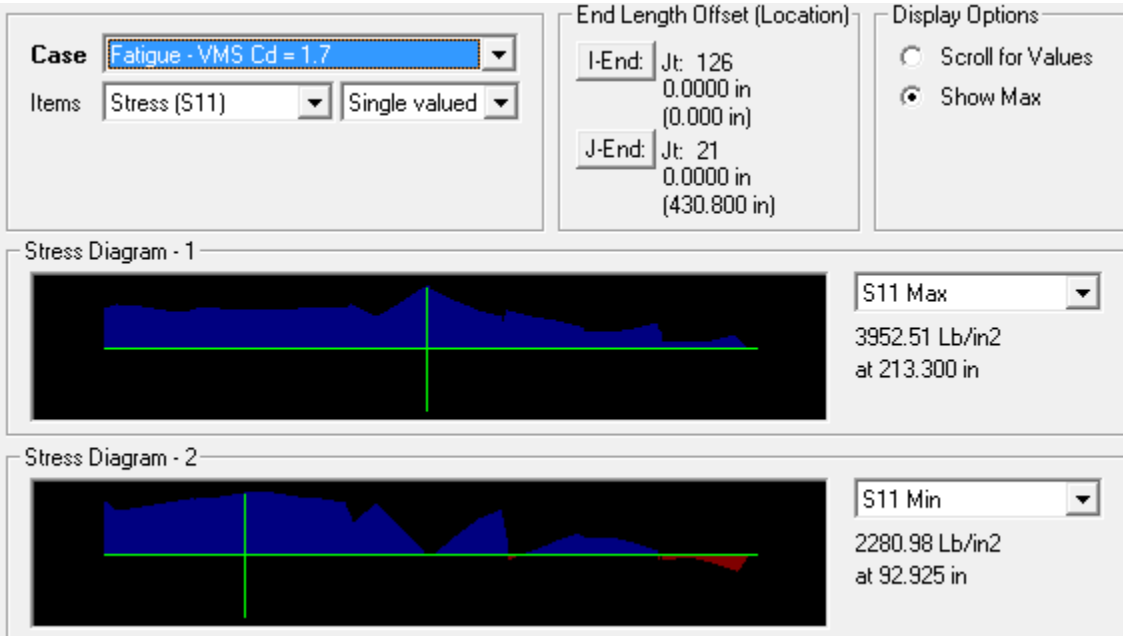
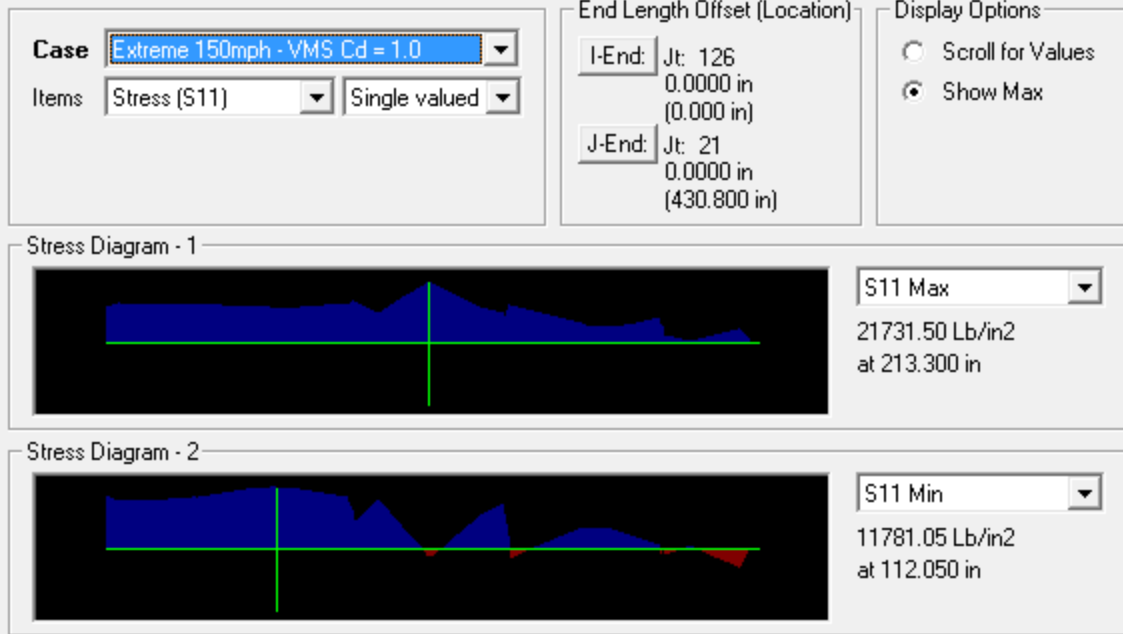
Case Extreme 90mph - VMS Cd = 1.22 Items Stress (S11) Single valued	End Length Offset (Location) I-End: Jt: 126 0.0000 in (0.000 in)	Display Options <input type="radio"/> Scroll for Values <input checked="" type="radio"/> Show Max
	J-End: Jt: 21 0.0000 in (430.800 in)	



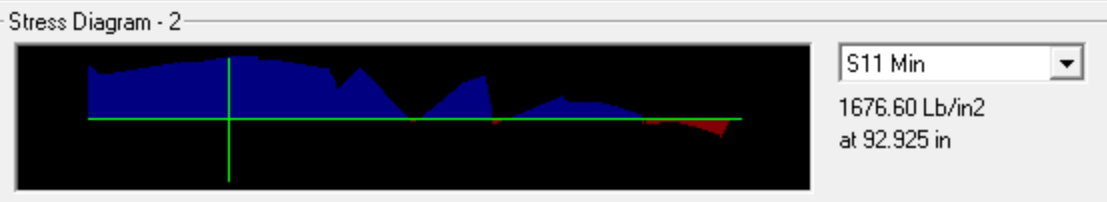
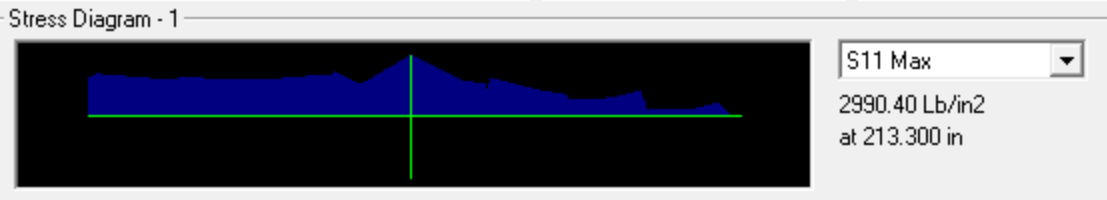
Case Extreme 90mph - VMS Cd = 1.0 Items Stress (S11) Single valued	End Length Offset (Location) I-End: Jt: 126 0.0000 in (0.000 in)	Display Options <input type="radio"/> Scroll for Values <input checked="" type="radio"/> Show Max
	J-End: Jt: 21 0.0000 in (430.800 in)	



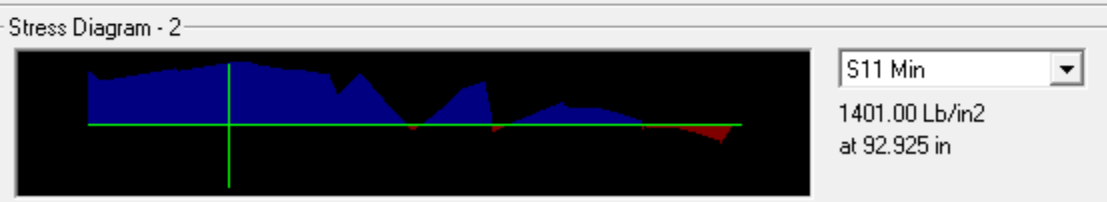
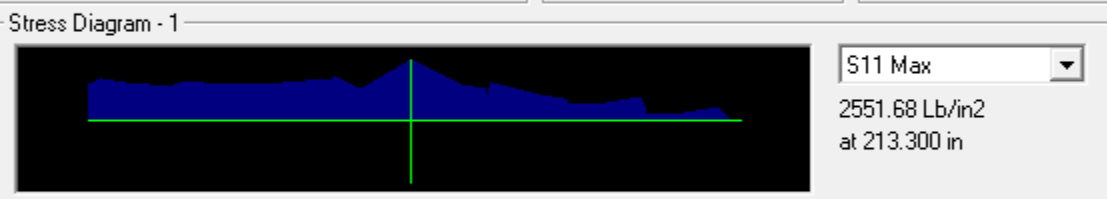




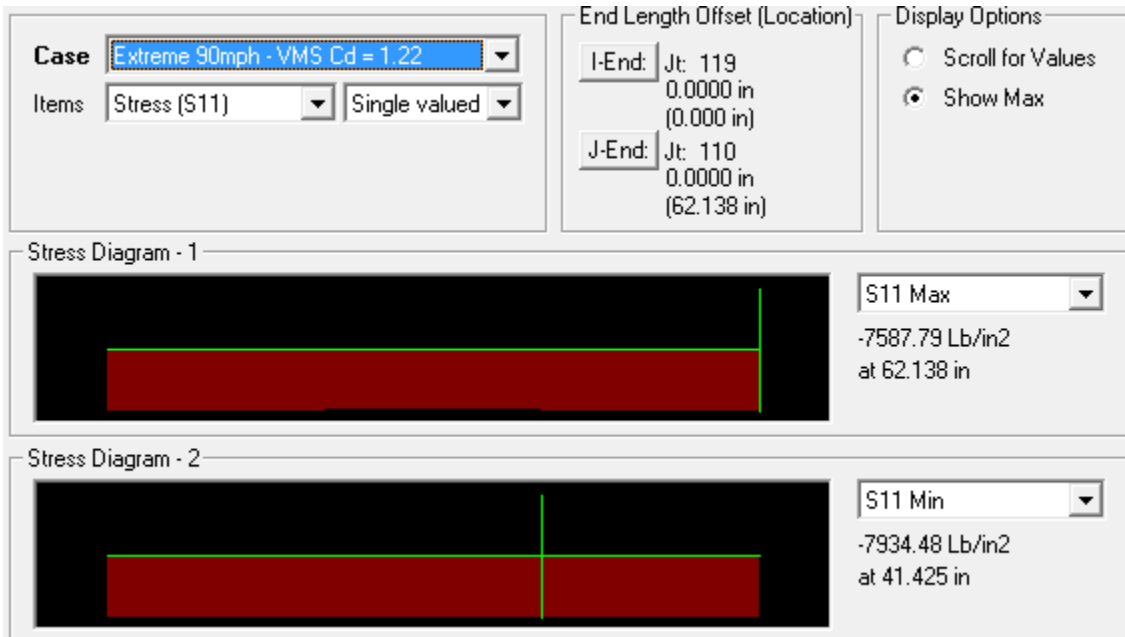
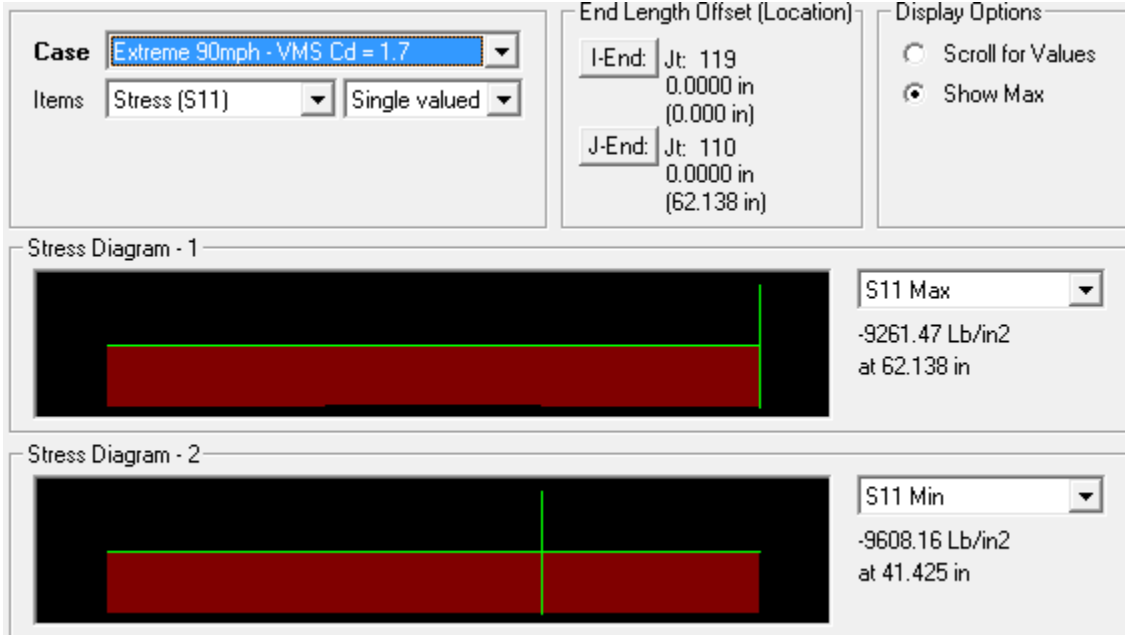
Case Fatigue - VMS Cd = 1.22 Items Stress (S11) Single valued	End Length Offset (Location) I-End: Jt: 126 0.0000 in (0.000 in) J-End: Jt: 21 0.0000 in (430.800 in)	Display Options <input type="radio"/> Scroll for Values <input checked="" type="radio"/> Show Max
--	--	--

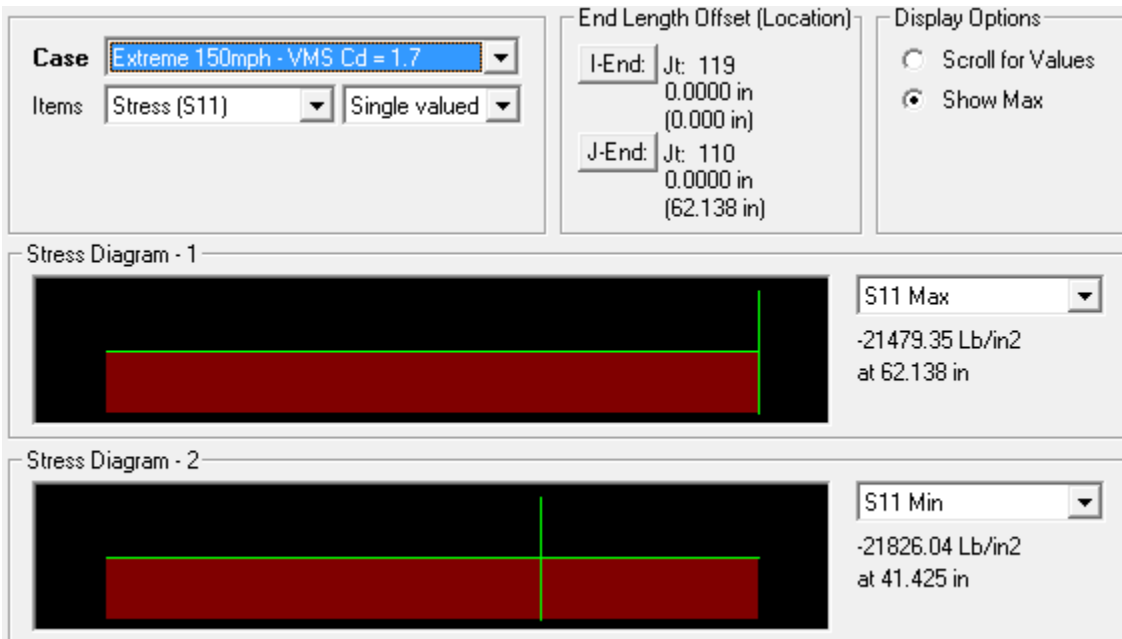
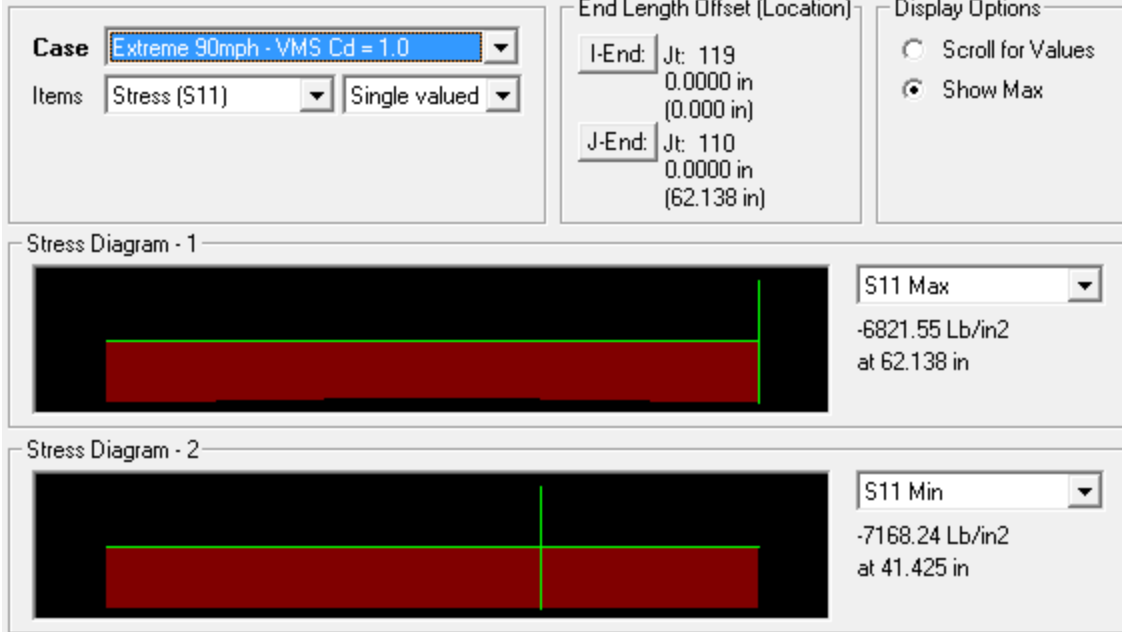


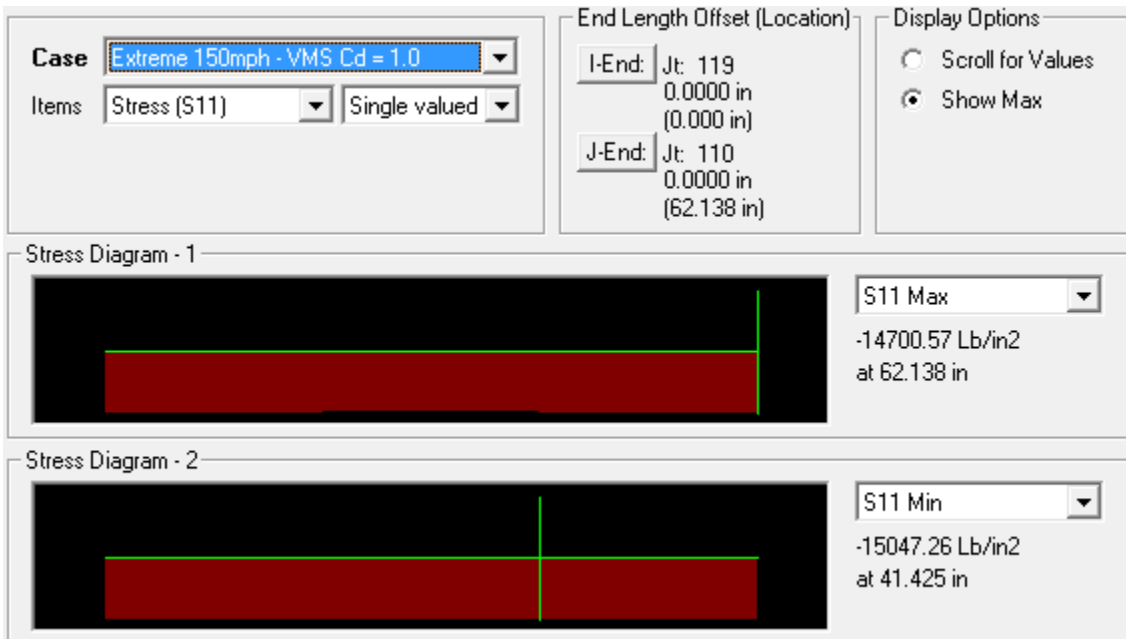
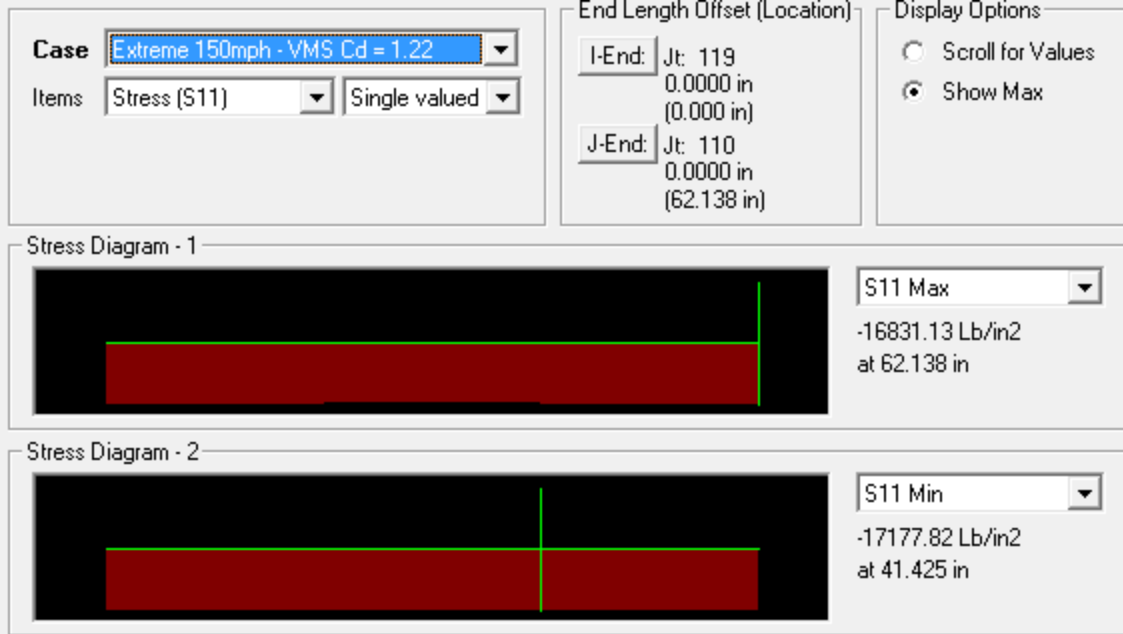
Case Fatigue - VMS Cd = 1.0 Items Stress (S11) Single valued	End Length Offset (Location) I-End: Jt: 126 0.0000 in (0.000 in) J-End: Jt: 21 0.0000 in (430.800 in)	Display Options <input type="radio"/> Scroll for Values <input checked="" type="radio"/> Show Max
---	--	--



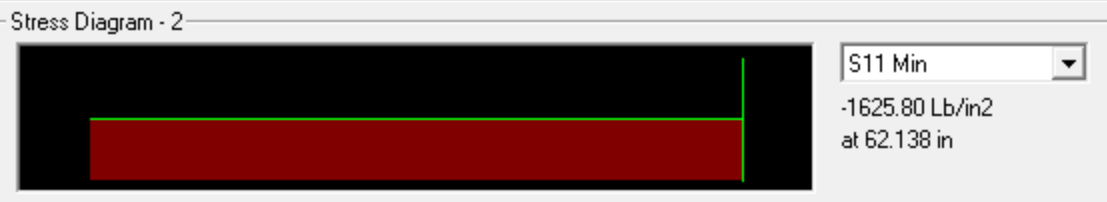
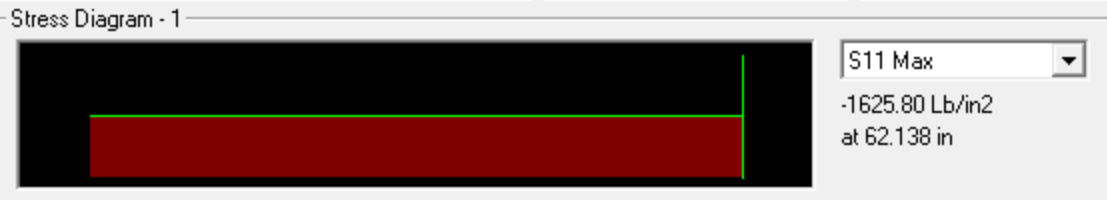
Diagonal 1



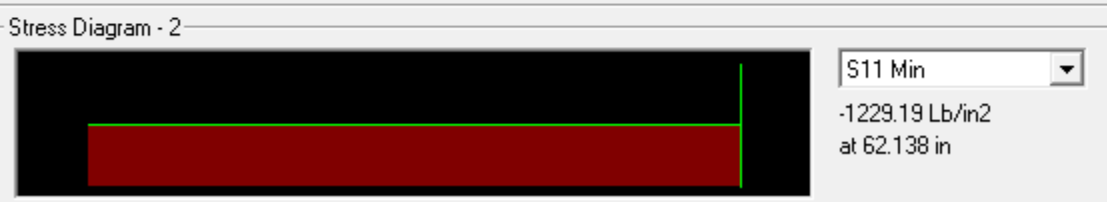
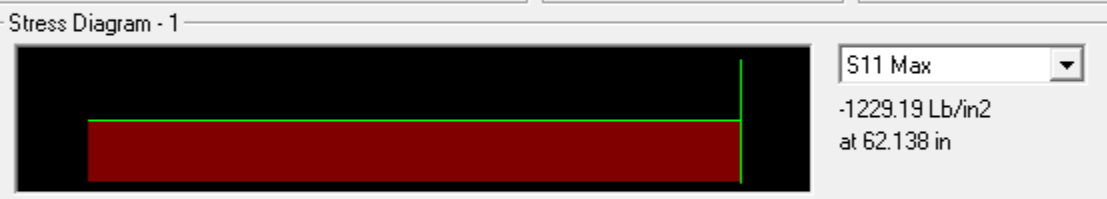


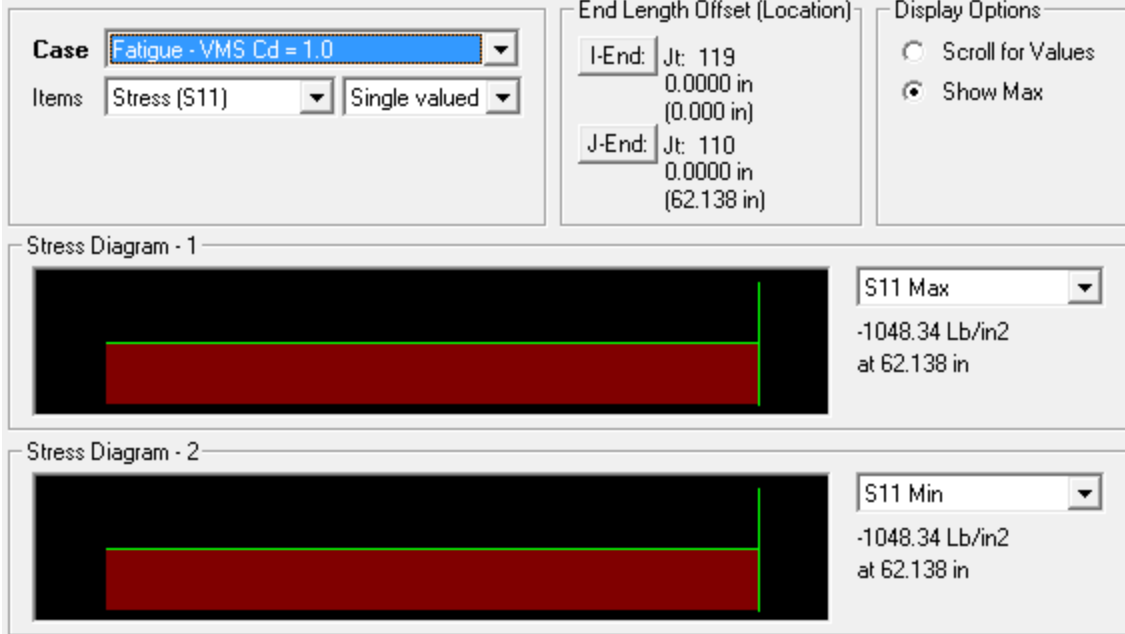


Case Fatigue - VMS Cd = 1.7 Items Stress (S11) Single valued	End Length Offset (Location) I-End: Jt: 119 0.0000 in (0.000 in)	Display Options <input type="radio"/> Scroll for Values <input checked="" type="radio"/> Show Max
	J-End: Jt: 110 0.0000 in (62.138 in)	

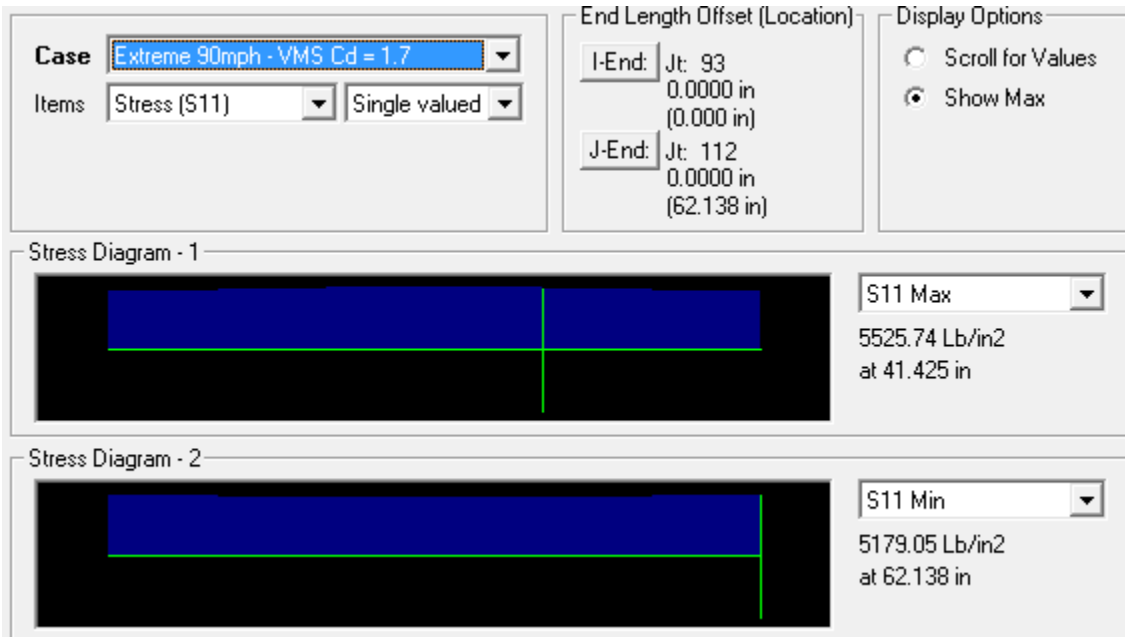


Case Fatigue - VMS Cd = 1.22 Items Stress (S11) Single valued	End Length Offset (Location) I-End: Jt: 119 0.0000 in (0.000 in)	Display Options <input type="radio"/> Scroll for Values <input checked="" type="radio"/> Show Max
	J-End: Jt: 110 0.0000 in (62.138 in)	

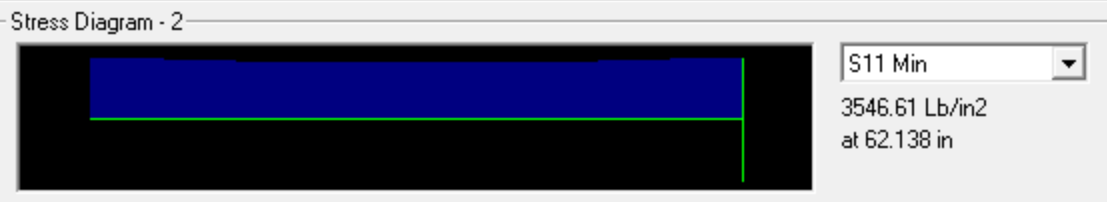
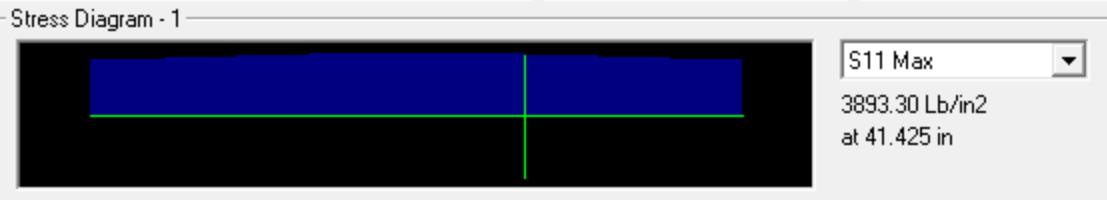




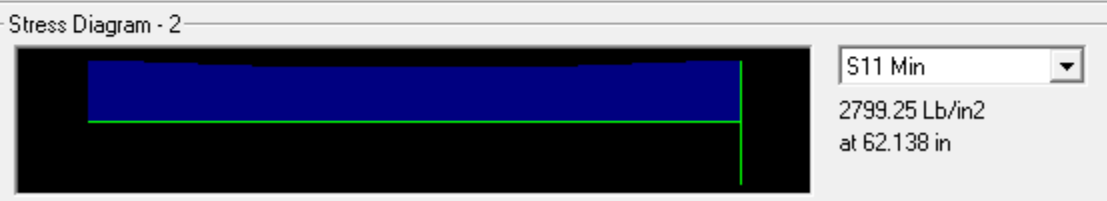
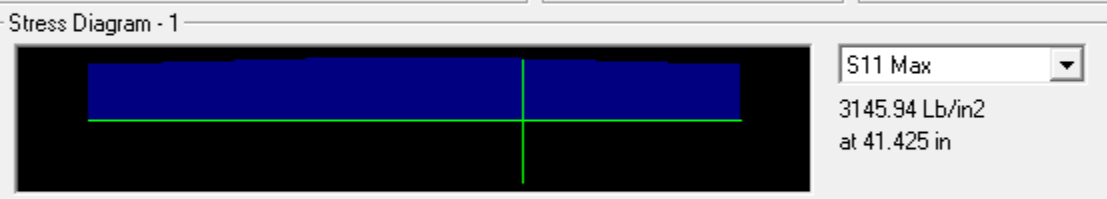
Diagonal 2

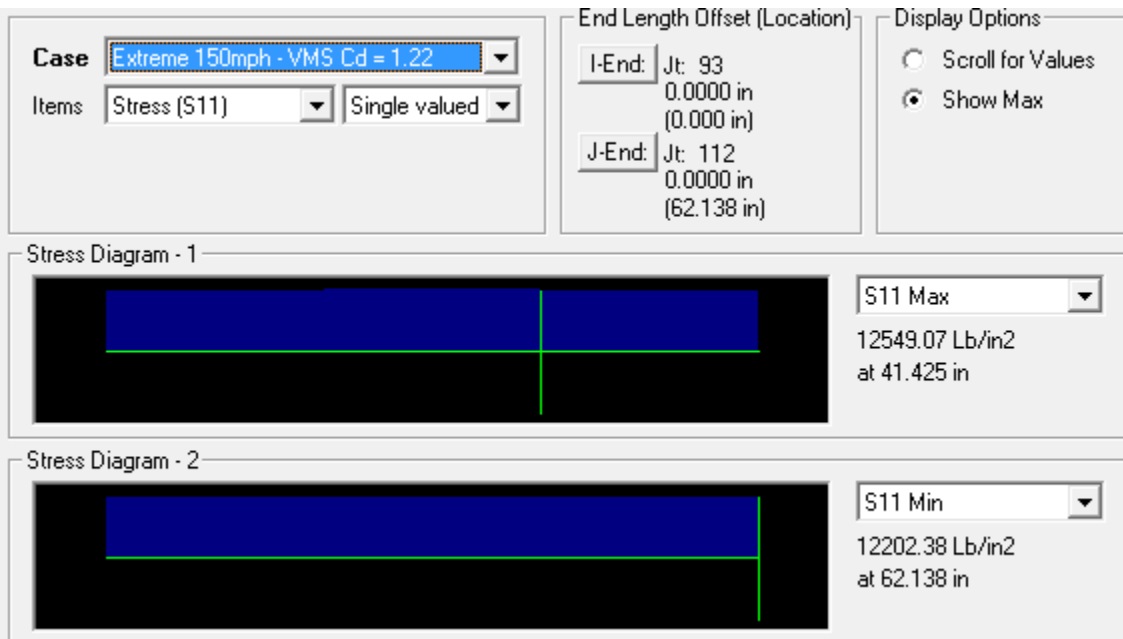
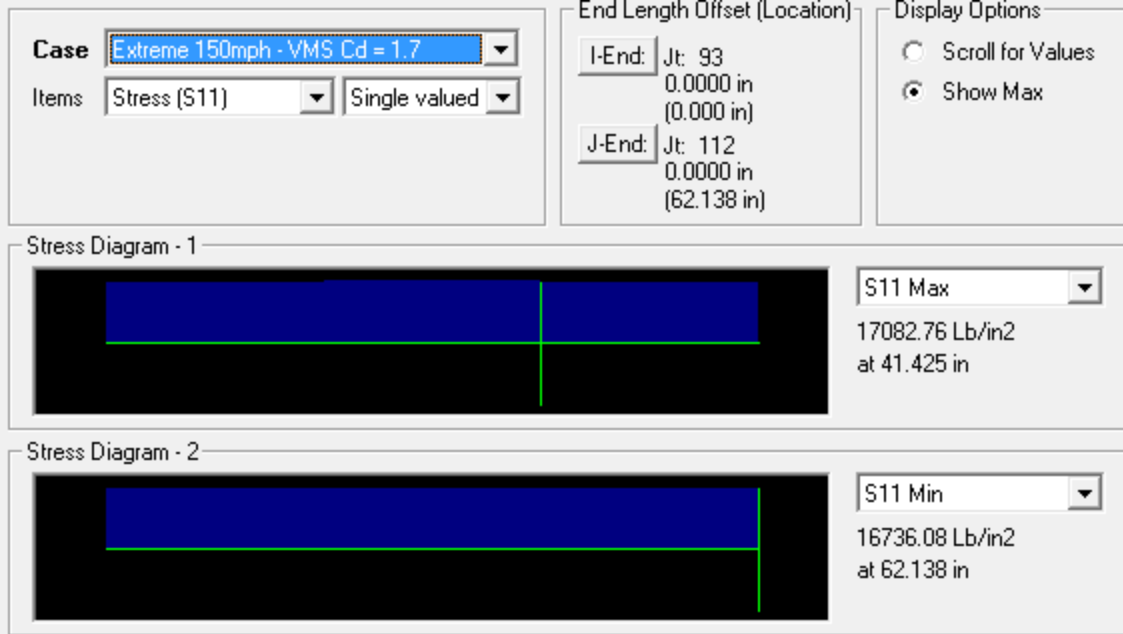


Case Extreme 90mph - VMS Cd = 1.22 Items Stress (S11) Single valued	End Length Offset (Location) I-End: Jt: 93 0.0000 in (0.000 in)	Display Options <input type="radio"/> Scroll for Values <input checked="" type="radio"/> Show Max
	J-End: Jt: 112 0.0000 in (62.138 in)	




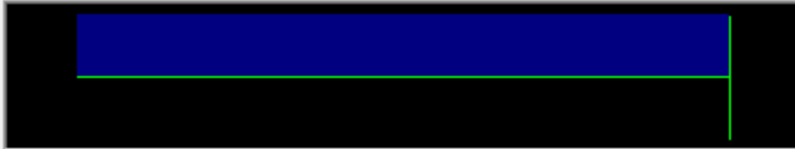
Case Extreme 90mph - VMS Cd = 1.0 Items Stress (S11) Single valued	End Length Offset (Location) I-End: Jt: 93 0.0000 in (0.000 in)	Display Options <input type="radio"/> Scroll for Values <input checked="" type="radio"/> Show Max
	J-End: Jt: 112 0.0000 in (62.138 in)	

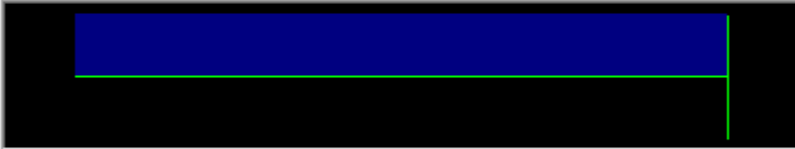





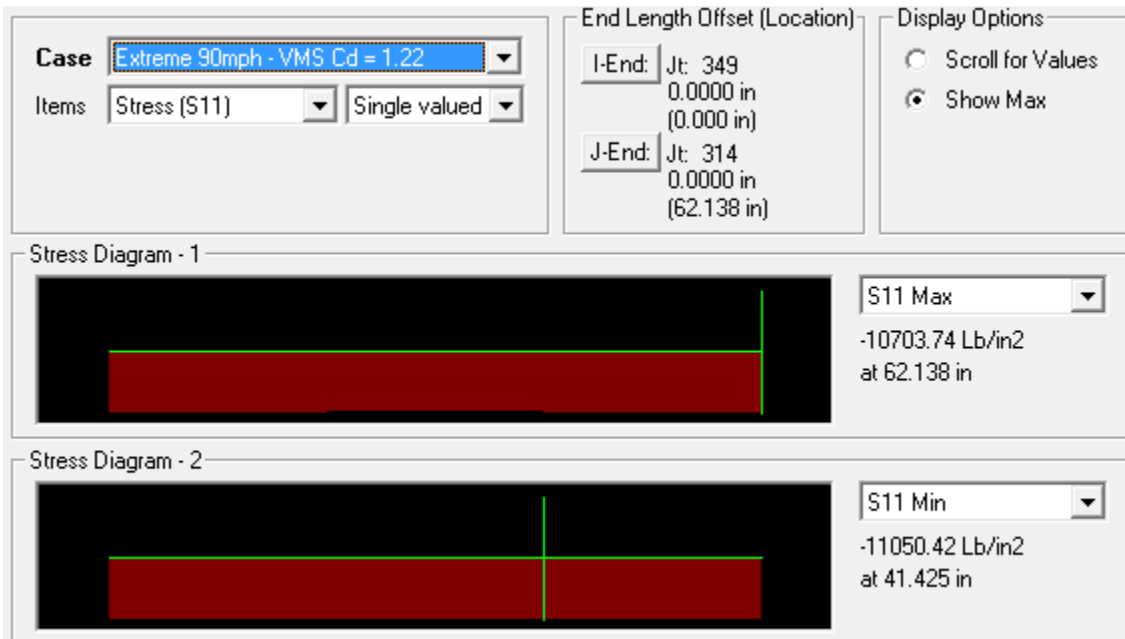
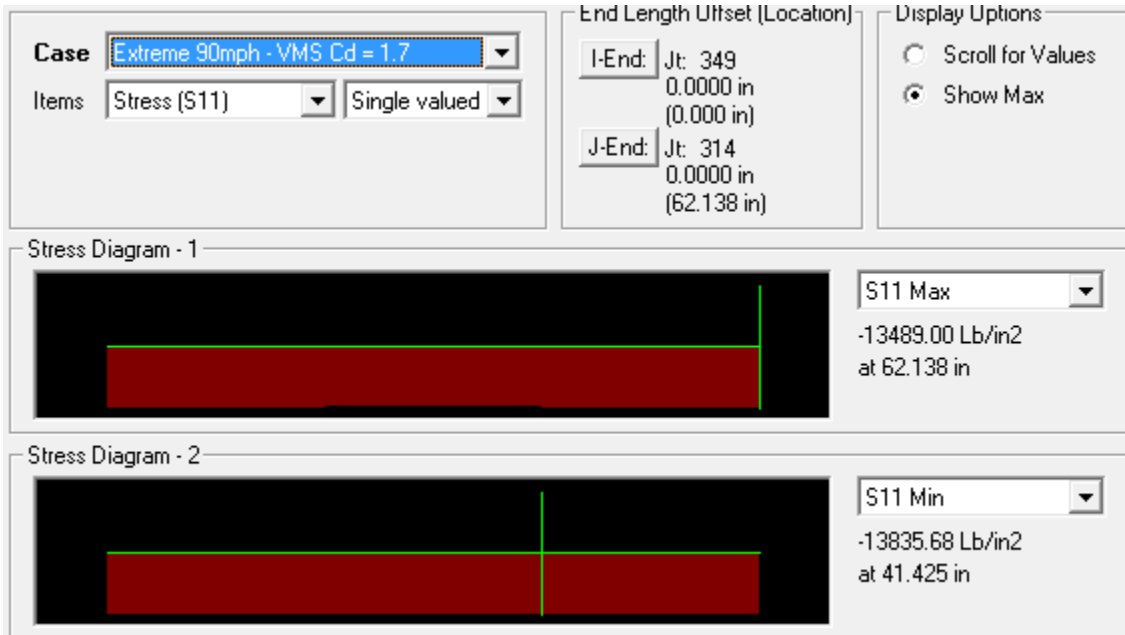
Case Extreme 150mph - VMS Cd = 1.0 Items Stress (S11) Single valued	End Length Offset (Location) I-End: Jt: 93 0.0000 in (0.000 in) J-End: Jt: 112 0.0000 in (62.138 in)	Display Options <input type="radio"/> Scroll for Values <input checked="" type="radio"/> Show Max
Stress Diagram - 1 		
		S11 Max 10470.99 Lb/in2 at 41.425 in
Stress Diagram - 2 		
		S11 Min 10124.31 Lb/in2 at 62.138 in

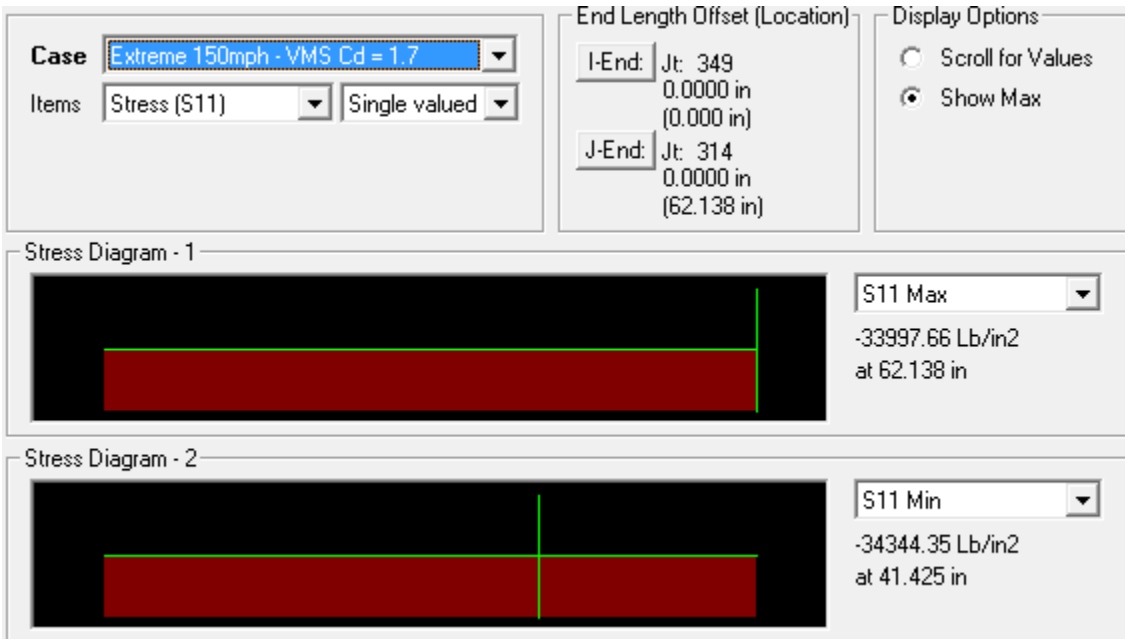
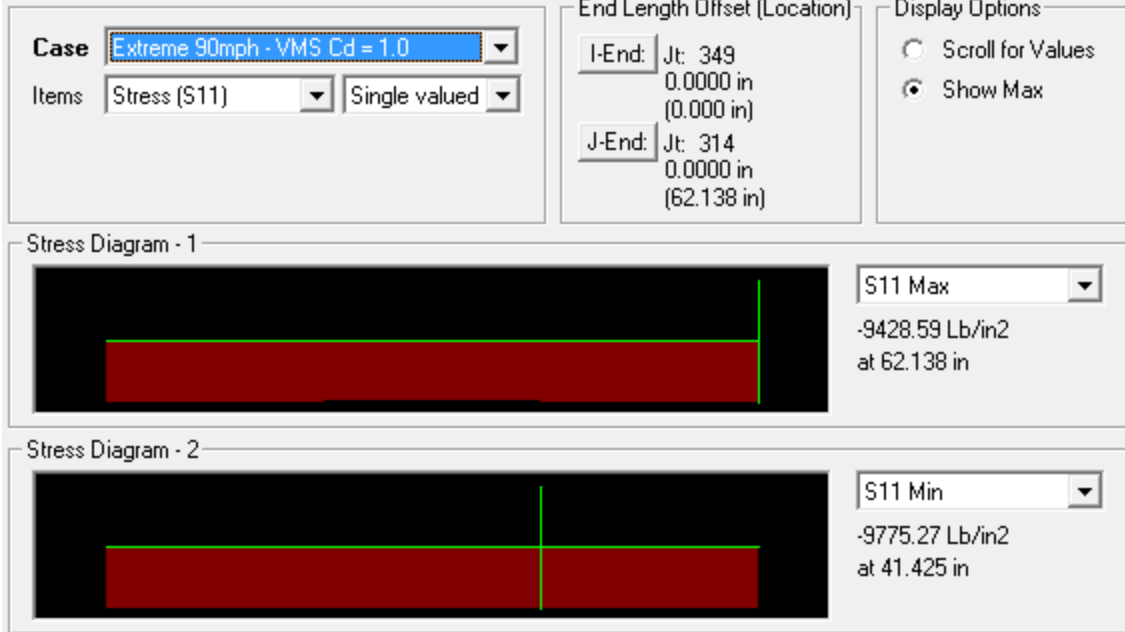
Case Fatigue - VMS Cd = 1.7 Items Stress (S11) Single valued	End Length Offset (Location) I-End: Jt: 93 0.0000 in (0.000 in) J-End: Jt: 112 0.0000 in (62.138 in)	Display Options <input type="radio"/> Scroll for Values <input checked="" type="radio"/> Show Max
Stress Diagram - 1 		
		S11 Max 1536.85 Lb/in2 at 62.138 in
Stress Diagram - 2 		
		S11 Min 1536.85 Lb/in2 at 62.138 in

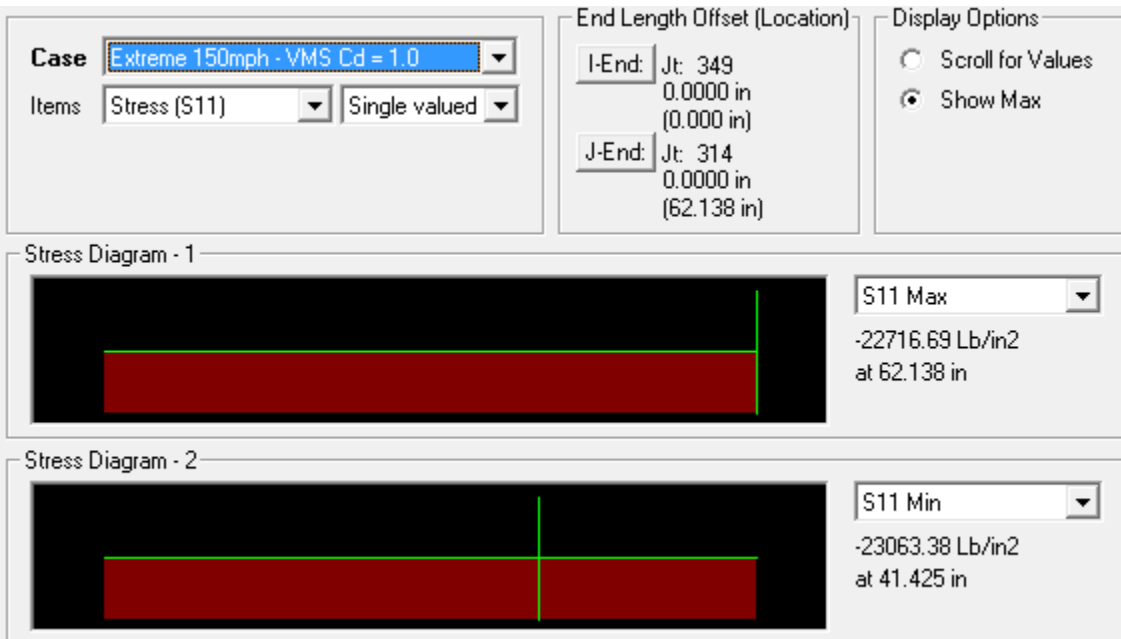
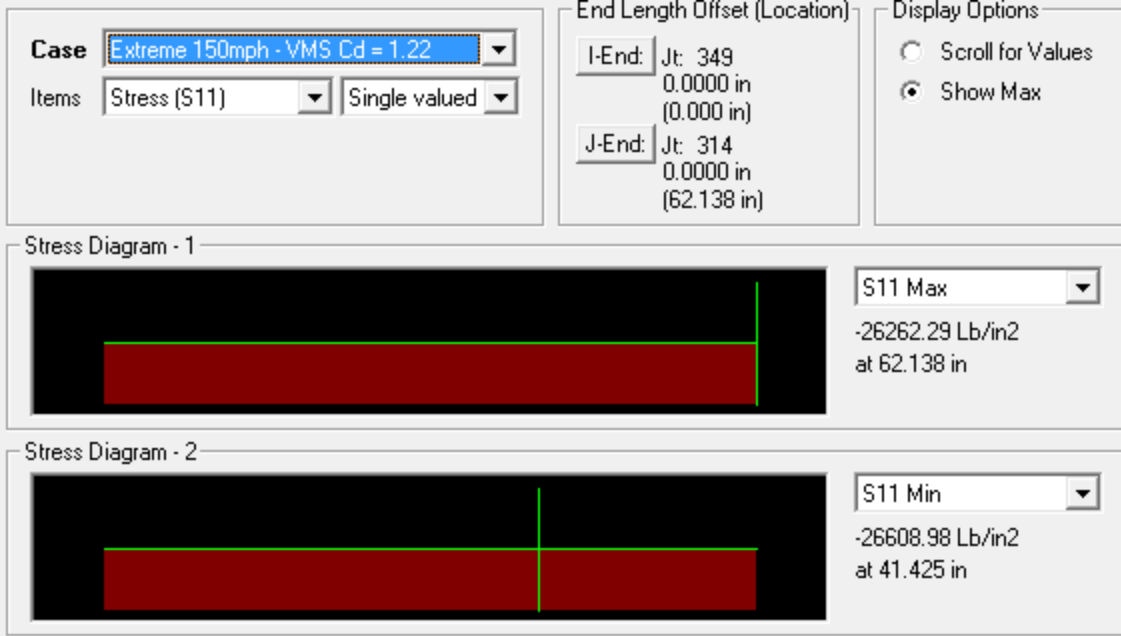
Case Fatigue - VMS Cd = 1.22 Items Stress (S11) Single valued	End Length Offset (Location) I-End: Jt: 93 0.0000 in (0.000 in) J-End: Jt: 112 0.0000 in (62.138 in)	Display Options <input type="radio"/> Scroll for Values <input checked="" type="radio"/> Show Max
Stress Diagram - 1 		
		S11 Max 1150.02 Lb/in2 at 62.138 in
Stress Diagram - 2 		
		S11 Min 1150.02 Lb/in2 at 62.138 in

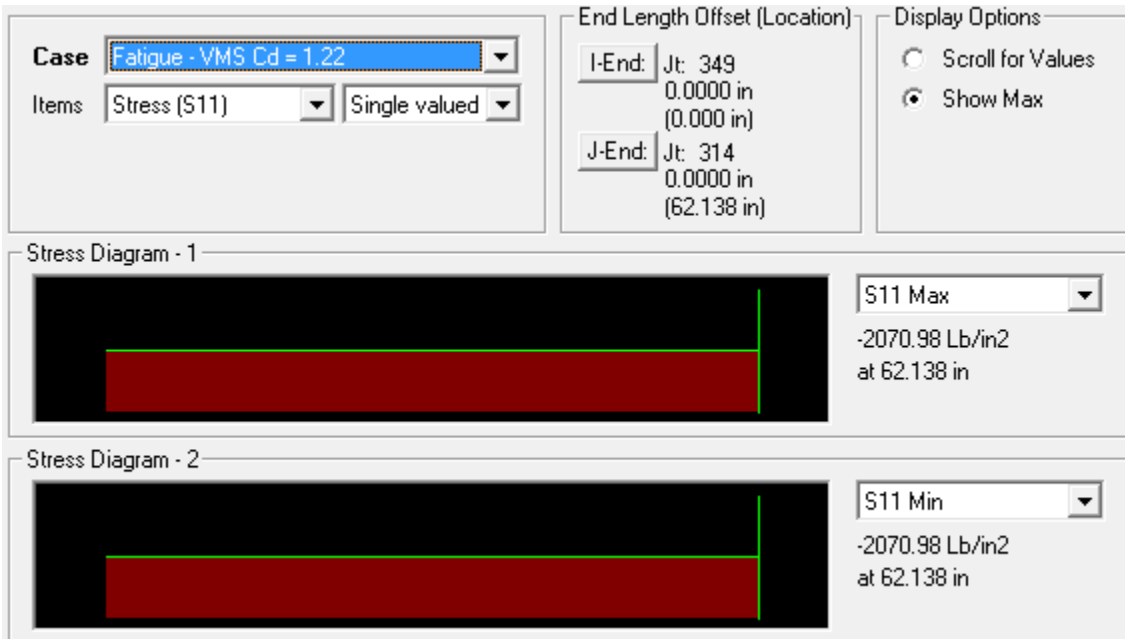
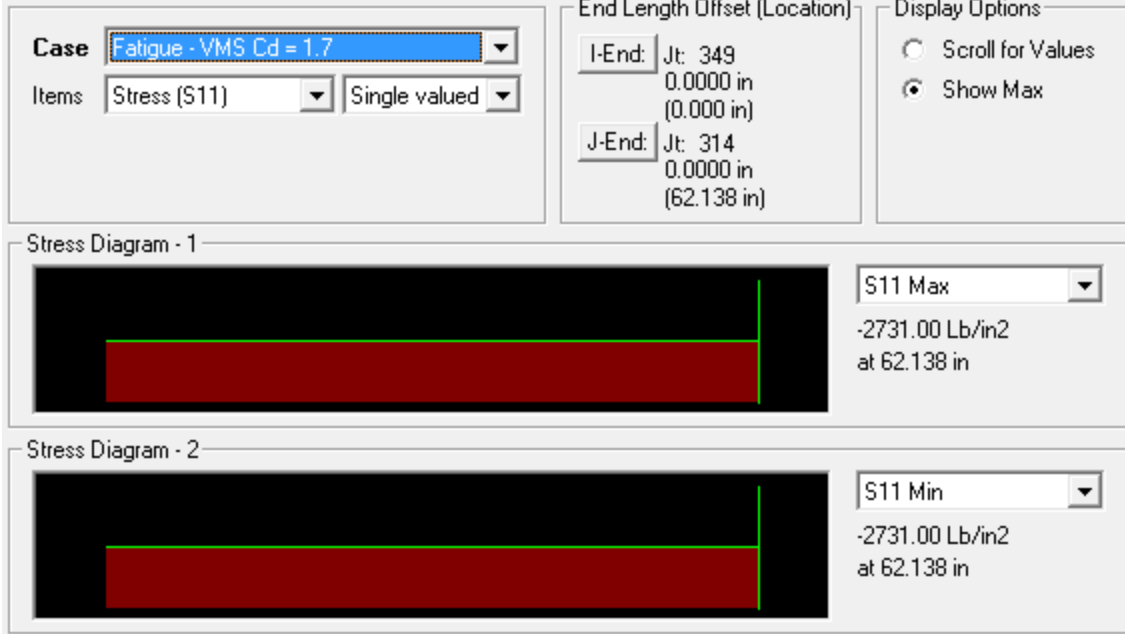
Case Fatigue - VMS Cd = 1.0 Items Stress (S11) Single valued	End Length Offset (Location) I-End: Jt: 93 0.0000 in (0.000 in) J-End: Jt: 112 0.0000 in (62.138 in)	Display Options <input type="radio"/> Scroll for Values <input checked="" type="radio"/> Show Max
Stress Diagram - 1 		
		S11 Max 973.62 Lb/in2 at 62.138 in
Stress Diagram - 2 		
		S11 Min 973.62 Lb/in2 at 62.138 in

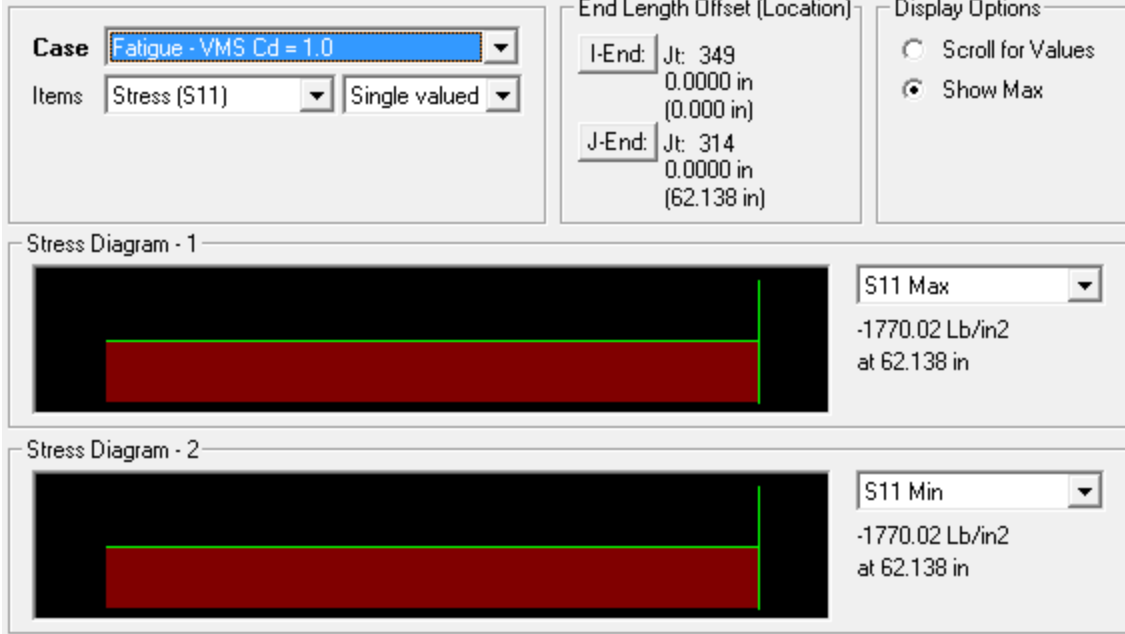
Diagonal 3



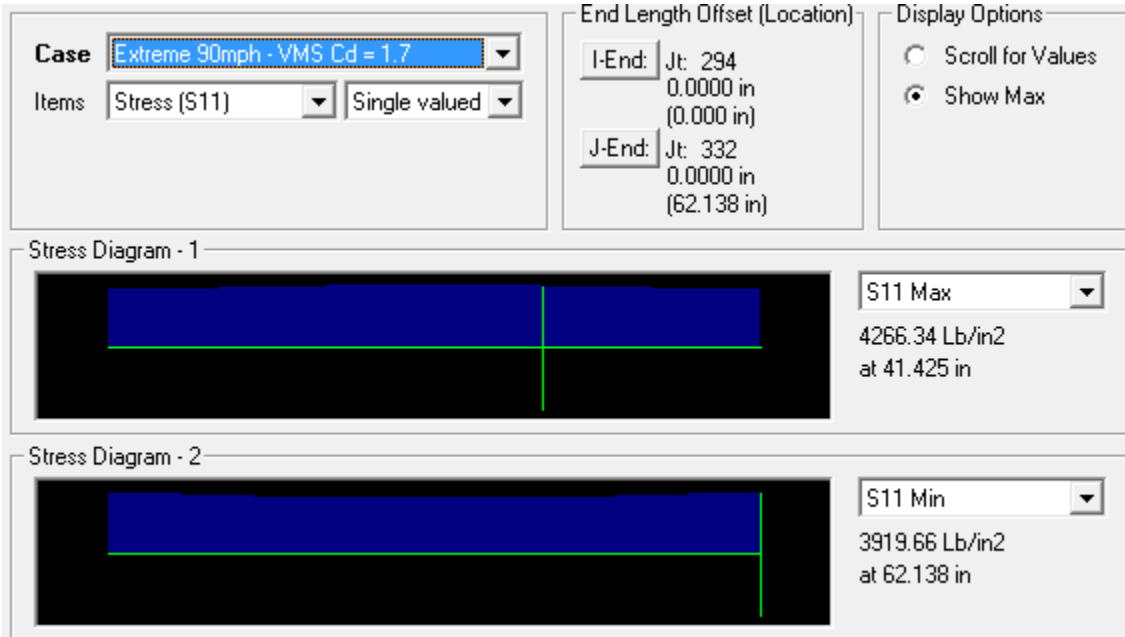




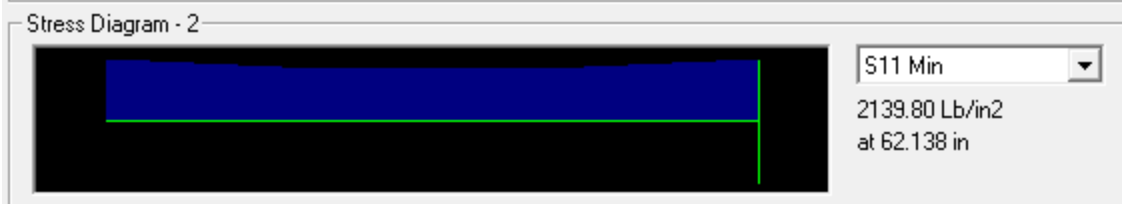
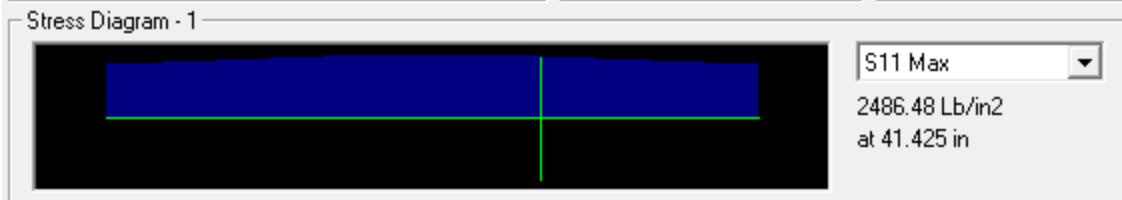




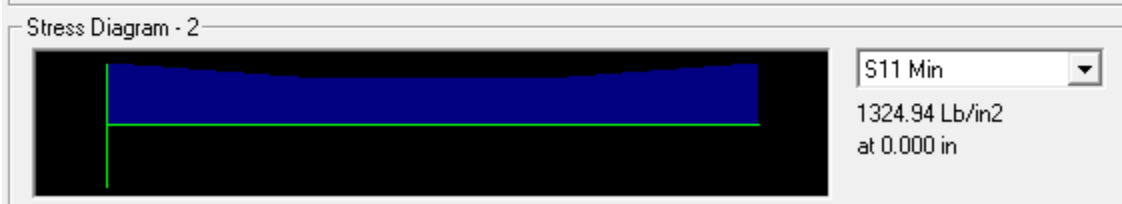
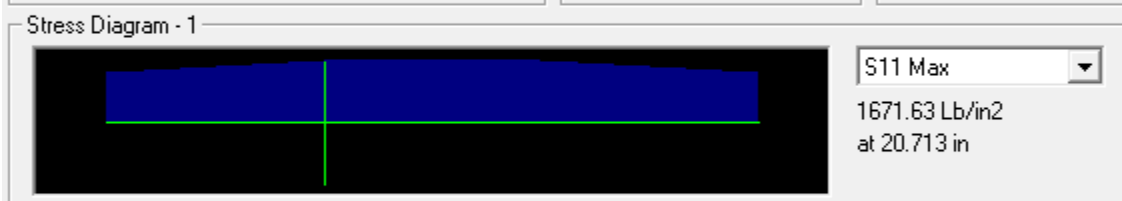
Diagonal 4



Case Extreme 90mph - VMS Cd = 1.22 Items Stress (S11) Single valued	End Length Offset (Location) I-End: Jt: 294 0.0000 in (0.000 in) J-End: Jt: 332 0.0000 in (62.138 in)	Display Options <input type="radio"/> Scroll for Values <input checked="" type="radio"/> Show Max
--	--	--




Case Extreme 90mph - VMS Cd = 1.0 Items Stress (S11) Single valued	End Length Offset (Location) I-End: Jt: 294 0.0000 in (0.000 in) J-End: Jt: 332 0.0000 in (62.138 in)	Display Options <input type="radio"/> Scroll for Values <input checked="" type="radio"/> Show Max
---	--	--




Case: Extreme 150mph - VMS Cd = 1.7
 Items: Stress (S11) Single valued

End Length Offset (Location)
 I-End: Jt: 294
 0.0000 in
 (0.000 in)
 J-End: Jt: 332
 0.0000 in
 (62.138 in)

Display Options
 Scroll for Values
 Show Max


Stress Diagram - 1

 S11 Max
 16178.68 Lb/in2
 at 41.425 in

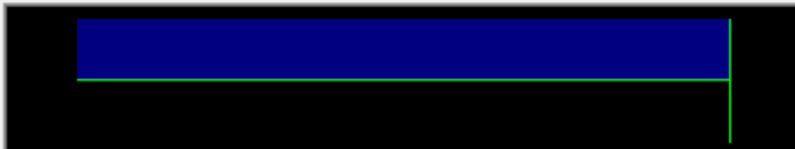
Stress Diagram - 2

 S11 Min
 15831.99 Lb/in2
 at 62.138 in

Case: Extreme 150mph - VMS Cd = 1.22
 Items: Stress (S11) Single valued

End Length Offset (Location)
 I-End: Jt: 294
 0.0000 in
 (0.000 in)
 J-End: Jt: 332
 0.0000 in
 (62.138 in)

Display Options
 Scroll for Values
 Show Max

Stress Diagram - 1

 S11 Max
 11235.57 Lb/in2
 at 41.425 in

Stress Diagram - 2

 S11 Min
 10888.88 Lb/in2
 at 62.138 in

Case: Extreme 150mph - VMS Cd = 1.0

Items: Stress (S11) Single valued

End Length Offset (Location):
 I-End: Jt: 294
 0.0000 in
 (0.000 in)
 J-End: Jt: 332
 0.0000 in
 (62.138 in)

Display Options:
 Scroll for Values
 Show Max

Stress Diagram - 1

S11 Max
 8969.83 Lb/in²
 at 41.425 in

Stress Diagram - 2

S11 Min
 8623.15 Lb/in²
 at 62.138 in

Case: Fatigue - VMS Cd = 1.7

Items: Stress (S11) Single valued

End Length Offset (Location):
 I-End: Jt: 294
 0.0000 in
 (0.000 in)
 J-End: Jt: 332
 0.0000 in
 (62.138 in)

Display Options:
 Scroll for Values
 Show Max

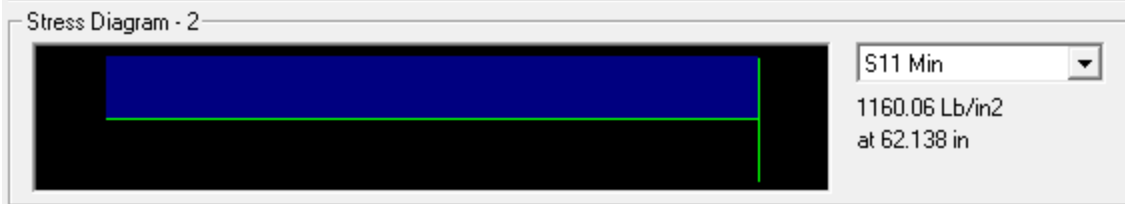
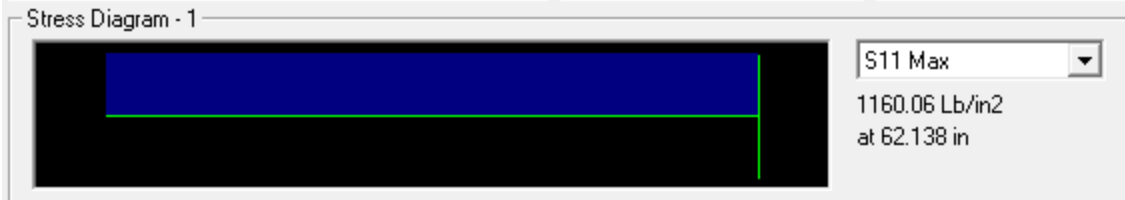
Stress Diagram - 1

S11 Max
 1581.83 Lb/in²
 at 62.138 in

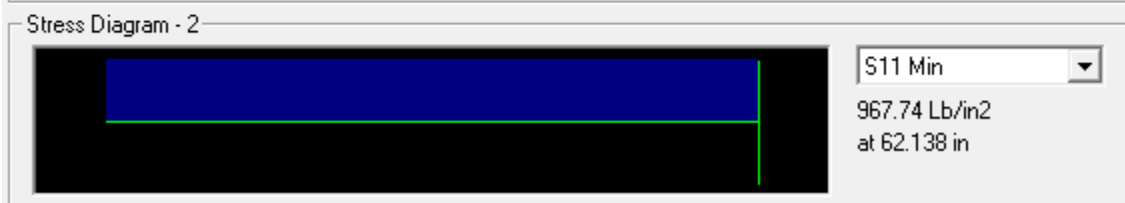
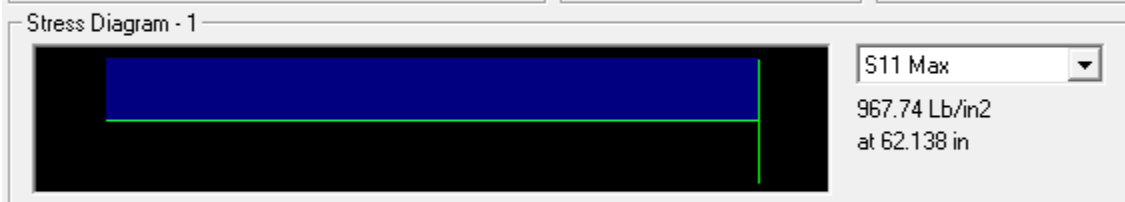
Stress Diagram - 2

S11 Min
 1581.83 Lb/in²
 at 62.138 in

Case Fatigue - VMS Cd = 1.22 Items Stress (S11) Single valued	End Length Offset (Location) I-End: Jt: 294 0.0000 in (0.000 in) J-End: Jt: 332 0.0000 in (62.138 in)	Display Options <input type="radio"/> Scroll for Values <input checked="" type="radio"/> Show Max
--	--	--

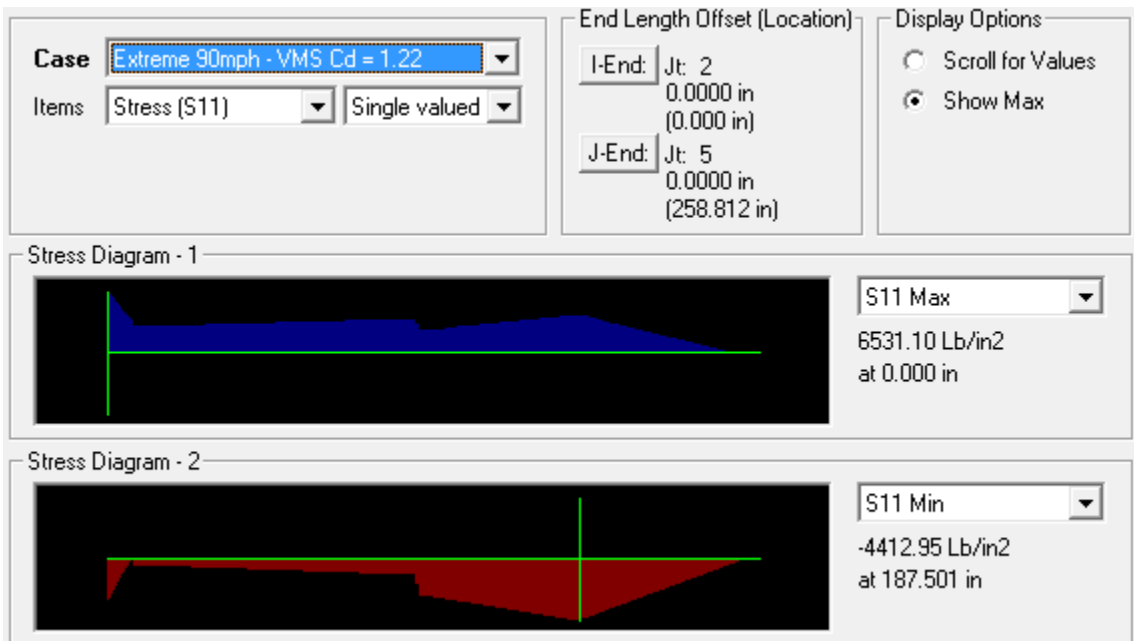
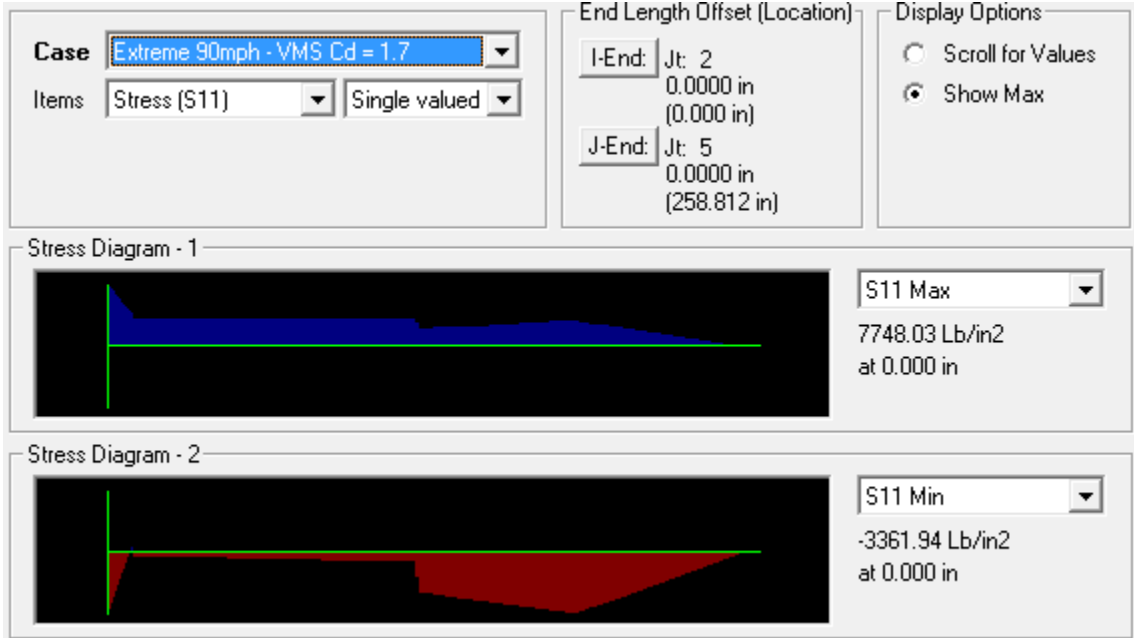


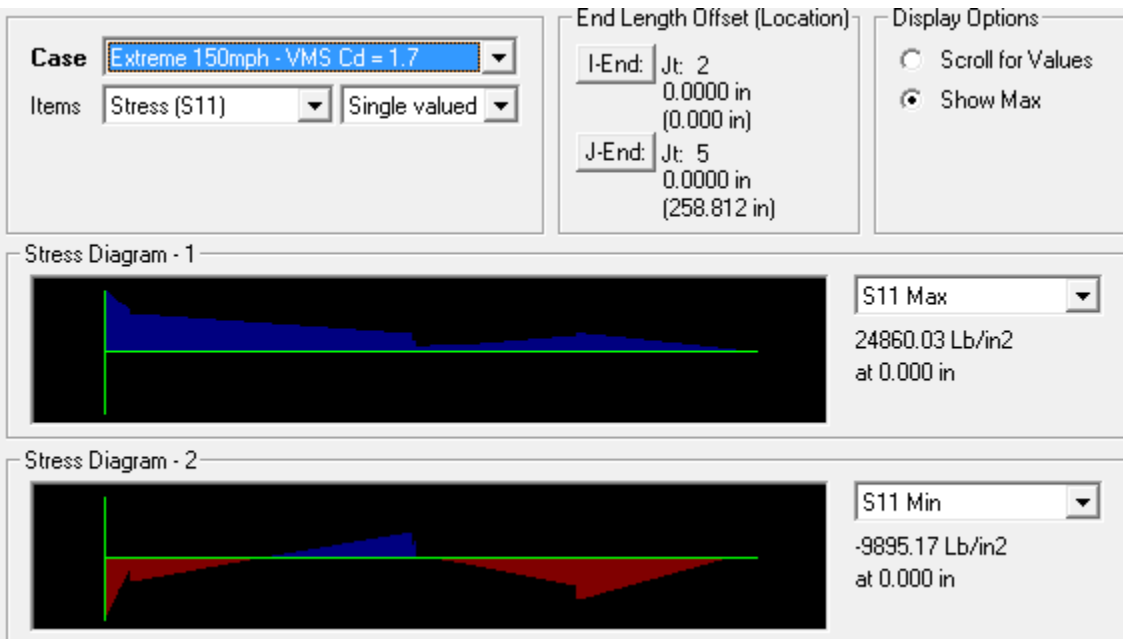
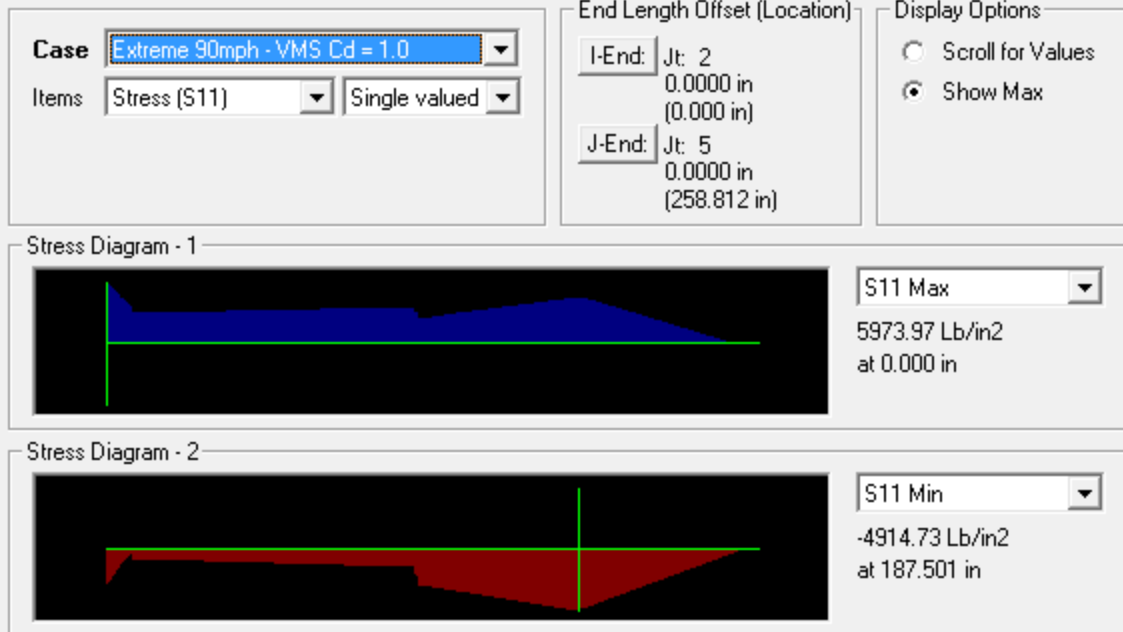
Case Fatigue - VMS Cd = 1.0 Items Stress (S11) Single valued	End Length Offset (Location) I-End: Jt: 294 0.0000 in (0.000 in) J-End: Jt: 332 0.0000 in (62.138 in)	Display Options <input type="radio"/> Scroll for Values <input checked="" type="radio"/> Show Max
---	--	--



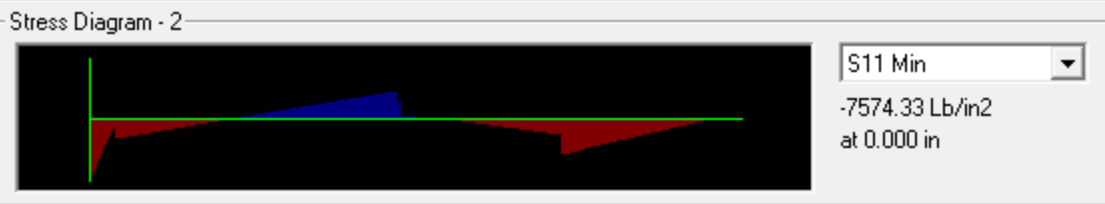
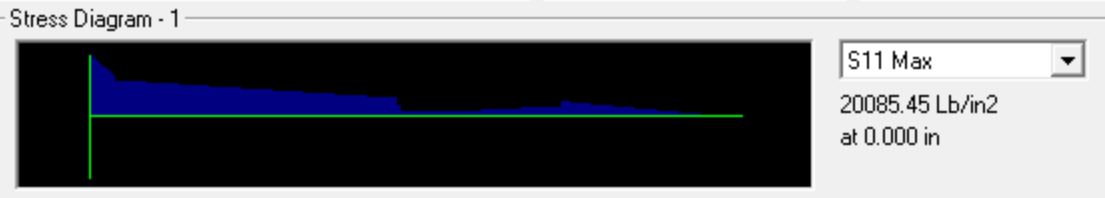
Structure B – Birmingham VMS Structure

Upright 1

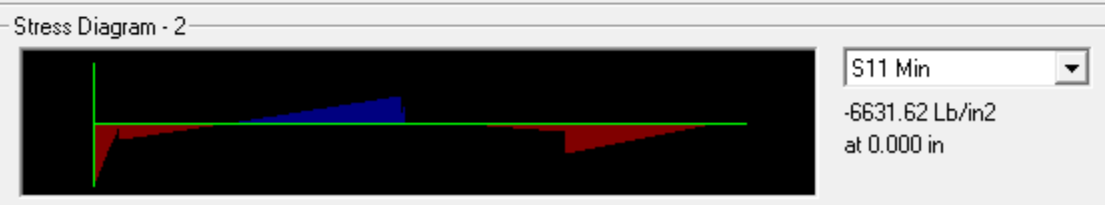
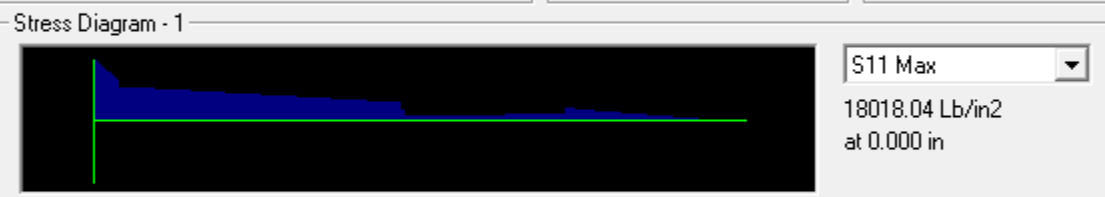




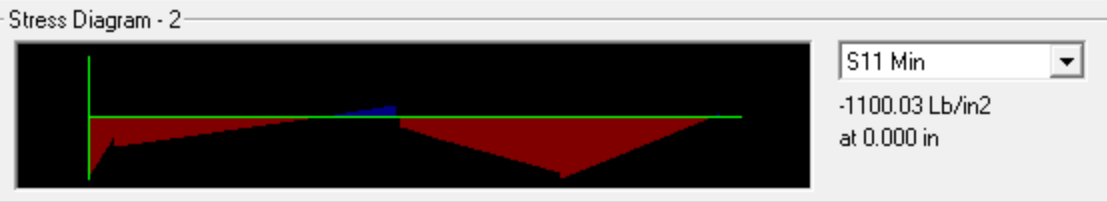
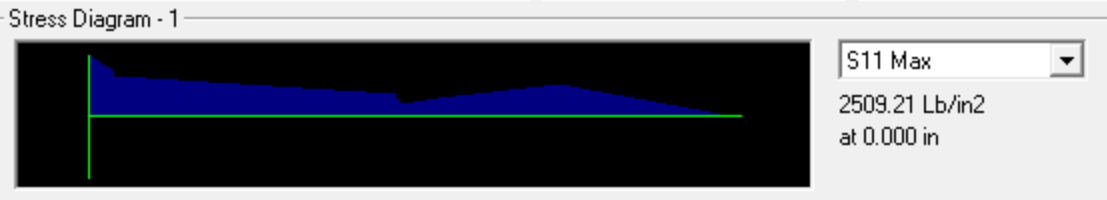
Case Extreme 150mph - VMS Cd = 1.22 Items Stress (S11) Single valued	End Length Offset (Location) I-End: Jt: 2 0.0000 in (0.000 in) J-End: Jt: 5 0.0000 in (258.812 in)	Display Options <input type="radio"/> Scroll for Values <input checked="" type="radio"/> Show Max
---	---	--



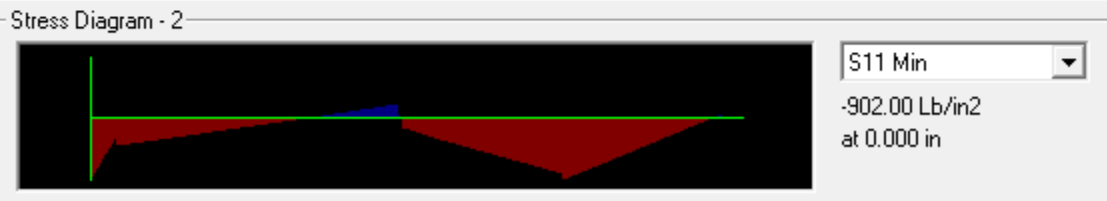
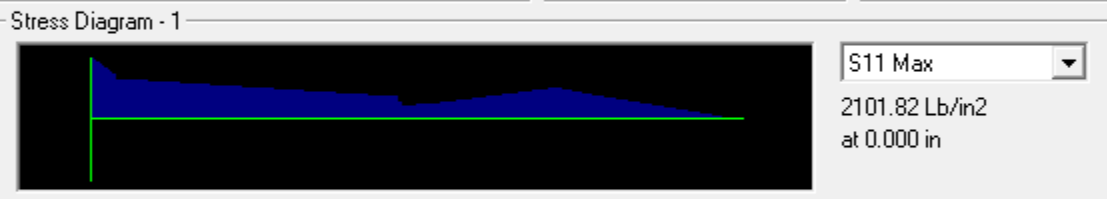
Case Extreme 150mph - VMS Cd = 1.0 Items Stress (S11) Single valued	End Length Offset (Location) I-End: Jt: 2 0.0000 in (0.000 in) J-End: Jt: 5 0.0000 in (258.812 in)	Display Options <input type="radio"/> Scroll for Values <input checked="" type="radio"/> Show Max
--	---	--

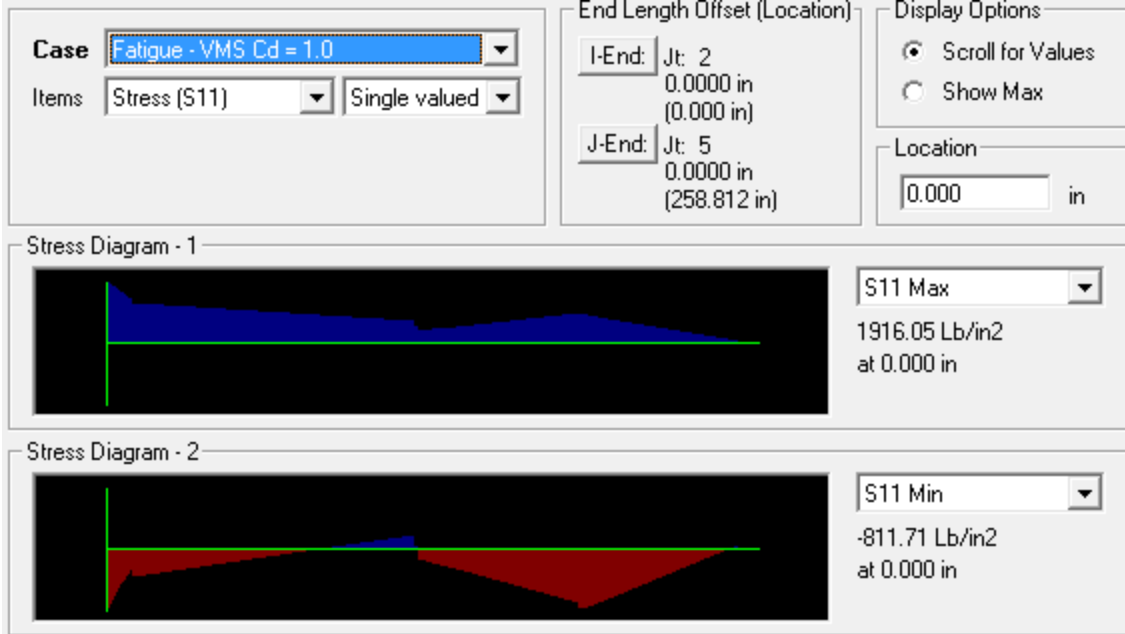


Case Fatigue - VMS Cd = 1.7 Items Stress (S11) Single valued	End Length Offset (Location) I-End: Jt: 2 0.0000 in (0.000 in) J-End: Jt: 5 0.0000 in (258.812 in)	Display Options <input checked="" type="radio"/> Scroll for Values <input type="radio"/> Show Max Location 0.000 in
--	---	---

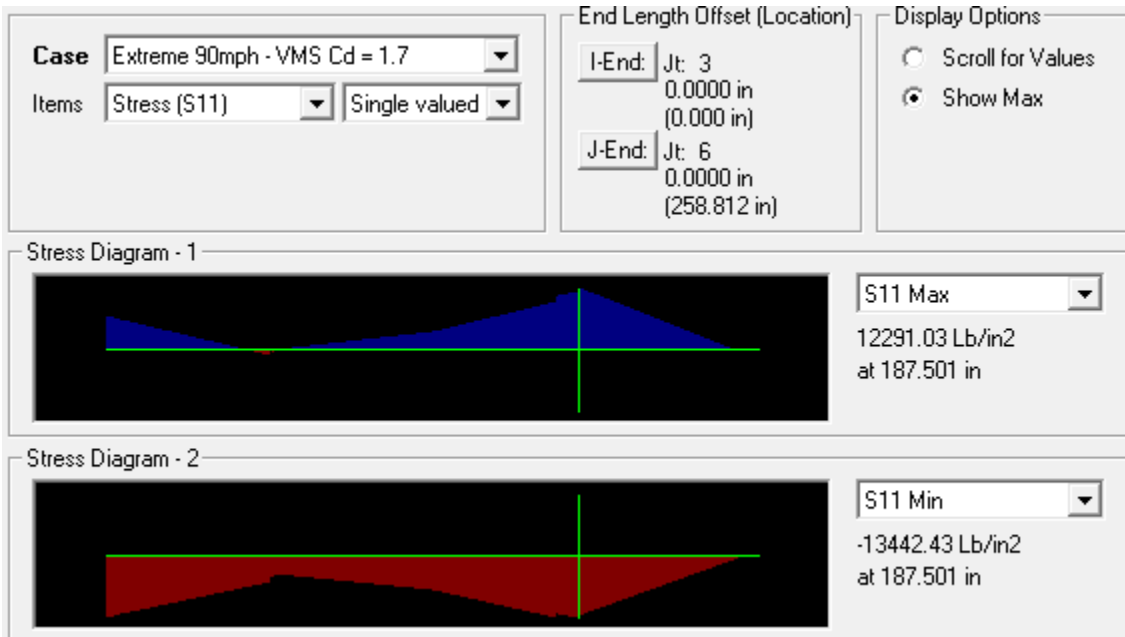


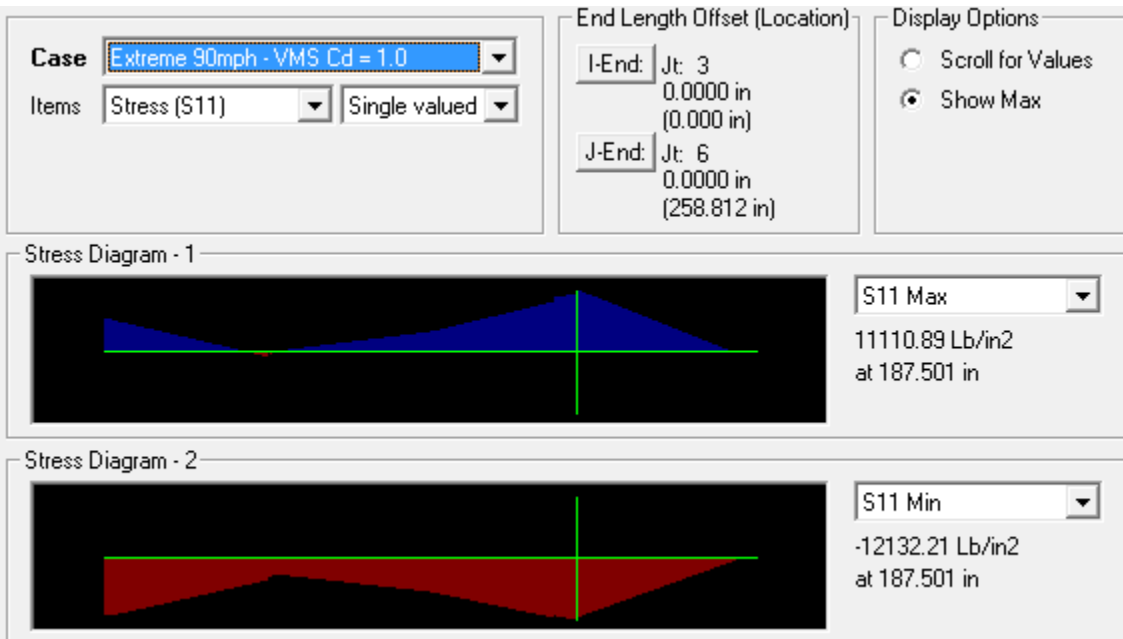
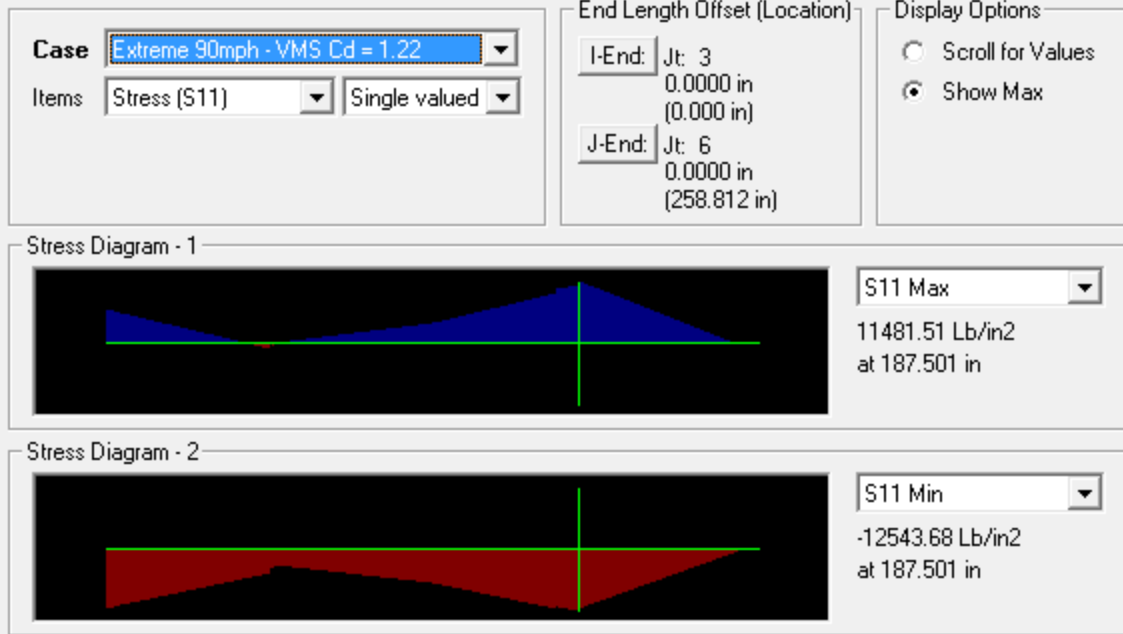
Case Fatigue - VMS Cd = 1.22 Items Stress (S11) Single valued	End Length Offset (Location) I-End: Jt: 2 0.0000 in (0.000 in) J-End: Jt: 5 0.0000 in (258.812 in)	Display Options <input checked="" type="radio"/> Scroll for Values <input type="radio"/> Show Max Location 0.000 in
---	---	---

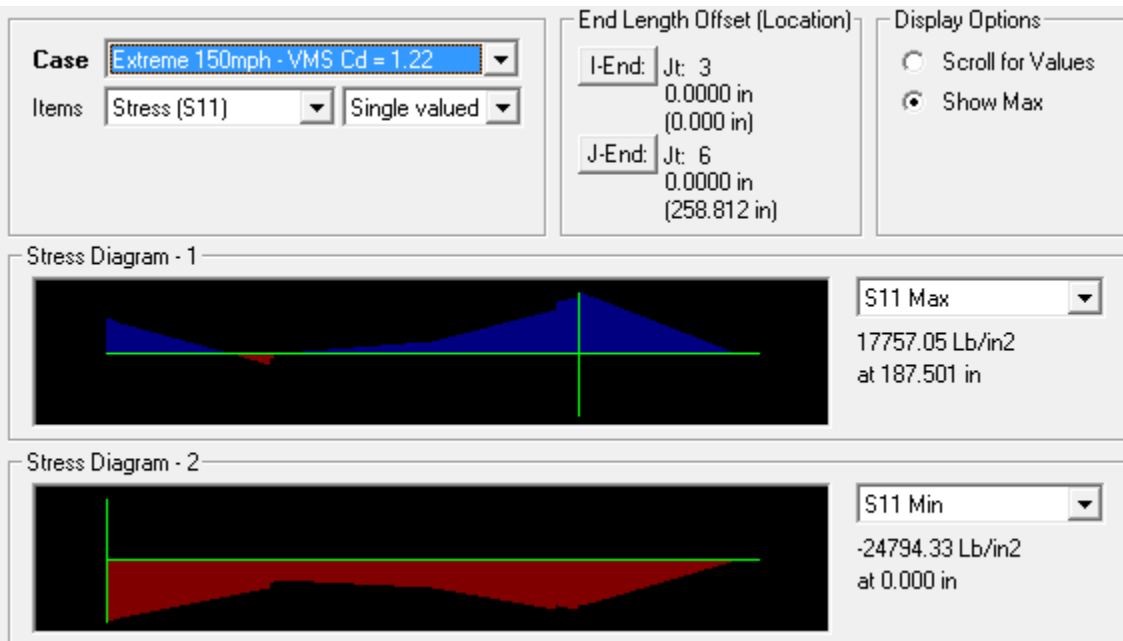
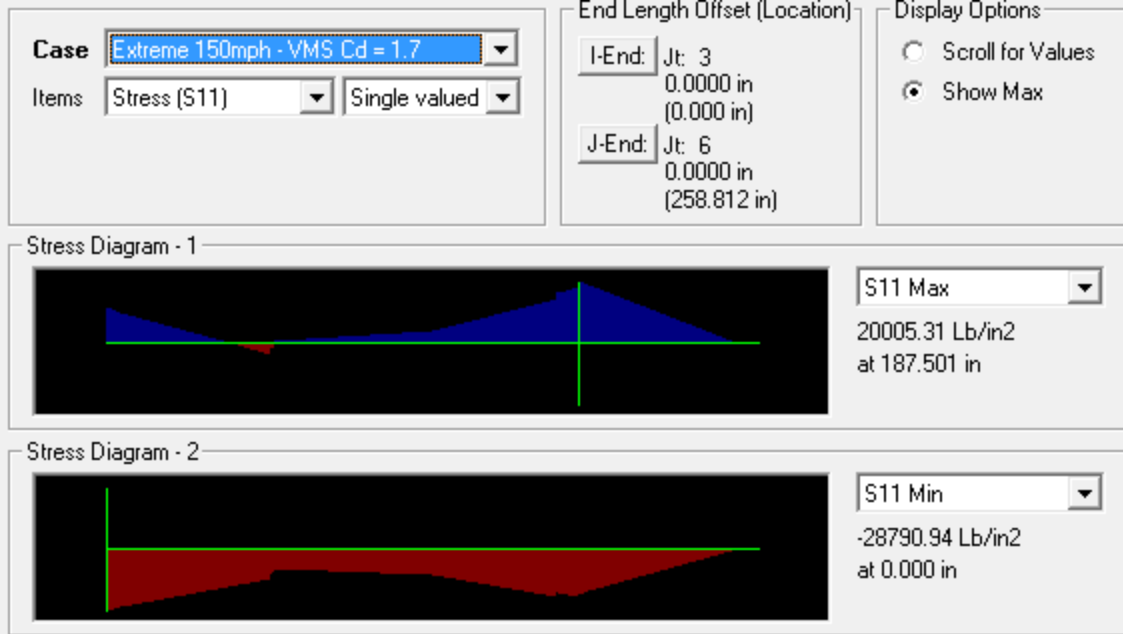


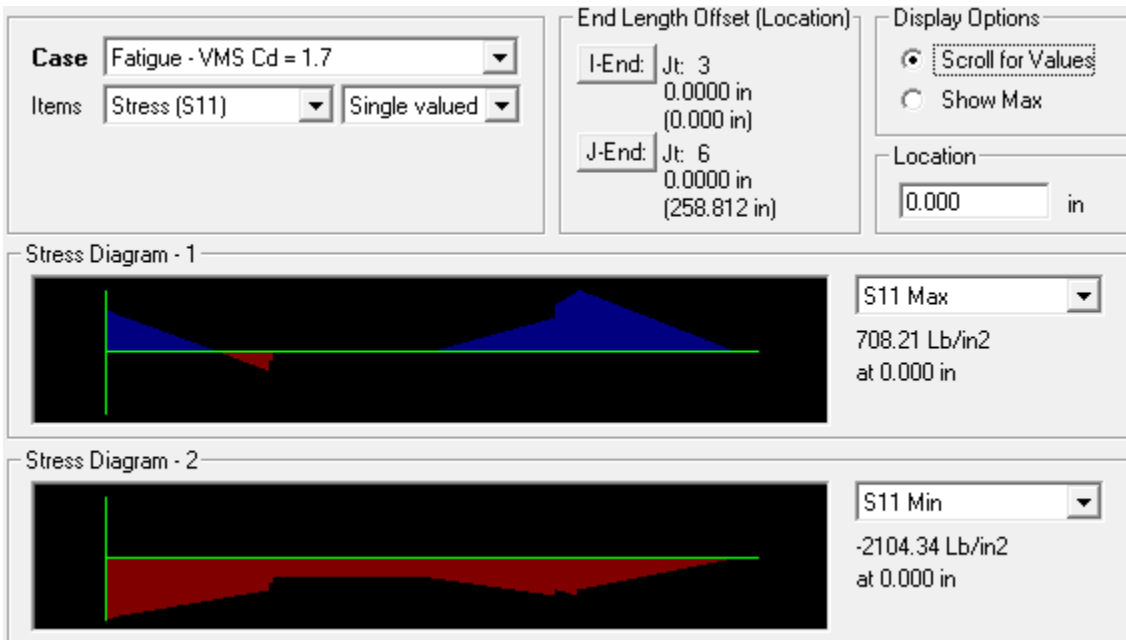
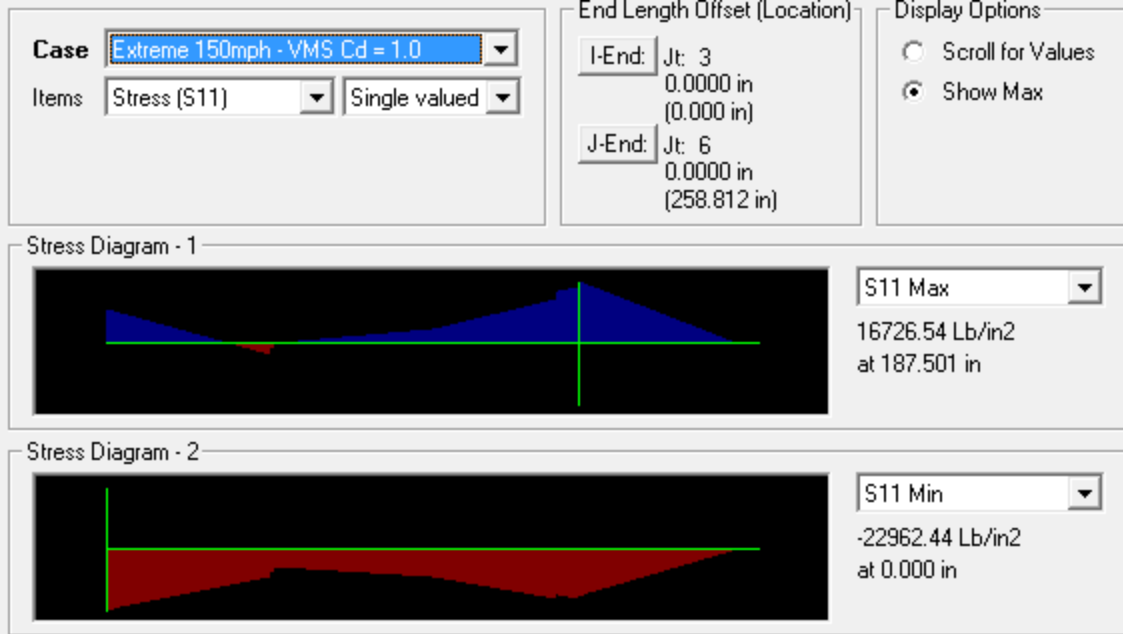


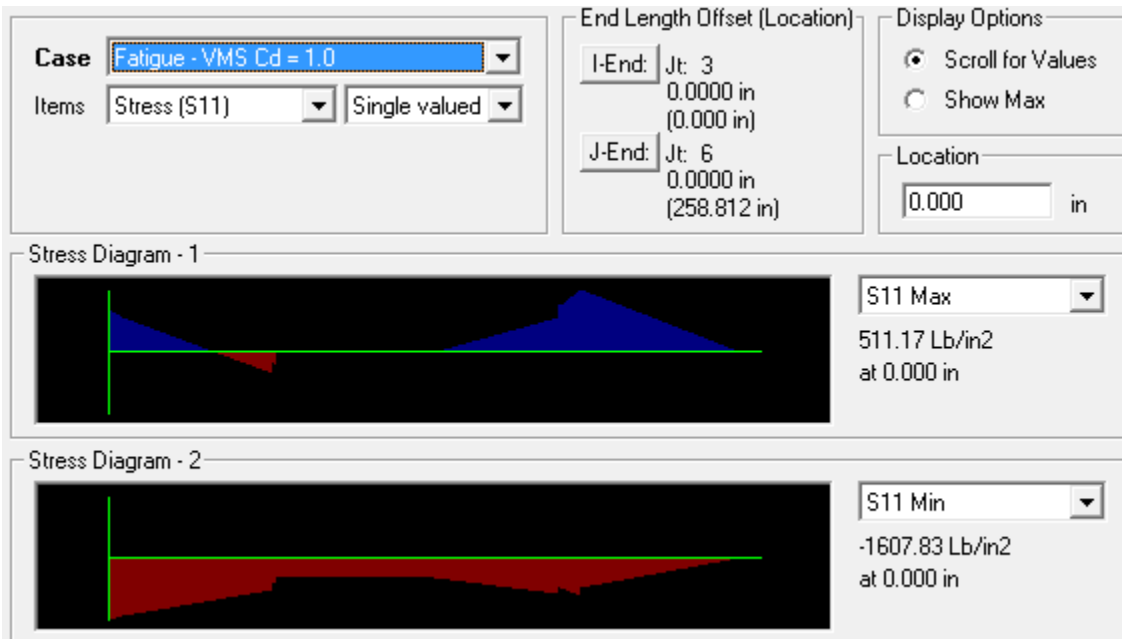
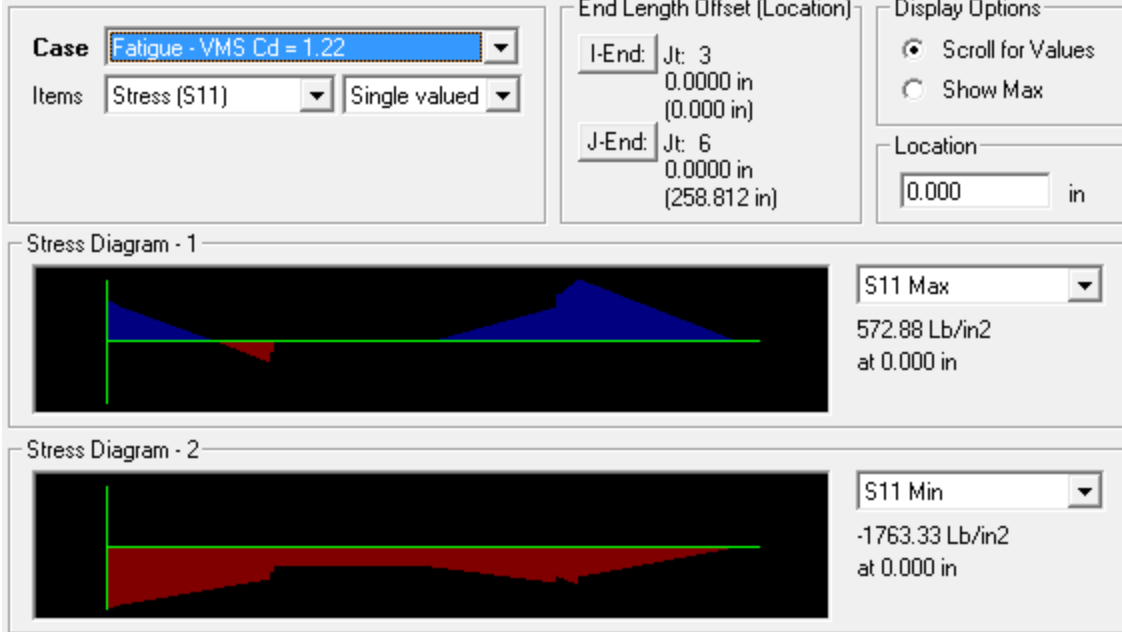
Upright 2





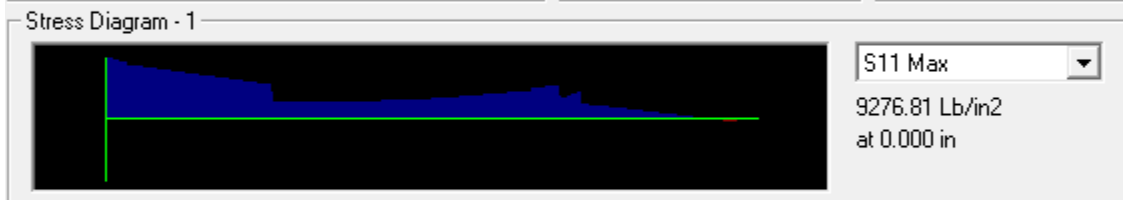




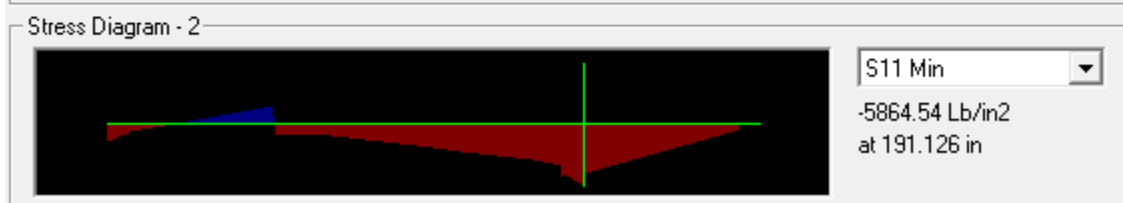
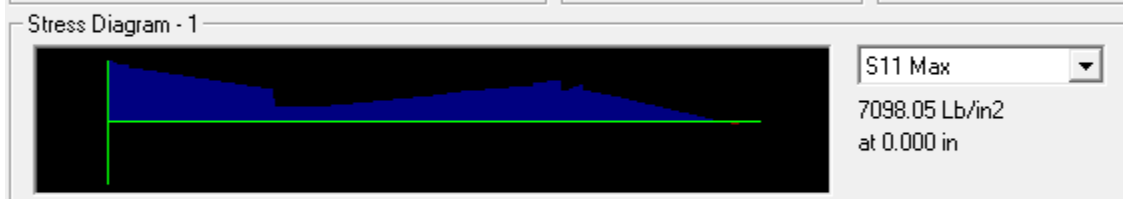


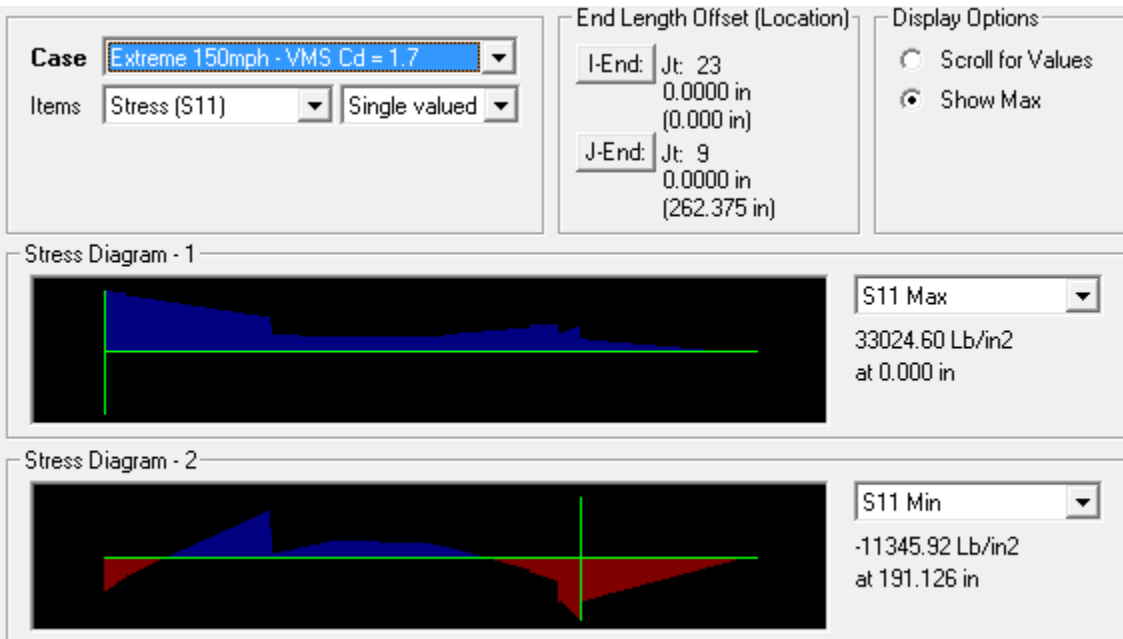
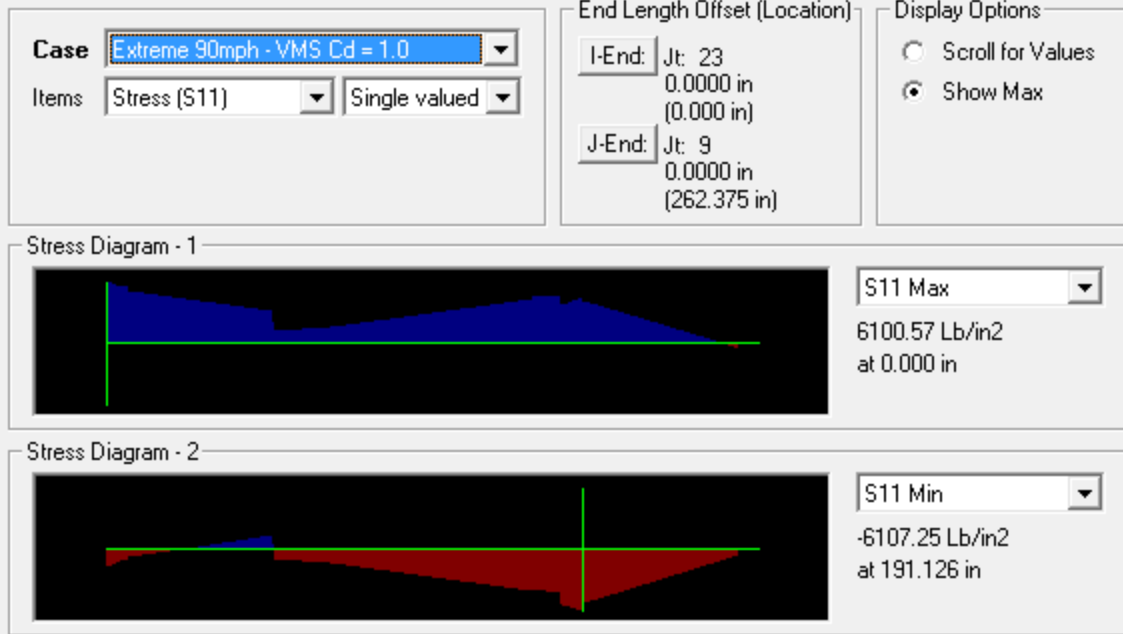
Upright 3

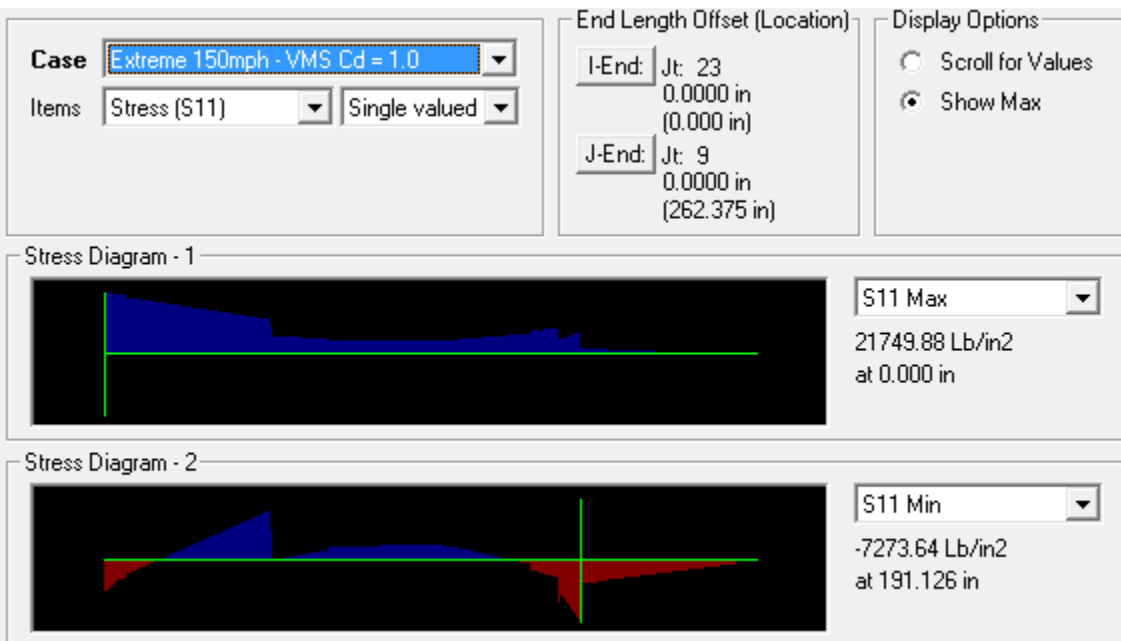
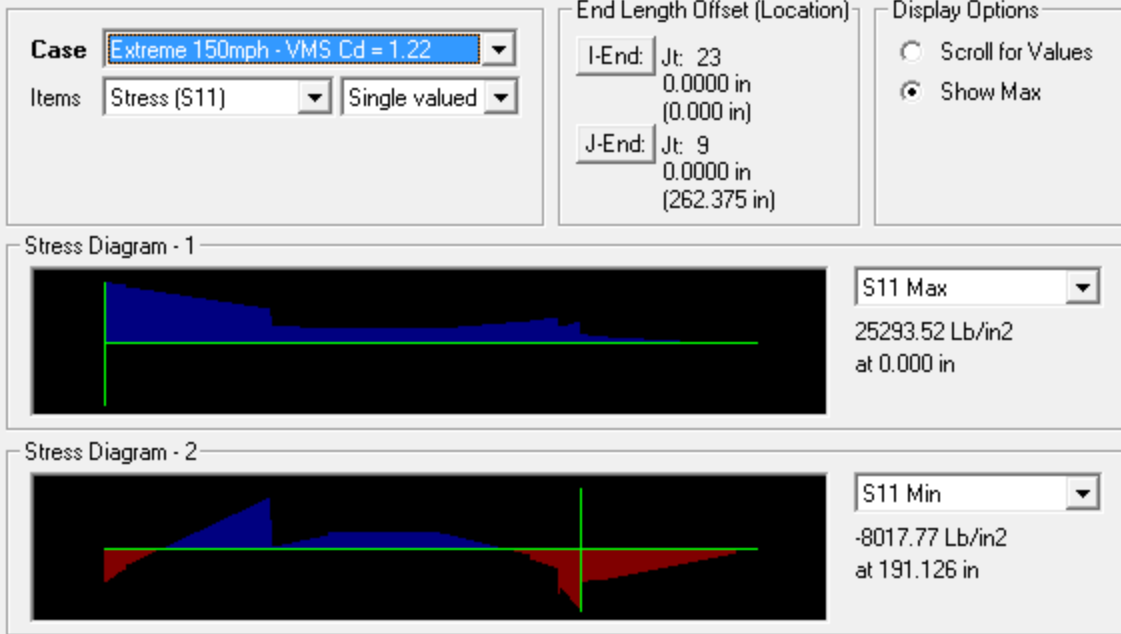
Case Extreme 90mph - VMS Cd = 1.7 Items Stress (S11) Single valued	End Length Offset (Location) I-End: Jt: 23 0.0000 in (0.000 in) J-End: Jt: 9 0.0000 in (262.375 in)	Display Options <input type="radio"/> Scroll for Values <input checked="" type="radio"/> Show Max
---	--	--



Case Extreme 90mph - VMS Cd = 1.22 Items Stress (S11) Single valued	End Length Offset (Location) I-End: Jt: 23 0.0000 in (0.000 in) J-End: Jt: 9 0.0000 in (262.375 in)	Display Options <input type="radio"/> Scroll for Values <input checked="" type="radio"/> Show Max
--	--	--

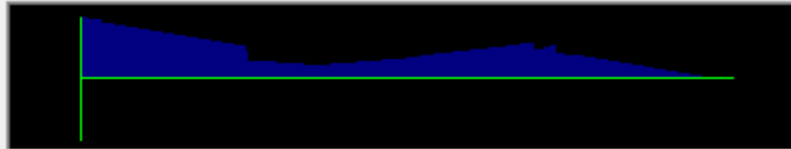






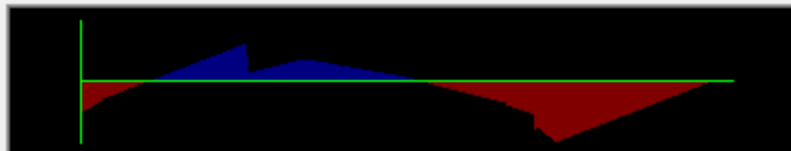
Case Fatigue - VMS Cd = 1.7 Items Stress (S11) Single valued	End Length Offset (Location) I-End: Jt: 23 0.0000 in (0.000 in) J-End: Jt: 9 0.0000 in (262.375 in)	Display Options <input checked="" type="radio"/> Scroll for Values <input type="radio"/> Show Max Location 0.000 in
---	--	---

Stress Diagram - 1



S11 Max
 3286.01 Lb/in2
 at 0.000 in

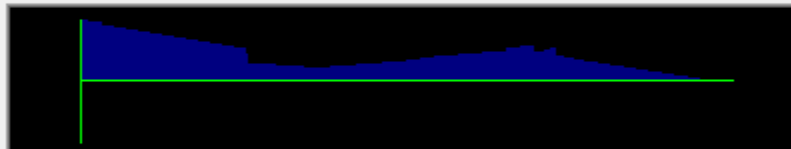
Stress Diagram - 2



S11 Min
 -716.72 Lb/in2
 at 0.000 in

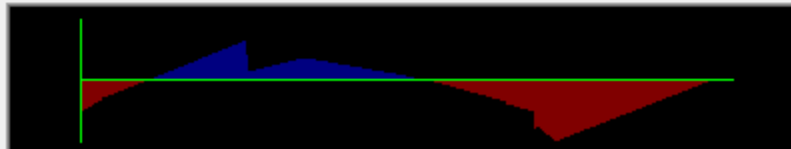
Case Fatigue - VMS Cd = 1.22 Items Stress (S11) Single valued	End Length Offset (Location) I-End: Jt: 23 0.0000 in (0.000 in) J-End: Jt: 9 0.0000 in (262.375 in)	Display Options <input checked="" type="radio"/> Scroll for Values <input type="radio"/> Show Max Location 0.000 in
--	--	---

Stress Diagram - 1

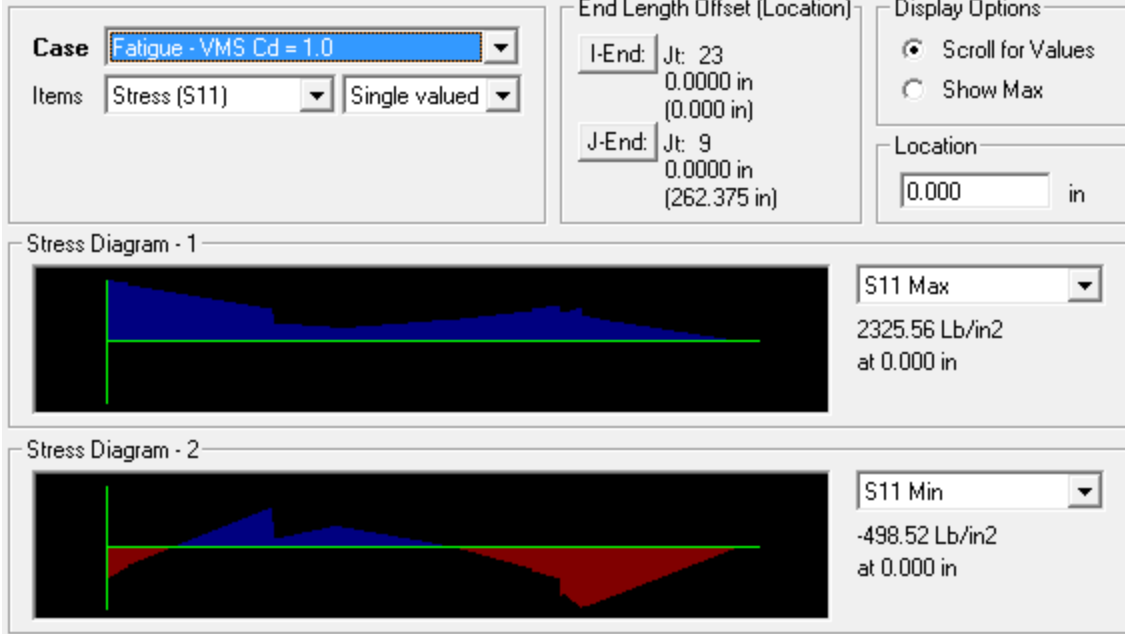


S11 Max
 2626.36 Lb/in2
 at 0.000 in

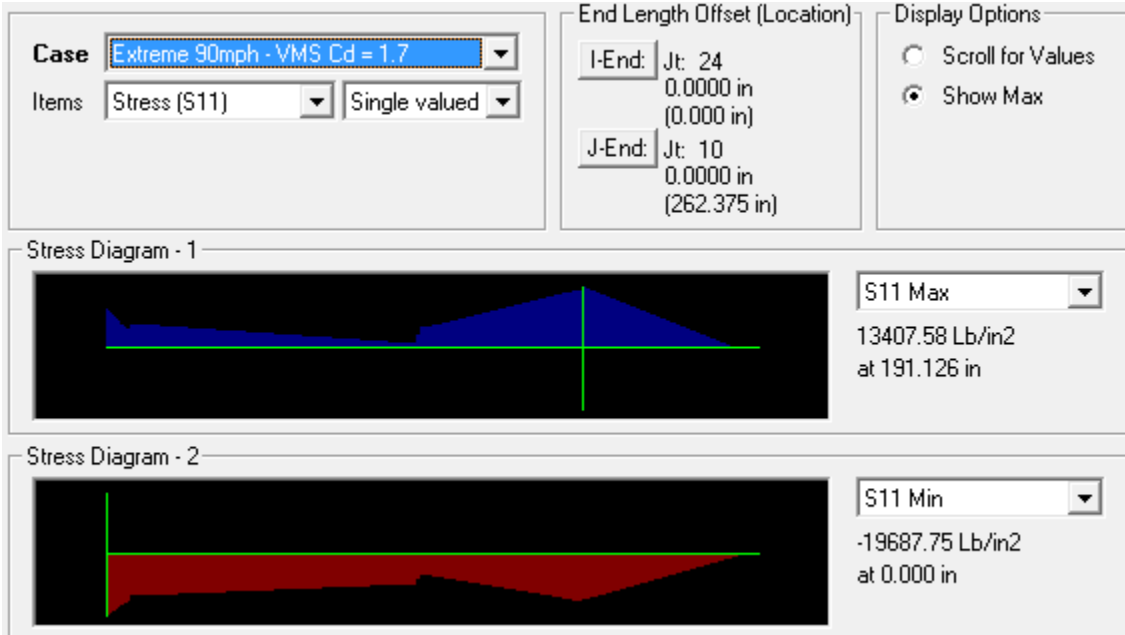
Stress Diagram - 2

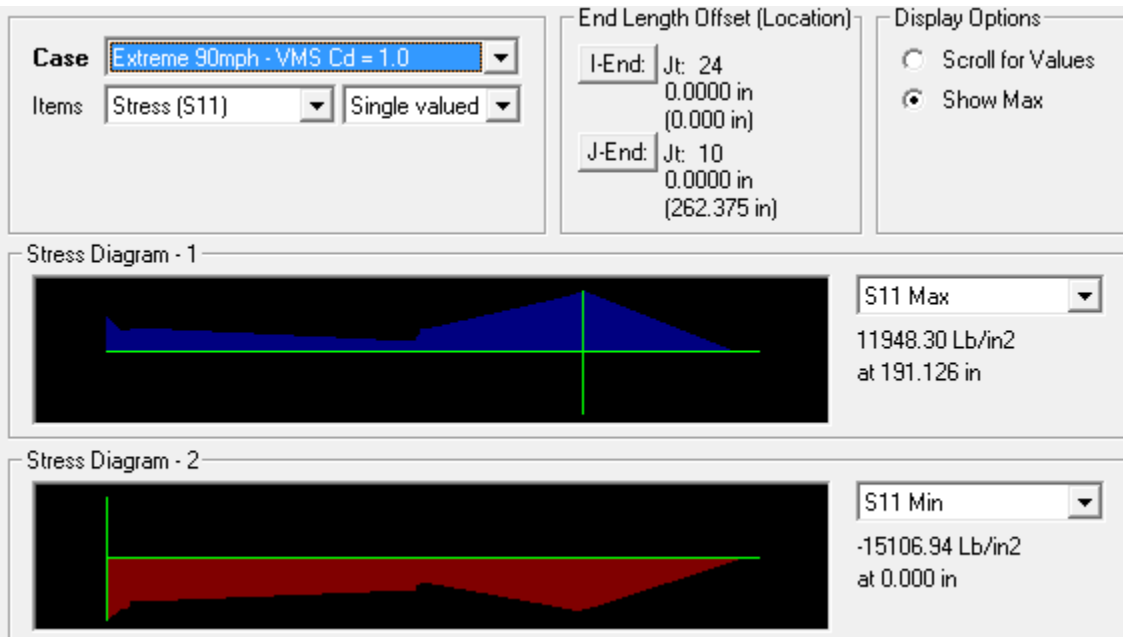
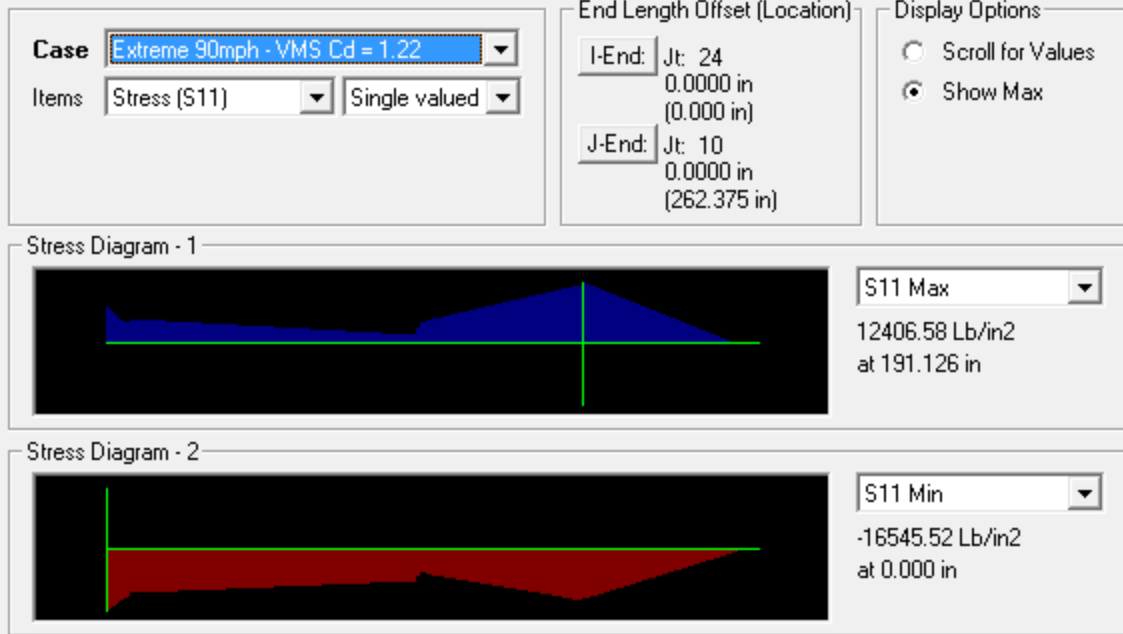


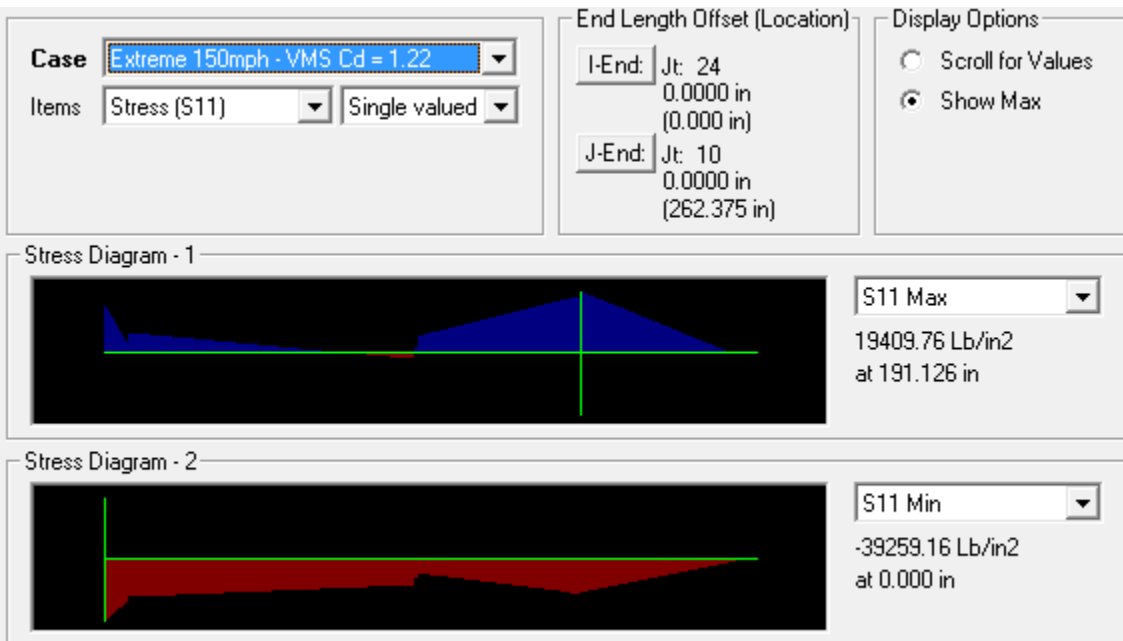
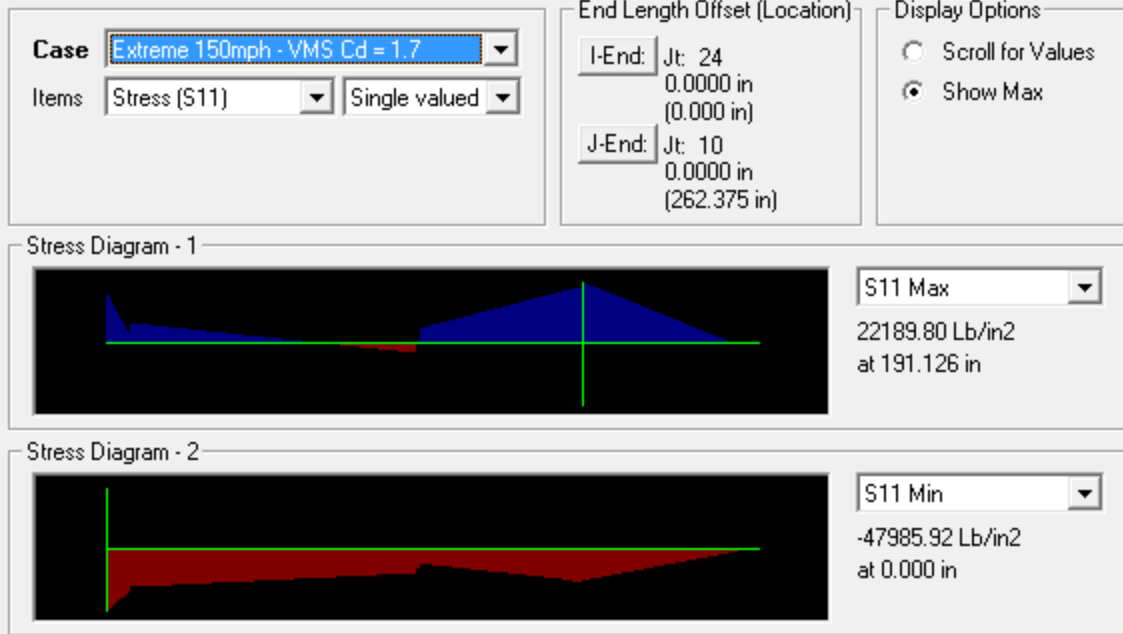
S11 Min
 -566.85 Lb/in2
 at 0.000 in



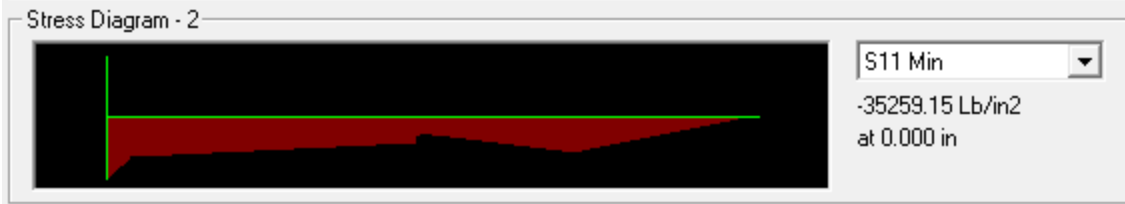
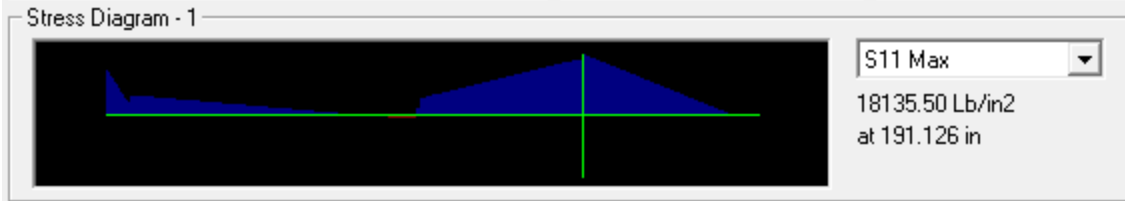
Upright 4



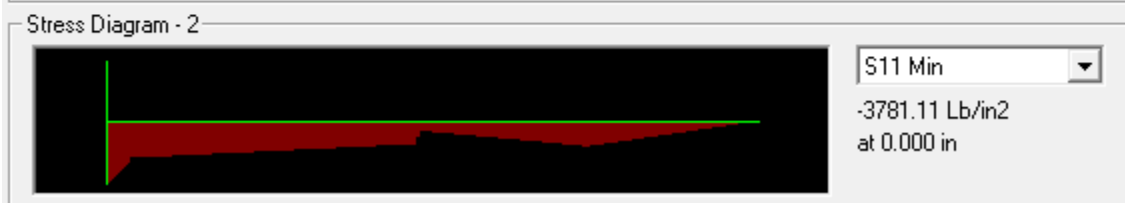
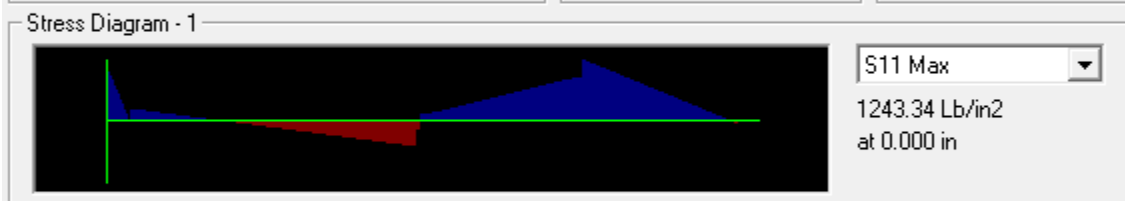




Case Extreme 150mph - VMS Cd = 1.0 Items Stress (S11) Single valued	End Length Offset (Location) I-End: Jt: 24 0.0000 in (0.000 in) J-End: Jt: 10 0.0000 in (262.375 in)	Display Options <input type="radio"/> Scroll for Values <input checked="" type="radio"/> Show Max
--	---	--



Case Fatigue - VMS Cd = 1.7 Items Stress (S11) Single valued	End Length Offset (Location) I-End: Jt: 24 0.0000 in (0.000 in) J-End: Jt: 10 0.0000 in (262.375 in)	Display Options <input checked="" type="radio"/> Scroll for Values <input type="radio"/> Show Max Location 0.000 in
---	---	---



Case: **Fatigue - VMS Cd = 1.22**

Items: Stress (S11) | Single valued

End Length Offset (Location):
 I-End: Jt: 24
 0.0000 in
 (0.000 in)
 J-End: Jt: 10
 0.0000 in
 (262.375 in)

Display Options:
 Scroll for Values
 Show Max

Location:
 0.000 in

Stress Diagram - 1

S11 Max
 999.60 Lb/in²
 at 0.000 in

Stress Diagram - 2

S11 Min
 -3036.51 Lb/in²
 at 0.000 in

Case: **Fatigue - VMS Cd = 1.0**

Items: Stress (S11) | Single valued

End Length Offset (Location):
 I-End: Jt: 24
 0.0000 in
 (0.000 in)
 J-End: Jt: 10
 0.0000 in
 (262.375 in)

Display Options:
 Scroll for Values
 Show Max

Location:
 0.000 in

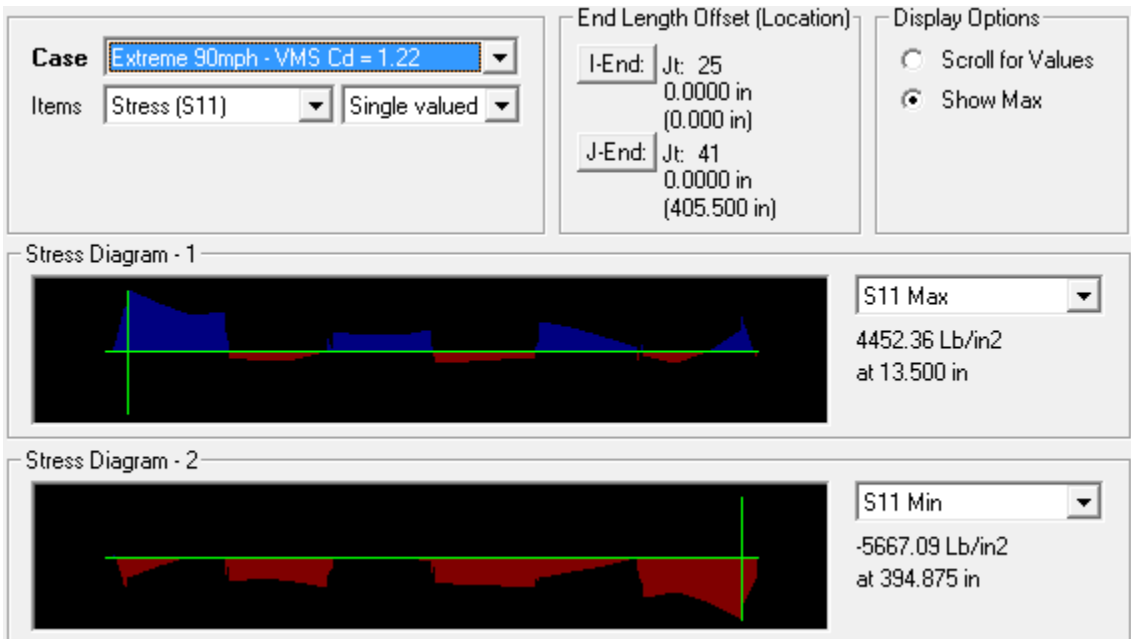
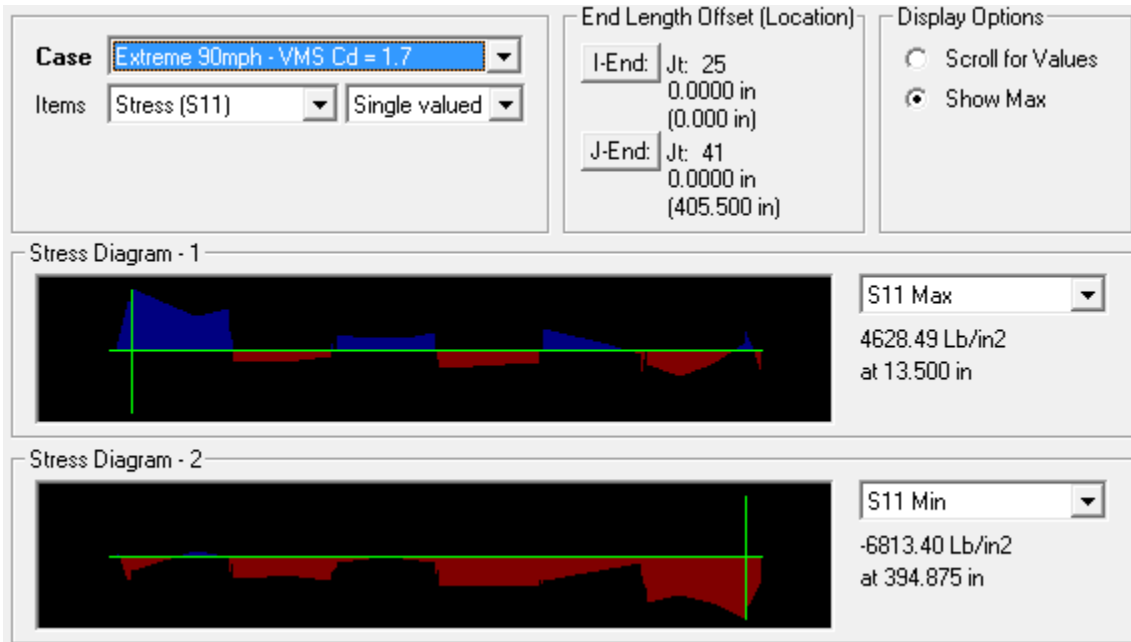
Stress Diagram - 1

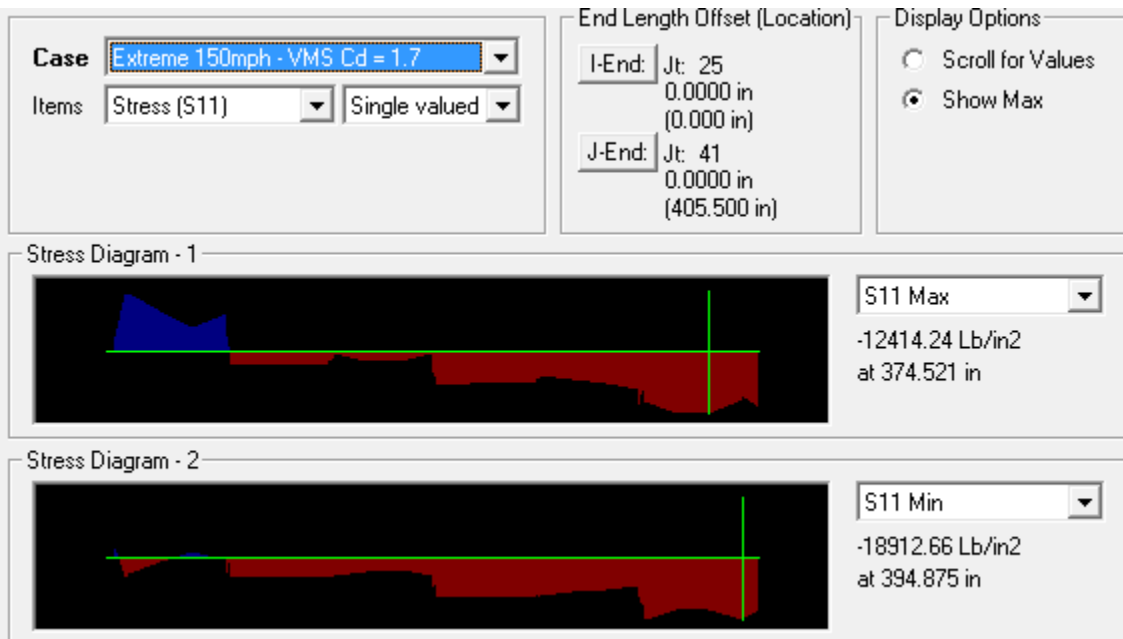
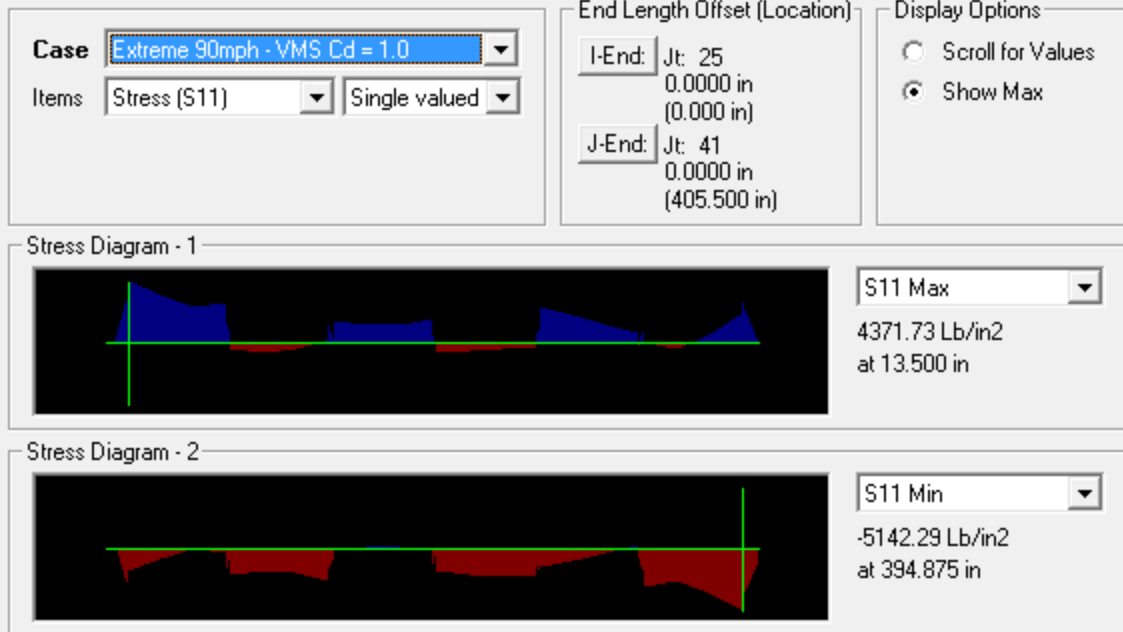
S11 Max
 888.46 Lb/in²
 at 0.000 in

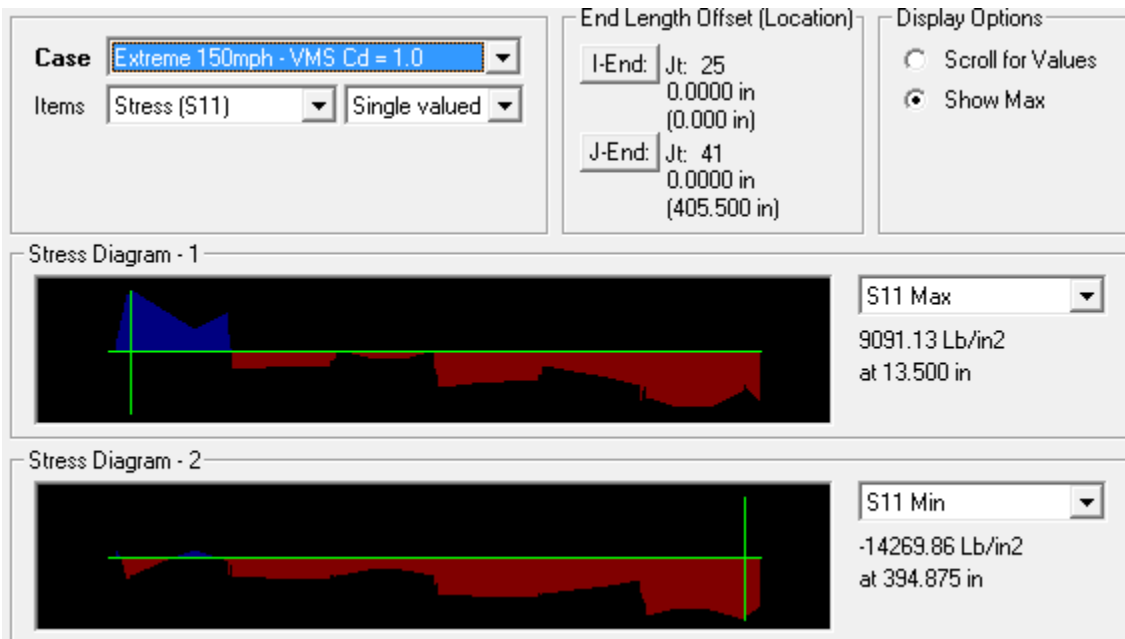
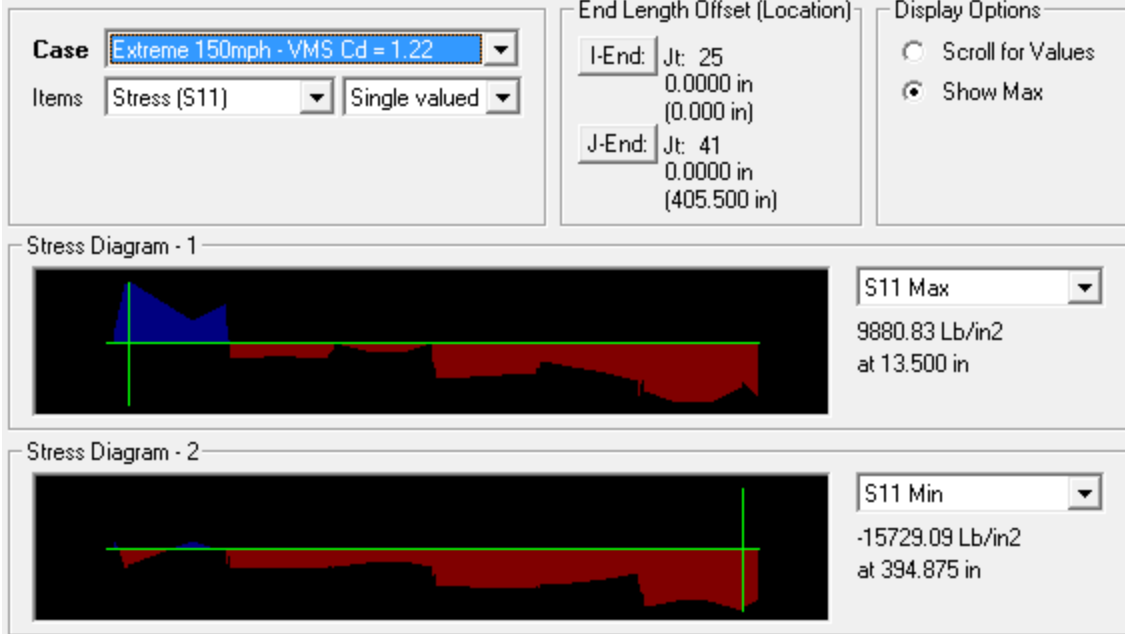
Stress Diagram - 2

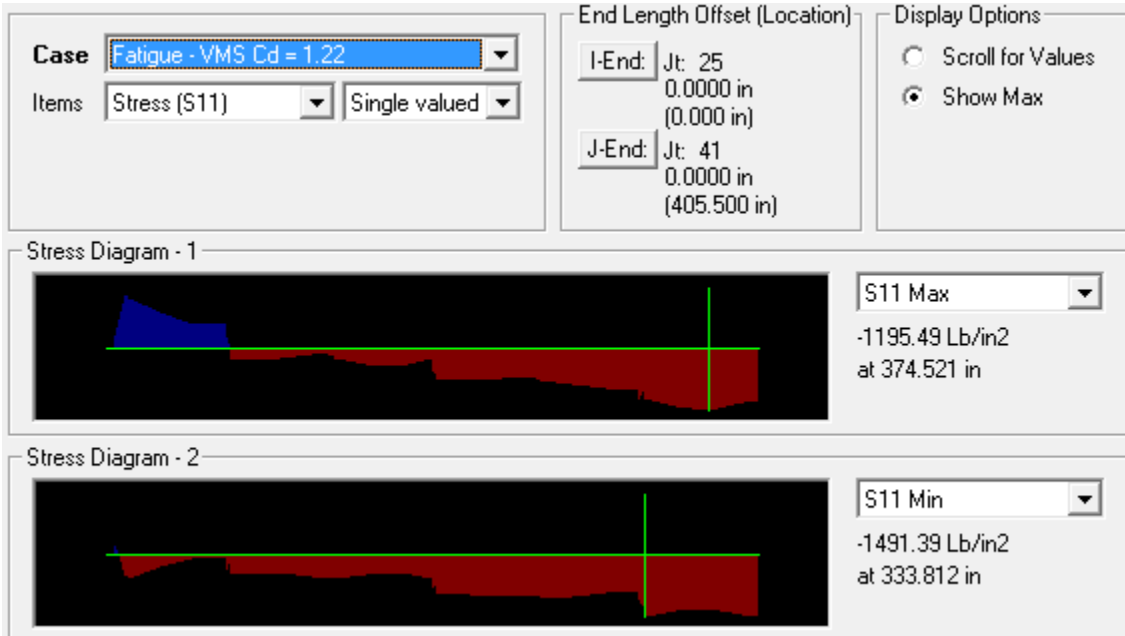
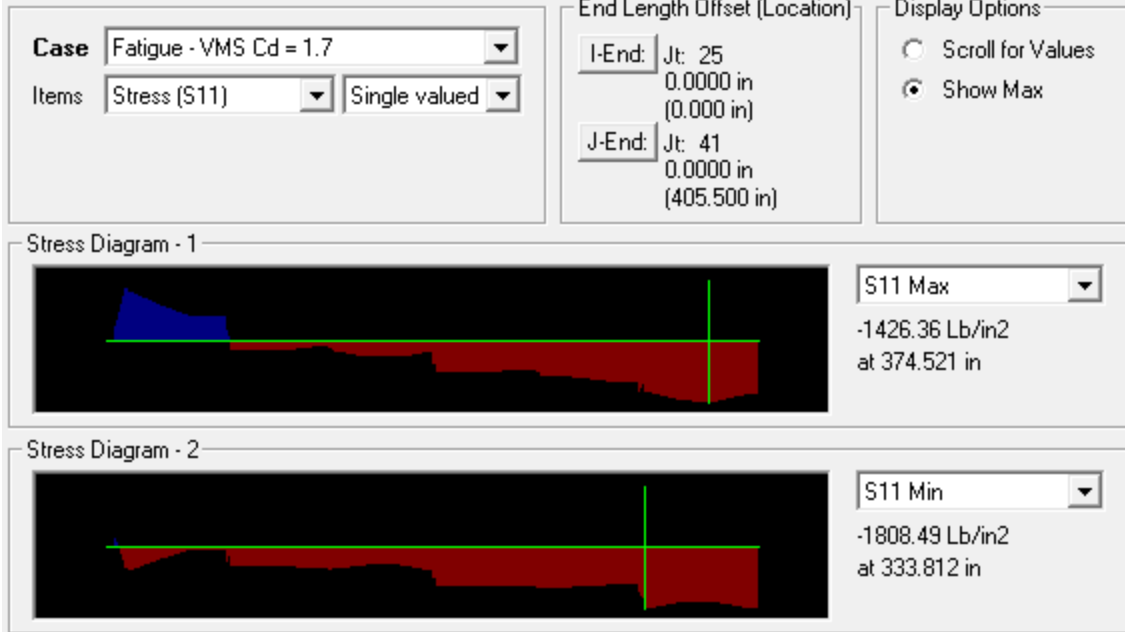
S11 Min
 -2696.97 Lb/in²
 at 0.000 in

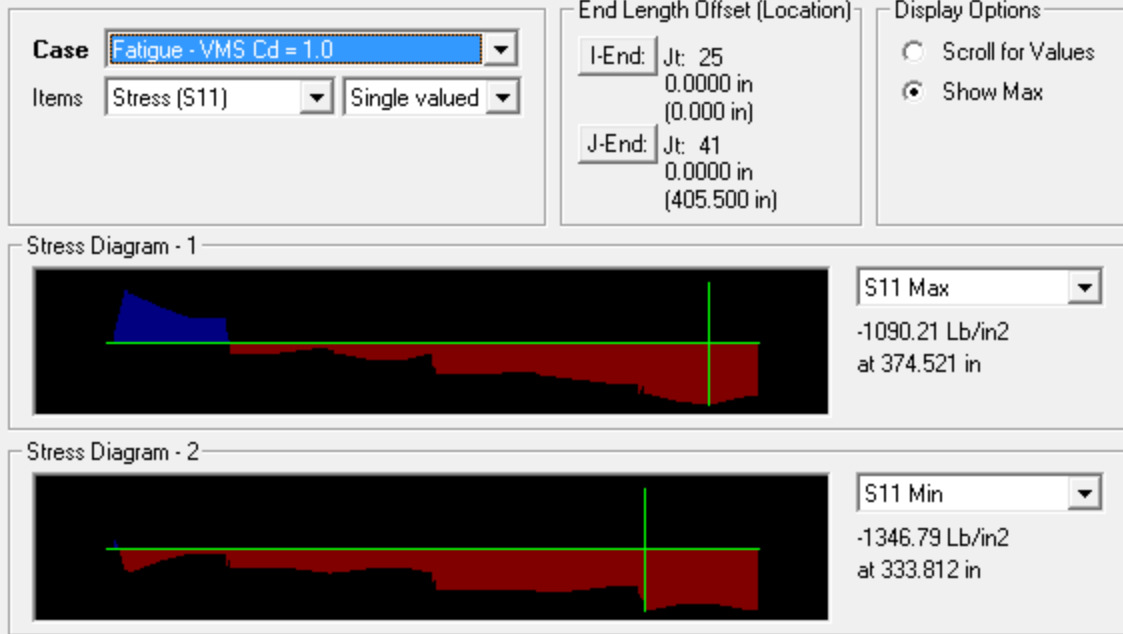
Chord 1a



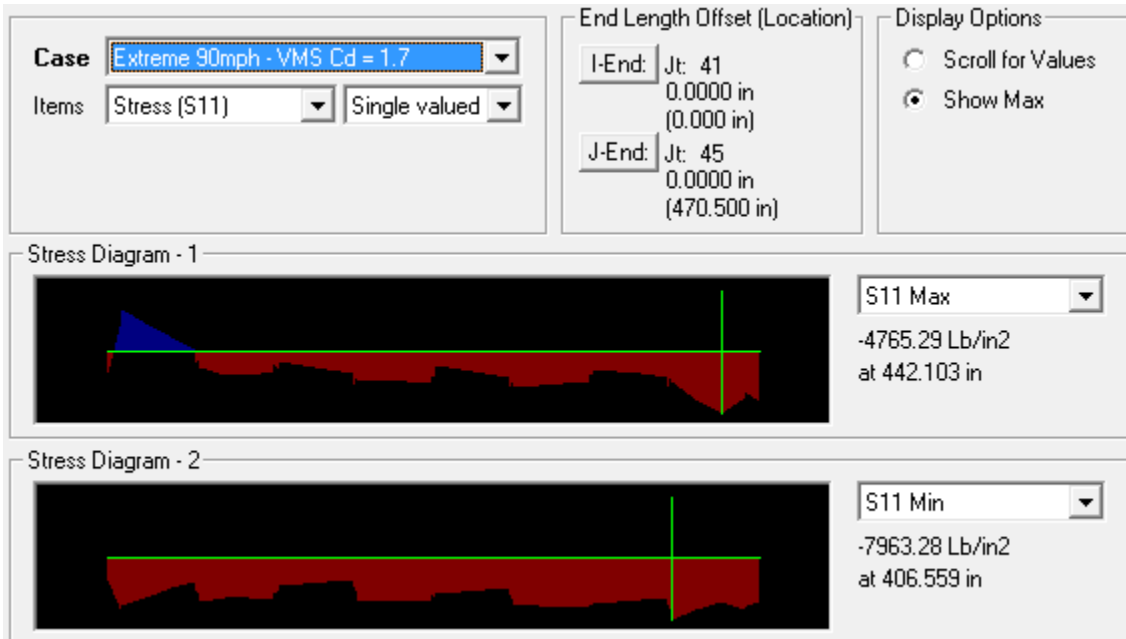


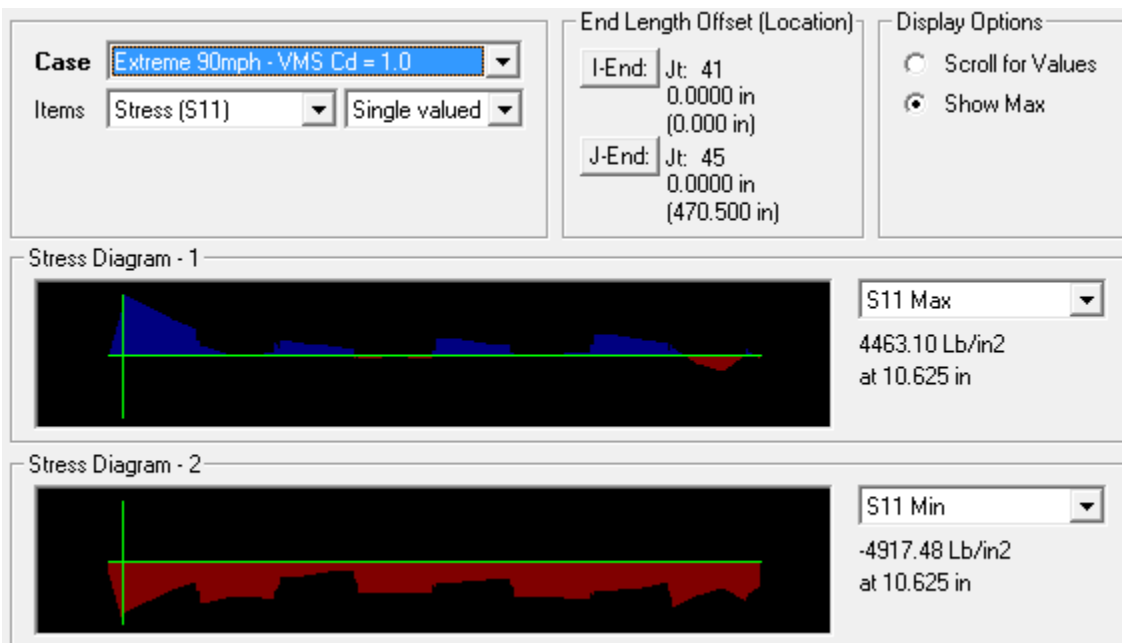
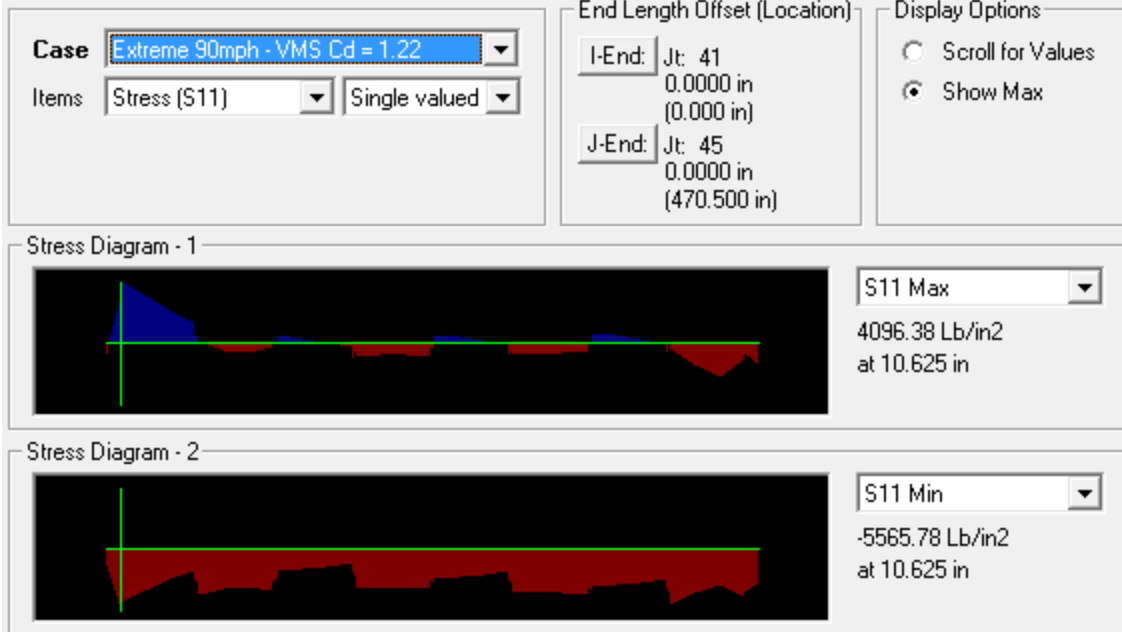


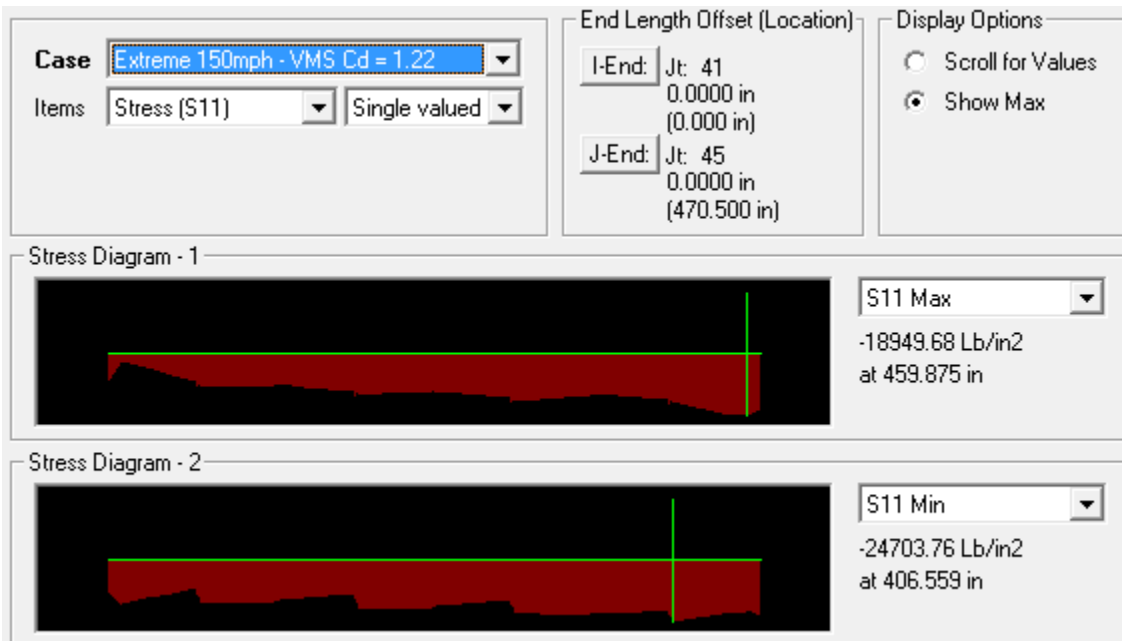
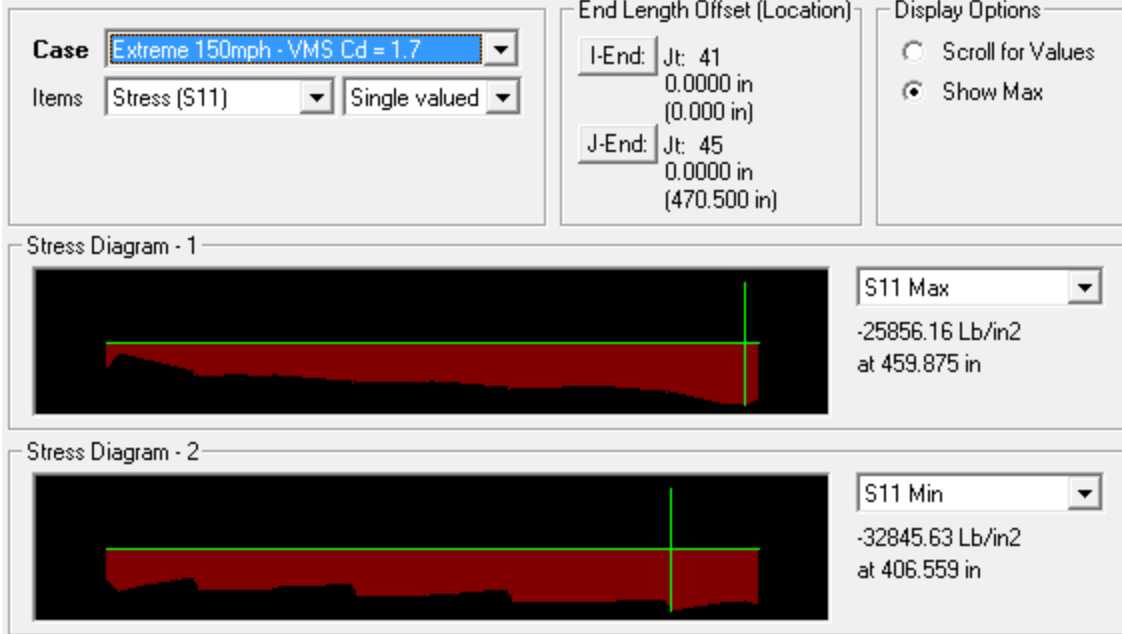






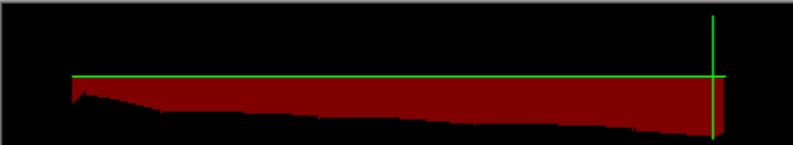
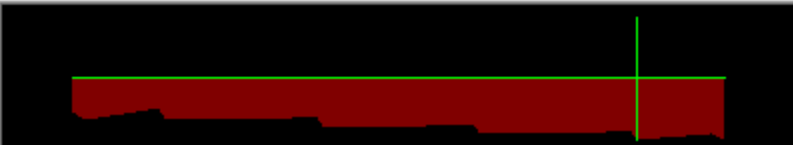
Chord 1b

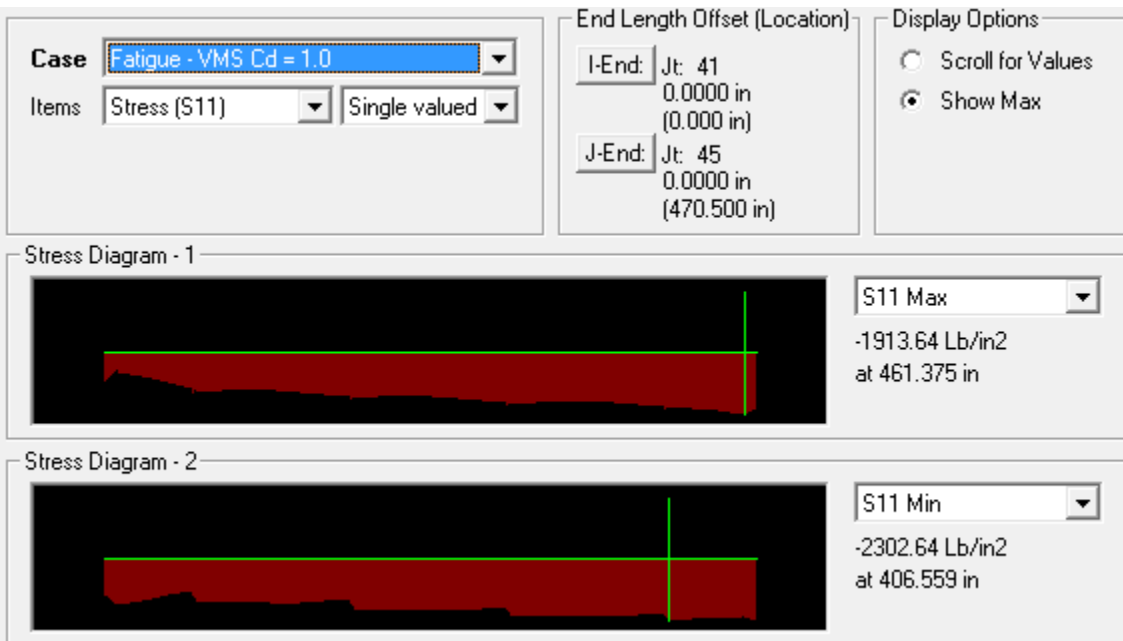
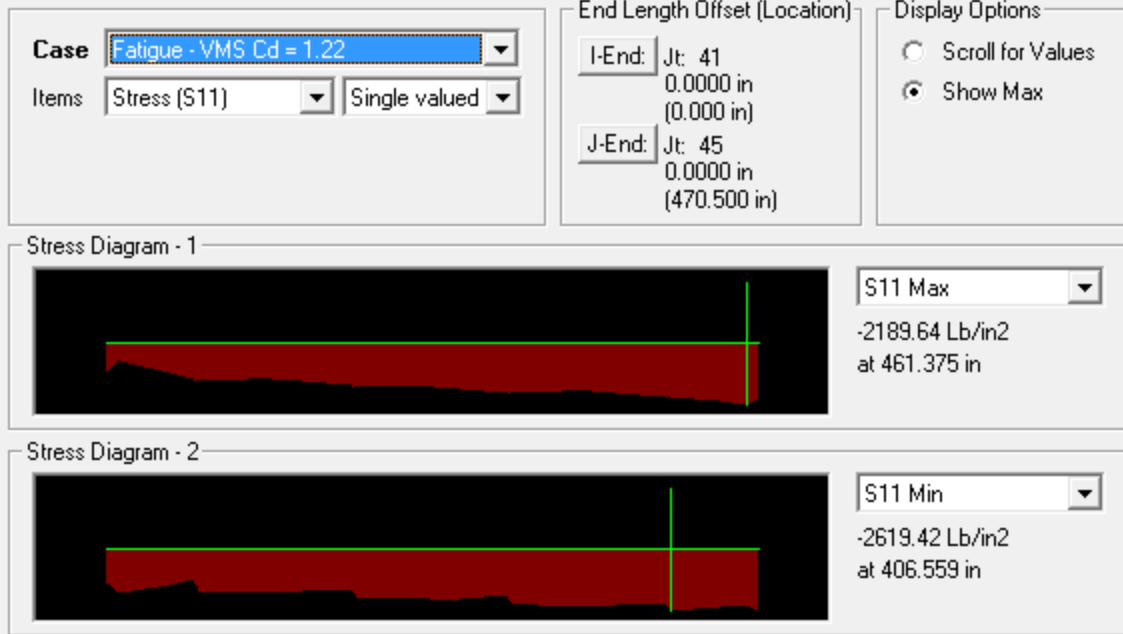




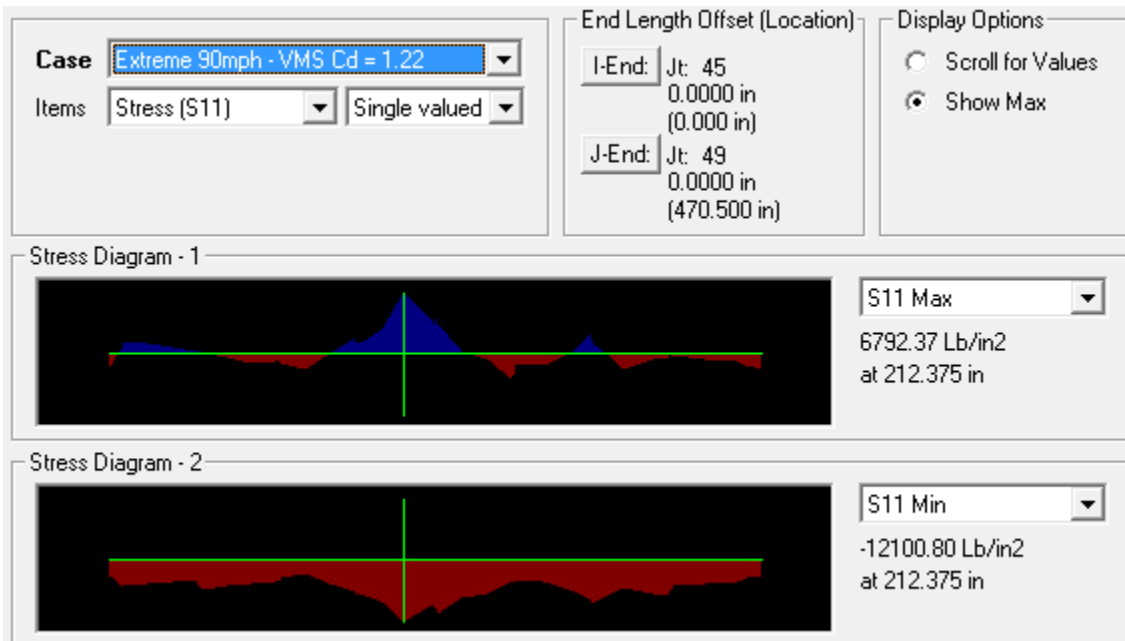
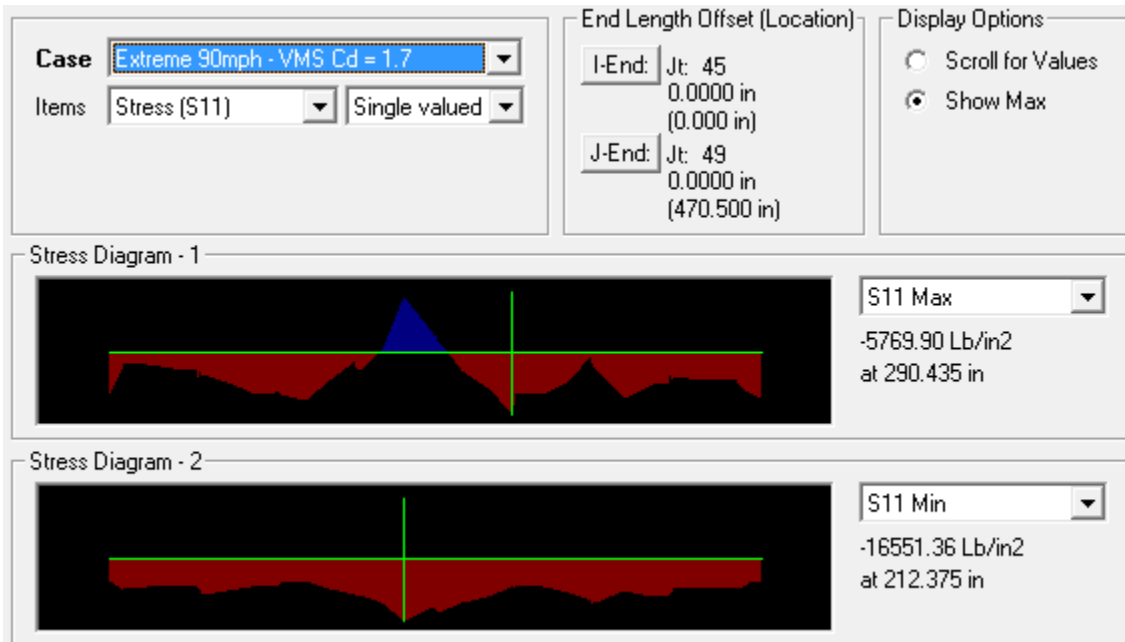


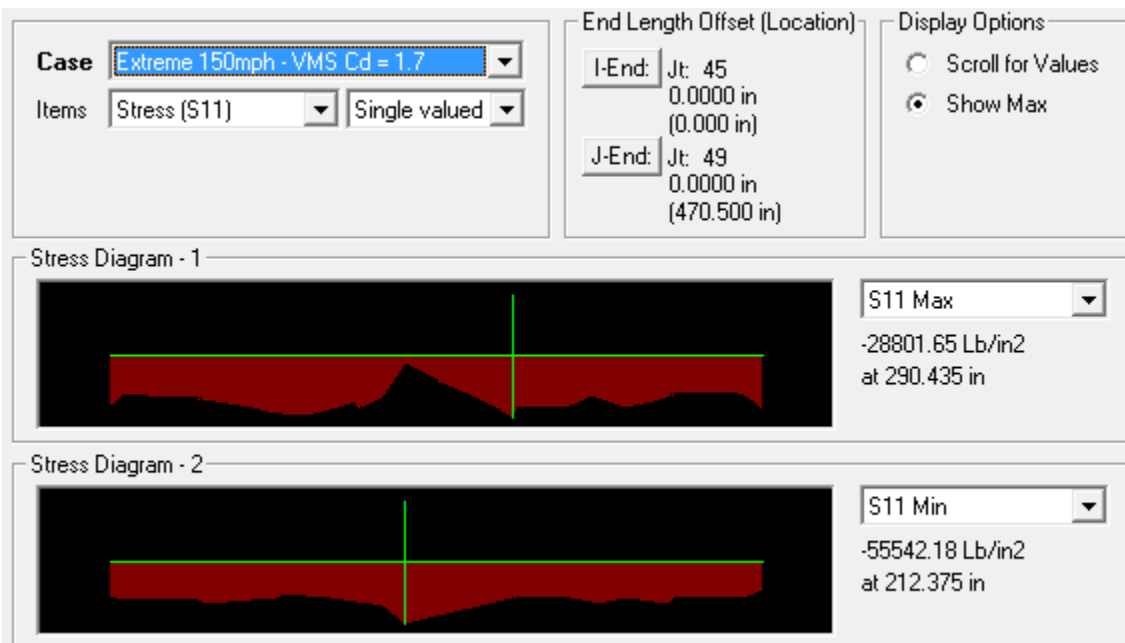
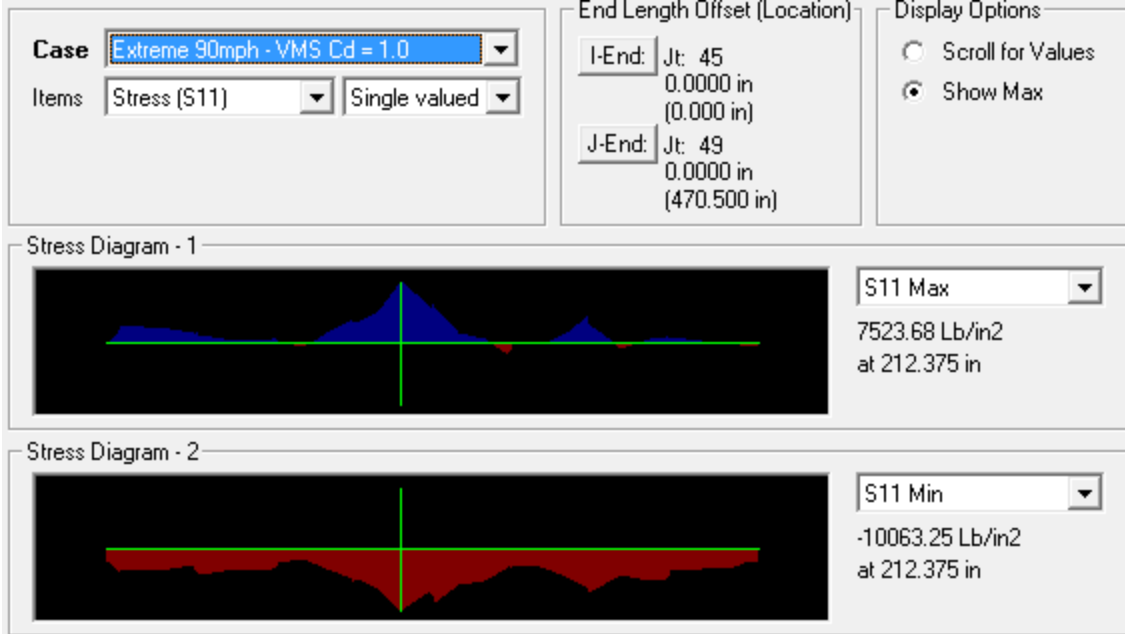
Case Extreme 150mph - VMS Cd = 1.0 Items Stress (S11) Single valued	End Length Offset (Location) I-End: Jt: 41 0.0000 in (0.000 in) J-End: Jt: 45 0.0000 in (470.500 in)	Display Options <input type="radio"/> Scroll for Values <input checked="" type="radio"/> Show Max	
Stress Diagram - 1 			S11 Max -15784.01 Lb/in2 at 459.875 in
Stress Diagram - 2 			S11 Min -20971.84 Lb/in2 at 406.559 in

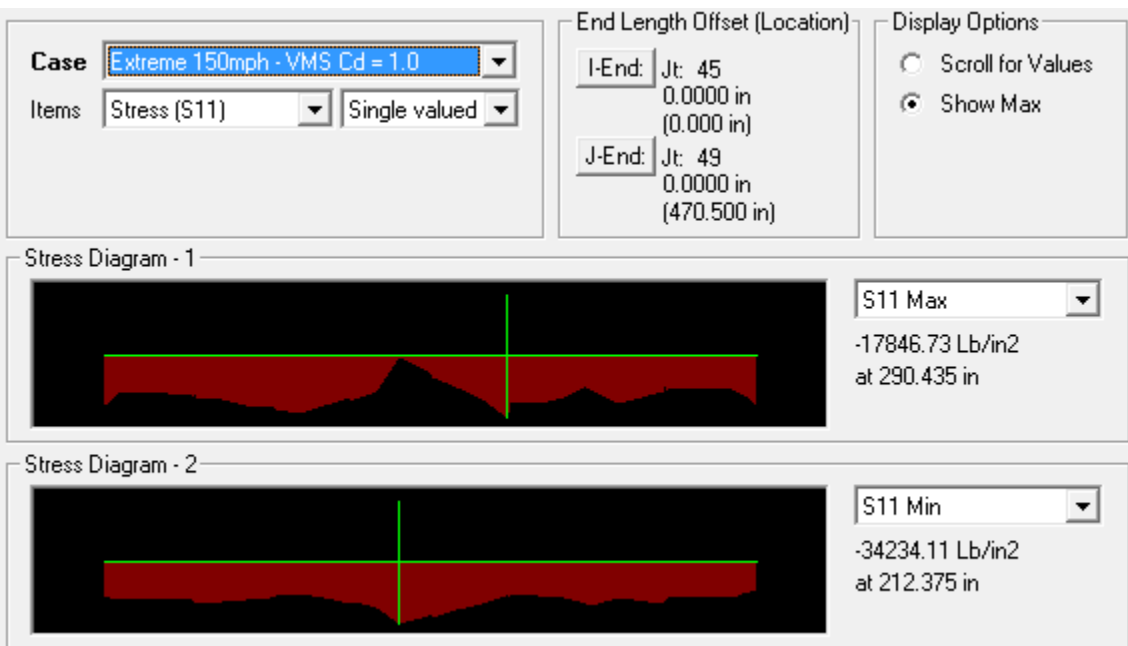
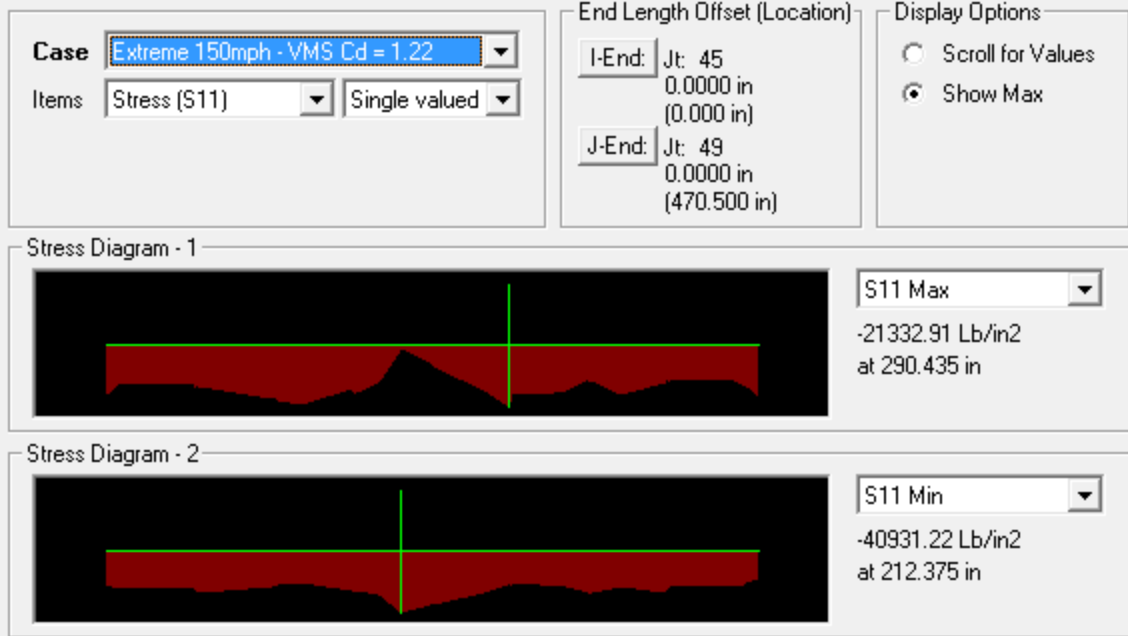
Case Fatigue - VMS Cd = 1.7 Items Stress (S11) Single valued	End Length Offset (Location) I-End: Jt: 41 0.0000 in (0.000 in) J-End: Jt: 45 0.0000 in (470.500 in)	Display Options <input type="radio"/> Scroll for Values <input checked="" type="radio"/> Show Max	
Stress Diagram - 1 			S11 Max -2794.91 Lb/in2 at 461.375 in
Stress Diagram - 2 			S11 Min -3314.12 Lb/in2 at 406.559 in



Chord 1c







Case Fatigue - VMS Cd = 1.7

Items Stress (S11) Single valued

End Length Offset (Location)

I-End: Jt: 45
0.0000 in
(0.000 in)

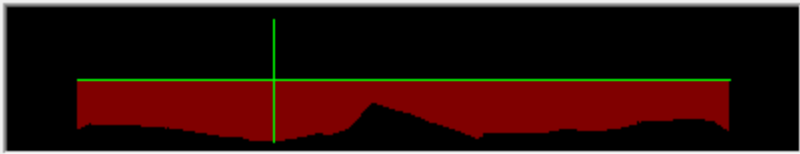
J-End: Jt: 49
0.0000 in
(470.500 in)

Display Options

Scroll for Values

Show Max

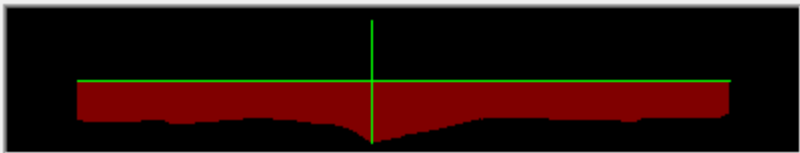
Stress Diagram - 1



S11 Max

-3098.55 Lb/in²
at 141.603 in

Stress Diagram - 2



S11 Min

-5342.51 Lb/in²
at 212.375 in

Case Fatigue - VMS Cd = 1.22

Items Stress (S11) Single valued

End Length Offset (Location)

I-End: Jt: 45
0.0000 in
(0.000 in)

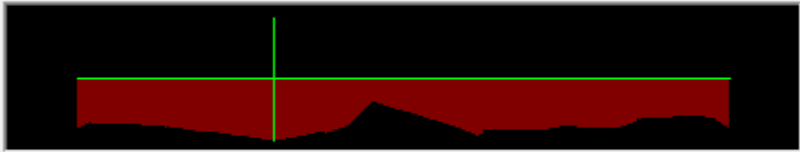
J-End: Jt: 49
0.0000 in
(470.500 in)

Display Options

Scroll for Values

Show Max

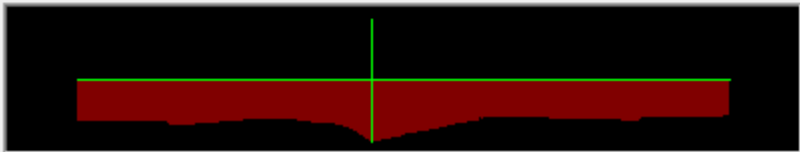
Stress Diagram - 1



S11 Max

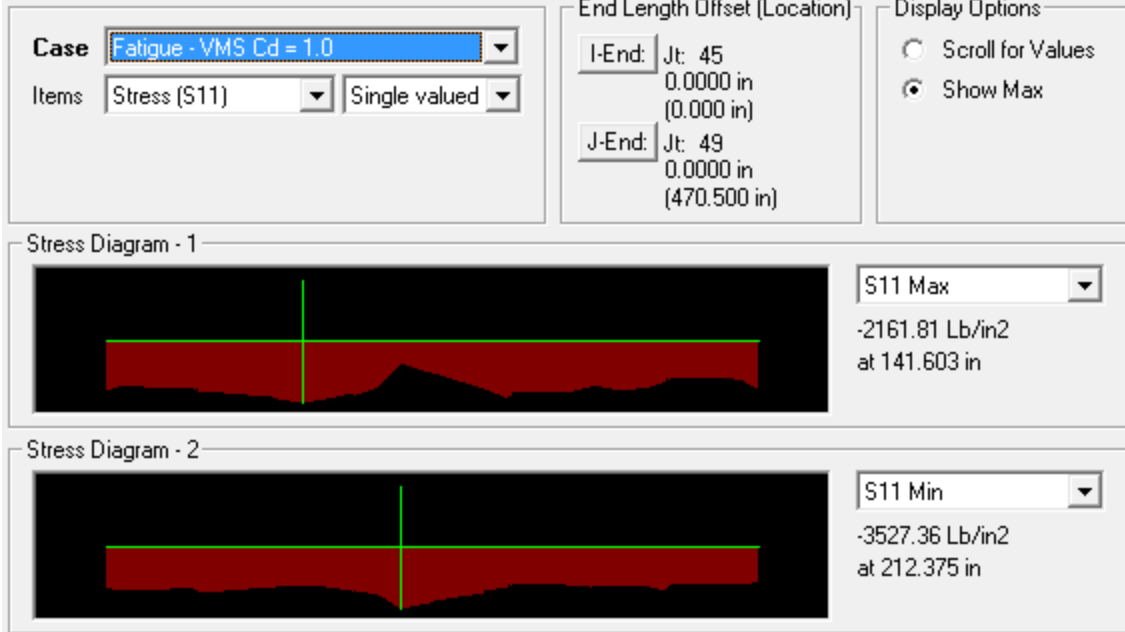
-2463.52 Lb/in²
at 141.603 in

Stress Diagram - 2

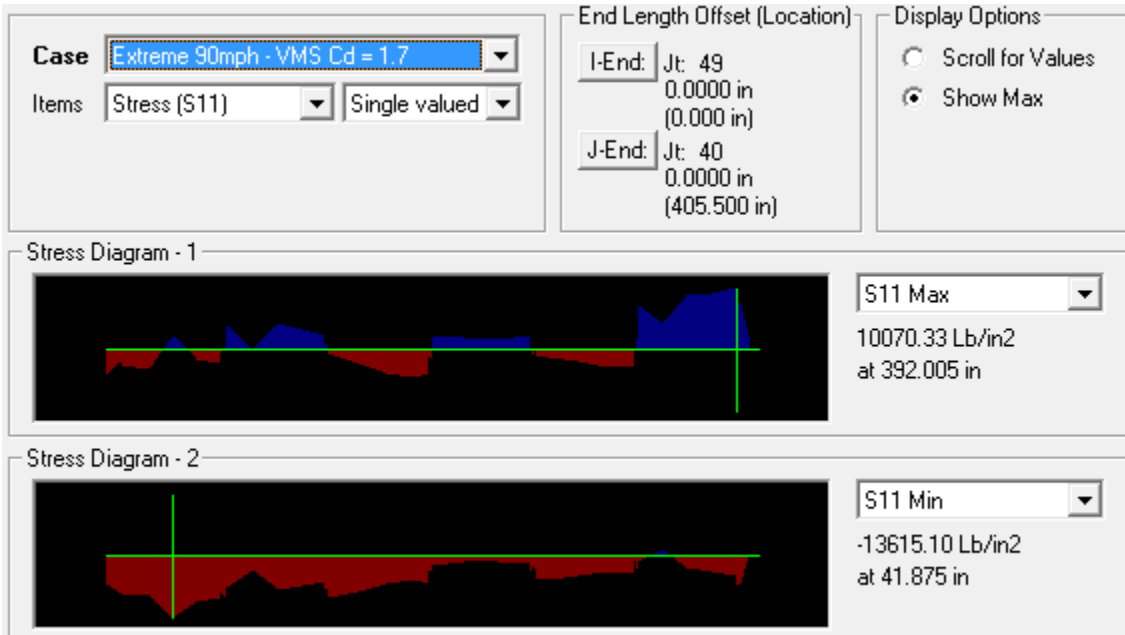


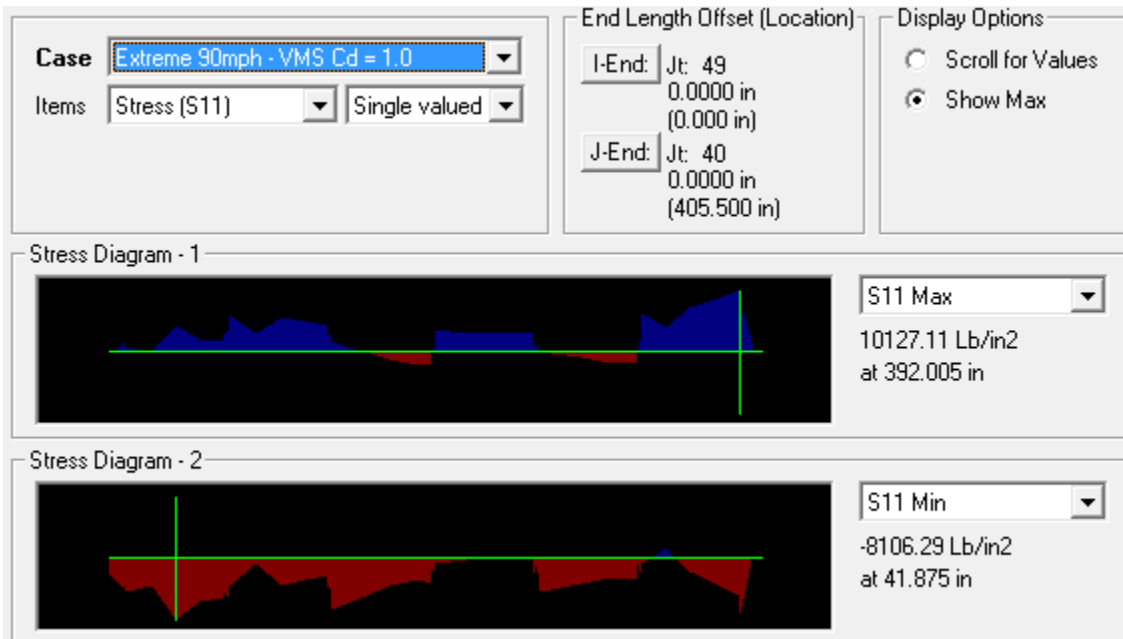
S11 Min

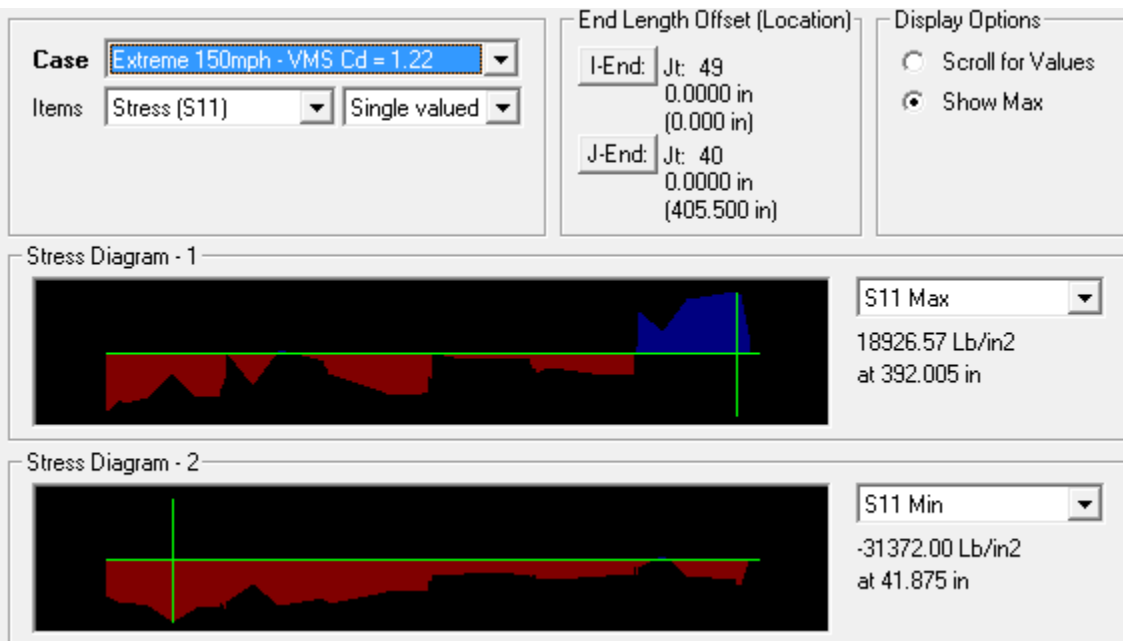
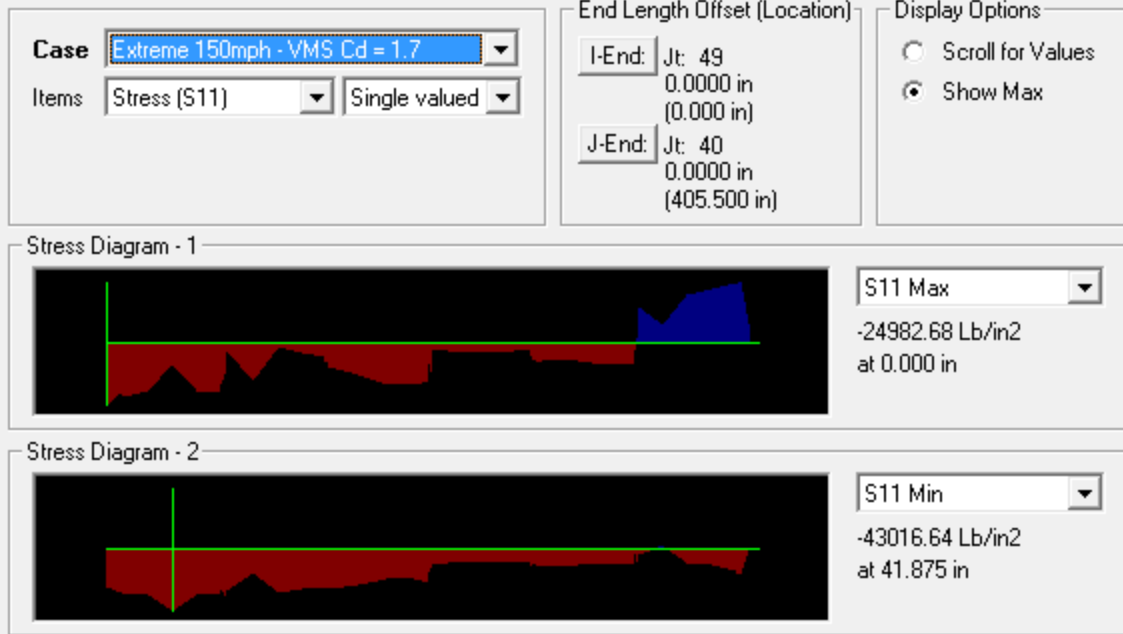
-4095.84 Lb/in²
at 212.375 in

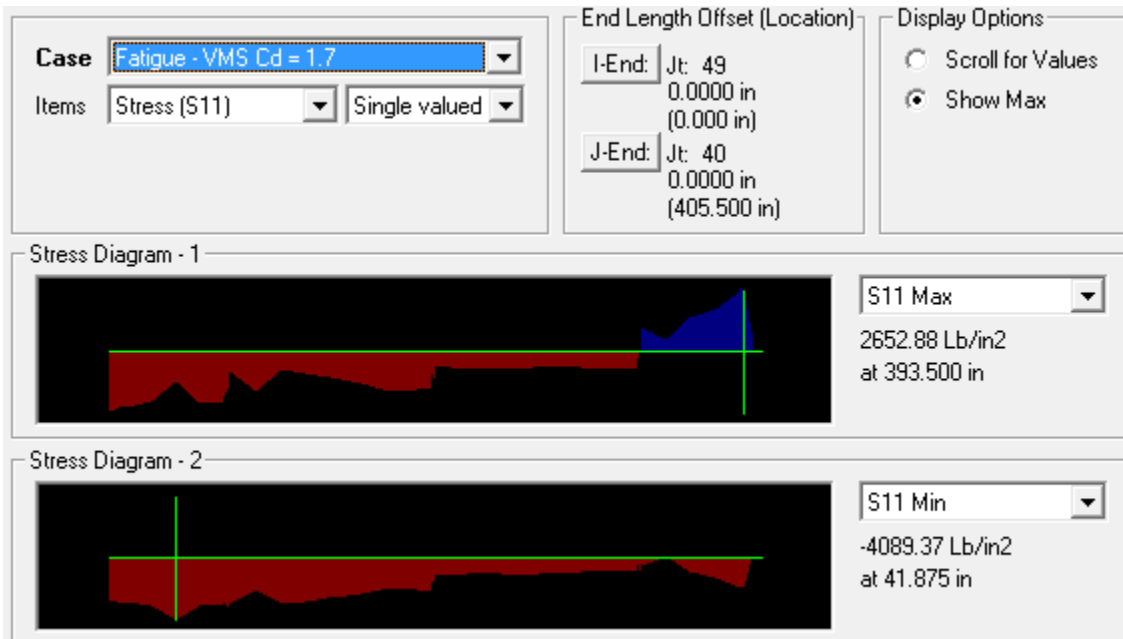
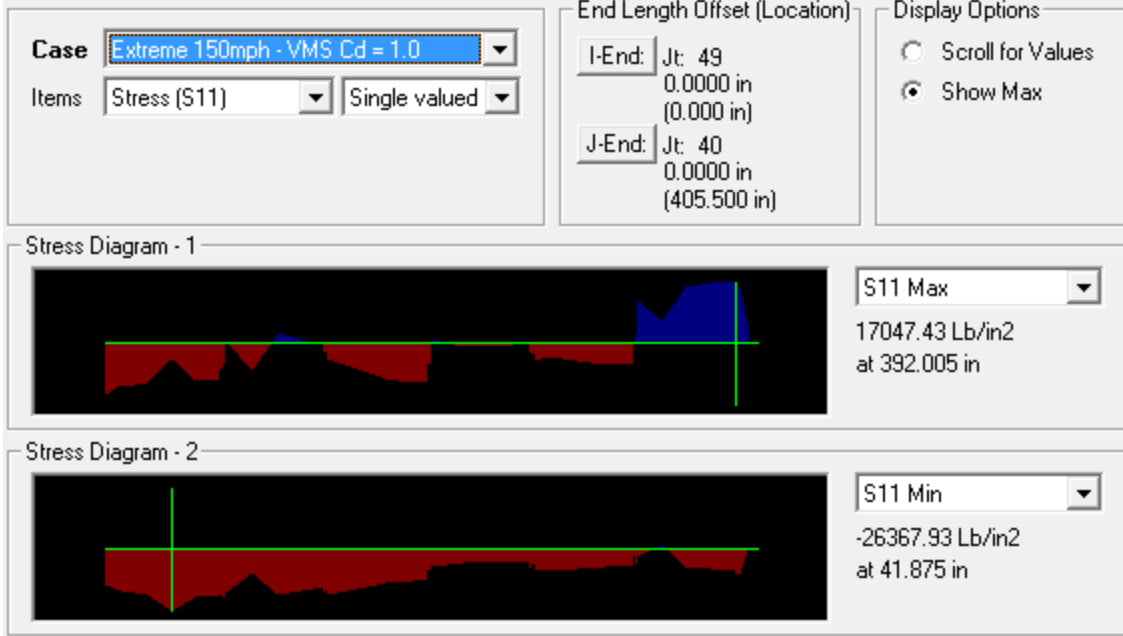


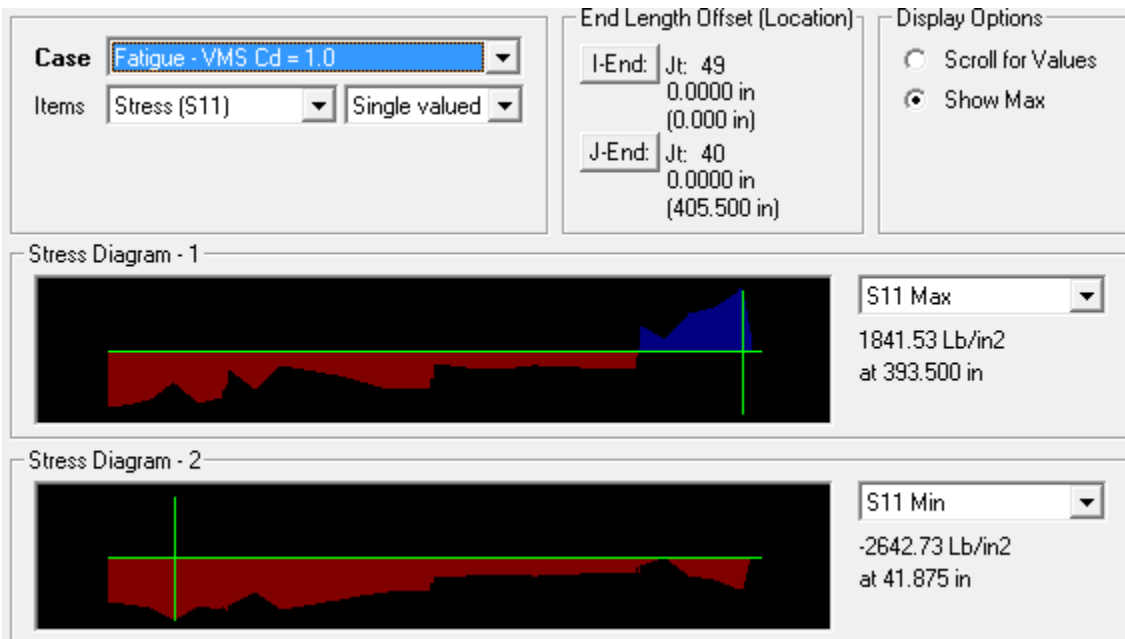
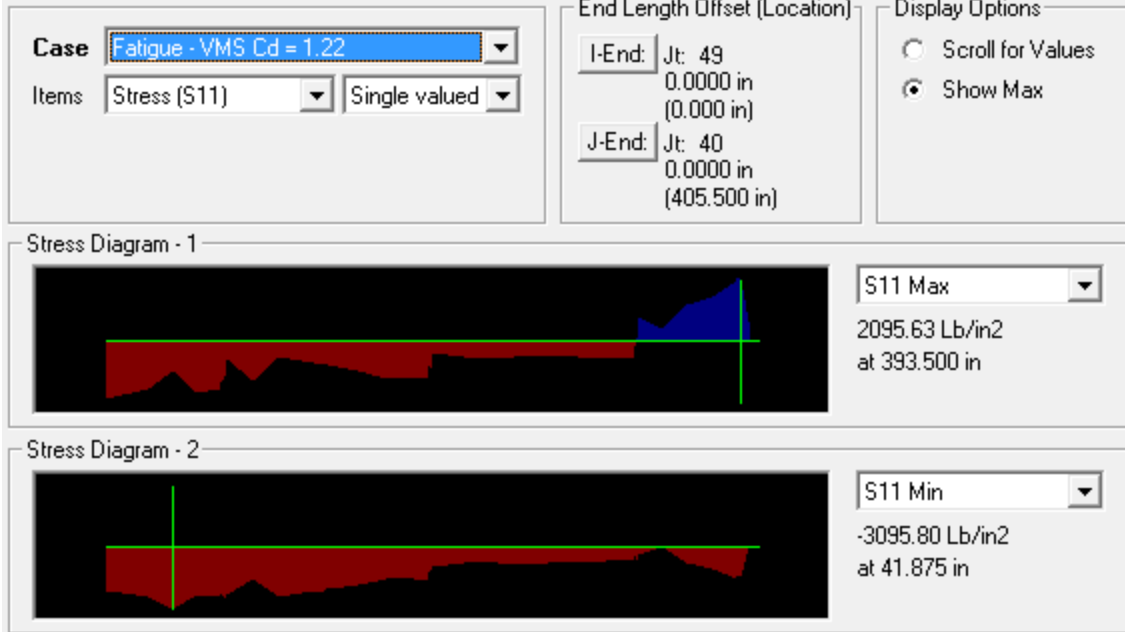
Chord 1d



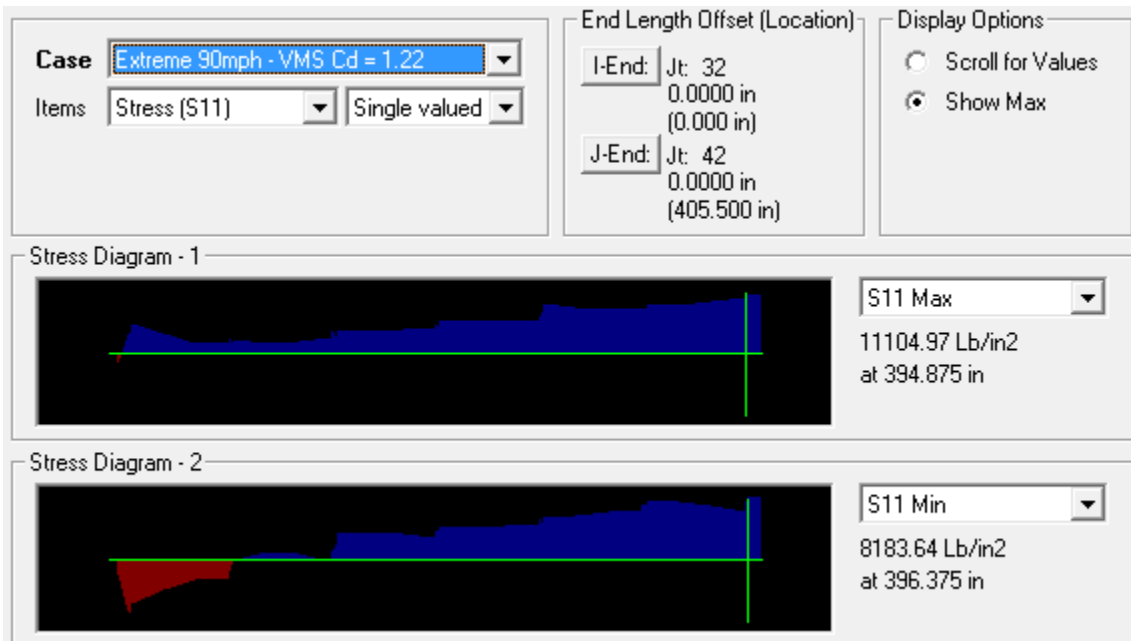
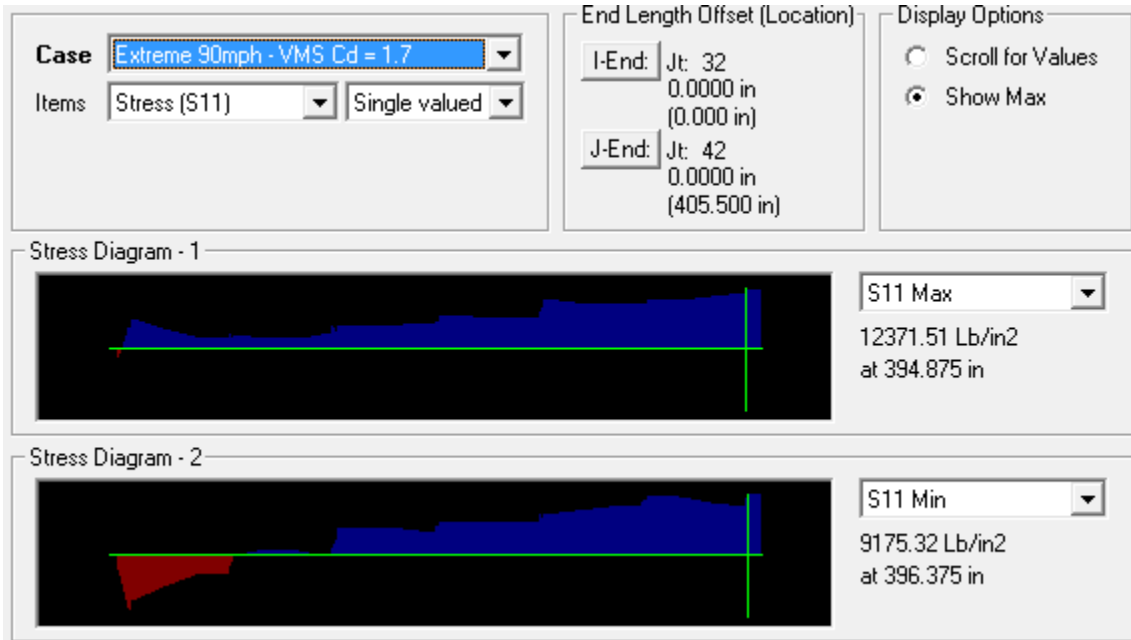


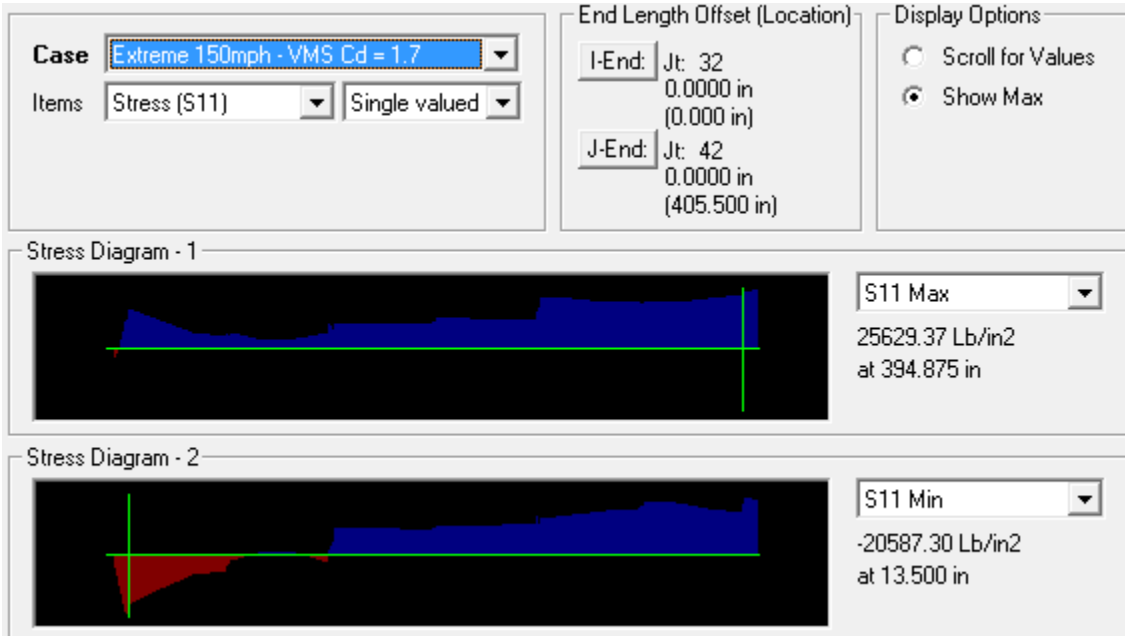
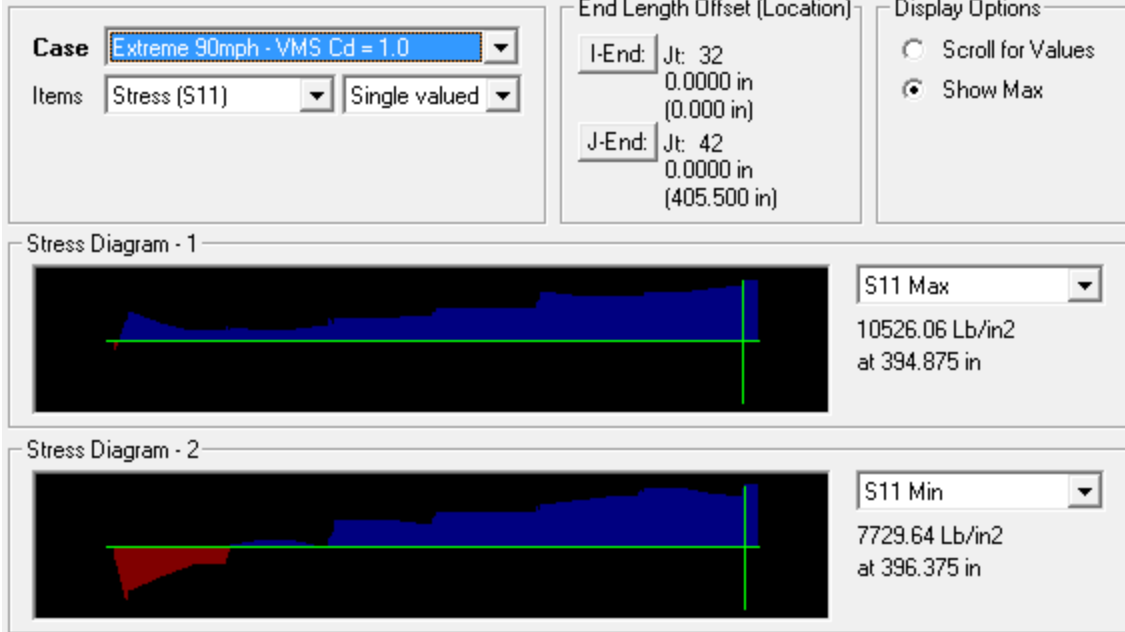


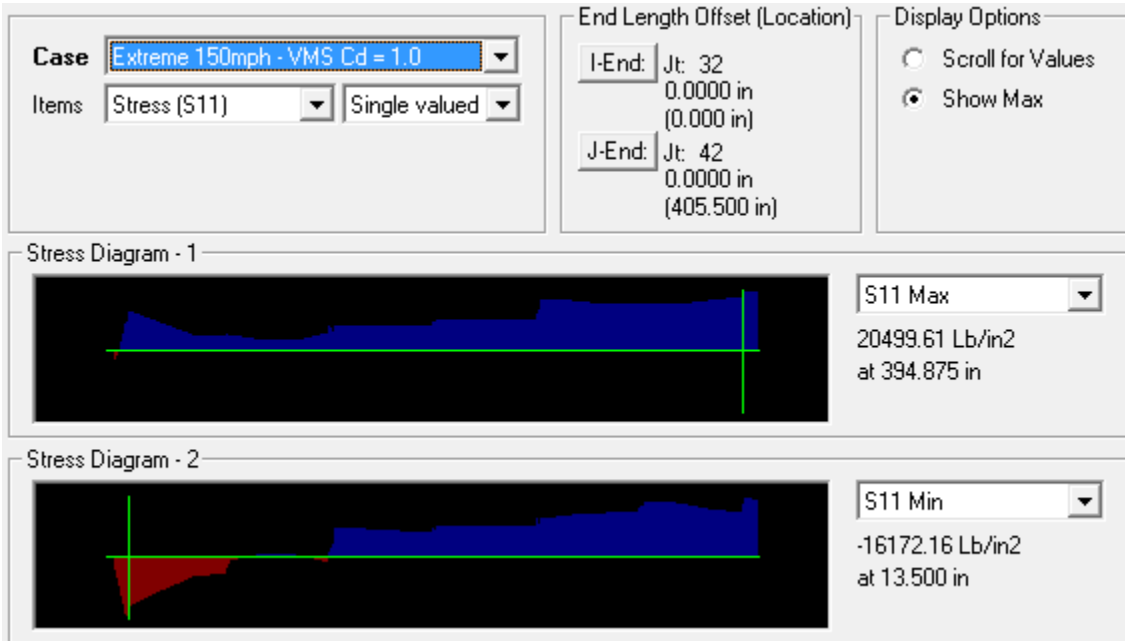
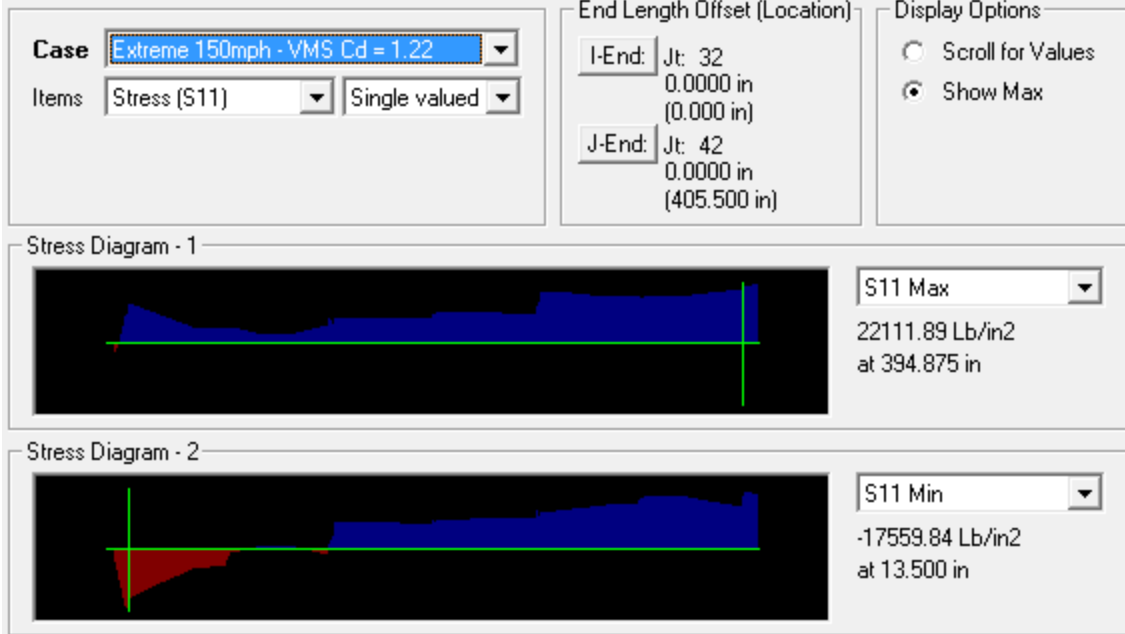


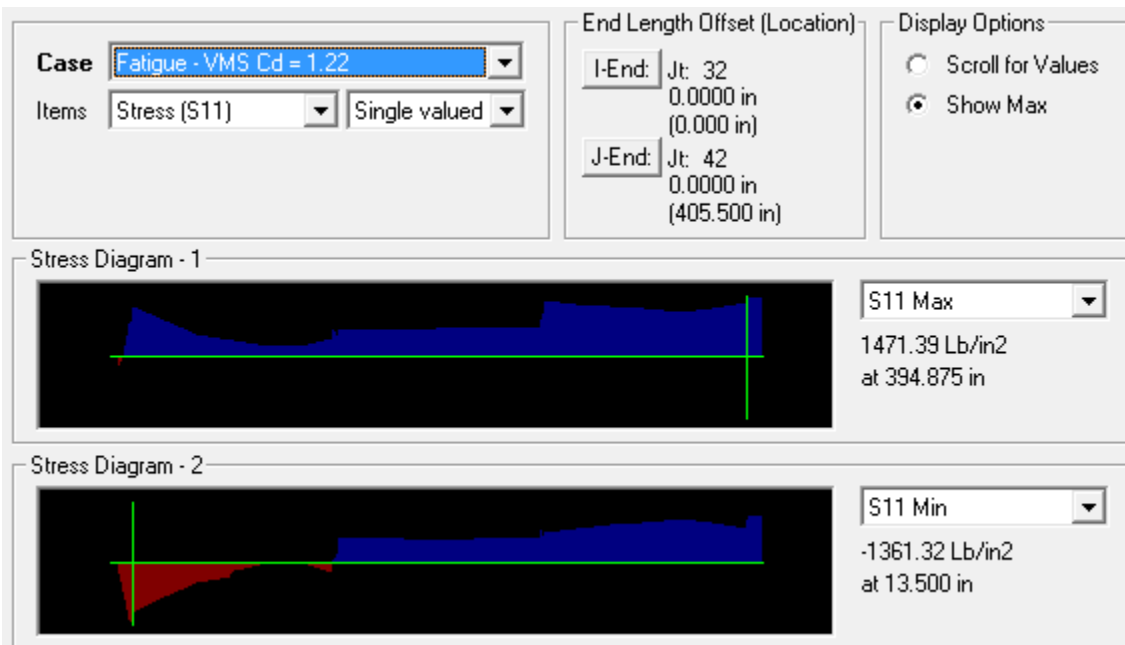
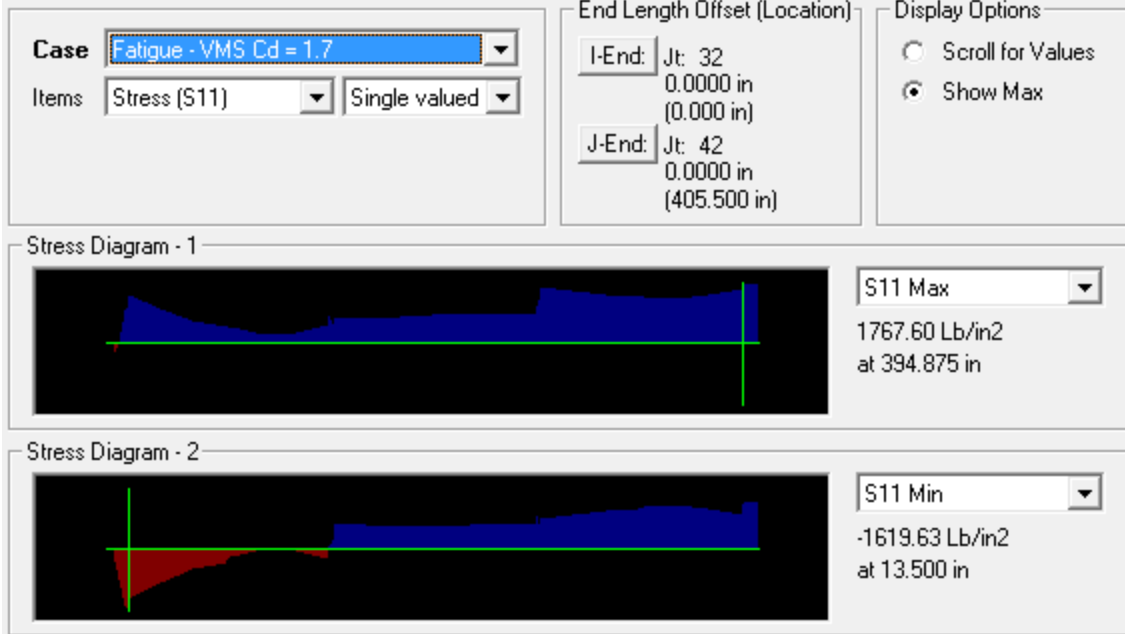


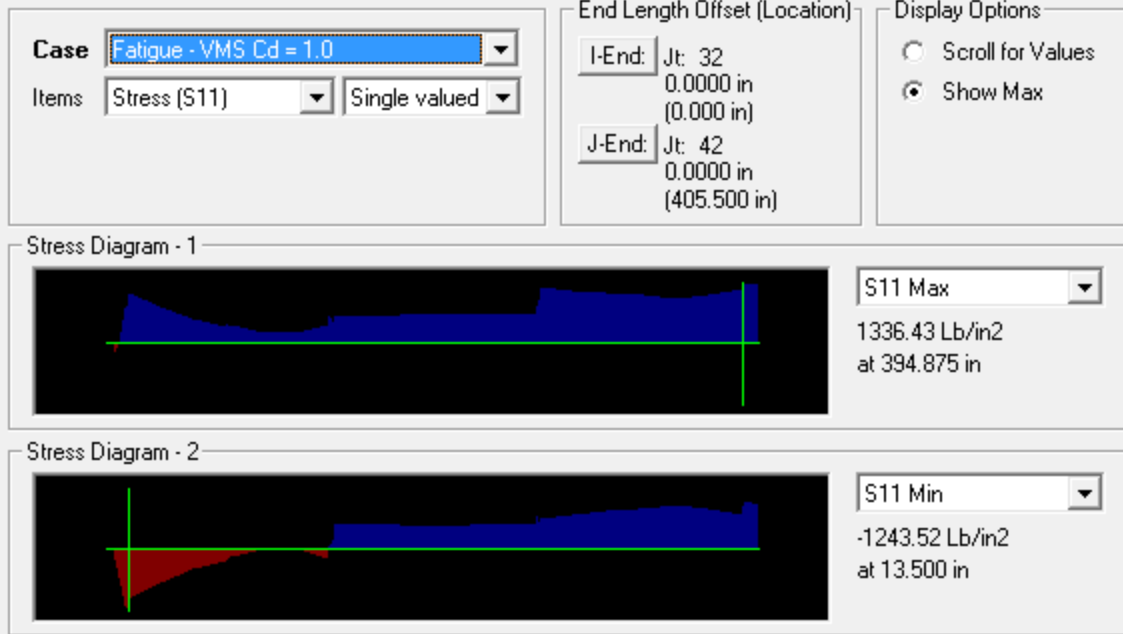
Chord 2a



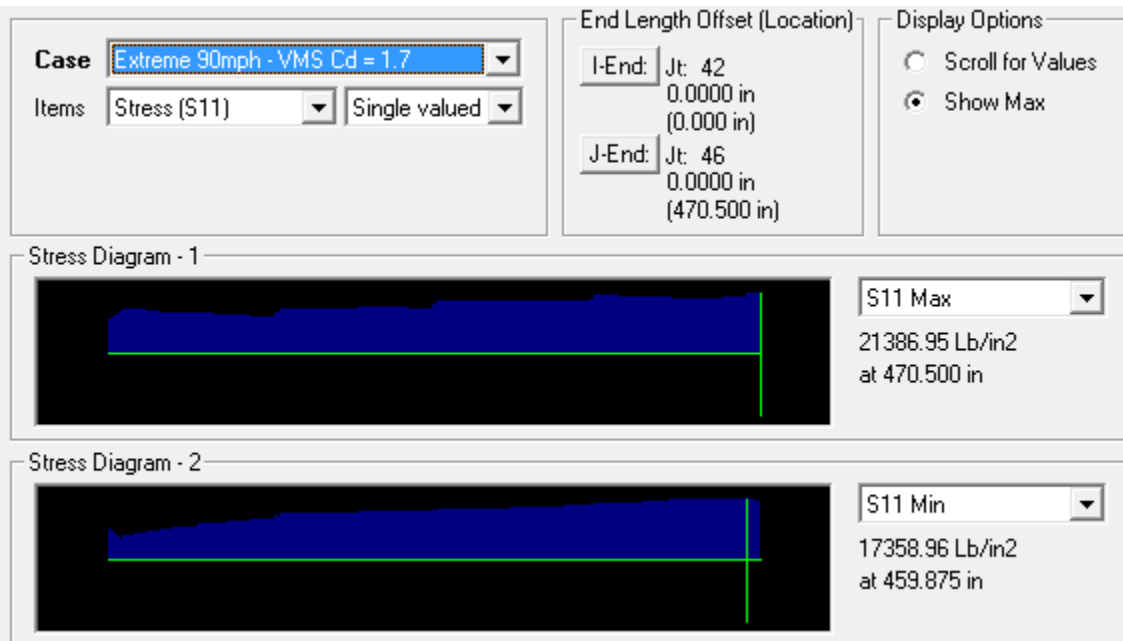




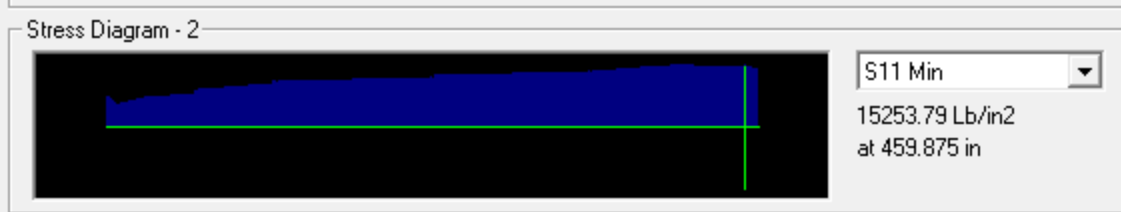
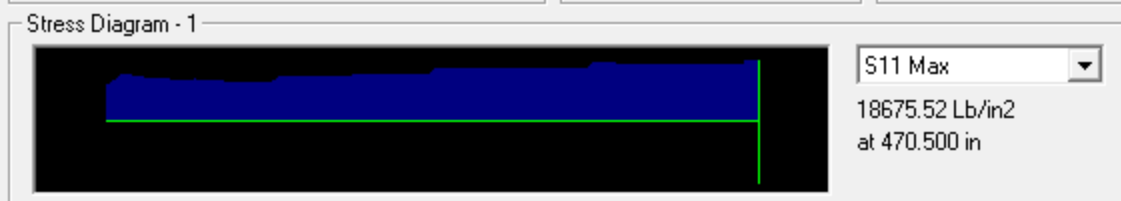




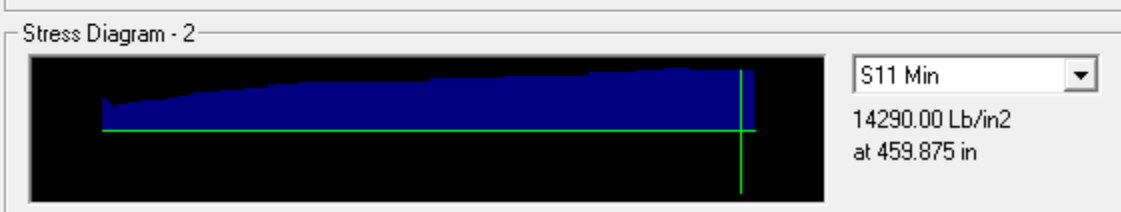
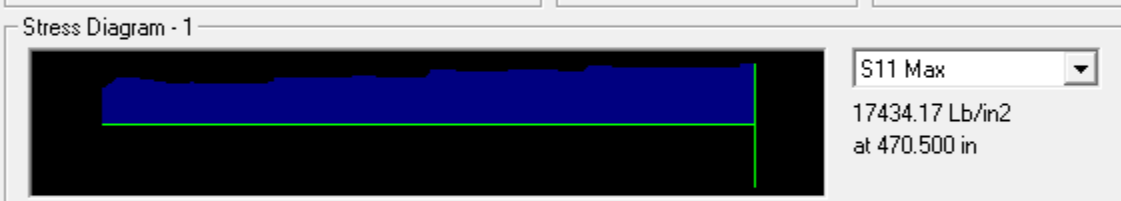
Chord 2b

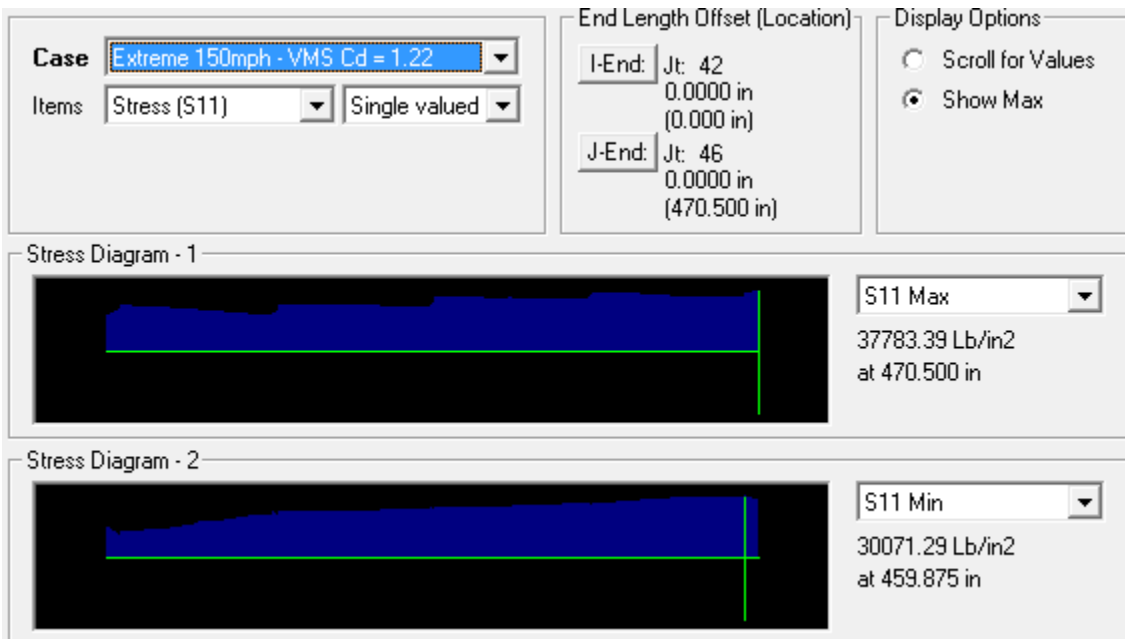
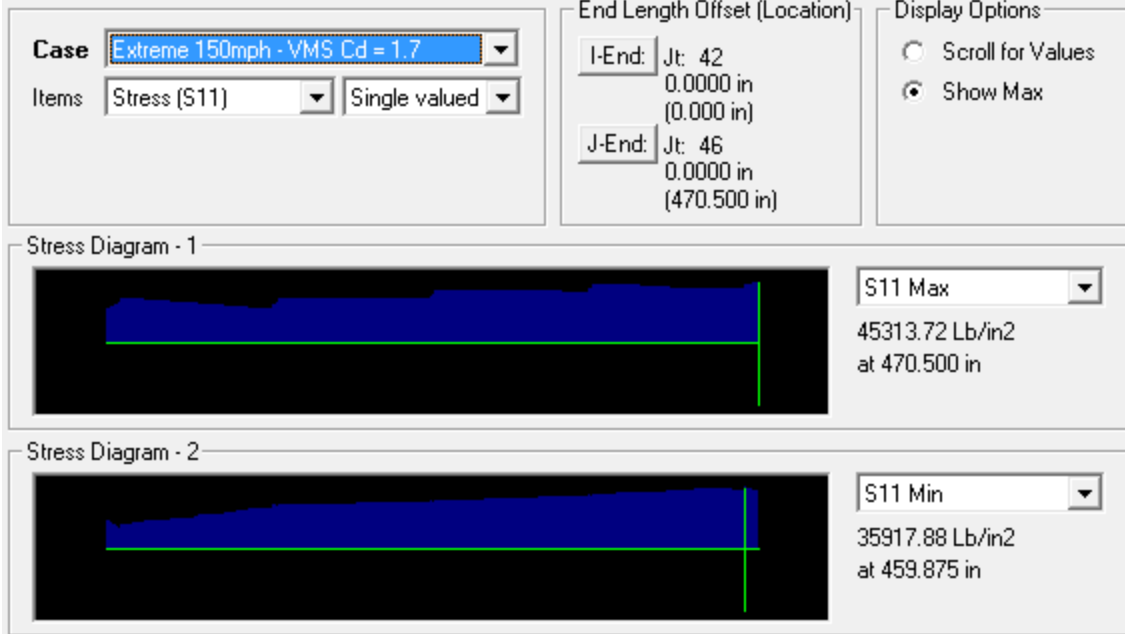


Case Extreme 90mph - VMS Cd = 1.22 Items Stress (S11) Single valued	End Length Offset (Location) I-End: Jt: 42 0.0000 in (0.000 in) J-End: Jt: 46 0.0000 in (470.500 in)	Display Options <input type="radio"/> Scroll for Values <input checked="" type="radio"/> Show Max
--	---	--

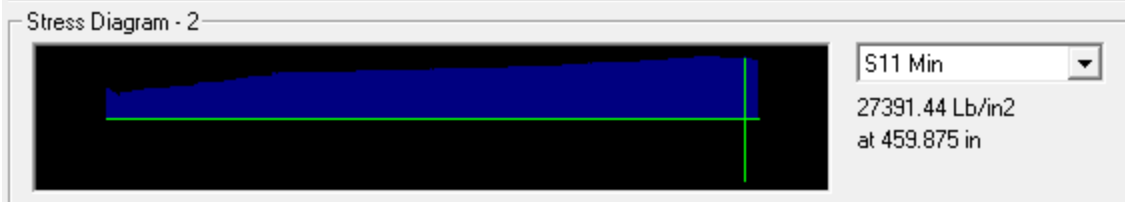
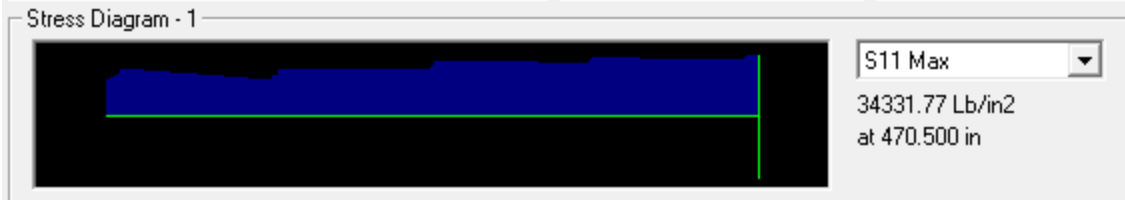


Case Extreme 90mph - VMS Cd = 1.0 Items Stress (S11) Single valued	End Length Offset (Location) I-End: Jt: 42 0.0000 in (0.000 in) J-End: Jt: 46 0.0000 in (470.500 in)	Display Options <input type="radio"/> Scroll for Values <input checked="" type="radio"/> Show Max
---	---	--

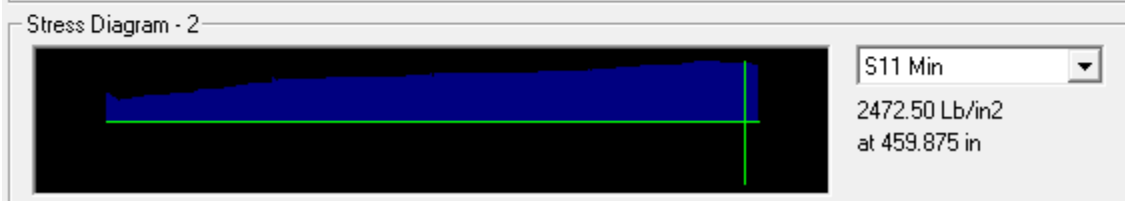
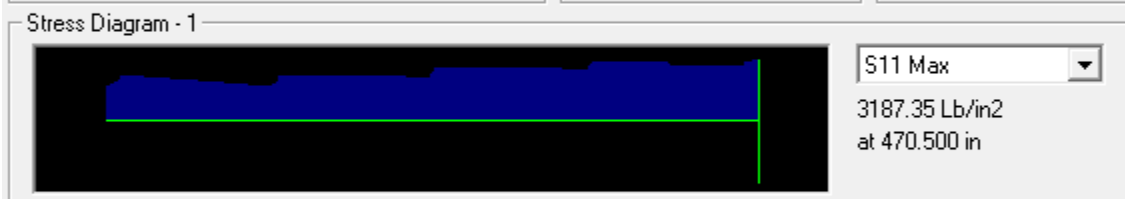


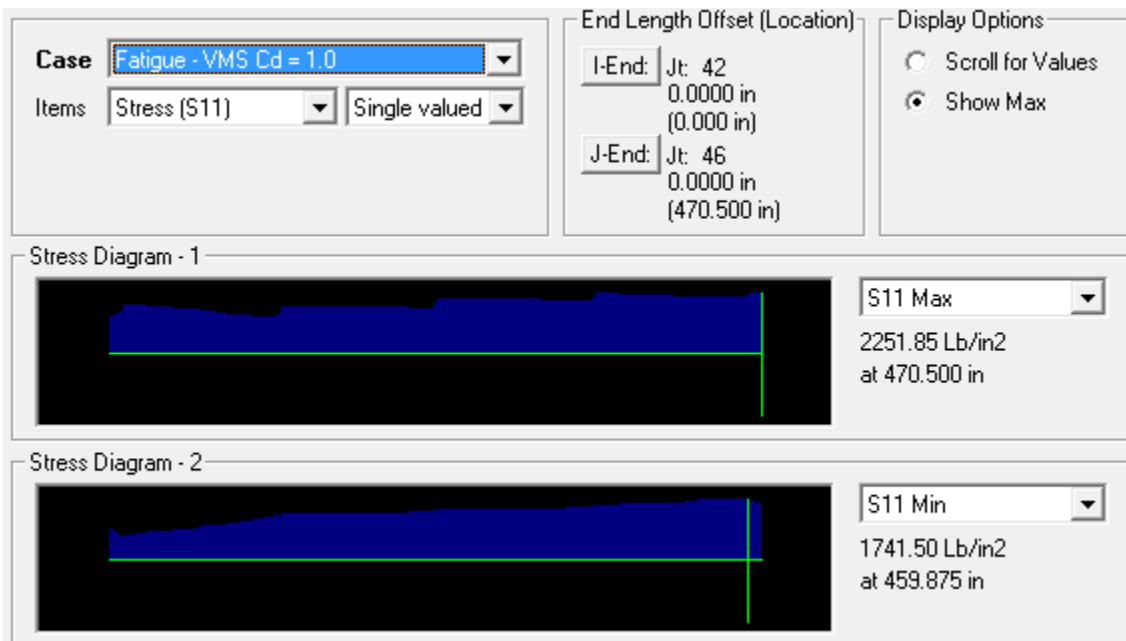
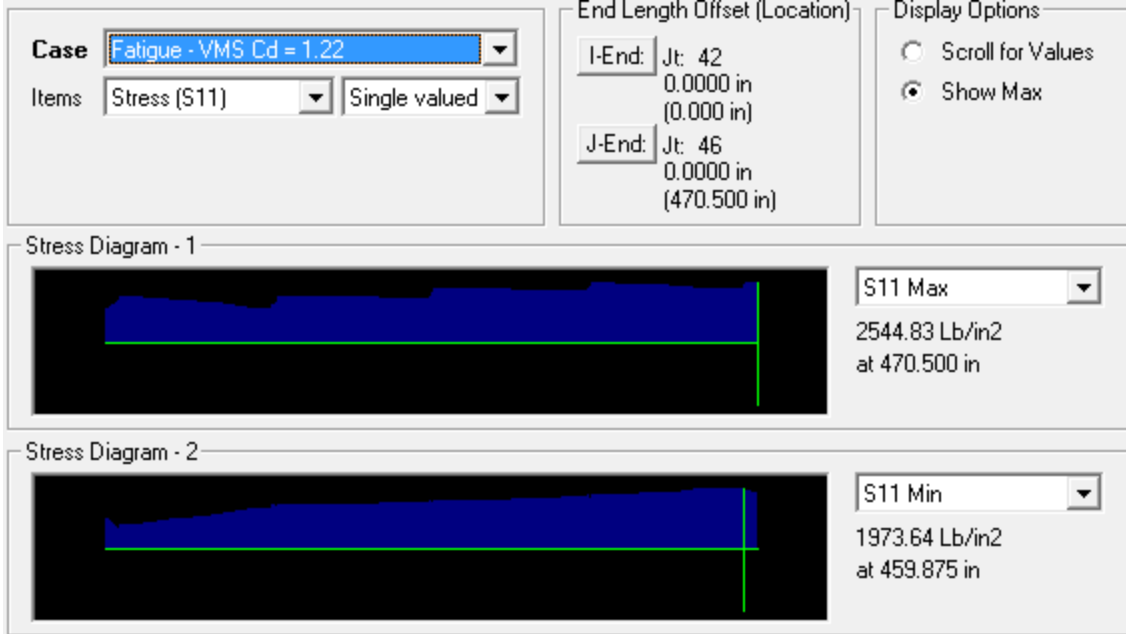


Case Extreme 150mph - VMS Cd = 1.0 Items Stress (S11) Single valued	End Length Offset (Location) I-End: Jt: 42 0.0000 in (0.000 in) J-End: Jt: 46 0.0000 in (470.500 in)	Display Options <input type="radio"/> Scroll for Values <input checked="" type="radio"/> Show Max
--	---	--

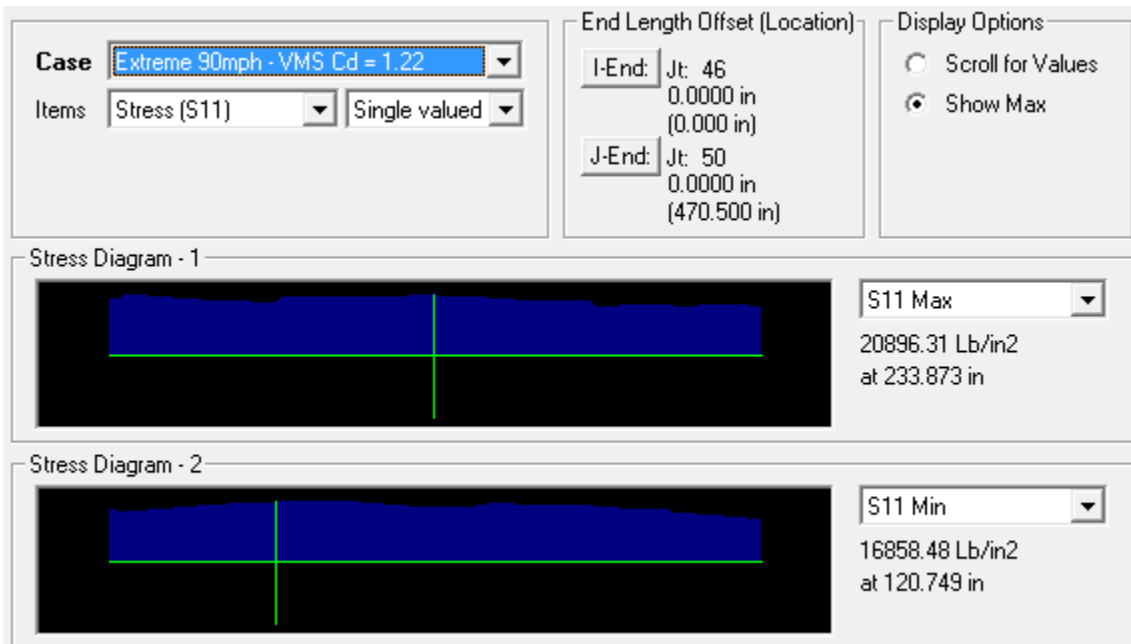
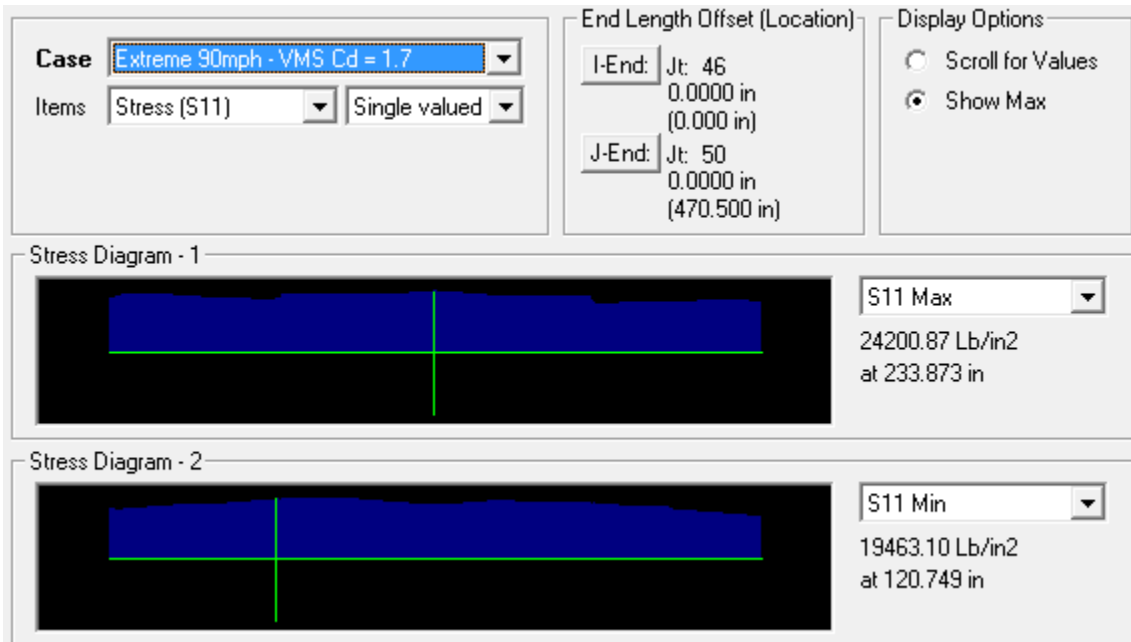


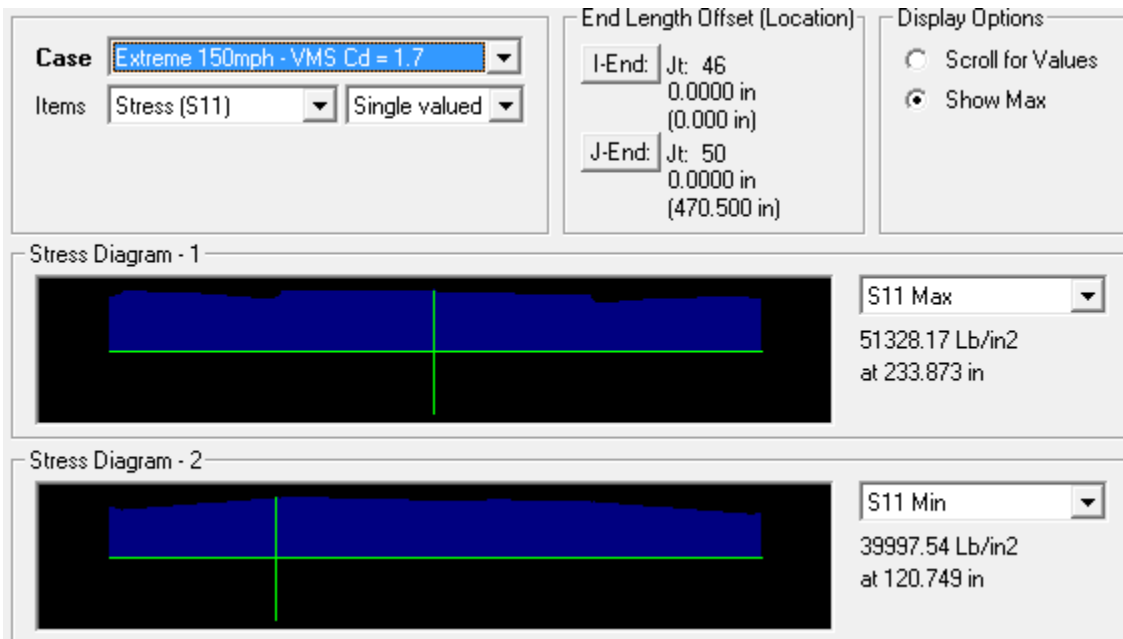
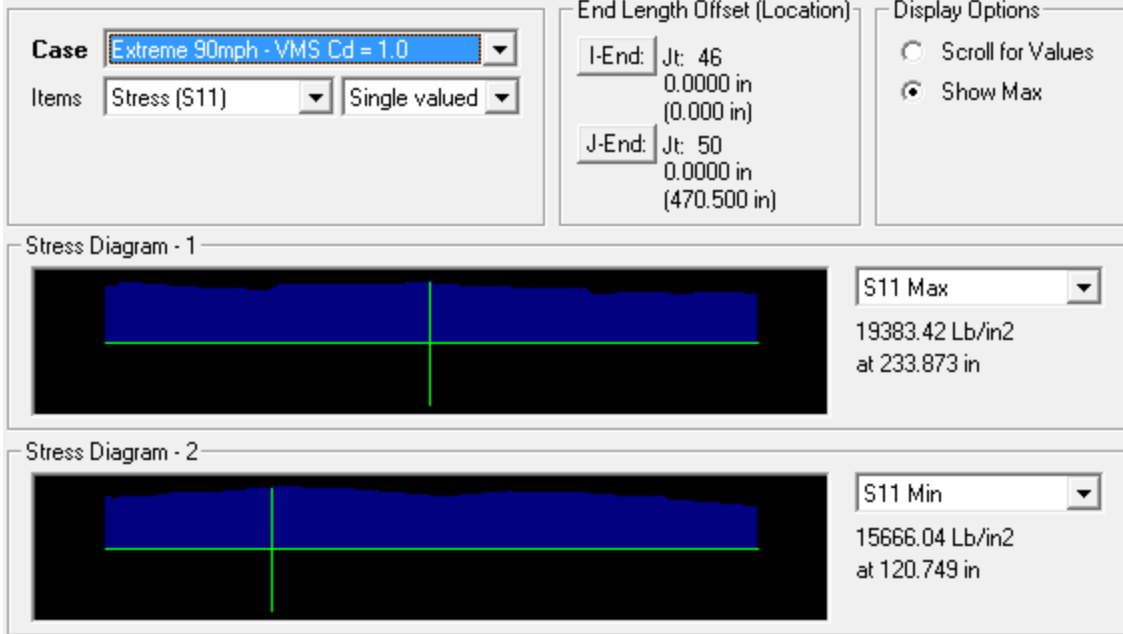
Case Fatigue - VMS Cd = 1.7 Items Stress (S11) Single valued	End Length Offset (Location) I-End: Jt: 42 0.0000 in (0.000 in) J-End: Jt: 46 0.0000 in (470.500 in)	Display Options <input type="radio"/> Scroll for Values <input checked="" type="radio"/> Show Max
---	---	--

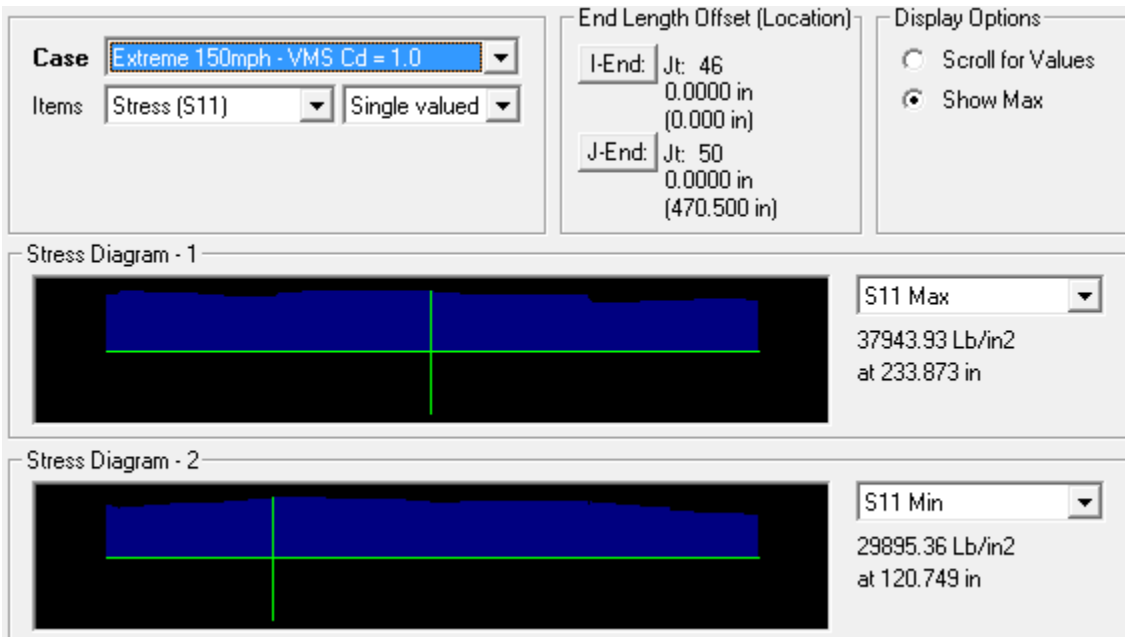
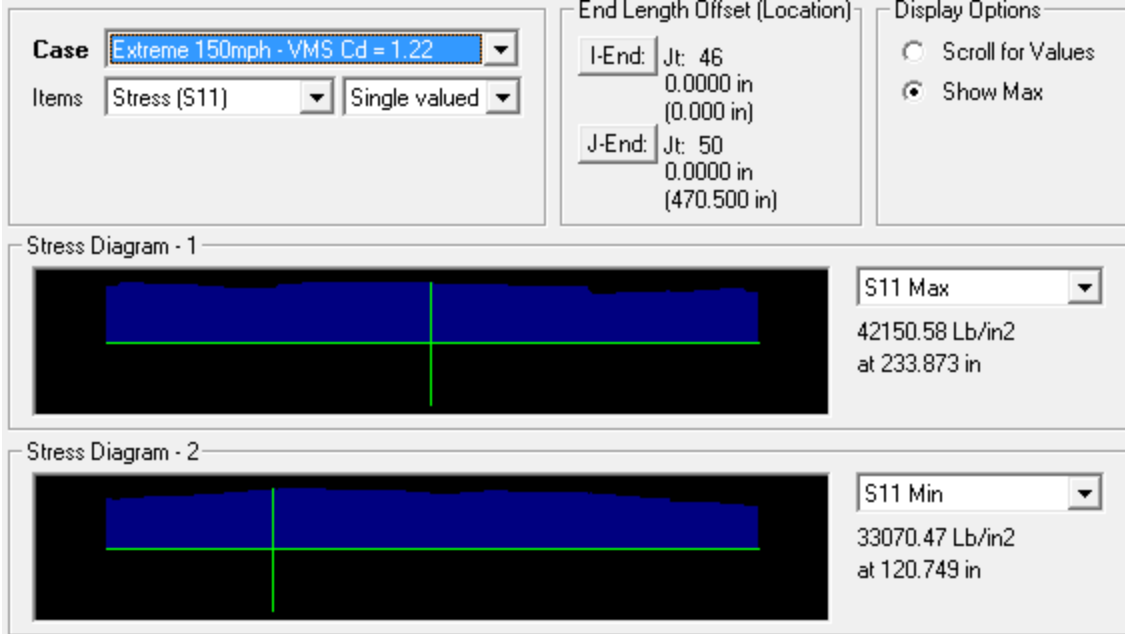


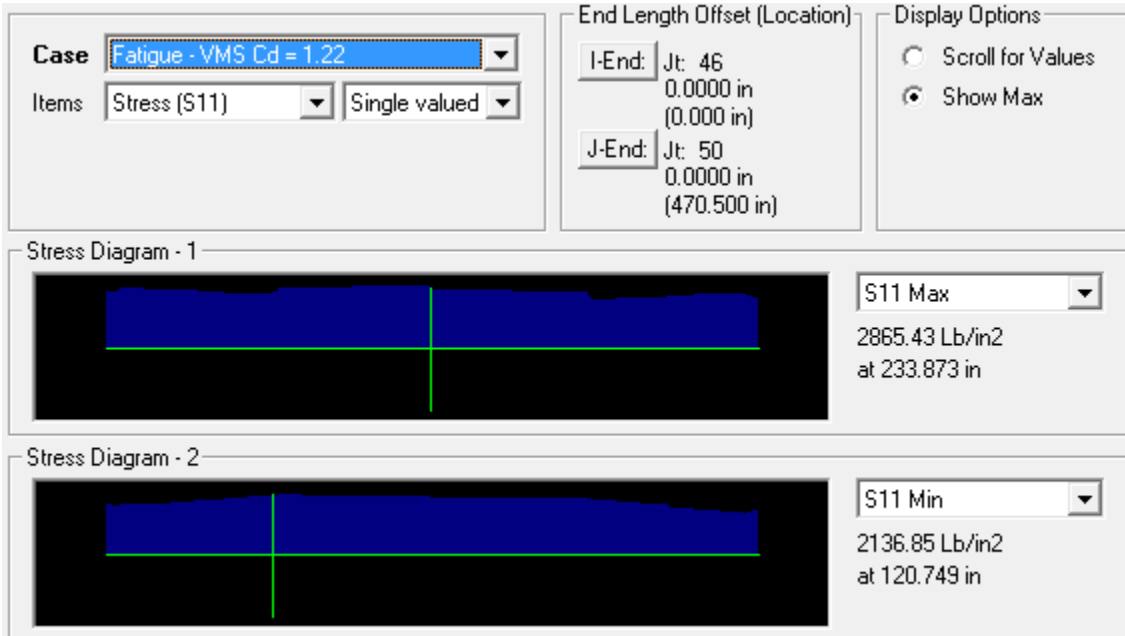
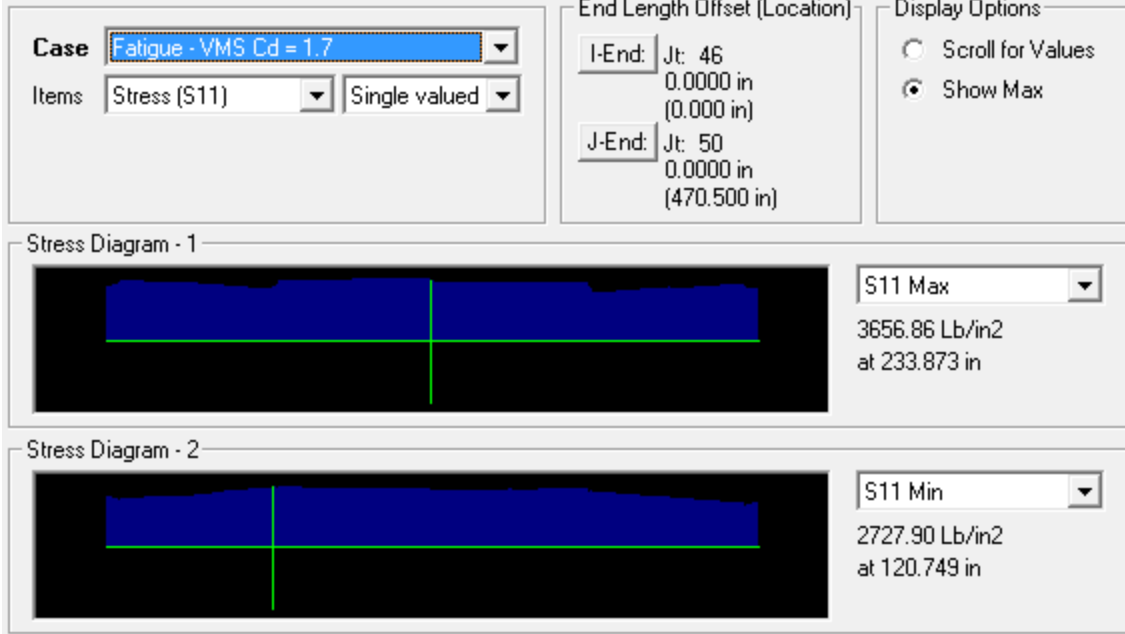


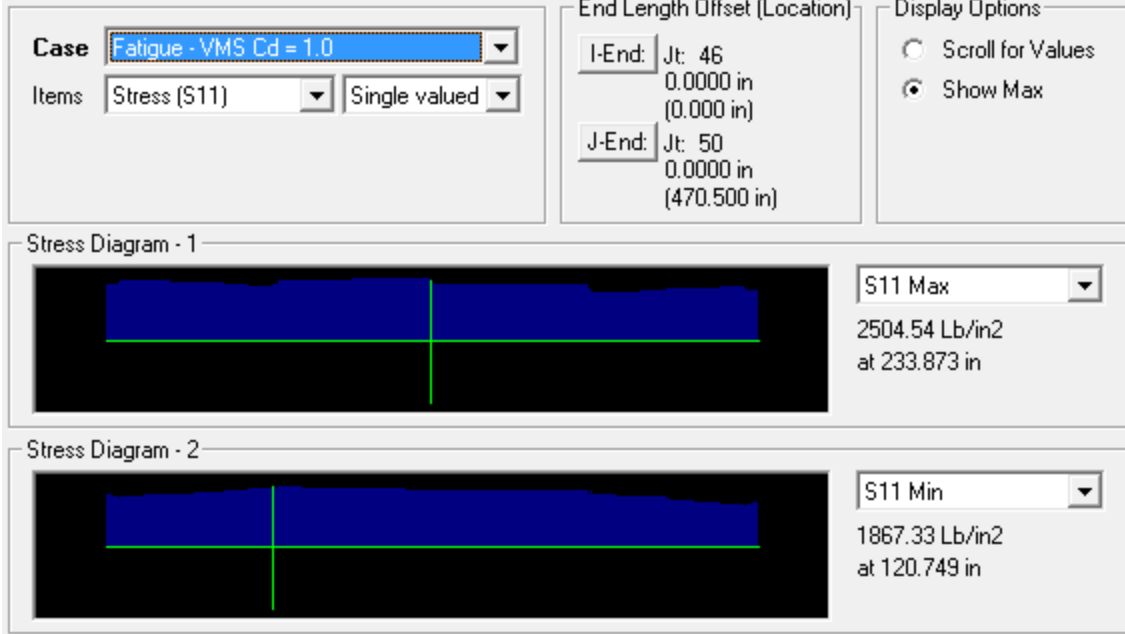
Chord 2c



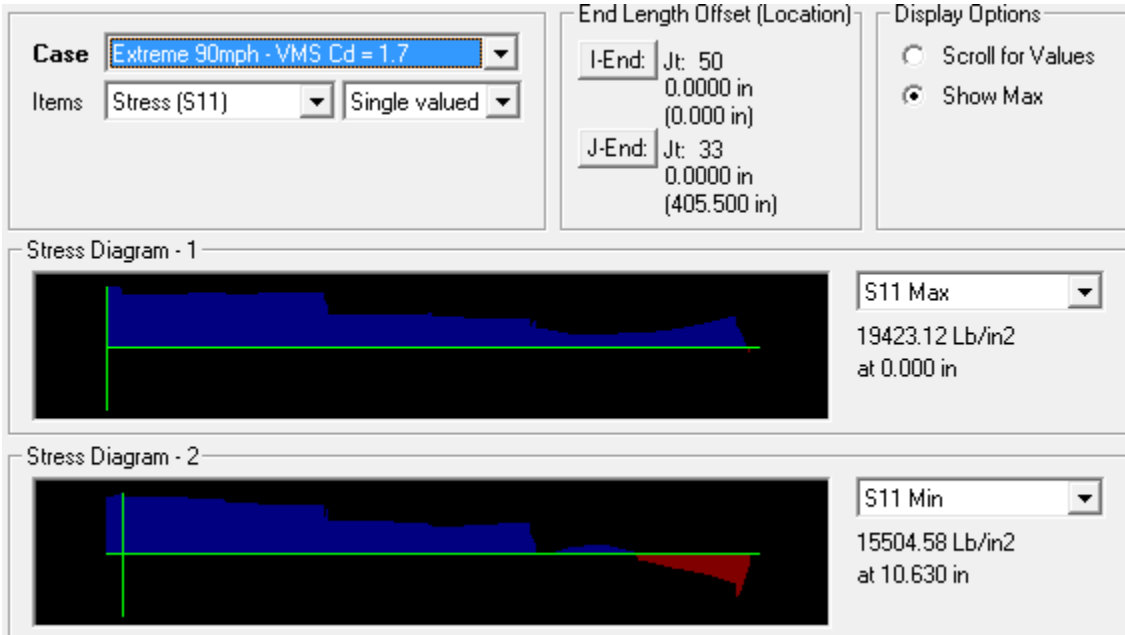


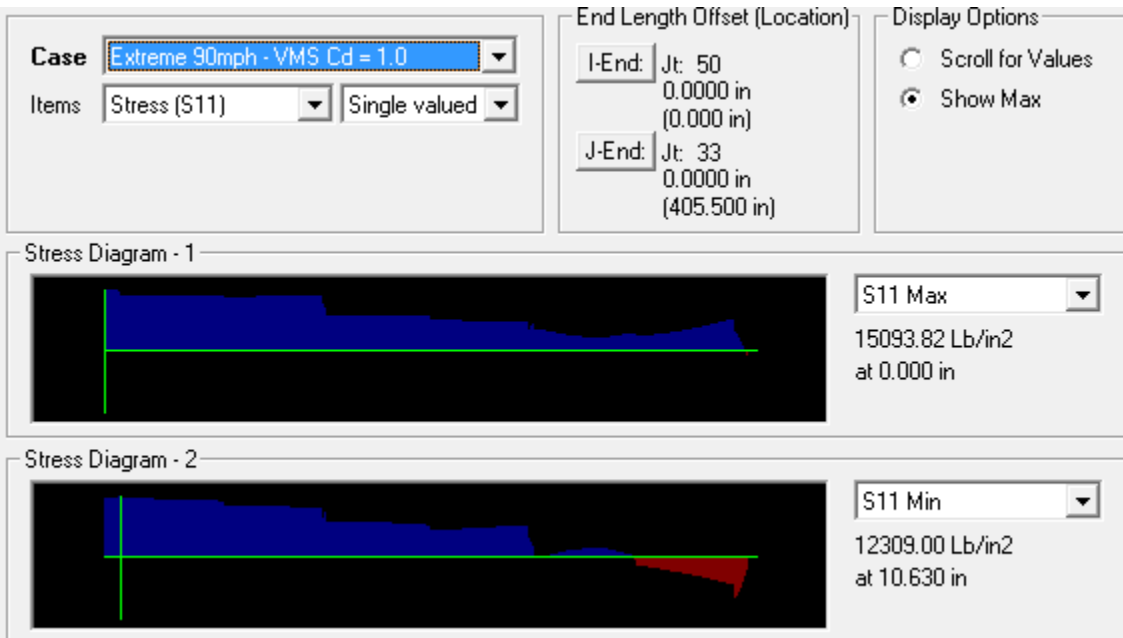
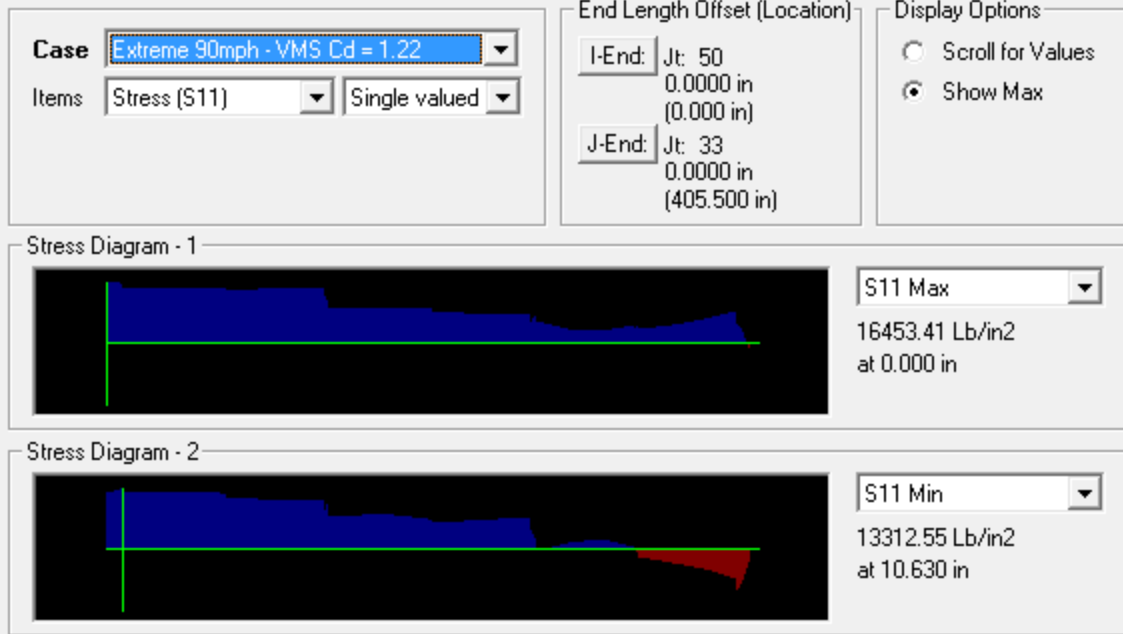


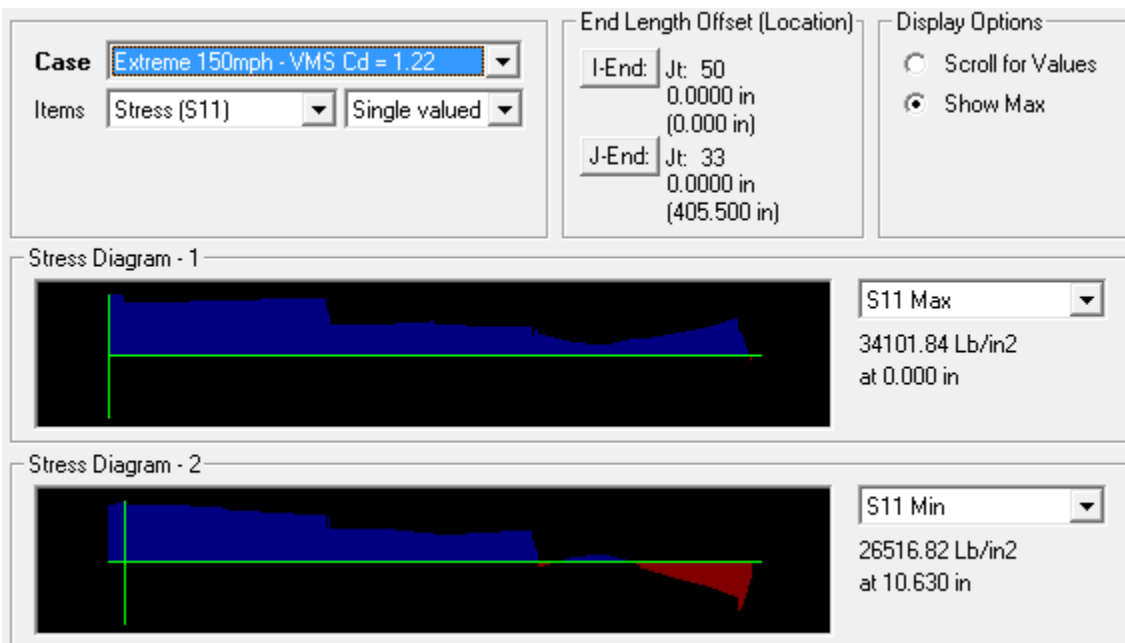
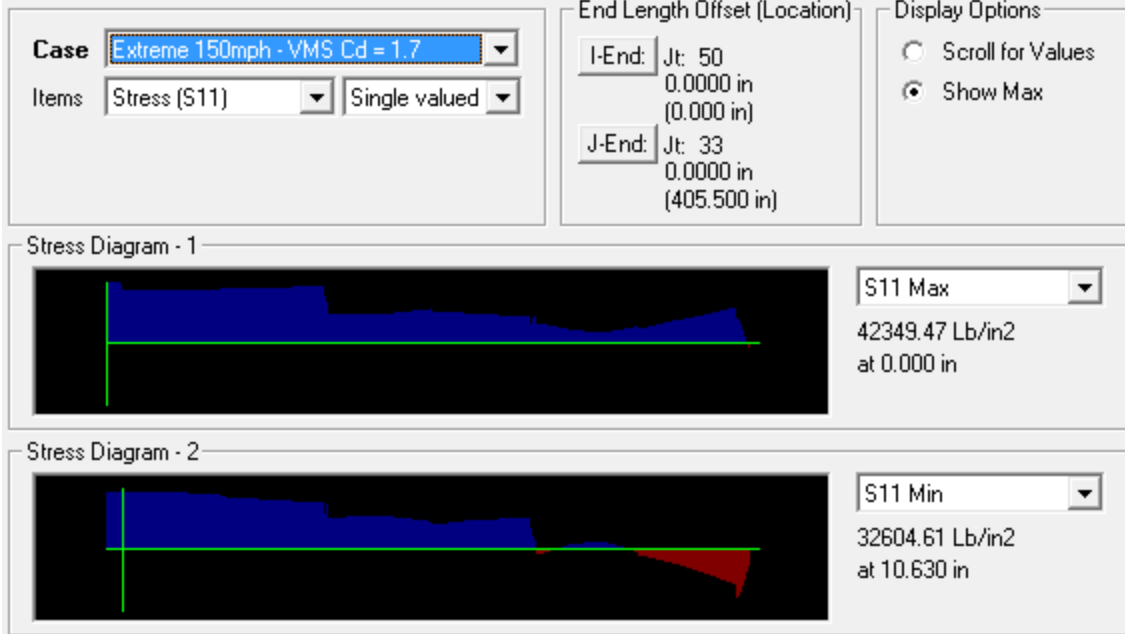


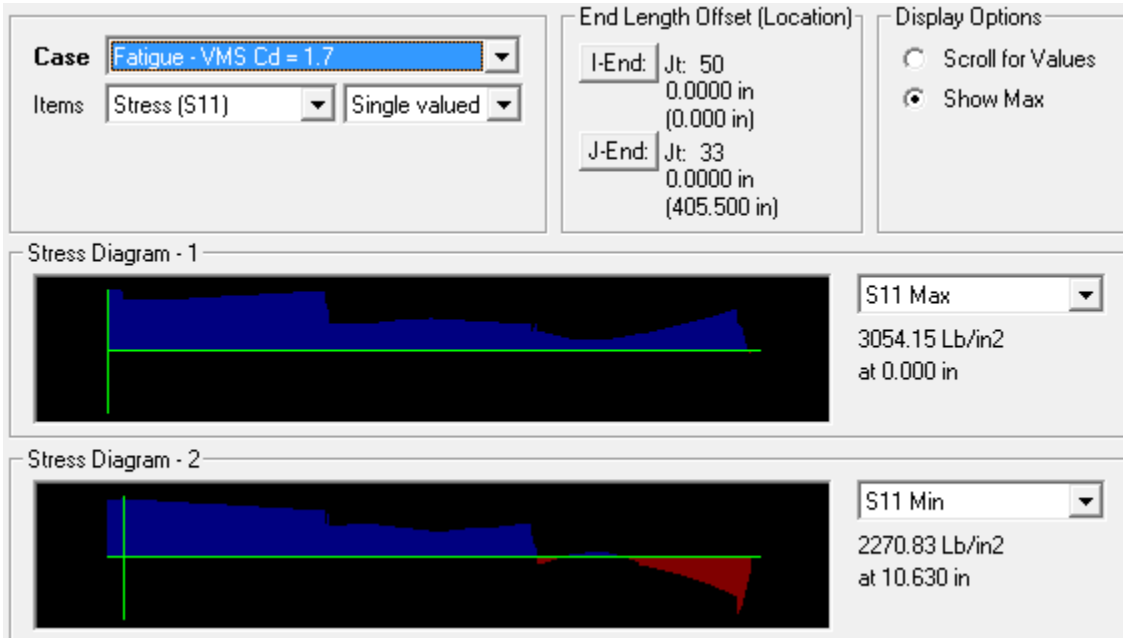
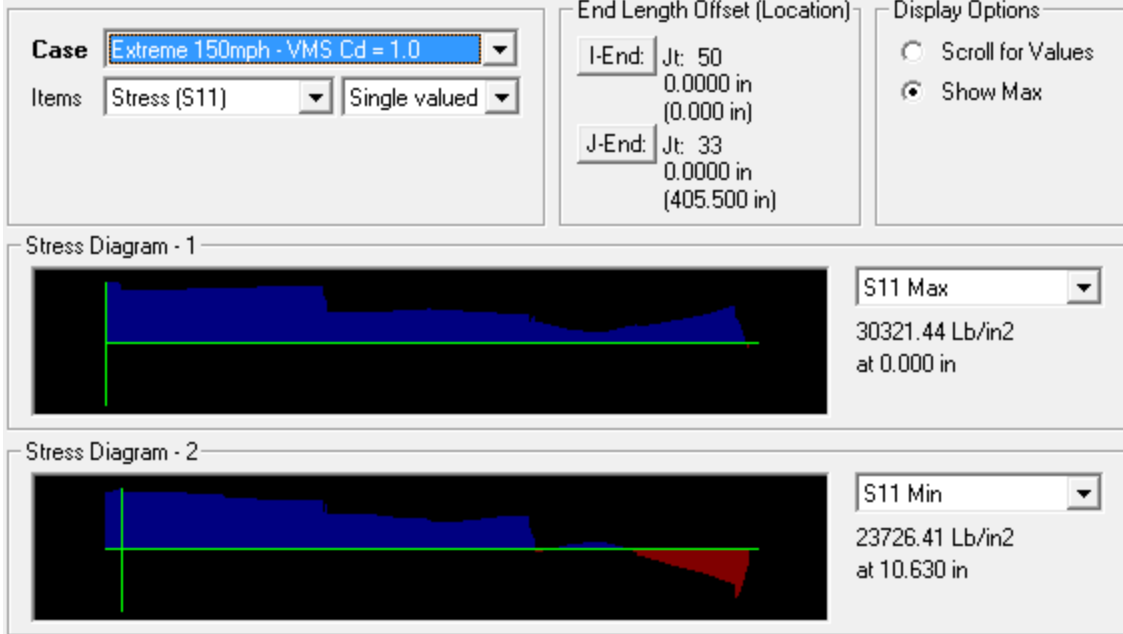


Chord 2d

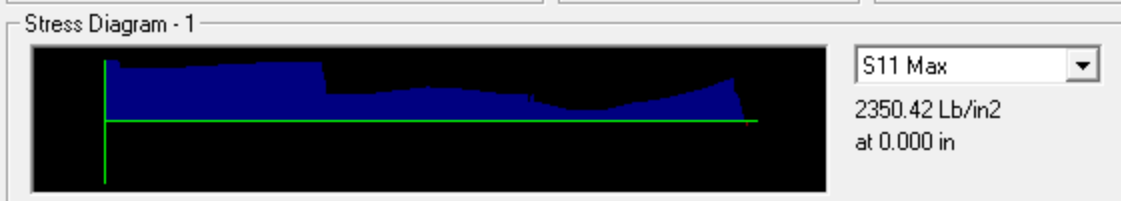




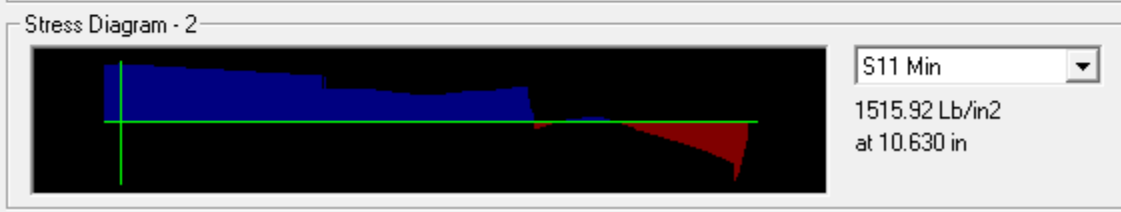
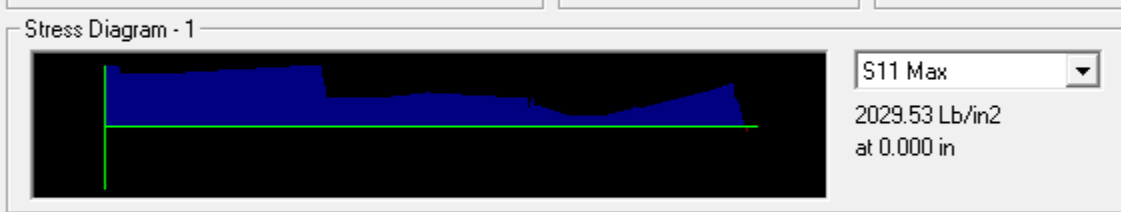




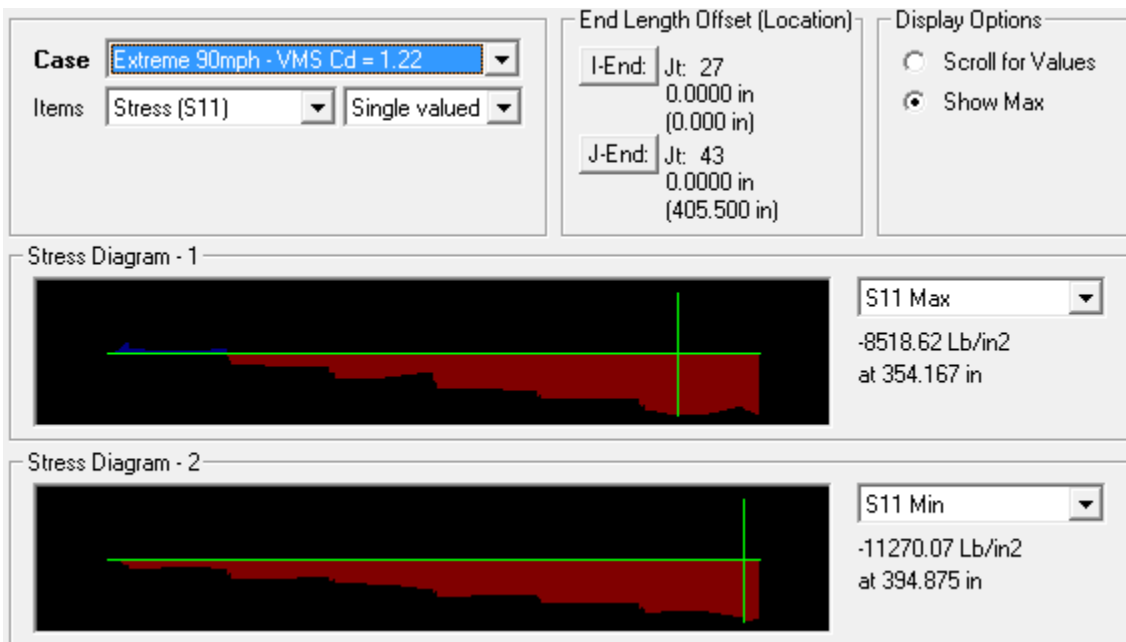
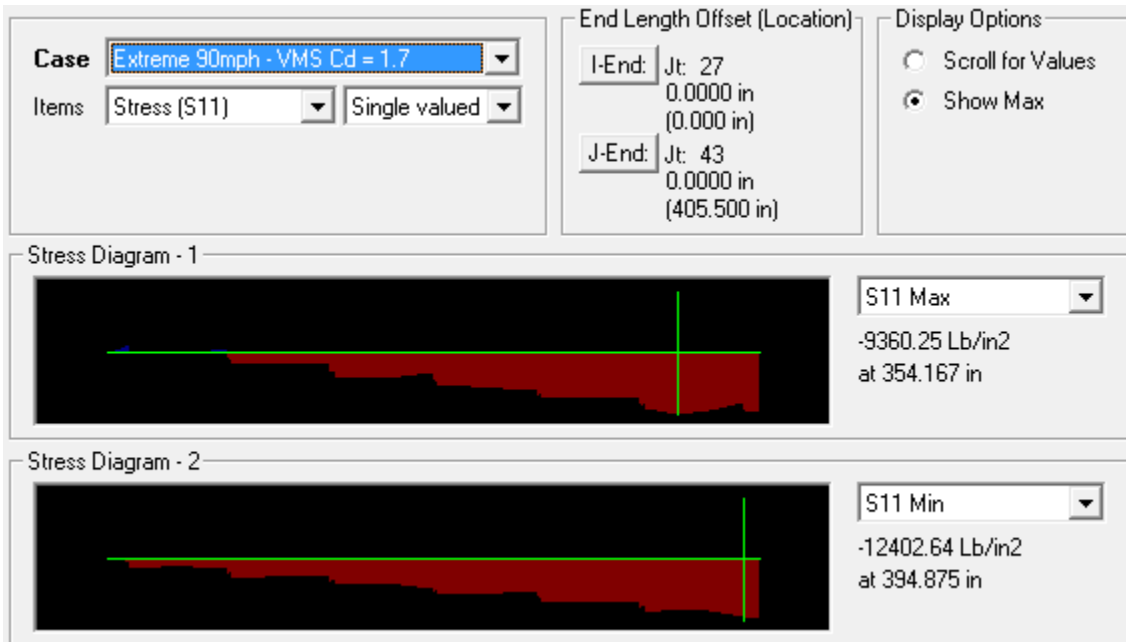
Case Fatigue - VMS Cd = 1.22 Items Stress (S11) Single valued	End Length Offset (Location) I-End: Jt: 50 0.0000 in (0.000 in) J-End: Jt: 33 0.0000 in (405.500 in)	Display Options <input type="radio"/> Scroll for Values <input checked="" type="radio"/> Show Max
--	---	--

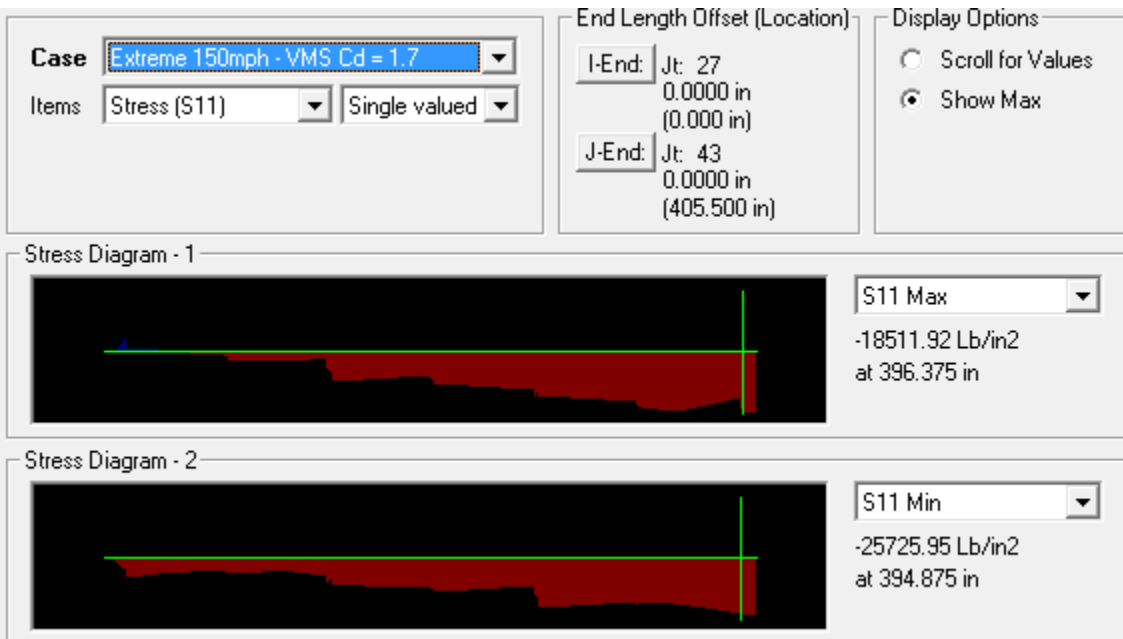
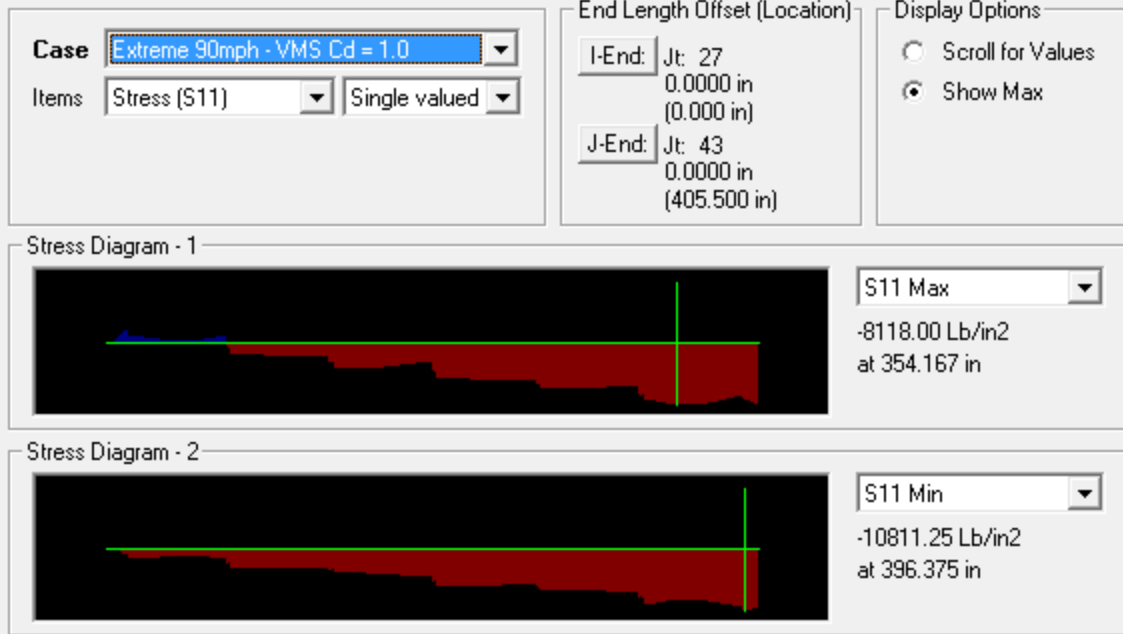


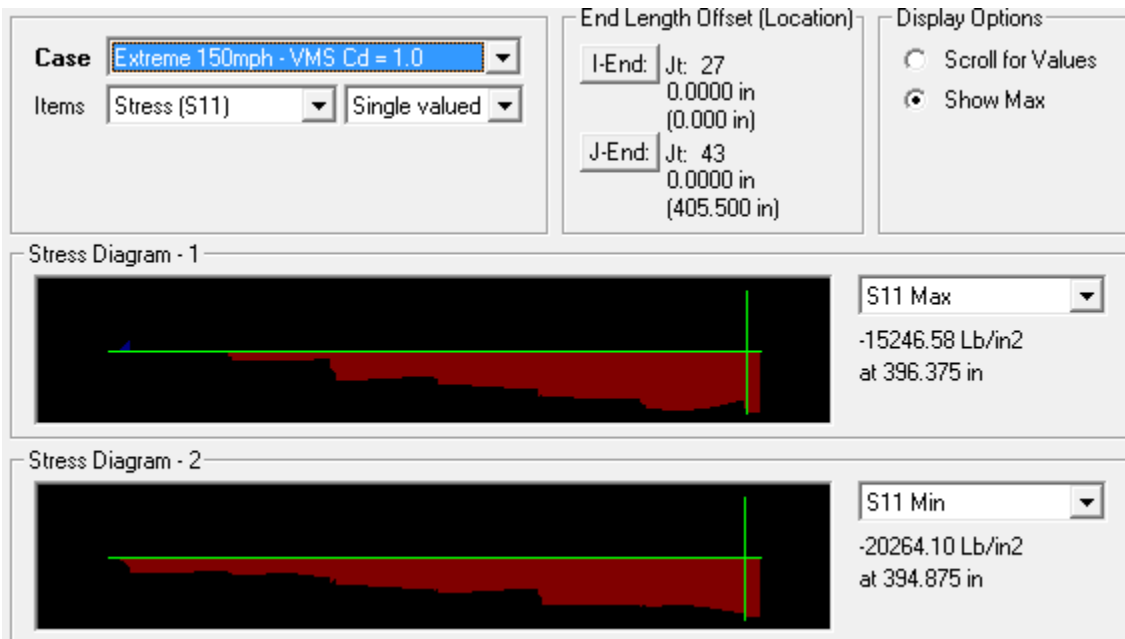
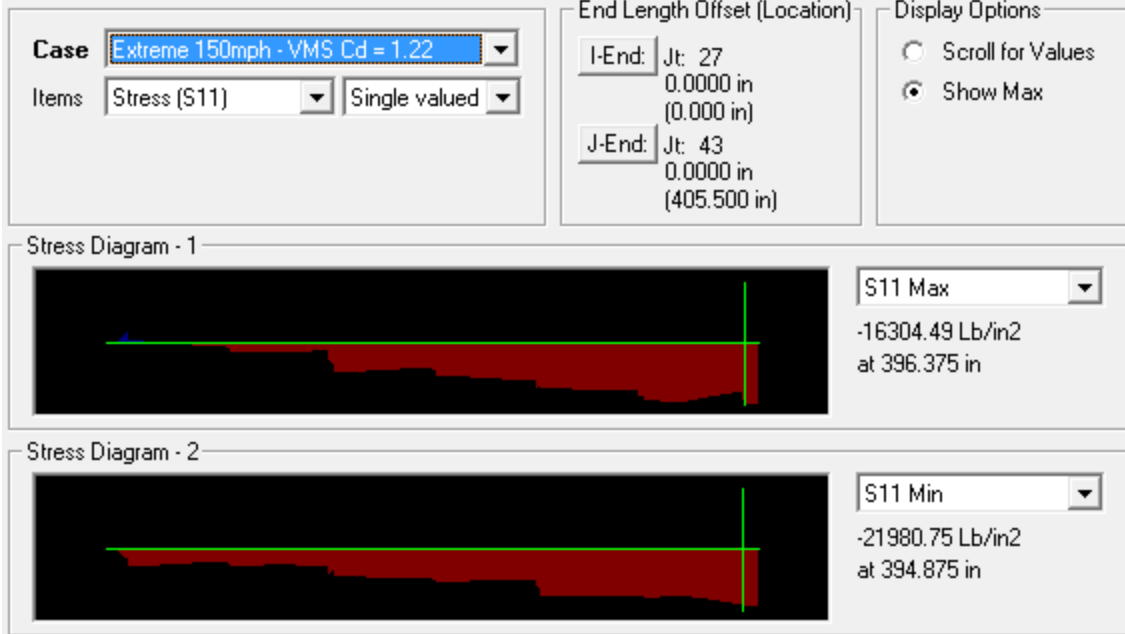
Case Fatigue - VMS Cd = 1.0 Items Stress (S11) Single valued	End Length Offset (Location) I-End: Jt: 50 0.0000 in (0.000 in) J-End: Jt: 33 0.0000 in (405.500 in)	Display Options <input type="radio"/> Scroll for Values <input checked="" type="radio"/> Show Max
---	---	--

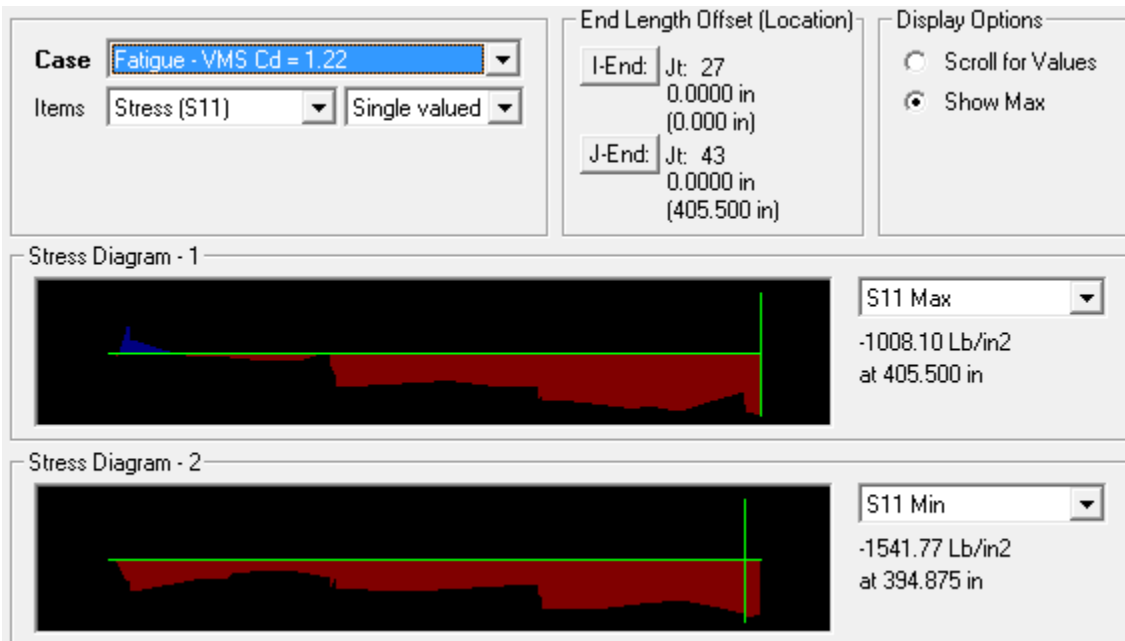
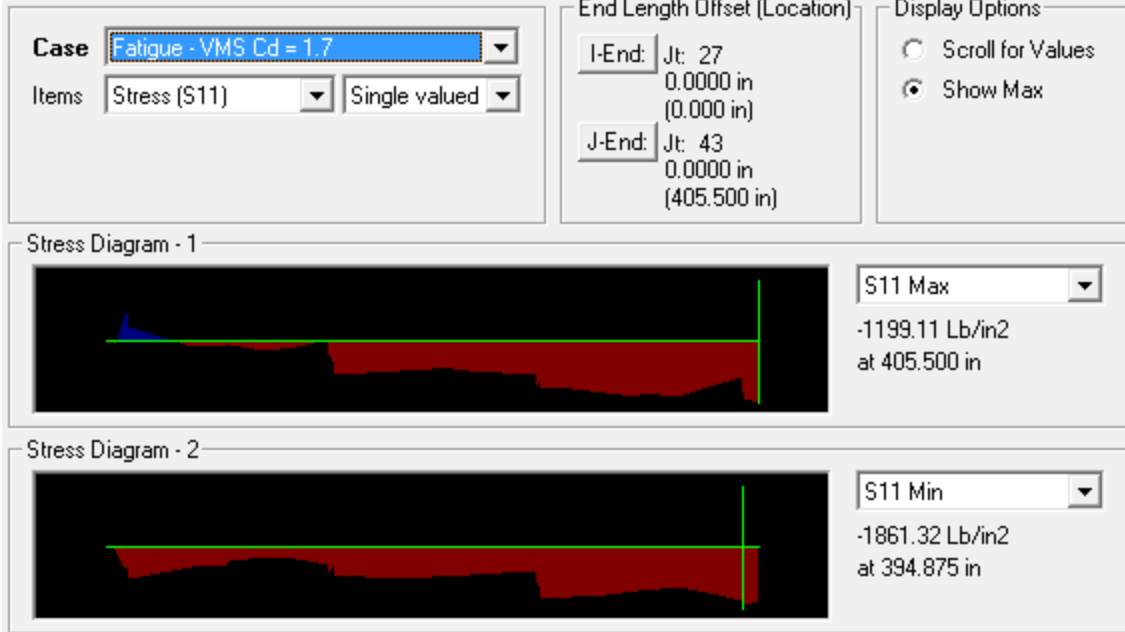


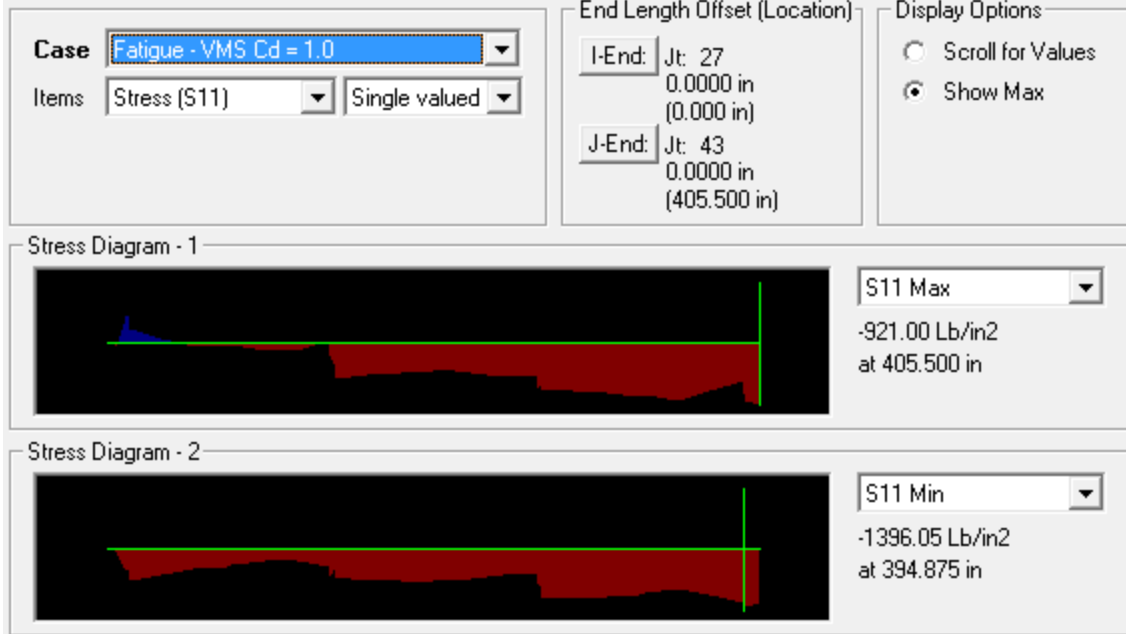
Chord 3a



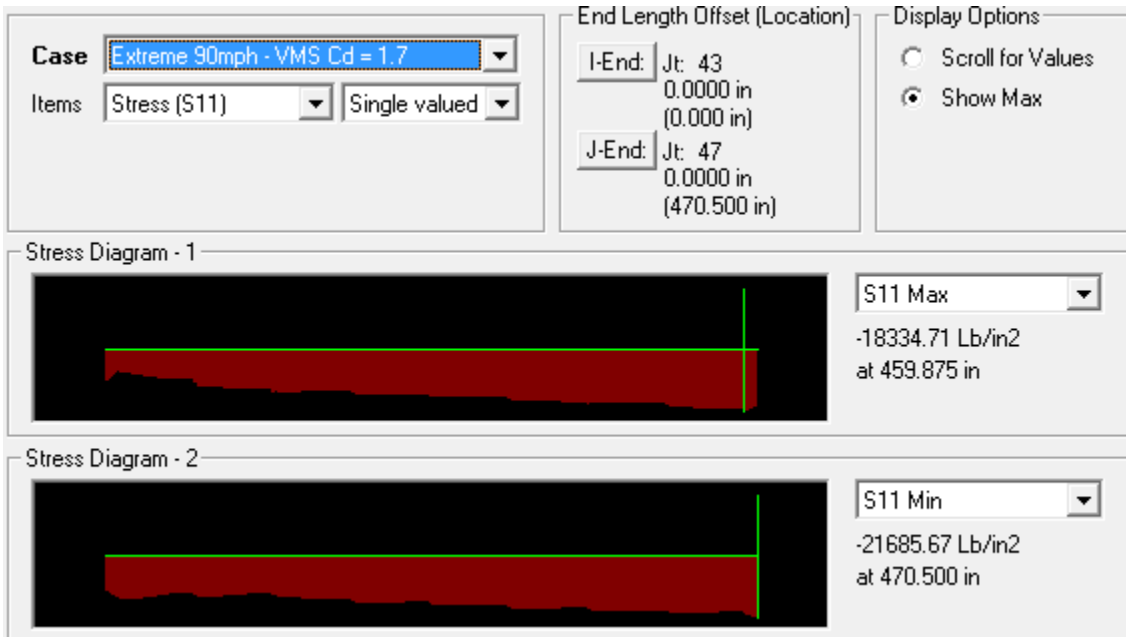


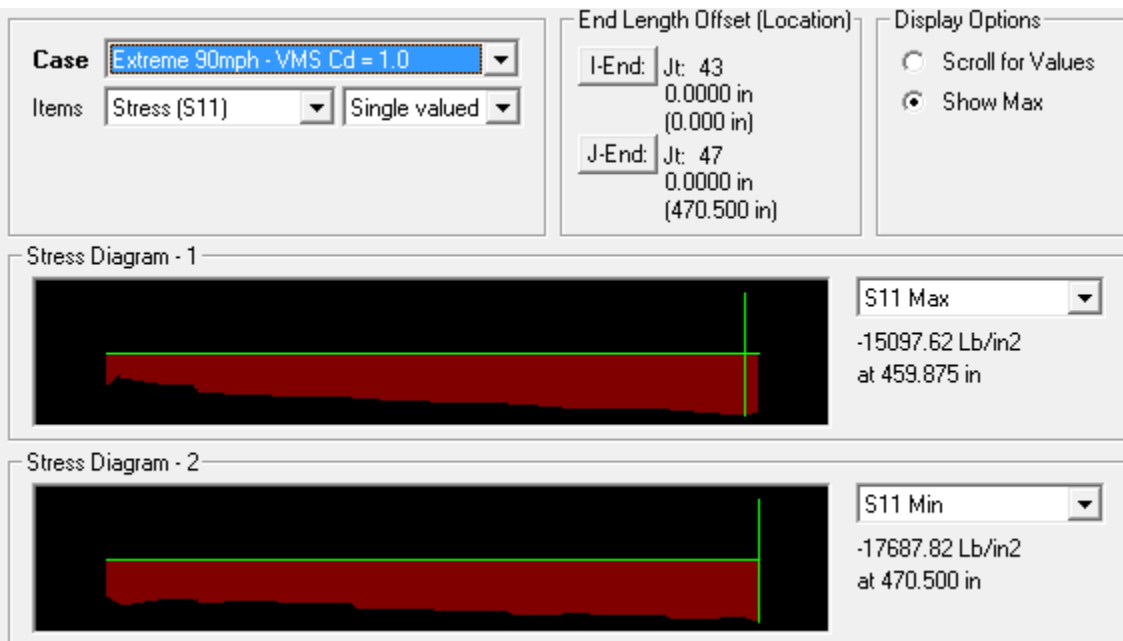
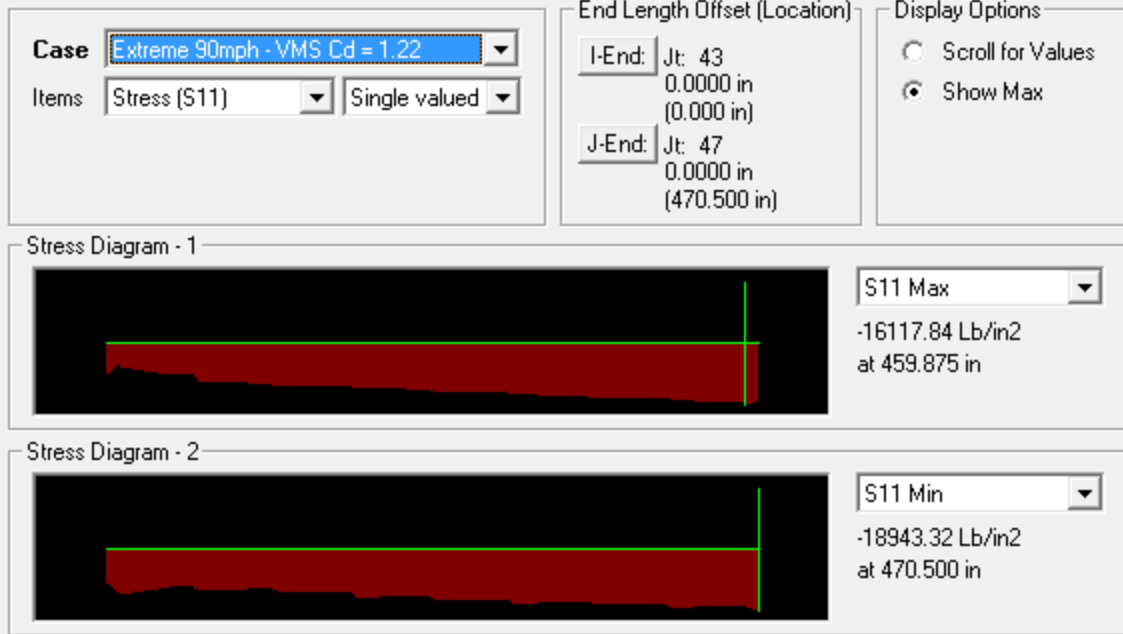










Chord 3b

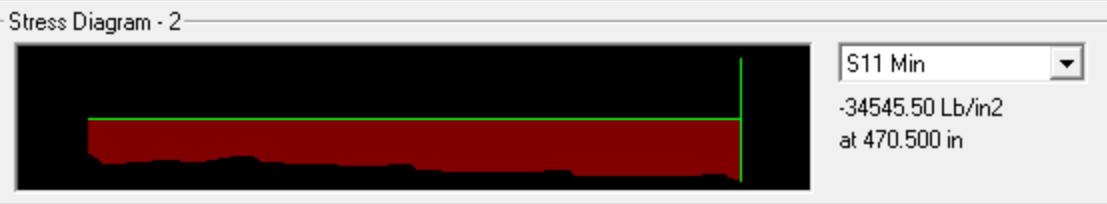
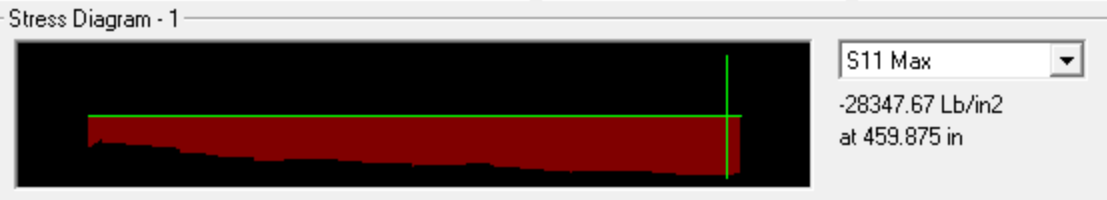




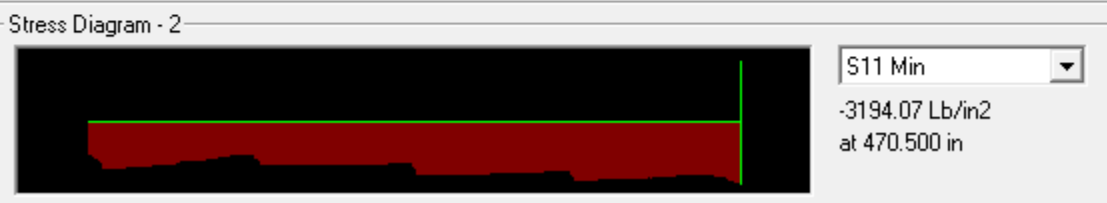
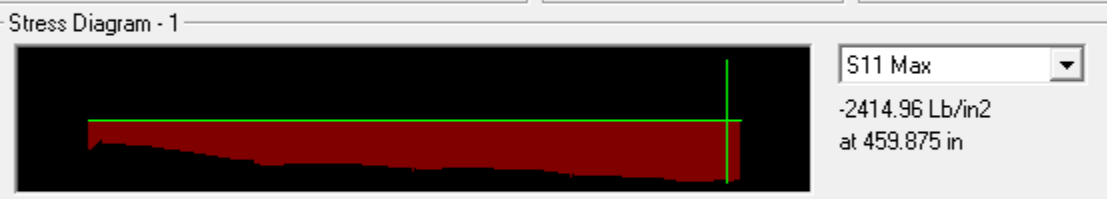
Case Extreme 150mph - VMS Cd = 1.7 Items Stress (S11) Single valued	End Length Offset (Location) I-End: Jt: 43 0.0000 in (0.000 in) J-End: Jt: 47 0.0000 in (470.500 in)	Display Options <input type="radio"/> Scroll for Values <input checked="" type="radio"/> Show Max
Stress Diagram - 1 		
		S11 Max -36604.31 Lb/in2 at 459.875 in
Stress Diagram - 2 		
		S11 Min -45652.67 Lb/in2 at 470.500 in

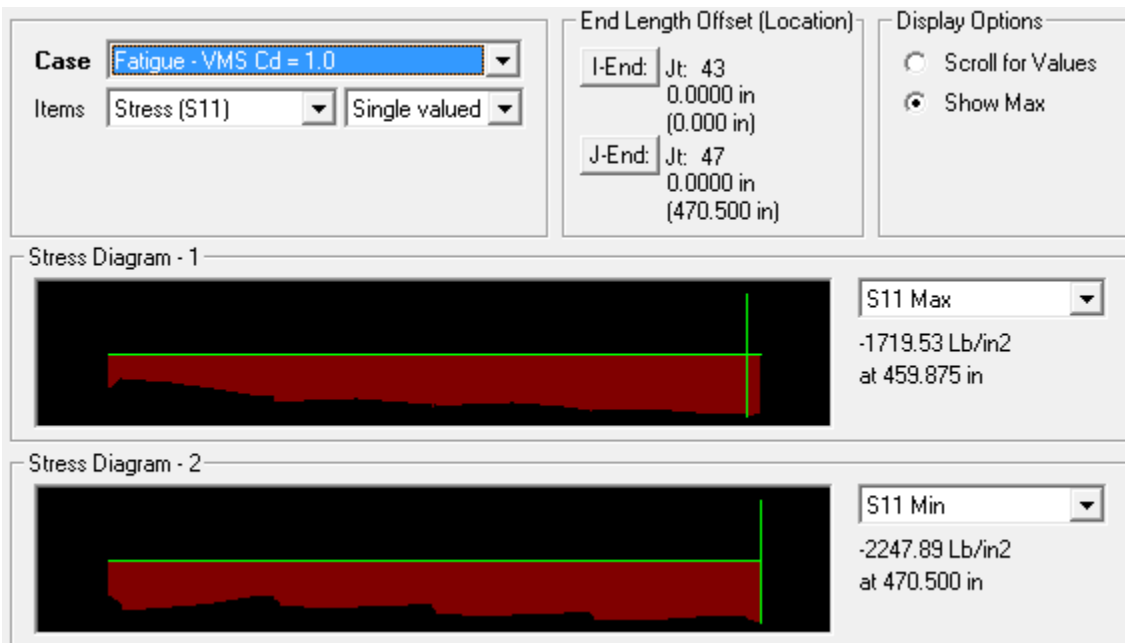
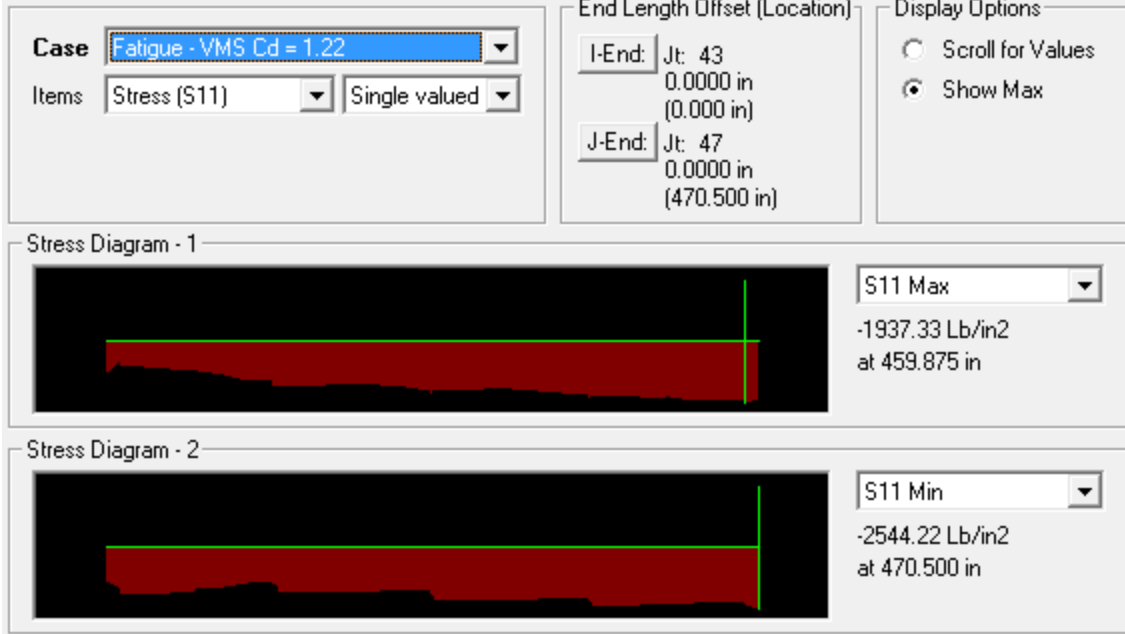
Case Extreme 150mph - VMS Cd = 1.22 Items Stress (S11) Single valued	End Length Offset (Location) I-End: Jt: 43 0.0000 in (0.000 in) J-End: Jt: 47 0.0000 in (470.500 in)	Display Options <input type="radio"/> Scroll for Values <input checked="" type="radio"/> Show Max
Stress Diagram - 1 		
		S11 Max -31006.50 Lb/in2 at 459.875 in
Stress Diagram - 2 		
		S11 Min -38036.47 Lb/in2 at 470.500 in

Case Extreme 150mph - VMS Cd = 1.0 Items Stress (S11) Single valued	End Length Offset (Location) I-End: Jt: 43 0.0000 in (0.000 in) J-End: Jt: 47 0.0000 in (470.500 in)	Display Options <input type="radio"/> Scroll for Values <input checked="" type="radio"/> Show Max
--	---	--

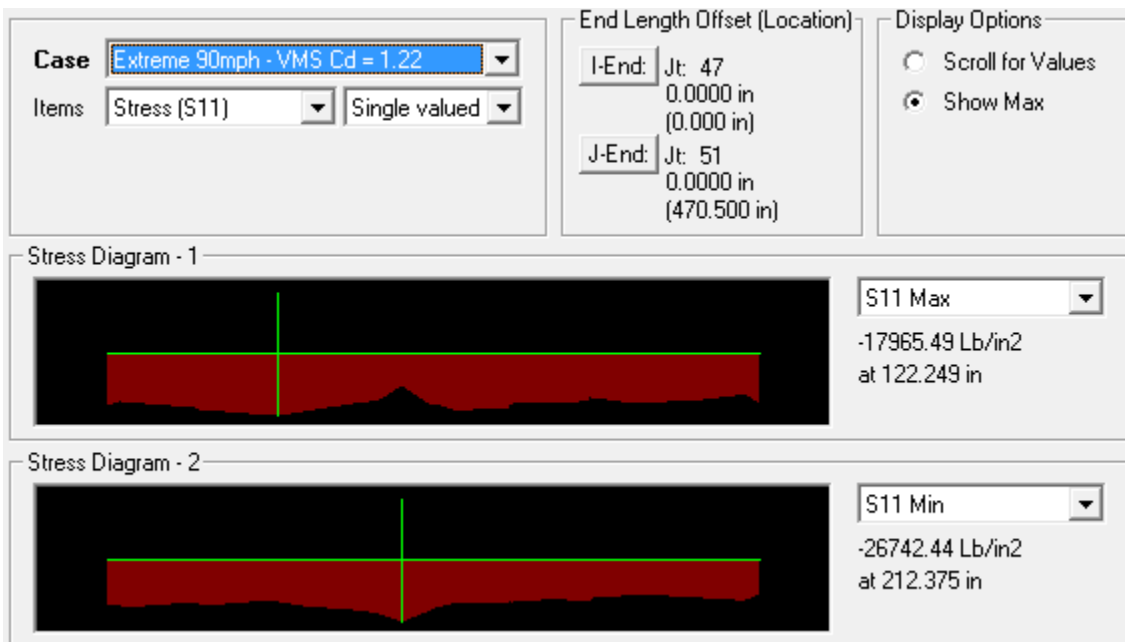
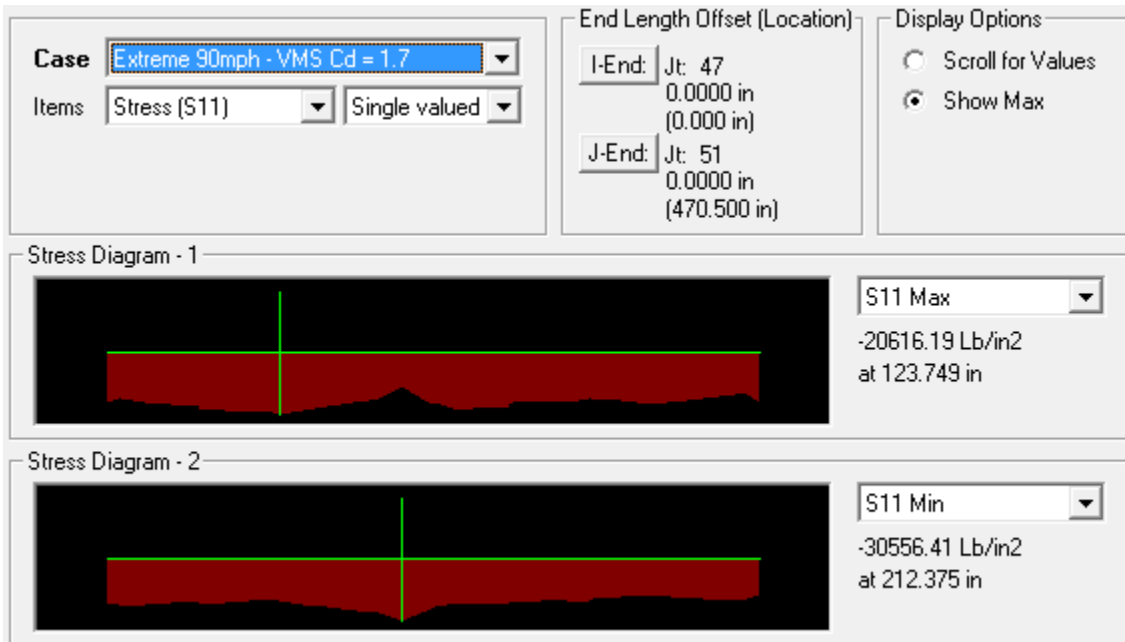


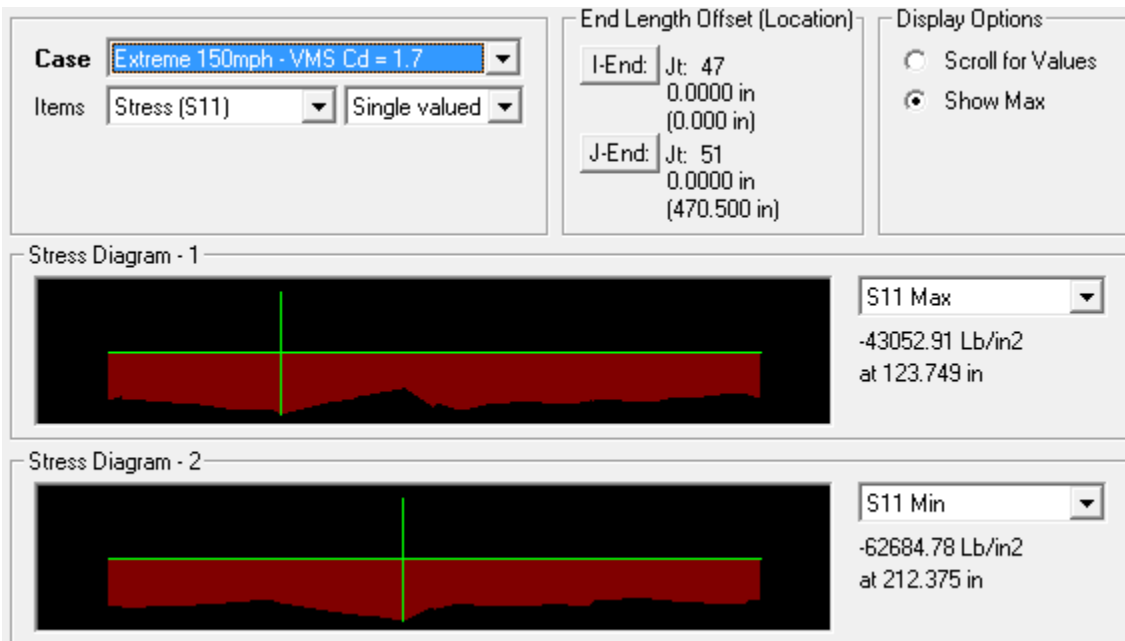
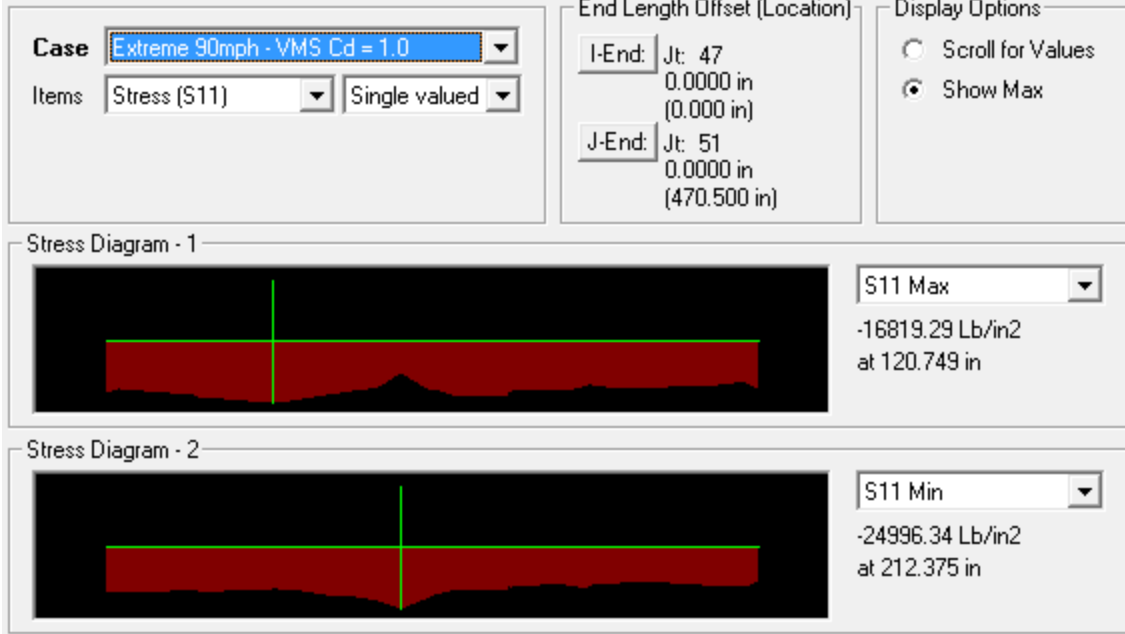
Case Fatigue - VMS Cd = 1.7 Items Stress (S11) Single valued	End Length Offset (Location) I-End: Jt: 43 0.0000 in (0.000 in) J-End: Jt: 47 0.0000 in (470.500 in)	Display Options <input type="radio"/> Scroll for Values <input checked="" type="radio"/> Show Max
---	---	--





Chord 3c





Case Extreme 150mph - VMS Cd = 1.22

Items Stress (S11) Single valued

End Length Offset (Location)

I-End: Jt: 47
0.0000 in
(0.000 in)

J-End: Jt: 51
0.0000 in
(470.500 in)

Display Options

Scroll for Values

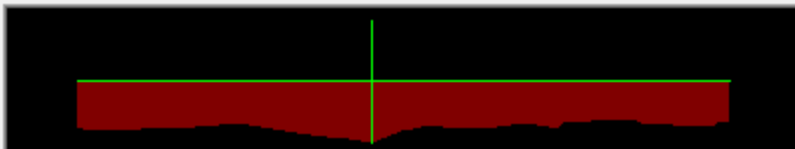
Show Max

Stress Diagram - 1



S11 Max
-35452.56 Lb/in2
at 123.749 in

Stress Diagram - 2



S11 Min
-50900.47 Lb/in2
at 212.375 in

Case Extreme 150mph - VMS Cd = 1.0

Items Stress (S11) Single valued

End Length Offset (Location)

I-End: Jt: 47
0.0000 in
(0.000 in)


J-End: Jt: 51
0.0000 in
(470.500 in)

Display Options

Scroll for Values

Show Max

Stress Diagram - 1

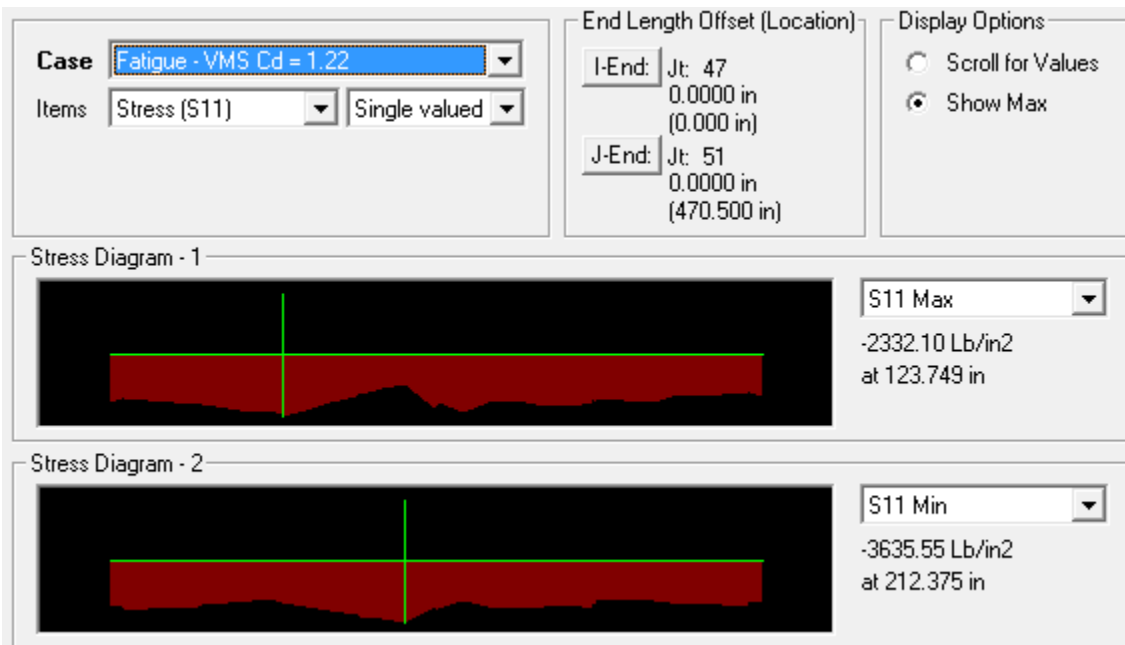
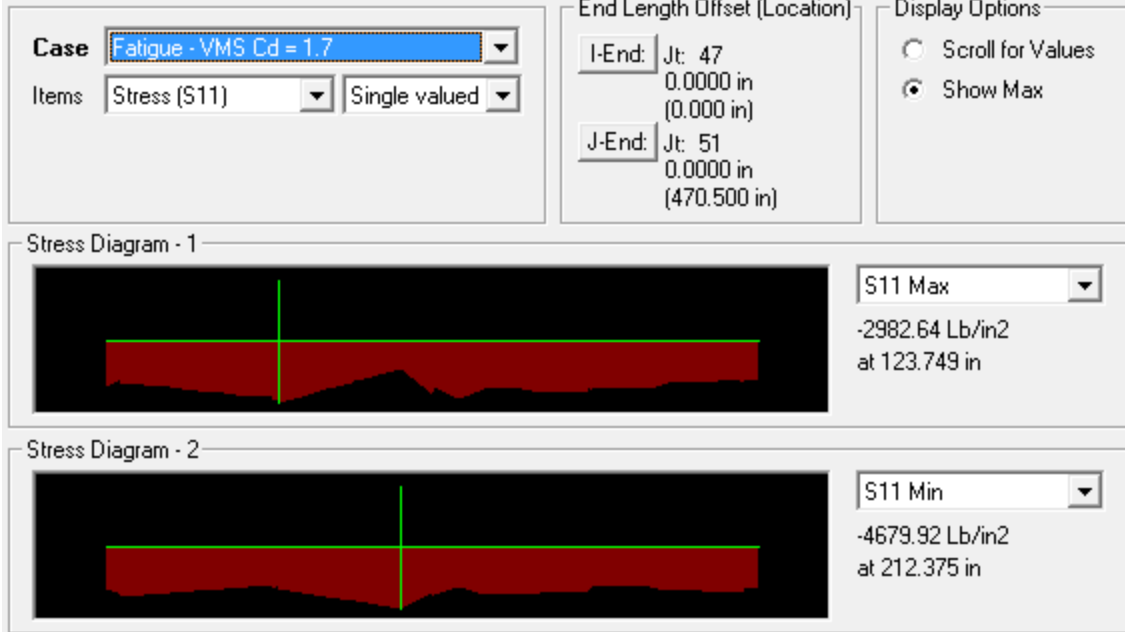


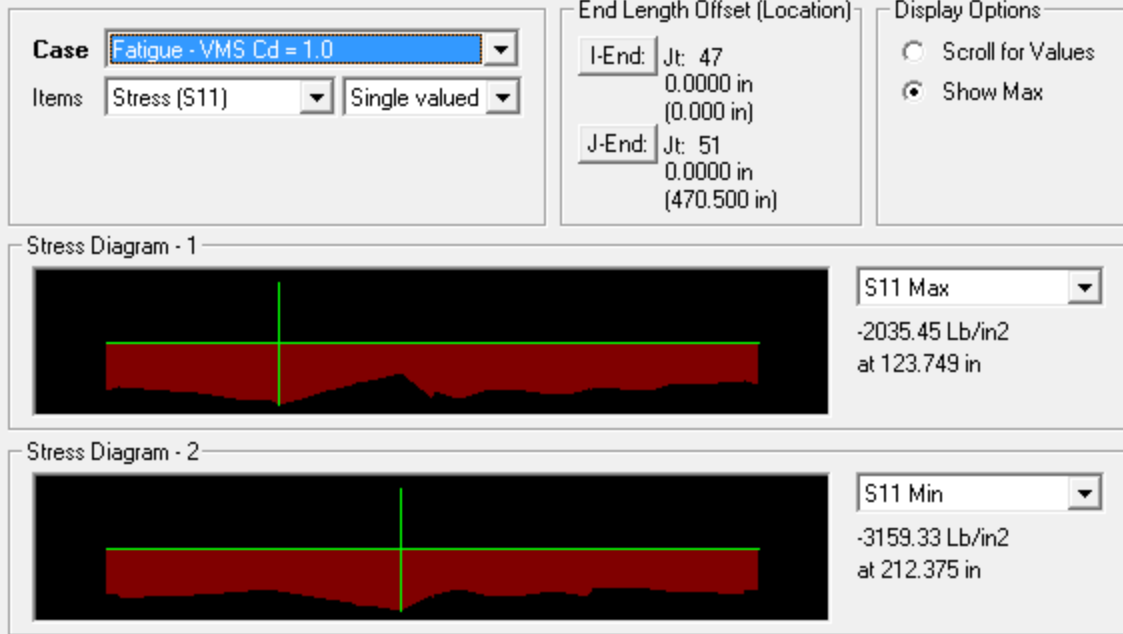
S11 Max
-31957.86 Lb/in2
at 123.749 in

Stress Diagram - 2

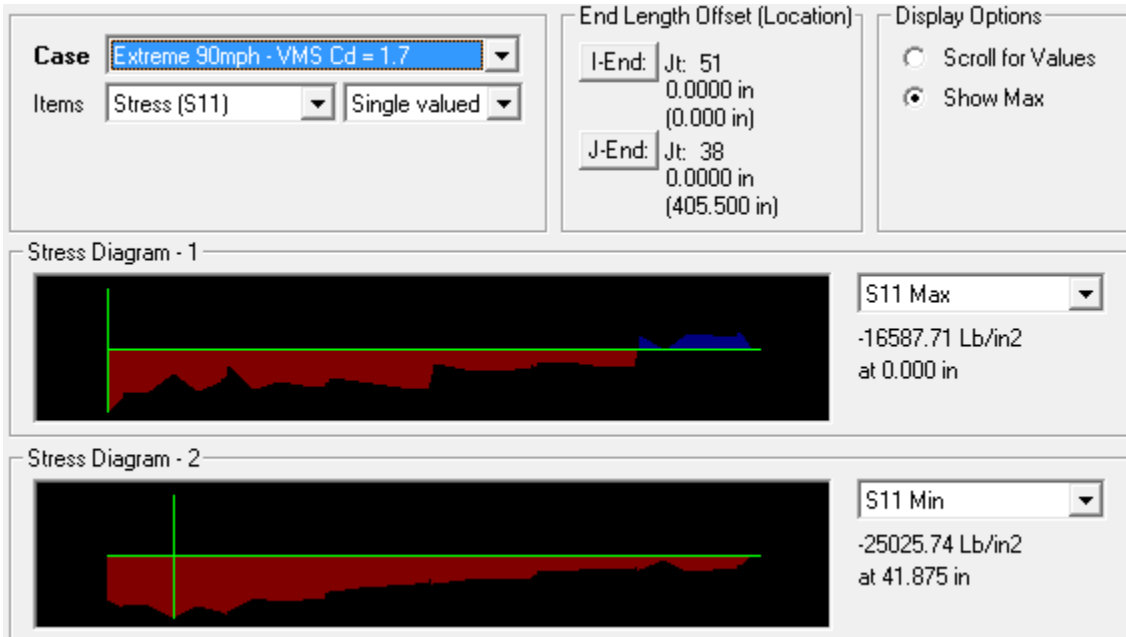


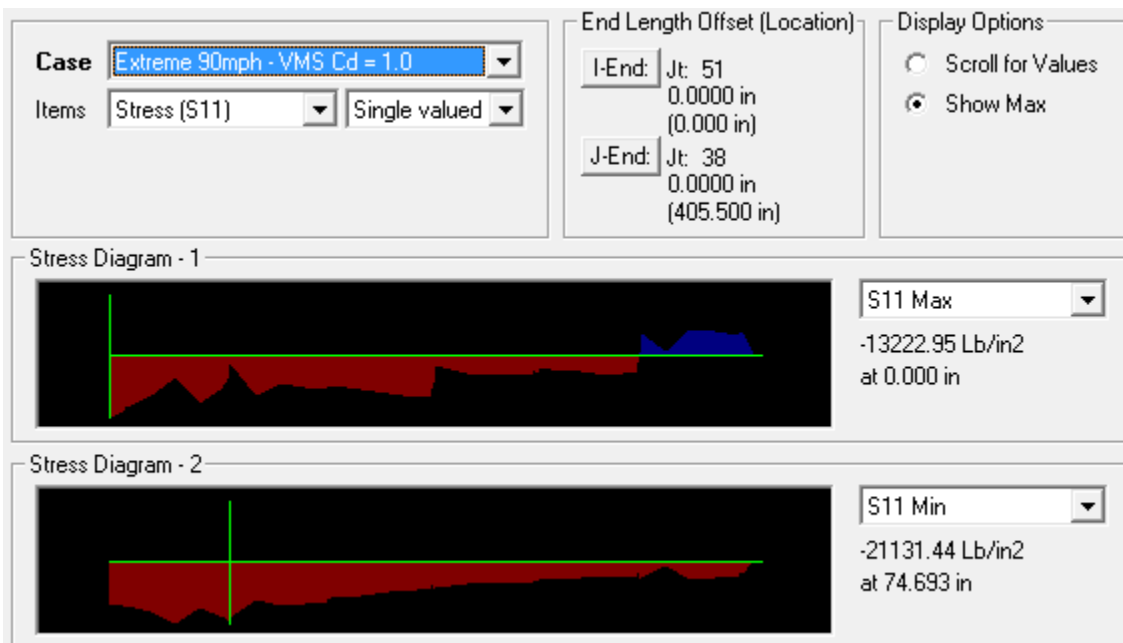
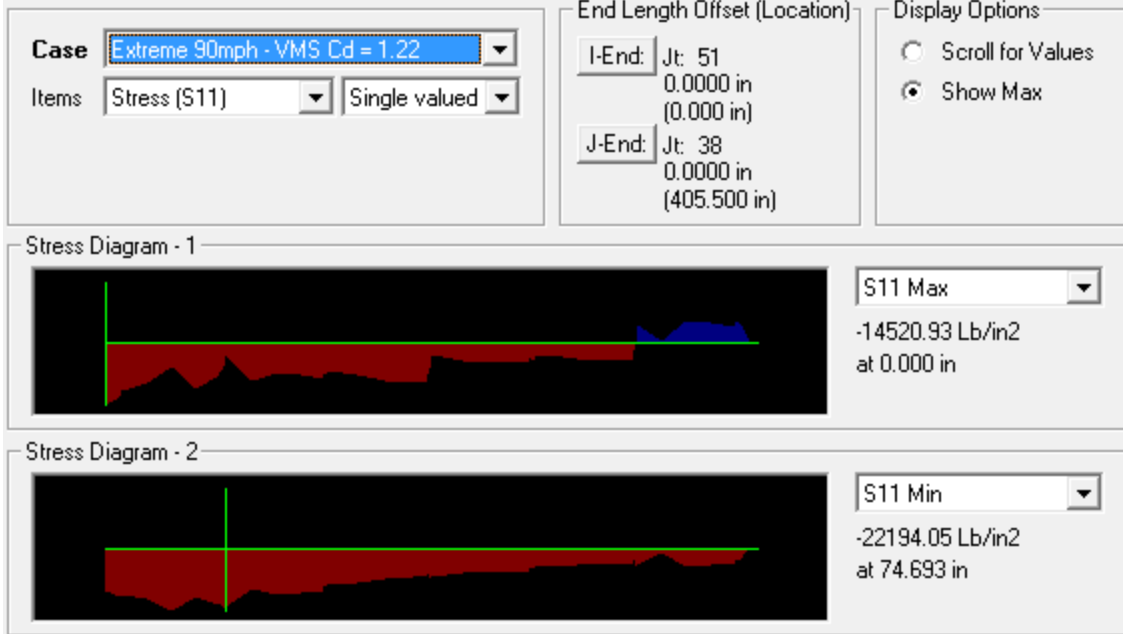
S11 Min
-46045.35 Lb/in2
at 212.375 in

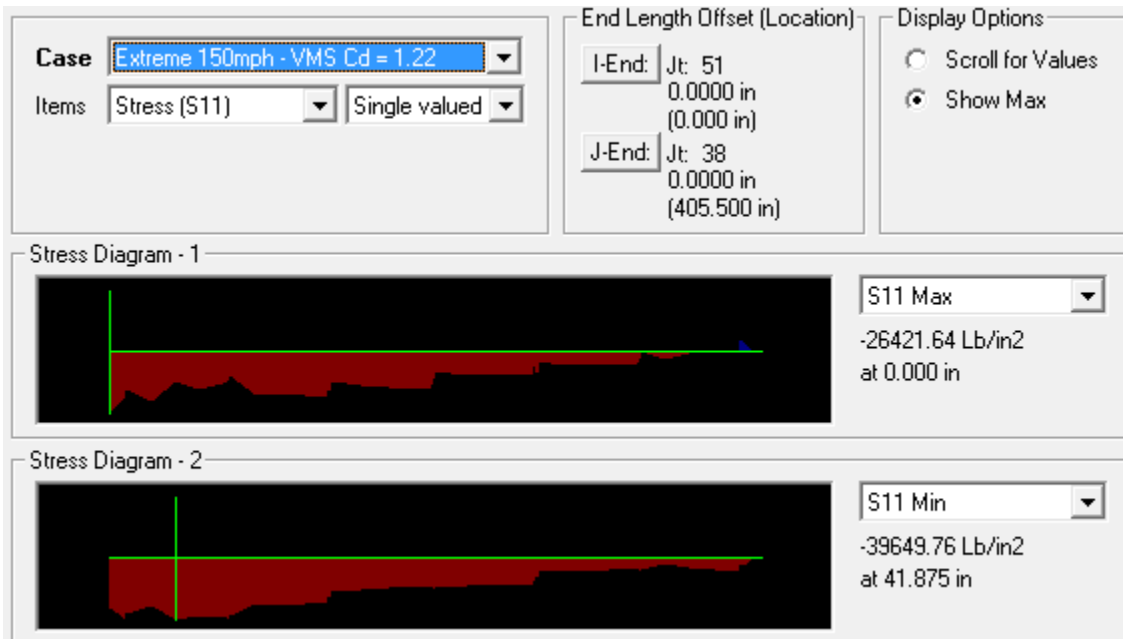
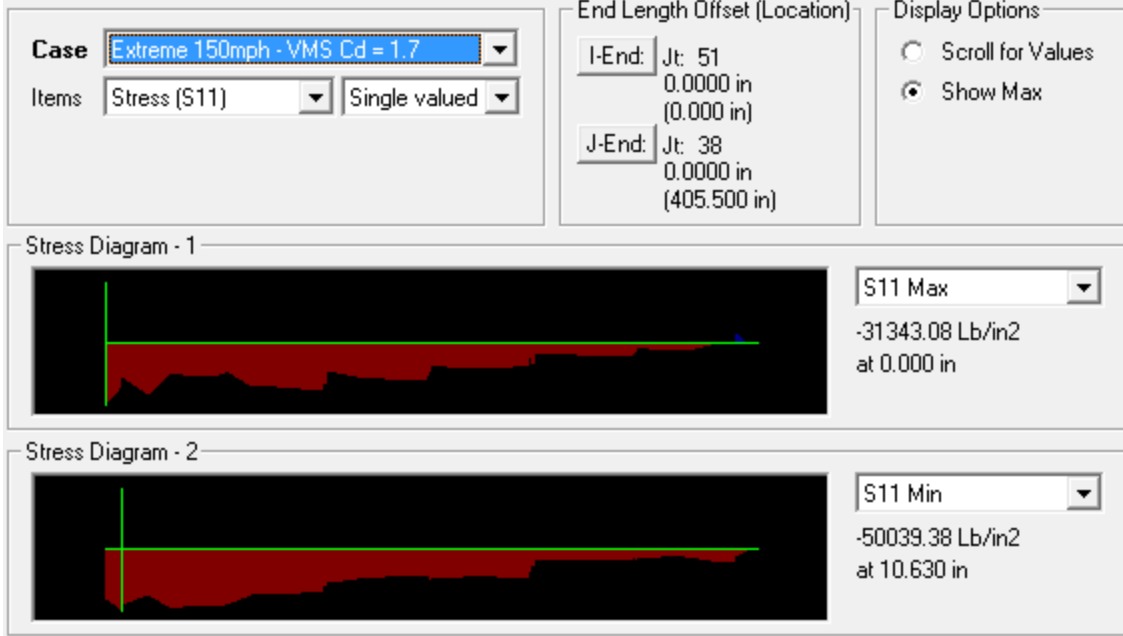


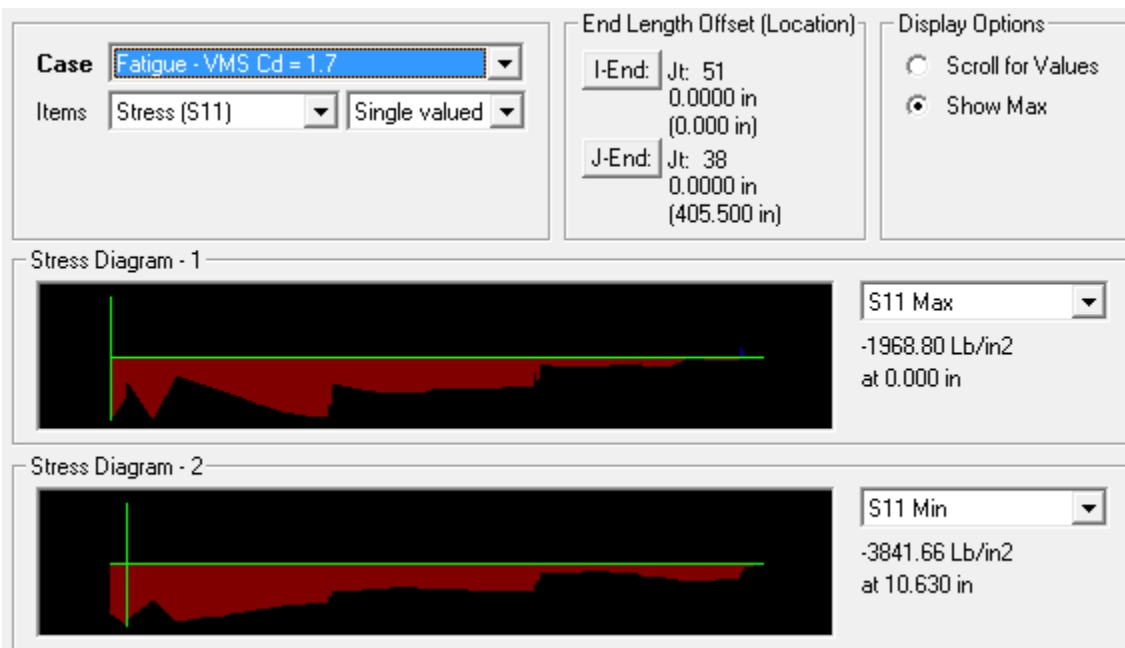
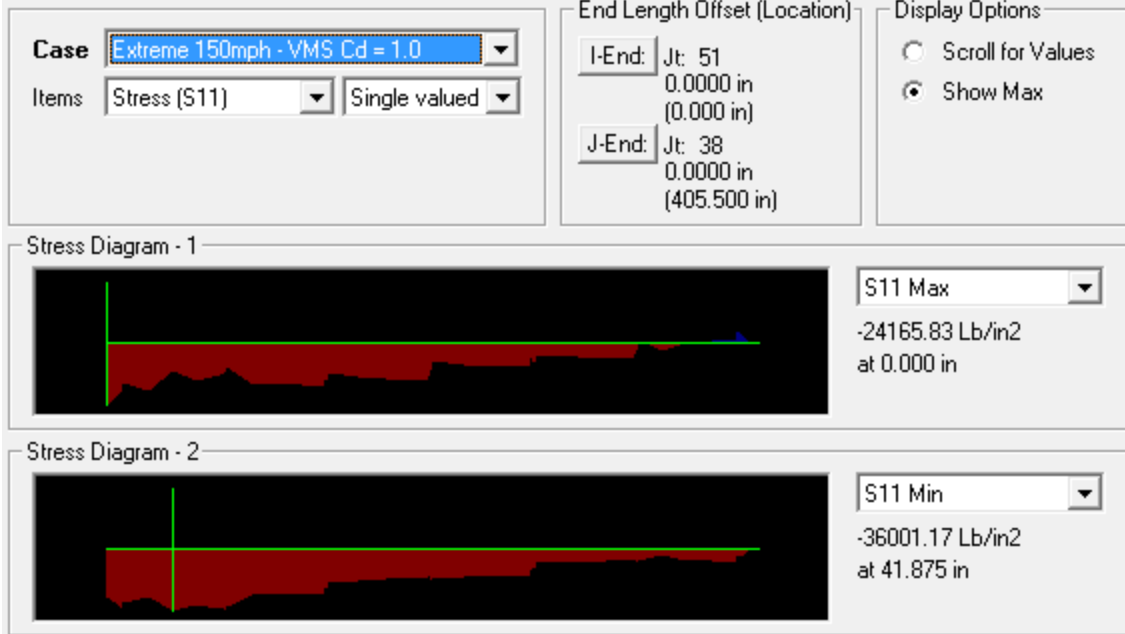


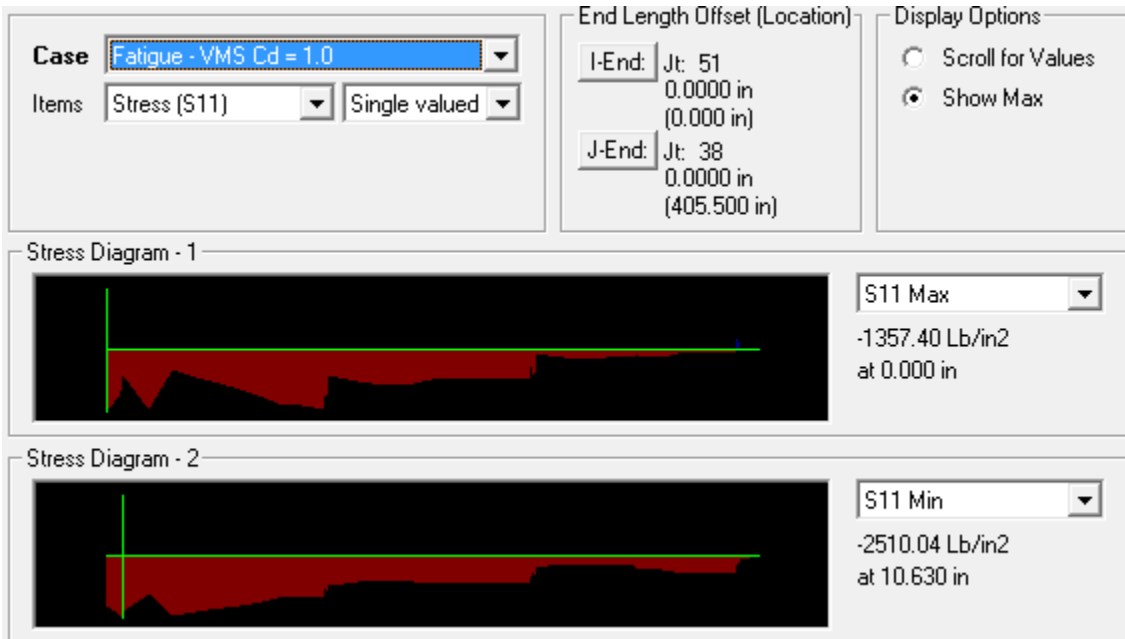
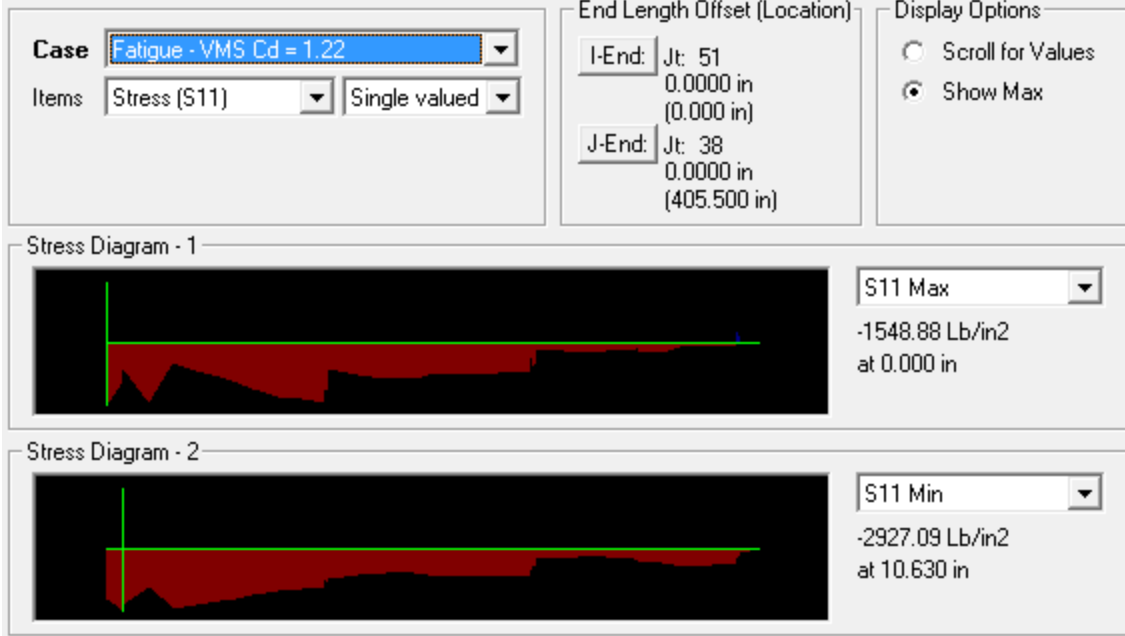
Chord 3d



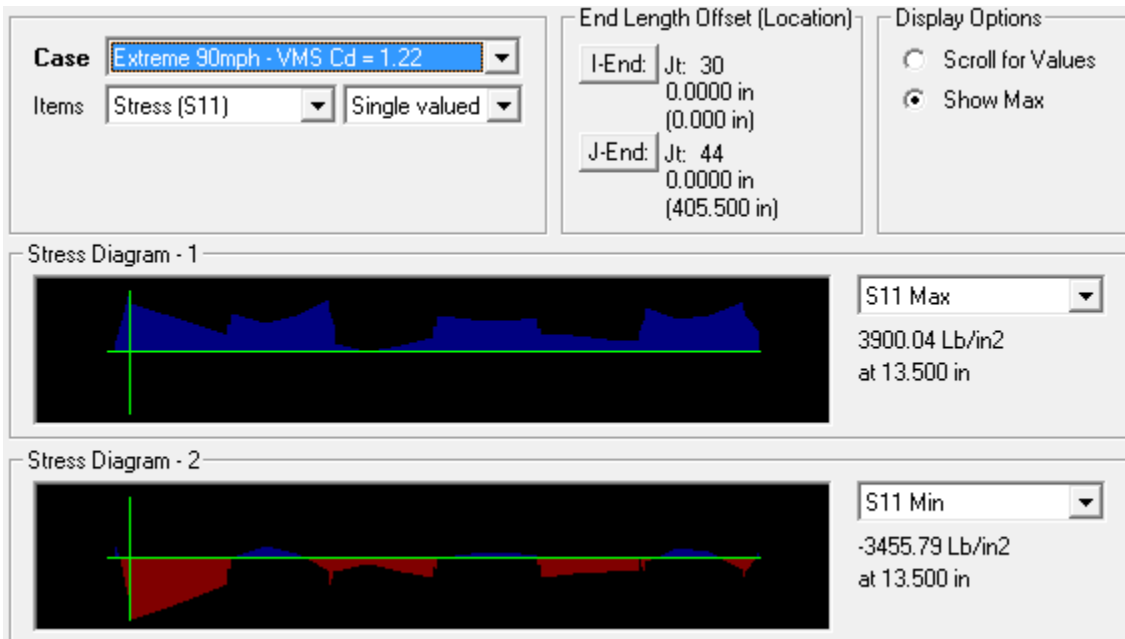
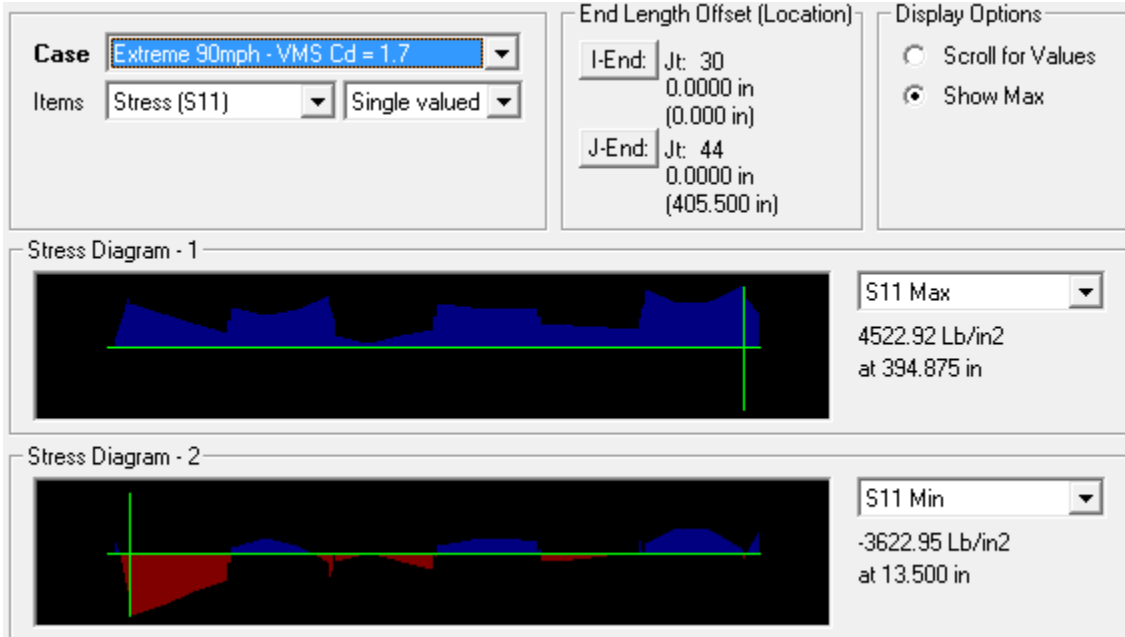


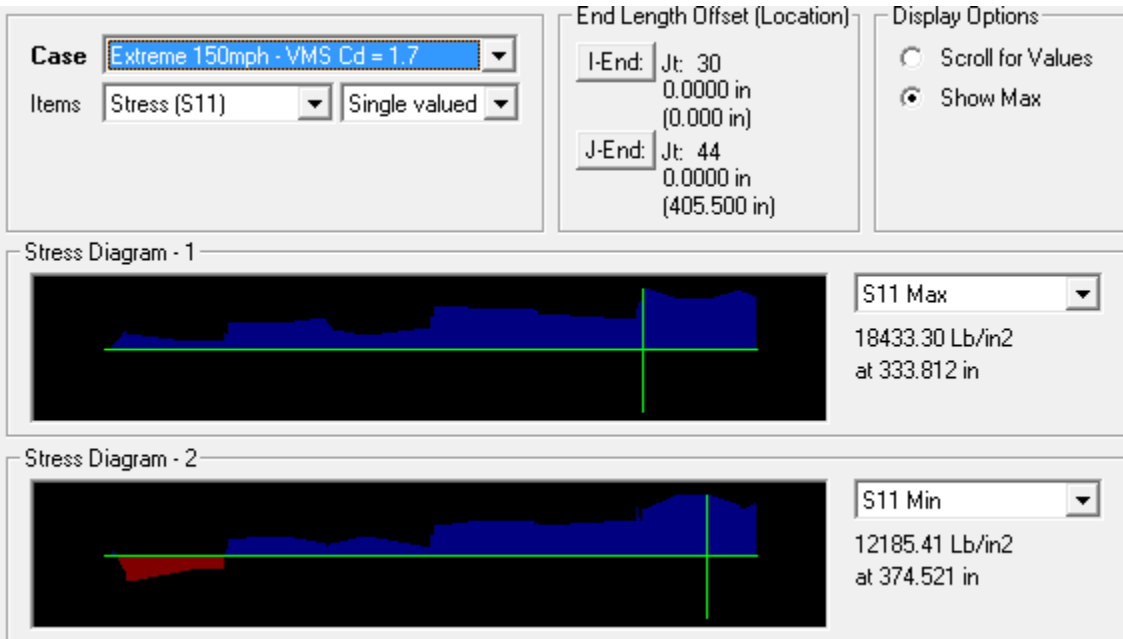
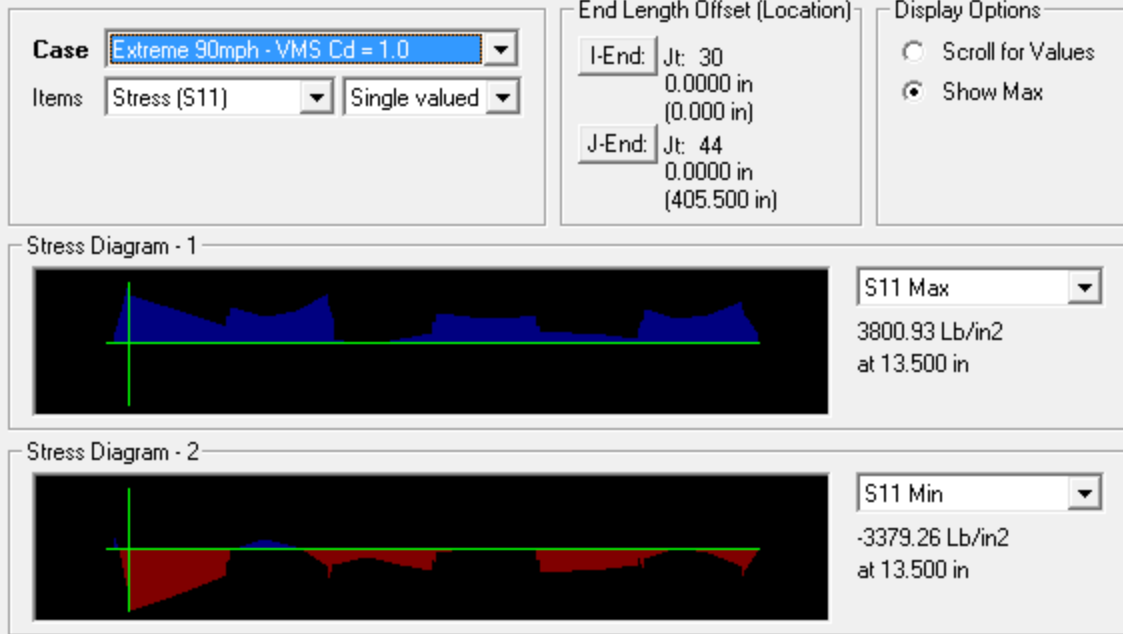


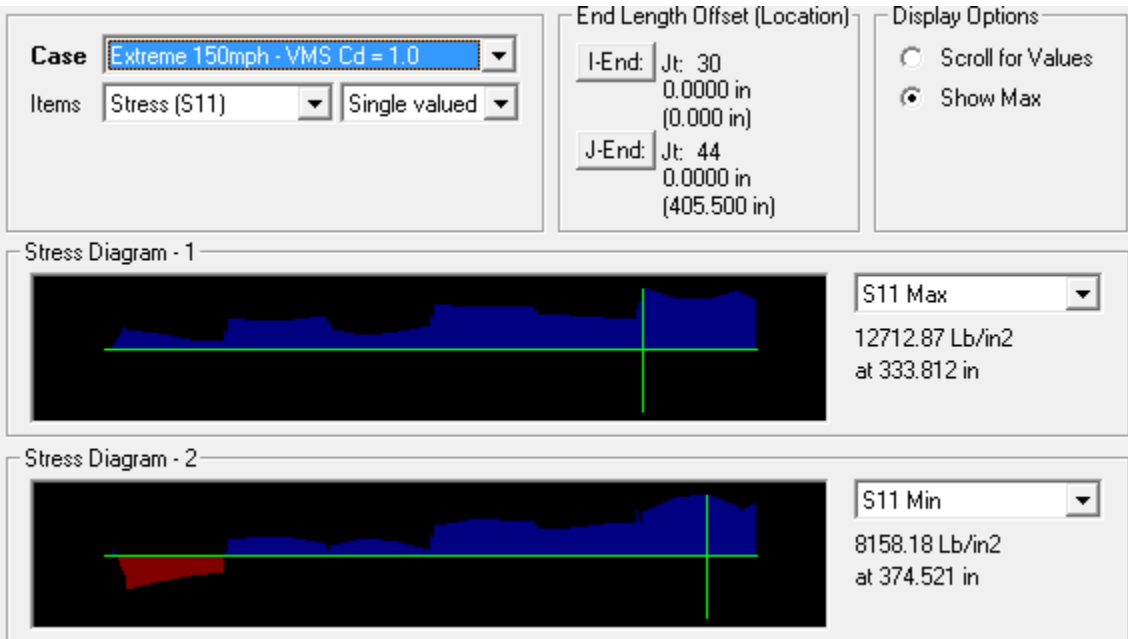
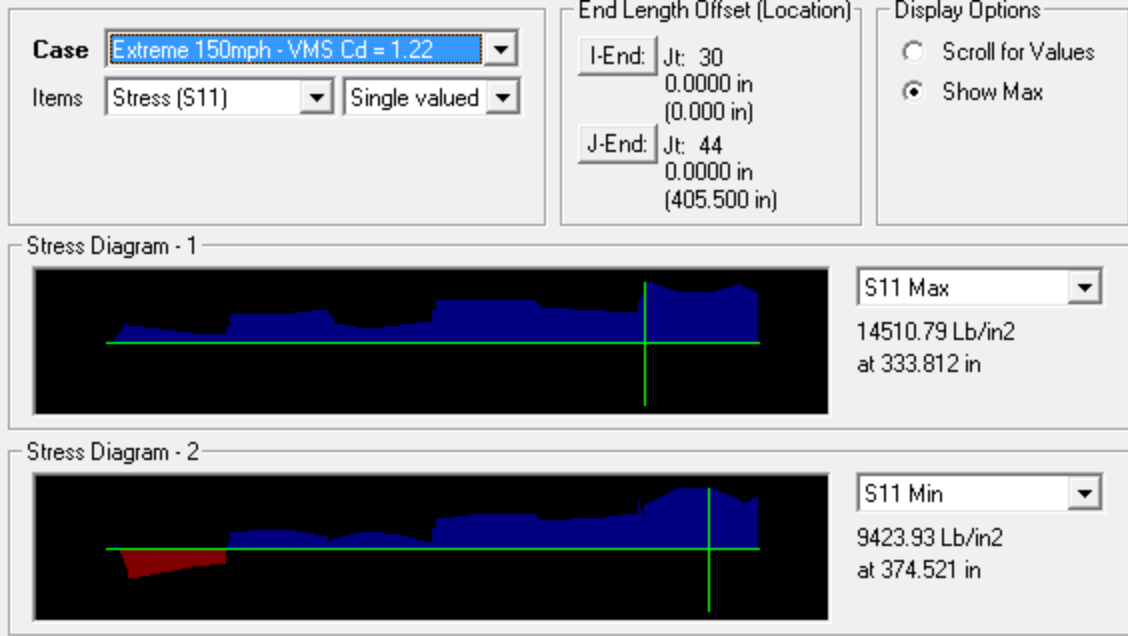


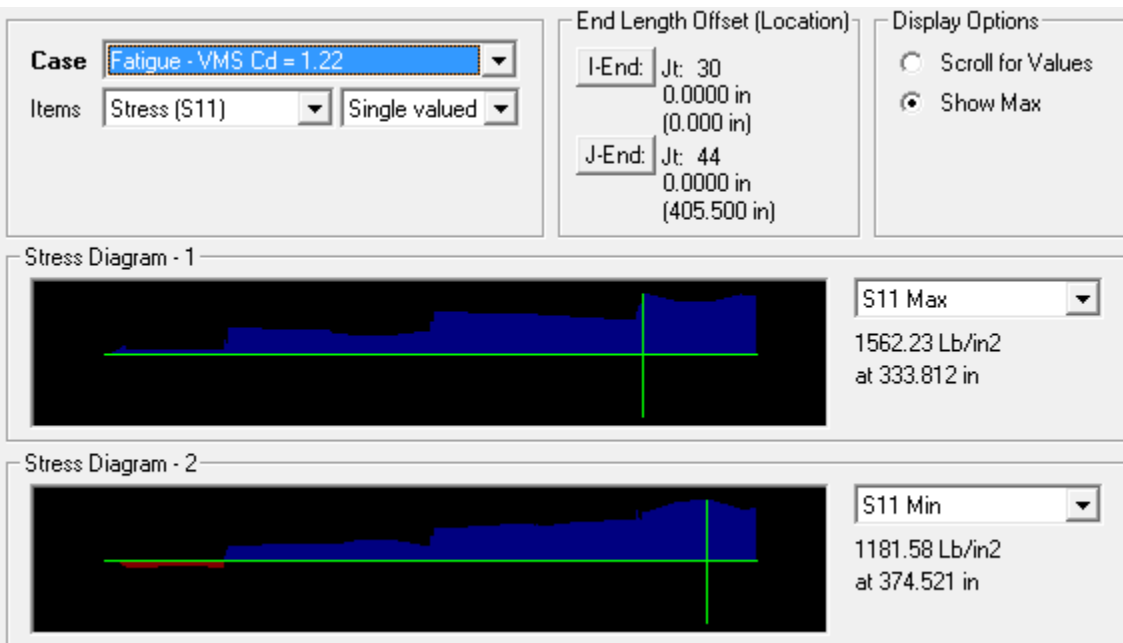
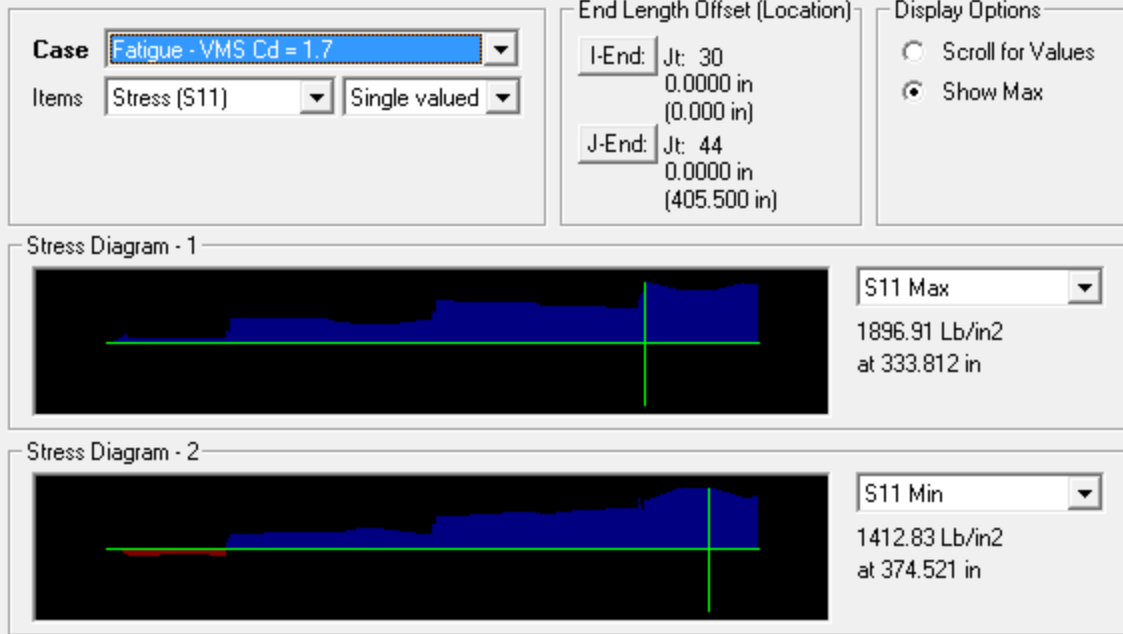


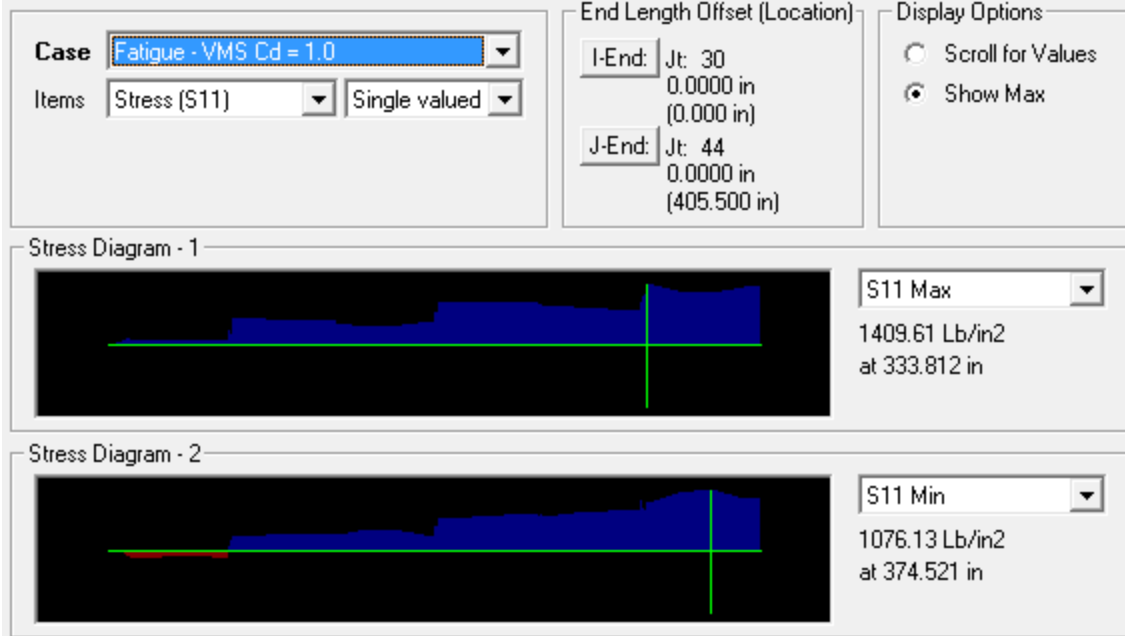
Chord 4a



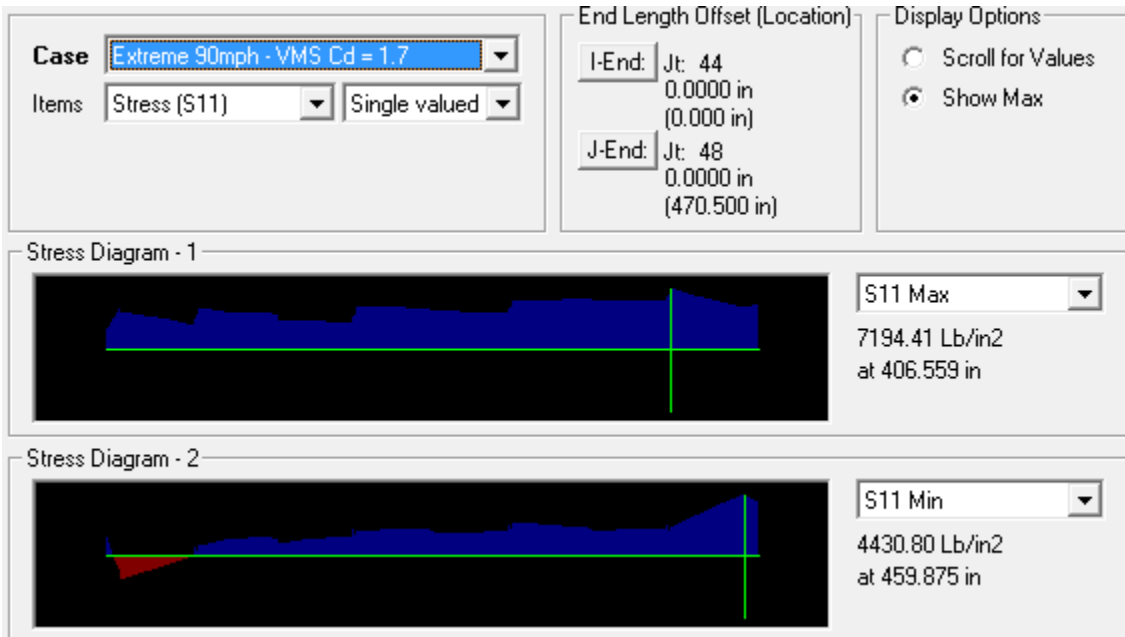








Chord 4b



Case Extreme 90mph - VMS Cd = 1.22 Items Stress (S11) Single valued	End Length Offset (Location) I-End: Jt: 44 0.0000 in (0.000 in) J-End: Jt: 48 0.0000 in (470.500 in)	Display Options <input type="radio"/> Scroll for Values <input checked="" type="radio"/> Show Max
--	---	--

Stress Diagram - 1



S11 Max
 4196.67 Lb/in²
 at 406.559 in

Stress Diagram - 2



S11 Min
 -2198.22 Lb/in²
 at 10.625 in

Case Extreme 90mph - VMS Cd = 1.0 Items Stress (S11) Single valued	End Length Offset (Location) I-End: Jt: 44 0.0000 in (0.000 in) J-End: Jt: 48 0.0000 in (470.500 in)	Display Options <input type="radio"/> Scroll for Values <input checked="" type="radio"/> Show Max
---	---	--

Stress Diagram - 1

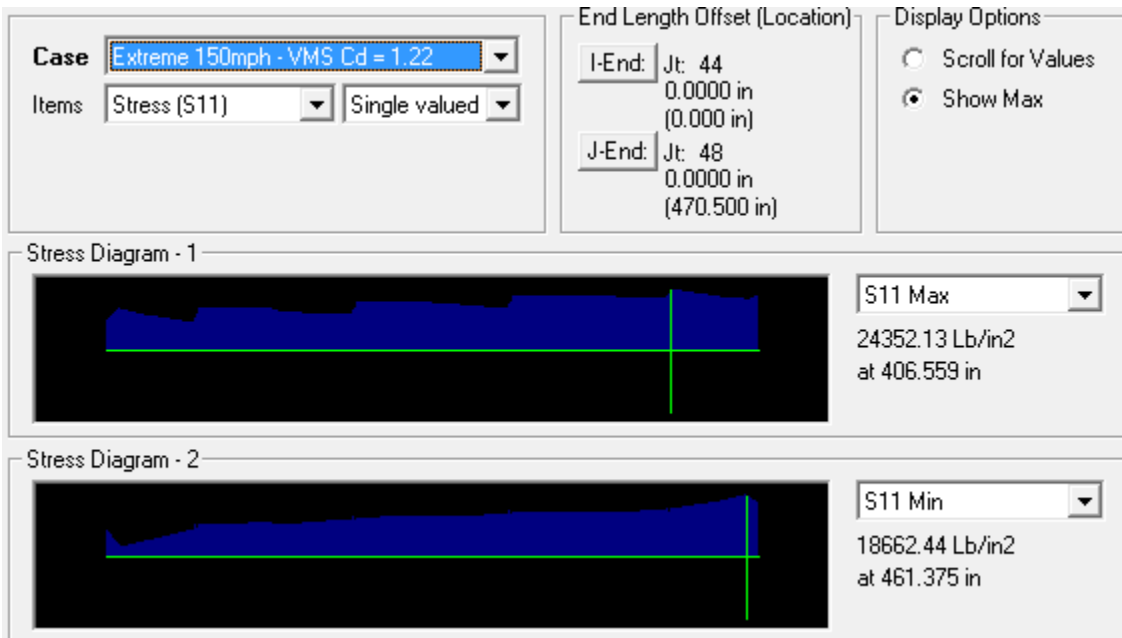
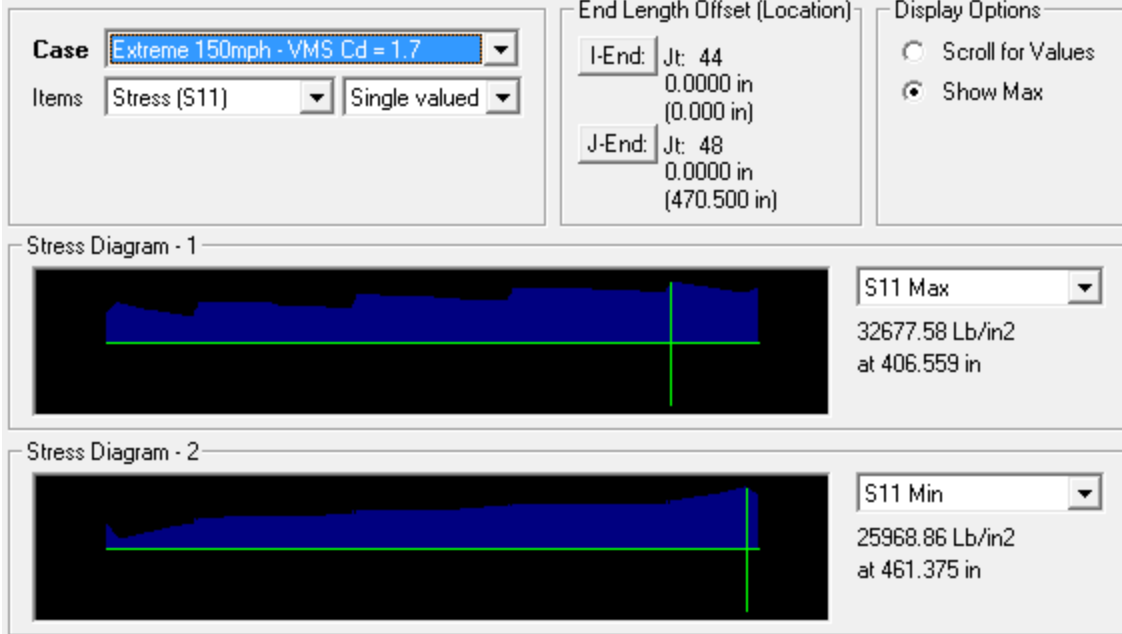


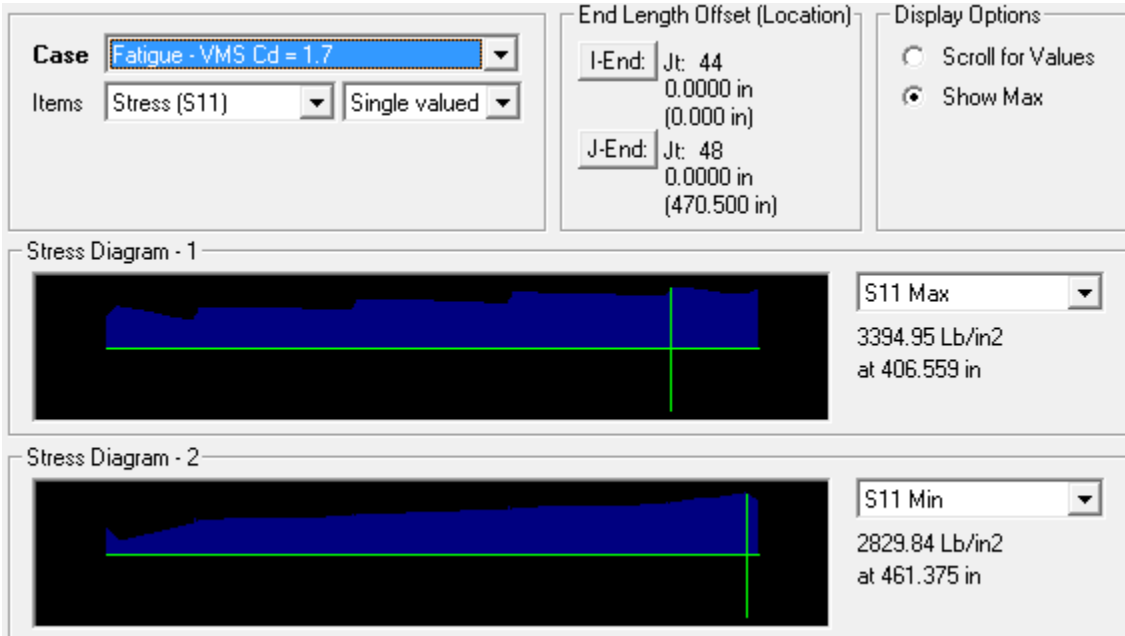
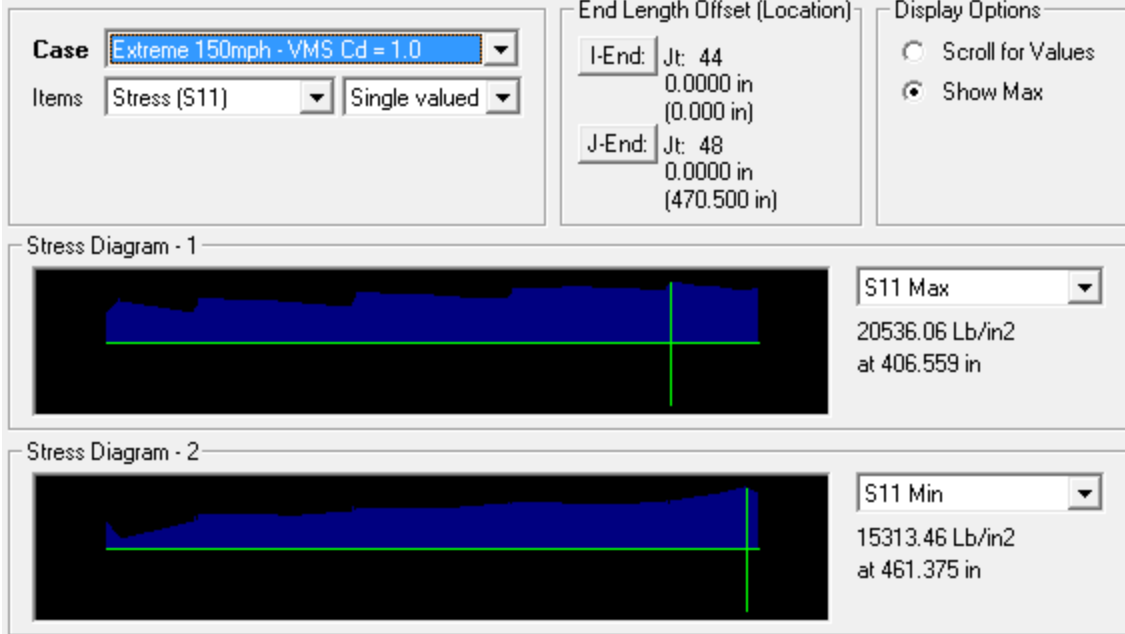
S11 Max
 2834.27 Lb/in²
 at 406.559 in

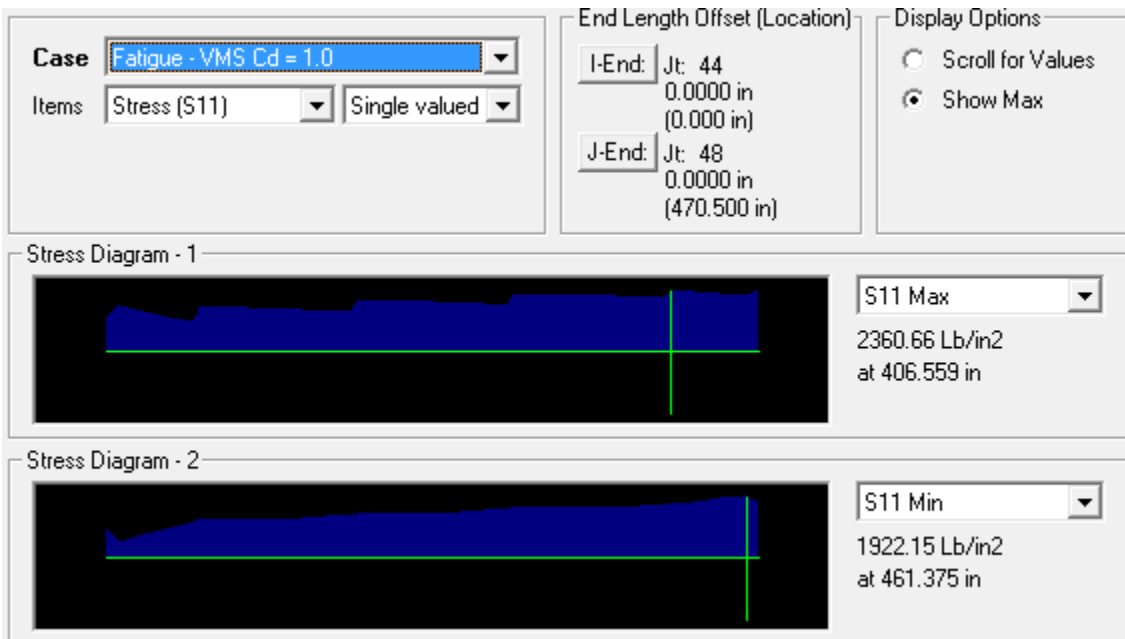
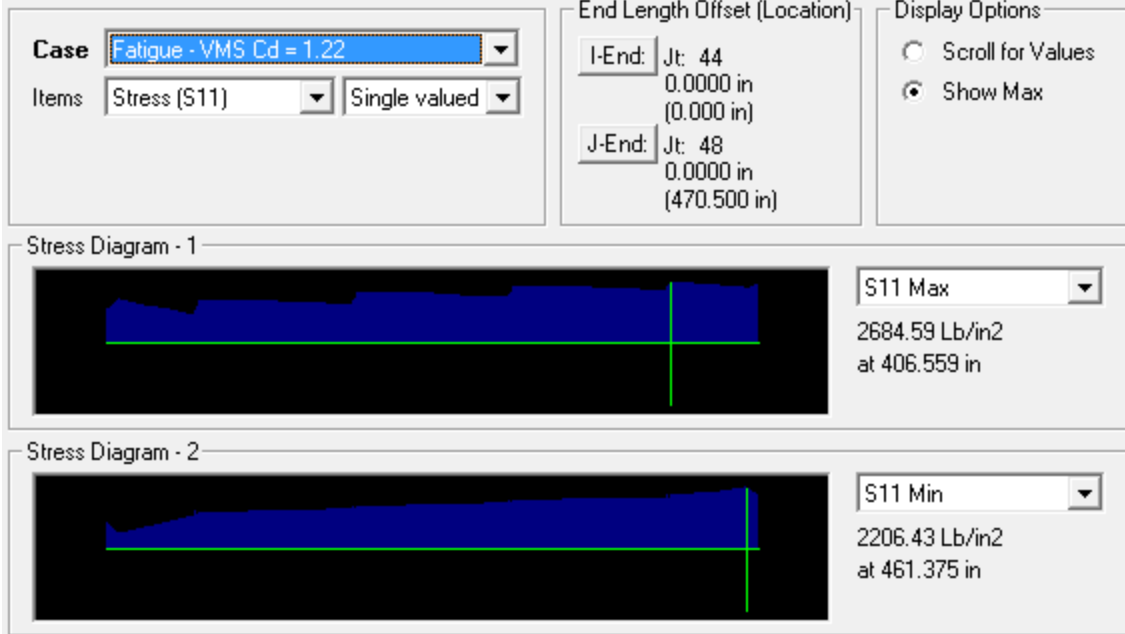
Stress Diagram - 2



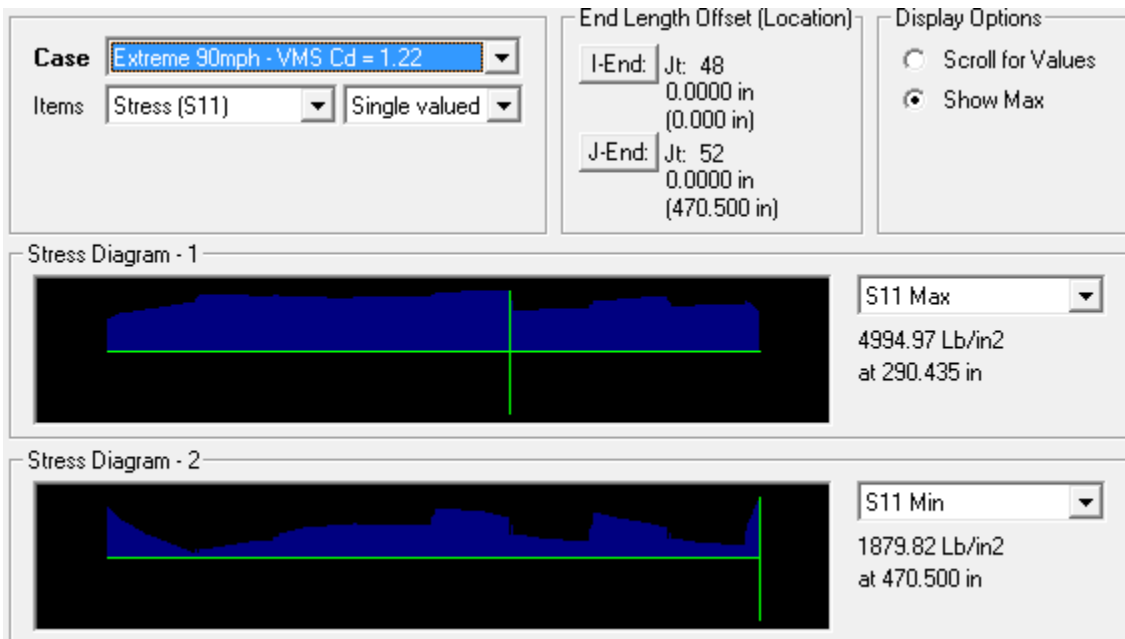
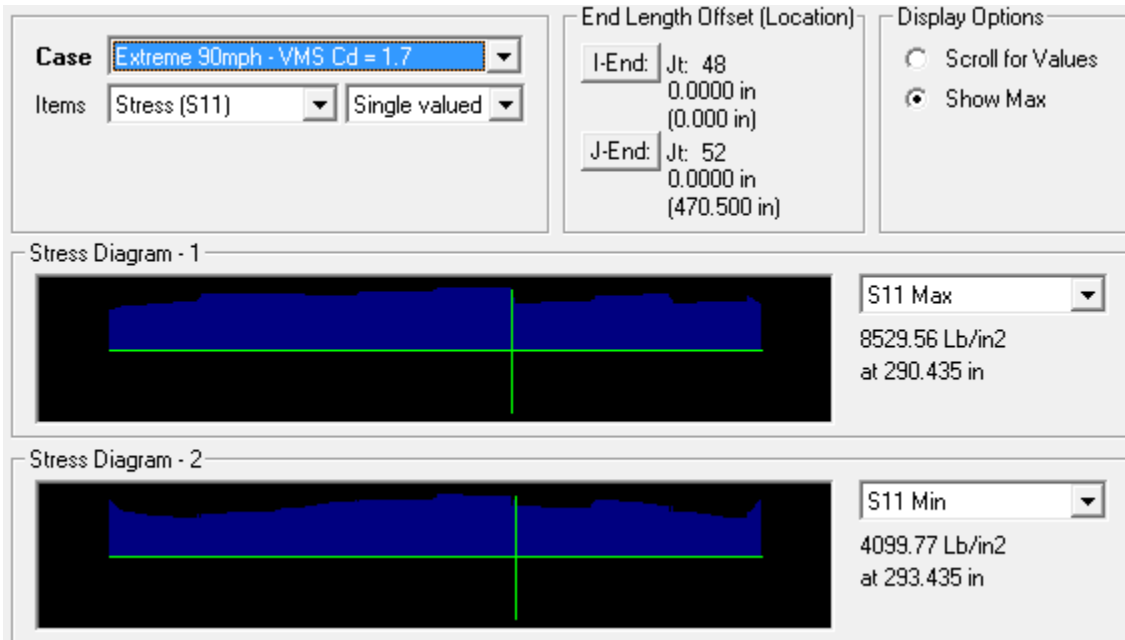
S11 Min
 -2447.62 Lb/in²
 at 10.625 in



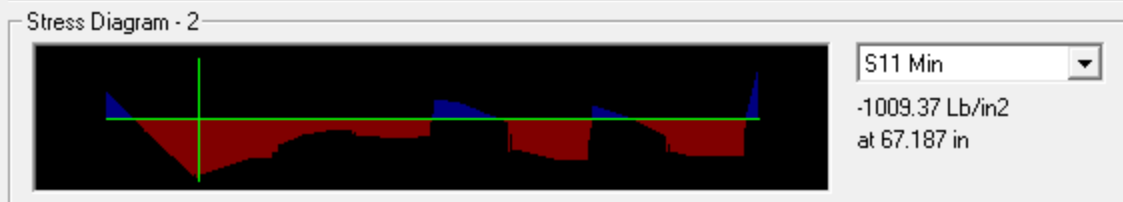
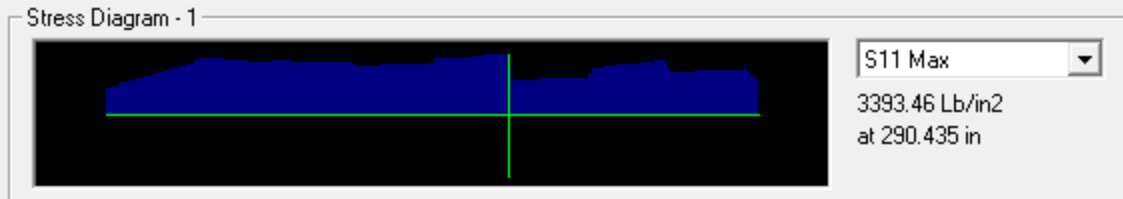




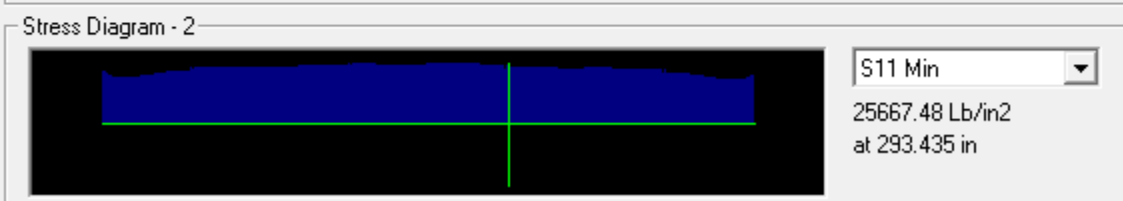
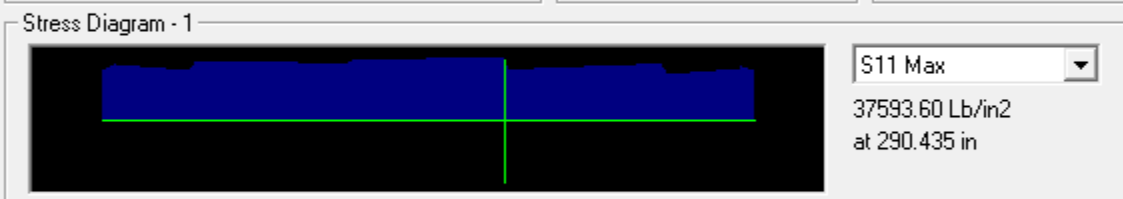
Chord 4c



Case Extreme 90mph - VMS Cd = 1.0 Items Stress (S11) Single valued	End Length Offset (Location) I-End: Jt: 48 0.0000 in (0.000 in) J-End: Jt: 52 0.0000 in (470.500 in)	Display Options <input type="radio"/> Scroll for Values <input checked="" type="radio"/> Show Max
---	---	--

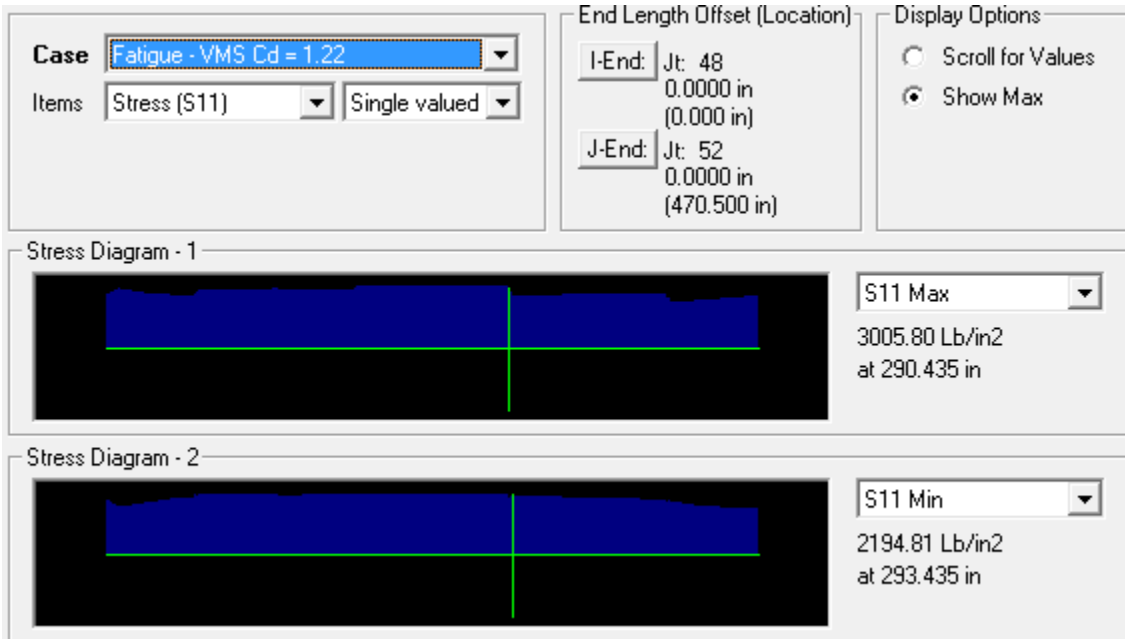
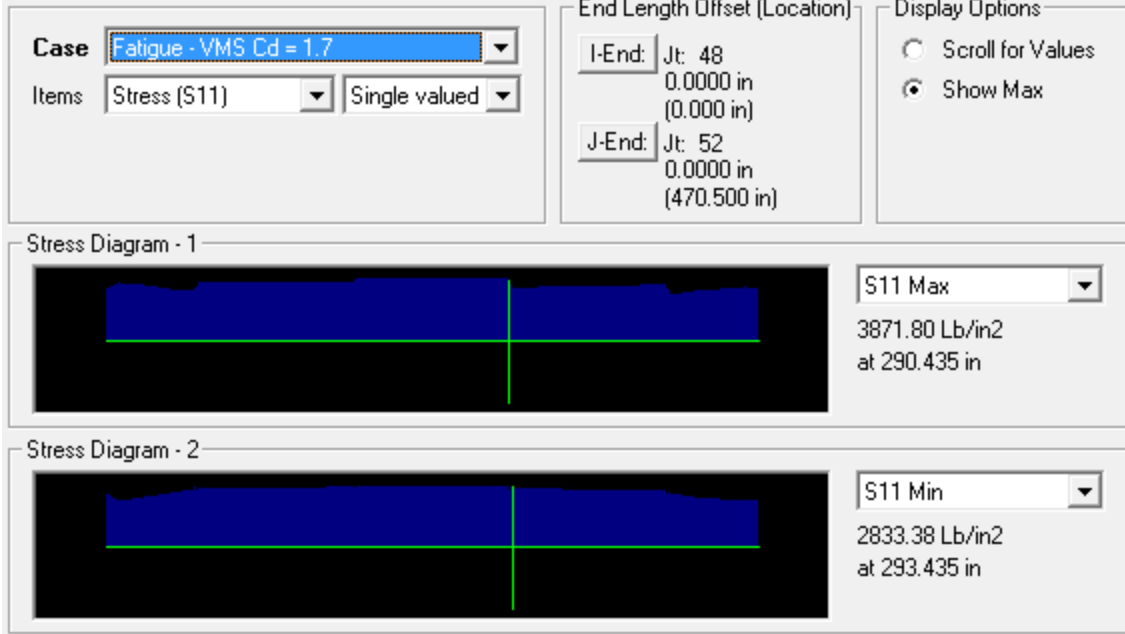


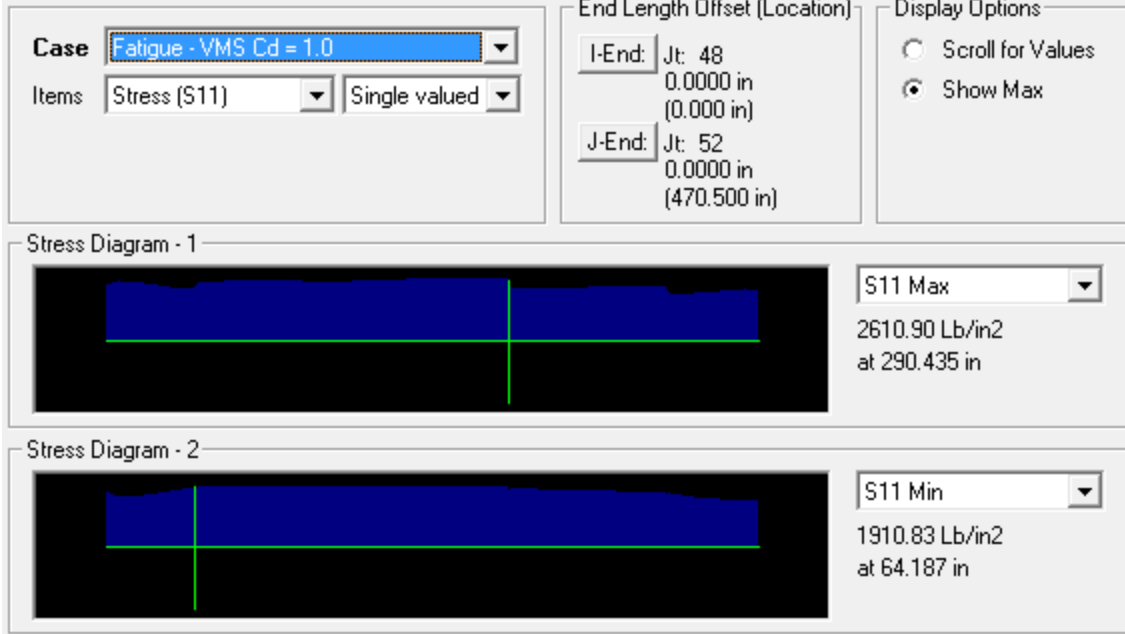
Case Extreme 150mph - VMS Cd = 1.7 Items Stress (S11) Single valued	End Length Offset (Location) I-End: Jt: 48 0.0000 in (0.000 in) J-End: Jt: 52 0.0000 in (470.500 in)	Display Options <input type="radio"/> Scroll for Values <input checked="" type="radio"/> Show Max
--	---	--



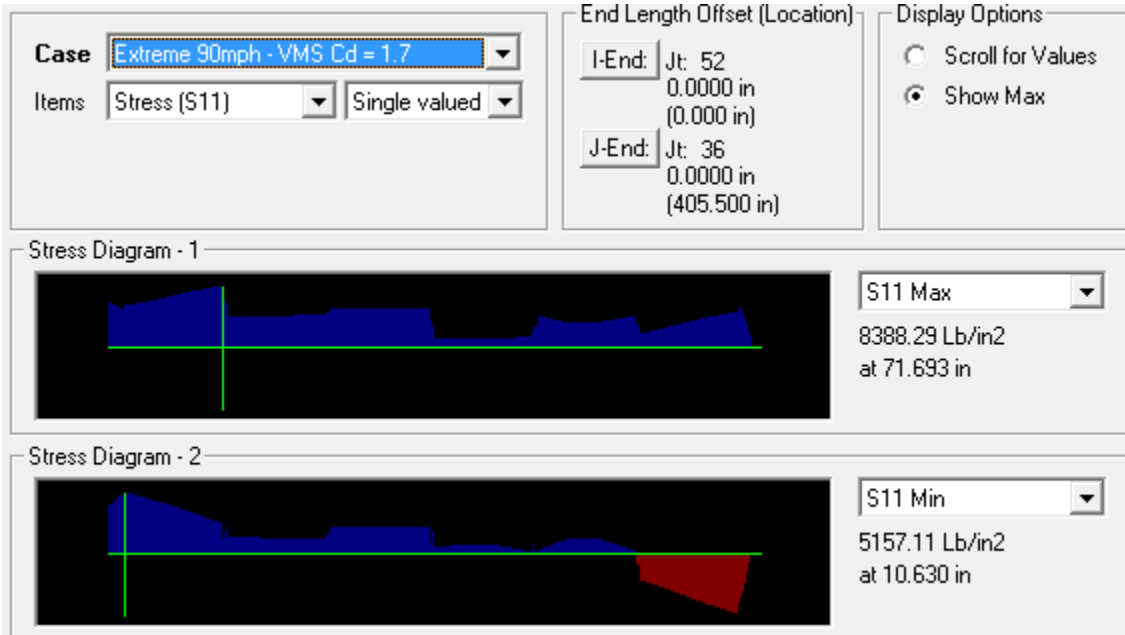
Case Extreme 150mph - VMS Cd = 1.22 Items Stress (S11) Single valued	End Length Offset (Location) I-End: Jt: 48 0.0000 in (0.000 in) J-End: Jt: 52 0.0000 in (470.500 in)	Display Options <input type="radio"/> Scroll for Values <input checked="" type="radio"/> Show Max
Stress Diagram - 1 		
Stress Diagram - 2 		

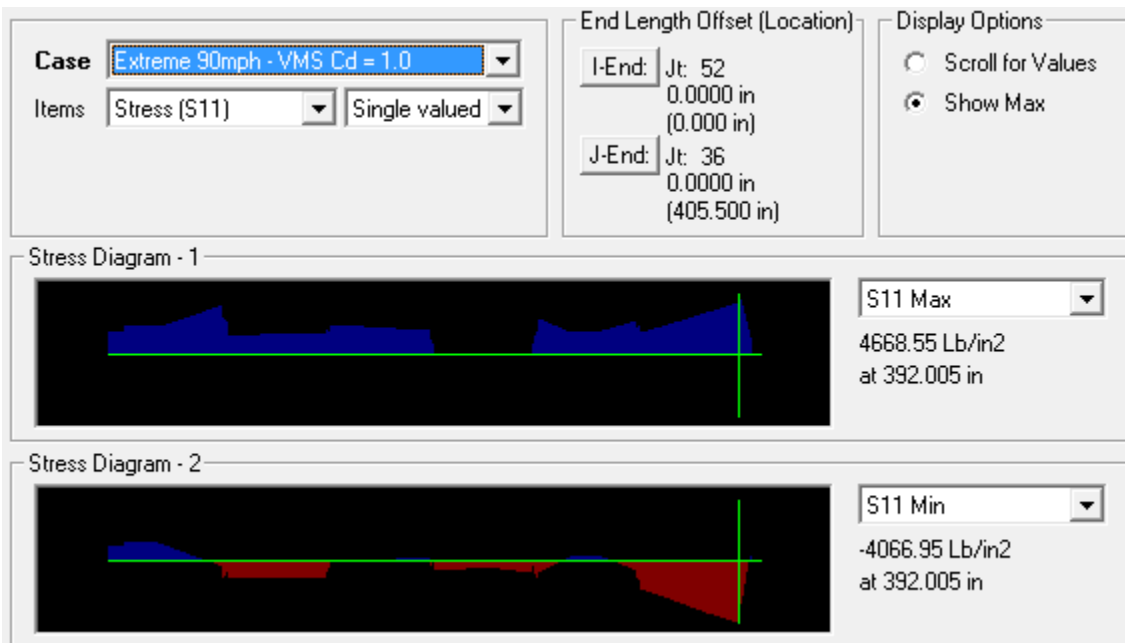
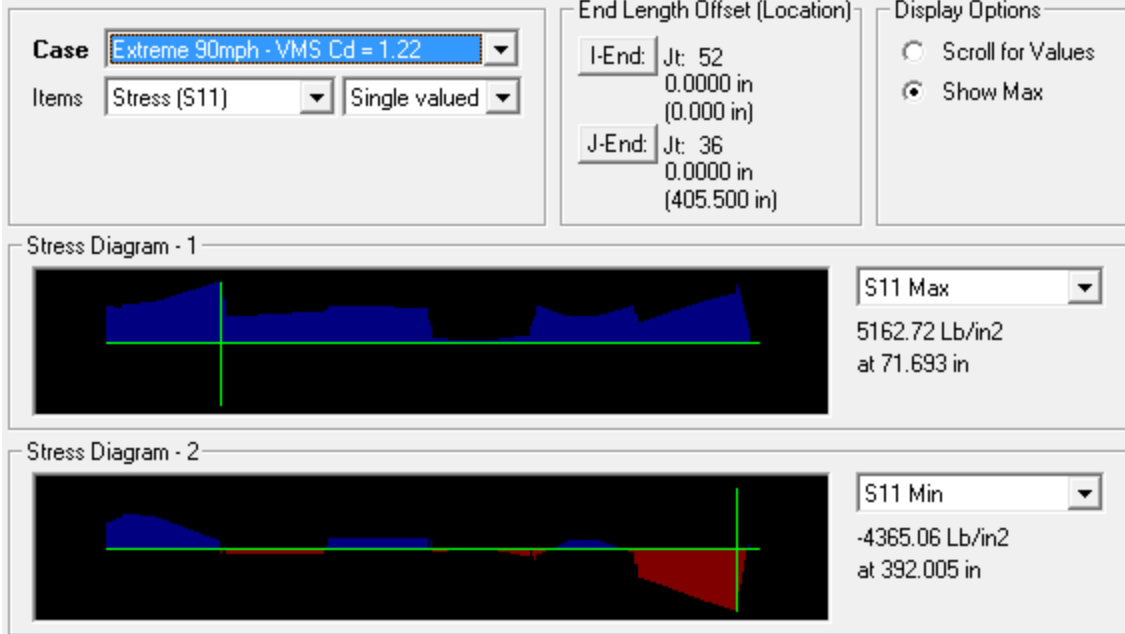
Case Extreme 150mph - VMS Cd = 1.0 Items Stress (S11) Single valued	End Length Offset (Location) I-End: Jt: 48 0.0000 in (0.000 in) J-End: Jt: 52 0.0000 in (470.500 in)	Display Options <input type="radio"/> Scroll for Values <input checked="" type="radio"/> Show Max
Stress Diagram - 1 		
Stress Diagram - 2 		





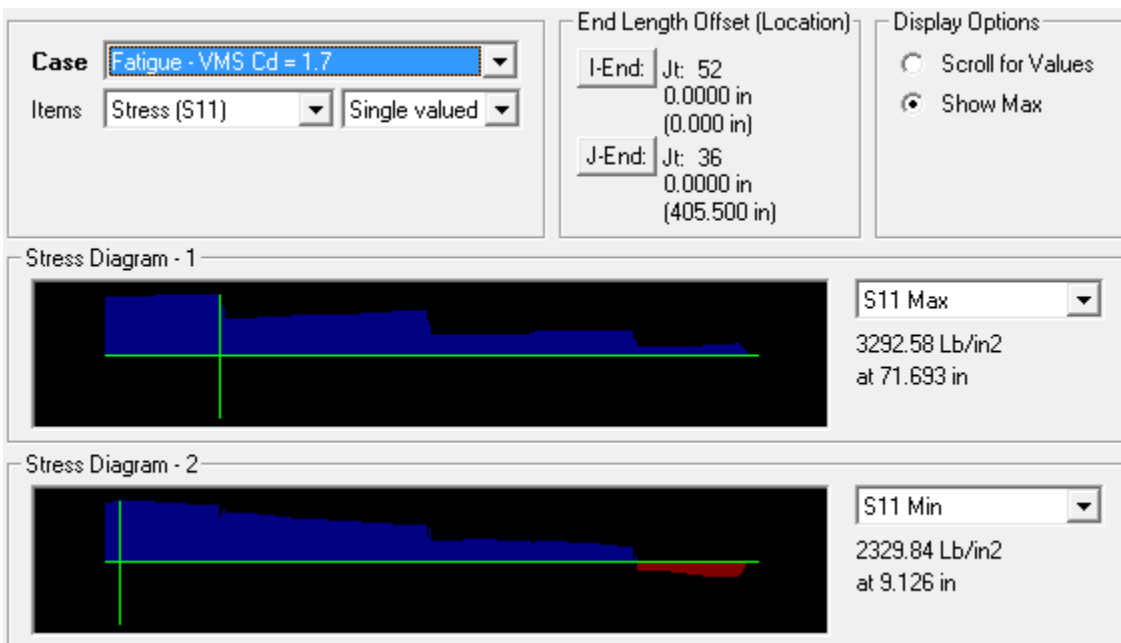
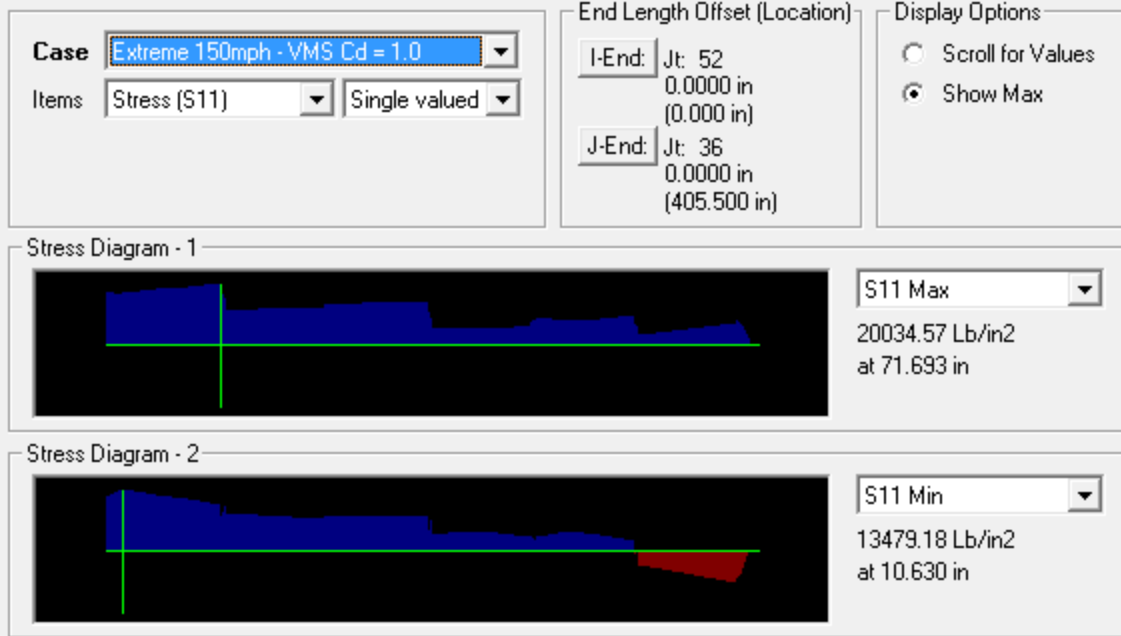
Chord 4d



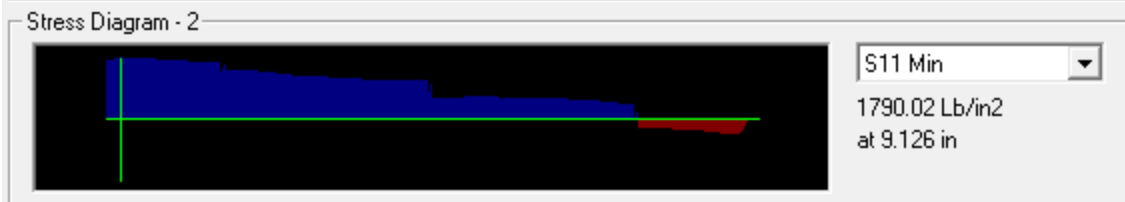
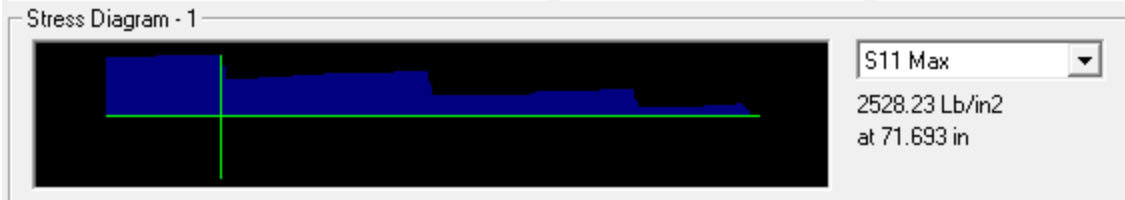


Case Extreme 150mph - VMS Cd = 1.7 Items Stress (S11) Single valued	End Length Offset (Location) I-End: Jt: 52 0.0000 in (0.000 in) J-End: Jt: 36 0.0000 in (405.500 in)	Display Options <input type="radio"/> Scroll for Values <input checked="" type="radio"/> Show Max
Stress Diagram - 1 		
Stress Diagram - 2 		

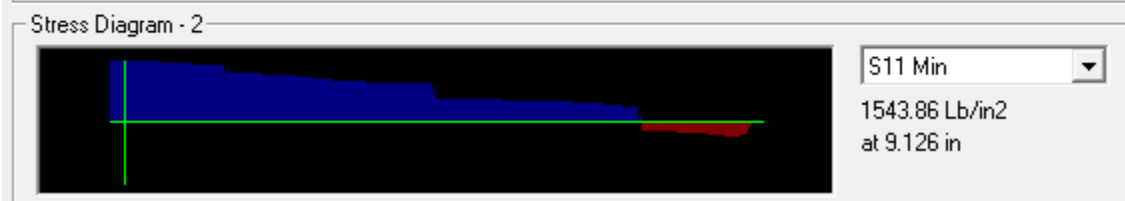
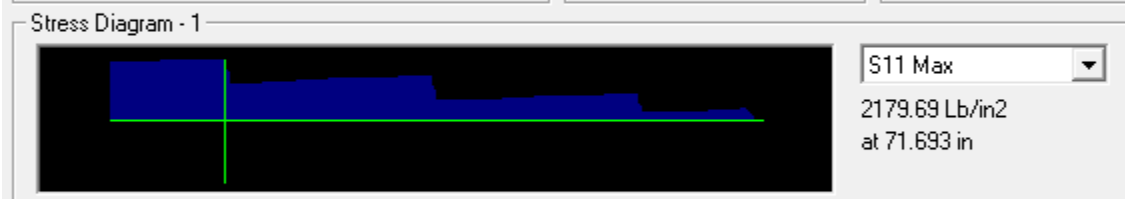
Case Extreme 150mph - VMS Cd = 1.22 Items Stress (S11) Single valued	End Length Offset (Location) I-End: Jt: 52 0.0000 in (0.000 in) J-End: Jt: 36 0.0000 in (405.500 in)	Display Options <input type="radio"/> Scroll for Values <input checked="" type="radio"/> Show Max
Stress Diagram - 1 		
Stress Diagram - 2 		



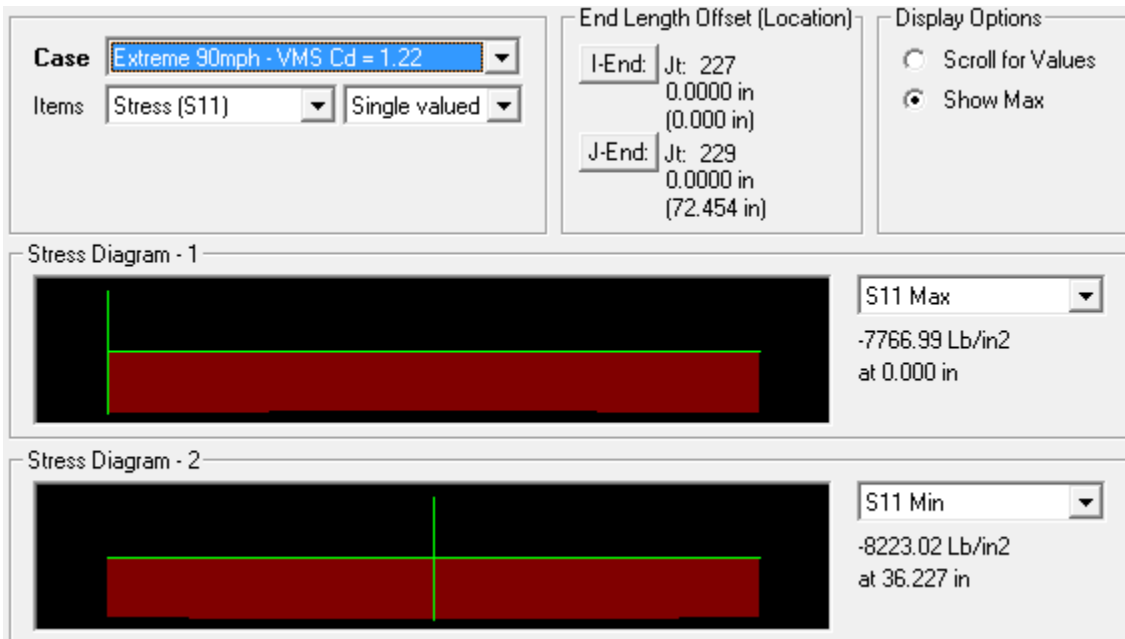
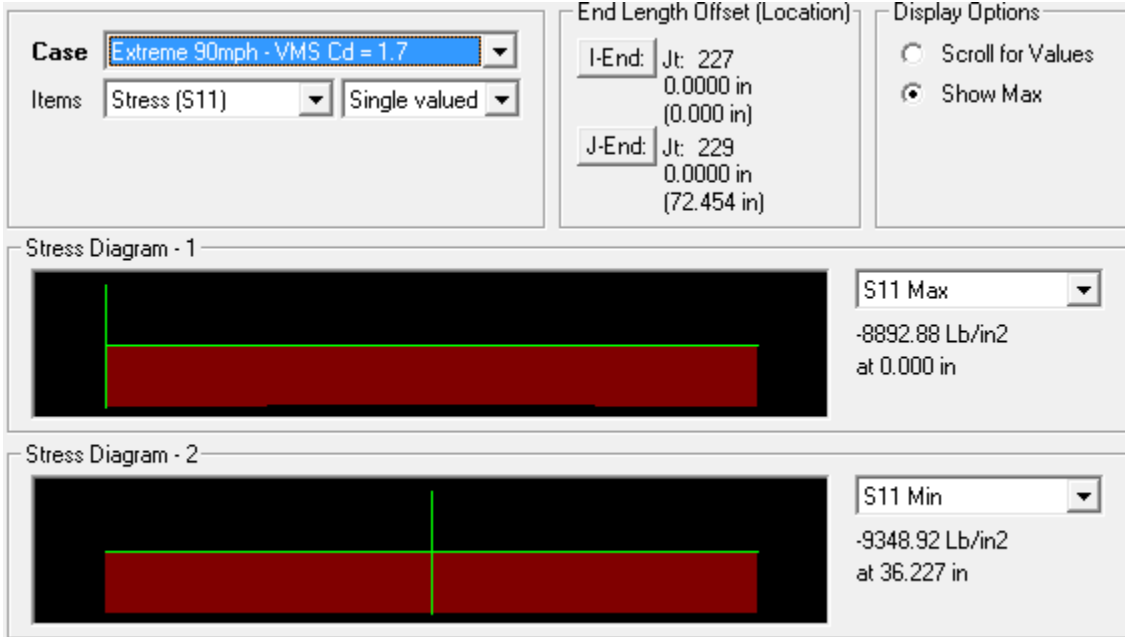
Case Fatigue - VMS Cd = 1.22 Items Stress (S11) Single valued	End Length Offset (Location) I-End: Jt: 52 0.0000 in (0.000 in) J-End: Jt: 36 0.0000 in (405.500 in)	Display Options <input type="radio"/> Scroll for Values <input checked="" type="radio"/> Show Max
--	---	--

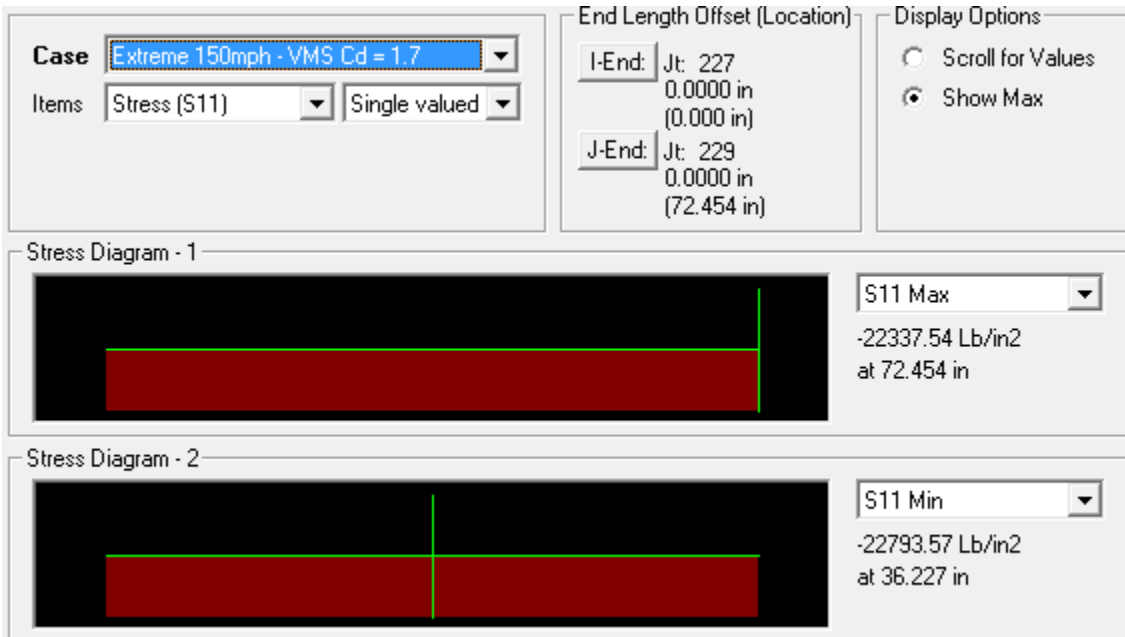
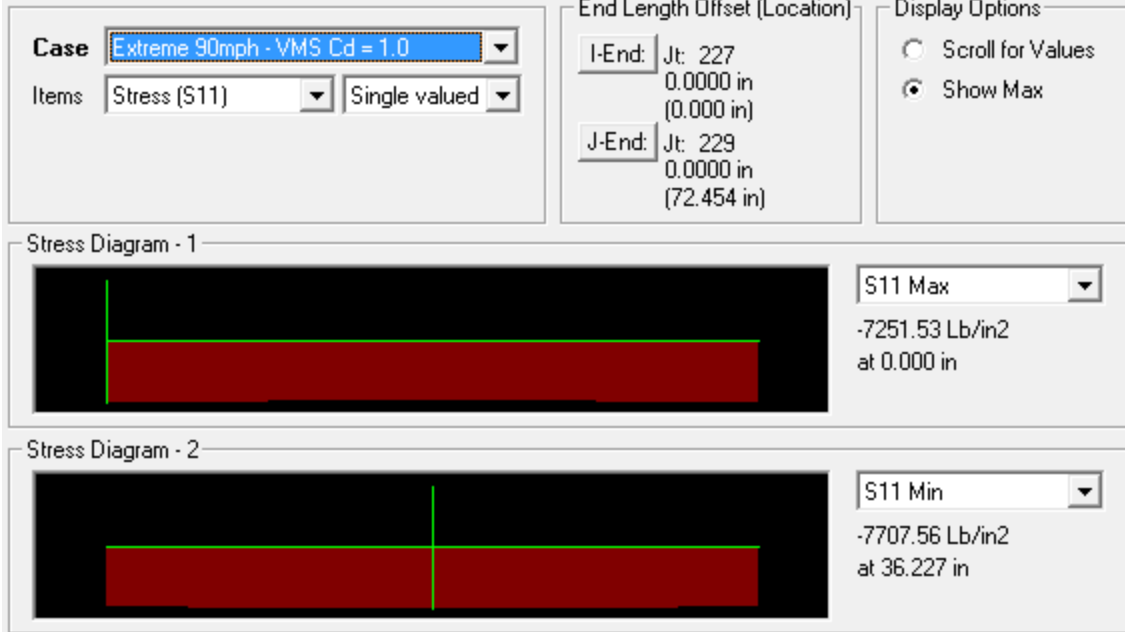


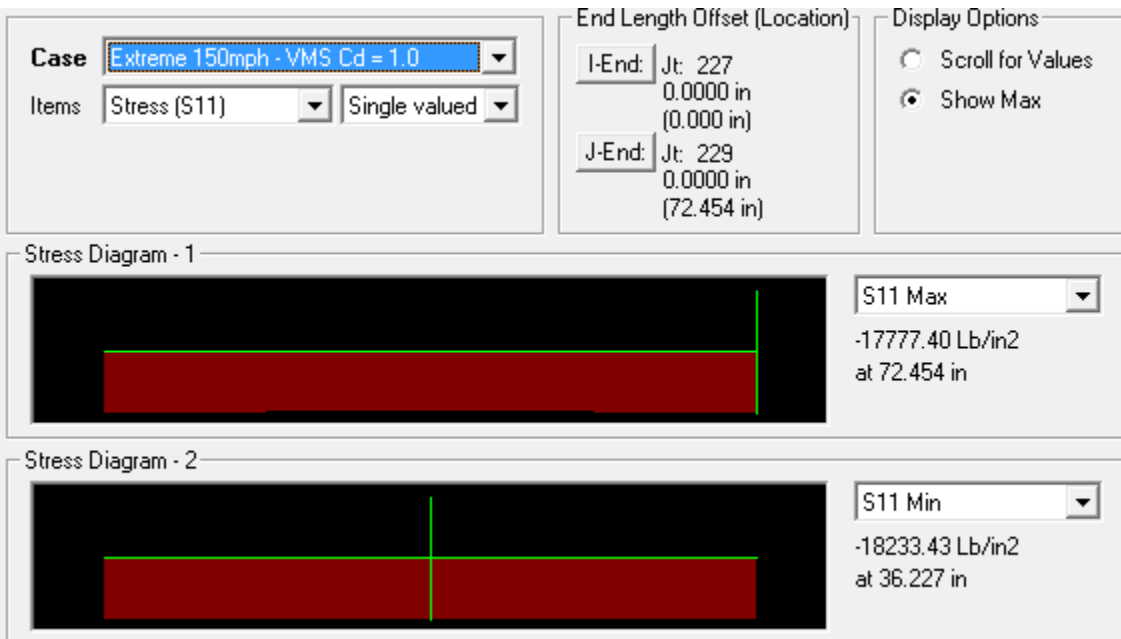
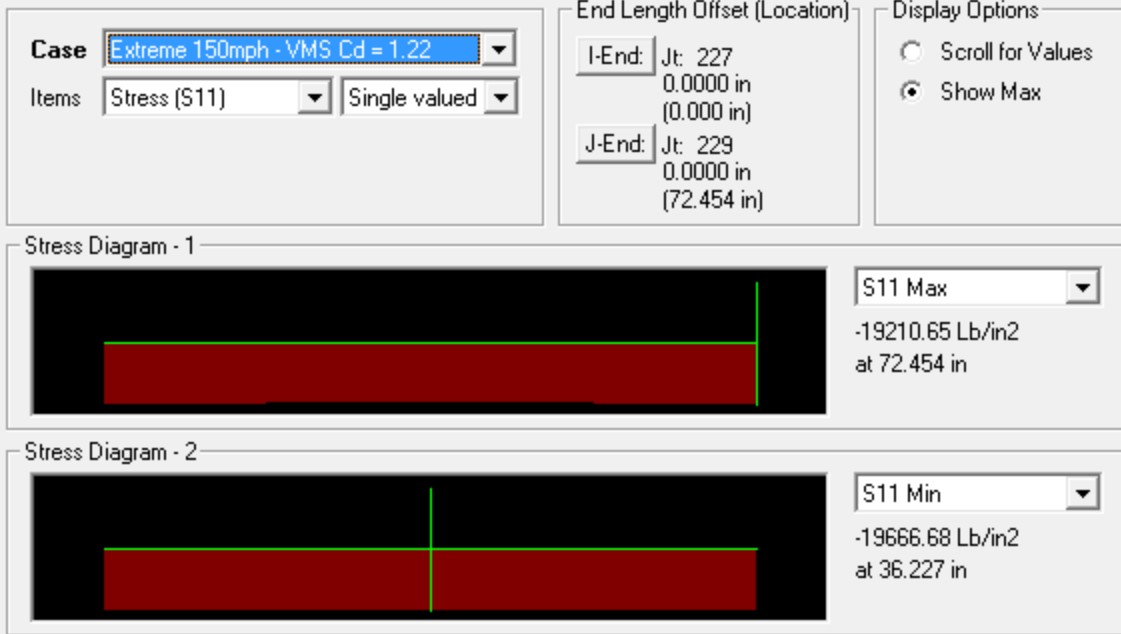
Case Fatigue - VMS Cd = 1.0 Items Stress (S11) Single valued	End Length Offset (Location) I-End: Jt: 52 0.0000 in (0.000 in) J-End: Jt: 36 0.0000 in (405.500 in)	Display Options <input type="radio"/> Scroll for Values <input checked="" type="radio"/> Show Max
---	---	--

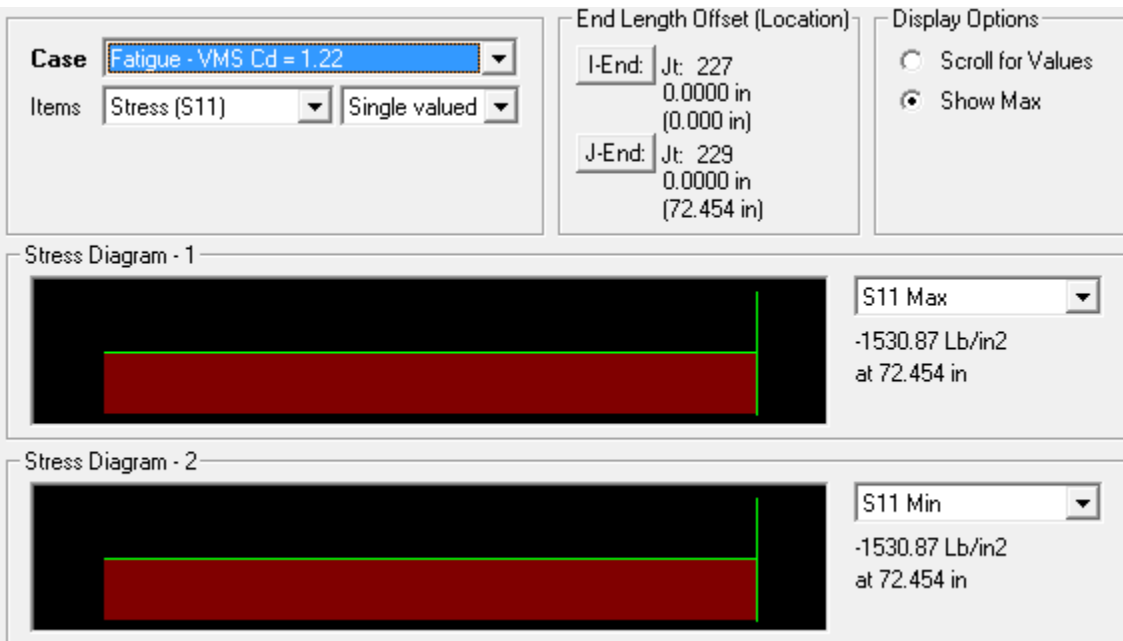
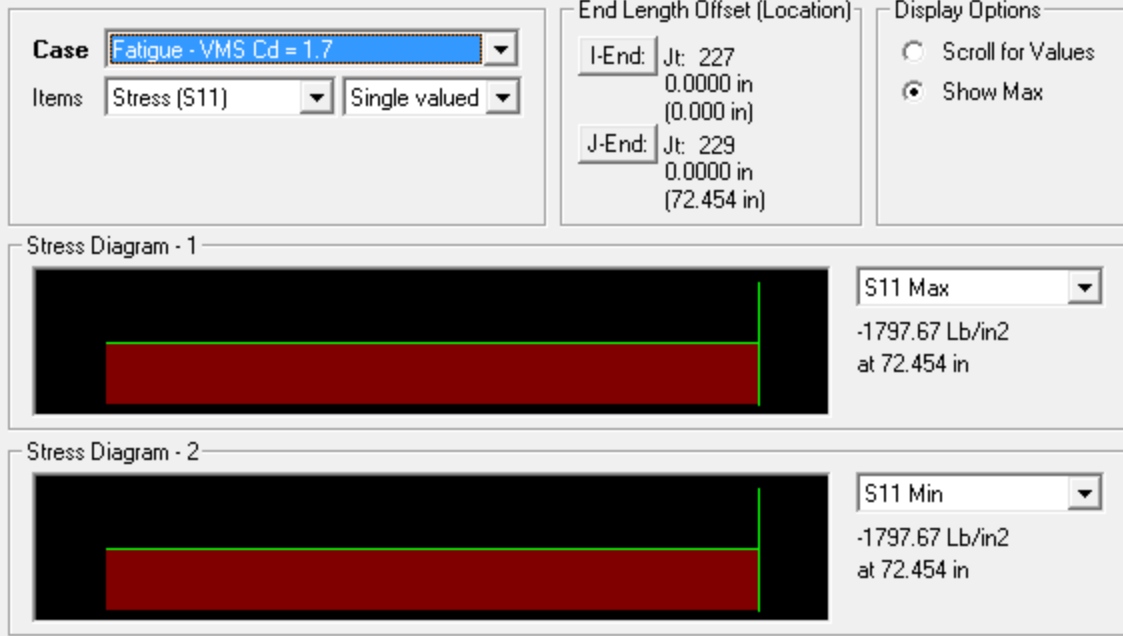


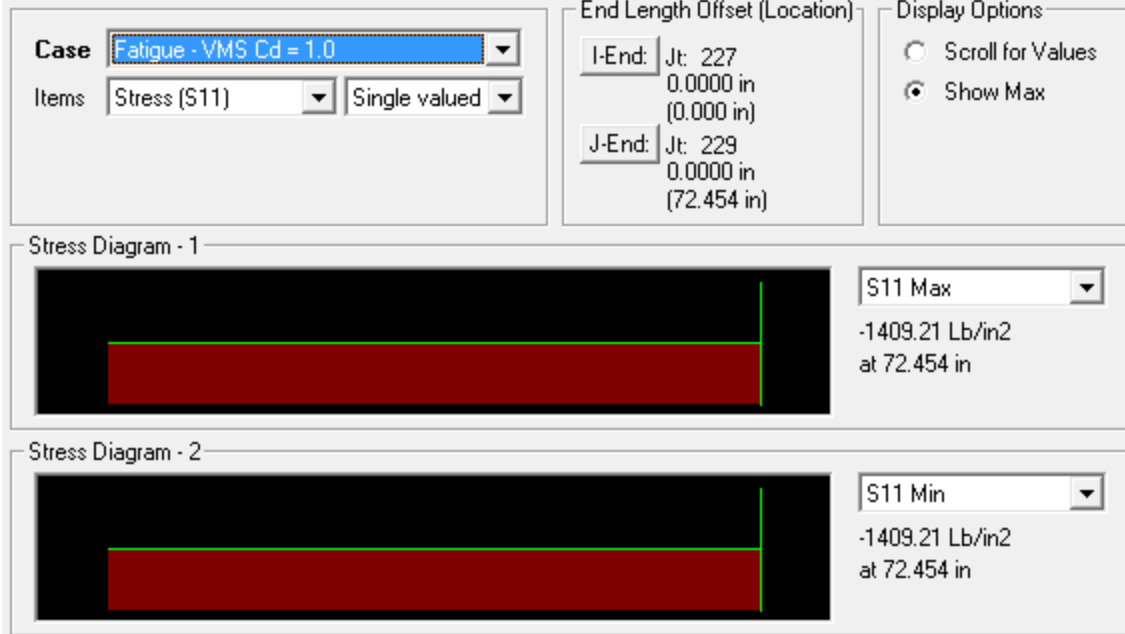
Diagonal 1



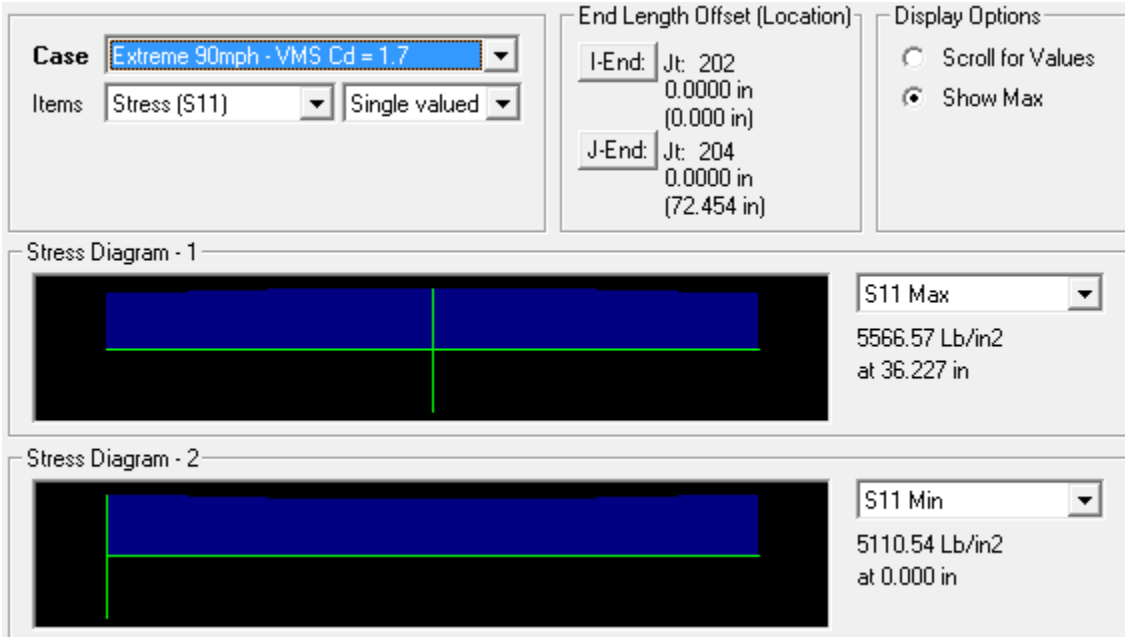


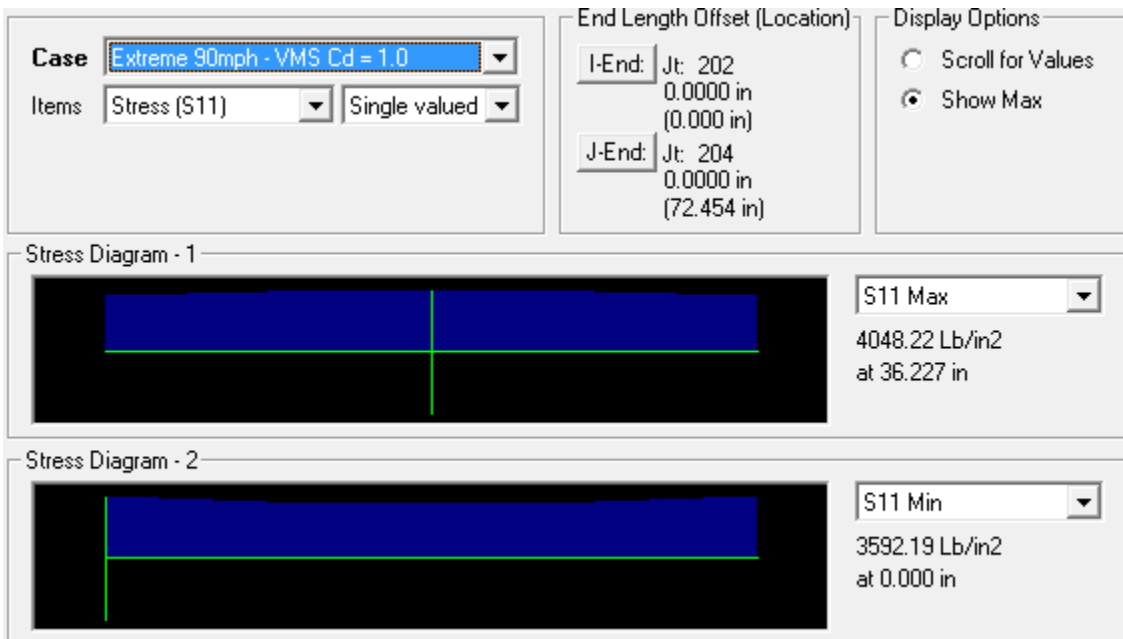
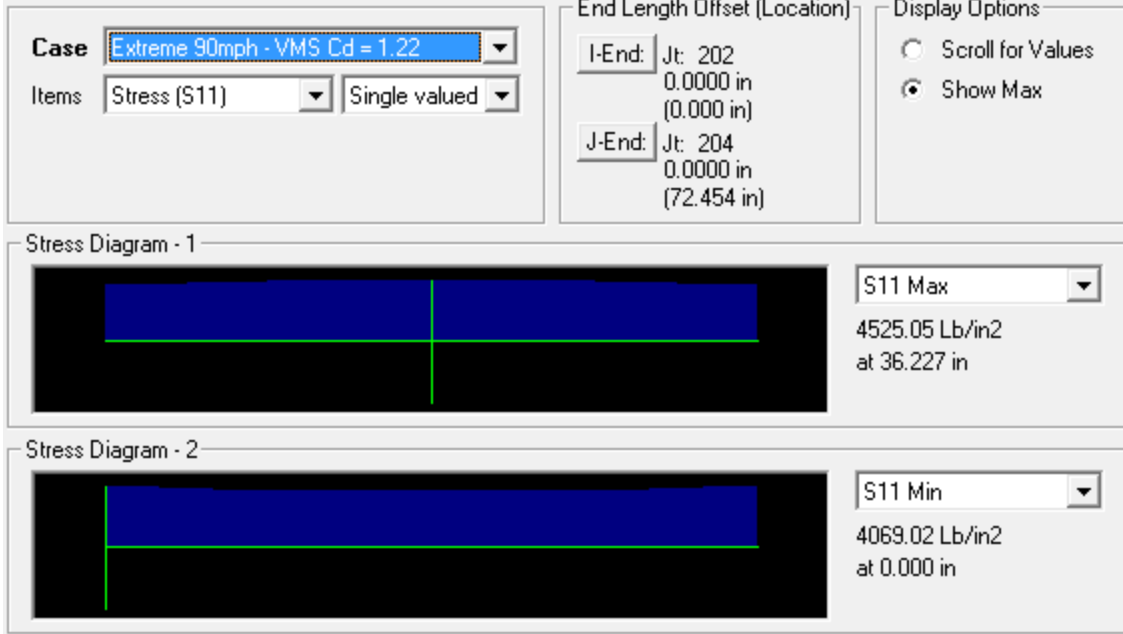






Diagonal 2

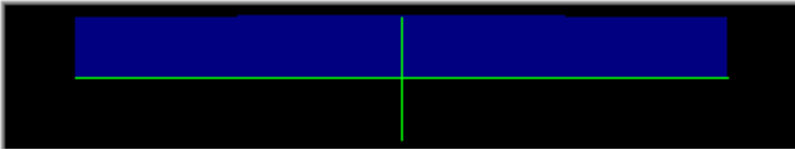





Case: Extreme 150mph - VMS Cd = 1.7
 Items: Stress (S11) Single valued

End Length Offset (Location)
 I-End: Jt: 202
 0.0000 in
 (0.000 in)
 J-End: Jt: 204
 0.0000 in
 (72.454 in)

Display Options
 Scroll for Values
 Show Max

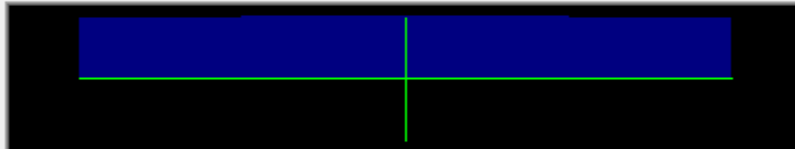
Stress Diagram - 1

 S11 Max
 16996.75 Lb/in2
 at 36.227 in

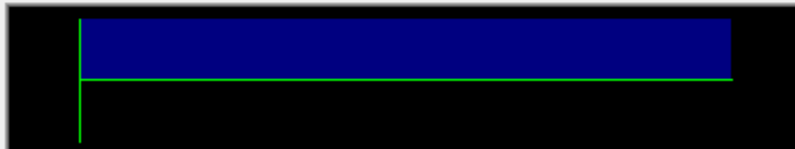
Stress Diagram - 2

 S11 Min
 16540.71 Lb/in2
 at 72.454 in

Case: Extreme 150mph - VMS Cd = 1.22
 Items: Stress (S11) Single valued

End Length Offset (Location)
 I-End: Jt: 202
 0.0000 in
 (0.000 in)
 J-End: Jt: 204
 0.0000 in
 (72.454 in)

Display Options
 Scroll for Values
 Show Max

Stress Diagram - 1

 S11 Max
 14104.18 Lb/in2
 at 36.227 in

Stress Diagram - 2

 S11 Min
 13648.15 Lb/in2
 at 0.000 in

Case Extreme 150mph - VMS Cd = 1.0

Items Stress (S11) Single valued

End Length Offset (Location)

I-End: Jt: 202
0.0000 in
(0.000 in)

J-End: Jt: 204
0.0000 in
(72.454 in)

Display Options

Scroll for Values

Show Max

Stress Diagram - 1

S11 Max

12778.35 Lb/in2
at 36.227 in

Stress Diagram - 2

S11 Min

12322.31 Lb/in2
at 0.000 in

Case Fatigue - VMS Cd = 1.7

Items Stress (S11) Single valued

End Length Offset (Location)

I-End: Jt: 202
0.0000 in
(0.000 in)

J-End: Jt: 204
0.0000 in
(72.454 in)

Display Options

Scroll for Values

Show Max

Stress Diagram - 1

S11 Max

1516.50 Lb/in2
at 72.454 in

Stress Diagram - 2

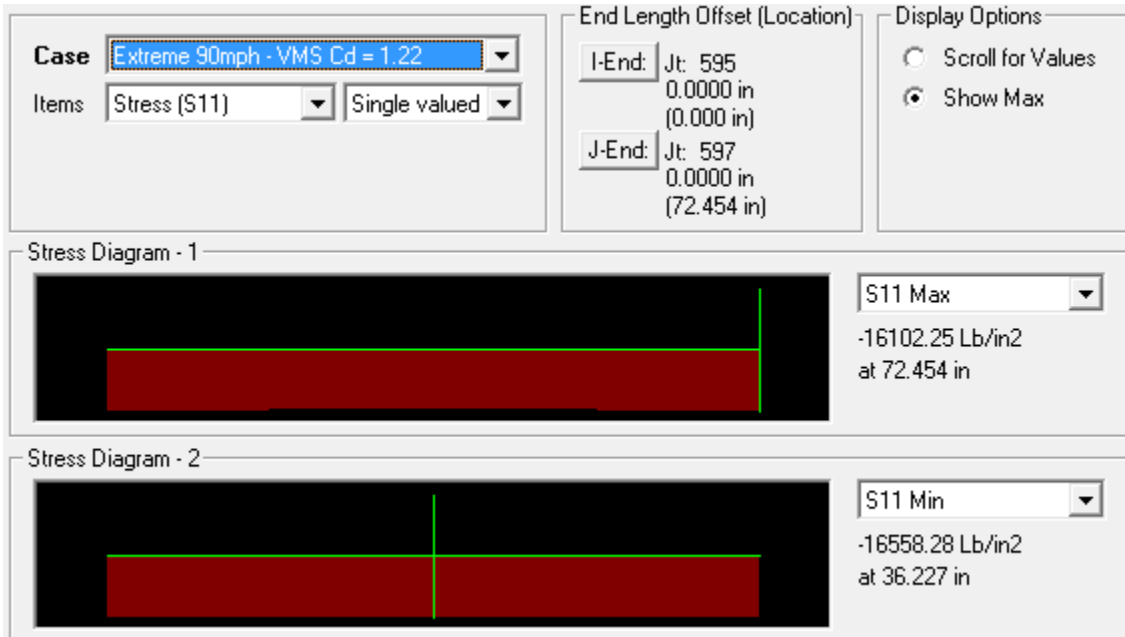
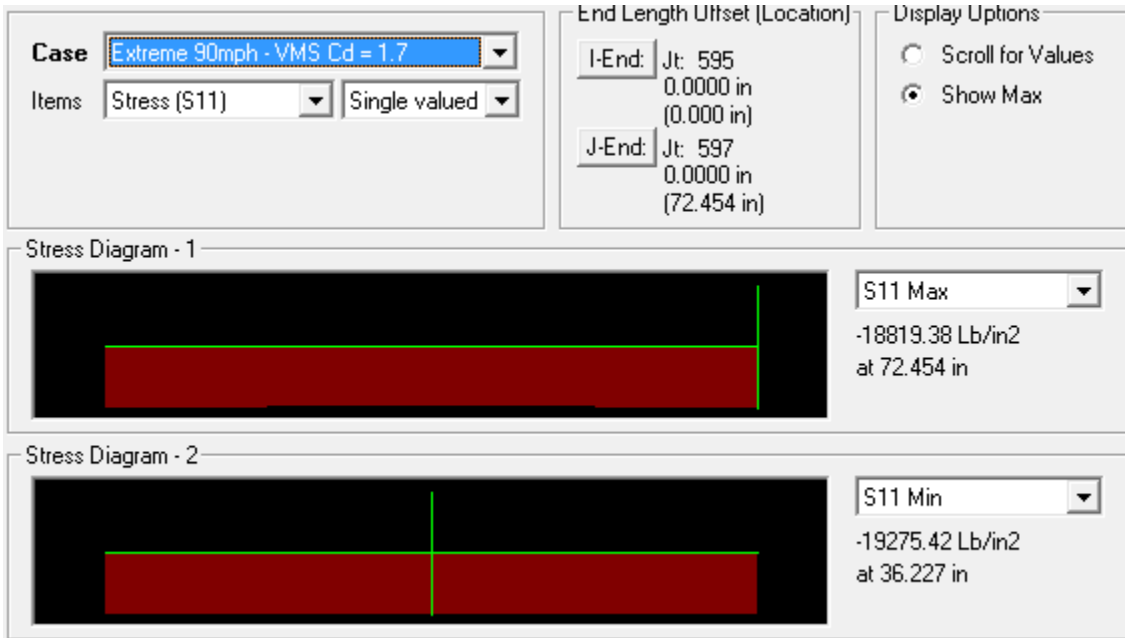
S11 Min

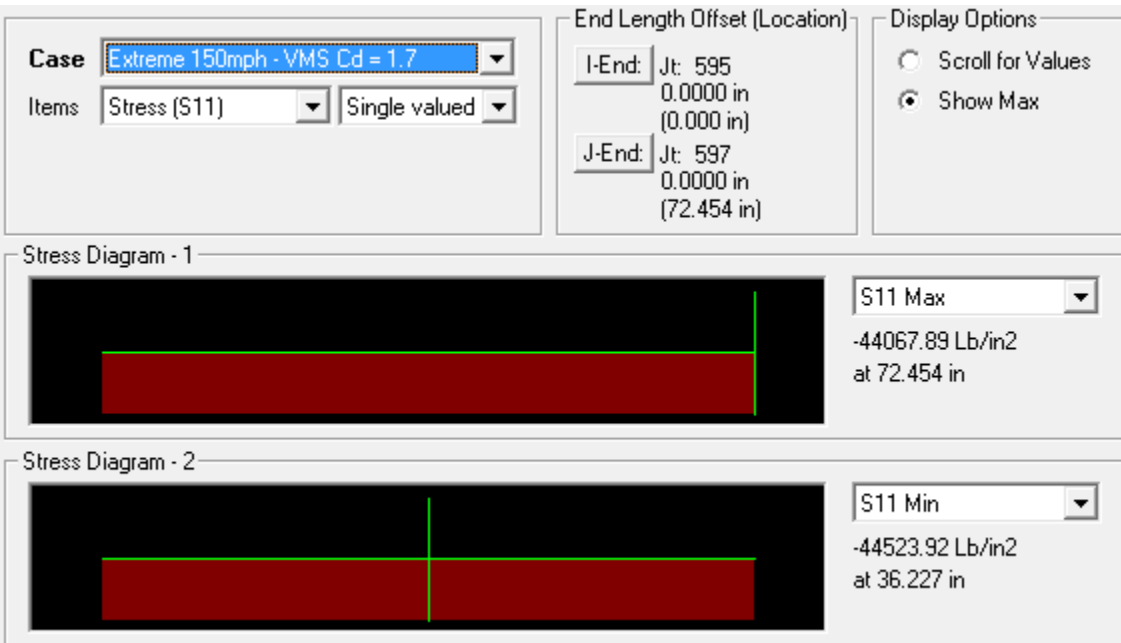
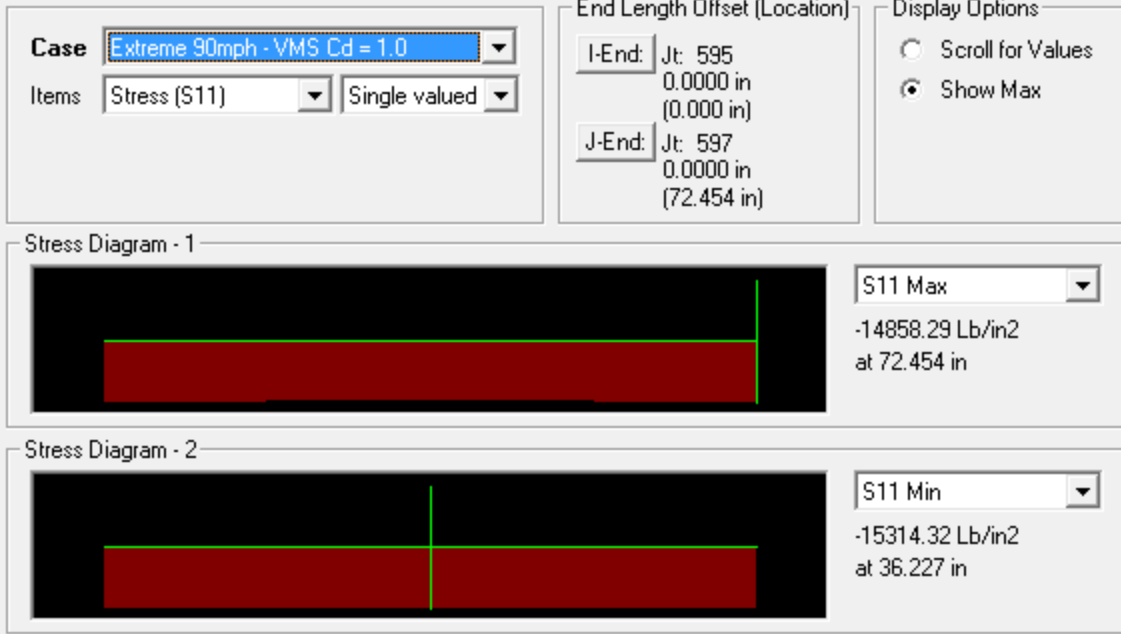
1516.50 Lb/in2
at 72.454 in

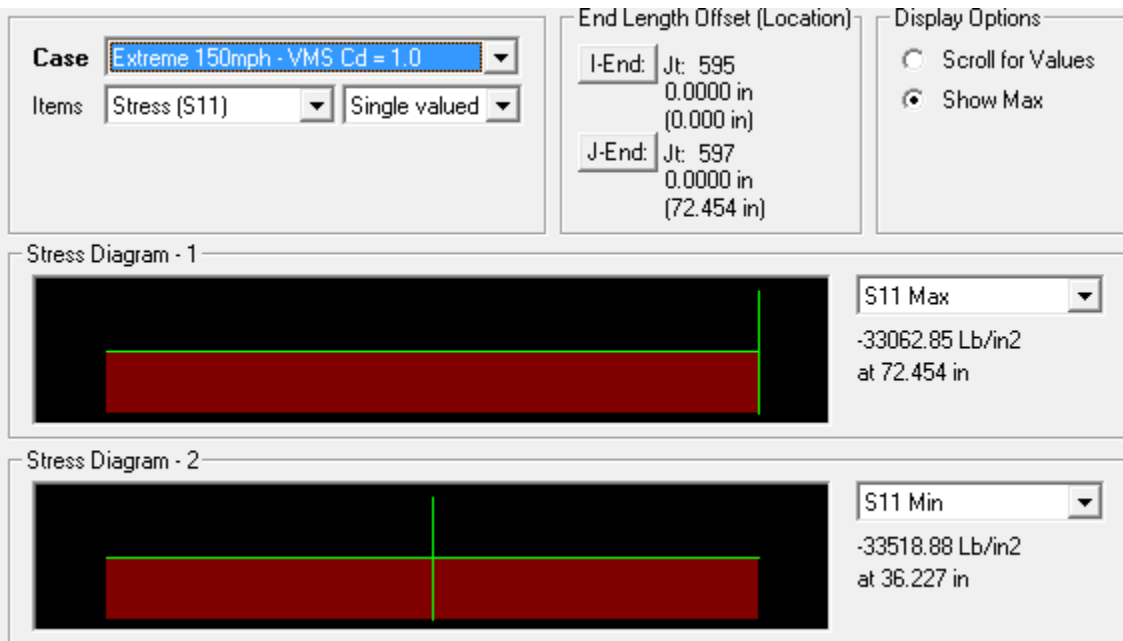
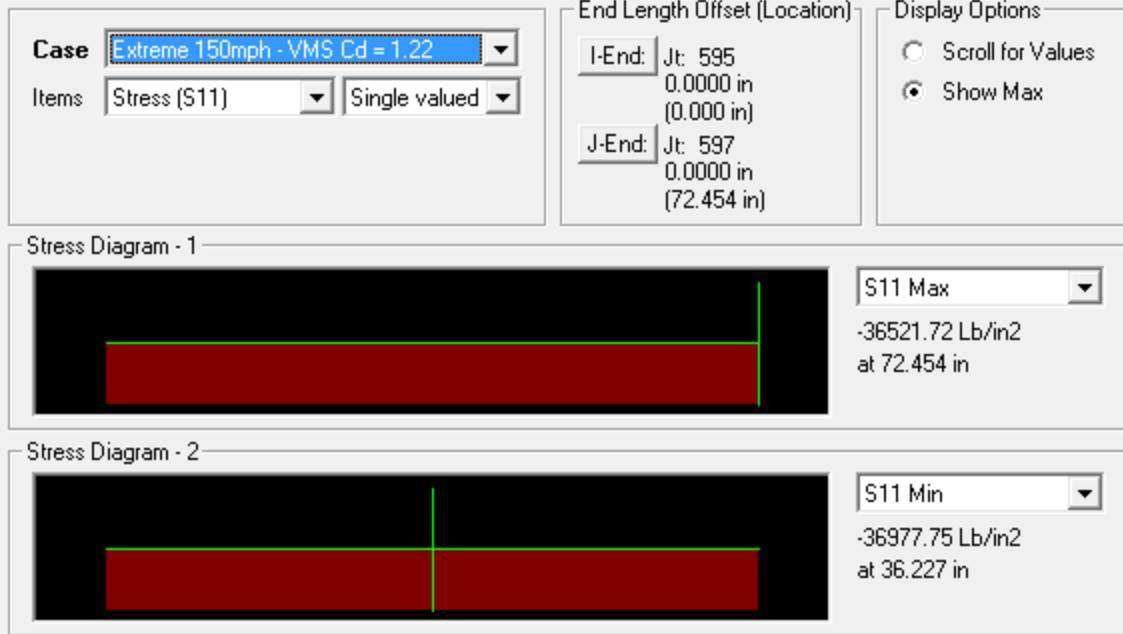
Case Fatigue - VMS Cd = 1.22 Items Stress (S11) Single valued	End Length Offset (Location) I-End: Jt: 202 0.0000 in (0.000 in) J-End: Jt: 204 0.0000 in (72.454 in)	Display Options <input type="radio"/> Scroll for Values <input checked="" type="radio"/> Show Max
Stress Diagram - 1 		
		S11 Max 1269.69 Lb/in2 at 72.454 in
Stress Diagram - 2 		
		S11 Min 1269.69 Lb/in2 at 72.454 in

Case Fatigue - VMS Cd = 1.0 Items Stress (S11) Single valued	End Length Offset (Location) I-End: Jt: 202 0.0000 in (0.000 in) J-End: Jt: 204 0.0000 in (72.454 in)	Display Options <input type="radio"/> Scroll for Values <input checked="" type="radio"/> Show Max
Stress Diagram - 1 		
		S11 Max 1157.15 Lb/in2 at 72.454 in
Stress Diagram - 2 		
		S11 Min 1157.15 Lb/in2 at 72.454 in

Diagonal 3

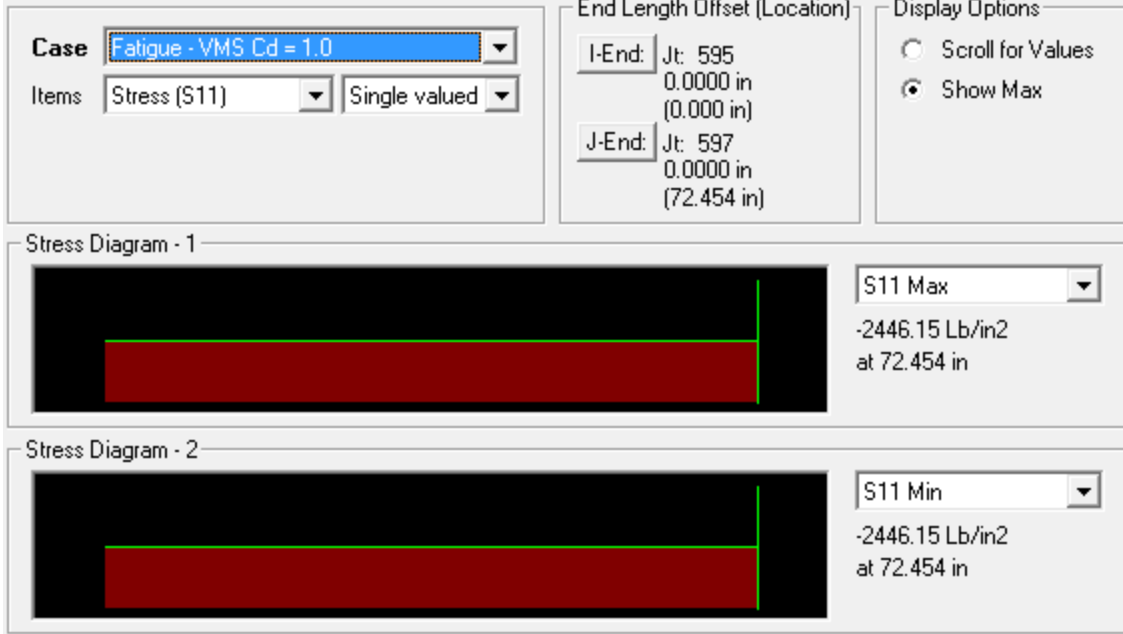




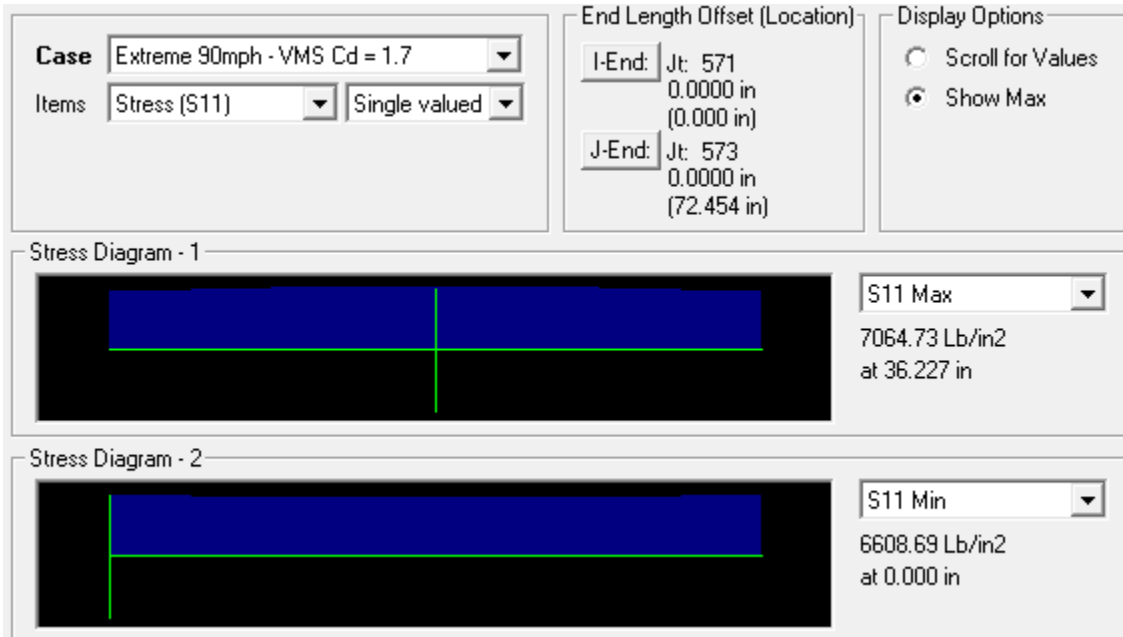


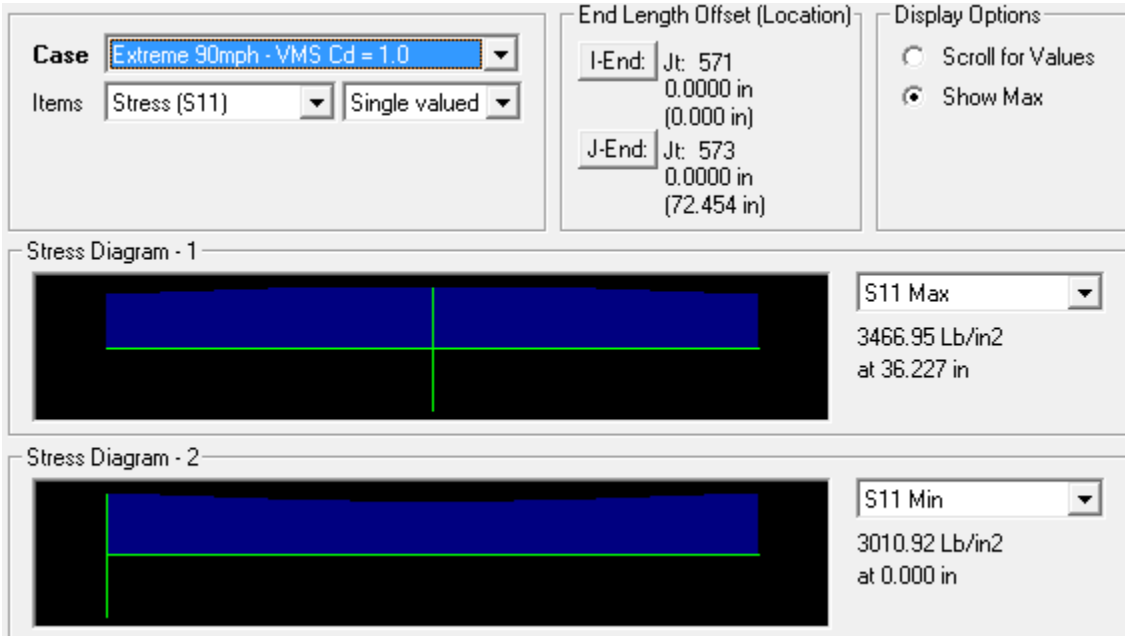
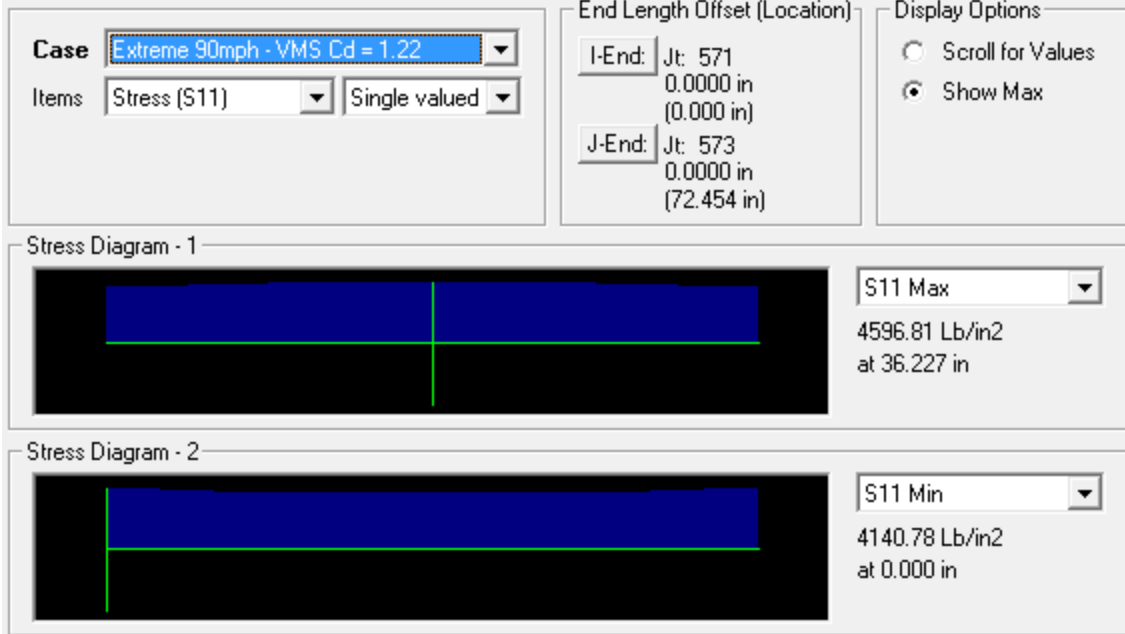
Case Fatigue - VMS Cd = 1.7 Items Stress (S11) Single valued	End Length Offset (Location) I-End: Jt: 595 0.0000 in (0.000 in) J-End: Jt: 597 0.0000 in (72.454 in)	Display Options <input type="radio"/> Scroll for Values <input checked="" type="radio"/> Show Max
Stress Diagram - 1 		
		S11 Max -3383.63 Lb/in2 at 72.454 in
Stress Diagram - 2 		
		S11 Min -3383.63 Lb/in2 at 72.454 in

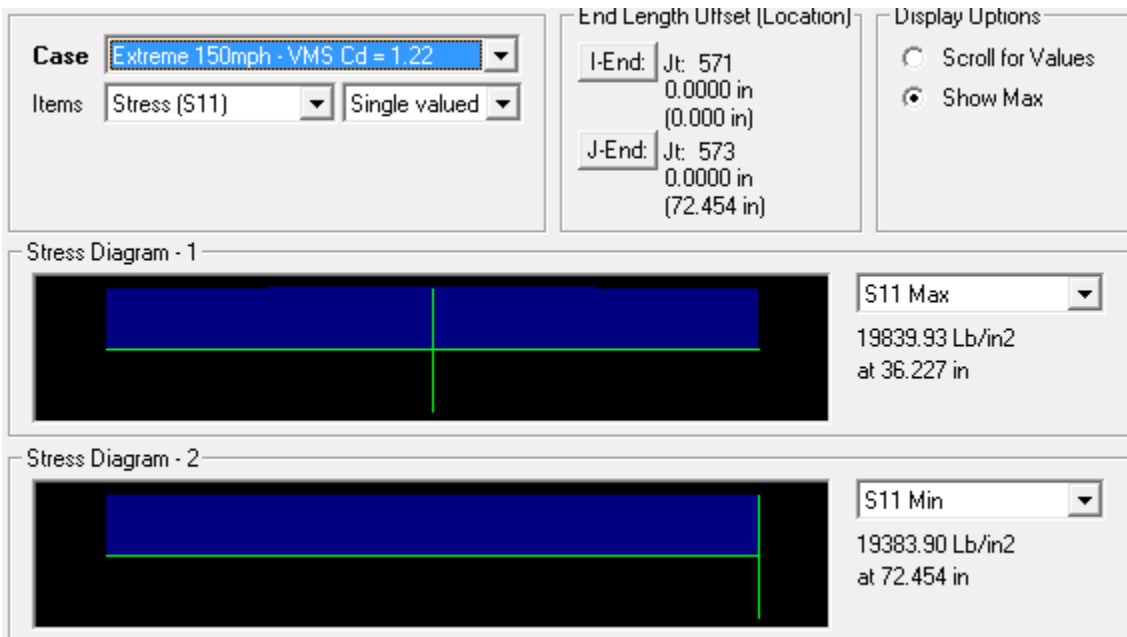
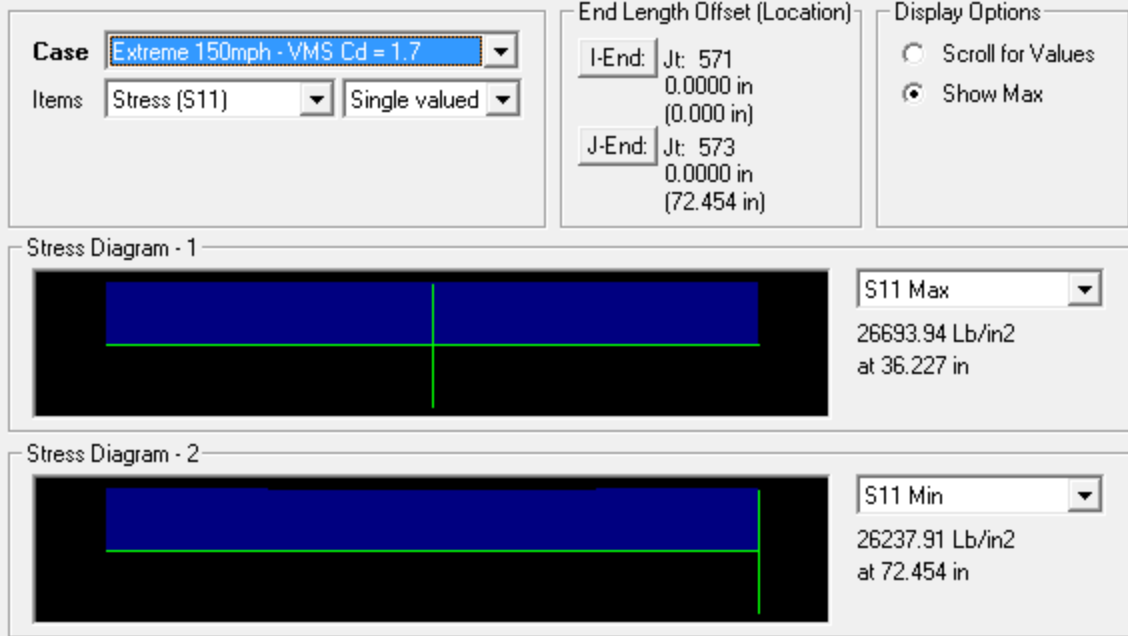
Case Fatigue - VMS Cd = 1.22 Items Stress (S11) Single valued	End Length Offset (Location) I-End: Jt: 595 0.0000 in (0.000 in) J-End: Jt: 597 0.0000 in (72.454 in)	Display Options <input type="radio"/> Scroll for Values <input checked="" type="radio"/> Show Max
Stress Diagram - 1 		
		S11 Max -2739.76 Lb/in2 at 72.454 in
Stress Diagram - 2 		
		S11 Min -2739.76 Lb/in2 at 72.454 in



Diagonal 4







Case Extreme 150mph - VMS Cd = 1.0

Items Stress (S11) Single valued

End Length Offset (Location)

I-End: Jt: 571
0.0000 in
(0.000 in)

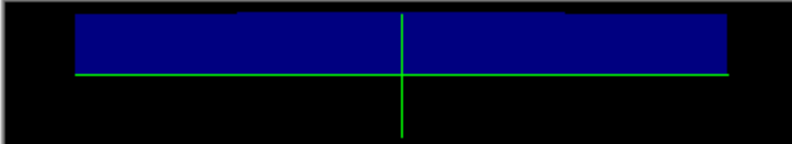
J-End: Jt: 573
0.0000 in
(72.454 in)

Display Options

Scroll for Values

Show Max


Stress Diagram - 1



S11 Max

16698.31 Lb/in2
at 36.227 in

Stress Diagram - 2



S11 Min

16242.28 Lb/in2
at 72.454 in

Case Fatigue - VMS Cd = 1.7

Items Stress (S11) Single valued

End Length Offset (Location)

I-End: Jt: 571
0.0000 in
(0.000 in)

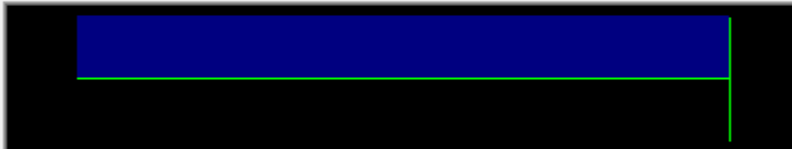
J-End: Jt: 573
0.0000 in
(72.454 in)

Display Options

Scroll for Values

Show Max

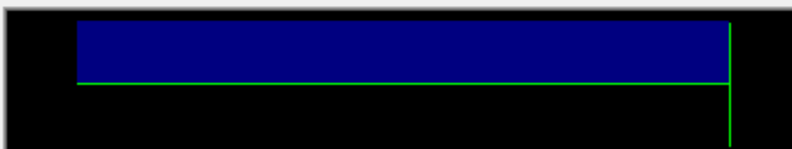
Stress Diagram - 1



S11 Max



2608.44 Lb/in2
at 72.454 in


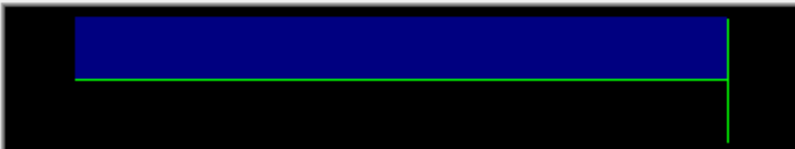
Stress Diagram - 2



S11 Min

2608.44 Lb/in2
at 72.454 in

Case Fatigue - VMS Cd = 1.22 Items Stress (S11) Single valued	End Length Offset (Location) I-End: Jt: 571 0.0000 in (0.000 in) J-End: Jt: 573 0.0000 in (72.454 in)	Display Options <input type="radio"/> Scroll for Values <input checked="" type="radio"/> Show Max
Stress Diagram - 1 		
		S11 Max 2023.63 Lb/in2 at 72.454 in
Stress Diagram - 2 		
		S11 Min 2023.63 Lb/in2 at 72.454 in

Case Fatigue - VMS Cd = 1.0 Items Stress (S11) Single valued	End Length Offset (Location) I-End: Jt: 571 0.0000 in (0.000 in) J-End: Jt: 573 0.0000 in (72.454 in)	Display Options <input type="radio"/> Scroll for Values <input checked="" type="radio"/> Show Max
Stress Diagram - 1 		
		S11 Max 1756.95 Lb/in2 at 72.454 in
Stress Diagram - 2 		
		S11 Min 1756.95 Lb/in2 at 72.454 in